КАЗАХСКИЙ НАЦИОНАЛЬНЫЙ УНИВЕРСИТЕТ имени АЛЬ-ФАРАБИ

ИНСТИТУТ ВЫЧИСЛИТЕЛЬНЫХ ТЕХНОЛОГИЙ
СИБИРСКОГО ОТДЕЛЕНИЯ РАН

ISSN 1560-7534
ISSN 1563-0285

СОВМЕСТНЫЙ ВЫПУСК

по материалам международной научной конференции
"Вычислительные и информационные технологии в науке, технике и образовании"
(CITech-2015)
(24-27 сентября 2015 года)

ВЫЧИСЛИТЕЛЬНЫЕ ТЕХНОЛОГИИ

Том 20

ВЕСТНИК КАЗНУ им. АЛЬ-ФАРАБИ

Серия математика, механика и информатика № 3 (86)

ЧАСТЬ II

АЛМАТЫ – НОВОСИБИРСК, 2015

Вычислительные Технологии

2015

Том 20

Computational Technologies

2015
Vol 20

ВЕСТНИК КАЗНУ 2015

Серия математика, механика и информатика № 3 (86)

Научное издание

Вестник КазНУ
Серия математика, механика, информатика
№ 3(86) 2015

ИБ № 8515

Подписано 14.04.2015 г. Формат 60x84 1/8. Бумага офсетная.
Печать цифровая. Объем 30,5 п.л. Тираж 500 экз. Заказ № 2618.
Казахского национального университета им. аль-Фараби.
050040, г. Алматы, пр. аль-Фараби, 71, КазНУ.
Отпечатано в типографии издательского дома «Қазақ университеті».
Издательский дом «Қазақ университеті»

The BULLETIN of KAZNU

Mathematics, Mechanics and Informatics Issue

2015

№ 3 (86)

Table of Contents

Session III. Mathematical modeling of technological processes

Session III. Mathematical modeling of technological processes

Optimal Stabilization of the Spacecraft's Rotational Motion on Finite Time Interval *

Shamshi Aipanov and Zainel Murzabekov

Research Institute for Mathematics and Mechanics,
Al-Farabi Kazakh National University,
Al-Farabi ave. 71, 050040 Almaty, Kazakhstan
{aipanov,murzabekov-zein}@mail.ru

Abstract. The problem of optimal damping the rotational motion of a spacecraft (SC) considered as a solid body and described by Euler's dynamic equations has been studied. It is required to transfer the SC with ellipsoid-constrained input to a state of rest in a given time interval. Optimal control problem on a finite time interval with fixed endpoints of trajectories and constrained input is solved in this paper by using Lagrange multipliers of a special form, that allows to construct an optimal feedback control. An example which shows the effectiveness of the proposed method for solving the problem is considered. A high accuracy transfer of a system to a state of rest and a high-speed performance of the algorithm is attained due to analytical solving possibility of some matrix differential equations (for instance, Riccati equations) taking into account the skew-symmetry property of the system.

Keywords: spacecraft, rotational motion, ellipsoid-constrained input, bilinear-quadratic optimal control problem, skew-symmetric system, method of Lagrange multipliers.

1 Introduction

Optimal control problems for dynamic systems with fixed endpoints of trajectories are frequently met in practice. These are, for example, control problems for space vehicles, aircrafts, robotic manipulators, electric power systems, etc. In these problems it is required to transfer the system from the given initial state to the desired final state within the finite interval of time, minimizing fuel or energy cost. Frequently we come across problems with box- or ellipsoid-constraints on control values.

Various mathematical formulations of the optimal control problems as well as their classification and applications are provided in [1]-[4]. Detailed surveys of models and methods used in modern optimal control theory are presented in [5], [6].

An optimal control problem for dynamic systems can be stated as a problem of finding an open-loop (programmed) control $u(t)$ or designing a closed-loop (synthesizing) control $u(x,t)$, where x is a state-vector, t is a current time. Note that feedback control plays a particularly important role for stochastic control systems [7], [8]. In the first case, the problem can be solved by using Pontryagin maximum principle [9], [10]. However, this approach gives only the necessary conditions of optimality, and this circumstance limits its possibilities for wide range applications. Besides, here arises a two-point boundary problem for ODEs which leads to some computational difficulties connected with quickly growing solutions [11]. In the second case, Bellman's dynamic programming method [12], [13] or Krotov's sufficient conditions of optimality [14] can be used. But in these methods we come across the complexities related to the choice of corresponding Bellman's or Krotov's functions.

* This work is supported by the the Science Committee of the RK Ministry of Education and Science under Grant No. 1625/GF3.

Note that the peculiarity of the problem under consideration consists in that the trajectories of the system should pass through given points at the initial and final time moments, i.e. left and right ends of the system trajectories are fixed. The problem with fixed right endpoints can be reduced to the problem with free right endpoints taking into account a trajectory deviation from the desired terminal point as a penalty in an objective functional. However, in order to provide sufficiently high precision of hitting the system into the given final state, one should assign sufficiently high values of a penalty function; this may lead to prevailing of a penalty over the initial target. That's why here we solve the optimal control problem without using penalty functions.

The method for solving the optimal control problem presented in the given article is based on Lagrange multipliers [15]. We'll use multipliers of special form [16], which make possible to obtain feedback optimal control and transfer the system to the desired state at the final time moment.

The paper is organized as follows. Mathematical statement of the optimal control problem for the SC's rotational motion with fixed endpoints of trajectories and ellipsoid-constrained input is given in Section 2. Section 3 is devoted to solving the problem by using the method of Lagrange multipliers. In Section 4, a numerical example will be presented to illustrate the effectiveness of the proposed algorithm. Finally, we draw some concluding remarks in Section 5.

2 Problem Statement

The rotational motion of a SC considered as a solid body is described by the Euler dynamic equations [17]:

$$\begin{aligned} J_1\dot{\omega}_1(t) &= (J_2 - J_3)\omega_2(t)\omega_3(t) + M_1(t), \\ J_2\dot{\omega}_2(t) &= (J_3 - J_1)\omega_1(t)\omega_3(t) + M_2(t), \\ J_3\dot{\omega}_3(t) &= (J_1 - J_2)\omega_1(t)\omega_2(t) + M_3(t), \end{aligned} \tag{1}$$

where $\omega_i(t)$ are components of $\omega(t)$, an angular velocity vector; $M_i(t)$ are projections of $M(t)$, a principal moment of external forces; J_i are projections of a principal central moment of inertia of the body. Note that the right-hand sides of the differential equations (1) are bilinear functions of $\omega_i(t)$, $(i = 1, 2, 3)$.

Let the condition

$$\omega(t_0) = (\omega_1(t_0), \omega_2(t_0), \omega_3(t_0))^T = \omega_0, \tag{2}$$

defining the SC rotation at initial moment t_0 be given for the system (1). Consider the problem of optimal damping the initial rotation of a SC within the given time interval $[t_0, t_f]$ in such a way that the angular velocity at the final moment t_f be equal to zero:

$$\omega(t_f) = 0. \tag{3}$$

We'll consider the case of constrained control, supposing that the input $M(t) = (M_1(t), M_2(t), M_3(t))^T$ can take values in the set U, given in the form of ellipsoid:

$$M(t) \in U = \{M = (M_1, M_2, M_3)^T \mid \sqrt{M^T D M} \le d_0\}, \quad t \in [t_0, t_f], \tag{4}$$

where D is a positive-definite diagonal matrix; $d_0 > 0$; a superscript T denotes the transpose.

Let the objective functional be given by

$$\begin{aligned} J(M(\cdot)) = \frac{1}{2}\int_{t_0}^{t_f} \big\{\alpha^2 \left[J_1^2(t)\omega_1^2(t) + J_2^2(t)\omega_2^2(t) + J_3^2(t)\omega_3^2(t)\right] + \\ M_1^2(t) + M_2^2(t) + M_3^2(t)\big\}\, dt \to \inf_M, \end{aligned} \tag{5}$$

where $\alpha > 0$ is a given parameter. The quadratic functional (5) corresponds to the objective of minimization the cost for control action and dampening the SC (the damping speed of the SC rotational motion is regulated by using the parameter α).

It's required to find the control input $M(t) = (M_1(t), M_2(t), M_3(t))^T$, satisfying the constraint (4), that transfers the system (1) from the initial state (2) to the state of rest (3) within the finite time interval of $[t_0, t_f]$ and minimizes the objective functional (5).

It turned out, that the considered problem solving can be appreciably simplified, if one reduces the system (1) to the form with skew-symmetric matrix. For this purpose let's make the change of variables [2]:

$$L_i(t) = J_i\omega_i(t), \quad (i = 1, 2, 3),$$

where $L_i(t)$ are components of $L(t)$, an angular momentum of the SC. Then the system (1) can be presented in the form

$$\dot{x}(t) = A(x(t))x(t) + Bu(t), \quad t \in [t_0, t_f], \tag{6}$$

where the state vector $x(t) = (L_1(t), L_2(t), L_3(t))^T$, the control vector $u(t) = (M_1(t), M_2(t), M_3(t))^T$,

$$A(x(t)) = \begin{pmatrix} 0 & L_3(t)/J_3 & -L_2(t)/J_2 \\ -L_3(t)/J_3 & 0 & L_1(t)/J_1 \\ L_2(t)/J_2 & -L_1(t)/J_1 & 0 \end{pmatrix}, \quad B = \begin{pmatrix} 1\,0\,0 \\ 0\,1\,0 \\ 0\,0\,1 \end{pmatrix}.$$

Here the matrix $A(x(t))$, depending on the state vector $x(t)$, is skew-symmetric:

$$A^T(x(t)) = -A(x(t)). \tag{7}$$

The initial and final conditions (2), (3) can be rewritten in the form

$$x(t_0) = (J_1\omega_1(t_0), J_2\omega_2(t_0), J_3\omega_3(t_0))^T = x_0, \quad x(t_f) = 0. \tag{8}$$

From (4) we have that the control $u(t)$ should satisfy the ellipsoid-constraint

$$u^T(t)Du(t) \le d_0^2, \quad x \in [t_0, t_f]. \tag{9}$$

The quadratic objective functional (5) will has the form

$$J(u(\cdot)) = \frac{1}{2}\int_{t_0}^{t_f} \left[x^T(t)Qx(t) + u^T(t)Du(t)\right] dt \to \inf_u, \tag{10}$$

where

$$Q = \begin{pmatrix} \alpha^2 & 0 & 0 \\ 0 & \alpha^2 & 0 \\ 0 & 0 & \alpha^2 \end{pmatrix}, \quad R = \begin{pmatrix} 1\,0\,0 \\ 0\,1\,0 \\ 0\,0\,1 \end{pmatrix}.$$

Thus, we get the bilinear-quadratic optimal control problem (6), (8)-(10) on a finite time interval for the system with fixed endpoints of trajectories and ellipsoid-constrained input.

3 Problem Solving

For arbitrary continuous function $x(\cdot)$ and arbitrary piecewise continuous function $u(\cdot)$ defined in the time interval $[t_0, t_f]$ we construct the Lagrange functional

$$L(x(\cdot), u(\cdot)) = \int_{t_0}^{t_f} \left\{ \frac{1}{2} x^T(t) Q x(t) + \frac{1}{2} u^T(t) R u(t) + \right.$$
$$\left. \lambda_0^T(t)[A(t)x(t) + Bu(t) - \dot{x}(t)] + \frac{1}{2}\lambda(t)\left[u^T(t)Du(t) - d_0^2\right] \right\} dt, \tag{11}$$

where a vector $\lambda_0(x(t), t)$ is a Lagrange multiplier that removes the differential constraint (6); a scalar $\lambda(t) \geq 0$ is a Lagrange multiplier that removes the inequality constraint (9) for control values. We'll use a multiplier $\lambda_0(t)$ of the special form

$$\lambda_0(t) = \lambda_0(x(t), t) = K(t)x(t) + q(t), \quad t \in [t_0, t_f],$$

where $K(t)$ is a symmetric matrix, $q(t)$ is a vector [16].

Let's introduce the function

$$V(x, t) = \frac{1}{2} x^T K(t) x + x^T q(t)$$

(note that the gradient $\nabla_x V(x, t) = \lambda_0(x, t)$). Then the functional (11) can be written as

$$L(x(\cdot), u(\cdot)) = V(x(t_0), t_0) - V(x(t_f), t_f) + \int_{t_0}^{t_f} M(x(t), u(t), t)\, dt,$$

where

$$M(x, u, t) = \frac{1}{2} x^T Q(t) x + \frac{1}{2} u^T R u + [K(t)x + q(t)]^T [A(t)x + Bu + f(t)] +$$
$$\frac{1}{2} x^T \dot{K}(t) x + x^T \dot{q}(t) + \frac{1}{2}\lambda(t)\left[u^T D(t) u - d_0^2\right].$$

We choose a control u so that the function $M(x, u, t)$ attains a minimum with respect to u and x for all $t \in [t_0, t_f]$. From this we obtain the formula for the input $u(t)$ and differential equations for matrix $K(t)$ and vector $q(t)$. The control $u(t) = u(x(t), t)$ can be presented in the form

$$u(x(t), t) = -[R + \lambda(t)D]^{-1} B^T [K(t)x(t) + q(t)] = w(x(t), t) + v(x(t), t), \tag{12}$$

where

$$w(x(t), t) = -R^{-1}(t)[K(t)x(t) + q(t)],$$
$$v(x(t), t) = \left\{ \left[[I + \lambda(t) R^{-1}(t) D \right]^{-1} - I \right\} w(x(t), t), \tag{13}$$

I is an identity matrix. Note that at $\lambda(t) = 0$ we have $v(x(t), t) = 0$. As matrices R, D are positive-definite and $\lambda(t) \geq 0$, then inverse matrices in (12), (13) exist for all $t \in [t_0, t_f]$. The control (12) depends on matrix $K(t)$, vector $q(t)$ and Lagrange multiplier $\lambda(t)$, which we have to define.

Substituting the control (12) into (6), we obtain the differential equation

$$\dot{x}(t) = [A(t) - SK(t)]x(t) + Bv(x(t), t) - Sq(t), \quad x(t_0) = x_0, \tag{14}$$

where $S = BR^{-1}B^T$.

We have also the following differential equations for determining $K(t)$ and $q(t)$:

$$\dot{K}(t) = -A^T(t)K(t) - K(t)A(t) + K(t)SK(t) - Q, \quad K(t_f) = K_f, \tag{15}$$

$$\dot{q}(t) = -[A(t) - SK(t)]^T q(t) + W^{-1}(t)Bv(x(t), t), \quad q(t_0) = q_0, \tag{16}$$

where matrix $W(t)$ is the solution of the differential equation

$$\dot{W}(t) = [A(t) - SK(t)]W(t) + W(t)[A(t) - SK(t)]^T - S, \quad W(t_f) = 0. \tag{17}$$

Taking into account the skew-symmetry property of the matrix $A(t) = A(x(t))$ (see (7)) it can be shown that the matrix

$$K(t) \equiv K_f = \begin{pmatrix} \alpha & 0 & 0 \\ 0 & \alpha & 0 \\ 0 & 0 & \alpha \end{pmatrix}, \quad t \in [t_0, t_f] \tag{18}$$

satisfies the Riccati equation (15). Using (18) and the skew-symmetry property of the matrix $A(t) = A(x(t))$, we also find the solution to the equation (17):

$$W(t) = \left[\frac{e^{2\,\alpha(t_f - t)} - 1}{2\,\alpha}\right] \cdot I.$$

It can be shown that under the initial condition $q(t_0) = q_0$ for the differential equation (16) chosen by

$$q(t_0) = W^{-1}(t_0)x_0 = \left[\frac{2\,\alpha}{e^{2\,\alpha(t_f - t_0)} - 1}\right] \cdot x_0,$$

we have $x(t_f) = 0$.

We choose Lagrange multiplier $\lambda(t) \geq 0$ so that the following equality (so called complementary slackness condition)

$$\lambda(t)\left[u^T(x(t), t)Du(x(t), t) - d_0^2\right] = 0, \quad t \in [t_0, t_f] \tag{19}$$

will be satisfied. If the inequality

$$w^T(x(t), t)Dw(x(t), t) - d_0^2 \leq 0, \tag{20}$$

holds true, then we can take $\lambda(t) = 0$. In this case $u(x(t), t) = w(x(t), t)$ and for this control law the constraint (9) will be met on the strength of (20). If the inequality

$$w^T(x(t), t)Dw(x(t), t) - d_0^2 > 0,$$

is valid, then scalar $\lambda = \lambda(t)$ should be chosen from the equation

$$\delta(\lambda) = u^T(x(t), t)Du(x(t), t) - d_0^2 = 0. \tag{21}$$

It can be shown that there exists a unique root $\lambda > 0$ of the equation (21). Hence, due to choice of the corresponding value of Lagrange multiplier $\lambda(t) \geq 0$ we satisfy the constraint (9) and complementary slackness condition (19) for each moment $t \in [t_0, t_f]$. The equation (21) can be solved by using the well-known numerical methods (for example, the bisection method [18]).

Thus, the optimal trajectory $x(t)$ for the problem (6), (8)-(10) is defined by integrating the system of differential equations (14), (16) over the time interval $[t_0, t_f]$; the optimal control $u(x(t), t)$ is calculated by (12).

4 Example: Optimal Damping of Spacecraft Rotation

To solve the problem (1)-(5) of optimal damping SC's initial rotation using constrained control input in a finite time interval, the program for realising the algorithm described in previous section has been written in FORTRAN. The numerical computations were carried out for the following initial data: the SC's rotation stop is implemented in time interval $[t_0, t_f] = [0,\ 400\ \text{s}]$; the value $d_0 = 25\ \text{N}\cdot\text{m}$ is given for the constraint (4); the parameter α in the objective functional (5) is taken to be $\alpha = 10^{-2}$; the principal central moments of inertia of the SC are equal

$$J_1 = 0.5 \cdot 10^5\ \text{kg}\cdot\text{m}^2, \quad J_2 = 2.0 \cdot 10^5\ \text{kg}\cdot\text{m}^2, \quad J_3 = 1.5 \cdot 10^5\ \text{kg}\cdot\text{m}^2;$$

the initial conditions

$$\omega_1(0) = 0.05\ \text{s}^{-1}, \quad \omega_2(0) = 0.02\ \text{s}^{-1}, \quad \omega_3(0) = -0.02\ \text{s}^{-1};$$

the final conditions

$$\omega_1(t_f) = \omega_2(t_f) = \omega_3(t_f) = 0.$$

The numerical computations results are presented in the graphical form in Figs. 1-3. The graphs of angular velocity vector's components variation are presented in Fig. 1. The results of calculations have shown the very high accuracy transfer of the SC to rest. The following values of angular velocity vector's components at final moment t_f are obtained:

$$\begin{gathered}\omega_1(t_f) \approx -0.7779 \cdot 10^{-17}\ \text{s}^{-1}, \quad \omega_2(t_f) \approx -0.5294 \cdot 10^{-17}\ \text{s}^{-1}, \\ \omega_3(t_f) \approx -0.1448 \cdot 10^{-16}\ \text{s}^{-1}.\end{gathered} \tag{22}$$

In Fig. 2 the graphs of control inputs $M_i(t)$, $(i = 1, 2, 3)$ are presented. As shown in Fig. 3 the constraint

$$|M(t)| = \sqrt{M_1^2(t) + M_2^2(t) + M_3^2(t)} \le d_0, \quad t \in [t_0, t_f] \tag{23}$$

holds true.

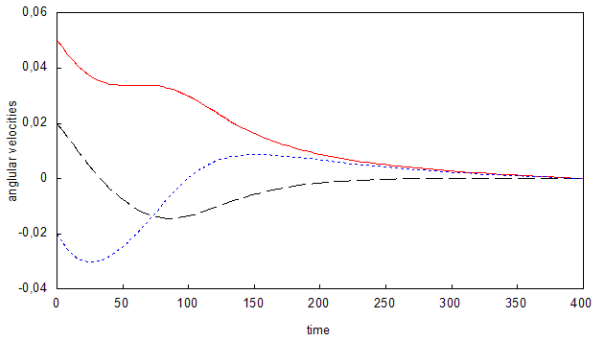

Fig. 1. Graphs of angular velocities (—— $\omega_1(t)$, – – – $\omega_2(t)$, - - - - $\omega_3(t)$)

The numerical computation results show that the found control input $M(t) = (M_1(t), M_2(t), M_3(t))^T$ provides the high accuracy transfer of the system to the final state (see (22)). Moreover, the optimal control $M(t)$ satisfies the constraint (4). As shown in Fig. 3, at the beginning of the interval, in $[t_0, t_1]$, $t_1 \approx 125\ s$, the control takes values on the boundary of the set U, then in the interval $[t_1, t_f]$ the control is inside the set U.

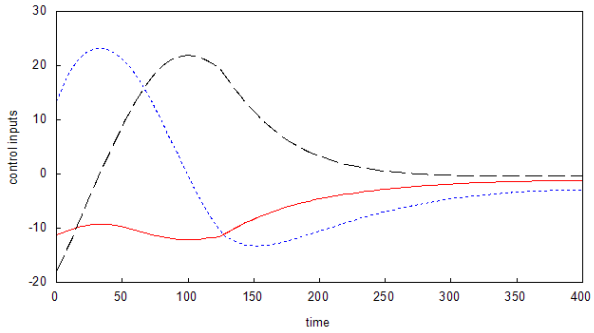

Fig. 2. Graphs of control inputs (—— $M_1(t)$, – – – $M_2(t)$, - - - - $M_3(t)$)

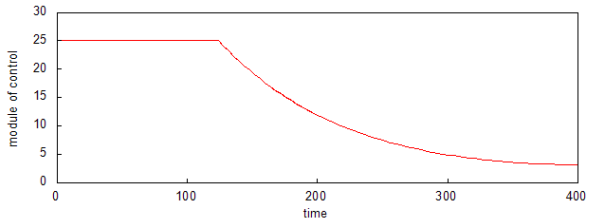

Fig. 3. Graph for the module of control $|M(t)|$

Note that in the case when the control values are interior points of the set U, we have $v(x(t), t) \equiv 0$, $t \in [t_1, t_f]$ in the formula for optimal control (12). At that the conjugate equation (16) has the form

$$\dot{q}(t) = -[A(t) - SK(t)]^T q(t),$$

i.e. the calculation of the inverse matrix $W^{-1}(t)$ in the right-hand side of the differential equation (16) isn't necessary in the interval $t \in [t_1, t_f]$.

5 Conclusion

In this work, the method for solving the bilinear-quadratic problem of optimal control for the skew-symmetric system with ellipsoid-constrained input is suggested. The peculiarity of the problem consists in that left and right ends of trajectories are fixed; it is required to transfer the system from the initial state $x(t_0) = x_0$ to the origin $x(t_f) = 0$ using the closed-loop control within the fixed time interval $[t_0, t_f]$.

The numerical example considered in the previous section demonstrates an effectiveness of the proposed method. The high accuracy transfer of the SC to the final state $\omega(t_f) = 0$ is attained due to the analytical solving the differential equations (15), (17) for determining the matrices $K(t)$, $W(t)$.

References

1. Bryson, A.E., Ho, Y.-C.: Applied Optimal Control: Optimization, Estimation and Control. Taylor & Francis Inc., Washington (1988)
2. Athans, M., Falb, P.L.: Optimal Control: An Introduction to the Theory and its Applications. Dover Publications Inc., New York (2006)
3. Ben-Asher, J.Z.: Optimal Control with Aerospace Applications. AIAA Inc., Reston (2010)
4. Geering, H.P.: Optimal Control with Engineering Applications. Springer-Verlag, Berlin-Heidelberg (2007

5. Kurzhanskii, A.B.: Differential Equations in Controls Synthesis Problems: I. Ordinary Systems. Diff. Eq. 41(1), 10-21 (2005)
6. Todorov, E.: Optimal Control Theory. In: Doya, K., et al. (eds) Bayesian Brain: Probabilistic Approaches to Neural Coding, pp. 269-298. MIT Press, Cambridge (2006)
7. Lindquist, A.: On Feedback Control of Linear Stochastic Systems. SIAM J. Control 11(2), 323-343 (1973)
8. Fleming, W.H., Rishel, R.W.: Deterministic and Stochastic Optimal Control. Springer-Verlag, New York-Heidelberg-Berlin (1975)
9. Pontryagin, L.S., Boltyanskii, V.G., Gamkrelidze, R.V., Mishchenko, E.F.: The Mathematical Theory of Optimal Processes. L.S. Pontryagin Selected Works, vol. 4. Gordon & Breach Science Publishers, Montreux (1986)
10. Ross, I.M.: A Primer on Pontryagin's Principle in Optimal Control. Collegiate Publishers, San Francisco (2009)
11. Abramov, A.A.: Numerical Stability of a Method for Transferring Boundary Conditions. Comput. Math. and Math. Phys. 46(3), 382-387 (2006)
12. Bellman, R.: Dynamic Programming. Dover Publications Inc., New York (2003)
13. Bellman, R., Kalaba, R.: Dynamic Programming and Modern Control Theory. Academic Press, New York (1966)
14. Krotov, V.F.: Global Methods in Optimal Control Theory. In: Kurzhanskii, A.B. (ed.) Advances in Nonlinear Dynamics and Control: A Report from Russia. Progress in Systems and Control Theory, vol. 17, pp. 74-121. Birkhäuser, Boston (1993)
15. Alekseev, V.M., Tikhomirov, V.M., Fomin, S.V.: Optimal Control. Consultants Bureau, New York (1987)
16. Murzabekov, Z.N.: Sufficient Conditions for Optimality of Dynamic Systems with Fixed Endpoints. Math. J. 4(2), 52-59 (2004) (in Russian)
17. Thomson, W.T.: Introduction to Space Dynamics. Dover Publications Inc., Mineola (1986)
18. Burden, R.L., Faires, J.D.: Numerical Analysis. Brooks/Cole, Cengage Learning, Boston (2011)

A Source Identification Problem Related to Mathematical Model of Laser Surface Heating. Numerical Results

Muhtarbay Otelbaev[1], Alemdar Hasanov[2], Bakytzhan Akpayev[1], Rakymzhan Kanseytov[1]

[1]L.N. Gumilev Eurasian National University, Satpayev Street 2, Astana 01008, Kazakhstan
[2]Izmir University, 35350 Uckuyular, Izmir, Turkey
alemdar.hasanoglu@izmir.edu.tr

Abstract. A mathematical for the two-dimensional modelling of the laser surface heating for the hardening of metallic materials is proposed. The model is governed by the heat equation $u_t - \Delta u = m(t)\delta(x - \omega(t))$, $(x,t) \in \Omega \subset R^2$, satisfying the initial $u(x,0) = g(x)$ and boundary $u(x,t) = 0$, $x \in \partial\Omega$, conditions. The pair of source terms $\langle m(t), \omega(t)\rangle$ is assumed to be unknown. The two valued ($m(t) = 0$ or $m(t) = m_0 > 0$) function $m(t)$ is treated to be as the intensity of the laser beam, and the function $\omega(t)$ describes the laser beam trajectory. The identification problem consists of determining the pair of source terms $\langle m(t), \omega(t)\rangle$ such that the corresponding heat function $u(x,t)$ satisfies the condition $\|u - v\|_{L_2(\Omega)} \leq \varepsilon$, where the smooth function $v(x,t)$ is assumed to be known (experimentally), and $\varepsilon > 0$ is a given in advance parameter. The structure of the optimal trajectory is also described.

Keywords: laser surface hardening, optimal trajectory, heat equation, best approximation

1 Introduction

Laser surface hardening treatment has gained a great industrial interest as a manufacturing technology during last decades (see, [2-4], [7-8], and references therein). One of distingushed feature of this technology is the possibility of integrating the heating source directly on the production line. During the heat treatment of large surfaces, the laser beam trajectory must be organized in order to cover the whole surface of a material with sequential passes, having different laser beam intensities $m(t)$. These passes compose the trajectory $\omega(t)$ of laser surface hardening. However different trajectiries lead to different laser surface hardening. Moreover interactons of these passes lead to the tempering of the previously hardened material. Hence various optimization problems related to determination the best laser beam path strategy arise. In this context, the present paper deals with the problem of identification laser beam intensity $m(t)$ and trajectory $\omega(t)$ in the heat equation $u_t - \Delta u = m(t)\delta(\omega(t) - x)$, corresponding to a given in advance temperatura distribution $v(x,t)$.

In this paper we study the following mathematical model of laser surface heating for the hardening of metallic materials:

$$\begin{cases} u_t - \Delta u = m(t)\delta_\gamma(x - \omega(t)), \quad (x,t) \in \Omega_T := \Omega \times (0,T]; \\ u(x,0) = u_0(x), \quad x \in \Omega \subset R^2; \\ u(x,t) = 0, \quad x \in \Gamma := \partial\Omega \times (0,T). \end{cases} \tag{1}$$

Here $\Omega \subset R^2$ is a domain with a piecewise smooth boundary. Below we will assume, without loss of generality, that this domain contains in the unit square: $\Omega \subset [0,1] \times [0,1]$. The functions $u_0(x) > 0$ and $m(t)$ are defined to be an initial temperature and the intensity of the laser beam, respectively. The intensity function $m(t)$ is assumed to be the two valued one, i.e. $m(t) = m_0 > 0$ or $m(t) = 0$. This class of functions will be defined to be as $\mathcal{M}$. The vector function $\omega(t) =$

$(\omega_1(t), \omega_2(t))$ describes the laser beam trajectory. The function $\delta_\gamma(x)$ describes the pointwise source located at the point $x \in \Omega$:

$$\delta_\gamma(x) = \delta_{\gamma,1}(x_1)\delta_{\gamma,1}(x_2), \quad \delta_{\gamma,1}(y) = \begin{cases} \frac{1}{\gamma}, & |y| \le \frac{\gamma}{2}, \\ 0, & |y| > \frac{\gamma}{2}. \end{cases} \tag{2}$$

When the laser beam impinges on the surface $\Omega \subset [0,1] \times [0,1]$ of a workpiece, part of its energy is absorbed by the surface and suddenly turns into thermal energy. If this absorbed energy is high enough, heat generated in this region at a rate higher than the rate at which it flows to the bulk of the material by conduction. In this curcumstances, the temperature $u(x,t)$ of the surface increases very quickly. Moving the workpiece with respect to the laser source along the trajectory $\omega(t)$, a point on the surface of the workpiece within the beam track is rapidly heated as the laser approaches it and passes, and is rapidly cooled by heat conduction to the bulk of material after the beam has passed. By optimal selecting the parameters $\langle m(t), \omega(t)\rangle$, i.e. the source terms, the heating (as well as the cooling) of the metallic material may be controlled in order to obtain a siutable treatment. The presented results show how the mathematical model can be usefully employed in the prediction of the time dependent temperature distribution arising on the workpiece.

The paper is organized as follows. Formulation of the source identification problem and the main result related to existence of a solution is given in Section 2. In Section 3 some auxiliary results and the proof of the main theorem are derived. In Section 4 program code is written.

2 Problem formulation and the main result

Let $\varepsilon > 0$ be a given in advance arbitrary small parameter, and $v(x,t)$ is the given heat function (temperature distribution), corresponding to the required (siutable) treatment of a metallic material. Evidently the heat function $v(x,t)$ is the solution of the heat conduction problem

$$\begin{cases} v_t - \Delta v = F(x,t), & (x,t) \in \Omega_T, \\ v(x,0) = u_0(x), & x \in \Omega, \\ v(x,t) = 0, & x \in \Gamma, \end{cases} \tag{3}$$

with the appropiate source term $F(x,t)$.

The *source identification problem (SIP)* consists of finding such a pair of source terms $W := \langle m(t), \omega(t)\rangle$, where $m(t) \in \mathcal{M}$, $\omega(t) = (\omega_1(t), \omega_2(t))$, that the corresponding solution of the heat conduction problem (1) satisfies the condition

$$\sup_{t\in[0,T]} \|v(\cdot,t;F) - u(\cdot,t;W)\|_{L_2(\Omega)} \le \varepsilon. \tag{4}$$

According to [5], the pair $W := \langle m(t), \omega(t)\rangle$ is defined to be a quasi-solution of SIP.

We will assume that this source function in (3) satisfies the following conditions:

$$\begin{cases} F(x,t) \in C^1(\overline{\Omega} \times (0,T]); \\ 0 < F(x,t) \le m_0(1-\theta), \quad \theta \in (0,1). \end{cases} \tag{5}$$

Hence SIP can be reformulated as follows. Find such a pair of source terms $\langle m(t), \omega(t)\rangle$, where $m(t) \in \mathcal{M}$, $\omega(t) = (\omega_1(t), \omega_2(t))$, that the corresponding solution of the heat conduction problem (1) satisfies the condition

$$\sup_{t\in[0,T]} \|v(\cdot,t;F) - u(\cdot,t;W)\|_{L_2(\Omega)} \le \varepsilon. \tag{6}$$

Evidently, for $\varepsilon = 0$ the above problem may not have a solution, due to measurement errors. Therefore for purposes of applications it is enough to show that for any given $\varepsilon > 0$ the problem has at least one solution.

The main result of the study can be formulated as the following

Theorem 1. *Let $\Omega \subset [0,1] \times [0,1]$ is a domain with a piecewise smooth boundary $\partial\Omega$. Assume that $u_0(x) > 0$, $m(t) \in \mathcal{M}$, $\omega(t) = (\omega_1(t), \omega_2(t))$ is a continuous vector function, and $\delta_\gamma(y)$ is defined by (2). Suppose that the source function $F(x,t)$ in the heat conduction problem (3) is of $C^1(\overline{\Omega} \times (0,T])$ and satisfies condition (4). Then SIP has a solution.*

Besides of the existence result, our aim is also to show the construction of the optimal laser beam intensity function $m(t)$, as well the optimal laser beam trajectory $\omega(t) = (\omega_1(t), \omega_2(t))$.

Without loss of generality, assume that the closure $\overline{\Omega}$ of the domain Ω contains in the unit square: $\overline{\Omega} \subset [0,1]^2$. Let $\{S_n\}$, $S_n := \{(x_1, x_2) \in \mathcal{R}^2 : \ |x_i - \mathring{x}_{i,n}| < \gamma/2, \ i = 1,2\}$ be a family of squares with the length $\gamma > 0$ and center at $\mathring{x}_n := (\mathring{x}_{1,n}, \mathring{x}_{2,n})$. Denote by $\mathcal{K}_\square := \{S_n\}$, $n = \overline{1,M}$, the finite cover of the compact $\overline{\Omega}$, satisfying the following conditions:

$$\begin{cases} \textbf{(i)} & \forall n, p = \overline{1,M}, \ n \neq p, \quad S_n \cap S_p = \emptyset; \\ \textbf{(ii)} & \Omega \subset \bigcup_{n=1}^{n=M} S_n. \end{cases}$$

Let us introduce now the *uniform coarse grid* $\mathcal{W}_\mathcal{T} := \{T_k \in [0,T] : T_0 = 0, \ T_k = k\mathcal{T}, \ k = \overline{1,N}\}$, with the grid parameter $\mathcal{T} = T/N$. Denote by $\mathcal{I}_k := [T_{k-1}, T_k]$ the subintervals in this grid. Further, introduce in each subinterval $\mathcal{I}_k := [T_{k-1}, T_k]$, $k = \overline{1,N}$, the *non-uniform fine grid* $\omega^{(k)} := \{t_{k,j} \in [T_{k-1}, T_k] : t_{k,0} = T_{k-1}, \ t_{k,1} < t_{k,2} < ... < t_{k,2M} = T_k\}$. We define the fine intervals $\mathcal{I}_{k,j} := [t_{k,j-1}, t_{k,j}]$, $j = \overline{1,2M}$, in two groups, with the odd and even subscripts: $\mathcal{I}_{k,2j-1}$, $\mathcal{I}_{k,2j}$, $j = \overline{1,2M}$.

The two valued function $m(t) \in \mathcal{M}$ will be constructed in each interval $\mathcal{I}_k := [T_{k-1}, T_k]$, $k = \overline{1,N}$ of the coarse grid $\mathcal{W}_\mathcal{T}$ as follows:

$$m(t) = \begin{cases} m_0, & t \in \mathcal{I}_{k,2i-1} := [t_{k,2(i-1)}, t_{k,2i-1}], \\ 0, & t \in \mathcal{I}_k \setminus \mathcal{I}_{k,2i-1}, \quad i = \overline{1,M}. \end{cases} \tag{7}$$

As a result the function $m(t) \in \mathcal{M}$ will be obtained as a piecewise constant function in each interval $\mathcal{I}_k := [T_{k-1}, T_k]$.

Let us construct now the vector-function $\omega(t)$, which is simulating the the trajectory of the workpiece move with respect to the laser source. According to the considered physical model, a point on the surface of the workpiece within the beam track is rapidly heated as the laser approaches it and passes. Hence for each time interval $\mathcal{I}_k := [T_{k-1}, T_k]$, $k = \overline{1,N}$, the finite cover $\mathcal{K}_\square := \{S_n\}$, $n = \overline{1,M}$, of the surface Ω will be heated by the laser beam sequentially, step by step, acting each S_n. Specifically, we assume that

$$\omega(t) = \mathring{x}_n := (\mathring{x}_{1,n}, \mathring{x}_{2,n}), \quad t \in \mathcal{I}_{k,2n-1}, \quad n = 1,2,...,M,$$

identifying each square S_n, with the center at $\mathring{x}_n$, and odd number subinterval $\mathcal{I}_{k,2n-1}$.

3 Some preliminary results

Lemma 1. *Let conditions of Theorem 1 hold. Then for any $\varepsilon_1 > 0$ there exist a pair $< m(t), \omega(t) >$ such that $\forall [t_1, t_2] \subset [0,T]$ the estimate holds:*

$$\sup_{x \in \overline{\Omega}} \left| \int_{t_1}^{t_2} [F(x,t) - m(t)\delta_\gamma(x - \omega(t))] \, dt \right| \leq \varepsilon_1.$$

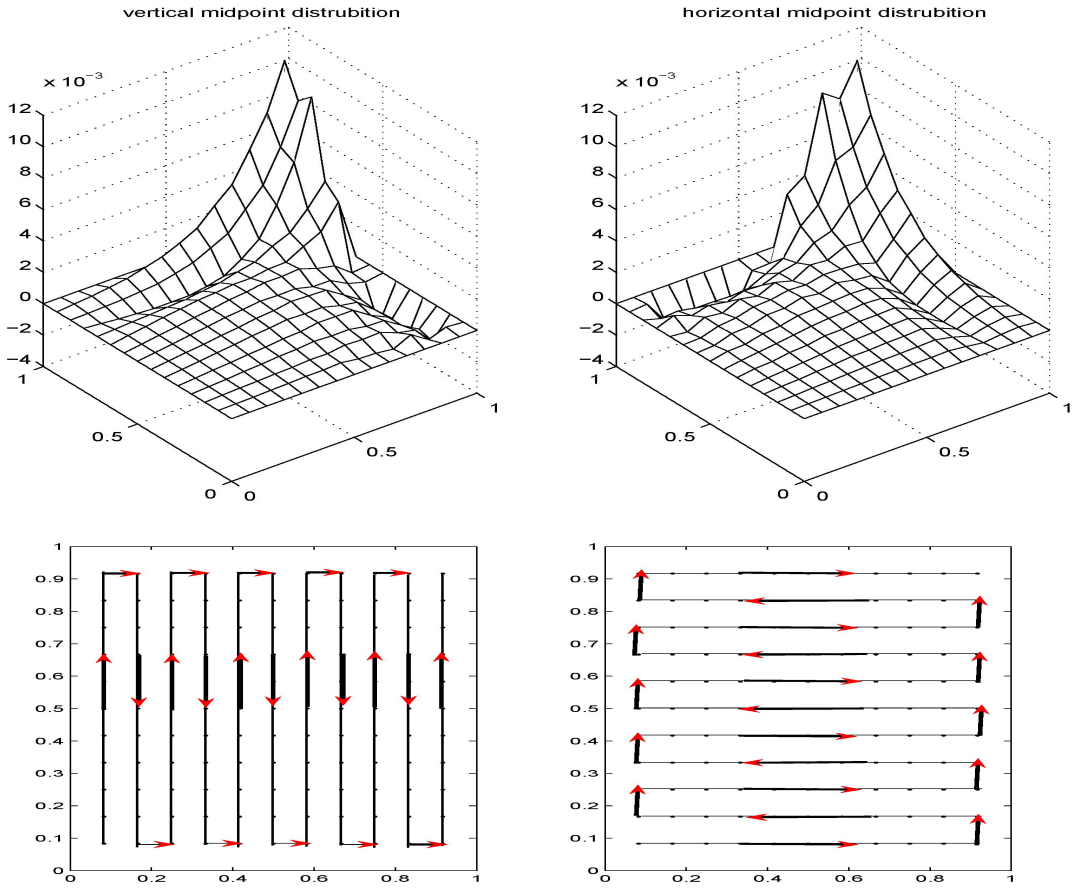

Fig. 1. Computed of heat functions (upper figures) corresponding to different laser beam trajectories (below figures)

Proof. Let for $j = 1, ..., M-1$ the length $d := d_{k,2j} > 0$ of each subinterval with even subscripts are chosen to be equal and satisfy $d < \theta\tau/(M-1)$. We define the length of the last subscript subinterval $\mathcal{I}_{k,2M}$ as follows:

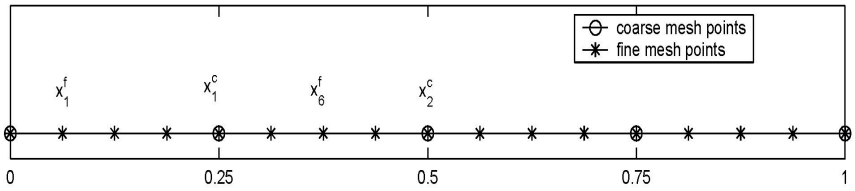

Fig. 2. The geometry of the coarse-fine time grids/intervals

$$d_{k,2M} = \tau - d(M-1) - \sum_{j=1}^{M} d_{k,2j-1} > 0, \ k = 1, ..., N \tag{8}$$

By the above construction of the vector-function $\omega(t)$, we have $\omega(t_{k,2j-1}) = \mathring{x}_j$, $\omega(t_{k,2j}) = \mathring{x}_{j+1}$, $j = 1, 2, ..., M-1; \omega(t_{k,2M-1}) = \mathring{x}_M$, $\omega(T_k) = \mathring{x}_1$ and $\omega(t) = x_j$, $t \in \mathcal{I}_{k,2j-1}$, $j = 1, 2, ..., M$. Using the condition $m(t) = m_0$ in $\mathcal{I}_{k,2i-1}$, we can show that the lengths of these subintervals with odd subscripts satisfy the following condition:

$$\frac{m_0}{\gamma^2} d_{k,2j-1} = \tau F(\mathring{x}_j, \mathring{T}_k), \quad j = \overline{1, M}, \quad \mathring{T}_k = 0.5(T_{k-1} + T_k). \tag{9}$$

Then, due to $meas\mathcal{I}_{k,j} = \tau$ for all $k = 1, 2, ..., N$, this condition with (8) will imply the condition:

$$d(M-1) + \frac{\gamma^2\tau}{m_0} \sum_{j=1}^{M} F(\mathring{x}_j, \mathring{T}_k) < \tau. \tag{10}$$

Indeed, by condition (5) there exists $\theta \in (0, 1)$ such that $0 < F(x, t) \le m_0(1-\theta)$. Hence condition (10) holds, if

$$d(M-1) + (1-\theta)M\gamma^2\tau < \tau. \tag{11}$$

But $M\gamma^2 \le 1$, due to $\Omega \subset [0, 1]^2$, and $d < \theta\tau/(M-1)$, by the above construction. This means the fulfilment of inequality (11), and hence condition (9).

Thus the construction of the parameters $d > 0$, $d_{k,2j-1}$ and $d_{k,2M}$, $k = \overline{1, N}$; $j = \overline{1, M}$ is completed.

Let now $m(t)$ and $\omega(t)$ be the above constructed functions. Assume that $t_1, t_2 \in (0, T]$, $0 \le t_1 < t_2 \le T$, are two arbitrary chosen values of the time variable $t \in (0, T]$, and consider the integral:

$$R_{t_1,t_2}(x) := \int_{t_1}^{t_2} [F(x, t)dt - m(t)\delta_\gamma(x - \omega(t))]dt$$

Evidently there exists such a positive integers k_1 and k_2 that $t_1 \in \mathcal{I}_{k_1}$ and $t_2 \in \mathcal{I}_{k_2+1}$. Then we can estimate the above integral as follows:

$$|R_{t_1,t_2}(x)| \le \int_{t_1}^{T_{k_1}} |F(x,t) - m(t)\delta_\gamma(x-\omega(t))|dt + \int_{T_{k_2}}^{t_2} |F(x,t) - m(t)\delta_\gamma(x-\omega(t))|dt + \sum_{k=k_1}^{k_2} \int_{\mathcal{I}_k} |F(x,t) - m(t)\delta_\gamma(x-\omega(t))|dt \quad (12)$$

We estimate the first right hand side integrals as follows:

$$\int_{t_1}^{T_{k_1}} |F(x,t) - m(t)\delta_\gamma(x-\omega(t))|dt \le \int_{t_1}^{T_{k_1}} |F(x,t)|dt + m_0 \int_{t_1}^{T_{k_1}} \delta_\gamma(x-\omega(t))|dt \le m_0\tau(1-\theta+\gamma^{-2})$$

The similar estimate holds for the second right hand side integral of (12), with the same constant $m_0\tau(1-\theta+\gamma^{-2}) > 0$. Adding and subtracting the term $F(\mathring{x}_j, \mathring{T}_k)$ we estimate the third right hand side integral as follows:

$$\sum_{k=k_1}^{k_2} \int_{\mathcal{I}_k} |F(x,t) - m(t)\delta_\gamma(x-\omega(t))|dt$$

$$\le \sum_{k=k_1}^{k_2} \int_{\mathcal{I}_k} |F(x,t) - F(\mathring{x}_j, \mathring{T}_k)|dt + \sum_{k=k_1}^{k_2} \int_{\mathcal{I}_k} |F(\mathring{x}_j, \mathring{T}_k) - m(t)\delta_\gamma(x-\omega(t))|dt \le 2(k_2-k_1)m_0\tau,$$

since the last right hand side integral is zero according to (9). Taking into account these estimates in (12) we conclude

$$|R_{t_1,t_2}(x)| \le 2m_0\tau[1-\theta+\gamma^{-2}+(k_2-k_1)],\ \theta \in (0,1),\ k_2 > k_1. \quad (13)$$

Since $\tau \sim N^{-1}$ is an arbitrary parameter, assuming $\varepsilon_1 = 2m_0\tau[1-\theta+\gamma^{-2}+(k_2-k_1)]$ we complete the proof of Lemma 1. □

Lemma 2. *Let conditions of Theorem 1 hold. Assume that $\langle m(t), \omega(t)\rangle$ is the pair satisfying the assertion of Lemma 1. Denote by $\tilde{F}(x,t) = F(x,t) - m(t)\delta_\gamma(x-\omega(t))$ the source term of the problem*

$$\begin{cases} \tilde{u}_t - \Delta\tilde{u} = \tilde{F}(x,t), & (x,t) \in \Omega_T, \\ \tilde{u}|_{t=0} = \tilde{u}|_{\partial\Omega} = 0, \end{cases} \quad (14)$$

where $F(x,t)$ is the source term of problem (3). Then for the Fourier coefficients $\tilde{u}_n(t)$ of the solution $\tilde{u}(x,t)$ of problem (14) with respect to the orthonormal basis $\{\phi_n\}_{n=1}^{\infty}$ the following estimate holds:

$$|\tilde{u}_n(t)| \le \tilde{C}_u \min\{\varepsilon_1, (\gamma n)^{-1}\},\ n = 1, 2, \dots, \quad (15)$$

where $\gamma > 0$ and $\varepsilon_1 > 0$ the parameters defined in (2) and Lemma 1, respectively, and the constant $\tilde{C}_u$ doesn't depend on $\varepsilon_1 > 0$.

Proof. Let $\tilde{u}(x,t)=\sum_{n=1}^{\infty}\tilde{u}_n(t)\phi_n(x)$ be the Fourier series solution of problem (14) with respect to the orthonormal basis $\{\phi_n\}_{n=1}^{\infty}$. Then for each $n=1,2,...$ the Fourier coefficients $\tilde{u}_n(t)$ satisfies the following problem

$$\begin{cases}\dot{\tilde{u}}_n(t)-\lambda_n\tilde{u}_n(t)=\tilde{F}_n(t),\\ \tilde{u}_n(0)=0,\end{cases} \tag{16}$$

where λ_n are eigenvalues of the Dirichlet problem for the Laplace operator, and

$$\tilde{F}(x,t)=\sum_{n=1}^{\infty}\tilde{F}_n(t)\phi_n(x),\quad \tilde{F}_n(t)=\int_{\Omega}\tilde{F}(\xi,t)\phi_n(\xi)d\xi$$

We transform the solution of problem (16) as follows:

$$\begin{aligned}\tilde{u}_n(t)=\int_0^t e^{-\lambda_n(t-\eta)}\tilde{F}_n(\eta)&=\int_0^t e^{-\lambda_n(t-\eta)}\left(\int_{\Omega}\tilde{F}(\xi,\eta)\phi_n(\xi)d\xi\right)d\eta\\ &=\int_{\Omega}\left(\int_0^t e^{-\lambda_n(t-\eta)}\tilde{F}(\xi,\eta)d\eta\right)\phi_n(\xi)d\xi.\end{aligned} \tag{17}$$

Let us estimate the integral term inside the brackets. Using Lemma 1 and the formula for integration by parts we get:

$$\begin{aligned}\left|\int_0^t e^{-\lambda_n(t-\eta)}\tilde{F}(\xi,\eta)d\eta\right|&=\left|\int_0^t e^{-\lambda_n(t-\eta)}d\int_0^{\eta}\tilde{F}(\xi,\tau)d\tau\right|\\ &=\left|\int_0^t\tilde{F}(\xi,\eta)d\eta-\lambda_n e^{-\lambda_n t}\int_0^t\left(\int_0^{\eta}\tilde{F}(\xi,\tau)d\tau\right)e^{\lambda_n\eta}d\eta\right|\\ \le\varepsilon_1+\varepsilon_1\lambda_n e^{-\lambda_n t}\int_0^t e^{\lambda_n\eta}d\eta&=\varepsilon_1+\varepsilon_1 e^{-\lambda_n t}(e^{\lambda_n t}-1)\le 2\varepsilon_1,\quad\forall t\in(0,T].\end{aligned}$$

Taking into account this estimate in (17) we conclude:

$$|\tilde{u}_n(t)|\le 2\varepsilon_1\int_{\Omega}|\phi_n(x)|dx\le 2(meas\ \Omega)^{1/2}\varepsilon_1\left|\int_{\Omega}\phi_n^2(x)dx\right|^{1/2}\le 2(meas\ \Omega)^{1/2}\varepsilon_1,$$

for all $n=1,2,....$

On the other hand,

$$|\tilde{u}_n(t)|=\left|\int_0^t e^{-\lambda_n(t-\eta)}\tilde{F}_n(\eta)d\eta\right|\le e^{-\lambda_n t}\sup_{\eta\in[0,t]}|\tilde{F}_n(\eta)|\int_0^t e^{\lambda_n\eta}d\eta\le\frac{1}{\lambda_n}\sup_{\eta\in[0,t]}|\tilde{F}_n(\eta)|.$$

Estimating $\tilde{F}_n(t)$ we get.

$$\begin{aligned}|\tilde{F}_n(\eta)|^2=\left|\int_{\Omega}\tilde{F}(\xi,t)\phi_n(\xi)d\xi\right|^2&\le\left(\int_{\Omega}|\tilde{F}(\xi,t)|^2d\xi\right)\left(\int_{\Omega}|\phi_n(\xi)|^2d\xi\right)\\ =\left(\int_{\Omega}|F(\xi,t)-m(t)\delta_{\gamma}(\xi-\omega(t))|^2d\xi\right)&\le\left(2\int_{\Omega}|F(\xi,t)|^2d\xi+2\int_{\Omega}|m(t)\delta_{\gamma}(\xi-\omega(t))|^2d\xi\right)\\ &\le C_0+C_1\gamma^{-2}\le C_2\gamma^{-2}.\end{aligned}$$

Using the well-known property of the eigenvalue $\lambda_n\approx n$, for the Fourier coefficients $\tilde{u}_n(t)$, $n=1,2,...$, we obtain the second estimate

$$|\tilde{u}_n(t)|\le C_3(\gamma n)^{-1}. \tag{18}$$

This completes the proof. □

4 Proof of the main result

Let $\tilde{u}(x,t) = u(x,t) - v(x,t;W)$ be the solution of problem (14) with the source term $\tilde{F}(x,t) = F(x,t) - m(t)\delta_\gamma(x-\omega(t))$. Then

$$\tilde{u}(x,t) = \sum_{n=1}^{\infty} \tilde{u}_n(t)\phi_n(x), \quad \tilde{u}_n(t) = \int_\Omega \tilde{u}(\xi,t)\phi_n(\xi)d\xi$$

and we have

$$\|\tilde{u}(\cdot,t)\|^2_{L_2(\Omega)} := \int_\Omega \left|\sum_{n=1}^{\infty} y_n(t)\phi_n(x)\right|^2 dx = \left(\sum_{n=1}^{\infty}|y_n(t)|^2\right)\left(\int_\Omega |\phi_n(x)|^2 dx\right)$$

Then

$$\|y(\cdot,t)\|^2_{L_2(\Omega)} = \int_\Omega \left|\sum_{n=1}^{\infty} y_n(t)\phi_n(x)\right|^2 dx = \left(\sum_{n=1}^{\infty}|y_n(t)|^2\right)\left(\int_\Omega |\phi_n(x)|^2 dx\right)$$

$$= \sum_{n=1}^{\infty}|y_n(t)|^2 \le \sum_{n:\varepsilon_1 \le n^{-1}\gamma^{-1}} |y_n(t)|^2 + \sum_{n:\varepsilon_1 > n^{-1}\gamma^{-1}} |y_n(t)|^2$$

$$\le \varepsilon_1^2 \sum_{n=1}^{[\varepsilon_1^{-1}\gamma^{-1}]} 1 + \sum_{n=[\varepsilon_1^{-1}\gamma^{-1}]+1}^{\infty} n^{-2}\gamma^{-2} < \varepsilon_1^2\varepsilon_1^{-1}\gamma^{-1} + \gamma^{-2}\frac{2}{[\varepsilon_1^{-1}\gamma^{-1}]+1} < \varepsilon_1\gamma^{-1} + \gamma^{-2}\frac{4}{\varepsilon_1^{-1}\gamma^{-1}},$$

i.e.

$$\sup_{t\in[0,T]} \|y(\cdot,t)\|_{L_2(\Omega)} \le \varepsilon_3, \quad \varepsilon_3 = \sqrt{5\varepsilon_1\gamma^{-1}}.$$

Theorem 1 is proved. □

5 Program code

```
#include<iostream>
#include<iomanip>
#include<cmath>
using namespace std;

int main() {
    const int N=2,M=9;
    int L=2*M*N;

    double wx[M][M];
    double wy[M][M];

    wx[0][0]=0.05;
    wy[0][0]=0.25;
```

```
float length[L],intensity[L],m0=1, gamma=0.1;

for (int i=0;i<L;i++){
        if (i%2!=0) {
            length[i]=0.001;
            intensity[i]=m0;
        }
        else {
            length[i]=0.002;
            intensity[i]=0;
        }
}
cout<<"i"<<"  intencity"<<endl;
for(int i=0,k=0;i<2*M;i++) {
        cout<<k<<"  "<<intensity[i]<<"  "<<endl;
        k++;
}

for(int i=0;i<sqrt(M);i++) {
    if(i==0) {
        for(int j=0;j<sqrt(M);j++)
            wx[i][j]=wx[0][0]+j*gamma;
    } else {
        for(int j=0;j<sqrt(M);j++)
            wx[i][j]=wx[i-1][j];
    }
}

for(int j=0;j<sqrt(M);j++) {
    if(j==0) {
        for(int i=0;i<sqrt(M);i++)
            wy[i][j]=wy[0][0]-i*gamma;
    } else {
        for(int i=0;i<sqrt(M);i++)
            wy[i][j]=wy[i][j-1];
    }
}

for(int i=1;i<sqrt(M);i+=2) {
    for(int j=0,k=(int)sqrt(M)-1;j<sqrt(M);j++) {
        wx[i][j]=wx[i-1][k];
        k--;
    }
}

cout<<"i"<<"     x"<<"     y"<<endl;
for(int i=0,k=0;i<sqrt(M);i++) {
```

```
        for(int j=0;j<sqrt(M);j++) {
            cout<<k<<"  "<<wx[i][j]<<"  "<<wy[i][j]<<endl;
            k++;
        }
    }

    return 0;
}
```

(Example from Kanseytov R., Yensebek N. (2015), Astana)

6 Conclusion

Formulation of the source identification problem and the main result related to existence of a solution are given. Some auxiliary results and the proof of the main theorem are derived. The program code is written.

References

1. O. Alifanov, Inverse Heat Transfer Problems, Springer, Berlin (1994).
2. V. Colombo, A. Mentrelli and T. Trombetti, Time-dependent 3-D modelling of laser surface heating for the hardening of metallic materials, The European Physical Journal D - Atomic, Molecular, Optical and Plasma Physics, 27(3) (2003), pp. 239-246.
3. A. M. Gadgiev, A. I. Gasanov (Hasanov), A. G. Fatullaev, Mathematical modelling of laser metal processing, Matem. Mod., 3 (1) (1991), pp. 18–24.
4. L. Grum, Comparison of different techniques of laser surface hardening, Journal of Achievements in Materials and Manufacturing Engineering, 24(1) (2007), pp. 17-25.
5. V.K. Ivanov, V.V. Vasin, V.P. Tanana, Theory of Linear Ill-Posed Problems and Its Applications, Nauka, Moscow, 1978.
6. M. Otelbaev, A. Hasanov, B. Akpaev, A control problem related to pointwise heat source, Dokladi Russian Academy of Sciences, Ser. Mathematics, (2010) (to appear).
7. M. Renardy, J. Rogers, Introduction to Partial Differential Equations, Springer-Verlag, New York, 1993.
8. G. Tani, L. Orazi, A. Fortunato, Prediction of hypo eutectoid steel softening due to tempering phenomena in laser surface hardening, CIRP Annals - Manufacturing Technology, 57(1), (2008), pp. 209-212.
9. G. Tani, L. Orazi, A. Fortunato, A. Fortunato, G. Campana, A. Ascari, G. Cuccolini, Optimization strategies of laser hardening of hype-eutectoc steel, Manufacturing Systems and Technologies for the New Frontier, Proceedings of the 41st CIRP Conference on Manufacturing Systems (Eds.: M. Mitsuishi, K. Ueda, F. Kimura), May 26-28, 2008, Tokyo, Japan.

Economic Solution of the Spatially Two-Dimensional Nonlinear Mathematical A1 Model

Maksat Kalimoldayev[1], Alexandra Alexeyeva[2], Keylan Alimhan[3], and Gulshat Amirkhanova[1]

[1]Institute of Information and Computational Technologies, Pushkina 125, Almaty, Kazakhstan
[2]Institute of Mathematics and Mathematical Modelling, Pushkina 125, Almaty, Kazakhstan
[3] L.N. Gumilyov Eurasian National University, Astana, Kazakhstan,
School of Science and Engineering, Tokyo Denki University, Saitama, Japan
mnk@ipic.kz,alankritalalita@gmail.com,keylan@live.jp,gulshat.aa@gmail.com

Abstract. In this article, the (2+1)-dimensional nonlinear mathematical A1 model, generalizing the Korteweg-de Vries equation, was considered. Its conservation laws were presented, an auxiliary linear system was considered, the zero curvature condition was defined, it connects the auxiliary linear system with this model. The direct scattering problem for this model was solved. For a given function the components of the scattering matrix were defined. In this paper we explained the economic meaning of (2+1)-dimensional nonlinear mathematical A1 model. The definition of economic soliton as a solution to the mathematical model was given. Economic sense of the method of direct scattering problem, corresponding to the positive analytical approach to the economy, is described.

Keywords: economic soliton, generalized Korteweg-de Vries (2+1)-dimensional nonlinear mathematical A1 model, direct scattering problem, positive approach

1 Introduction.

Solitons occur as private regular localized stable solutions of nonlinear evolution equations, such as Korteweg-de Vries equation, the nonlinear Schrцdinger equation, sine-Gordon equation, and their multidimensional analogues.

Classical Korteweg-de Vries equation [1]

$$u_t + u_{xxx} + 6uu_x = 0\ , \tag{1}$$

where $u = u(x,t)$ is sufficiently smooth real function describes both weak hydromagnetic long waves in plasma and waves on water [2] and weakly nonlinear ion-acoustic pressure waves in a plasma [3]. Korteweg-de Vries equation is called universal mathematical model because it describes many of the physical problems of nonlinear waves in different physical environments.

Multidimensional analogues of Korteweg-de Vries equation is also universal. For example, Kadomtsev-Petviashvili equation [4]

$$(u_{xxx} + 6uu_x + u_x + u_t)_x - u_{yy} = 0\ , \tag{2}$$

where $u = u(x,y,t)$ is a sufficiently smooth function, it was obtained for weakly nonlinear long waves in dispersing medium.

Tapert and Varma [5] and Narayanamurti and Varma [6] obtained the equation (2) in the study of the thermal pulse propagation in solids. Kako and Roulendz obtained equation (2) for the two-dimensional propagation of ion-acoustic solitons [7].

The universal nature of the multi-dimensional analogues of Korteweg-de Vries equation allows to abstract from specific physical conditions and find its new multidimensional generalizations, based on the properties of soliton equations.

It is known that soliton equations have the following properties [8]:

1. soliton equation has an infinite number of conservation laws;
2. it has a solution in the form of solitary waves – solitons;
3. if soliton equation admits solutions such as solitary waves, it must accept solutions, which represent a nonlinear superposition of N solitary waves for arbitrary N;
4. it is also exactly integrable in the sense of infinite-dimensional generalization of completely integrable Hamiltonian system. All known soliton equations have Hamiltonian structures, and an infinite set of integrals of motion are in involution (i.e. Poisson bracket disappears);
5. there is a canonical transformation (the inverse scattering method – ISM), which transforms the soliton equation into infinite system of equations with variables of action-angle type, each soliton equation can be integrated in a trivial way (from the condition of zero curvature implies the existence of an infinite number of conservation laws);
6. it has the Hirota's property, has bilinear forms, which gives the opportunity to build N-soliton solutions (non-linear superposition of N solitons);
7. Painleve property (a test that shows that the nonlinear equation is completely integrable).

Veselov-Novikov equation [9]:

$$u_t = (uv)_z + (u\bar{v})_z + u_{zzz} + u_{\bar{z}\bar{z}\bar{z}} \ ,$$

where $v_z = -3u_z, z = x + iy$, and $u = u(z,t)$ are enough smooth function, it was obtained as a two-dimensional integrable extension of the Korteweg-de Vries equation.

Nizhnik L.P. proposed spatial two-dimensionalization of modified Korteweg-de Vries equation [10]:

$$u_t = u_{xxx} + u_{yyy} + (vu)_y + (wu)_x - \frac{1}{2}(v_y + w_x)u \ , \tag{3}$$

where $v_x = 3\left(u^2\right)_y$, $w_y = 3\left(u^2\right)_x$, and $u = u(x,y,t)$ are a sufficiently smooth function. Equation (3) was obtained on the basis of the possible existence of equation (3) of the Lax pair, which allows us to solve the equation (3) with the inverse scattering method.

2 (2+1)-dimensional nonlinear mathematic model A1 generalizing Korteweg-de Vries equation.

Alexeyeva A. presented the class of the spatially two-dimensional nonlinear mathematical models A1-A14 and AI-AXII [11], generalizing the classical Korteweg-de Vries equation (1).

In particular, the (2+1)-dimensional nonlinear A1 equation has the form [11]:

$$\Psi_t + \Psi_{xyy} + 2[\Psi^2]_y + [UV]_y = 0 \ , \tag{4}$$

where $V_x = \Psi_y$, $U_y = \Psi_x$, and $\Psi = \Psi(x,y,t)$ is a sufficiently smooth complex-valued function.

Integrability of the (2+1)-dimensional nonlinear A1 equation proves the existence of a hierarchy of auxiliary linear systems [12]:

$$\begin{cases} \varphi_x = U_0\varphi + \lambda\varphi \\ \varphi_t = \lambda\varphi_y + A\varphi + \lambda B\varphi, \end{cases}$$

$$\begin{cases} \varphi_x = U_0\varphi + \lambda\varphi \\ \varphi_t = \lambda\varphi_y + A\varphi + \lambda B\varphi + \lambda^2 C\varphi, \end{cases}$$

$$\begin{cases} \varphi_x = U_0\varphi + \lambda\varphi \\ \varphi_t = \lambda\varphi_y + A\varphi + \lambda B\varphi + \lambda^2 C\varphi + \lambda^3 D\varphi \ , \end{cases}$$

...

where

$$U_0 = \begin{pmatrix} 0 & \Psi \\ \bar{\Psi} & 0 \end{pmatrix}, \varphi = \begin{pmatrix} \varphi_1 \\ \varphi_2 \end{pmatrix} ,$$

$$A = \begin{pmatrix} 0 & -\Psi_{xy} - 2\Psi^2 - \partial_x^{-1}(\Psi_y)\,\partial_y^{-1}(\Psi_x) \\ -\bar{\Psi}_{xy} - 2\bar{\Psi}^2 - \partial_x^{-1}(\bar{\Psi}_y)\,\partial_y^{-1}(\bar{\Psi}_x) & 0 \end{pmatrix} ,$$

$$B = \begin{pmatrix} i & -2i\partial_x^{-1}\Psi - \partial_x^{-1}(\Psi_y) \\ 2i\partial_x^{-1}\bar{\Psi} - \partial_x^{-1}(\bar{\Psi}_y) & -i \end{pmatrix} ,$$

$$C = D = \ldots = \begin{pmatrix} i & -2i\partial_x^{-1}\Psi \\ 2i\partial_x^{-1}\bar{\Psi} & -i \end{pmatrix} .$$

$\lambda_t = \lambda\lambda_y$, $\lambda = \lambda(y,t)$ - spectral parameter, complex valued function $\Psi = \Psi(x,y,z) \in C^\infty(R^1 \times R^1 \times R^1_+)$ and decreases with all its partial derivatives faster than any power of $|x|^{-1}$.

The compatibility conditions for the above systems are as follows:

$$U_0 t - Ax + [U_0, A] = 0 .$$

where $[U_0, A] = U_0,\ A - AU_0$.

Equation (4) has the bilinear H1 form [13]:

$$\left(D_x D_t + D_x^2 D_y^2\right)(\varphi \circ \varphi) = 0 , \tag{5}$$

where

$$(D_x D_t)(\varphi \circ \varphi) = 2\left(\varphi_{xt}\varphi - \varphi_x\varphi_t\right) ,$$

$$\left(D_x^2 D_y^2\right)(\varphi \circ \varphi) = 2\left(\varphi_{xxyy}\varphi - 2\varphi_{xxy}\varphi_y + \varphi_{xx}\varphi_{yy} - 2\varphi_{xyy}\varphi_x + 2\varphi_{xy}^2\right) .$$

$\varphi = \varphi(x,y,t)$ is a sufficiently smooth complex-valued function.

(2+1)-dimensional nonlinear A1 equation is a generalization of the classical Korteweg-de Vries equation (1).

(2+1)-dimensional bilinear H1 form (5) is a generalization of the classical Hirota H operator [1]:

$$\left(D_x D_t + D_x^4\right)(f \circ f) = 0 ,$$

where

$$(D_x^m D_t^n)(F \circ G) = (\partial_x - \partial_{x'})^m (\partial_t - \partial_{t'})^n F(x,t)\, G\left(x',t'\right)/_{x'=x,t'=t} , \tag{6}$$

$f(x,t)$ is a sufficiently smooth real function. Bilinear operator (6) has the following properties [1]:

1) $D_x^m(a \circ 1) = \partial_x^m a$,
2) $D_x^m(a \circ b) = (-1)^m D_x^m(a \circ b)$,
3) $D_x^m(a \circ a) = 0,\ m = 2k+1,\ k \in Z$,
4) $D_x^m D_t^n(e^{k_1 x - \omega_1 t} \circ e^{k_2 x - \omega_2 t}) = (k_1 - k_2)^m(\omega_2 - \omega_1)^n e^{(k_1+k_2)x - (\omega_1+\omega_2)t}$.

Below under $\ln\varphi$ we mean a function $\ln\varphi = \ln|\varphi| + i\arg\varphi,\ -\pi < \arg\varphi < \pi$ i.e. the main part of a multi-valued function

$$\ln\varphi = \ln|\varphi| + i\arg\varphi + 2k\pi,\ \ -\pi < \arg\varphi < \pi, k \in Z .$$

Consequently, actual range of the φ function represents one sheet of the Riemann surface, i.e. complex plane with the cut along the negative semiaxis and punctured origin of coordinates.

Using Hirota method for (2+1)-dimensional nonlinear A1 equation were built 1-, 2-, and N-soliton solutions [14].

1-soliton solution of the (2+1)-dimensional nonlinear A1 equation:

$$\Psi = 2(\ln\varphi)_{xy}$$
$$\varphi = 1 + \exp\{\alpha x + \beta y - \alpha\beta^2 t + \gamma\} ,$$

where $\varphi = \varphi(x, y, t)$ is a sufficiently smooth complex-valued function, α, β, γ are constants.

2-soliton solution of the (2+1)-dimensional nonlinear A1 equation:

$$\Psi = 2(\ln\varphi)_{xy}$$
$$\varphi = 1 + \exp\{\eta_1\} + \exp\{\eta_2\} + \exp\{\eta_1 + \eta_2 + A_{12}\} ;$$
$$\eta_j = \alpha_j x_j + \beta_j y - \alpha_j\beta_j^2 t + \gamma_j, \;\; j = \overline{1,2} ;$$
$$\exp\{A_{12}\} = \frac{\beta_1 - \beta_2}{\beta_1 + \beta_2} \cdot \frac{\alpha_1\alpha_2(\beta_1 - \beta_2) + (\alpha_1 - \alpha_2)(\beta_1\alpha_2 + \beta_2\alpha_1)}{\alpha_1\alpha_2(\beta_1 + \beta_2) + (\alpha_1 + \alpha_2)(\beta_1\alpha_2 + \beta_2\alpha_1)} ;$$

where $\varphi = \varphi(x, y, t)$ is an enough smooth complex-valued function, α_j, β_j, γ_j, $j = 1, 2$ are constants, $\beta_1 \neq \beta_2$.

N-soliton solution of the (2+1)-dimensional nonlinear A1 equation:

$$\Psi = 2(\ln\varphi)_{xy}$$
$$\varphi_N = \sum_{\mu^*=0,1} \exp\left(\sum_{i=1}^{N} \mu_i\eta_i + \sum_{1\le i<j}^{N} \mu_i\mu_j A_{ij}\right) ,$$

where μ^* appears in all sets as $\mu_j = 0, 1$; $j = \overline{1, N}$;

$$\eta_j = \alpha_j x + \beta_j y - \alpha_j\beta_j^2 t + \gamma_j, \;\; j = \overline{1, N} ;$$
$$\exp\{A_{ij}\} = \frac{\beta_i - \beta_j}{\beta_i + \beta_j} \cdot \frac{\alpha_i\alpha_j(\beta_i - \beta_j) + (\alpha_i - \alpha_j)(\beta_i\alpha_j + \beta_j\alpha_i)}{\alpha_i\alpha_j(\beta_i + \beta_j) + (\alpha_i + \alpha_j)(\beta_i\alpha_j + \beta_j\alpha_i)}, \beta_1 \neq \beta_2 ,$$

where $\varphi = \varphi(x, y, t)$ is a sufficiently smooth complex-valued function, α_j, β_j, γ_j, $j = \overline{1, N}$ are constants.

This work will present conservation law for the (2+1)-dimensional nonlinear mathematical A1 model, consideration of the direct scattering problem and application of the (2+1)-dimensional mathematical A1 model to nonlinear economic processes and phenomena.

3 Conception of the soliton and economic soliton.

Mathematically soliton means a localized nonlinear wave, which behaves like a particle. It interacts with the similars and asymptotically recovers its original shape with the possible displacement of phases.

Solitons are studied in the oceans (wandering waves, tsunami, vortex solitons) in solid crystalline solids (dislocations, domain walls) in magnetic materials (solitons in ferromagnets, electromagnetic solitons) in optical fibers (optical soliton soliton network) in the atmosphere

of Earth and other planets (Rossby soliton, red spot of Jupiter) in galaxies (black holes) in living organisms (nerve impulses, breathers, intellektony, membrony) and the economy (economic soliton).

Sometimes soliton is defined as a regular localized sustainable solution of the nonlinear differential equation [15].

A wide variety of systems, including a social-economic, may be stable localized formation. In organizational and economic forms such as the shadow economy and marginal urban societies, appears the soliton's characteristics [16]. The collective behavior of subjects of economy has nonlinear wave character. Therefore there is the issue of providing its structural and local stability arises [17]. Both of the above-mentioned forms are resistant to external influences and have other soliton's properties. Note that not every solution of the (2+1)-dimensional nonlinear mathematical A1 model is a soliton. Likewise, not every collective formation has the characteristics of a soliton.

Under the economic soliton means "the form of behavior of the microsubjects' economy, a feature which is a stable tendency of microsubjects to certain activities and continuous reproduction of the functional qualities of this collective formation" [17]. For soliton formation imposed certain conditions on the function $\Psi = \Psi(x, y, t)$, which determines the behavior of the individual. Probability wave – nonlinear wave which characterizing the behavior of the microsubjects of economy. Then the probability density $\rho(x, y, t) = |\Psi(x, y, t)|^2$ determines getting the individual to the certain point of economic space. Therefore, "in a particular area of economic space the soliton in the economy can be considered as a stable localization of the probability density of the getting microeconomic subjects to this area" [16].

4 Direct scattering problem for the (2+1)-dimensional nonlinear mathematical A1 model.

Consider the (2+1)-dimensional nonlinear A1 equation:

$$\Psi_t + \Psi_{xyy} + 2\left[\Psi^2\right]_y + [UV]_y = 0 \,,$$
$$V_x = \Psi_y,\ U_y = \Psi_x \,,$$

where complex-valued function $\Psi = \Psi(x, y, t) \in C^\infty(R^1 \times R^1 \times R^1_+)$, R^1 is the set of real numbers, R^1_+ is a positive semiaxis, and the function $\Psi(x, y, t)$ decreases with all its derivatives faster than any power of $|x|^{-1}$ [19].

Conservation law for the (2+1)-dimensional nonlinear A1 equation has the form:

$$\frac{\partial T}{\partial t} + divF = 0 \,,$$

where $divF = \frac{\partial F_1}{\partial x} + \frac{\partial F_2}{\partial y}$; T is density, $F = (F_1, F_2)$ is a flow similar to a fluid flow;

$$T = \Psi + C_1 \,;$$
$$F_1 = \Psi_{yy} + C_2 \,;$$
$$F_2 = 2\Psi^2 + UV + C_3 \,;$$

C_i, $i = \overline{1,3}$ are arbitrary constants.

The method of direct scattering problem for the (2+1)-dimensional nonlinear mathematical A1 model consists of the following steps:

1) An auxiliary linear system, Lax pair for the (2+1)-dimensional nonlinear mathematical A1 model is constructed.

2) The compatibility equation of the auxiliary linear system of the (2+1)-dimensional nonlinear mathematical A1 model is determined, it is the conditions of zero curvature.

3) For the first equation of the auxiliary linear system spectral problem is considered.

4) For a given function we find the components of the scattering matrix at fixed y and t.

5) Using the second equation for the auxiliary linear system we reconstruct the evolution of the components of the scattering matrix and discrete spectrum of variables y and t.

So, for the (2+1)-dimensional nonlinear mathematical A1 model we consider an auxiliary linear system of the form

$$\begin{cases} \varphi_x = P\varphi, \\ \varphi_t = Q_1\varphi + \lambda I\varphi_y, \end{cases} \tag{7}$$

where $\varphi = colon\,(\varphi_1, \varphi_2)$; $P = P_1 + \lambda P_2$,

$$P_1 = \begin{pmatrix} 0 & \Psi \\ \bar{\Psi} & 0 \end{pmatrix}, P_2 = \begin{pmatrix} -i & 0 \\ 0 & i \end{pmatrix}, I = \begin{pmatrix} 1 & 0 \\ 0 & 1 \end{pmatrix},$$

$$Q_1 = A + \lambda B\,,$$

$$A = \begin{pmatrix} 0 & -\Psi_{xy} - 2\Psi^2 - UV \\ -\bar{\Psi}_{xy} - 2\bar{\Psi}^2 - \bar{U}\bar{V} & 0 \end{pmatrix},$$

$$B = \begin{pmatrix} i & -2i\partial_x^{-1}\Psi - V \\ 2i\partial_x^{-1}\bar{\Psi} - \bar{V} & -i \end{pmatrix},$$

$\lambda_t = \lambda\lambda_y$, $\lambda = \lambda\,(y,t)$ is a spectral parameter, $\lambda = \xi_1 + i\xi_2$, $Re\lambda = \xi_1$, $Im\lambda = \xi_2$.

The compatibility conditions for the auxiliary linear system (5) and (2+1)-dimensional mathematical A1 model (4) has the form:

$$P_1 t - Ax + [P_1, A] = 0\,,$$

where $[P_1, A] = P_1 A - AP_1$.

Rapid decrease allows to define u, $\bar{u}$, v, $\bar{v}$ eigenfunctions with the following boundary conditions at fixed y and t

$$u \sim \begin{pmatrix} e^{-iRe\lambda x} \\ 0 \end{pmatrix} \text{at} \quad x \to -\infty,$$

$$\bar{u} \sim \begin{pmatrix} e^{-iRe\lambda x} \\ 0 \end{pmatrix} \text{ at} \quad x \to -\infty,$$

$$v \sim \begin{pmatrix} 0 \\ e^{iRe\lambda x} \end{pmatrix} \text{ at} \quad x \to +\infty,$$

$$\bar{v} \sim \begin{pmatrix} -e^{-iRe\lambda x} \\ 0 \end{pmatrix} \text{ at} \quad x \to +\infty.$$

For the spectral problem

$$\varphi_x = P_1\varphi + \lambda P_2\varphi \tag{8}$$

for a given solution of $\varphi = \varphi(x, y, t)$ at fixed y and t will be found the components of the scattering matrix:

$$S(\lambda) = \begin{pmatrix} a(\lambda) & b(\lambda) \\ \bar{b}(\bar{\lambda}) & -\bar{a}(\bar{\lambda}) \end{pmatrix}$$

Matrix $S(\lambda)$ describes the function φ. $\frac{1}{a(\lambda)}$ is the transmission coefficient, $\frac{b(\lambda)}{a(\lambda)}$ is reflection coefficient.

Next, we will omit the dependence of the functions of the y and t.

Assume, that φ and $\bar{\varphi}$ are the solution of the spectral problem (8):

$$\varphi = \varphi(x, Re\lambda) = colon(\varphi_1(x, Re\lambda), \varphi_2(x, Re\lambda)) ,$$
$$\bar{\varphi} = \bar{\varphi}(x, Re\lambda) = colon(\bar{\varphi}_1(x, Re\lambda), \bar{\varphi}_2(x, Re\lambda)) .$$

Then

$$\frac{d}{dx} W(\varphi, \bar{\varphi}) = 0 ,$$

where $W(\varphi, \bar{\varphi})$ is the Wronskian of φ and $\bar{\varphi}$:

$$W(\varphi, \bar{\varphi}) = \varphi_1 \bar{\varphi}_2 - \varphi_2 \bar{\varphi}_1 .$$

As $W(u, \bar{u}) = -1$ and $W(v, \bar{v}) = 1$, v and $\bar{v}$ decisions are linearly independent, so we can express u and $\bar{u}$ functions through v and $\bar{v}$:

$$u = a(Re\lambda)\bar{v} + b(Re\lambda)v$$
$$\bar{u} = -\bar{a}(Re\lambda)v + \bar{b}(Re\lambda)\bar{v}$$

or

$$\begin{pmatrix} u \\ \bar{u} \end{pmatrix} = \begin{pmatrix} a(Re\lambda) & b(Re\lambda) \\ \bar{b}(Re\lambda) & -\bar{a}(Re\lambda) \end{pmatrix} \begin{pmatrix} \bar{v} \\ v \end{pmatrix}$$

wherein

$$a(Re\lambda)\bar{a}(Re\lambda) + b(Re\lambda)\bar{b}(Re\lambda) = 1 .$$

We now establish the analytic properties of the scattering matrix.

If Ψ and $\bar{\Psi}$ are absolutely integrable, i.e. Ψ, $\bar{\Psi} \in L_1$, the $u(x, \lambda)e^{i\lambda x}$ and $v(x, \lambda)e^{-i\lambda x}$ functions are analytic in the upper halfplane and the $\bar{u}(x, \bar{\lambda})e^{-i\bar{\lambda}x}$ and $\bar{v}(x, \bar{\lambda})e^{i\bar{\lambda}x}$ functions are analytic in the lower halfplane, where

$$u(x, \lambda) = colon(u_1(x, \lambda), u_2(x, \lambda)) ,$$
$$v(x, \lambda) = colon(v_1(x, \lambda), v_2(x, \lambda)) .$$

Then the function

$$a(\lambda) = W(u(x, \lambda), v(x, \lambda)) = u_1(x, \lambda)v_2(x, \lambda) - u_2(x, \lambda)v_1(x, \lambda)$$

is analytic in the upper halfplane, and the function

$$\bar{a}(\bar{\lambda}) = W(\bar{u}(x, \bar{\lambda}), v(x, \bar{\lambda})) = \bar{u}_1(x, \bar{\lambda})\bar{v}_2(x, \bar{\lambda}) - \bar{u}_2(x, \bar{\lambda})\bar{v}_1(x, \bar{\lambda})$$

is analytic in the lower halfplane.

Functions

$$b(\lambda) = -W(u(x,\lambda), \bar{v}(x,\bar{\lambda})) ,$$
$$\bar{b}(\bar{\lambda}) = -W(\bar{u}(x,\bar{\lambda}), v(x,\lambda))$$

are, generally speaking, do not have the analytic properties.

To establish the analytic properties of the scattering matrix we represent the function $u(x,\lambda) = colon(u_1(x,\lambda),\ u_2(x,\lambda))$ in the form of the integral equation.

$$u_1(x,\lambda)e^{i\lambda x} = 1 + \int_{-\infty}^{x} M(x,z_1,\lambda)u_1(z_1,\lambda)e^{i\lambda z_1}dz_1 , \tag{9}$$

$$u_2(x,\lambda)e^{i\lambda x} = \int_{-\infty}^{x} e^{2i\lambda(x-z_1)}\bar{\Psi}(z_1)u_1(z_1,\lambda)e^{i\lambda z_1}dz_1 , \tag{10}$$

$$M(x,z_1,\lambda) = \bar{\Psi}(z_1)\int_{z_1}^{x} e^{2i\lambda(z_2-z_1)}\Psi(z_2)dz_2 . \tag{11}$$

Following [1] we can show absolute convergence, limitations of $u_1(x,\lambda)e^{i\lambda z}$, $u_2(x,\lambda)e^{i\lambda z}$ functions and their derivatives with respect to λ, that sets the analyticity of $u_1(x,\lambda)e^{i\lambda z}$ and $u_2(x,\lambda)e^{i\lambda z}$ functions in the upper halfplane $Im(\lambda) > 0$.

At Ψ , $\bar{\Psi} \in L_1$ and additional conditions on Ψ and $\bar{\Psi}$ functions:

$$\left|\bar{\Psi}(x)\right| \le Ce^{-2K|x|} ,$$
$$|\Psi(x)| \le Ce^{-2K|x|} ,$$

where C, K $(K > 0)$ are constants, we obtain analyticity of the vector functions, $u(x,\lambda)e^{i\lambda x}$, $v(x,\lambda)e^{-i\lambda x}$ and $a(\lambda)$ for all $Im(\lambda) > -K$, while the vector functions $\bar{u}(x,\bar{\lambda})e^{-i\bar{\lambda}x}$ and $\bar{v}(x,\bar{\lambda})e^{i\bar{\lambda}x}$ and $\bar{a}(\bar{\lambda})$ are analytic for all $Im(\lambda) < K$. Besides $b(\lambda)$ and $\bar{b}(\bar{\lambda})$ are analytic in the strip $-K < Im(\lambda) < K$.

In order to obtain an asymptotic expansion for large λ in the upper halfplane, we integrate (9)-(11) by parts, we obtain:

$$u_1(x,\lambda)e^{i\lambda x} = 1 - \frac{1}{2i\lambda}\int_{-\infty}^{x} \bar{\Psi}(z_1)dz_1 + O(\lambda^2) ,$$

$$u_2(x,\lambda)e^{i\lambda x} = -\frac{1}{2i\lambda}\bar{\Psi}(x) + O(\lambda^{-2}) ,$$

$$v_1(x,\lambda)e^{-i\lambda x} = \frac{1}{2i\lambda}\Psi(x) + O(\lambda^{-2}) ,$$

$$v_2(x,\lambda)e^{-i\lambda x} = -\frac{1}{2i\lambda}\int_{x}^{\infty} \bar{\Psi}(z)\Psi(z)dz + O(\lambda^{-2}) .$$

For the coordinates of vector functions

$$\bar{u}(x,\bar{\lambda}) = colon(\bar{u}_1(x,\bar{\lambda}), \bar{u}_2(x,\bar{\lambda})) ,$$
$$\bar{v}(x,\bar{\lambda}) = colon(\bar{v}_1(x,\bar{\lambda}), \bar{v}_2(x,\bar{\lambda}))$$

for all λ lying in the lower halfplane we obtain an asymptotic expansion:

$$\bar{u}_1(x,\bar{\lambda})e^{i\bar{\lambda}x} = 1 - \frac{1}{2i\bar{\lambda}}\Psi(x) + O(\lambda^2) ,$$

$$\bar{u}_2(x,\bar{\lambda})e^{-i\bar{\lambda}x} = -1 - \frac{1}{2i\bar{\lambda}}\int_{-\infty}^{x}\Psi(z_1)\bar{\Psi}(z_1)dz_1 + O(\bar{\lambda}^2) ,$$

$$\bar{v}_1(x,\bar{\lambda})e^{-i\bar{\lambda}x} = 1 + \frac{1}{2i\bar{\lambda}}\int_{x}^{\infty}\Psi(z_1)\bar{\Psi}(z_1)dz_1 + O(\bar{\lambda}^2) ,$$

$$\bar{v}_2(x,\bar{\lambda})e^{-i\bar{\lambda}x} = -\frac{1}{2i\bar{\lambda}}\bar{\Psi}(x) + O(\lambda^{-2}) .$$

Then for $|\lambda| \to \infty$ in the corresponding halfplanes we have asymptotic expansions for $a(\lambda)$ and $\bar{a}(\bar{\lambda})$:

$$a(\lambda) = 1 - \frac{1}{2i\lambda}\int_{-\infty}^{\infty}\Psi(z_1)\bar{\Psi}(z_1)dz_1 + O(\lambda^2) ,$$

$$\bar{a}(\bar{\lambda}) = 1 - \frac{1}{2i\bar{\lambda}}\int_{-\infty}^{\infty}\Psi(z_1)\bar{\Psi}(z_1)dz_1 + O(\bar{\lambda}^{-2}) .$$

If Ψ and $\bar{\Psi}$ not too small, the spectral problem

$$\varphi_x = P_1\varphi + \lambda P_2\varphi$$

can have discrete eigenvalues when $a(\lambda)$ has zeros in the upper halfplane, $(Im(\lambda) > 0)$ and $\bar{a}(\bar{\lambda})$ has zeros in the lower halfplane $(Im(\lambda) < 0)$.

Let us assume that Ψ and $\bar{\Psi}$ decrease sufficiently rapidly at $|x| \to \infty$ i.e.

$$\int_{-\infty}^{\infty}|z_1|^n|\Psi(z_1)|dz_1 < \infty ,$$

$$\int_{-\infty}^{\infty}|z_1|^n|\bar{\Psi}(z_1)|dz_1 < \infty$$

for all n. Then $a(\lambda)$, $\bar{a}(\bar{\lambda})$, $b(\lambda)$, $\bar{b}(\bar{\lambda})$ are entire functions. In this case we can continue $b(\lambda)$, $\bar{b}(\bar{\lambda})$ and get $\gamma_k(\lambda) = b(\lambda_k)$ and $\bar{\gamma}_k(\bar{\lambda}) = \bar{b}(\bar{\lambda}_k)$.

Then the functions $a(\lambda)$, $\bar{a}(\bar{\lambda})$ are analytic in the upper and lower halfplanes, respectively, and on the real axis. Therefore $a(\lambda)$ has only a finite number of zeros at $Im(\lambda) > 0$ [18].

Let λ_k, $k = \overline{1,N}$ are zeros $a(\lambda)$ in the upper halfplane $(Im(\lambda) > 0)$, where N is the number of bound states. At $\lambda = \lambda_k$, $k = \overline{1,N}$ we have a relationship:

$$u(x,\lambda) = \gamma_k(\lambda)v(x,\lambda), \gamma_k(\lambda) = b(\lambda_k), k = \overline{1,N} .$$

Let $\bar{\lambda}_k$, $k = \overline{1,N}$ are zeros of $\bar{a}(\bar{\lambda})$ in the lower halfplane. Then for $\overline{\lambda} = \overline{\lambda}_k$, $k = \overline{1,N}$ we have bound states:

$$\bar{u}(x,\bar{\lambda}) = \bar{\gamma}_k(\bar{\lambda})\bar{v}(x,\bar{\lambda}), \bar{\gamma}_k(\bar{\lambda}) = \bar{b}(\bar{\lambda}_k), k = \overline{1,N} .$$

Using the second equation of the auxiliary linear system (7)

$$\varphi_t = \lambda\varphi_y + A\varphi + B\lambda\varphi , \tag{12}$$

where the spectral parameter $\lambda = \lambda(x,y,t)$ satisfies the differential equation:

$$\lambda_t = \lambda\lambda_y \ , \tag{13}$$

we restore the dependence of the $S(\lambda)$ scattering matrix on the variables y and t.

The equation (13) has two solutions:

$$\lambda(y,t) = \lambda_1 = const \ ,$$

$$\lambda(y,t) = \lambda_2(y,t) = \frac{y + c_1 + ic_2}{t_0 - t} \ ,$$

where c_1, c_2, t_0 are some real constants.

The scattering matrix

$$S\left(\lambda\right) = \begin{pmatrix} a\left(\lambda\right) & b\left(\lambda\right) \\ \bar{b}\left(\bar{\lambda}\right) & -\bar{a}\left(\bar{\lambda}\right) \end{pmatrix}$$

by (12) satisfies the evolution equation

$$S_t = \lambda S_y \tag{14}$$

From which we obtain the evolution on the x, y and t of the transition coefficients and discrete spectrum

$$a(x,y,t,\lambda) = a(x, y + \lambda t, \lambda) \ ,$$

$$b(x,y,t,\lambda) = b(x, y + \lambda t, \lambda) \ ,$$

$$\gamma_j(x,y,t,\lambda_j) = \gamma_j(x, y + \lambda_j t, \lambda_j), j = \overline{1,N} \ .$$

From (14) we see that the components of the scattering matrix $S(\lambda)$ satisfy the evolution equations

$$b_t = \lambda b_y \ ,$$

$$a_t = \lambda a_y \ ,$$

$$(\gamma_j)_t = \lambda(\gamma_j)_y \ .$$

Thus, for the (2+1)-dimensional nonlinear mathematical A1 model we built auxiliary linear system, the condition of zero curvature, for the first equation of the auxiliary linear system we considered spectral problem, for a given function φ we obtain the components of the scattering matrix and discrete spectrum for fixed y and t. Using the second equation of the auxiliary linear system, we restored the evolution of the data of the scattering matrix and discrete spectrum on the variables y and t.

5 The economic meaning of the direct scattering problem for the (2+1)-dimensional mathematical A1 mode.

Spatially two-dimensional nonlinear mathematical A1 model (4) adequately describes the objective reality of any economic phenomenon or process. It is known [17] that the behavior of the microsubjects of economy has wave character. Here, the function $\Psi = \Psi\left(x,y,t\right)$ is the wave function describing the state of the economy microsubject, x, y are the potentials of collective economic interactions; t is the time factor, which serves as a transformation parameter;

$\rho(x,y,t) = |\Psi(\mathrm{x},\mathrm{y},\mathrm{t})|^2$ is the density of the probability of micro-economic subject in given point of economic space at a given time. The wave function of the economic $\Psi = \Psi(x,y,t)$ is equal to the probability amplitude of finding the microeconomic subject at a particular point in economic space each time point t . Potentials of the collective economic interactions x and y are characteristic of the collective economic field, which, in turn, is the result of the aggregation of individual economic fields.

(2+1)-dimensional nonlinear mathematical A1 model describes a change in x and y potentials whereby eigenvalues λ_j, $j = \overline{1,N}$ of $\Psi = \Psi(x,y,t)$ function satisfy the evolution equation $\lambda_t = \lambda\lambda_y$. Hence the transformation of $\Psi = \Psi(x,y,t)$ function defined by the change in the x and y potentials of collective interactions. In turn, the change in the x and y potentials of collective interaction is caused by the evolution of the function $\Psi = \Psi(x,y,t)$.

The solution of (2+1)-dimensional nonlinear mathematical A1 model by direct scattering problem is that for a given initial value of $\Psi = \Psi(x,y,t)$ function recovering the so-called scattering data, i.e. all λ_j, $j = \overline{1,N}$ eigenvalues and components of the scattering matrix will also change. Thus soliton will form only if the function $\Psi = \Psi(x,y,t)$ is deformed in accordance with the equation (4).

If to apply the method of direct scattering problem to the economic problems, it will conform to the implementation of a positive approach to economic policy.

In particular, the requirement to assess the consequences of any predefined permanent economic activities, such as budget, formally corresponds to the solution of the direct problem of scattering. I.e. data recovery in the scattering matrix for a given function $\Psi = \Psi(x,y,t)$ in advance on the collective interactions of x and y. This interpretation of the direct scattering problem method is consistent with the positive analytical approach in the economy.

6 Conclusion.

Thus, we examined the (2+1)-dimensional nonlinear mathematical A1 model, generalizing the Korteweg-de Vries equation. Showed its conservation laws, considered the auxiliary linear system for it, determined the conditions of zero curvature, which connects the auxiliary linear system with this model. Solved a direct scattering problem for this model. For a given function defined components of the scattering matrix, restored the evolution of the scattering matrix on the variables y and t.

Explained the economic meaning of (2+1)-dimensional nonlinear mathematical A1 model. Defined an economic soliton as solution of this mathematical model. Explain the economic meaning of the method of direct scattering problem corresponding to the positive analytical approach in the economy.

References

1. Ablowitz, M., Sigur, X.: Solitons and the inverse scattering method, 477 p. Moscow (1987) (in Russian)
2. Gardner, C.S. and Morikawa, G.M.: Similarity in the asymptotic behavious of collision free hydromagnetic wave and water waves. In: Report NYO-9082. Cjurant Inst. of Math. Sciences (1969)
3. Washimi, M. and Taniuti, T.: Propagation of ion acoustic solitary waves of small amplitude. In: Phys. Rev. Lett., vol. 17, pp. 996-998 (1966)
4. Kadomtsev, B.B., Petviashvili, V.I.: On the stability of solitary waves in a medium with weak dispersion. In: DAN SSSR, vol. 192, pp. 753-756 (1970) (in Russian)
5. Tappert, F. and Varma, C.M.: Asymptotic theory of self - trapping of heat pulses in solids. In: Phys. Rev. Lett., vol. 25, pp. 1108-1111 (1970)
6. Narayanamyrti V. and Varma C. M.: Nonlinear propagation of heat pulses in solids. In: Phys. Rev. Lett., vol. 25, pp. 1105-1108 (1970)

7. Kako, M. and Rowland, G.: Two dimensional stability of ion acoustic solitons. In: Plasma Phisics, vol. 18, pp. 165-170 (1976)
8. Newell, A.: Solitons in mathematics and physics (trans. from English) 326 p. Moscow (1989) (in Russian)
9. Veselov, A.P., Novikov, S.P.: Finite-two-dimensional potential Schrödinger operators. Explicit formulas and evolution equations. In: DAN SSSR, vol. 279, pp.20 (1984) (in Russian)
10. Nizhnik, L.P.: Inverse scattering problems of hyperbolic equations. 232 p. Kiev (1991) (in Russian)
11. Alexeyeva, A.V.: (2+1)-dimensional analogs of the Korteweg-de Vries equation. In: International Journal of Contemorary Mathematics, vol.3, № 1-2, pp. 47-55 (2012)
12. Alekseyeva, A.V.: (2+1)-dimensional model of the Korteweg-de Vries equation and its integrability. In: Bulletin of the MES, № 3, pp. 12-15 (2006) (in Russian)
13. Alekseyeva, A.V.: Hirota method for (2+1)-dimensional bilinear H1 form. In: Proceedings of the MES. Series of Physics and Mathematics, № 5, pp. 27-33 (2012) (in Russian)
14. Alekseyeva, A.V.: N-soliton solutions of the (2+1)-dimensional nonlinear A1 equation. In: Proceedings of the X International correspondence scientific-practical conference "Scientific debate: Innovation in the Modern World", pp. 6-15. Moscow (2013) (in Russian)
15. Shikin, G.: Fundamentals of the theory of solitons in the general theory of relativity, pp.3. Moscow (1995) (in Russian)
16. Ogorodnikova, T.V.: Economic soliton as stable form of collective wave behavior of microeconomic subjects (2004) (in Russian)
17. Ogorodnikova, T.V.: The formalization of the wave soliton of the collective economic behavior (in Russian)
18. Ablowitz, M. J. , Kaup, D. J., Newell, A. C. and Segur, H.: The Inverse Scattering transform–Fourier analysis for Nonlinear Problems. In: Stud. Appl. Math, vol. 53, pp. 249-315 (1974)
19. Tahtadzhan L .A., Fadeev L.D.: The Hamiltonian approach in the theory of solitons, 527 p. Moscow (1986) (in Russian)

Construction of Mathematical Model, Compression of Rubber-Metal Supports and Behavior of Rubber Layer

Ruslan Askarbekov

Kyrgyz State Technical University,
Mira avenue 66, 720044 Bishkek, Kyrgyzstan
askarbekovu@gmail.com
http://www.kstu.kg

Abstract. Rubber-metal supports (RMS) apply under vertical compression load, because they can withstand many times over higher load compared with conventional frictional contact system. The particular importance in this case are questions related to the strength of the RMS under compression which reaches 100 MPa. In this article I built a model the deformation of RMS in Matlab. Also I used the analytical model for building according to the compression rubber layer under the influence of a uniform load.

Keywords: Rubber, rubber-metal supports, Caushy tensor, compression

1 Introduction

Rubber constructions are widely used in various fields of modern technology as elastic hinges and supports, dampers and vibration isolation devices, compensators of various kinds of deformations and so on. Rubber elements are superior to traditional systems for the same purpose in many respects - simple design, reliability, size, cost, and others.

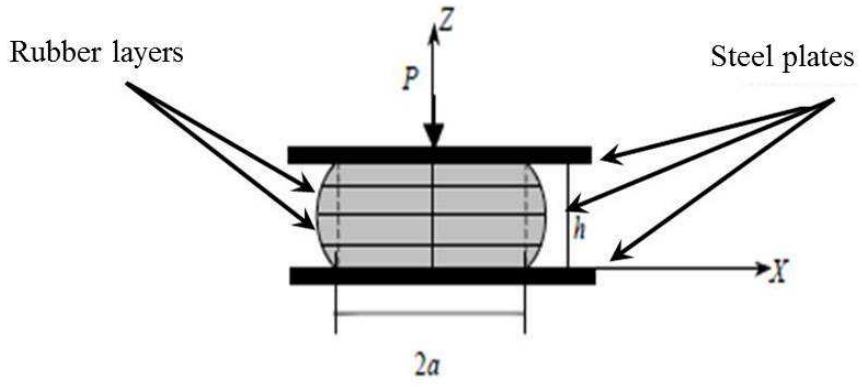

Fig. 1. The compression of rubber layer in rubber-metal shock absorber

2 Material and methods

The RMS supports are compressed under load to determine the modulus of elasticity, shear modulus and rubber stiffness. RMS test carried out at the press machine UM-100 in the laboratory of the department "Mechanics and Industrial Engineering"in KSTU, the applied load was 6 tons. Loads are increased gradually. RMS has the following geometrical characteristics:

diameter - 0.105 m, height - 0.1 m. The rubber layers are compressed and on around the edges is bulges, during loading (Fig. 2 and 3). Metal plate is uniformly distributes all load and does not participate in the compression process, practically. The results of the experiment shown on graphs 4-7, also in data table.

Figure 1: The rubbe-metal elements

Figure 2: Compresion of the RMS2 and RMS3

Fig. 2.

To comparison of the results and estimate parameters is needed carrying out an experiment. Since the deformation of the rubber layer depends on the technology of the rubber composition and manufacturing rubber elements.[2] When loading the sample, were observed external defects (cracks) in the rubber layers of RMS. Temperature during the experiment was equal to room temperature and 20 degrees Celsius.

Many experiments have shown that the mechanical properties of the elements of the RMS may differ significantly from the mechanical properties of rubber, from which they are made.[3] The reason for this difference is due

to the presence of the so-called form factor. This is especially observed in the effect of compressive strain. Using of a new method of determining the stress-strain state of the RMS are shown below. This method is based on the use of the Cauchy tensor.

σ, MPa	RMS №2	RMS №3
	ε	ε
1,13	0,09	0,075
2,27	0,16	0,13
3,40	0,24	0,17
4,53	0,29	0,2
5,66	0,33	0,23
6,80	0,36	0,26

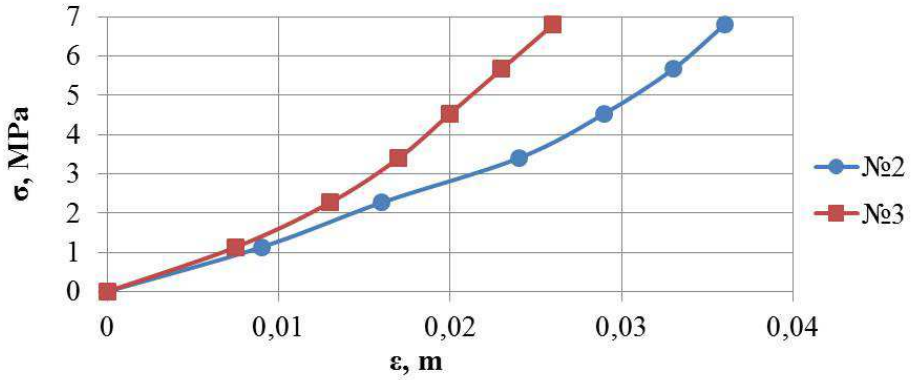

Fig. 3. Diagram of stress and strain in a single-layer rubber (RMS2), and a two-layer rubber (RMS3).

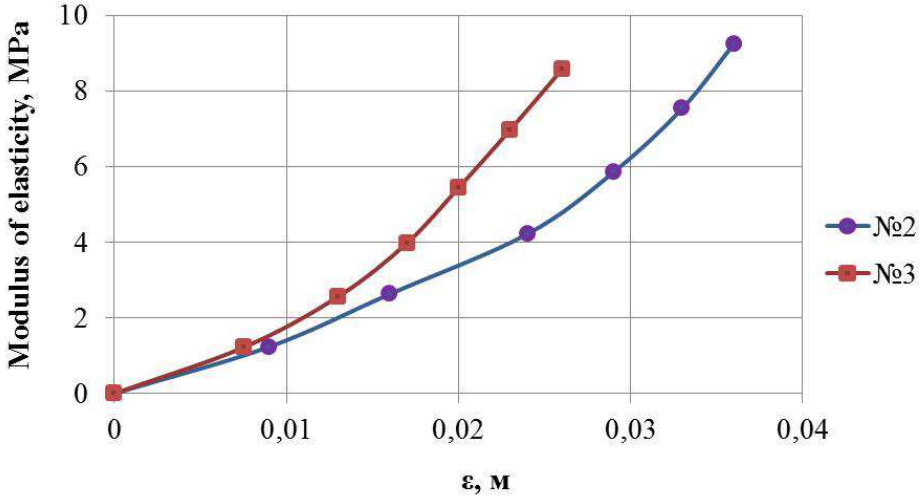

Fig. 4. The dependence of the elastic modulus from the deformation in a single-layer rubber (RMS2), and a two-layer rubber (RMS3).

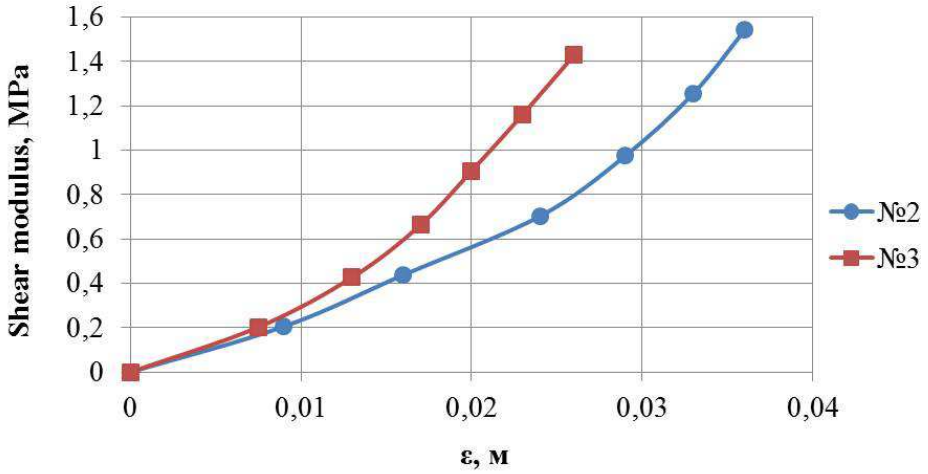

Fig. 5. The dependence of the shear modulus from the deformation in a single-layer rubber (RMS2), and a two-layer rubber (RMS3).

3 Determination of the displacement and deformation of RMS in the Matlab using the Cauchy tensor

Let the known solution of the static boundary value problem. It is easily determined from the strain [1]

$$\varepsilon_{ij} = \frac{1}{E}\left(-\nu\delta_{ij}\sigma_{kk} + (1+\nu)\sigma_{ij}\right) \tag{1}$$

Next we define the displacement by the formulas Cesaro.

$$u_i(x)=u_i(x^0)+\omega_{ij}(x^0)(x_j-x_j^0)+\frac{1}{E}\int_\ell(\varepsilon_{ik}(y)+(x_j-y_j)(\varepsilon_{ki,j}(y)-\varepsilon_{kj,i})))dy_k,$$

where l - in line $\mathbf{V}$, x_0 - the starting point of the line, $u_i(x^0), \varpi_{ij}(x^0)$ - integration constants. Generally speaking, more convenient to use this formula, and its transformed view.

$$u_i(x)= u_i(x^0) + \omega_{ij}(x^0)\,(x_j- x_j^{\,0}) +$$

$$\frac{1}{E}\int_\ell(-\nu\delta_{ik}\sigma_{tt} + (1+\nu)(\sigma_{ik} + (x_j - y_j)(-\nu(\delta_{ki}\sigma_{tt,j} - \delta_{kj}\sigma_{tt,i}) + (1+\nu)(\sigma_{ki,j} - \sigma_{kj,i})))dy_k$$

In this equation $u_i(x^0), \varpi_{ij}(x^0)$ are arbitrary constants. They are do not correspond to causing a deformation of movements (parallel translation and rotation of rigid body). In what follows may be excluded from consideration such movements. In this case

$$u_i(x) = \frac{1}{E}\int_l(-\nu\delta_{ik}\sigma_{tt} + (1+\nu)(\sigma_{ik} + (x_j - y_j)(-\nu(\delta_{ki}\sigma_{tt,j}) + (1+\nu)(\sigma_{ki,j} - \sigma_{kj,i}))))\,dy_k \tag{2}$$

As shown in Figure 7, the vectors

$$z_i = x_i - u_i(x), \quad x_i \in V, \quad z_i = x_i - u_i(x), \quad x_i \in S, \tag{3}$$

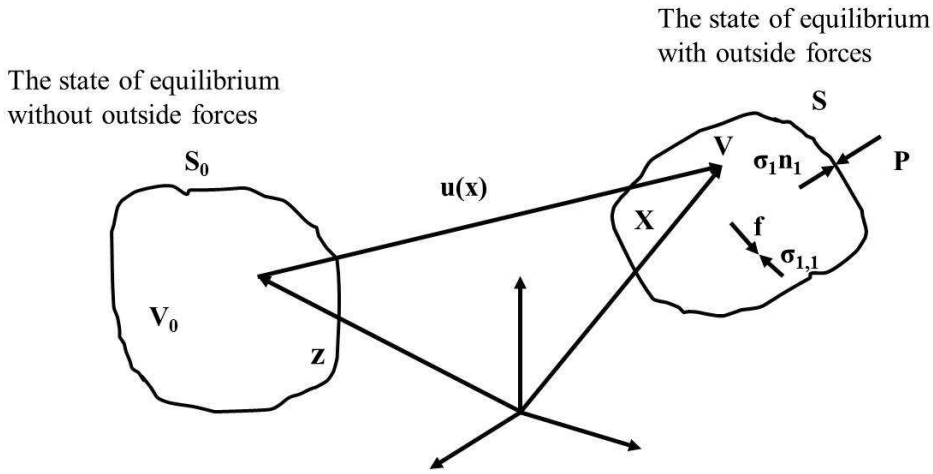

Fig. 6.

define some area V_0 and its surface S_0. (V_0, S_0), obviously the state of equilibrium without any external forces.

Comparing condition of the static boundary value problem is called further for sake of brevity (V_0, S_0),. Vectors value $u(x)$ of the decision does not move the body. The body occupies an area V, bounded by the surface S, to solutions and remains the same even after the decision. Determine the coordinates $z_i(3)$ to compare the state there is some mathematical transformation of the field (V, S). Field $u_i(x)$ determines the relative change of coordinates, deformation components, rotation and tension of these condition. This relativity can be represented as

$$x_i\text{-}z_i = u_i(x), \quad \varepsilon_{ij}(x)\text{-}\varepsilon_{ij}(z) = (u_{i,j}+u_{j,i})/2, \quad \omega_{ij}(x)\text{-}\omega_{ij}(z) = (u_{i,j}-u_{j,i})/2,$$
$$\sigma_{ij}(x) = \lambda\delta_{ij}u_{k,k} + \mu(u_{i,j}+u_{j,i}). \qquad (4)$$

Here $x_i, \varepsilon_{ij}(x), \varpi_{ij}(x), \sigma_{iy}(x)$ refer to the position of equilibrium with the outside forces, and $z_i, \varepsilon_{ij}(z), \varpi_{ij}(z)$ - the position of equilibrium without external forces. Field $u_i(x)$ only converts (V, S) in (V_0, S_0), therefore it determines the only the relative change of coordinates, strains and stresses compared these states. In a Cartesian coordinate system, the axis of which is denoted by x_1, x_2, x_3, deformed body occupies an area V.

4 Results

Let the is known only Cauchy tensor

$$\varepsilon_{ij} = c\times$$
$$\begin{pmatrix} \sin x_2 \cos x_3 & \frac{1}{2}(\sin x_2 \sin x_3 + x_1 \cos x_2 \cos x_3) & \frac{1}{2}(\cos x_2 - x_1 \sin x_2 \sin x_3) \\ \frac{1}{2}(\sin x_2 \sin x_3 + x_1 \cos x_2 \cos x_3) & x_1 \cos x_2 \sin x_3 & \frac{1}{2}x_1 \sin x_2(\cos x_3 - 1) \\ \frac{1}{2}(\cos x_2 - x_1 \sin x_2 \sin x_3) & \frac{1}{2}x_1 \sin x_2(\cos x_3 - 1) & 0 \end{pmatrix}.$$

This model is realized in Matlab, used by when determining strained deformed condition RMS. Below are the results of calculation.

First need to build a layered element of rubber-metal support. Then on the displaced points we obtain the final form and strain state of the RMS as shown in Figure 8. Figure 9 shows the initial and deformed condition of RMS with two layers of rubber.

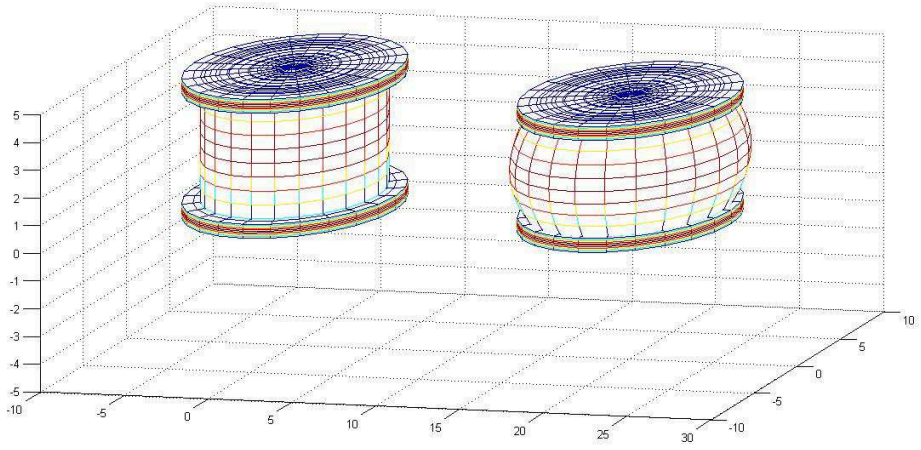

Fig. 7. The deformed condition RMS with a single layer of rubber in compression.

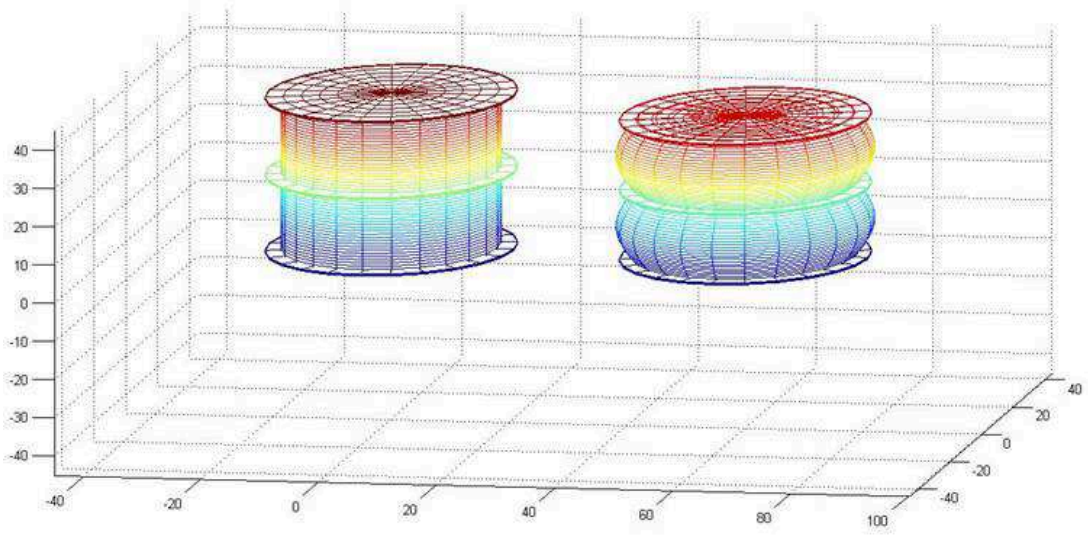

Fig. 8. The deformed condition RMS with two layers of rubber in compression.

5 Conclusion

In matlab, these elements are constructed from the original state, ie, without load and under load application. When the applied load as shown in Figure rubber elements are compressed. Displacements obtained by using the analytical equations and on the figure show complete similarity with the real model. Thus model 3-dimensional constructions under the influence of static forces are deformed.

References

1. Zhakypbek A.B., Duishenaliev T.B.: A new outlook on some of the basics of mechanics rigid body. Bishkek (1999)
2. Nowacki V.: Theory of elasticity. M., Mir (1975)
3. Rubber.: Test methods. /Tutorial. Manual for schools/Edited by IV Vinogradskaya. - Leningrad (1968)

Mass Conservation and Pressure Equations for the Sequential Chemical Compositional Simulation

B.E. Bekbauov[1], A. Kaltayev[1], Zh. Baishemirov[2], A.T. Rakhymova[2]

[1]Al-Farabi Kazakh National University, Almaty, Kazakhstan,
[2]Abai Kazakh National Pedagogical University,
Institute of Information and Computational Technologies, Almaty, Kazakhstan
bakhbergen.bekbauov@kaznu.kz

Abstract. In this paper we studied a new mathematical formulation for the chemical compositional reservoir simulation. A comparison with UTCHEM simulator has also been performed of Alkaline-Surfactant-Polymer (ASP) Flooding.

Keywords: Chemical flooding, Alkaline-Surfactant-Polymer, Mass Conservation

1 Introduction

Chemical flooding is one of the most promising and broadly applied EOR processes. Its commercial implementation has been facing several technical, operational and economic challenges. Chemical flooding is further subdivided into polymer flooding, surfactant flooding, alkaline flooding, miscellar flooding, and alkaline-surfactant-polymer (ASP) flooding. ASP flooding is a form of chemical enhanced oil recovery method that can allow operators to extend reservoir pool life and extract incremental reserves currently inaccessible by conventional methods. In the ASP flooding process, surfactants are chemicals that used to reduce the interfacial tension between the involved fluids, increasing oil mobility. Alkali reduces adsorption of the surfactant on the rock surfaces and reacts with acids in the oil to create natural surfactant. Polymer improves the sweep efficiency. Lots of compositional models investigated in the open literature [1-9] have some limitations for applicability like single species, equilibrium mass transfer, and lack of modeling miscibility which occurs during surfactant flooding. The basic equations used in UTCHEM model that describe multiphase, multicomponent flow in permeable media are the species-conservation equations, pressure (an overall mass-continuity) equation, and energy conservation equations. Chen et al. [10] presented a numerical approach based on a formulation that solves both pressure and compositions implicitly. Though the approach was claimed to be sequential and extended from the IMPEC (implicit pressure and explicit composition) approach used in UTCHEM model [11], the mathematical formulations for the governing equations did not undergo any change in their model. The system of species conservation equations was solved implicitly for the overall concentration of each component. In this work we introduce a new approach to model the reduction in pore volume due to adsorption that satisfies the continuity equation. In certain situations, such as significant change in the effective pore size, these enhancements are essential to properly model the physical phenomena occurring in petroleum reservoirs. In addition, this new approach for modeling the adsorption effect on the transport of a component makes it possible to develop a new mathematical formulation for the sequential chemical compositional reservoir simulation. The innovation is the development of a new mathematical formulation of the mass conservation and pressure equations for the sequential chemical compositional simulation. We have noticed that the net loss of components by fluids is not equal to gain of the same components by fluid phase. Since the model derivation is quite long, we have not provided it in this work. Using the newly developed

model we simulated ASP flooding process and compared the simulation results with that of UTCHEM simulator.

2 Mathematical model

The mathematical formulation developed in the scope of this work is extended from the UTCHEM model formulation for use in chemical flooding studies. Accumulation terms in the species-conservation equations used in UTCHEM model account for the reduction in pore volume caused by adsorption. During the process of this research, it was revealed that this commonly used approach estimates the adsorption effect on the transport of a component reasonably well but it does not satisfy the species-conservation equation. Since the total mass conservation equation follows from summing the species-conservation equations over all components, the obtained equation violates the principle of total mass conservation as well. With these as governing equations, several simulators have been developed during recent years to model chemical compositional phenomena in petroleum reservoirs.

Let us consider overall compositional balance equations:

$$\frac{\partial}{\partial t}\left[\phi\rho_i\left(\sum_{\alpha=1}^{n_p} S_\alpha c_{i\alpha} + \hat{c}_i\right)\right] + \nabla\cdot\phi\rho_i\sum_{\alpha=1}^{n_p}(S_\alpha c_{i\alpha}\overrightarrow{u_\alpha}) - \nabla\cdot\sum_{\alpha=1}^{n_p}\left[K_{i\alpha}^{=}\cdot\nabla(\phi\rho_i S_\alpha c_{i\alpha})\right] =$$

$$= -k_i\phi\rho_i\left(\sum_{\alpha=1}^{n_p} S_\alpha c_{i\alpha} + \hat{c}_i\right) + Q_i, i = 1, ..., n_c - components \tag{1}$$

where

$\alpha = 1, ..., n_p$ is phases, ϕ is porosity, ρ_i is density of component, $K_{i\alpha}^{=}$ is absolute permeability, S_α is saturation of α phase, $\tilde{c_i}$ is overall concentration, $c_{i\alpha}$ is concentration of component i in α phase,$\overrightarrow{u_\alpha}$ is velocity of phase, Q_i is source / sink term, $-k_i\phi\rho_i\left(\sum_{\alpha=1}^{n_p} S_\alpha c_{i\alpha} + \hat{c}_i\right)$ is radioactive decay, k_i is coefficient of radioact decay

In our approach, the porosity ϕ is related to the original porosity ϕ_R as follows:

$$\phi = \phi_R(1 - \sum_{i=1}^{n_{c\nu}}\hat{c}_i)[1 + c_r(p_1 - p_s)] \tag{2}$$

For a slightly compressible fluid, the component density ρ_i can be written as:

$$\rho_i = \rho_{iR}[1 + c_i^0(p_1 - p_R)], i = 1, ..., n_c \tag{3}$$

ρ_{iR} is reference density, ρ_i is density of component

We define the overall concentration

$$\tilde{c_i} = \sum_{\alpha=1}^{n_p} S_\alpha c_{i\alpha} + \hat{c}_i, i = 1, ..., n_c \tag{4}$$

Since reference density ρ_{iR} is constant for each component we can divide through both sides of equation (1) by ρ_{iR}. In terms of the dimensionless density $\bar{\rho}_i = \rho_i/\rho_{iR}$. Then equation (1)can be written as:

$$\frac{\partial(\phi\bar{\rho}_i\tilde{c}_i)}{\partial t} + \nabla\cdot\phi\bar{\rho}_i\sum_{\alpha=1}^{n_p}(S_\alpha c_{i\alpha}\overrightarrow{u} - \nabla\cdot\sum_{\alpha=1}^{n_p}[K^{=}_{i\alpha}\cdot\nabla(\phi\bar{\rho}_i S_\alpha c_{i\alpha})] =$$

$$= -k_i\phi\bar{\rho}_i\tilde{c}_i + \frac{Q_i}{\rho_{iR}}.i = 1,...,n_c \tag{5}$$

The phase velocity from Darcy's law is

$$\overrightarrow{u_\alpha} = -\frac{k^{=}k_{r\alpha}}{\phi S_{\alpha\mu_\alpha}}(\nabla p_\alpha - \gamma_\alpha\nabla Z), = 1,...,n_p isphases \tag{6}$$

where

p_α is pressure, $\gamma_\alpha\nabla Z$ is gravity effect, $k^{=}$ is absolute permeability, $k_{r\alpha}$ is relative permeability, μ_α is viscosity of α phase

By substituting Eq. (2,3,4) into the the Eq. (5) and carrying out time derivation we obtain the continuity equation in the following form

$$\phi_R[1 + c_f(p_1 - p_S)]F_t(\tilde{c}_i,\hat{c}_i) + \phi_R c_t\frac{\partial p_1}{\partial t} +$$

$$+\nabla\cdot\left\{\phi\sum_{\alpha=1}^{n_p}\left(S_\alpha\overrightarrow{u_\alpha}\sum_{i=1}^{n_c}[1 + c_i^0(p_1 - p_R)]c_{i\alpha}\right)\right\} = \sum_{i=1}^{n_c}\frac{Q_i}{\rho_{iR}} \tag{7}$$

$$\sum_{i=1}^{n_c}\sum_{\alpha=1}^{n_p}[K^{=}_{i\alpha}\cdot\nabla(\phi\bar{\rho}_i S_\alpha c_{i\alpha})] = 0$$

$$\sum_{i=1}^{n_c} k_i\phi\bar{\rho}_i\tilde{c}_i = 0$$

ϕ_R is original porosity, c_f is compressibility of rock, c_i^0 is compressibility of component i, $p_{c\alpha 1} = p_\alpha - p_1$ is capillary pressure, p_R is reference pressure, p_1 is pressure of water, p_s is pressure of rock, c_t is total compressibility, F_t is a known (source type) function that is determined using the values from the previous time step

The pressure equation is developed by substituting Darcy's law (Eq. (6)) for the phase flux term of equation above, using the definition of capillary pressure $p_{c\alpha 1} = p_\alpha - p_1, \alpha = 2,...,n_p$ The pressure equation in terms of the reference phase (phase 1) pressure is

$$\phi_R c_t\frac{\partial p_1}{\partial t} - \nabla\cdot k^{=}\lambda_{rTc}\nabla p_1 = \nabla\cdot k^{=}\sum_{\alpha=2}^{n_p}\lambda_{r\alpha c}\nabla p_{c\alpha 1} -$$

$$-\nabla \cdot \overline{k} \sum_{\alpha=1}^{n_p} \lambda_{r\alpha c} \gamma_\alpha \nabla Z - \phi_R [1 + c_f (p_1 - p_s)] F_t(\tilde{c}_i, \hat{c}_i) + \sum_{i=1}^{n_c} \frac{Q_i}{\rho_{iR}} \tag{8}$$

where

$\lambda_{r\alpha c} = \lambda_{r\alpha} \sum_{i=1}^{n_c} \bar{\rho}_i c_{i\alpha}$ is relative mobility

and

$\lambda_{rTc} = \sum_{\alpha=1}^{n_p} \lambda_{r\alpha c}$ is total relative mobility.

Statement of the problem. We examine ASP flooding within the reservoir of 623.2, 623.2 and 40 ft for x,y and z directions, respectively (number of grids - 19x19x3). Reservoir properties: fluid consists of 11 components (water, oil, surfactant, polymer, anion, calcium, Mg, CO3, Na, H+, acid), porosity - 30%, permeability - 1648 mD, depth - 4150 ft and initial water saturation - 0.3.

3 Results and Discussion

At the current initial stage of the development process our main goal is to evaluate whether our recently developed initial version of the mathematical formulation is appropriate for simulating the mechanism of ASP flooding. Since there is no analytical solution available for the chemical compositional problem under consideration, the verification test is based on the comparison with simulator, UTCHEM. Comparative studies show that the results obtained from IMPEC implementation of the newly proposed formulation are similar with that of UTCHEM simulator.

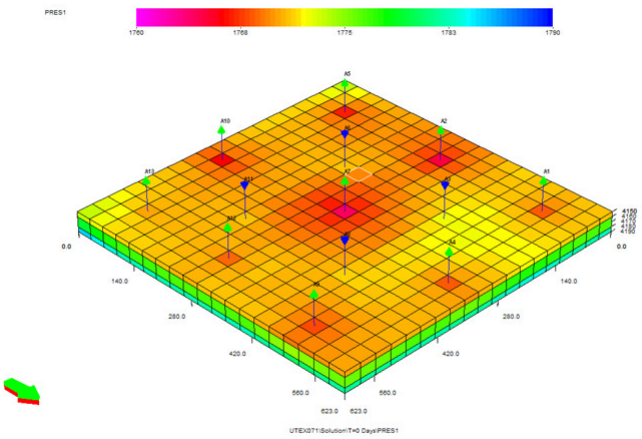

Fig. 1. The computational domain

The matches between old and new formulations' numerical results for the matched variables are shown in Figs. 2-7 for the injected pore volume in the range 0-1.0 PV.

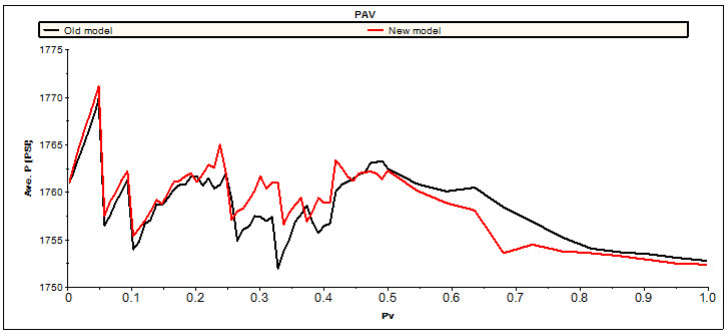

Fig. 2. Average pressure vs. pore volume

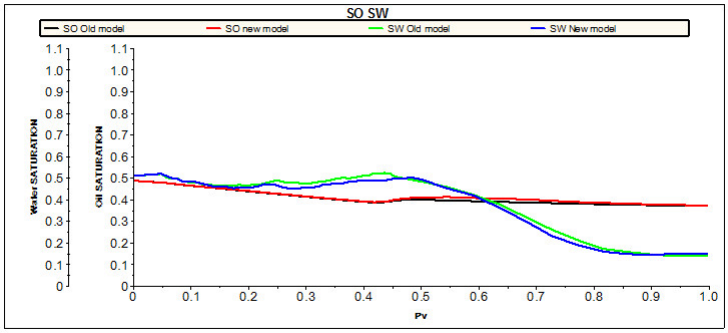

Fig. 3. Oil and water saturation vs. pore volume

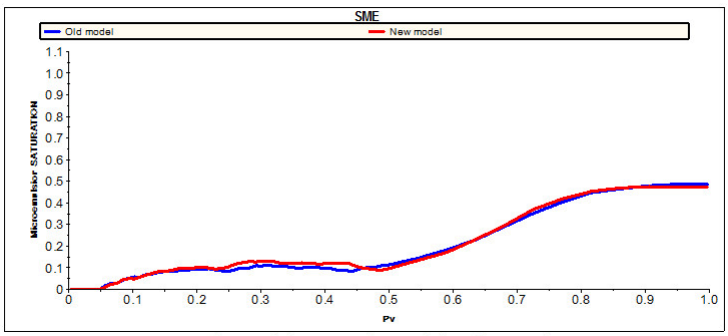

Fig. 4. Microemulsion saturation vs. injected pore volume

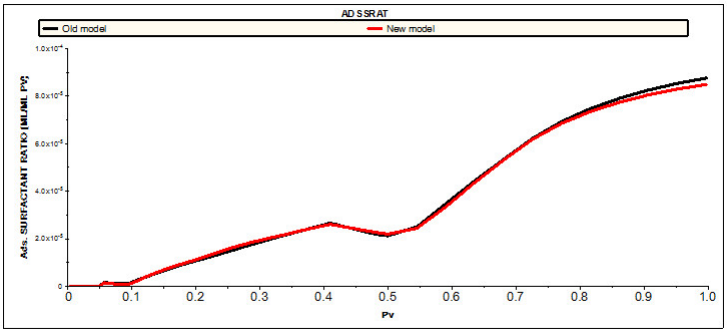

Fig. 5. Adsorbed surfactant ratio (ML per ML of pore volume) vs. injected pore volume

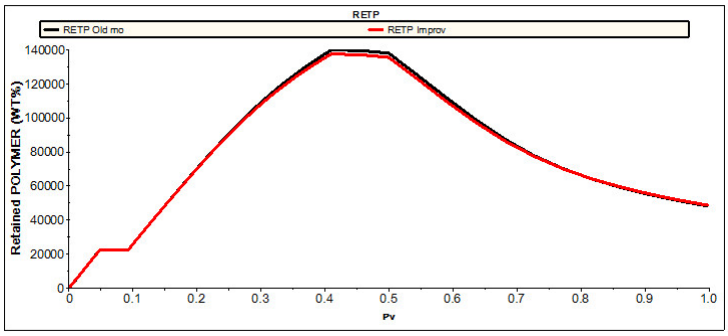

Fig. 6. Retained polymer vs. injected pore volume

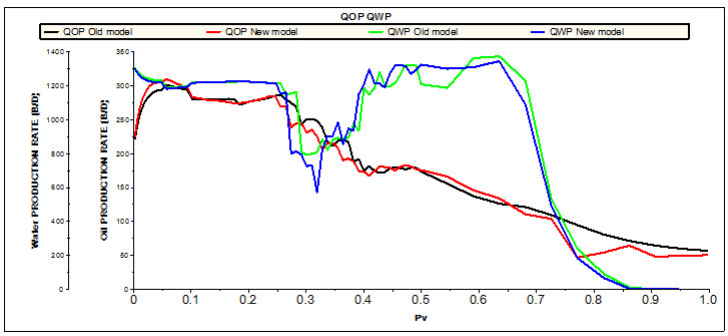

Fig. 7. Oil and water production rate

4 Conclusion

The mathematical formulation developed in the scope of this work is extended from the UTCHEM model formulation for use in chemical flooding studies. A comparison with UTCHEM has also been performed. Comparative studies show that the results obtained from IMPEC implementation of the newly proposed formulation are in a good agreement with that of UTCHEM simulator. In the scope of this research work, through its application to the above-mentioned numerical experiment and comparisons with UTCHEM model results, the newly developed formulation has proven to be applicable and accurate.

Acknowledgment. This paper was supported by the Ministry of Science and Education of the Republic of Kazakhstan through the Research Project No. 0128 GF4.

References

1. Baehr, A. L. and M. Y. Corapcioglu.: "Groundwater Contamination by Petroleum Products: 2. Numerical Solution,"Water Resour. Res., 23(10), 201 (1987)
2. Mayer, A. S. and C. T. Miller.: "A Compositional Model for Simulating Multiphase Flow, Transport and Mass Transfer in Groundwater Systems,"paper presented at the Eighth International Conference on Computational Methods in Water Resources, Venice, Italy, June 11-15 (1990)
3. Sleep, B. E. and J. F. Sykes. : "Compositional Simulation of Groundwater Contamination by Organic Compounds: 1. Model Development and Verification,"Water Resour. Res., 29(6), 1697-1708, June (1993)
4. Abriola, L. M. and G. F. Pinder.: "Two-Dimensional Numerical Simulation of Subsurface Contamination by Organic Compounds - A Multiphase Approach,"Proceedings of Specialty Conference on Computer Applications in Water Resources, ASCE (1985)
5. Abriola, L. M. and G. F. Pinder.: "A Multiphase Approach to the Modeling of Porous Media Contamination by Organic Compounds: 2. Numerical Simulation,"Water Resources Res., 21 (1), 19.Faust, J. C., J. H. Guswa and J. W. Mercer. 1989. "Simulation of Three-Dimensional Flow of Immiscible Fluids within and Below the Saturated Zone,"Water Resour. Res., 25(12), 2449 (1985)
6. Letniowski, F. W. and P. A. Forsyth.: "A Control Volume Finite Element Approach for Three-Dimensional NAPL Groundwater Contamination,"University of Waterloo, Ontario, Canada, Dept. of Computer Science, Report No. CS90-21, May (1990)
7. Sleep, B. E. and J. F. Sykes.: "Numerical Simulation of Three-Phase Multi-Dimensional Flow in Porous Media,"Computational Methods in Subsurface Hydrology, G. Gambolati et al. (eds.), Springer- Verlag, Berlin (1990)
8. Kalurachchi, J. J. and J. C. Parker.: "Modeling Multicomponent Organic Chemical Transport in Three-Phase Porous Media,"J. of Contaminant Transport, 5, 349 (1990)
9. Z. Chen, Y. Ma, and G. Chen.: A sequential numerical chemical compositional simulator. Transport in Porous Media 68, 389-411 (2007)
10. Delshad, M., Pope, G.A., Sepehrnoori, K.: UTCHEM Version-9.0, Technical Documentation, Center for Petroleum and Geosystems Engineering. The University of Texas at Austin, Texas, July (2000)

Numerical Simulation of the Combustion in Planar Shear Layer

Ye. Belyayev, A. Kaltayev, and A. Naimanova

Al-Farabi Kazakh National University, Al-Farabi Ave 71, Almaty, 050040, Kazakhstan
Institute of Mathematics and Mathematical Modelling MES RK, Pushkin str. 12, Almaty, 050010, Kazakhstan
yerzhan.belyayev@gmail.com

Abstract. Numerical study of two-dimensional supersonic hydrogen-air mixing and combustion in free shear layer is performed. The system of Naveir-Stokes equations for multispecies reacting flow is solved using ENO scheme of third-order in accuracy. In order to produce the roll-up and pairing of vortex rings, an unsteady boundary condition is applied at the inlet plane. At the outflow, the non-reflecting boundary condition is taken. The influence of different Mach numbers on the formation of vorticity structures and shear layer growth rate are studied. The obtained results are compared with available experimental data and the numerical results of other authors. For the description of reaction pathways of hydrogen, a seven species chemical reaction model by Jachimowski is adopted.

Keywords: Supersonic shear flow, mixing layer, ENO scheme, hydrogen combustion

1 Introduction

Free shear flows are of importance due to their occurrence in a broad number of engineering applications such as combustion, propulsion and environmental flows. A thorough understanding of the dynamics of free shear flows is required in order to understand their effects on the processes involved in these applications. Planar shear layers have been studied extensively, both experimentally and computationally, over the last two decades. The gas-dynamical structure of mixing between two parallel super-subsonic flows has been comprehensively studied by many investigators. Nowadays, there is a large number of works on experimental [1-2], analytical [3-4] and numerical [5-8] study of this problem in the view of above physical effects as separately as with including all of them. Experimental efforts to study the roll of large scale structures and growth mechanisms in compressible mixing layer have been done in sufficient details by researchers [1-2]. There is a great deal of researches devoted to the turbulence problem and influence of turbulence quantities on the mixing and vorticity formation [2,6]. Understanding the mechanisms of particle movement in free shear flows is very important for many technological applications. These include many propulsion and energy conversion systems such as gas turbines and rocket engines. There are also many physiological and environmental situations involving two-phase turbulent flows. In the present study, the third order essentially non-oscillatory (ENO) finite difference scheme is adopted to solve the system of Favre-averaged Navier-Stokes equations to supersonic planar shear layer. A Lagrangian approach is used to trace the particles which are moved in gas flow. The inflow physical parameters profile across the non-premixed hydrogen (fuel) and air stream at the splitter plate leading edge is assumed to vary smoothly according to a hyperbolic-tangent function (Fig. 1).

1.1 Mathematical model

The non-dimensional governing Navier-Stokes equations is:

$$\frac{\partial \boldsymbol{U}}{\partial t} + \frac{\partial \left(\boldsymbol{E} - \boldsymbol{E}_v\right)}{\partial x} + \frac{\partial \left(\boldsymbol{F} - \boldsymbol{F}_v\right)}{\partial y} = 0 \,. \tag{1}$$

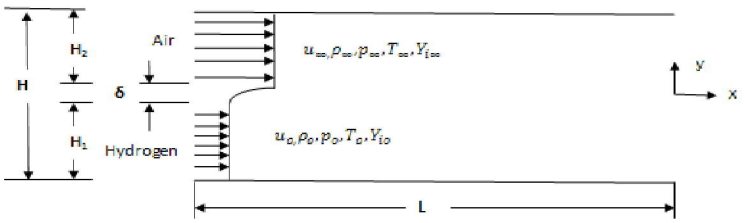

Fig. 1. An illustration of the flow configuration

where the vector of the dependent variables and the vector fluxes are given as

$$\boldsymbol{U} = (\rho, \rho u, \rho v, E_t, \rho Y_k)^T \ ,$$
$$\boldsymbol{E} = \left(\rho u, \rho u^2 + p, \rho uv, (E_t + p)\, u, \rho u Y_k\right)^T \ ,$$
$$\boldsymbol{F} = \left(\rho v, \rho uv, \rho v^2 + p, (E_t + p)\, v, \rho v Y_k\right)^T \ ,$$

$$\boldsymbol{E}_v = (0, \tau_{xx}, \tau_{xy}, u\tau_{xx} + v\tau_{xy} - q_x, J_{kx})^T$$
$$\boldsymbol{F}_v = (0, \tau_{xy}, \tau_{yy}, u\tau_{xy} + v\tau_{yy} - q_y, J_{ky})^T$$

Here, the viscous stresses, thermal conduction, and diffusion flux of species are:

$$\tau_{xx} = \frac{\mu}{Re}\left(2u_x - \frac{2}{3}(u_x + v_y)\right);$$
$$\tau_{yy} = \frac{\mu}{Re}\left(2v_y - \frac{2}{3}(u_x + v_y)\right);$$
$$\tau_{xy} = \tau_{yx} = \frac{\mu}{Re}(u_y + v_x);$$

$$q_x = \frac{\mu}{\Pr Re}\frac{\partial T}{\partial x} + \frac{1}{\gamma_\infty M_\infty^2}\sum_{k=1}^{N} h_k J_{xk};$$
$$q_y = \frac{\mu}{\Pr Re}\frac{\partial T}{\partial y} + \frac{1}{\gamma_\infty M_\infty^2}\sum_{k=1}^{N} h_k J_{yk};$$

$$J_{kx} = -\frac{\mu}{ScRe}\frac{\partial Y_k}{\partial x}, \quad J_{ky} = -\frac{\mu}{ScRe}\frac{\partial Y_k}{\partial y}.$$

Y_k - is the mass fraction of k^{th} species. The thermal equation for multi-species gas is:

$$p = \frac{\rho T}{\gamma_\infty M_\infty^2 W}, \quad W = \left(\sum_{k=1}^{N}\frac{Y_k}{W_k}\right)^{-1}, \quad \sum_{k=1}^{N} Y_k = 1 \tag{2}$$

where W_k is the molecular weight of the species. The equation for a total energy is given by

$$E_t = \frac{\rho h}{\gamma_\infty M_\infty^2} - p + \frac{1}{2}\rho\left(u^2 + w^2\right) \tag{3}$$

The enthalpy of the gas mixture is calculated according to $h = \sum_{k=1}^{N} Y_k h_k$, with specific enthalpy of k^{th} species evaluated suing $h_k = h_k^0 + \int_{T_0}^{T} c_{pk} dT$.

The specific heat at constant pressure for each component c_{pk} is:

$$c_{pk} = C_{pk}/W, \quad C_{pk} = \sum_{i=1}^{5} \bar{a}_{ki} T^{(i-1)}, \quad \bar{a}_{jk} = a_{jk} T_\infty^{j-1}$$

where the molar specific heat C_{pk} is given in terms of the fourth degree polynomial with respect to temperature, consistent with the JANAF Thermochemical Tables [7,10].

1.2 Initial and boundary conditions

At the entrance:

$$u_1 = M_0\sqrt{\frac{\gamma_0 R_0 T_0}{W_0}}, \quad w_1 = 0, \quad p_1 = p_0, \quad T_1 = T_0, \quad Y_{k1} = Y_{k0}, \quad k = k_0, \varepsilon = \varepsilon_0$$
$$at\ x = 0, 0 \le z < H_1,$$
$$u_2 = M_\infty\sqrt{\frac{\gamma_\infty R_0 T_\infty}{W_\infty}}, w_2 = 0, p_2 = p_\infty, T_2 = T_\infty, Y_{k2} = Y_{k\infty}, k = k_\infty, \varepsilon = \varepsilon_\infty$$
$$at\ x = 0, H_1 + \delta \le z \le H_2.$$

In the region of $H_1 \le z \le H_1 + \delta$ all physical variables are varied smoothly from hydrogen (fuel) flow to air flow using a hyperbolic-tangent function of any variable φ, so the inflow profiles are defined by

$$\phi(z) = 0.5\left(\phi_2 + \phi_1\right) + 0.5\left(\phi_2 - \phi_1\right)\tanh\left(0.5z/\theta\right) at x = 0, 0 \le z \le H.$$

where $\phi = (u, v, p, T, Y_k, k, \varepsilon)$, θ - is the momentum thickness. The pressure is assumed to be uniform across the shear layer. On the lower and upper boundary the condition of symmetry are imposed. At the outflow, the non-reflecting boundary condition is used.

1.3 Method of solution

The numerical scheme to solve the two-phase equations is based on a Eulerian-Lagrangian formulation. The numerical solution of RANS equations is performed in two steps. The first-step solves for the gas dynamic parameters (ρ, u, w, E_t) and second-step solves for the species $(Y_k, k = 1, 7)$ with mass source terms. The approximation of convection terms is performed by the ENO-scheme of third-order accuracy [8]. The ENO scheme is constructed on the basis of Godunov method, where piecewise polynomial function is defined by the Newton's formula of the third degree. In approximation of derivatives of diffusion terms, second-order central-difference operators are used. The system of the finite difference equations are solved by using matrix sweep method. Then it is necessary to define Jacobian matrix which in the case of the thermally perfect gas represents difficult task. This problem is connected by explicit representation of

pressure through the unknown parameters. Here pressure is determined by using the following formula

$$p = (\bar{\gamma} - 1)\left[E_t - \frac{1}{2}\rho\left(u^2 + w^2\right) - \rho\frac{h_0}{\gamma_\infty M_\infty^2}\right] + \frac{\rho T_0}{M_\infty^2 W}$$

where $\bar{\gamma} = h_{sm}/e_{sm}$ is an effective adiabatic parameter of the gas mixture, $h_{sm} = \sum_{i=1}^{N} Y_i \int_{T_0}^{T} c_{p_i} dT$, $e_{sm} = \sum_{i=1}^{N} Y_i \int_{T_0}^{T} c_{v_i} dT$, are the enthalpy and internal energy of the mixture minus the heat and energy of formation; $T_0 = 293K$ to the standard temperature of formation. The system of the original equations is solved by the use of the Euler method.

1.4 Results and discussion

The free shear layer of hydrogen-air turbulent flows mixing and combustion are numerically studied. The simulations are performed in a rectangular domain of $4cm$ in stream-wise direction and $1.5cm$ in transverse direction. The splitter plate thickness is $0.1cm$, and at the trailing edge is $0.0045cm$. At the inflow plane, hydrogen enters from the lower half and air enters from the upper half. A $401x151$ grid with stretching at the entrance and mixing layer was used. The hydrogen flow parameters are $M_0 = 1.4(M_0 = 1.1)$, $T_0 = 400K$, $P_0 = 101320Pa$ and air flow parameters are $M_\infty = 1.8(M_\infty = 1.4)$, $T_\infty = 1300K$, $P_\infty = 101320Pa$. For the description of reaction pathways of hydrogen, a seven species chemical reaction model by Jachimowski is taken [10].

The process of ignition represented in the Figure 2-3 are different for given cases. From isolines of water vapor concentration $H2O$ Figure 2-b, 3-b are visible the ignition delay time is $t = 1.25mks$ for result with smaller parameter, while for large Mach numbers are $t = 5.35mks$. The temperature in the ignition region for both cases Figure 2-a, 3-a is equal to $0.97(1261K)$. As a identifier of the given mixture ignition it was taken the main product - water vapor $H2O$ with the value approximately 0.2 percent of initial oxidant fracture.

References

1. Papamoschou, D., Roshko, A.: Journal Fluid Mechanics. 197, 453–477 (1988)
2. Elliot, G.S., Samimy, M.: Physics Fluids. 2 , p.1231–1240, (1990).
3. Cheng, T.S., Lee, K.S.: International Journal of Heat and Fluid Flow. 26, p.755–770,(2005).
4. Tang, W., Komerath, N.M., Sankar, L.N.: Journal Propulsion. 6, N 4, p. 455–460, (1990).
5. Reichert, R.S., Biringen, S.: Mechanics Research Communications. 34, p. 249–259, (2007).
6. Xiao-Tian Shi, Jun Chen, Wei-Tao Bi, Chi-Wang Shu, Zhen-Su She: Acta Mech. Sin. 27, p.318–329, (2011).
7. Kee, R. J., Rupley, F. M., Miller, J. A. CHEMKIN-II: a Fortran chemical kinetic package for the analysis of gas-phase chemical kinetics. SANDIA Report SAND89-8009 (1989).
8. Bruel, P., Naimanova, A. Zh.: Thermoph. and Aeromech. 17, No. 4, p.531–542, (2010).
9. Zhou H., Flamant G., Gauthier D., Lu J.: International journal of multiphase flow. 28, p.1801–1821, (2002).
10. Belyayev Ye., Kaltayev A., Naimanova A. Zh. Supersonic Flow with Perpendicular Injection of a Hydrogen. Proceedings of 2010 2nd International Conference on Computer Engineering and Technology, Vol. 5, Mechanical and Aerospace Engineering, V5-531-534, (2010).

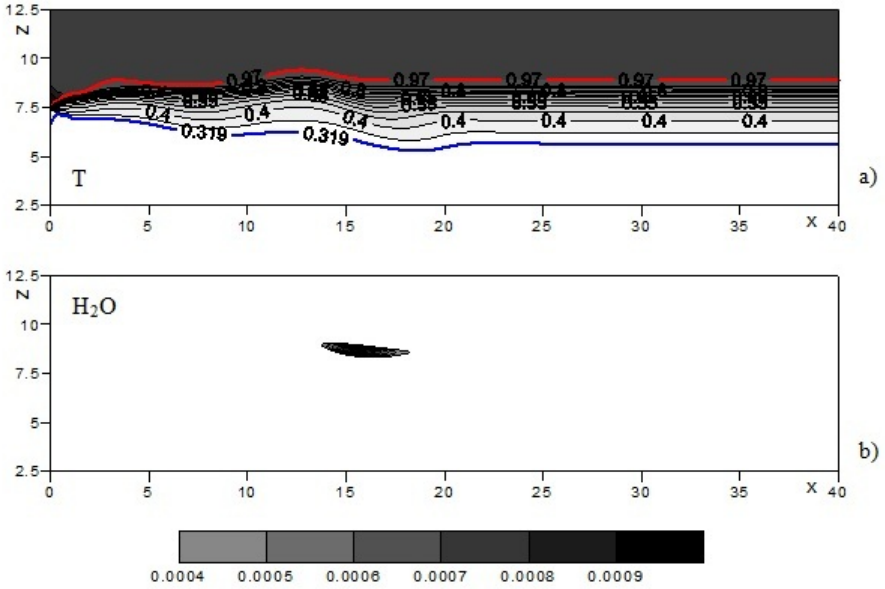

Fig. 2. The temperature field a) and formation of water vapor b) for $M_0 = 1.1$, $M_\infty = 1.4$

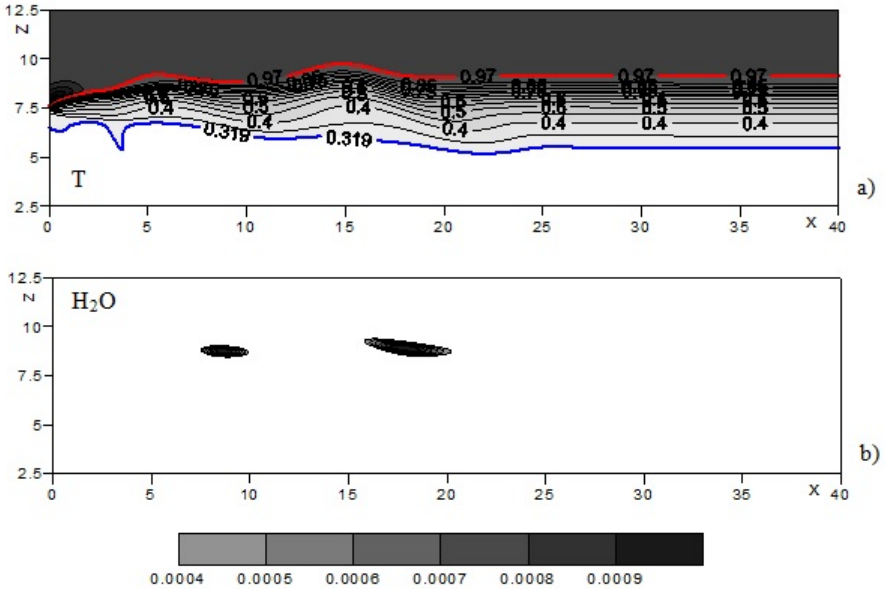

Fig. 3. The temperature field a) and formation of water vapor b) for $M_0 = 1.4$, $M_\infty = 1.8$

Numerical Simulation of the Mixing in Planar Shear Layer

Altyn Makasheva, Yerzhan Belyayev, and Asel Beketaeva

Institute of Mathematics and Mathematical Modelling MES RK, Pushkin str. 12, Almaty, 050010, Kazakhstan
Al-Farabi Kazakh National University, Al-Farabi Ave 71, Almaty, 050040, Kazakhstan
altyn-mak@mail.ru,turbulch@yahoo.com,azimaras@mail.ru

Abstract. Simulated the quasi-2D supersonic turbulent hydrogen-air mixing in the free shear layer. The system of the Favre-Averaged Navier-Stokes equations for the multispecies flow is solved using the ENO scheme third order accuracy. The main system equations is closed by k-? two-equation turbulence models. The dispersion of the particles is simulated following their trajectories in the shear layer with Euler method. In order to produce the roll-up and pairing vortex rings, an unsteady boundary condition is applied at the inlet plane. The influence of different Mach numbers on the formation of the vorticity structures and the shear layer growth rate are studied. The obtained results are compared with the experimental data and the numerical results of other authors. The numerical simulation of the particle dispersion in the shear layer with the large scale vortical structure is performed. The shear layer problem for the monatomic (air) gas has been tested by the following parameters: $M_0 = 0.51$, $T_0 = 285.07K$, $p_0 = 56088.91Pa$, $M_\infty = 1.8$, $T_\infty = 176.58K$, $p_\infty = 54648.65Pa$. The computational grid is 526x201. The channel height and length are 8 cm and 50 cm, respectively. The splitter plate thickness is 0.3175 cm, and edge of nozzle is 0.05 cm. The initial momentum thickness is 0.05 cm. It was obtained the shear layer growth in terms of momentum and vorticity thickness is agreed with experimental data.

Keywords: Supersonic shear flow, mixing layer, ENO scheme, turbulence model

1 Introduction

Free shear flows are of importance due to their occurrence in a broad number of engineering applications such as combustion, propulsion and environmental flows. A thorough understanding of the dynamics of free shear flows is required in order to understand their effects on the processes involved in these applications. Planar shear layers have been studied extensively, both experimentally and computationally, over the last two decades. The gas-dynamical structure of mixing between two parallel super-subsonic flows has been comprehensively studied by many investigators. Nowadays, there is a large number of works on experimental [1-2], analytical [3-4] and numerical [5-8] study of this problem in the view of above physical effects as separately as with including all of them. Experimental efforts to study the roll of large scale structures and growth mechanisms in compressible mixing layer have been done in sufficient details by researchers [1-2]. There is a great deal of researches devoted to the turbulence problem and influence of turbulence quantities on the mixing and vorticity formation [2,6]. Understanding the mechanisms of particle movement in free shear flows is very important for many technological applications. These include many propulsion and energy conversion systems such as gas turbines and rocket engines. There are also many physiological and environmental situations involving two-phase turbulent flows. In the present study, the third order essentially non-oscillatory (ENO) finite difference scheme is adopted to solve the system of Favre-averaged Navier-Stokes equations to supersonic planar shear layer. A Lagrangian approach is used to trace the particles which are moved in gas flow. The inflow physical parameters profile across the non-premixed hydrogen (fuel) and air stream at the splitter plate leading edge is assumed to vary smoothly according to a hyperbolic-tangent function (Fig. 1).

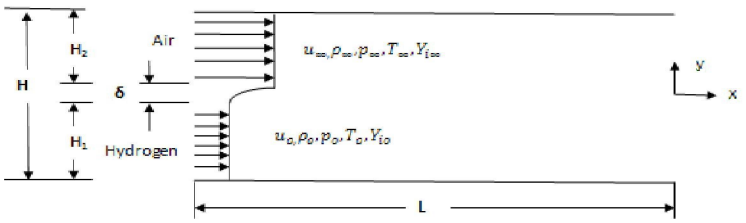

Fig. 1. An illustration of the flow configuration

1.1 Mathematical model

The non-dimensional governing Favre-averaged Navier-Stokes equations is:

$$\frac{\partial \boldsymbol{U}}{\partial t} + \frac{\partial \left(\boldsymbol{E} - \boldsymbol{E}_v\right)}{\partial x} + \frac{\partial \left(\boldsymbol{F} - \boldsymbol{F}_v\right)}{\partial y} + \frac{\partial \left(\boldsymbol{G} - \boldsymbol{G}_v\right)}{\partial z} = 0\,. \tag{1}$$

where the vector of the dependent variables and the vector fluxes are given as

$$\begin{aligned}
\boldsymbol{U} &= \left(\rho, \rho u, \rho v, \rho w, E_t, \rho Y_k\right)^T\,, \\
\boldsymbol{E} &= \left(\rho u, \rho u^2 + p, \rho uv, \rho uw, \left(E_t + p\right)u, \rho u Y_k\right)^T\,, \\
\boldsymbol{F} &= \left(\rho v, \rho uv, \rho v^2 + p, \rho vw, \left(E_t + p\right)v, \rho v Y_k\right)^T\,, \\
\boldsymbol{G} &= \left(\rho w, \rho uw, \rho vw, \rho w^2 + p, \left(E_t + p\right)w, \rho w Y_k\right)^T\,,
\end{aligned}$$

$$\boldsymbol{E}_v = \left(0, \tau_{xx}, \tau_{xz}, u\tau_{xx} + w\tau_{xz} - q_x, J_{kx}, \frac{1}{Re}\left(\mu_l + \frac{\mu_t}{\sigma_k}\right)\frac{\partial k}{\partial x}, \frac{1}{Re}\left(\mu_l + \frac{\mu_t}{\sigma_\varepsilon}\right)\frac{\partial \varepsilon}{\partial x}\right)^T$$

$$\boldsymbol{F}_v = \left(0, \tau_{xz}, \tau_{zz}, u\tau_{xz} + w\tau_{zz} - q_z, J_{kz}, \frac{1}{Re}\left(\mu_l + \frac{\mu_t}{\sigma_k}\right)\frac{\partial k}{\partial z}, \frac{1}{Re}\left(\mu_l + \frac{\mu_t}{\sigma_\varepsilon}\right)\frac{\partial \varepsilon}{\partial z}\right)^T$$

$$\boldsymbol{W} = \left(0, 0, 0, 0, 0, \left[P_k - \rho\varepsilon\left(1 + \alpha M_t^2\right) + D\right], \left[C_{\varepsilon 1}P_k\varepsilon/k - C_{\varepsilon 2}f_{\varepsilon 2}\rho\varepsilon^2/k\right]\right)^T$$

Here, the viscous stresses, thermal conduction, and diffusion flux of species are:

$$\begin{aligned}
\tau_{xx} &= \frac{1}{Re}\left(\mu_l + \frac{\mu_t}{\sigma_k}\right)\left(2u_x - \frac{2}{3}\left(u_x + w_z\right)\right); \\
\tau_{zz} &= \frac{1}{Re}\left(\mu_l + \frac{\mu_t}{\sigma_k}\right)\left(2w_z - \frac{2}{3}\left(u_x + w_z\right)\right); \\
\tau_{xz} &= \tau_{zx} = \frac{1}{Re}\left(\mu_l + \frac{\mu_t}{\sigma_k}\right)\left(u_z + w_x\right);
\end{aligned}$$

$$q_x = \frac{1}{\Pr Re}\left(\mu_l + \frac{\mu_t}{\sigma_k}\right)\frac{\partial T}{\partial x} + \frac{1}{\gamma_\infty M_\infty^2}\sum_{k=1}^{N} h_k J_{xk};$$

$$q_z = \frac{1}{\Pr Re}\left(\mu_l + \frac{\mu_t}{\sigma_k}\right)\frac{\partial T}{\partial z} + \frac{1}{\gamma_\infty M_\infty^2}\sum_{k=1}^{N} h_k J_{zk};$$

$$J_{kx} = -\frac{1}{ScRe}\left(\mu_l + \frac{\mu_t}{\sigma_k}\right)\frac{\partial Y_k}{\partial x}, \quad J_{kz} = -\frac{1}{ScRe}\left(\mu_l + \frac{\mu_t}{\sigma_k}\right)\frac{\partial Y_k}{\partial z}.$$

Parameters of the turbulence are:

$$P_k = \tau_{txx}\frac{\partial u}{\partial x} + \tau_{txz}\frac{\partial u}{\partial z} + \tau_{tzx}\frac{\partial w}{\partial x} + \tau_{tzz}\frac{\partial w}{\partial z};$$

$$\tau_{txx} = \frac{\mu_t}{Re}\left(2\frac{\partial u}{\partial x} - \frac{2}{3}\left(\frac{\partial u}{\partial x} + \frac{\partial w}{\partial z}\right)\right); \quad \tau_{txz} = \frac{\mu_t}{Re}\left(\frac{\partial u}{\partial z} + \frac{\partial w}{\partial x}\right);$$

$$\tau_{tzz} = \frac{\mu_t}{Re}\left(2\frac{\partial w}{\partial z} - \frac{2}{3}\left(\frac{\partial u}{\partial x} + \frac{\partial w}{\partial z}\right)\right);$$

$$M_t^2 = 2 \cdot M_\infty^2 \cdot k/T;$$

$$f_{\varepsilon 2} = 1 - 0.3 \cdot \exp\left(-Re_t^2\right); \quad Re_t = Re\left(\frac{\rho k^2}{\mu_l \varepsilon}\right);$$

$$C_{\varepsilon 1} = 1.44; C_{\varepsilon 2} = 1.92; \sigma_k = 1.0; \sigma_\varepsilon = 1.3,$$

where k, ε - turbulent kinetic energy, rate of dissipation of turbulent kinetic energy. P_k - is turbulence production term, μ_t - is the turbulence Mach number.

Y_k - is the mass fraction of k^{th} species. The thermal equation for multi-species gas is:

$$p = \frac{\rho T}{\gamma_\infty M_\infty^2 W}, \quad W = \left(\sum_{k=1}^{N}\frac{Y_k}{W_k}\right)^{-1}, \quad \sum_{k=1}^{N} Y_k = 1 \tag{2}$$

where W_k is the molecular weight of the species. The equation for a total energy is given by

$$E_t = \frac{\rho h}{\gamma_\infty M_\infty^2} - p + \frac{1}{2}\rho\left(u^2 + w^2\right) \tag{3}$$

The enthalpy of the gas mixture is calculated according to $h = \sum\limits_{k=1}^{N} Y_k h_k$, with specific enthalpy of k^{th} species evaluated suing $h_k = h_k^0 + \int\limits_{T_0}^{T} c_{pk} dT$.

The specific heat at constant pressure for each component c_{pk} is:

$$c_{pk} = C_{pk}/W, \quad C_{pk} = \sum_{i=1}^{5} \bar{a}_{ki} T^{(i-1)}, \quad \bar{a}_{jk} = a_{jk} T_\infty^{j-1}$$

where the molar specific heat C_{pk} is given in terms of the fourth degree polynomial with respect to temperature, consistent with the JANAF Thermochemical Tables [7,10].

The coefficient of viscosity is represented in the form of the sum of μ_l - molecular viscosity and μ_t - turbulent viscosity: $\mu = \mu_l + \mu_t$, where μ_t is defined according to $k - \varepsilon$ model with compressibility correction. The mixture averaged molecular viscosity is evaluated using from Wilke's formula.

In the present study the particles system is considered, with the following assumptions:

1) The particles are rigid spheres with diameter d_p and ρ_p density;

2) The effect of particles on the fluid is negligible.

In agree with assumption the non-dimensional Lagrangian particle equation are:

$$\frac{d\,\boldsymbol{u}_p}{d\,t} = D_p\left(\boldsymbol{u} + \boldsymbol{u}' - \boldsymbol{u}_p\right) \tag{4}$$

Where $\overrightarrow{u}_p$ and $\overrightarrow{u'}$ is the velocity vector for a particle and turbulent fluctuating component are respectively; and D_p is the drag function:

$$D_p = \frac{3}{8}\frac{\rho}{\rho_p}\frac{|\boldsymbol{u} + \boldsymbol{u}' - \boldsymbol{u}_p|}{r_p}\left(\boldsymbol{u} + \boldsymbol{u}' - \boldsymbol{u}_p\right)\cdot C_D \tag{5}$$

The drag coefficient C_D is given by

$$C_D = \begin{cases} \frac{24}{Re_p}\left(1 + \frac{1}{6}Re_p^{2/3}\right), & Re_p \le 1000 \\ 0,424, & Re_p > 1000 \end{cases} \tag{6}$$

where $Re_p = \frac{2\rho|\boldsymbol{u}+\boldsymbol{u}'-\boldsymbol{u}_p|}{\mu}$.

The particle position can be obtained by integrating the following equation:

$$\frac{d\overrightarrow{x}_p}{dt} = \overrightarrow{u}_p \tag{7}$$

1.2 Initial and boundary conditions

At the entrance:

$$u_1 = M_0\sqrt{\frac{\gamma_0 R_0 T_0}{W_0}}, \quad w_1 = 0, \quad p_1 = p_0, \quad T_1 = T_0, \quad Y_{k1} = Y_{k0}, \quad k = k_0, \varepsilon = \varepsilon_0$$
$$at\ x = 0, 0 \le z < H_1,$$
$$u_2 = M_\infty\sqrt{\frac{\gamma_\infty R_0 T_\infty}{W_\infty}}, w_2 = 0, p_2 = p_\infty, T_2 = T_\infty, Y_{k2} = Y_{k\infty}, k = k_\infty, \varepsilon = \varepsilon_\infty$$
$$at\ x = 0, H_1 + \delta \le z \le H_2.$$

In the region of $H_1 \le z \le H_1 + \delta$ all physical variables are varied smoothly from hydrogen (fuel) flow to air flow using a hyperbolic-tangent function of any variable φ, so the inflow profiles are defined by

$$\phi(z) = 0.5\left(\phi_2 + \phi_1\right) + 0.5\left(\phi_2 - \phi_1\right)\tanh\left(0.5z/\theta\right) at x = 0, 0 \le z \le H.$$

where $\phi = (u, v, p, T, Y_k, k, \varepsilon)$, θ - is the momentum thickness. The pressure is assumed to be uniform across the shear layer. On the lower and upper boundary the condition of symmetry are imposed. At the outflow, the non-reflecting boundary condition is used.

1.3 Method of solution

The numerical scheme to solve the two-phase equations is based on a Eulerian-Lagrangian formulation. The numerical solution of RANS equations is performed in two steps. The first-step solves for the gas dynamic parameters (ρ, u, w, E_t) and second-step solves for the species $(Y_k, k = 1, 7)$ with mass source terms. The approximation of convection terms is performed by the ENO-scheme of third-order accuracy [8]. The ENO scheme is constructed on the basis of Godunov method, where piecewise polynomial function is defined by the Newton's formula of the

third degree. In approximation of derivatives of diffusion terms, second-order central-difference operators are used. The system of the finite difference equations are solved by using matrix sweep method. Then it is necessary to define Jacobian matrix which in the case of the thermally perfect gas represents difficult task. This problem is connected by explicit representation of pressure through the unknown parameters. Here pressure is determined by using the following formula

$$p = (\bar{\gamma} - 1)\left[E_t - \frac{1}{2}\rho\left(u^2 + w^2\right) - \rho\frac{h_0}{\gamma_\infty M_\infty^2}\right] + \frac{\rho T_0}{M_\infty^2 W}$$

where $\bar{\gamma} = h_{sm}/e_{sm}$ is an effective adiabatic parameter of the gas mixture, $h_{sm} = \sum\limits_{i=1}^{N} Y_i \int\limits_{T_0}^{T} c_{p_i} dT$, $e_{sm} = \sum\limits_{i=1}^{N} Y_i \int\limits_{T_0}^{T} c_{v_i} dT$, are the enthalpy and internal energy of the mixture minus the heat and energy of formation; $T_0 = 293K$ to the standard temperature of formation. The system of the original equations is solved by the use of the Euler method.

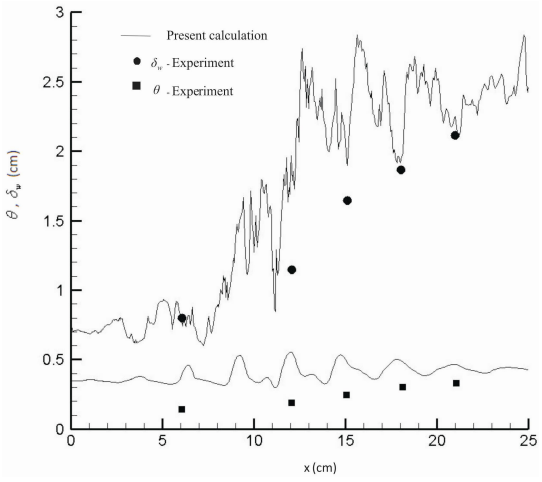

Fig. 2. Comparison of present calculation with experimental data by the growth of momentum and vorticity thickness

Starting at time $t = 0$, the gas-phase equations are integrated to simulate the dynamics of large scale vertical structures. At a specified time during this simulation, the particle injection is started. The trajectories of various are tracked by solving equations (4)-(7).

1.4 Results and discussion

Previously the shear layer problem for monatomic (air) gas has been tested by the following parameters: $M_0 = 0.51$, $T_0 = 285.07K$, $P_0 = 56088.91Pa$, $M_\infty = 1.8$, $T_\infty = 176.58K$, $P_\infty = 54648.65Pa$. The computational grid is 526x201. The channel height and length were 8 cm and 50 cm, respectively. The splitter plate thickness is 0.3175 cm, and at the trailing edge is 0.05 cm. The initial momentum thickness $\theta = \int\limits_{-\infty}^{+\infty}\left(\frac{\rho}{\rho_\infty}u^*\left(1-u^*\right)dz\right)$ is 0.05 cm. The geometrical parameters above are taken from experimental work of Samimy and Elliot [7]. Experiment was conducted in tunnel, present calculation performed for planar channel to estimate the behavior of turbulence quantities. Fig. 2 shows ($M_c = 0.51$) the comparison of the calculated distributions of

longitudinal (axial) mean velocity, variation of the momentum (θ) and vorticity (δ_w) thicknesses with the experimental data [7]. The non-dimensional variables $u^* = \frac{(u-u_0)}{(u_\infty - u_0)}$, $z^* = \frac{(z-z_c)}{\delta_w}$, $\theta = \int\limits_{-\infty}^{+\infty} \left(\frac{\rho}{\rho_\infty} u^* (1-u^*)\, dz \right)$, $\delta_w = \frac{(u_\infty - u_0)}{(\partial u/\partial z)_{\max}}$ are defined accordingly the experiments [3-4]. Fig. 2 indicates that the shear layer growth in terms of momentum and vorticity thickness is predicted reasonably accurate by the present algorithm, as compared to experimental data.

The comparison of calculated transverse distribution of the normalized streamwise mean velocity and Reynolds stress $-\overline{u'v'}/(u_\infty - u_o)^2$ at the longitudinal position x=12 cm with experimental measurements as shown in Figure 3 suggest that in the fully developed region for $x \geq 12$ cm the mean flow is self-similar.

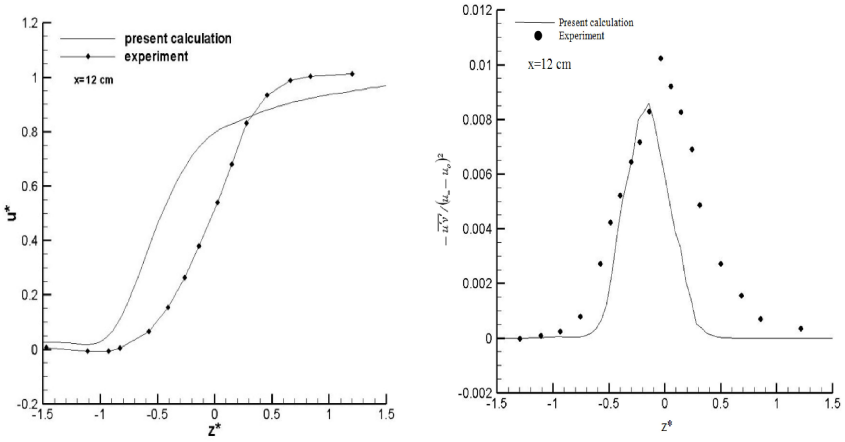

Fig. 3. Comparison of present calculation with experimental data by longitudinal mean velocity profile and Reynolds stress at the longitudinal position $x = 12$ cm in the shear layer

References

1. Papamoschou, D., Roshko, A.: Journal Fluid Mechanics. 197, 453–477 (1988)
2. Elliot, G.S., Samimy, M.: Physics Fluids. 2 , p.1231–1240, (1990).
3. Cheng, T.S., Lee, K.S.: International Journal of Heat and Fluid Flow. 26, p.755–770,(2005).
4. Tang, W., Komerath, N.M., Sankar, L.N.: Journal Propulsion. 6, N 4, p. 455–460, (1990).
5. Reichert, R.S., Biringen, S.: Mechanics Research Communications. 34, p. 249–259, (2007).
6. Xiao-Tian Shi, Jun Chen, Wei-Tao Bi, Chi-Wang Shu, Zhen-Su She: Acta Mech. Sin. 27, p.318–329, (2011).
7. Kee, R. J., Rupley, F. M., Miller, J. A. CHEMKIN-II: a Fortran chemical kinetic package for the analysis of gas-phase chemical kinetics. SANDIA Report SAND89-8009 (1989).
8. Bruel, P., Naimanova, A. Zh.: Thermoph. and Aeromech. 17, No. 4, p.531–542, (2010).
9. Zhou H., Flamant G., Gauthier D., Lu J.: International journal of multiphase flow. 28, p.1801–1821, (2002).
10. Belyayev Ye., Kaltayev A., Naimanova A. Zh. Supersonic Flow with Perpendicular Injection of a Hydrogen. Proceedings of 2010 2nd International Conference on Computer Engineering and Technology, Vol. 5, Mechanical and Aerospace Engineering, V5-531-534, (2010).

On the Account of Distributed Inertia of Rod Mechanism in Plane and Spatial Motion

I.R. Bismildin and Y.S. Temirbekov

Al-Farabi Kazakh National University, Almaty, Kazakhstan,
Almaty Technological University, Almaty, Kazakhstan
mech.math360@gmail.com,temirbekove@mail.ru

Abstract. To reduce inertia of moving links into resultant force and moment vectors and to represent center of mass as node in finite element models are widely-used in mechanical calculations of linkage mechanisms. Considering distributed inertia of motion makes possible to create more precise finite element models in spatial linkage structures. By algebraically summing all the distributed inertial loads acting in both directions, perpendicular and along the axis of a constant cross section link, we can show that their intensity varies linearly along the length of link. Using this approach together with Chasles' theorem for a point of free rigid body in projections onto the moving axes in the finite element method for rectilinear homogeneous rod, we reach to a more precise finite element model considering analytically distributed inertia of motion. Besides, we obtained sub vectors in known FEM (Finite Element Method) matrix relation which binds the generalized reaction forces acting at the contact points of the rod element with nodal generalized elastic movements. These sub vectors includes the weight and inertia of a distributed spatial movement of link.

Keywords: distributed inertia, finite-element method, model, force

1 Introduction

Since the 60s of XX century, and to the present time in applied problems of mechanics and physics has become very popular so-called finite element method (FEM).

Its development based on structural analysis, a technique for static analysis of constructions. At the beginning the field of FEM application was limited to calculation of the elastic strain fields of static systems. Later, it became applicable to such problems as the dynamics of elastic systems, heat transfer, fluid dynamics and electrodynamics. Rapid development of the method in the beginning was due to its clarity of discretization idea, which is nicely described at [1], [2]. Lets consider the application of FEM in problems of kinematics and dynamics of linkages. Inertia is the resistance of any physical object to any change in its state of motion, including changes to its speed and direction. Inertia of a solid body has distributed over its mass nature. In currently used FEM models in the dynamics of linkage systems inertia of the links is considered as reduced to the center of mass the force and moment, and the center of mass itself is considered as a node. Such simplified approach works fine in quasi-static regimes, where velocities of links motions are low enough to consider them as set of step by step movements. But in dynamic regimes the influence of inertial forces to the links motion is more significant. And author's of this study consider presenting the inertia in a more complex form. Thereby, our intention to solve this problem encouraged us to invent a new finite element models which are analytically includes the distributed inertia of links in motion.

2 Plane approach

Let's consider a plane-parallel motion the k-th link of mechanism with respect to a fixed coordinate system OXY illustrated in Fig.1. Let us also to introduce a system of coordinates

$OX'Y'$, the position of which relative to the fixed coordinates system OXY, determined by the angle of inclination θ_k of the rod.

At the point P_k of the hinge joint which connect the k-th link with the (k-1)-th link, we introduce two local coordinate systems: the moving with the associated joint and the axes remaining parallel to the axes of the coordinate system OXY, and the $PX'_kY'_k$ rigidly connected to the link. Let the k-th link of mechanism with a constant cross-section, moves plane-parallel

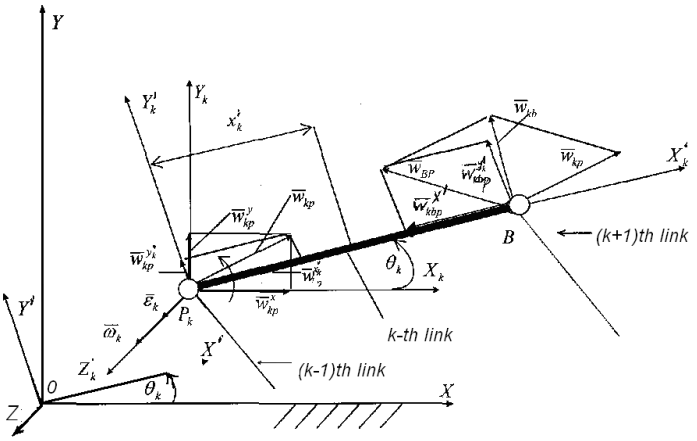

Fig. 1. Plane-parallel motion the k-th link of mechanism

way relative to the fixed OXY coordinate system .

At the specific position θ_k of the mechanism, acceleration components of the point P_k in coordinate system OXY are $\overline{w}^x_{kp}$ and $\overline{w}^y_{kp}$, $\overline{\omega}_k$, $\overline{\varepsilon}_k$ are angular velocity and acceleration respectively.

Lets find the components of $\overline{w}_{kp}$ acceleration vector to respect the $OX'Y'$ coordinate system:

$$\begin{Bmatrix} w^{x'}_{kp} \\ w^{y'}_{kp} \end{Bmatrix} = \begin{bmatrix} \cos\theta_k & \sin\theta_k \\ -\sin\theta_k & \cos\theta_k \end{bmatrix} \begin{Bmatrix} w^{x}_{kp} \\ w^{y}_{kp} \end{Bmatrix}$$

It's known that plane-parallel motion of solid body consist of translational motion and rotational motion about pole. The full acceleration of point B of the k-th link consist of acceleration of the pole P_k , and of acceleration of the point B in it rotational movement with the link about this pole.

If the motion is accelerated, then $\overline{w}^{y'_k}_{kbp}$ vector oriented perpendicularly to axis of the link in direction of rotation. The $\overline{w}^{x'_k}_{kbp}$ vector is always directed from the point B to the pole P_k.

Their values are respectively $\overline{w}^{y'_k}_{kbp} = l_k\varepsilon_k$ and $\overline{w}^{x'_k}_{kbp} = l_k\omega_k^2$.

Components of acceleration vector of the point B in coordinates system $OX'Y'$ in matrix form is:

$$\begin{Bmatrix} w^{x'}_{b} \\ w^{y'}_{b} \end{Bmatrix} = \begin{Bmatrix} w^{x'}_{kp} \\ w^{y'}_{kp} \end{Bmatrix} + \begin{Bmatrix} w^{x'}_{kbp} \\ w^{y'}_{kbp} \end{Bmatrix}$$

$$\begin{Bmatrix} w^{x'}_{b} \\ w^{y'}_{b} \end{Bmatrix} = \begin{bmatrix} \cos\theta_k & \sin\theta_k \\ -\sin\theta_k & \cos\theta_k \end{bmatrix} \begin{Bmatrix} w^{x}_{kp} \\ w^{y}_{kp} \end{Bmatrix} + \begin{Bmatrix} -l_k w_k^2 \\ l_k w_k \end{Bmatrix}$$

If area of link's cross-section is constant, then we able to consider the dead load as uniformly distributed load with intensity:

$$q_{cb}^{k} = \gamma_k A_k$$

γ_k – specific weight of link k, A_k – the cross-section of the link k

For the further calculations, lets expand this load into two directions: co-directionally and perpendicularly to axis of the link illustrated in Fig.1 and Fig.2

$$\begin{Bmatrix} q_{cb}^{x'} \\ q_{cb}^{y'} \end{Bmatrix} = \begin{bmatrix} \cos\theta_k & \sin\theta_k \\ -\sin\theta_k & |\cos\theta_k| \end{bmatrix} \begin{Bmatrix} 0 \\ -q_{cb}^{k} \end{Bmatrix}$$

The numerical values of the intensity of these loads diagrams correspond to the ordinates of these loads, and the directions are shown as the arrows.

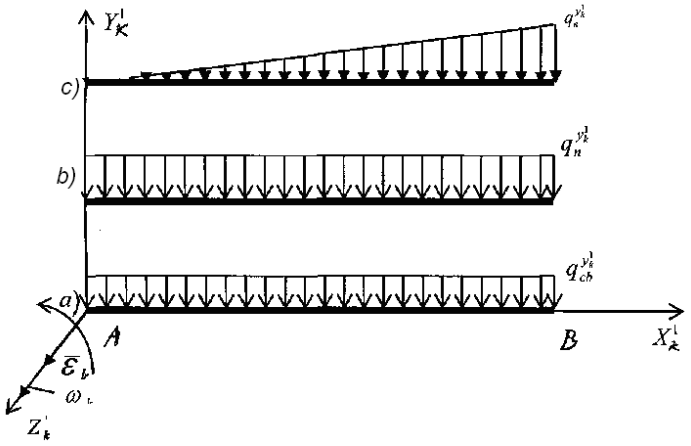

Fig. 2. Co-directionally expanded loads

Acceleration of translational motion of the link generates inertial forces of acceleration equal to:

$$q_n^{x'_k} = -\frac{\gamma_k A_k}{g} \overline{w}_{kp}^{x'_k},$$
$$q_n^{y'_k} = -\frac{\gamma_k A_k}{g} \overline{w}_{kp}^{y'_k}$$

where g - is acceleration of gravity.

Because of the rotational movement of link k with angular velocity $\overline{w}_k$ around the pole P_k, there is produces triangle shape distributed loads with the intensity active along the axis of the link:

$$q_b^{x'_k} = \frac{\gamma_k A_k}{g} \omega_k^2 x'_k$$

Same way:

$$q_b^{y'_k} = -\frac{\gamma_k A_k}{g} \varepsilon_k^{x'_k}$$

These loads are always active in perpendicular way to the axis of the link and opposite directed to $\varepsilon_k \times l_k$

Algebraically summing up all the loads acting in the direction of the axis will see that in the intensification of the total load varies in length unit linearly and is defined by the following expression:

$$q_y\left(x'_k\right) = a_{kq} + b_{kq} x'_k$$

where $a_{kq} = -\gamma_k A_k \cos\theta_k - \frac{\gamma_k A_k}{g} w_{kp}^{y'_k}$, $b_{kq} = -\frac{\gamma_k A_k}{g}\varepsilon_k$

Similarly, summing all the forces active along the axis of the link (in the direction of the axis X'_k) we see that their intensity is also changing along the length of link linearly, and is expressed by the equation:

$$q_x\left(x'_k\right) = a_{kn} + b_{kn}x'_k$$

where $a_{kn} = -\gamma_k A_k \sin\theta_k - \frac{\gamma_k A_k}{g} w_{kp}^{x'_k}$, $b_{kn} = -\frac{\gamma_k A_k}{g}\omega_k^2$.

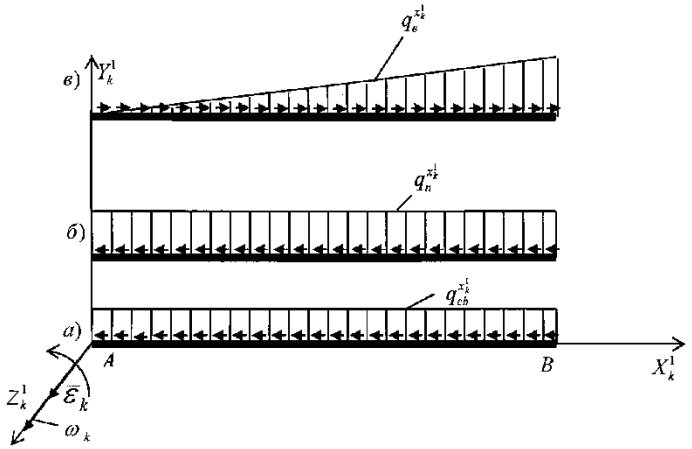

Fig. 3. Perpendicularly to axis expanded loads

Thereby, the intensity of the forces of inertia and gravity of the rod have a well-defined analytical expression. Using this and finite element method (FEM) for the straight rod, we have a more accurate finite element model, which analytically includes distributed inertia of plane motion. Equations of equilibrium of the rod element are:

$$\frac{dN}{dx} + q_x = \frac{dN}{dx} + a_n + b_n x = 0, \quad \frac{dQ_y}{dx} + q_y = \frac{dQ_y}{dx} + a_q + b_q x = 0$$

Equations of compatibility of strains and displacement are:

$$\varepsilon_x = \frac{du}{dx}, \quad \chi = \frac{d\phi}{dx}, \quad \kappa_y = -\frac{d^2 w_z}{dx^2}, \quad \kappa_z = -\frac{d^2 w_y}{dx^2}.$$

Relations between deformations and internal strains are:

$$N = EF\varepsilon_x, \quad M = GJ_\chi, \quad M_y = EJ_y\kappa_y.$$

If the link length is l, and displacements u_o, w_{yo}, w_{zo}, u_l, w_{yl}, w_{zl} and rotations $\phi_o, \phi_{yo}, \phi_{zo}, \phi_l, \phi_{yl}, \phi_{zl}$ are given at the end section of the rod, then solving for the elastic

displacement we have:

$$Q_{yo} = -\frac{EJ_z}{l^3}(2w_{yo} + l\phi_{zo} - 2w_{yl} + l\phi_{zl}) + \frac{a_q l}{2} + \frac{3b_q l^2}{20}$$
$$Q_{yl} = -\frac{1}{l^3}EJ_z(2w_{yo} + l\phi_{zo} - 2w_{yl} + l\phi_{zl}) - \frac{a_q l}{2} - \frac{7b_q l^2}{20}$$
$$M_{zo} = -\frac{1}{l^2}EJ_z(6w_{yo} + 4l\phi_{zo} - 6w_{yl} + 2l\phi_{zl}) - \frac{a_q l}{12} - \frac{b_q l^3}{30}$$
$$M_{zl} = -\frac{1}{l^2}EJ_z(6w_{yo} + 2l\phi_{zo} - 6w_{yl} + 4l\phi_{zl}) - \frac{a_q l}{12} - \frac{b_q l^3}{20}$$
$$Q_{zo} = -\frac{1}{l^3}EJ_z(2w_{yo} + l\phi_{zo} - 2w_{yl} + l\phi_{zl})$$
$$Q_{zl} = -\frac{1}{l^3}EJ_z(2w_{yo} + l\phi_{zo} - 2w_{yl} + l\phi_{zl})$$
$$M_{yo} = -\frac{1}{l^2}EJ_z(-6w_{yo} + 4l\phi_{zo} + 6w_{yl} + 2l\phi_{zl})$$
$$M_{yl} = -\frac{1}{l^2}EJ_z(-6w_{yo} + 4l\phi_{zo} + 6w_{yl} + 2l\phi_{zl})$$
$$N_0 = EF\left[\frac{u_l - u_o}{l} + \frac{a_n l}{2EF} + \frac{b_n l}{EF}\right]$$
$$N_l = EF\left[\frac{u_l - u_o}{l} - \frac{a_n l}{2EF} - \frac{b_n l}{EF}\right]$$
$$M_o = \frac{GJ_z}{l}(\phi_l - \phi_o)$$
$$M_l = \frac{GJ_z}{l}(\phi_l - \phi_o)$$

Having considered external and internal geometric and force factors now we have the basic equations of equilibrium of FEM for the straight rod:

$$\begin{Bmatrix} \overrightarrow{R}_\xi^{ij} \\ \overrightarrow{R}_\xi^{ji} \end{Bmatrix} = \begin{bmatrix} B_{11}^{ij} & B_{12}^{ij} \\ B_{21}^{ij} & B_{22}^{ij} \end{bmatrix} \begin{Bmatrix} \overrightarrow{U}_\xi^{ij} \\ \overrightarrow{U}_\xi^{ji} \end{Bmatrix} + \begin{Bmatrix} \overrightarrow{Q}^{ij} \\ \overrightarrow{Q}^{ji} \end{Bmatrix}$$

This equation establishes relation between the generalized reactive forces

$$\overrightarrow{R}_\xi^{ij} = [\overrightarrow{R}_{1N\xi}^{ij}, \overrightarrow{R}_{2N\xi}^{ij}, \overrightarrow{R}_{3N\xi}^{ij}, \overrightarrow{R}_{1M\xi}^{ij}, \overrightarrow{R}_{2M\xi}^{ij}, \overrightarrow{R}_{3M\xi}^{ij}]^T$$

which acting in the nodes of rod with the nodal displacements

$$\overrightarrow{U}_\xi^{ij} = [u_1^{ij}, u_2^{ij}, u_3^{ij}, \phi_1^{ij}, \phi_2^{ij}, \phi_3^{ij}]^T$$

and

$$\overrightarrow{U}_\xi^{ji} = [u_1^{ji}, u_2^{ji}, u_3^{ji}, \phi_1^{ji}, \phi_2^{ji}, \phi_3^{ji}]^T$$

The square sub-matrix $[B_{kl}^{ij}]$, $(k = 1..2, l = 1..2)$ of stiffness matrix $[B^{ij}]$ of the rod element is constant, and now we have the sub-vectors $\overrightarrow{Q}^{ij}$ and $\overrightarrow{Q}^{ji}$ analytically containing not only the

weight but also the distributed inertia of plane-parallel movement of the rod.

$$\overrightarrow{Q}^{ij} = \begin{Bmatrix} -\frac{a_n l}{2} - \frac{b_n l^2}{2} \\ -\frac{a_q l}{2} - \frac{3b_q l^2}{20} \\ 0 \\ 0 \\ 0 \\ -\frac{a_q l^2}{12} - \frac{b_q l^3}{30} \end{Bmatrix} \tag{1}$$

$$\overrightarrow{Q}^{ji} = \begin{Bmatrix} -\frac{a_n l}{2} - \frac{b_n l^2}{2} \\ -\frac{a_q l}{2} - \frac{7b_q l^2}{20} \\ 0 \\ 0 \\ 0 \\ \frac{a_q l^2}{12} + \frac{b_q l^3}{30} \end{Bmatrix} \tag{2}$$

3 Spatial approach

Now consider the spatial movement of the k-th rod relative to the fixed coordinate system $OXYZ$.

Theorem 1. *A free body displacement can be produced by a translation along a line (called its screw axis) followed by a rotation about that line.*

Then the acceleration of any point M of free rigid body in projections onto the moving axes $P_k X'_k Y'_k Z'_k$ has the form:

$$\begin{cases} w_{x_k} = w_{Pxk} + \frac{\omega_{y_k}}{dt} z_k - \frac{\omega_{z_k}}{dt} y_k + \omega_{x_k}(\omega_{x_k} x_k + \omega_{y_k} y_k + \\ +\omega_{z_k} z_k) - \omega_k^2 x_k, \\ w_{y_k} = w_{Pyk} + \frac{\omega_{z_k}}{dt} x_k - \frac{\omega_{x_k}}{dt} z_k + \omega_{y_k}(\omega_{x_k} x_k + \omega_{y_k} y_k + \\ +\omega_{z_k} z_k) - \omega_k^2 y_k, \\ w_{z_k} = w_{Pzk} + \frac{\omega_{x_k}}{dt} x_k - \frac{\omega_{y_k}}{dt} z_k + \omega_{z_k}(\omega_{x_k} x_k + \omega_{y_k} y_k + \\ +\omega_{z_k} z_k) - \omega_k^2 z_k \end{cases}$$

Where $w_{P_{xk}}$,$w_{P_{yk}}$, $w_{P_{zk}}$ are projections of acceleration $\overline{w}_{P_k}$ of pole P_k in $P_k X'_k Y'_k Z'_k$. In this case centers of gravity of cross-sections of the link are set axially $P_k X'_k$, therefore, coordinates of point are $x_k = x'_k$,$y_k = z_k = 0$. Then

$$\begin{cases} w_{x_k} = w_{Pxk} + \omega_{x_k}^2 - \omega_k^2 x_k \\ w_{y_k} = w_{Pyk} + \frac{d\omega_{z_k}}{dt} x_k + \omega_{y_k}\omega_{x_k} x_k \\ w_{z_k} = w_{Pzk} - \frac{d\omega_{y_k}}{dt} x_k + \omega_{x_k}\omega_{z_k} x_k \end{cases}$$

Because of the acceleration w_{x_k} distributed inertial forces appears along $P_k X_k$, intensity of the total load changes long the link linearly:

$$q_k x_k = a_{kn} + b_{kn} x_k$$

$a_{kn} = -\gamma_k A_k \sin\theta_k - \frac{\gamma_k A_k}{g} w_{P_{xk}}$
$b_{kn} = -\frac{\gamma_k A_k}{g}\omega_{x_k}^2 + \frac{\gamma_k A_k}{g}\omega_k^2$

Algebraically summing up all the loads acting on the link in the plane $P_k X_k Y_k$, we find that the intensity of the total load varies along the length of the straight-line link linearly determined by the following expression:

$q_k^y x_k = a_{kq}^y + b_{kq}^y x_k$
$a_{kq}^y = -\gamma_k A_k \cos\theta_k - \frac{\gamma_k A_k}{g} w_{P_{yk}}$
$b_{kq}^y = -\frac{\gamma_k A_k}{g}\frac{d\omega_{z_k}}{dt} x_k - \frac{\gamma_k A_k}{g}\omega_{y_k}\omega_{x_k} x_k$

here θ_k - is the angle of inclination of link k in OXY plane.

Same way:

$q_k^z x_k = a_{kq}^z + b_{kq}^z x_k$
$a_{kq}^z = -\gamma_k A_k \cos\theta_k - \frac{\gamma_k A_k}{g} w_{P_{zk}}$
$b_{kq}^z = -\frac{\gamma_k A_k}{g}\frac{d\omega_{y_k}}{dt} x_k - \frac{\gamma_k A_k}{g}\omega_{z_k}\omega_{x_k} x_k$

Equilibrium equations of element of the rod for spatial case:

$$\frac{dN}{dx} + q_x = \frac{dN}{dx} + a_n + b_n x = 0$$
$$\frac{dQ_y}{dx} + q_y = \frac{dQ_y}{dx} + a_q + b_q x = 0$$
$$\frac{dQ_z}{dx} + q_z = 0$$
$$\frac{dM}{dx} + m = 0$$
$$\frac{dM_y}{dx} - Q_z = 0$$
$$\frac{dM_z}{dx} - Q_y = 0$$

If the link length is l, and displacements $u_o, w_{yo}, w_{zo}, u_l, w_{yl}, w_{zl}$ and rotations $\phi_o, \phi_{yo}, \phi_{zo}, \phi_l, \phi_{yl}, \phi_{zl}$ are given at the end section of the rod, then solving for the elastic displacement for spatial case we have:

$$Q_{yo} = -\frac{6EJ_z}{l^3}(2w_{yo} + l\phi_{zo} - 2w_{yl} + l\phi_{zl}) + \frac{a_q^y l}{2} - \frac{3b_q^y l^2}{20}$$
$$Q_{yl} = -\frac{6EJ_z}{l^3}(2w_{yo} + l\phi_{zo} - 2w_{yl} + l\phi_{zl}) - \frac{a_q^y l}{2} - \frac{7b_q^y l^2}{20}$$
$$M_{zo} = -\frac{EJ_z}{l^3}(6w_{yo} + 4l\phi_{zo} - 6w_{yl} + 2l\phi_{zl}) - \frac{a_q^y l^2}{12} - \frac{b_q^y l^3}{30}$$

$$M_{zl} = -\frac{EJ_z}{l^3}(6w_{yo} + 2l\phi_{zo} - 6w_{yl} + 4l\phi_{zl}) - \frac{a_q^y l^2}{12} - \frac{b_q^y l^3}{20}$$
$$Q_{zo} = -\frac{6EJ_z}{l^3}(2w_{yo} + l\phi_{zo} - 2w_{yl} + l\phi_{zl}) + \frac{a_q^z l}{2} + \frac{3b_q^z l^2}{20}$$
$$Q_{zl} = -\frac{6EJ_z}{l^3}(2w_{yo} + l\phi_{zo} - 2w_{yl} + l\phi_{zl}) - \frac{a_q^z l}{2} - \frac{7b_q^z l^2}{20}$$
$$M_{yo} = -\frac{EJ_z}{l^3}(-6w_{yo} + 4l\phi_{zo} + 6w_{yl} + 2l\phi_{zl}) - \frac{a_q^z l^2}{12} - \frac{7b_q^z l^3}{30}$$
$$M_{yl} = -\frac{EJ_z}{l^3}(-6w_{yo} + 4l\phi_{zo} + 6w_{yl} + 2l\phi_{zl}) - \frac{a_q^z l^2}{12} - \frac{7b_q^z l^3}{20}$$
$$N_0 = EF\left[\frac{u_l - u_o}{l} + \frac{a_n l}{2EF} + \frac{b_n l}{EF}\right]$$
$$N_l = EF\left[\frac{u_l - u_o}{l} - \frac{a_n l}{2EF} - \frac{b_n l}{EF}\right]$$
$$M_o = \frac{GJ_z}{l}(\phi_l - \phi_o) + \frac{ml}{2}$$
$$M_l = \frac{GJ_z}{l}(\phi_l - \phi_o) - \frac{ml}{2}$$

The sub-vectors Q^{ij} Pë Q^{ji} now analytically containing not only the weight but also the distributed inertia of spatial movement of the rod are:

$$\overrightarrow{Q}^{ij} = \begin{Bmatrix} -\frac{a_{kn}l}{2} - \frac{b_{kn}l^2}{2} \\ -\frac{a_{kq}^y l}{2} - \frac{3b_{kq}^y l^2}{20} \\ -\frac{a_{kq}^z l}{2} - \frac{3b_{kq}^z l^2}{20} \\ \frac{ml}{2} \\ \frac{a_{kq}^z l^2}{12} + \frac{3b_{kq}^z l^3}{30} \\ -\frac{a_{kq}^y l^2}{12} - \frac{3b_{kq}^y l^3}{30} \end{Bmatrix} \quad (3)$$

$$\overrightarrow{Q}^{ji} = \begin{Bmatrix} -\frac{a_{kn}l}{2} - \frac{b_{kn}l^2}{2} \\ -\frac{a_{kq}^y l}{2} - \frac{7b_{kq}^y l^2}{20} \\ -\frac{a_{kq}^z l}{2} - \frac{7b_{kq}^z l^2}{20} \\ -\frac{ml}{2} \\ -\frac{a_{kq}^z l^2}{12} - \frac{3b_{kq}^z l^3}{30} \\ \frac{a_{kq}^y l^2}{12} + \frac{3b_{kq}^y l^3}{30} \end{Bmatrix} \quad (4)$$

4 Implementation

Developed model of the finite elements has been tested in Class IV Mechanism elastic oscillations problem.

Class IV spatial mechanism with external prismatic pair are simulated with the help of spatial finite bar elements assembly. They are rigidly connected with each other and revolute and prismatic kinematic pairs in the way providing possibility to take into account any changes in mechanism geometry. Each link is considered as one or several series-connected finite bar elements with equal longitudinal cross-section. The input shaft is considered to be connected

with the inertia-type flywheel and this provides absence of unwanted fluctuations of the input angular velocity. In this case the input crank is regarded as a uniformly rotating overhanging beam. This assumption is made only for simplification of computations.

The kinematics of the considered Class IV lever rigid link mechanism (Figure 4) in contrast to the kinematics of the similar II class mechanisms does not have any analytical solutions. Consequently it cannot be directly considered in deriving a differential equation system of the mechanism finite element model elastic oscillations: i.e. by considering geometric constraints in kinetic and potential energy expressions and generalized force vector. Therefore positions, displacements, velocities and accelerations analysis problems for rigid link mechanisms shall be solved at each time step. Mechanism kinematics analysis depends upon its input motion characteristics and its geometry. Let us assume that values of the input link angular velocity and acceleration are equal, for example, $\omega_1 = 100s^{-1}$ and $\varepsilon_1 = 0s^{-2}$.

The coordinates of the mechanism stationary base member for crank mounting: $X_0 = 0.0$, $Y_0 = 0.0$, $Z_0 = 0.0$.

Links length: $L_{1-3} = 0.17m$, $L_{5-8} = 0.17m$, $L_{5-9} = 0.20m$, $L_{8-9} = 0.258m$, $L_{13-17} = 0.39m$, $L_{14-18} = 0.50m$, $L_{21-23} = 0.10m$, $L_{22-23} = 0.10m$, $L_{23-24} = 0.05m$, $L_{24-25} = 0.05m$.

Links move in the planes parallel to global plane OXZ. Lengths of links connecting axes are: $L_{3-5} = 0.02m$, $L_{8-13} = 0.02m$, $L_{9-14} = 0.02m$, $L_{17-21} = 0.02m$, $L_{18-22} = 0.02m$. The revolute kinematic pair axes are oriented in parallel to OY axis. Letters L_{i-j} are used to denote a link, axis or the part of thereof and its corresponding length with from the node "i"till the node "j". The analysis of positions revealed that when the initial pitch angle of the crank is equal to zero then the considered mechanism is available in four assemblies. For further analysis the 2-nd assembly of the mechanism will be used. The finite element model nodes displacements, velocities and accelerations are analyzed to determine the estimated positions of the considered mechanism assembly. In the general case, the inertial forces of finite bar elements of the link in plane-parallel motion with the plane of symmetry parallel to motion plane may be reduced to the inertial force P_u applied to the link centre of mass M_u: $P_u = -m \cdot W_s$, $Mu = -J_s\varepsilon$, where m $[kg]$ is the link mass, W_s $[m/sec^{-2}]$ is the link centre of mass vector, J_s $[kg \cdot m^2]$ is the link moment of inertia about the axis crossing the centre of mass and perpendicular to the link motion plane, ε $[c^{-2}]$ is the link angular acceleration. Taking into consideration the above said, each link shall be considered as one or several series-connected finite bar elements with equal longitudinal cross-section in order to take into account the inertia of motion of the entire mechanism. Then for the finite element model (Figure 5) of the considered mechanism the forces and the moments of the inertia forces of the links shall be applied: in the node 2 to the link L_{1-3}, in the node 6 to the link L_{5-8}, in the node 7 to the link L_{5-9}, in the node 10 to the link L_{8-9}, in the node 15 to the link L_{13-17}, in the node 16 to the link L_{14-18}, in the node 23 to sliding block composed of the assembly of the finite bar elements L_{21-23}, L_{22-23}, L_{23-24} and L_{24-24}; and in the nodes 4, 11, 12, 19, 20 it shall be applied to the axes of rotation L_{3-5}, L_{8-13}, L_{9-14}, L_{17-21}, L_{18-22}. Let us assume that cross-sections of all links and axes are rectangular with the width of 0.01m and height of 0.02m. The weight forces of link and axes are also applied to the discrete mass points.

Finite element model consists of 26 Finite bar elements connected by 25 nodes. Elasticity characteristics are taken as equal for all links and axes: elasticity modulus is $E = 2 \cdot 10^{11}$ $[Pa]$, the Poisson ratio is $\mu = 0.3$, specific weight of material is $\rho = 5850[kg/m^3]$ and corresponds to elasticity characteristics of steel. Time step is equal to $\Delta t = 0.0005235$ $[sec]$.

Finite bar elements (BFE) models and corresponding node numbers: BFE 1: nodes 1 and 2, BFE 2: nodes 2 and 3, BFE 3: nodes 3 and 4, BFE 4: nodes 4 and 5, BFE 5: nodes 5 and 6, BFE 6: nodes 5 and 7, BFE 7: nodes 6 and 8, BFE 8: nodes 7 and 9, BFE 9: nodes 8 and 10,

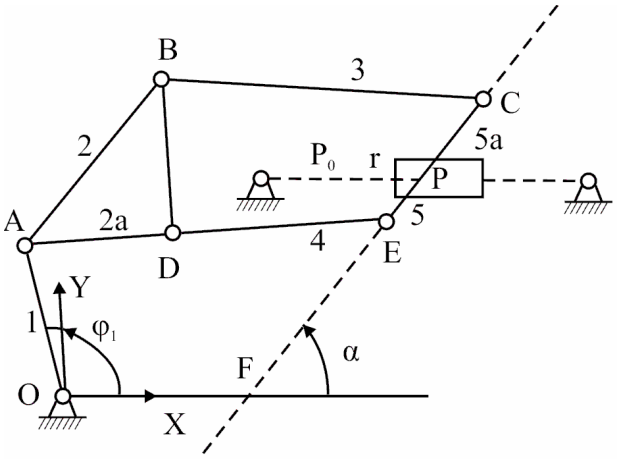

Fig. 4. Planar scheme of Class IV mechanism with external prismatic pair

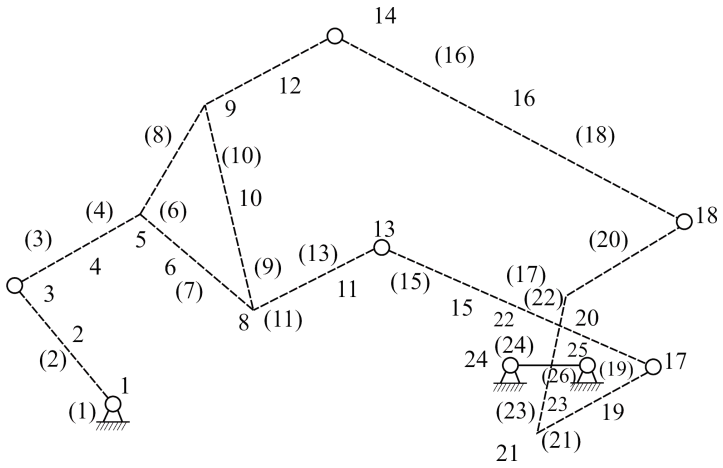

Fig. 5. Finite Element Model of Class IV spatial mechanism with external prismatic pair

BFE 10: nodes 9 and 10, BFE 11: nodes 8 and 11, BFE 12: nodes 9 and 12, BFE 13: nodes 11 and 13, BFE 14: nodes 12 and 14, BFE 15: nodes 13 and 15,BFE 16: nodes 14 and 16, BFE 17: nodes 15 and 17, BFE 18: nodes 16 and 18, BFE 19: nodes 17 and 19, BFE 20: nodes 18 and 20, BFE 21: nodes 19 and 21, BFE 22: nodes 20 and 22, BFE 23: nodes 21 and 23, BFE 24: nodes 22 and 23, BFE 25: nodes 23 and 24, BFE 26: nodes 23 and 25.

Global displacements of finite element model nodes in the Figure 5 are numbered in the way allowing describing mechanism deformation and providing compatibility between finite bar elements in the nodes with allowance for availability of 5 class kinematic pairs in some of them. For example, for node 3 global the degrees of freedom U_{13}, U_{14}, U_{15} are used to describe global node linear shifts. Other two independent displacements U_{16}, U_{18} in the node 3 are required to describe its angular displacements (angles of rotation) about the global axes OX and OZ.

Angular displacement U_{17} about the global axis OY in the node 3 is not available. Exclusion of such displacement from degrees of freedom of the finite element model simulates hinged connection in the node 3 with the axis permanently oriented parallel to global axis OY. The same can be said for degrees of freedom U_{77}, U_{83}, U_{101}, U_{107} simulating hinged connection in nodes 13, 14, 17 and 18 of the mechanism model. Generally, the formula $N_i = 6 \cdot n_u - i$, $(i = 0, 1, 2, 3, 4, 5)$, where is the node number; n_5, n_4, n_3 are the numbers of the degrees of freedom that correspond

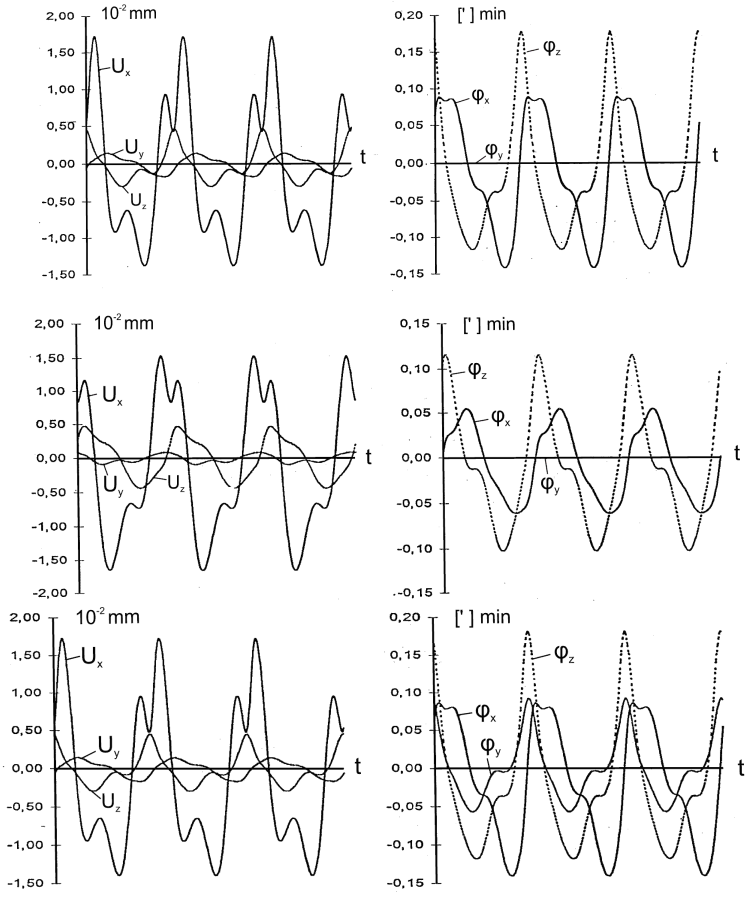

Fig. 6. Global Linear Vibrations and Angular Flexural Oscillations in the Finite Element Mechanism Model (FEMM) Nodes 17, 18, 19, correspondingly

to linear displacements along coordinate axes; n_2, n_1, n_0 are the numbers of the degrees of freedom that correspond to the angular displacements along coordinate axes, is used to simplify determination of the number of degree of freedom and its correspondence to the finite element model node number.

Figure 6 shoes the elastic linear and angular oscillations profiles of the mechanism finite element model nodes 17, 18, 19 versus positions they would have in case of the rigid link model of the mechanism.

5 Conclusions

Thereby, we got a new analytical expressions of inertial forces intensity and weights of the links for two cases of motion: plane parallel (1,2) and spatial (3,4). This is one of the few analysis of distributed inertia forces in a spatial mechanism, and allow to achieve optimum dynamic response of the linkage in design stage. Described model has been aplied for dynamic computition of elastic oscillations of the structure of Class IV mechanism with external prismatic pair. The obtained results bring us to conclusion on effectiveness of the proposed method, algorithm and computer software in terms of their application in numerical simulation of high-class mechanisms elastic oscillations. Our future work will be developing more precise methods of calculation structural strength and stiffness of linkages. There will be considered a more general case, when the linkage units have linearly changing variable cross-section.

References

1. Zienkiewicz O.PY. and McGrau H. The finite element in engineering science. *London*, 1971.
2. Bathe K.J. and Wilson E.L. Numerical Methods in Finite Element Analysis. Prentice-Hall, 1976.
3. Bathe K.J. Finite Element Procedures. Cambridge, 2006.
4. Reddy, J.N. An Introduction to the Finite Element Method (Third ed.). McGraw-Hill., 2006.
5. Zienkiewicz O.C., Taylor R.L. and Zhu J.Z. The Finite Element Method: Its Basis and Fundamentals (Sixth ed.). Butterworth-Heinemann., 2005.
6. Solin P., Segeth K. and Dolezel I. Higher-Order Finite Element Methods. Chapman and Hall/CRC Press., 2003.

On Some Properties of Signals with Finite Fourier-Walsh Spectrum

Nurzhan Bokayev, Zhalgas Mukanov, and Talgat Akhazhanov

L.N. Gumilyov Eurasian national university, Mechanics and Mathematics department,
Satpayev Str. 2, 010008 Astana, Republic of Kazakhstan
bokayev2011@yandex.ru,mukanovj@mail.ru,talgat_a2008@mail.ru
http://www.enu.kz/en/

Abstract. In this paper we present a multiple analog of the well-known sampling theorem (Kotelnikov-Shannon's theorem) on the representation of functions with finite Fourier spectrum through its values at equidistant points for Walsh-Fourier transformations. It follows that a signal with a finite spectrum Walsh is a step function.

Keywords: Walsh functions, Walsh-Fourier transformation, Fourier-Walsh spectrum

1 Introduction

For a number $x \in R_+$ and natural number n, we set

$$x_n \equiv [2^n x] \,(\mathrm{mod}\ 2),\ x_{-n} \equiv [2^{1-n} x] \,(\mathrm{mod}\ 2), \tag{1}$$

where $[a]$ is the integer part of the number a, and the numbers x_n and x_{-n} are equal to 0 or 1 by definition [1]. It is easy to see that the equality

$$x = \sum_{i=1}^{+\infty} 2^{i-1} x_{-i} + \sum_{i=1}^{+\infty} \frac{x_i}{2^i} \tag{2}$$

is true. Wherein

$$[x] = \sum_{i=1}^{+\infty} 2^{i-1} x_{-i}, x = x - [x] = \sum_{i=1}^{+\infty} \frac{x_i}{2^i}. \tag{3}$$

Note that $x_{-i} = 0$ for $i \geq i(x)$. If the number $x \in R_+$ is binary rational, then $x_i = 0$ for $i \geq i_0(x)$, that is, in this case, the second series of the right-hand side of (2) and (3) is a finite sum [1].

We now introduce the operation $\oplus$ on the set R_+ as follows. If the numbers $x, y \in R_+$ presented in the form (2), then we set

$$x \oplus y = \sum_{i=1}^{+\infty} 2^{i-1} |x_{-i} - y_{-i}| + \sum_{i=1}^{+\infty} \frac{|x_i - y_i|}{2^i}. \tag{4}$$

Obviously, $x \oplus y \in R_+$. The first of the series in the right-hand side of equation (4) is a finite sum. If x is binary rational, then the second row in (4) is also a finite sum [2]

Since $x_{-i} = 0$ for $i \geq i(x) \in N$, the nonnegative integer number

$$t(x, y) = \sum_{i=1}^{+\infty} (x_n y_{-n} + x_{-n} y_n)$$

is defined for $(x,y) \in R_+ \times R_+$. Generalized Walsh functions are defined for $(x,y) \in R_+ \times R_+$ by the equality

$$\psi_y(x) \equiv \psi(x,y) = (-1)^{t(x,y)}. \tag{5}$$

We also need the following properties of generalized Walsh functions [3, Chap.9]:

$$\psi_y(x) = \psi_x(y),\ \psi_y(x) = \pm 1 \quad \text{for} \quad (x,y) \in R_+ \times R_+$$

$$\psi_y(x) = \psi_{[y]}(y)\psi_{[x]}(y), \quad \psi_0(x) \equiv 1, \quad x,y \in R_+ \tag{6}$$

We denote by $D\left(x,x'\right) \equiv \int_0^{x'} \chi\left(x,t\right) dt$ - generalized Walsh-Dirichlet kernel.

As usual, we denote by $L(R_+)$ the space of functions f measurable on R_+ with respect to the Lebesgue measure with the finite norm

$$\|f\|_{L(R_+)} = \int_{R_+} |f(x)|\, dx.$$

We denote by $L^\infty(R_+)$ the space of essentially bounded on R_+ functions with the norm

$$\|f\|_{L^\infty(R_+)} = ess \sup_{x \in R_+} |f(x)|.$$

We denote by N (respectively Z) the set of all natural (respectively integer) numbers.

The Fourier-Walsh transform $F[f] \equiv \tilde{f}$ of a function $f \in L(R_+)$ is defined by the equality

$$F[f] \equiv \tilde{f} = \int\limits_{R_+} \psi(x,y) f(y) dy. \tag{7}$$

It was first defined in the work of N.J.Fine [2]. Since $f \in L(R_+)$ and $|\psi(x,y)| \equiv 1$, the integral of the right-hand side of (7) converges absolutely and uniformly on R_+.

A function $f : R_+ \to R_+$ is called dyadic-continuous at a point $x \in R_+$ if, for any $\varepsilon > 0$, there exists $\delta > 0$ such that $|f(x \oplus y) - f(x)| < \varepsilon$ for $0 < y < \delta$. A function $f : R_+ \to R_+$ is called uniformly dyadic-continuous at a point $x \in R_+$ if, for any $\varepsilon > 0$, there exists $\delta > 0$ such that $|f(x \oplus y) - f(x)| < \varepsilon$ for all $x \in R_+$ and for $0 < y < \delta$.

Here we cite the well-known Kotelnikov-Shannon's theorem for signal with a finite spectrum. Under the spectrum of the signal is understood trigonometric Fourier transform.

Theorem A. Let the signal $f(t)$ has finite spectrum: $\hat{f}(w) = 0$ при $|w| > a$. Then we have formula

$$f(t) = \sum_{k=-\infty}^{+\infty} f\left(\frac{\pi}{a}k\right) \frac{\sin a\left(t - \frac{\pi}{a}k\right)}{a\left(t - \frac{\pi}{a}k\right)}.$$

This sampling theorem means that any signal $s(t)$, whose spectrum contains components with frequencies above a certain value $\omega_B = 2\pi f_B$, there can be no loss of information represented by its discrete samples $\{s\,(kT)\}$, taken with an interval T, satisfying the following inequality:

$$T \leq \frac{1}{2\Gamma_B} = \frac{\pi}{\omega_B}$$

The two-dimensional analogue of this theorem is also known. Kotelnikov-Shannon's formula shows that the recovery message describing the function $f(t)$ with finite spectrum, concentrated in the frequency band $|\omega| < a$, enough to pass through the communication channel only discrete values $f\left(\frac{\pi}{a}k\right)$ (the reference values). The following analogue of the above theorem for functions

of several variables with finite spectrum Fourier-Walsh. Now we prove a multiple analog of this theorem for a signal with a finite Walsh spectrum.

Theorem 1. Let function $f(x_1,...,x_n) \in L_1\left(R_+^n\right)$ dyadic-continuous on R_+^n and his Fourier-Walsh transform $f(y_1,...,y_n)$ has finite support.

$$\widehat{f}(y_1,...,y_n) = 0$$

for $y_i > \delta_i$, where

$$\delta_i < 2^r, i = 1,...,n$$

Then the function $f(x_1,...,x_n)$ can be uniquely recovered by its values at the lattice points

$$\overline{x_k} = \left(\frac{k_1}{2^{r_1}}, \frac{k_2}{2^{r_2}}, ..., \frac{k_n}{2^{r_n}}\right), k_j = 0,1,2,..., j = 1,2,...,$$

by the formula

$$f(x_1,...,x_n) = \frac{1}{2^{r_1+...+r_n}} \sum_{k=0}^{\infty} ... \sum_{k=0}^{\infty} f\left(\frac{k_1}{2^{r_1}}, \frac{k_2}{2^{r_2}}, ..., \frac{k_n}{2^{r_n}}\right) \prod_{i=1}^{n} D\left(\frac{k_i}{2^{r_i}} \oplus x_i, 2^{r_i}\right), \tag{8}$$

Proof.

For brevity, we give the proof for the case of a function of two variables.

Since the function $\widehat{f}(y_1,...,y_n)$ has finite support, then $\widehat{f}(y_1,...,y_n) \in L_1\left(R_+^n\right)$. Therefore

$$f(x_1,x_2) = \lim_{\min k_i \to \infty} \int_0^{2^{k_1}} \int_0^{2^{k_2}} \widehat{f}(y_1,y_2)\,\chi(x_1,y_1)\,\chi(x_2,y_2)\,dy_1dy_2 =$$

$$= \int_0^{2^{r_1}} \int_0^{2^{r_2}} \widehat{f}(y_1,y_2)\,\chi(x_1,y_1)\,\chi(x_2,y_2)\,dy_1dy_2 \tag{9}$$

Note that the system functions

$$\phi_{\nu_1,\nu_2}^{r_1,r_2}(y_1,y_2) = \frac{1}{\sqrt{2^{r_1+r_2}}} \chi\left(\frac{\nu_1}{2^{r_1}}, y_1\right) \chi\left(\frac{\nu_2}{2^{r_2}}, y_2\right)$$

are orthonormal and bounded on $[0,2^{r_1}) \times [0,2^{r_2})$. Given that $\widehat{f}(y_1,y_2) = 0$ for $y_j > 2^{r_j}, j = 1,2$ we expand the function $\widehat{f}(y_1,y_2)$ in a Fourier series to respect system $\{\phi_{\nu_1,\nu_2}^{r_1,r_2}(y_1,y_2)\}$:

$$\widehat{f}(y_1,y_2) \approx \sum_{\nu_1=0}^{\infty} \sum_{\nu_2=0}^{\infty} b_{\nu_1,\nu_2} \phi_{\nu_1,\nu_2}^{r_1,r_2}(y_1,y_2), \tag{10}$$

where

$$f(x_1,x_2) = \int_0^{2^{r_1}} \int_0^{2^{r_2}} \widehat{f}(y_1,y_2)\,\phi_{\nu_1,\nu_2}^{r_1,r_2}(y_1,y_2)\,dy_1dy_2 =$$

$$= \frac{1}{\sqrt{2^{r_1+r_2}}} \int_0^{2^{r_1}} \int_0^{2^{r_2}} \widehat{f}(y_1,y_2)\,\chi\left(\frac{\nu_1}{2^{r_1}}, y_1\right) \chi\left(\frac{\nu_2}{2^{r_2}}, y_2\right) dy_1dy_2. \tag{11}$$

From (10) and (11) it follows that

$$b_{\nu_1,\nu_2}(y_1,y_2) = \frac{1}{\sqrt{2^{r_1+r_2}}} f\left(\frac{\nu_1}{2^{r_1}}, \frac{\nu_2}{2^{r_2}}\right), \nu_j = 0,1,2,..., j = 1,2.$$

Therefore, according to (10)

$$\widehat{f}(y_1,y_2)\approx\sum_{\nu_1=0}^{\infty}\sum_{\nu_2=0}^{\infty}\frac{1}{2^{r_1+r_2}}f\left(\frac{\nu_1}{2^{r_1}},\frac{\nu_2}{2^{r_2}}\right)\chi\left(\frac{\nu_1}{2^{r_1}},y_1\right)\chi\left(\frac{\nu_2}{2^{r_2}},y_2\right) \tag{12}$$

Further, from (10) and (12) we have

$$f(x_1,x_2)=\int_0^{2^{r_1}}\int_0^{2^{r_2}}\chi(x_1,y_1)\chi(x_2,y_2)\sum_{\nu_1=0}^{\infty}\sum_{\nu_2=0}^{\infty}\frac{1}{2^{r_1+r_2}}f\left(\frac{\nu_1}{2^{r_1}},\frac{\nu_2}{2^{r_2}}\right)\chi\left(\frac{\nu_1}{2^{r_1}},y_1\right)\chi\left(\frac{\nu_2}{2^{r_2}},y_2\right)dy_1dy_2=$$

$$=\frac{1}{2^{r_1+r_2}}\sum_{\nu_1=0}^{\infty}\sum_{\nu_2=0}^{\infty}f\left(\frac{\nu_1}{2^{r_1}},\frac{\nu_2}{2^{r_2}}\right)\int_0^{2^{r_1}}\int_0^{2^{r_2}}\chi\left(\frac{\nu_1}{2^{r_1}}\oplus x_1,y_1\right)\chi\left(\frac{\nu_2}{2^{r_2}}\oplus x_2,y_2\right)dy_1dy_2=$$

$$=\frac{1}{2^{r_1+r_2}}\sum_{\nu_1=0}^{\infty}\sum_{\nu_2=0}^{\infty}f\left(\frac{\nu_1}{2^{r_1}},\frac{\nu_2}{2^{r_2}}\right)D\left(\frac{\nu_1}{2^{r_1}}\oplus x_1,2^{r_1}\right)D\left(\frac{\nu_2}{2^{r_2}}\oplus x_2,2^{r_2}\right),$$

where $D\left(x,x^{'}\right)\equiv\int_0^{x^{'}}\chi(x,t)\,dt$- generalized Walsh-Dirichlet kernel.

Theorem 1 is proved.

The following theorems are the properties of signals with a finite spectrum Walsh.

Theorem 2. Let the function $f(\overline{x})\in L_1\left(R_+^n\right)$ dyadic-continuous on R_+^n and its Fourier-Walsh transform $\widehat{f}(\overline{y})$ has a finite support $\widehat{f}(y_1,...,y_n)=0$ при $y_j\geq 2^{r_j}$, $j=1,...,n$. Then $f(\overline{x})$ - step function that is constant on the intervals $\overline{r}$-th rank,

$$\Delta_{\nu}(\overline{r})=\left[\frac{\nu_1}{2^{r_1}},\frac{\nu_1+1}{2^{r_1}}\right]\times\left[\frac{\nu_2}{2^{r_2}},\frac{\nu_2+1}{2^{r_2}}\right]\times...\times\left[\frac{\nu_n}{2^{r_n}},\frac{\nu_n+1}{2^{r_n}}\right].$$

This follows from theorem 1, given that

$$D\left(\frac{\nu_i}{2^{r_i}}\oplus x_i,2^{r_i}\right)=\begin{cases}2^{r_i},0\leq\frac{\nu_i}{2^{r_i}}\oplus x_i<\frac{1}{2^{r_i}}\\ 0,\frac{1}{2^{r_i}}\leq\frac{\nu_i}{2^{r_i}}\oplus x_i<\infty\end{cases}$$

Theorem 3. If the function $f(\overline{x})\in L_1\left(R_+^n\right)$ be step and constant on the intervals $\overline{r}$-th rank $\Delta_{\nu}(\overline{r})$, then Fourier-Walsh transform $\widehat{f}(\overline{y})$ finite, i.e.

$$\widehat{f}(y_1,...,y_n)=0$$

при $y_j\geq 2^{r_j}$, $j=1,...,n$.

Proof.

The step function and constant on the intervals $\overline{r}$-th rank $\Delta_{\nu}(\overline{r})$, can be represented as a series of

$$f(x_1,x_2)=\sum_{\nu_1=0}^{\infty}\sum_{\nu_2=0}^{\infty}c_{\nu_1,\nu_2}\frac{1}{2^{r_1+r_2}}D\left(2^{r_1},\frac{\nu_1}{2^{r_1}}\oplus x_1\right)D\left(2^{r_2},\frac{\nu_2}{2^{r_2}}\oplus x_2\right),$$

where c_{ν_1,ν_2} constant. Therefore

$$f(y_1,y_2)=\int_0^{\infty}\int_0^{\infty}f(t_1,t_2)\chi(t_1,y_1)\chi(t_2,y_2)\,dt_1dt_2=$$

$$=\frac{1}{2^{r_1+r_2}}\sum_{\nu_1=0}^{\infty}\sum_{\nu_2=0}^{\infty}c_{\nu_1,\nu_2}\int_{0\leq\frac{\nu_1}{2^{r_1}}\oplus t_1<\frac{1}{2^{r_1}}}\int_{0\leq\frac{\nu_1}{2^{r_1}}\oplus t_1<\frac{1}{2^{r_1}}}\chi(t_1,y_1)\chi(t_2,y_2)\,dt_1dt_2.$$

Assumed that $\frac{\nu_i}{2^{r_i}} \oplus t_i = \nu_i$, i.e. $t_i = \frac{\nu_i}{2^{r_i}} \oplus \nu_i$, $i = 1, 2$, we have

$$\widehat{f}(y_1, y_2) = \sum_{\nu_1=0}^{\infty} \sum_{\nu_2=0}^{\infty} c_{\nu_1,\nu_2} \chi\left(\frac{\nu_1}{2^{r_1}}, y_1\right) \chi\left(\frac{\nu_2}{2^{r_2}}, y_2\right) \int_0^{\frac{1}{2^{r_1}}} \int_0^{\frac{1}{2^{r_2}}} \chi(\nu_1, y_1) \chi(\nu_2, y_2) \, d\nu_1 d\nu_2.$$

Further, given that

$$\int_0^{\frac{1}{2^{r_i}}} \chi(\nu_i, y_i) \, d\nu_i = o, i = 1, 2$$

we have $\widehat{f}(y_1, y_2) = 0$ for $y_j \geq 2^{r_j}$, $j = 1, 2$.

Theorem 3 is proved.

Note that the analogues of theorems 1 and 3 for the one-dimensional multiplicative transformation was previously proved by S.Yu.Zolotareva (1980 r.,[4]), and theorem 2 is proved by M.S.Bespalov (1982 r.,[5]).

References

1. Golubov, B., Elements of dyadic analysis. URSS/LKI, Moscow (2007) (in Russian)
2. Fine, N.J.: The generalized Walsh functions. Trans. Amer. Math. Soc. 69, 66–77 (1950)
3. Schipp, F., Wade, W.R., and Simon P.: Walsh Series. Akad. Kiado, Budapest (1990)
4. Zolotareva, S.Yu.: Frequency properties of multiplicative Fourier transform. M. MIET, 82–93 (1980) (in Russian)
5. Bespalov, M.S.: Multiplicative Fourier Transforms on L^p. Manuscript No. 100-82 submitted to VINITI, Moscow (1981)

A Vorticity Based Model of Isotropic Turbulence

Amitabha Chanda

Faculty (Retd.), Indian Statistical Institute
Presently Visiting Faculty, UCSTA, University of Calcutta, India
amitabha39@yahoo.co.in;amitabha39@gmail.com

Abstract. It is argued that the transfer operator in the governing equation of isotropic turbulence is engaged in convective transfer of turbulent energy; and convective transfer is solely carried out by vortices. This understanding is used to find the form of longitudinal coorelation coefficient f in isotropic turbulence and hence that of the transverse coorelation coefficient g. With these solutions the general decay of isotropic turbulence is studied as against the the standard expressions of f and g. The new expressions are compared with the standard ones.

Keywords: Frequency, Convective transfer, Isotropic, Galilean invariance, Vorticity

1 Background of the study of turbulence

Study of Navier-Stokes equations for incompressible flow is being vigorously conducted almost for nine decades. Odqvist [1], Leray [2], Hopf [3] and Ladyzhenskaya [4] have done lot of theoretical studies. We would like to mention the contribution of Sedov [5] also. Above all the contribution of Kolmogorov [6] on turbulent flow guided by the NS equations opened a floodgate of research on turbulence, for both incompressible and compressible fluid. Contribution of Burger [7] and Taylor [8] are note worthy. Some of these studies are on the real field, some in wavenumber field. Significant studies of NS equations in wavenumber field have been carried out by Heisenberg [9], Kraichnan [10] and many others.

The Navier-Stokes equations for incompressible laminar flow are the starting point for turbulence study. Fluctuations in velocity and pressure fields are then superimposed on the laminar equations. Right from this point mathematicians have made an assumption. Principle of superposition, which is valid only in linear systems, is assumed to be valid in nonlinear system also. But the acceptance of the validity of the Principle of superposition in nonlinear system cannot not fully solve the problem of turbulence. Further assumptions are needed. To circumvent this difficulty, number of symmetry approximations are used. The most popular is isotropy.

1.1 Homogenous Isotropic turbulence

Homogenous Isotropic turbulence,(henceforth will be mentioned as Isotropic turbulence), is the simplest model and is being studied from many different angles. But even with consideration of isotropy NS equations cannot be solved. One has to make more simplifying assumption. Heisenberg solved the problem of isotropic turbulence in wavenumber field introducing a fictitious turbulent viscosity. He modeled this viscosity with energy density in wavenumber field and wavenumber as well using dimensional reasoning. The result obtained mathematically in the form of power law is found to be in conformity with the laboratory finding.

We again observe that assumptions are freely used to create models that fit with the experimental results. The success of a model to great extent depends upon its success to explain the experimental results with reasonable accuracy. In the present paper we would like to make a new type of assumption.

2 A suggested deviation from Karman-Howarth equation

2.1 The Karman-Howarth equation of isotropic turbulence

The equation representing homogeneous isotropic turbulence, developed by von Karman and Howarth [11] and popularly known as Karman-Howarth (K-H) equation is given below. Batchelor [12] has given a comprehensive discussion of N-H equation in his famous book.

$$\frac{\delta u^2 f(r)}{\delta t} = u^2(\frac{\delta}{\delta r} + \frac{4}{r})k(r) + 2\nu u^2(\frac{\delta^2}{\delta r^2} + \frac{4}{r}\frac{\delta}{\delta r})f(r) \tag{1}$$

In this equation **u**, **f** and **k**, respectively root mean square velocity, longitudinal correlation coefficient and third order moment are all functions of time. However it may be noted that (1) is not a solvable equation since it contains three variables. So we need further assumption.

If we restrict our study to steady state condition we are still left with two variables **f** and **k** in one equation i.e. an unsolvable situation. So some sort of modeling has to be done to relate **f** and **k**. In the present paper we are trying to suggest a new method to circumvent this problem of unsolvability.

We write the $N-S$ equations at two space points $\mathbf{x}$ and $\mathbf{x}'$, but at the same instant $\mathbf{t}$.

$$\begin{aligned} \frac{\delta u_i}{\delta t} + u_k\frac{\delta u_i}{\delta x_k} &= \nu\frac{\delta^2 u_i}{\delta x_k \delta x_k} \\ \frac{\delta u'_j}{\delta t} + u'_k\frac{\delta u'_j}{\delta x'_k} &= \nu\frac{\delta^2 u'_j}{\delta x'_k \delta x'_k} \end{aligned} \tag{2}$$

2.2 The role of vorticity

Let us now study the convective transfer operator. Tennekes & Lumley [12] have linked the convective transfer part with vorticity, based on pure mathematical reasoning. The details of the approach is given below.

$$\begin{aligned} u_k\frac{\delta u_i}{\delta x_k} &= u_k(\frac{\delta u_i}{\delta x_k} - \frac{\delta u_k}{\delta x_i}) + u_k\frac{\delta u_k}{\delta x_i} \\ &= 2u_k\tau_{ki} + \frac{1}{2}\frac{\delta u_k u_k}{\delta x_i} \end{aligned} \tag{3}$$

Here τ_{ki} is the rotation tensor and is given as below.

$$\tau_{ki} = \frac{1}{2}(\frac{\delta u_i}{\delta x_k} - \frac{\delta u_k}{\delta x_i}) \tag{4}$$

Vorticity again is linked with the rotation tensor in the following way.

$$\begin{aligned} \omega_j &= \epsilon_{jki}\frac{\delta u_i}{\delta x_k} \\ &= \frac{1}{2}\epsilon_{jki}(\frac{\delta u_i}{\delta x_k} + \frac{\delta u_k}{\delta x_i}) + \frac{1}{2}\epsilon_{jki}(\frac{\delta u_i}{\delta x_k} - \frac{\delta u_k}{\delta x_i}) \\ &= \epsilon_{jki}(s_{ki} + \tau_{ki}) \end{aligned} \tag{5}$$

s_{ki} is the symmetric strain tensor and τ_{ki} the antisymmetric rotation tensor. ϵ_{ijk} is a skew-symmetric tensor. Vorticity vector ω_j is also a skew-symmetric tensor. Hence ω_j is related to τ_{ki} only. So we have the following result.

$$\omega_j = \epsilon_{jki}\tau_{ki} \tag{6}$$

From (6) we now get

$$\tau_{ki} = -\frac{1}{2}\epsilon_{ijk}\omega_j \tag{7}$$

So (3) becomes

$$\frac{\delta u_k u_i}{\delta x_k} = -\epsilon_{ijk}u_k\omega_j + \frac{\delta e}{\delta x_i} = -(\omega \mathbf{Xu})_\mathbf{i} + \frac{\delta \mathbf{e}}{\delta \mathbf{x_i}} \tag{8}$$

Here $e = \frac{1}{2}u_k u_k$. Let us now take the first of equations (2) only for component 1 i.e. substituting i by 1.

$$\frac{\delta u_1}{\delta t} = (\omega \mathbf{Xu})_\mathbf{1} - \frac{\delta \mathbf{e}}{\delta \mathbf{x_1}} + \nu \frac{\delta^\mathbf{2} \mathbf{u_1}}{\delta \mathbf{x_k} \delta \mathbf{x_k}} \tag{9}$$

For the second point we get the similar equation.

$$\frac{\delta u_1'}{\delta t} = (\omega' \mathbf{Xu'})_\mathbf{1} - \frac{\delta \mathbf{e'}}{\delta \mathbf{x_1'}} + \nu \frac{\delta^\mathbf{2} \mathbf{u_1'}}{\delta \mathbf{x_k'} \delta \mathbf{x_k'}} \tag{10}$$

From (9) and (10) we get the following result.

$$\frac{\delta \overline{u_1 u_1'}}{\delta t} = \overline{(\omega \mathbf{Xu})_\mathbf{1} \mathbf{u_1'}} + \overline{(\omega' \mathbf{Xu_1'})\mathbf{u}}_1 + \frac{\delta}{\delta r}(\overline{eu_1'} - \overline{e'u_1}) + 2\nu[\frac{\delta^2}{\delta r^2} + \frac{4}{r}\frac{\delta}{\delta r}]\overline{u_1 u_1'} \tag{11}$$

Let us first examine the two terms $\overline{eu_1'}$ and $\overline{e'u_1}$. We examine the first one.

$$\begin{aligned} \overline{eu_1'} &= \frac{1}{2}\overline{u_k u_k u_1'} \\ &= \frac{1}{2}(\overline{u_1 u_1 u_1'} + \overline{u_2 u_2 u_1'} + \overline{u_3 u_3 u_1'}) \\ &= \frac{1}{2}(-2rD + rD + rD) = 0 \end{aligned} \tag{12}$$

Here D is a scalar. We can process the second one and again get to zero. So (11) reduces to the following form.

$$\frac{\delta \overline{u_1 u_1'}}{\delta t} = \overline{(\omega \mathbf{Xu})_\mathbf{1} \mathbf{u_1'}} + \overline{(\omega' \mathbf{Xu'})_\mathbf{1} \mathbf{u}}_1 + 2\nu[\frac{\delta^2}{\delta r^2} + \frac{4}{r}\frac{\delta}{\delta r}]\overline{u_1 u_1'} \tag{13}$$

If we now put K-H equation (1) and (13) side by side we may say that in (13) convective transport has been taken over by vorticity transport. This is our first finding.

At this stage we would like to refer to the findings of Jimenez et. al. [13]. Experimental results have shown that in isotropic turbulence vortices are more or less ellipsoidal. In the present case we are examining isotropic turbulence with near-zero separation distance between two probes. So we would like to consider that the statistical results are mostly affected by the small and medium eddies of near spherical shape. The term $(\omega \mathbf{Xu})_\mathbf{1}$ denotes the 1-component of the cross product of a polar velocity vector and an axial vorticity vector. In view of this finding and the first finding as above we would like to replace $(\omega \mathbf{Xu})_\mathbf{1}$by ωu_1. Here ω stands for the size of the average eddy. So (13) becomes

$$\frac{\delta \overline{u_1 u_1'}}{\delta t} = \overline{u_1 u_1' \omega} + \overline{u_1 u_1' \omega'} + 2\nu[\frac{\delta^2}{\delta r^2} + \frac{4}{r}\frac{\delta}{\delta r}]\overline{u_1 u_1'} \tag{14}$$

Since $r- > 0$ we would like to assume that the vortices are not only small, assumed earlier, but also are confined in a narrow zone. this has been observed by Brasseur and Lin [14] So, we

would like to assume ω and ω' are not only spherical, their sizes vary in anarrow range. With this assumption (14) becomes

$$\frac{\delta\overline{u_1u_1'}}{\delta t} = (\overline{u_1u_1'} + \overline{u_1u_1'})\overline{\omega} + 2\nu[\frac{\delta^2}{\delta r^2} + \frac{4}{r}\frac{\delta}{\delta r}]\overline{u_1u_1'} \tag{15}$$

We now rewrite (15) as below.

$$\frac{\delta\overline{u^2}f}{\delta t} + 2\overline{\omega}\,\overline{u^2}f = 2\nu\left[\frac{\delta^2}{\delta r^2} + \frac{4}{r}\frac{\delta}{\delta r}\right]\overline{u^2}f \tag{16}$$

3 Solution of equation (16) for steady state condition as $r \to 0$

For steady state condition (16) becomes

$$\overline{\omega}f = \nu\left[\frac{\delta^2}{\delta r^2} + \frac{4}{r}\frac{\delta}{\delta r}\right]f \tag{17}$$

We shall now try to solve the steady state equation (17) for steady state condition

$$rf_{rr} + 4f_r - \frac{\overline{\omega}}{\nu}rf = 0 \tag{18}$$

Let us now try to solve (18). We express $\mathbf{f}$ as $f = e^{\alpha r}\phi(r)$. We put this form in (18) and get $r\phi_{rr} + (2\alpha r + 4)\phi_r + \left(\alpha^2 - \frac{\overline{\omega}}{\nu}\right)r\phi + 4\alpha\phi = 0$. We now set the following condition. $\alpha^2 - \frac{\overline{\omega}}{\nu} = 0$ or $\alpha = \sqrt{\frac{\overline{\omega}}{\nu}}$. Using this condition in the equation we have $r\phi_{rr} + (2\alpha r + 4)\phi_r + 4\alpha c\phi = 0$.

We now put $r = c\tau$ in this equation and get $r\phi_{rr} + (2\alpha c\tau + 4)\phi_r + 4\alpha c\phi = 0$ Then after putting $2\alpha c = -1$ we get the following equation.

$$r\phi_{rr} + (4 - \tau)\phi_r - 2\phi = 0 \tag{19}$$

(20) is a Kummer's equation with a solution as below.

$$\phi = F(2, 4, \tau) \tag{20}$$

With (18) the final solution of (17) is given as

$$\begin{aligned} f &= e^{\alpha\tau}F(2,4,\tau) = exp\left\{\left(\frac{\overline{\omega}}{\nu}\right)^{\frac{1}{2}}r\right\}F(2,4,\tau) \\ &= exp\left\{\left(\frac{\overline{\omega}}{\nu}\right)^{\frac{1}{2}}r\right\}F\left\{2,4,-2\left(\frac{\overline{\omega}}{\nu}\right)^{\frac{1}{2}}r\right\} \\ &= exp\left\{\left(\frac{\overline{\omega}}{\nu}\right)^{\frac{1}{2}}r\right\}\Sigma_{n=0}^{\infty}\left[\frac{(2)_n}{(4)_n}\frac{1}{n!}\left\{-2\left(\frac{\overline{\omega}}{\nu}\right)^{\frac{1}{2}}r\right\}^n\right] \\ &= exp\left\{\left(\frac{\overline{\omega}}{\nu}\right)^{\frac{1}{2}}r\right\}\left[1 - \frac{2}{4}\left\{2\left(\frac{\overline{\omega}}{\nu}\right)^{\frac{1}{2}}r\right\} + \frac{2.3}{4.5}\frac{1}{2!}\left\{2\left(\frac{\overline{\omega}}{\nu}\right)r^2\right\} - \right] \end{aligned} \tag{21}$$

When r tends to zero the asymptotic form of (12) may be given as

$$\begin{aligned} f &= e^{\alpha\tau}F(2,4,\tau) \\ &= \left\{1+\left(\frac{\overline{\omega}}{\nu}^{\frac{1}{2}}\right)r\left\{1-\left(\frac{\overline{\omega}}{\nu}\right)^{\frac{1}{2}}r+\frac{3}{10}\frac{\overline{\omega}}{\nu}\right)r^2\right\} \\ &= 1-\frac{7}{10}(\frac{\overline{\omega}}{\nu})r^2 \\ &= 1-\frac{7}{10}\left(\frac{\overline{\omega}\lambda^2}{\nu}\right)(\frac{r}{\lambda})^2 \end{aligned} \tag{22}$$

In (22) we have nondimensionalised the distance r by Taylor's microscale λ. It may also be noted from (22) that as expected $\mathbf{f}$ is less than unity in the neighbourhood of $\mathbf{r}=\mathbf{0}$ and unity when $\mathbf{r}=\mathbf{0}$

4 Standard and the suggested forms of f : a comparative study

We would now make an attempt to compare the suggested form of $\mathbf{f}$ near $\mathbf{r}=\mathbf{0}$ (22) with the standard form given by Batchelor [14], as below.

$$\begin{aligned} f &= 1-\frac{1}{2\lambda^2}r^2 \\ &= 1-\frac{1}{2}(\frac{r}{\lambda})^2 \end{aligned} \tag{23}$$

Now let us compare (22) with (23). Doing so we get the following result.

A. In both the cases $f=1$ at $r=0$
B. In both the cases slope of f is negative everywhere.

The slopes of the standard f and the suggested f are as below.

$$\begin{aligned} f'_{standard} &= -\frac{1}{\lambda}(\frac{r}{\lambda}) \\ f'_{suggested} &= -\frac{7}{5\lambda}(\frac{\overline{\omega}\lambda^2}{\nu})(\frac{r}{\lambda}) \end{aligned} \tag{24}$$

It may be seen that the suggested form of f is of the same order with the standard one besides a modifying factor $\frac{\overline{\omega}\lambda^2}{\nu}$, which is a non-dimensional number. A simple graph is included at the bottom, comparing the two forms of f's with a value of the modifying factor, arbitrarily taken as unity. Now we shall like to get the forms of the tranverse correlation g from the standard and the suggested forms. These are as below.

$$g = f+\frac{1}{2}rf' \tag{25}$$

We shall now get the forms of g with the standard and suggested forms of f.

$$\begin{aligned} g_{standard} &= 1-(\frac{r}{\lambda})^2 \\ g_{suggested} &= 1-\frac{7}{5}(\frac{\overline{\omega}\lambda^2}{\nu})(\frac{r}{\lambda})^2 \end{aligned} \tag{26}$$

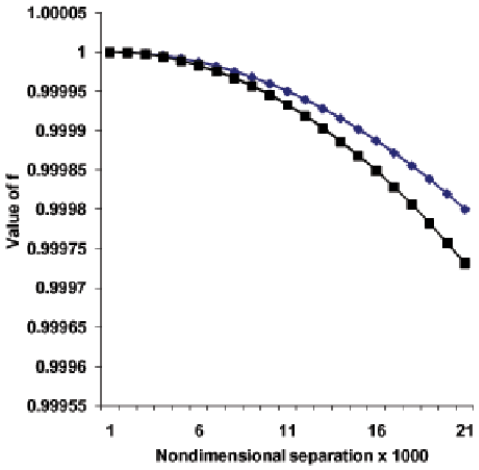

Fig. 1.

Acknowledgement

I acknowledge with thanks the active guidance given by R K Roychowdhury, Emeritus Professor of Indian Statistical Institute, a mathematician of international repute in handling KummerвЂ™s equation.

5 Discussion and comment

In this paper the author presents a new model of isotropic turbulence. It is argued that in isotropic turbulence convective transfer is basically carried out by eddies. This has been shown by comparing K-H equation with an equation, arrived through mathematical steps and without further assumption. From dimensional reasoning also vorticiy has the same dimension with convective operator. From all these findings we would like to conclude that eddies are the sources of fluctuations in the velocity field. In fact If the eddies disappear; disturbances in velocity field in isotropic turbulence are likely to disappear with the death of turbulence.

References

1. Odqvist, F.K.G. Math. Z. 32: 329-375 (1930)
2. Leray, J. J. Math. Pures Appl. 12:1-82. 1934a J. Math. Pures Appl. 13: 331-418 1934b Acta. Math. 63:193-248 (1933)
3. Hopf, E. Math. Ann. 117:764-775 (1941)
4. Ladyzhenskaya, O.A. Dokl. Acad. Nauk. SSSR 123:427-429 (1958)
5. Sedov, L.I. C.R. Acad. Sci. URSS. 42, 116. (1944)
6. Kolmogorov, A.N. C.R. Acad. Sci. URSS. 30, 301. 1941b C.R. Acad. Sci. URSS. 31, 538. (1941a)
7. Burger, J.M. Adv. Appl. Mech. 1, 171. (1948a)
8. Taylor, G.I. Proc. Roy. Soc. A, 151, 421. (1935a)
9. Heisenberg, W. Proc. Roy. Soc. A, 195, 402. (1948b)
10. von Karman, T & Howarth, L. Proc. Roy. Soc. A, 164, 192. (1938)
11. Batchelor, G.K. The theory of Homogenous turbulence, Cambridge University. (1959)
12. Tennekes, H. & Lumley, J.L. A first course in turbulence, The MIT Press, Cambridge, Massachussets & London (UK). (1972)
13. Jimenez, J., Wray, A.A., Saffman, P.G. & Rogallo, R.S. JFM, 255, 65-90. (1993)
14. Brasseur, J.G. & Lin, W. Fluid Dyn. Res., 36, 357-384. (2005)

An Inverse Problem for the Stokes Equations

G.M. Dairbaeva

Al-Farabi Kazakh National University, Almaty, Kazakhstan
lazat-dairbayeva@mail.ru

Abstract. We consider the initial boundary problem to the Stokes equations, which is ill-posed in this paper. The direct and adjoint problems are formulated to the original equations. Sobolev's space, space of traces of functions and their norms are considered. The definitions of generalized solutions to the direct and adjoint problems are given for the original equations. We consider the following approach: ill-posed problem is reduced to the inverse problem, which can be written in operator form $Aq = f$, then minimization of the objective functional $J(q) =< Aq - f, Aq - f >$. is researched. Formulation of the inverse problem to the direct problem is made for the Stokes equations. It is shown that the initial boundary value problem is reduced to the inverse problem with respect to well-posed problem for the original equations. It is shown that the inverse problem can be written as an operator equation. For numerical solving the direct and adjoint problems we use a finite element method, its application to ill-posed problems is new. For application of the finite element method a triangulation of the domain is made. The inverse problem is solved numerically using a combination of optimization method and finite element method. The estimation of the convergence rate of the algorithm with respect to the functional is found.

Keywords: Stokes equations, inverse problem, finite element method, optimization method.

1 The problem formulation

Let's consider the domain $\Omega = \{(x, y) \in R^2 : x \in (0, 1), y \in (0, 1)\}$. $\partial\Omega = \Gamma_0 \cup \Gamma_1$ is the boundary of Ω, where $\Gamma_1 = \{(1, y) : y \in [0, 1]\}$. Let's imagine the boundary Γ_0 as follows $\Gamma_0 = \Gamma_{01} \bigcup \Gamma_{02} \bigcup \Gamma_{03}$, where $\Gamma_{01} = \{(x, 0) : x \in [0, 1]\}$, $\Gamma_{02} = \{(0, y) : y \in [0, 1]\}$, $\Gamma_{03} = \{(x, 1) : x \in [0, 1]\}$. In the domain Ω we consider the initial boundary problem for the Stokes equations

$$\Delta u - \nabla p = 0, \tag{1}$$

$$div\, u = 0, \tag{2}$$

$$u\mid_{\Gamma_0} = \begin{cases} 0,\ if\ (x, y) \in \Gamma_{01} \bigcup \Gamma_{03}, \\ \varphi(y),\ if\ (x, y) \in \Gamma_{02}, \end{cases} \tag{3}$$

$$(pn - \frac{\partial u}{\partial n})\mid_{\Gamma_0} = f(x, y),\ (x, y) \in \Gamma_0, \tag{4}$$

where $u = (u_1, u_2)$ is velocity and p is pressure, $\varphi = (\varphi_1, \varphi_2)$, $f = (f_1, f_2)$ are given functions, $n = (n_1, n_2)$ is the outward unit normal to the boundary $\partial\Omega$.

We rewrite the problem (2)-(4) in the coordinate form

$$\Delta u_1 - p_x = 0,\ (x, y) \in \Omega \tag{5}$$

$$\Delta u_2 - p_y = 0,\ (x, y) \in \Omega \tag{6}$$

$$u_{1x} + u_{2y} = 0,\ (x,y) \in \Omega \tag{7}$$

$$u_l\ |_{\Gamma_0} = \begin{cases} 0,\ if\ (x,y) \in \Gamma_{01} \bigcup \Gamma_{03} \\ \varphi_l(y),\ if\ x,y) \in \Gamma_{02} \end{cases},\ \ l = 1,2, \tag{8}$$

$$\Gamma_{01}: \ \begin{cases} u_{1y}(x,0) = f_1(x,0),\ \ x \in (0,1) \\ -p(x,0) + u_{2y}(x,0) = f_2(x,0),\ \ x \in (0,1) \end{cases} \tag{9}$$

$$\Gamma_{02}: \ \begin{cases} -p(0,y) + u_{1x}(0,y) = f_1(0,y),\ \ y \in (0,1) \\ u_{2x}(0,y) = f_2(0,y),\ \ y \in (0,1) \end{cases} \tag{10}$$

$$\Gamma_{03}: \ \begin{cases} -u_{1y}(x,1) = f_1(x,1),\ \ x \in (0,1) \\ p(x,1) - u_{2y}(x,1) = f_2(x,1),\ \ x \in (0,1). \end{cases} \tag{11}$$

The problem (2)-(4) is ill-posed [1]. We can see below that it can be formulated as an inverse problem to some well-posed problem for the initial equations.

2 The direct problem formulation

Let's consider the Stokes system equations in the given domain Ω

$$\Delta u_1 - p_x = 0, \tag{12}$$

$$\Delta u_2 - p_y = 0, \tag{13}$$

$$u_{1x} + u_{2y} = 0, \tag{14}$$

with the following boundary conditions

$$u_l\ |_{\Gamma_0} = \begin{cases} 0,\ if\ (x,y) \in \Gamma_{01} \bigcup \Gamma_{03}, \\ \varphi_l(y),\ if\ \ (x,y) \in \Gamma_{02}, \end{cases}\ l = 1,2, \tag{15}$$

$$\Gamma_1: \ \begin{cases} p(1,y) - u_{1x}(1,y) = q_1(y),\ \ y \in (0,1) \\ -u_{2x}(1,y) = q_2(y),\ \ y \in (0,1), \end{cases} \tag{16}$$

The problem (12) - (16), where it is required to determine $u(x,y)$, $p(x,y)$ from the given function $q(y)$, we will be called direct.

So, we consider the Sobolev space $L_2(\Omega)$, $W_2^1(\Omega)$ with the appropriate norms

$$\|u\|_{L_2(\Omega)} = \left(\int\limits_\Omega u^2 dxdy \right)^{1/2},\ \|u\|_{W_2^1(\Omega)} = \left(\int\limits_\Omega u^2 dxdy + \int\limits_\Omega |\nabla u|^2 dxdy \right)^{1/2}.$$

Let's consider the space of traces of functions from $W_2^1(\Omega)$ and traces functions on $\partial\Omega$ and denote this space by $W_2^{1/2}(\partial\Omega)$ with the norm

$$\|u\|_{W_2^{1/2}(\partial\Omega)} = \left(\int\limits_{\partial\Omega} u^2 ds + \int\limits_{\partial\Omega} \int\limits_{\partial\Omega} \frac{|u(z) - u(h)|^2}{|z-h|^2} dsds \right)^{1/2}, \tag{17}$$

where $z = (x, y)$, $h = (u, v)$.

Restriction functions from $W_2^{1/2}(\partial\Omega)$ on the part of the border Γ_0 (Γ_{02}, Γ_1) we denote by $W_2^{1/2}(\Gamma_0)$, $\left(W_2^{1/2}(\Gamma_{02}), W_2^{1/2}(\Gamma_1)\right)$ with norm (17) where $\partial\Omega$ is replaced with Γ_0 (Γ_{02}, Γ_1).

We give the definition of a generalized solution to the direct problem (12) - (16).

Definition 1. Let $\varphi \in W_2^{1/2}(\Gamma_{02})$ and $q \in \left(W_2^{1/2}(\Gamma_1)\right)^*$. The set of functions (u, p) where $u \in W_2^1(\Omega)$, $p \in L_2(\Omega)$, is called the generalized solution to the direct problem (12) - (16), if the following conditions hold: $div\, u = 0$, (8) and for any $v = (v_1, v_2)$ such that $v \in W_2^1(\Omega)$ and $v|_{\Gamma_0} = 0$, satisfies the equality

$$-\int\limits_{\Omega} [u_{1x}v_{1x} + u_{2x}v_{2x} + u_{1y}v_{1y} + u_{2y}v_{2y} - p(v_{1x} + v_{2y})]\, dxdy + \\ + \int\limits_0^1 [q_1(y)v_1(1, y) + q_2(y)v_2(1, y)]dy = 0. \tag{18}$$

The direct problem (12) - (16) in the sense of the definition of the generalized solution is well-posed [2,3].

3 The inverse problem to the direct problem

Suppose that additional information is given about the solution to the direct problem (12) - (16) on the boundary Γ_0

$$\Gamma_{01}: \quad \begin{cases} u_{1y}(x, 0) = f_1(x, 0), \ x \in (0, 1), \\ -p(x, 0) + u_{2y}(x, 0) = f_2(x, 0), \ x \in (0, 1), \end{cases} \tag{19}$$

$$\Gamma_{02}: \quad \begin{cases} -p(0, y) + u_{1x}(0, y) = f_1(0, y), \ y \in (0, 1), \\ u_{2x}(0, y) = f_2(0, y), \ y \in (0, 1), \end{cases} \tag{20}$$

$$\Gamma_{03}: \quad \begin{cases} -u_{1y}(x, 1) = f_1(x, 1), \ x \in (0, 1), \\ p(x, 1) - u_{2y}(x, 1) = f_2(x, 1), \ x \in (0, 1). \end{cases} \tag{21}$$

The inverse problem. The inverse problem to the direct problem (12) - (16) is concluded in finding unknown function $q = (q_1(y), q_2(y))$ from the additional information (19) - (21).

We consider the operator

$$A: \quad q := (pn - \frac{\partial u}{\partial n})|_{\Gamma_1} \to f := (pn - \frac{\partial u}{\partial n})|_{\Gamma_0},$$

where (u, p) is a solution to the problem (12) - (16). Then the inverse problem (12) - (16), (19) - (21) can be written in the operator form

$$Aq = f, \tag{22}$$

where $A: \left(W_2^{1/2}(\Gamma_1)\right)^* \to \left(W_2^{1/2}(\Gamma_0)\right)^*$, $f = (f_1, f_2)$ is given function, $q = (q_1, q_2)$ - unknown function.

Let's write in the coordinate form

$$q_1(y) := p(1, y) - u_{1x}(1, y), \ \ y \in (0, 1), \ \ (\Gamma_1) \tag{23}$$

$$q_2(y) := -u_{2x}(1,y),\ \ y \in (0,1),\ \ (\Gamma_1) \tag{24}$$

$$(Aq_1)(x,y) = \begin{cases} u_{1y}(x,0),\ \ x \in (0,1),\ \ (\Gamma_{01}) \\ -p(0,y) + u_{1x}(0,y),\ \ y \in (0,1),\ \ (\Gamma_{02}) \\ -u_{1y}(x,1),\ \ x \in (0,1),\ \ (\Gamma_{03}) \end{cases} \tag{25}$$

$$(Aq_2)(x,y) = \begin{cases} -p(x,0) + u_{2y}(x,0),\ \ x \in (0,1),\ \ (\Gamma_{01}) \\ u_{2x}(0,y),\ \ y \in (0,1),\ \ (\Gamma_{02}) \\ p(x,1) - u_{2y}(x,1),\ \ x \in (0,1),\ \ (\Gamma_{03}) \end{cases} \tag{26}$$

here (u,p) is a solution to the direct problem (12) - (16).

To solve the equation (22) we apply the optimization method.

Consider the functional

$$J(q) = \|Aq - f\|^2_{L_2(\Gamma_0)} = \|Aq_1 - f_1\|^2_{L_2(\Gamma_0)} + \|Aq_2 - f_2\|^2_{L_2(\Gamma_0)}.$$

or

$$J(q_1,q_2) = \int_0^1 (u_{1y}(x,0) - f_1(x,0))^2 dx + \int_0^1 (-p(0,y) + u_{1x}(0,y) - f_1(0,y))^2 dy +$$

$$+ \int_0^1 (u_{1y}(x,1) + f_1(x,1))^2 dx + \int_0^1 (-p(x,0) + u_{2y}(x,0) - f_2(x,0))^2 dx +$$

$$+ \int_0^1 (u_{2x}(0,y) - f_2(0,y))^2 dy + \int_0^1 (p(x,1) - u_{2y}(x,1) - f_2(x,1))^2 dx.$$

We will solve the the problem (22) by minimizing the functional $J(q)$.

4 The adjoint problem

To apply the optimization method for solving the equation (22) let's consider the adjoint problem to the problem (12) - (16)

$$\Delta\psi_1 - \pi_x = 0,\ (x,y) \in \Omega, \tag{27}$$

$$\Delta\psi_2 - \pi_y = 0,\ (x,y) \in \Omega, \tag{28}$$

$$\psi_{1x} + \psi_{2y} = 0,\ (x,y) \in \Omega \tag{29}$$

with the following boundary conditions

$$\psi_1(x,y) = \mu_1(x,y),\ (x,y) \in \Gamma_0, \tag{30}$$

$$\psi_2(x,y) = \mu_2(x,y),\ (x,y) \in \Gamma_0, \tag{31}$$

$$\Gamma_1: \quad \begin{cases} \pi(1,y) - \psi_{1x}(1,y) = 0, \ y \in (0,1), \\ \psi_{2x}(1,y) = 0, \ y \in (0,1). \end{cases} \tag{32}$$

Definition 2. Let $\mu \in W_2^{1/2}(\Gamma_0)$. The set of functions (ψ, π), where $\psi = (\psi_1, \psi_2) \in W_2^1(\Omega)$, $\psi(x,y) \mid_{\Gamma_0} = \mu$, $\pi \in L_2(\Omega)$, will be called a generalized solution to the adjoint problem (27) - (32) if for any $v = (v_1, v_2)$ such that $v \in W_2^1(\Omega)$ и $v|_{\Gamma_0} = 0$, satisfies the equality

$$\int\limits_{\Omega} \left[\psi_{1x} v_{1x} + \psi_{2x} v_{2x} + \psi_{1y} v_{1y} + \psi_{2y} v_{2y} - \pi(v_{1x} + v_{2y})\right] dxdy = 0. \tag{33}$$

It is shown that the gradient of the functional $J(q)$ has the form

$$J'(q) = (J'_{q_1}(q), J'_{q_2}(q)),$$
$$J'_{q_1}(q) = \psi_1(x,y) \mid_{\Gamma_1}, J'_{q_2}(q) = \psi_2(x,y) \mid_{\Gamma_1} .$$

Thus $J'(q) = \psi \mid_{\Gamma_1}$, where $\psi(x,y)$ is a first component of the solution to the adjoint problem (27) - (32) such that in the boundary conditions (30), (31) the function $\mu(x,y)$ has the form

$$\mu(x,y) = 2\left[Aq - f\right](x,y), \ (x,y) \in \Gamma_0.$$

5 Computational algorithm for the inverse problem soluton

As an optimization method, we consider the method of Landweber

$$\begin{gathered} q_{n+1} = \ q_n - \ \alpha \ J' q_n, \\ q_0 \in \left(W_2^{1/2}(\Gamma_1)\right)^*, \quad \alpha \in \left(0, \|A\|^{-2}\right), \end{gathered} \tag{34}$$

where $q_n = (q_1^{(n)}, q_2^{(n)})$.

We give computational algorithm of the Landweber method:

1. We set the initial approximation $q_0 = (q_1^{(0)}, q_2^{(0)})$.
2. Suppose that q_n is known, we find the first component $u_n = (u_1^{(n)}, u_2^{(n)})$ of the generalized solution to the direct problem (12) - (16).
3. We find the first component $\psi_n(x,y) = (\psi_1^{(n)}, \psi_2^{(n)})$ of the generalized solution to the adjoint problem (27) - (32) with $\mu(x,y) = 2[Aq - f](x,y)$, $(x,y) \in \Gamma_0$.
4. We calculate the value of the functional $J(q_n) = \|Aq_n - f\|^2_{L_2(\Gamma_0)}$. If the functional $J(q_n)$ is not enough small, then we find the gradient of the functional $J'(q_n) = \psi_n \mid_{\Gamma_1}$.
5. We calculate the next approximation $q_{n+1} = q_n - \alpha J' q_n$.

The convergence of the above computational algorithm is proved similarly [1].

Theorem *(on the convergence with respect to the functional of Landweber's method)* Let $A : \left(W_2^{1/2}(\Gamma_1)\right)^* \to \left(W_2^{1/2}(\Gamma_0)\right)^*$ be the bounded linear operator. Assume that the problem $Aq = f$ with $f \in \left(W_2^{1/2}(\Gamma_0)\right)^*$ has an exact solution $q_e \in L_2(\Omega)$. Then, for any $q_0 \in \left(W_2^{1/2}(\Gamma_1)\right)^*$ and $\alpha \in \left(0, \|A\|^{-2}\right)$ the sequence q_n is defined by the equality

$$q_{n+1} = \ q_n - \ \alpha \ J' q_n, \ \ q_0 \in \left(W_2^{1/2}(\Gamma_1)\right)^*,$$

and converges with respect to the functional, and the estimate

$$J(q_n) \leq \frac{\|q_0 - q_T\|^2}{n\alpha(1 - \alpha\|A\|^2)}$$

holds.

From the algorithm of the Landweber method it can be seen that for the calculation of the approximate solution q_n for each n is necessary to solve the direct problem (12) - (16) and the adjoint problem (27) - (32). To solve the last problems we apply the finite element method [4].

The method of the finite elements (MFE). We illustrate a finite element method as an example of the direct problem. Consider MFE in the case piecewise-linear functions in the triangles. We perform triangulation of the given domain Ω, triangular grid cells are triangles.

Let's consider any triangle with given tops $P_0(x_0, y_0)$, $P_1(x_1, y_1)$, $P_2(x_2, y_2)$:
$\tau = \{(x, y) = P_0\lambda_0 + P_1\lambda_1 + P_2\lambda_2 : \quad \lambda_i \geq 0, \quad \lambda_0 + \lambda_1 + \lambda_2 = 1\}$,
$\lambda_i = \lambda_i(x, y), \quad i = 0, 1, 2.$

If we write down $\lambda_0 = 1 - \lambda_1 - \lambda_2$, then

$$\begin{gathered}\tau = \{(x, y) = P_0 + \lambda_1(P_1 - P_0) + \lambda_2(P_2 - P_0) : \ \lambda_i \geq 0, \ \lambda_1 + \lambda_2 \leq 1\}, \\ \lambda_i = \lambda_i(x, y), \quad i = 1, 2.\end{gathered} \tag{35}$$

From (35) we find

$$\lambda_1(x, y) = \frac{(x - x_0)(y_2 - y_0) - (y - y_0)(x_2 - x_0)}{\triangle},$$

$$\lambda_2(x.y) = \frac{(y - y_0)(x_1 - x_0) - (x - x_0)(y_1 - y_0)}{\triangle},$$

where $\triangle = (x_1 - x_0)(y_2 - y_0) - (y_1 - y_0)(x_2 - x_0)$.

On the triangle τ we consider linear function

$$v(x, y) = v_0 + \lambda_1(x, y)(v_1 - v_0) + \lambda_2(x, y)(v_2 - v_0), \ for\ any\ (x, y) \in \tau, \tag{36}$$

where $v(x, y) = (v_1(x, y), v_2(x, y))$, $v_0 = (v_1^{(0)}, v_2^{(0)})$, $v_1 = (v_1^{(1)}, v_2^{(1)})$, $v_2 = (v_1^{(2)}, v_2^{(2)})$.

The function $v(x, y)$ is determined uniquely by its values $v_0 = v(P_0)$, $v_1 = v(P_1)$, $v_2 = v(P_2)$.

Further, the domain of integration in equation (18) is a union of triangles, subintegral functions are replaced on the type formulas (36). We note that for the scalar function p in (36) we must take the scalar function.

6 Numerical results

For the numerical solution of direct and adjoint problems the finite element method was used, the number of the partition sides of the domain $n = 30$.

As a zero approximation of the inverse problem (22) is taken $q_{(1)0} = 0, q_{(2)0} = 0$. In the Landweber method parameter $\alpha = 0.01$. Fig. 1-Fig. 3 show the components of the exact solution to the direct problem (12) - (16). Fig. 4-Fig. 6 shows the components of the zero approximation to the direct problem (12) - (16). Fig. 7-Fig. 9 shows the components of an approximate solution to the direct problem at 1200 iterations. Fig. 10, Fig. 11 illustrate the error rate and the pressure p in the grid analog norm of the norm in $L_2(\Gamma_1)$, where the horizontal axis - iteration, vertical axis - error. Fig. 12, Fig. 13 show the components of the exact solution of the inverse problem

(22). Fig. 14, Fig. 15 show the components of the approximate solution at 1200 iterations of the inverse problem (22), and Fig. 16 – error q approximate solution of the inverse problem, where the horizontal axis - iteration, vertical axis- error. Fig. 17 shows the residual (the functional J) of the inverse problem (22), and the horizontal axis - iteration, vertical axis - residual.

7 Conclusion

It is shown that ill-posed problem to the Stokes equations is reduced to the inverse problem with respect to well-posed problem to the original equations. The inverse problem is solved numerically using a combination of optimization method and the finite element method. The estimate of convergence rate of the algorithm with respect to the functional was obtained.

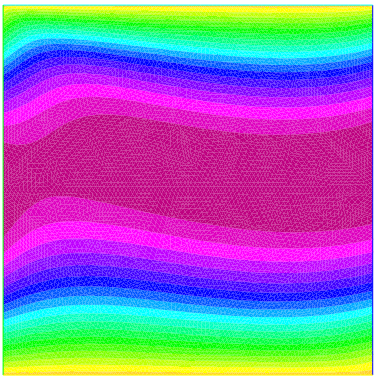

Fig. 1. The exact solution of the direct problem. Velocity $u_{(1)}$.

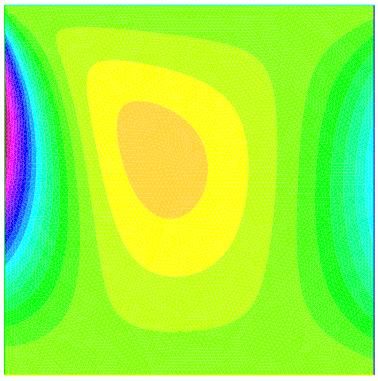

Fig. 2. The exact solution of the direct problem. Velocity $u_{(2)}$.

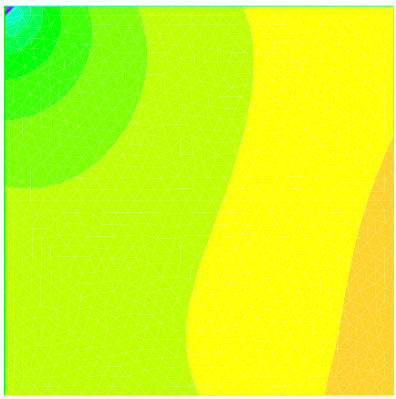

Fig. 3. The exact solution of the direct problem.Pressure p.

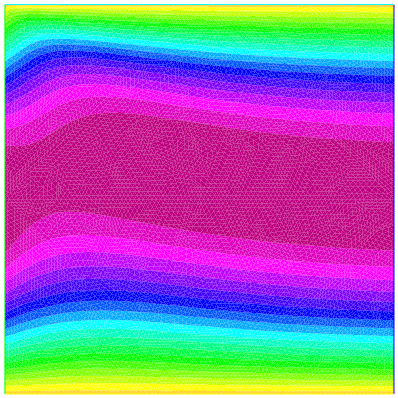

Fig. 4. The zero approximation to the solution of the direct problem. Velocity $u_{(1)0}$.

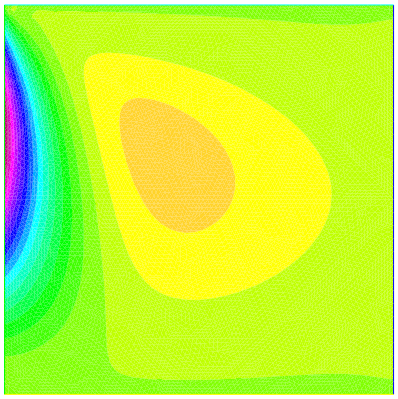

Fig. 5. The zero approximation to the solution of the direct problem. Velocity $u_{(2)0}$.

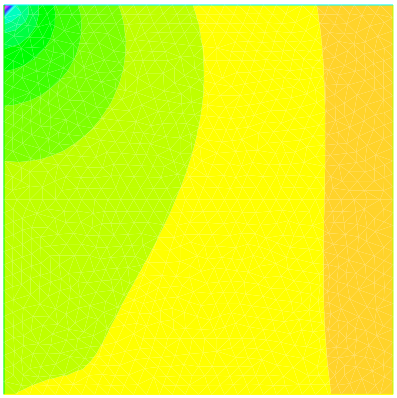

Fig. 6. The zero approximation to the solution of the direct problem. Pressure $p_{(0)}$.

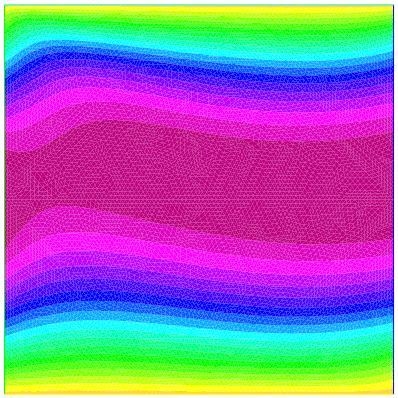

Fig. 7. The approximate solution of the direct problem. Velocity $u_{(1)}$.

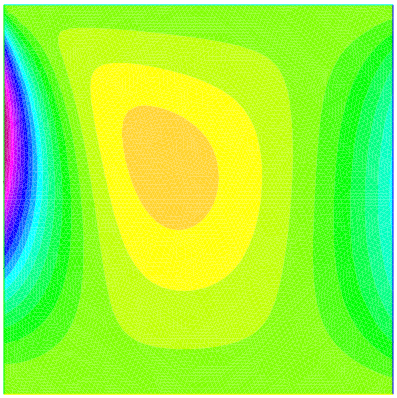

Fig. 8. The approximate solution of the direct problem. Velocity $u_{(2)}$.

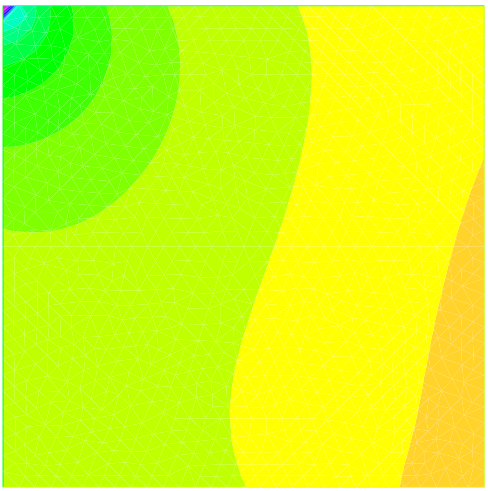

Fig. 9. The approximate solution of the direct problem. Pressure p.

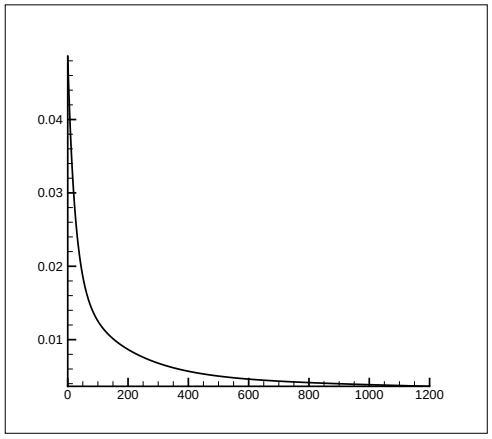

Fig. 10. The error rate on the number of iterations of u.

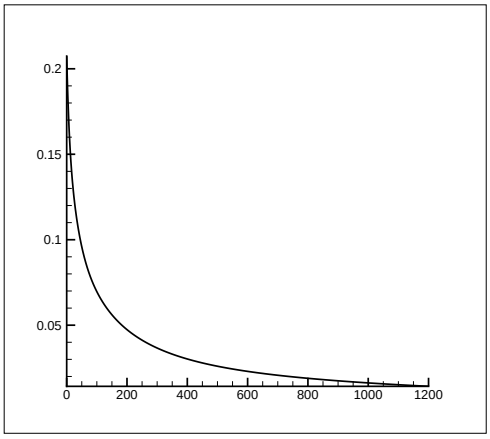

Fig. 11. The error of the pressure on the number of iterations.

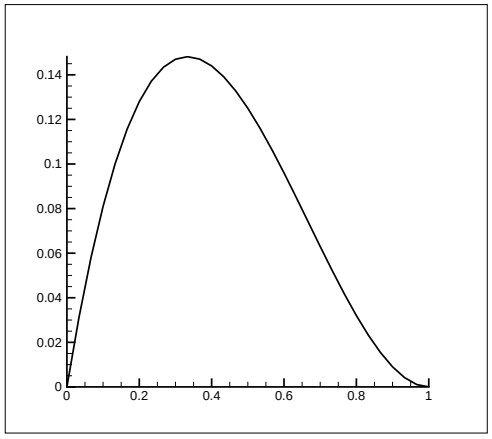

Fig. 12. The exact solution of the inverse problem. The first component q_1.

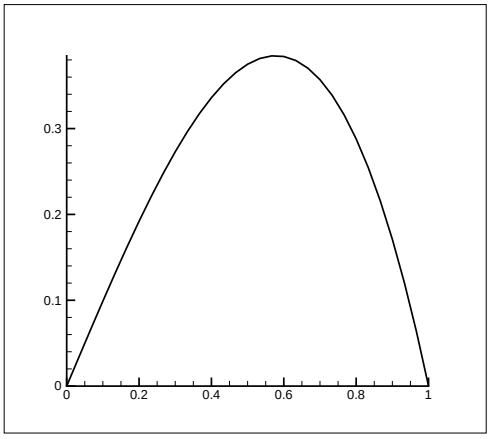

Fig. 13. The exact solution of the inverse problem. The second component q_2.

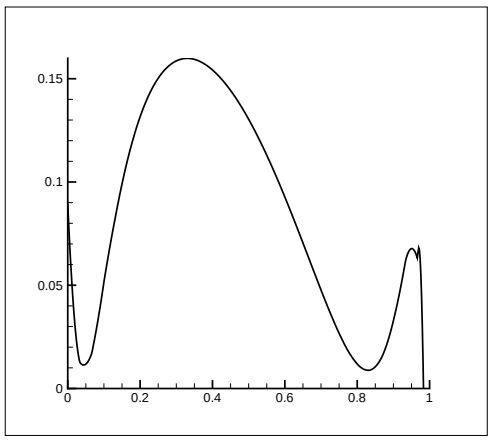

Fig. 14. The approximate solution of the inverse problem. The first component q_1.

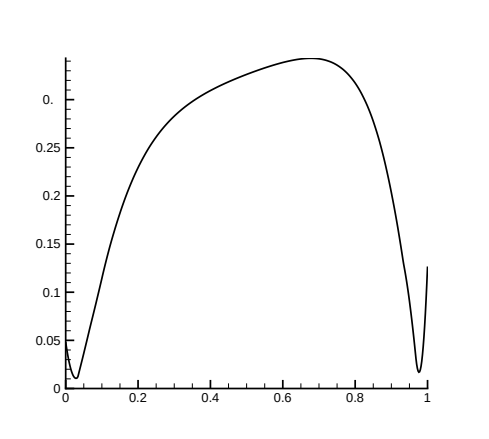

Fig. 15. The approximate solution of the inverse problem. The second component q_2.

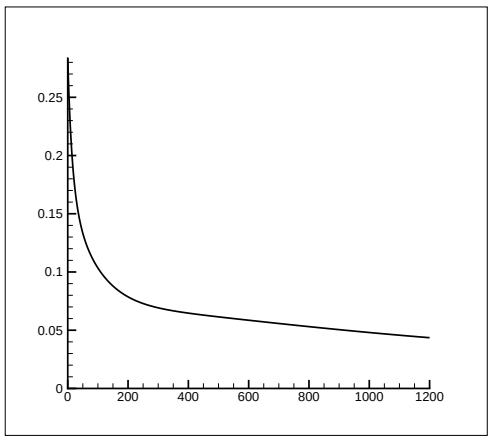

Fig. 16. The error of the approximate solution q_n on the number of iterations.

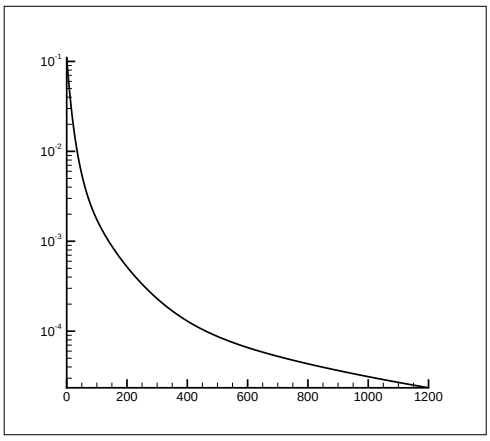

Fig. 17. The residual on the number of iterations (functional $J(q_n) = \|Aq_n - f\|^2$).

References

1. Kabanikhin, S.I.: Inverse and Ill-Posed Problems. Theory and Applications. De Gruyter, Germany (2011)
2. Ladyzhenskaja, O.A.: Matematicheskie voprosy dinamiki vjazkoj neszhimaemoj zhidkosti. Gosudarstvennoe izdatel'stvo fizko-matematicheskoj literatury. Moscow (1961)
3. Bastay, G., Johansson, T., Lesnik, D., Kozlov, K.: An Alternating Method for the Stationary Stokes System. ZAMM (Z. Angew. Math. Mech). 86, 268–280 (2006)
4. Segerlind,Larry J.: Applied finite element analysis. New York (1984)

Bending Vibration of Drill String

Askar Ibrayev[1], Abibulla Tyurekhodjayev[2]

[1]Eurasian National University named after L.N. Gumilev, Astana, Kazakhstan
[2]Kazakh National Technical University named after K.I. Satpayev, Almaty, Kazakhstan
askar.ibrayev@gmail.com,tyurekhodja@mail.ru

Abstract. The analytical solution of the bending vibration of drill string is obtained by using of the method of partial sampling of Tyurehodzhaev A.N., an. Obtained general solutions of the differential equation of bending and transverse vibrations of drill strings are used in practice, for example, in solving problems related oilfield business.

Keywords: Drill string, bending and transverse vibrations, drilling

1 Introduction

One of the important problems of the modern oil and gas production is to achieve of oil and gas pool by drilling wells. Bending and transverse vibration of the drill string is appeared during the drilling, which leads to wear and breakage of the drilling equipment.

In paper [1] the mathematical models of complex mechatronic drilling rig is constructed, drill string makes bending and torsional vibrations by the following power and resistance modulus. The investigated stability of the drill string is given in accordance with direct method of Lyapunov. Domain of stability is determined depending on the parameters of the drill string.

In paper [2] the computer simulation of phenomena of free bending vibrations of extreme length drill string is realized. The frequencies of the vibrations relative to the fixed and movable coordinate system at various characteristics of geometrical and physical parameters of the column are determined.

In this paper, analytical solution of bending and transverse vibrations of drill string is obtained by the method of partial discretization of nonlinear differential equations constructed by Tyurekhodjayev.

2 Problem statement

The equation of bending and transverse vibrations of drill string has the following form:

$$EJ\frac{\partial^4 y(x,t)}{\partial x^4}+\frac{\partial}{\partial x}\left[(F-p\,x)\frac{\partial y(x,t)}{\partial x}\right]+m\frac{\partial^2 y(x,t)}{\partial t^2}=0 \tag{1}$$

where $F=p\,l$, l – drill string length, p, m – weight and mass of the unit of drill string length.

Initial and boundary conditions:

$$t=0,\quad y(x,0)=\alpha(x),\quad \frac{\partial y(x,0)}{\partial t}=\gamma(x). \tag{2}$$

Boundary conditions can be written in the general form:

$$y(0,t)=f_1(t),\quad \frac{\partial y}{\partial x}(0,t)=f_2(t),\quad y(L,t)=f_3(t),\quad \frac{\partial^2 y}{\partial x^2}(L,t)=f_4(t). \tag{3}$$

3 Results and discussions

Differential equations with partial derivatives (1) can be written as follows:

$$\frac{\partial^4 y(x,t)}{\partial x^4} + \frac{p(L-x)}{EJ}\frac{\partial^2 y(x,t)}{\partial x^2} - \frac{p}{EJ} + \frac{m}{EJ}\frac{\partial y(x,t)}{\partial t^2} = 0. \tag{4}$$

Applying the Laplace-Carson integral transformation with respect to t to differential equations with partial derivatives (4) with taking into account the initial conditions (2) give it to an ordinary differential equation of the following form:

$$\frac{d^4\bar{y}(x,s)}{dx^4} + \frac{p(L-x)}{EJ}\frac{d^2\bar{y}(x,s)}{dx^2} - \frac{p}{EJ}\frac{d\bar{y}(x,s)}{dx} + \frac{m}{EJ}s^2\bar{y}(x,s) - s\cdot\bar{y}(x,0) - \bar{y}_s(x,0) = 0 \tag{5}$$

Applying to the equation (5) method of partial discretization of Tyurekhodjayev [3], we obtain:

$$\begin{aligned}\frac{d^4\bar{y}(x,s)}{dx^4} = -\frac{1}{2}\sum_{k=1}(x_k + x_{k+1})\Bigg\{\left[\frac{p(L-x)}{EJ}\frac{d^2\bar{y}(x,s)}{dx^2} - \frac{p}{EJ}\frac{d\bar{y}(x,s)}{dx} + \frac{m}{EJ}s^2\bar{y}(x,s)\right]\delta(x-x_k) - \\ \left[\frac{p(L-x_{k+1})}{EJ}\frac{d^2\bar{y}(x_{k+1},s)}{dx^2} - \frac{p}{EJ}\frac{d\bar{y}(x_{k+1},s)}{dx} + \frac{m}{EJ}s^2\bar{y}(x_{k+1},s)\right]\delta(x-x_{k+1})\Bigg\} + \\ + s\cdot\alpha(x) + \gamma(x),\end{aligned} \tag{6}$$

where $\delta(\xi)$ - delta function of Dirac.

Quadruply integrate equation (6) with respect to x:

$$\begin{aligned}\frac{d^3\bar{y}(x,s)}{dx^3} = -\frac{1}{2}\sum_{k=1}(x_k + x_{k+1})\Bigg\{\left[\frac{p(L-x)}{EJ}\frac{d^2\bar{y}(x,s)}{dx^2} - \frac{p}{EJ}\frac{d\bar{y}(x,s)}{dx} + \frac{m}{EJ}s^2\bar{y}(x,s)\right]H(x-x_k) - \\ \left[\frac{p(L-x_{k+1})}{EJ}\frac{d^2\bar{y}(x_{k+1},s)}{dx^2} - \frac{p}{EJ}\frac{d\bar{y}(x_{k+1},s)}{dx} + \frac{m}{EJ}s^2\bar{y}(x_{k+1},s)\right]H(x-x_{k+1})\Bigg\} + \\ + s\cdot\alpha_1(x) + \gamma_1(x) + A(s)\end{aligned} \tag{7}$$

$$\begin{aligned}\frac{d^2\bar{y}(x,s)}{dx^2} = -\frac{1}{2}\sum_{k=1}(x_k + x_{k+1})\times\Bigg\{\left[\frac{p(L-x)}{EJ}\frac{d^2\bar{y}(x,s)}{dx^2} - \frac{p}{EJ}\frac{d\bar{y}(x,s)}{dx} + \frac{m}{EJ}s^2\bar{y}(x,s)\right] \\ (x-x_k)H(x-x_k) - \left[\frac{p(L-x_{k+1})}{EJ}\frac{d^2\bar{y}(x_{k+1},s)}{dx^2} - \frac{p}{EJ}\frac{d\bar{y}(x_{k+1},s)}{dx} + \frac{m}{EJ}s^2\bar{y}(x_{k+1},s)\right] \\ (x-x_{k+1})H(x-x_{k+1})\Bigg\} + s\cdot\alpha_2(x) + \gamma_2(x) + A(s) + B(s).\end{aligned} \tag{8}$$

$$\begin{aligned}\frac{d\bar{y}(x,s)}{dx} = -\frac{1}{4}\sum_{k=1}(x_k + x_{k+1})\times\Bigg\{\left[\frac{p(L-x)}{EJ}\frac{d^2\bar{y}(x,s)}{dx^2} - \frac{p}{EJ}\frac{d\bar{y}(x,s)}{dx} + \frac{m}{EJ}s^2\bar{y}(x,s)\right] \\ (x-x_k)^2H(x-x_k) - \left[\frac{p(L-x_{k+1})}{EJ}\frac{d^2\bar{y}(x_{k+1},s)}{dx^2} - \frac{p}{EJ}\frac{d\bar{y}(x_{k+1},s)}{dx} + \frac{m}{EJ}s^2\bar{y}(x_{k+1},s)\right] \\ (x-x_{k+1})^2H(x-x_{k+1})\Bigg\} + s\cdot\alpha_3(x) + \gamma_3(x) + \frac{1}{2}A(s)x^2 + B(s)x + C(s),\end{aligned} \tag{9}$$

$$\bar{y}(x,s) = -\frac{1}{12}\sum_{k=1}(x_k + x_{k+1})\times$$
$$\left\{\left[\frac{p(L-x)}{EJ}\frac{d^2\bar{y}(x,s)}{dx^2} - \frac{p}{EJ}\frac{d\bar{y}(x,s)}{dx} + \frac{m}{EJ}s^2\bar{y}(x,s)\right](x-x_k)^3 H(x-x_k) -\right.$$
$$\left.\left[\frac{p(L-x_{k+1})}{EJ}\frac{d^2\bar{y}(x_{k+1},s)}{dx^2} - \frac{p}{EJ}\frac{d\bar{y}(x_{k+1},s)}{dx} + \frac{m}{EJ}s^2\bar{y}(x_{k+1},s)\right](x-x_{k+1})^3 H(x-x_{k+1})\right\}+$$
$$+ s\cdot\alpha_4(x) + \gamma_4(x) + \frac{1}{6}A(s)x^3 + \frac{1}{2}B(s)x^2 + C(s)x + D(s), \tag{10}$$

where

$$\begin{aligned}
\alpha_1(x) &= \int \alpha(x)dx, \qquad \gamma_1(x) = \int \gamma(x)dx,\\
\alpha_2(x) &= \int \alpha_1(x)dx, \qquad \gamma_2(x) = \int \gamma_1(x)dx,\\
\alpha_3(x) &= \int \alpha_2(x)dx, \qquad \gamma_3(x) = \int \gamma_2(x)dx,\\
\alpha_4(x) &= \int \alpha_3(x)dx, \qquad \gamma_4(x) = \int \gamma(x)_3dx,
\end{aligned} \tag{11}$$

$H(\zeta)$ - unit function of Heaviside.
Introduce the following notations:

$$q_k(s) = \textstyle\sum_{k=1}(x_k + x_{k+1})\left[\frac{p(L-x_k)}{EJ}\frac{d^2\bar{y}(x,s)}{dx^2} - \frac{p}{EJ}\frac{d\bar{y}(x,s)}{dx} + \frac{m}{EJ}s^2\bar{y}(x,s)\right],$$
$$q_{k+1}(s) = \textstyle\sum_{k=1}(x_k + x_{k+1})\left[\frac{p(L-x_{k+1})}{EJ}\frac{d^2\bar{y}(x_{k+1},s)}{dx^2} - \frac{p}{EJ}\frac{d\bar{y}(x_{k+1},s)}{dx} + \frac{m}{EJ}s^2\bar{y}(x_{k+1},s)\right]. \tag{12}$$

Boundary conditions (3) reduces to

$$y(0,s) = f_1(s), \quad \frac{\partial y}{\partial x}(0,s) = f_2(s), \quad y(L,s) = f_3(s), \quad \frac{\partial^2 y}{\partial x^2}(L,s) = f_4(s). \tag{13}$$

Equations (7) - (10) with taking into account (11), (12) can be written as follows:

$$\begin{cases}
\bar{y}'''(x,s) = -\frac{1}{2}q_k(s)H(x-x_k) + \frac{1}{2}q_{k+1}(s)H(x-x_{k+1}) + s\cdot\alpha_1(x) + \gamma_1(x) + A(s)\\
\bar{y}''(x,s) = -\frac{1}{2}q_k(s)(x-x_k)H(x-x_k) + \frac{1}{2}q_{k+1}(s)(x-x_{k+1})H(x-x_{k+1}) +\\
+s\cdot\alpha_2(x) + \gamma_2(x) + x\cdot A(s) + B(s)\\
\bar{y}'(x,s) = -\frac{1}{4}q_k(s)(x-x_k)^2H(x-x_k) + \frac{1}{4}q_{k+1}(s)(x-x_{k+1})^2H(x-x_{k+1}) +\\
+s\cdot\alpha_2(x) + \gamma_2(x) + \frac{x^2}{2}x\cdot A(s) + x\cdot B(s) + C(s)\\
\bar{y}(x,s) = -\frac{1}{12}q_k(s)(x-x_k)^3H(x-x_k) + \frac{1}{12}q_{k+1}(s)(x-x_{k+1})^3H(x-x_{k+1}) +\\
+\frac{x^3}{6}x\cdot A(s) + x\cdot B(s) + x\cdot C(s)
\end{cases} \tag{14}$$

Taking into account (12) from (14) we obtain the following expression:

$$\begin{aligned}
&\bar{y}'''(x,s) = -\frac{1}{2EJ}\sum_{k=1}(x_k + x_{k+1})\left\{[p(L-x_k)\bar{y}''(x_k,s) - p\bar{y}'(x_k,s) + ms^2\bar{y}(x_k,s)] \times\right.\\
&\left.\times H(x-x_k) - [p(L-x_{k+1})\bar{y}''(x_{k+1},s) - p\bar{y}'(x_{k+1},s) + ms^2\bar{y}(x_{k+1},s)]H(x-x_{k+1})\right\} +\\
&+s\cdot\alpha_1(x) + \gamma_1(x) + A(s)\\
&\bar{y}''(x,s) = -\frac{1}{2EJ}\sum_{k=1}(x_k + x_{k+1})\left\{[p(L-x_k)\bar{y}''(x_k,s) - p\bar{y}'(x_k,s) + ms^2\bar{y}(x_k,s)](x-x_k) \times\right.\\
&\left.\times H(x-x_k) - [p(L-x_{k+1})\bar{y}''(x_{k+1},s) - p\bar{y}'(x_{k+1},s) + ms^2\bar{y}(x_{k+1},s)](x-x_{k+1})\right\} +\\
&H(x-x_{k+1}) + s\cdot\alpha_2(x) + \gamma_2(x) + x\cdot A(s) + B(s)\\
&\bar{y}'(x,s) = -\frac{1}{4EJ}\sum_{k=1}(x_k + x_{k+1})\left\{[p(L-x_k)\bar{y}''(x_k,s) - p\bar{y}'(x_k,s) + ms^2 2\bar{y}(x_k,s)](x-x_k)^2 \times\right.\\
&\left.\times H(x-x_k) - [p(L-x_{k+1})\bar{y}''(x_{k+1},s) - p\bar{y}'(x_{k+1},s) + ms^2\bar{y}(x_{k+1},s)](x-x_{k+1})^2\right\} +\\
&H(x-x_{k+1}) + s\cdot\alpha_3(x) + \gamma_3(x) + \frac{x^2}{2}A(s) + x\cdot B(s) + C(s)
\end{aligned} \tag{15}$$

$$\begin{aligned}
&\bar{y}(x,s) = -\frac{1}{12EJ}\sum_{k=1}(x_k + x_{k+1})\left\{[p(L-x_k)\bar{y}''(x_k,s) - p\bar{y}'(x_k,s) + ms^2\bar{y}(x_k,s)](x-x_k)^2 \times\right.\\
&\left.\times H(x-x_k) - [p(L-x_{k+1})\bar{y}''(x_{k+1},s) - p\bar{y}'(x_{k+1},s) + ms^2\bar{y}(x_{k+1},s)](x-x_{k+1})^2\right\} +\\
&H(x-x_{k+1}) + s\cdot\alpha_3(x) + \gamma_3(x) + \frac{x^3}{6}A(s) + \frac{x^2}{2}B(s) + x\cdot C(s) + D(s)
\end{aligned}$$

From the equations (15) obtain system of equations relative to $\bar{y}'''(x,s)$, $\bar{y}''(x,s)$, $\bar{y}'(x,s)$ and $\bar{y}(x,s)$ the same for each point of x_k . Determine for the point x_1, $(x_1 < x < x_2)$, $x = z_1 = \dfrac{x_1 + x_2}{2}$

$$\begin{cases}
\bar{y}'''(x,s) = -\dfrac{1}{2EJ}(x_1+x_2)[p(L-x_1)\bar{y}''(x_1,s) - p\bar{y}'(x_1,s) + ms^2\bar{y}(x_1,s)] +\\
+s\cdot\alpha_1(z_1) + \gamma_1(z_1) + A(s),\\
\bar{y}''(x,s) = -\dfrac{1}{2EJ}(x_1+x_2)[p(L-x_1)\bar{y}''(x_1,s) - p\bar{y}'(x_1,s) + ms^2\bar{y}(x_1,s)](z_1-x_1) +\\
+s\cdot\alpha_2(z_1) + \gamma_2(z_1) + z_1\cdot A(s) + B(s),\\
\bar{y}'(x,s) = -\dfrac{1}{4EJ}(x_1+x_2)[p(L-x_1)\bar{y}''(x_1,s) - p\bar{y}'(x_1,s) + ms^2\bar{y}(x_1,s)](z_1-x_1)^2 +\\
+s\cdot\alpha_3(z_1) + \gamma_3(z_1) + \dfrac{z_1^2}{2}A(s) + z_1\cdot B(s) + C(s),\\
\bar{y}(x,s) = -\dfrac{1}{12EJ}[p(L-x_1)\bar{y}''(x_1,s) - p\bar{y}'(x_1,s) + ms^2\bar{y}(x_1,s)](z_1-x_1)^3 +\\
+s\cdot\alpha_4(z_1) + \gamma_4(z_1) + \dfrac{z_1^3}{6}A(s) + \dfrac{z_1^2}{2}B(s) + z_1\cdot C(s) + D(s),
\end{cases} \tag{16}$$

Equation (16) can be reduced to the form of the system of linear algebraic equations with four unknowns $\bar{y}'''(x_1,s)$, $\bar{y}''(x_1,s)$, $\bar{y}'(x_1,s)$ and $\bar{y}(x_1,s)$

$$\begin{cases} a_{11}\bar{y}'''(x_1,s)+b_{11}\bar{y}''(x_1,s)+c_{11}\bar{y}'(x_1,s)+d_{11}\bar{y}(x_1,s)=e_{11} \\ b_{21}\bar{y}''(x_1,s)+c_{21}\bar{y}'(x_1,s)+d_{21}\bar{y}(x_1,s)=e_{21} \\ b_{31}\bar{y}''(x_1,s)+c_{31}\bar{y}'(x_1,s)+d_{31}\bar{y}(x_1,s)=e_{31} \\ b_{41}\bar{y}''(x_1,s)+c_{41}\bar{y}'(x_1,s)+d_{41}\bar{y}(x_1,s)=e_{41}. \end{cases} \tag{17}$$

Where

$$\begin{aligned} a_{11} &= 1, \\ b_{11} &= \frac{p}{2EJ}(x_1+x_2)(L-x_1), \\ b_{21} &= 1+\frac{p}{2EJ}(x_1+x_2)(L-x_1)(z_1-x_1), \\ b_{31} &= \frac{p}{4EJ}(x_1+x_2)(L-x_1)(z_1-x_1)^2, \\ b_{41} &= \frac{p}{12EJ}(x_1+x_2)(L-x_1)(z_1-x_1)^3, \\ c_{11} &= -\frac{p}{2EJ}(x_1+x_2), \\ c_{21} &= -\frac{p}{2EJ}(x_1+x_2)(z_1-x_1), \\ c_{31} &= 1-\frac{p}{4EJ}(x_1+x_2)(z_1-x_1)^2, \\ c_{41} &= 1-\frac{p}{12EJ}(x_1+x_2)(z_1-x_1)^3, \\ d_{11} &= \frac{ms^2}{2EJ}(x_1+x_2), \\ d_{21} &= \frac{ms^2}{4EJ}(x_1+x_2)(z_1-x_1), \\ d_{31} &= \frac{ms^2}{4EJ}(x_1+x_2)(z_1-x_1)^2, \\ d_{41} &= 1+\frac{ms^2}{12EJ}(x_1+x_2)(z_1-x_1)^3, \\ e_{11} &= s\cdot\alpha_1(z_1)+\gamma_1(z_1)+A(s), \\ e_{21} &= s\cdot\alpha_2(z_1)+\gamma_2(z_1)+z_1\cdot A(s)+B(s), \\ e_{31} &= s\cdot\alpha_3(z_1)+\gamma_3(z_1)+\frac{z_1^2}{2}A(s)+z_1\cdot B(s)+C(s), \\ e_{41} &= s\cdot\alpha_4(z_1)+\gamma_4(z_1)+\frac{z_1^3}{6}A(s)+\frac{z_1^2}{2}B(s)+z_1\cdot C(s)+D(s). \end{aligned} \tag{18}$$

Further for each point of x_k we obtain the system of linear algebraic equations, which in general terms can be written as follows:

$$\begin{cases} a_{1k}\bar{y}'''(x_k,s)+b_{1k}\bar{y}''(x_k,s)+c_{1k}\bar{y}'(x_k,s)+d_{1k}\bar{y}(x_k,s)=e_{1k} \\ b_{2k}\bar{y}''(x_k,s)+c_{2k}\bar{y}'(x_k,s)+d_{2k}\bar{y}(x_k,s)=e_{2k} \\ b_{3k}\bar{y}''(x_k,s)+c_{3k}\bar{y}'(x_k,s)+d_{3k}\bar{y}(x_1,s)=e_{3k} \\ b_{4k}\bar{y}''(x_k,s)+c_{4k}\bar{y}'(x_k,s)+d_{4k}\bar{y}(x_k,s)=e_{4k}. \end{cases} \tag{19}$$

Find all values of $\bar{y}'''(x_k,s)$, $\bar{y}''(x_k,s)$, $\bar{y}'(x_k,s)$ and $\bar{y}(x_k,s)$, $k=\overline{1,n}$.

$$\bar{y}'''(x_k,s)=\frac{\begin{vmatrix} e_{1k} & b_{1k} & c_{1k} & d_{1k} \\ e_{2k} & b_{2k} & c_{2k} & d_{2k} \\ e_{3k} & b_{3k} & c_{3k} & d_{3k} \\ e_{4k} & b_{4k} & c_{4k} & d_{4k} \end{vmatrix}}{\begin{vmatrix} 1 & b_{1k} & c_{1k} & d_{1k} \\ 0 & b_{2k} & c_{2k} & d_{2k} \\ 0 & b_{3k} & c_{3k} & d_{3k} \\ 0 & b_{4k} & c_{4k} & d_{4k} \end{vmatrix}}, \bar{y}''(x_k,s)=\frac{\begin{vmatrix} 1 & e_{1k} & c_{1k} & d_{1k} \\ 0 & e_{2k} & c_{2k} & d_{2k} \\ 0 & e_{3k} & c_{3k} & d_{3k} \\ 0 & e_{4k} & c_{4k} & d_{4k} \end{vmatrix}}{\begin{vmatrix} 1 & b_{1k} & c_{1k} & d_{1k} \\ 0 & b_{2k} & c_{2k} & d_{2k} \\ 0 & b_{3k} & c_{3k} & d_{3k} \\ 0 & b_{4k} & c_{4k} & d_{4k} \end{vmatrix}},$$

$$\bar{y}'(x_k,s)=\frac{\begin{vmatrix} 1 & b_{1k} & e_{1k} & d_{1k} \\ 0 & b_{2k} & e_{2k} & d_{2k} \\ 0 & b_{3k} & e_{3k} & d_{3k} \\ 0 & b_{4k} & e_{4k} & d_{4k} \end{vmatrix}}{\begin{vmatrix} 1 & b_{1k} & c_{1k} & d_{1k} \\ 0 & b_{2k} & c_{2k} & d_{2k} \\ 0 & b_{3k} & c_{3k} & d_{3k} \\ 0 & b_{4k} & c_{4k} & d_{4k} \end{vmatrix}}, \quad \bar{y}(x_k,s)=\frac{\begin{vmatrix} 1 & b_{1k} & c_{1k} & e_{1k} \\ 0 & b_{2k} & c_{2k} & e_{2k} \\ 0 & b_{3k} & c_{3k} & e_{3k} \\ 0 & b_{4k} & c_{4k} & e_{4k} \end{vmatrix}}{\begin{vmatrix} 1 & b_{1k} & c_{1k} & d_{1k} \\ 0 & b_{2k} & c_{2k} & d_{2k} \\ 0 & b_{3k} & c_{3k} & d_{3k} \\ 0 & b_{4k} & c_{4k} & d_{4k} \end{vmatrix}}, \tag{20}$$

Define the coefficients for the point x_2, $(x_2<x<x_3)$, $x=z_2=\dfrac{x_2+x_3}{2}$

$$\begin{aligned} a_{11}&=1, \\ b_{11}&=\frac{p}{2EJ}(x_2+x_3)(L-x_2), \\ b_{21}&=1+\frac{p}{2EJ}(x_2+x_3)(L-x_2)(z_2-x_2), \\ b_{31}&=\frac{p}{4EJ}(x_2+x_3)(L-x_2)(z_2-x_2)^2, \\ b_{41}&=\frac{p}{12EJ}(x_2+x_3)(L-x_2)(z_2-x_2)^3, \\ c_{11}&=-\frac{p}{2EJ}(x_2+x_3), \\ c_{21}&=-\frac{p}{2EJ}(x_2+x_3)(z_2-x_2), \\ c_{31}&=1-\frac{p}{4EJ}(x_2+x_3)(z_2-x_2)^2, \\ c_{41}&=1-\frac{p}{12EJ}(x_2+x_3)(z_2-x_2)^3, \\ d_{11}&=\frac{ms^2}{2EJ}(x_2+x_3), \\ d_{21}&=\frac{ms^2}{4EJ}(x_2+x_3)(z_2-x_2), \end{aligned} \tag{21}$$

$$d_{31} = \frac{ms^2}{4EJ}(x_2 + x_3)(z_2 - x_2)^2,$$
$$d_{41} = 1 + \frac{ms^2}{12EJ}(x_2 + x_3)(z_2 - x_2)^3,$$
$$e_{11} = s \cdot \alpha_1(z_2) + \gamma_1(z_2) + A(s) -$$
$$-\frac{1}{2EJ}(x_1 + x_2)[p(L - x_1)\bar{y}''(x_1, s) - p\bar{y}'(x_1, s) + ms^2\bar{y}(x_1, s)],$$
$$e_{21} = s \cdot \alpha_2(z_2) + \gamma_2(z_2) + z_2 \cdot A(s) + B(s) -$$
$$-\frac{1}{2EJ}(x_1 + x_2)[p(L - x_1)\bar{y}''(x_1, s) - p\bar{y}'(x_1, s) + ms^2\bar{y}(x_1, s)](z_1 - x_1),$$
$$e_{31} = s \cdot \alpha_3(z_2) + \gamma_3(z_2) + \frac{z_2^2}{2}A(s) + z_2 \cdot B(s) + C(s) -$$
$$-\frac{1}{4EJ}(x_1 + x_2)[p(L - x_1)\bar{y}''(x_1, s) - p\bar{y}'(x_1, s) + ms^2\bar{y}(x_1, s)](z_1 - x_1)^2,$$
$$e_{41} = s \cdot \alpha_4(z_2) + \gamma_4(z_2) + \frac{z_2^3}{6}A(s) + \frac{z_2^2}{2}B(s) + z_2 \cdot C(s) + D(s) -$$
$$-\frac{1}{12EJ}[p(L - x_1)\bar{y}''(x_1, s) - p\bar{y}'(x_1, s) + ms^2\bar{y}(x_1, s)](z_1 - x_1)^3.$$

By mathematical induction we defined the coefficients for x_k when $k = \overline{3, n}$, $(x_k < x < x_{k+1})$, $x = y_k = \dfrac{x_k + x_{k+1}}{2}$,

$$\begin{aligned}
a_{1k} &= 1,\\
b_{1k} &= \frac{p}{2EJ}(x_k + x_{k+1})(L - x_k),\\
b_{2k} &= 1 + \frac{p}{2EJ}(x_k + x_{k+1})(L - x_k)(z_k - x_k),\\
b_{3k} &= \frac{p}{4EJ}((x_k + x_{k+1})(L - x_k)(z_k - x_k)^2,\\
b_{4k} &= \frac{p}{12EJ}((x_k + x_{k+1})(L - x_k)(z_k - x_k)^3,\\
c_{1k} &= -\frac{p}{2EJ}(x_k + x_{k+1}),\\
c_{2k} &= -\frac{p}{2EJ}((x_k + x_{k+1})(z_k - x_k),\\
c_{3k} &= 1 - \frac{p}{4EJ}(x_k + x_{k+1})(z_k - x_k)^2,\\
c_{4k} &= 1 - \frac{p}{12EJ}(x_k + x_{k+1})(z_k - x_k)^3,
\end{aligned} \tag{22}$$

$$d_{1k} = \frac{ms^2}{2EJ}(x_k + x_{k+1}),$$
$$d_{2k} = \frac{ms^2}{4EJ}(x_k + x_{k+1})(z_k - x_k),$$
$$d_{3k} = \frac{ms^2}{4EJ}(x_k + x_{k+1})(z_k - x_k)^2,$$
$$d_{4k} = 1 + \frac{ms^2}{12EJ}(x_k + x_{k+1})(z_k - x_k)^3,$$
$$e_{1k} = s \cdot \alpha_1(z_k) + \gamma_1(z_k) + A(s) -$$
$$-\frac{1}{2EJ}\sum_{i=1}^{k-2}(x_i + x_{i+1})\left\{[p(L - x_i)\bar{y}''(x_i, s) - p\bar{y}'(x_i, s) + ms^2\bar{y}(x_i, s)] - \right.$$
$$\left. - [p(L - x_{i+1})\bar{y}''(x_{i+1}, s) - p\bar{y}'(x_{i+1}, s) + ms^2\bar{y}(x_{i+1}, s)]\right\},$$
$$e_{2k} = s \cdot \alpha_2(z_k) + \gamma_2(z_k) + z_k \cdot A(s) + B(s) -$$
$$-\frac{1}{2EJ}\sum_{i=1}^{k-2}(x_i + x_{i+1})\left\{[p(L - x_i)\bar{y}''(x_i, s) - p\bar{y}'(x_i, s) + ms^2\bar{y}(x_i, s)] - \right.$$
$$\left. - [p(L - x_{i+1})\bar{y}''(x_{i+1}, s) - p\bar{y}'(x_{i+1}, s) + ms^2\bar{y}(x_{i+1}, s)]\right\},$$
$$e_{3k} = s \cdot \alpha_3(z_k) + \gamma_3(z_k) + \frac{z_k^2}{2}A(s) + z_k \cdot B(s) + C(s) -$$
$$-\frac{1}{2EJ}\sum_{i=1}^{k-2}(x_i + x_{i+1})\left\{[p(L - x_i)\bar{y}''(x_i, s) - p\bar{y}'(x_i, s) + ms^2\bar{y}(x_i, s)] - \right.$$
$$\left. - [p(L - x_{i+1})\bar{y}''(x_{i+1}, s) - p\bar{y}'(x_{i+1}, s) + ms^2\bar{y}(x_{i+1}, s)]\right\},$$
$$e_{4k} = s \cdot \alpha_4(z_k) + \gamma_4(z_k) + \frac{z_k^3}{6}A(s) + \frac{z_k^2}{2}B(s) + z_2 \cdot C(s) + D(s) -$$
$$-\frac{1}{2EJ}\sum_{i=1}^{k-2}(x_i + x_{i+1})\left\{[p(L - x_i)\bar{y}''(x_i, s) - p\bar{y}'(x_i, s) + ms^2\bar{y}(x_i, s)] - \right.$$
$$\left. - [p(L - x_{i+1})\bar{y}''(x_{i+1}, s) - p\bar{y}'(x_{i+1}, s) + ms^2\bar{y}(x_{i+1}, s)]\right\},$$

Substituting the finding coefficients in (20) we can obtain all values of $\bar{y}'''(x_k, s)$, $\bar{y}''(x_k, s)$, $\bar{y}'(x_k, s)$ and $\bar{y}(x_k, s)$, $k = \overline{1, n}$.

$$\Delta_1 = \begin{vmatrix} e_{1k} & b_{1k} & c_{1k} & d_{1k} \\ e_{2k} & b_{2k} & c_{2k} & d_{2k} \\ e_{3k} & b_{3k} & c_{3k} & d_{3k} \\ e_{4k} & b_{4k} & c_{4k} & d_{4k} \end{vmatrix} = \tag{23}$$

$$= e_{1k}(b_{2k}c_{3k}d_{4k} + b_{3k}c_{4k}d_{2k} + b_{4k}c_{2k}d_{3k} - b_{4k}c_{3k}d_{2k} - b_{3k}c_{2k}d_{4k} - b_{2k}c_{4k}d_{3k}) -$$
$$-e_{2k}(b_{1k}c_{3k}d_{4k} - b_{1k}c_{4k}d_{3k} - b_{3k}c_{1k}d_{4k} + b_{4k}c_{1k}d_{3k} + b_{3k}c_{4k}d_{1k} - b_{4k}c_{3k}d_{1k}) -$$
$$-e_{3k}(b_{1k}c_{4k}d_{2k} - b_{1k}c_{2k}d_{4k} - b_{4k}c_{1k}d_{2k} + b_{2k}c_{1k}d_{4k} + b_{4k}c_{2k}d_{1k} - b_{2k}c_{4k}d_{1k}) -$$
$$-e_{4k}(b_{1k}c_{2k}d_{3k} - b_{1k}c_{3k}d_{2k} - b_{2k}c_{1k}d_{3k} + b_{3k}c_{1k}d_{2k} + b_{2k}c_{3k}d_{1k} - b_{3k}c_{2k}d_{1k}) =$$
$$= e_{1k}g_{11}(x_k) - e_{2k}g_{12}(x_k) - e_{3k}g_{13}(x_k) - e_{4k}g_{14}(x_k).$$

$$\Delta_2 = \begin{vmatrix} 1 & e_{1k} & c_{1k} & d_{1k} \\ 0 & e_{2k} & c_{2k} & d_{2k} \\ 0 & e_{3k} & c_{3k} & d_{3k} \\ 0 & e_{4k} & c_{4k} & d_{4k} \end{vmatrix} = \tag{24}$$

$$= e_{2k}c_{3k}d_{4k} + e_{3k}c_{4k}d_{2k} + e_{4k}c_{2k}d_{3k} - e_{4k}c_{3k}d_{2k} - e_{3k}c_{2k}d_{4k} - e_{2k}c_{4k}d_{3k} =$$
$$= e_{2k}(c_{3k}d_{4k} - c_{4k}d_{3k}) + e_{3k}(c_{4k}d_{2k} - c_{2k}d_{4k}) + e_{4k}(c_{2k}d_{3k} - c_{3k}d_{2k}) =$$
$$= e_{2k}g_{21}(x_k) + e_{3k}g_{22}(x_k) + e_{4k}g_{23}(x_k).$$

$$\Delta_3 = \begin{vmatrix} 1 & b_{1k} & e_{1k} & d_{1k} \\ 0 & b_{2k} & e_{2k} & d_{2k} \\ 0 & b_{3k} & e_{3k} & d_{3k} \\ 0 & b_{4k} & e_{4k} & d_{4k} \end{vmatrix} = \tag{25}$$

$$= e_{3k}b_{2k}d_{4k} + e_{4k}b_{3k}d_{2k} + e_{2k}b_{4k}d_{3k} - e_{3k}b_{4k}d_{2k} - e_{4k}b_{2k}d_{3k} - e_{2k}b_{3k}d_{4k} =$$
$$= e_{2k}(b_{4k}d_{3k} - b_{3k}d_{4k}) + e_{3k}(b_{2k}d_{4k} - b_{4k}d_{2k}) + e_{4k}(b_{3k}d_{2k} - b_{2k}d_{3k}) =$$
$$= e_{2k}g_{31}(x_k) + e_{3k}g_{32}(x_k) + e_{4k}g_{33}(x_k).$$

$$\Delta_4 = \begin{vmatrix} 1 & b_{1k} & c_{1k} & e_{1k} \\ 0 & b_{2k} & c_{2k} & e_{2k} \\ 0 & b_{3k} & c_{3k} & e_{3k} \\ 0 & b_{4k} & c_{4k} & e_{4k} \end{vmatrix} = e_{2k}g_{41}(x_k) + e_{3k}g_{42}(x_k) + e_{4k}g_{43}(x_k). \tag{26}$$

$$\Delta = \begin{vmatrix} 1 & b_{1k} & c_{1k} & d_{1k} \\ 0 & b_{2k} & c_{2k} & d_{2k} \\ 0 & b_{3k} & c_{3k} & d_{3k} \\ 0 & b_{4k} & c_{4k} & d_{4k} \end{vmatrix} = \begin{vmatrix} b_{2k} & c_{2k} & e_{2k} \\ b_{3k} & c_{3k} & e_{3k} \\ b_{4k} & c_{4k} & e_{4k} \end{vmatrix} = b_{2k}c_{3k}d_{4k} + b_{3k}c_{4k}d_{2k} + b_{4k}c_{2k}d_{3k} - \tag{27}$$

$$-b_{4k}c_{3k}d_{2k} - b_{2k}c_{4k}d_{3k} - b_{3k}c_{2k}d_{4k} = G(x_k).$$

Where

$$
\begin{aligned}
&g_{11}(x_k) = b_{2k}c_{3k}d_{4k} + b_{3k}c_{4k}d_{2k} + b_{4k}c_{2k}d_{3k} - b_{4k}c_{3k}d_{2k} - b_{3k}c_{2k}d_{4k} - b_{2k}c_{4k}d_{3k},\\
&g_{12} = b_{1k}c_{3k}d_{4k} - b_{1k}c_{4k}d_{3k} - b_{3k}c_{1k}d_{4k} + b_{4k}c_{1k}d_{3k} + b_{3k}c_{4k}d_{1k} - b_{4k}c_{3k}d_{1k},\\
&g_{13} = b_{1k}c_{4k}d_{2k} - b_{1k}c_{2k}d_{4k} - b_{4k}c_{1k}d_{2k} + b_{2k}c_{1k}d_{4k} + b_{4k}c_{2k}d_{1k} - b_{2k}c_{4k}d_{1k},\\
&g_{14} = b_{1k}c_{2k}d_{3k} - b_{1k}c_{3k}d_{2k} - b_{2k}c_{1k}d_{3k} + b_{3k}c_{1k}d_{2k} + b_{2k}c_{3k}d_{1k} - b_{3k}c_{2k}d_{1k},\\
&g_{21}(x_k) = c_{3k}d_{4k} - c_{4k}d_{3k},\\
&g_{22}(x_k) = c_{4k}d_{2k} - c_{2k}d_{4k},\\
&g_{23}(x_k) = c_{2k}d_{3k} - c_{3k}d_{2k},\\
&g_{31}(x_k) = b_{4k}d_{3k} - b_{3k}d_{4k},\\
&g_{32}(x_k) = b_{2k}d_{4k} - b_{4k}d_{2k},\\
&g_{33}(x_k) = b_{3k}d_{2k} - b_{2k}d_{3k},\\
&g_{41}(x_k) = b_{3k}c_{4k} - b_{4k}c_{3k},\\
&g_{42}(x_k) = b_{4k}c_{2k} - b_{2k}c_{3k},\\
&g_{43}(x_k) = b_{2k}c_{3k} - b_{3k}c_{2k},\\
&G(x_k) = b_{2k}c_{3k}d_{4k} + b_{3k}c_{4k}d_{2k} + b_{4k}c_{2k}d_{3k} - b_{4k}c_{3k}d_{2k} - b_{2k}c_{4k}d_{3k} - b_{3k}c_{2k}d_{4k}.
\end{aligned}
\tag{28}
$$

Let's define the original expression (15)

$$
\begin{aligned}
&\bar{y}'''(x,t) = -\frac{1}{2EJ}\sum_{k=1}(x_k + x_{k+1})\left\{\left[p(L-x_k)\bar{y}''(x_k,t) - p\bar{y}'(x_k,t) + m\frac{\partial^2 y}{\partial t^2}(x_k,t)\right]\times\right.\\
&\left.\times H(x-x_k) - \left[p(L-x_{k+1})\bar{y}''(x_{k+1},t) - p\bar{y}'(x_{k+1},t) + m\frac{\partial^2 y}{\partial t^2}(x_{k+1},s)\right]H(x-x_{k+1})+\right\} +\\
&+L^{-1}(s\cdot\alpha_1(x) + \gamma_1(x) + A(s)),\\
&\bar{y}''(x,t) = -\frac{1}{2EJ}\sum_{k=1}(x_k + x_{k+1})\left\{\left[p(L-x_k)\bar{y}''(x_k,t) - p\bar{y}'(x_k,t) + m\frac{\partial^2 y}{\partial t^2}(x_k,t)\right]\times\right.\\
&\left.\times H(x-x_k) - \left[p(L-x_{k+1})\bar{y}''(x_{k+1},t) - p\bar{y}'(x_{k+1},t) + m\frac{\partial^2 y}{\partial t^2}(x_{k+1},s)\right]H(x-x_{k+1})+\right\} +\\
&+L^{-1}(s\cdot\alpha_2(x) + \gamma_2(x) + x\cdot A(s) + B(s)),\\
&\bar{y}'(x,t) = -\frac{1}{2EJ}\sum_{k=1}(x_k + x_{k+1})\left\{\left[p(L-x_k)\bar{y}''(x_k,s) - p\bar{y}'(x_k,t) + m\frac{\partial^2 y}{\partial t^2}(x_k,t)\right]\times\right.
\end{aligned}
\tag{29}
$$

$$\times H(x-x_k) - \left[p(L-x_{k+1})\bar{y}''(x_{k+1},t) - p\bar{y}'(x_{k+1},t) + m\frac{\partial^2 y}{\partial t^2}(x_{k+1},s)\right] H(x-x_{k+1})\Big\} +$$
$$+L^{-1}\left(s\cdot\alpha_3(x) + \gamma_3(x) + \frac{x^2}{2}A(s) + x\cdot B(s) + C(s)\right),$$
$$\bar{y}(x,t) = -\frac{1}{2EJ}\sum_{k=1}(x_k + x_{k+1})\left\{\left[p(L-x_k)\bar{y}''(x_k,t) - p\bar{y}'(x_k,t) + m\frac{\partial^2 y}{\partial t^2}(x_k,t)\right]\times\right.$$
$$\times H(x-x_k) - \left[p(L-x_{k+1})\bar{y}''(x_{k+1},t) - p\bar{y}'(x_{k+1},t) + m\frac{\partial^2 y}{\partial t^2}(x_{k+1},s)\right] H(x-x_{k+1})\Big\} +$$
$$+L^{-1}\left(s\cdot\alpha_4(x) + \gamma_4(x) + \frac{x^3}{6}A(s) + \frac{x^2}{2}B(s) + C(s) + D(s)\right).$$

Let's define the original coefficients (22)

When $k = \overline{3,n}$, $(x_k < x < x_k + 1)$, $x = y_k = \dfrac{x_k + x_{k+1}}{2}$,

$$\begin{aligned}
a_{1k} &= 1,\\
b_{1k} &= \frac{p}{2EJ}(x_k + x_{k+1})(L - x_k),\\
b_{2k} &= 1 + \frac{p}{4EJ}(x_k + x_{k+1})(L - x_k)(z_k - x_k),\\
b_{3k} &= \frac{p}{4EJ}((x_k + x_{k+1})(L - x_k)(z_k - x_k)^2,\\
b_{4k} &= \frac{p}{12EJ}((x_k + x_{k+1})(L - x_k)(z_k - x_k)^3,\\
c_{1k} &= -\frac{p}{2EJ}(x_k + x_{k+1}),\\
c_{2k} &= -\frac{p}{2EJ}((x_k + x_{k+1})(z_k - x_k),\\
c_{3k} &= 1 - \frac{p}{4EJ}(x_k + x_{k+1})(z_k - x_k)^2,\\
c_{4k} &= 1 - \frac{p}{12EJ}(x_k + x_{k+1})(z_k - x_k)^3,
\end{aligned} \tag{30}$$

$$d_{1k} = 0, \quad d_{2k} = 0, \quad d_{3k} = 0, \quad d_{4k} = 1e_{1k} = L^{-1}(s\cdot\alpha_1(z_k) + \gamma_1(z_k) + A(s)) -$$
$$-\frac{1}{2EJ}\sum_{i=1}^{k-2}(x_i + x_{i+1})\left\{\left[p(L-x_i)y''(x_i,t) - py'(x_i,t) + m\frac{\partial^2}{\partial t^2}y(x_i,t)\right] -\right.$$
$$-\left.\left[p(L-x_{i+1})\bar{y}''(x_{i+1},s) - p\bar{y}'(x_{i+1},t) + m\frac{\partial^2}{\partial t^2}\bar{y}(x_{i+1},t)\right]\right\},$$
$$e_{2k} = L^{-1}(s\cdot\alpha_2(z_k) + \gamma_2(z_k) + z_k\cdot A(s) + B(s)) -$$
$$-\frac{1}{2EJ}\sum_{i=1}^{k-2}(x_i + x_{i+1})\left\{\left[p(L-x_i)y''(x_i,t) - py'(x_i,t) + m\frac{\partial^2}{\partial t^2}y(x_i,t)\right] -\right.$$

$$- \left[p(L-x_{i+1})\bar{y}''(x_{i+1},t) - p\bar{y}'(x_{i+1},t) + m\frac{\partial^2}{\partial t^2}\bar{y}(x_{i+1},t)\right]\Bigg\},$$

$$e_{3k} = L^{-1}\left(s\cdot\alpha_3(z_k) + \gamma_3(z_k) + \frac{z_k^2}{2}A(s) + z_k\cdot B(s) + C(s)\right) -$$

$$-\frac{1}{2EJ}\sum_{i=1}^{k-2}(x_i + x_{i+1})\left\{\left[p(L-x_i)y''(x_i,t) - py'(x_i,t) + m\frac{\partial^2}{\partial t^2}y(x_i,t)\right] -\right.$$

$$\left. - \left[p(L-x_{i+1})\bar{y}''(x_{i+1},t) - p\bar{y}'(x_{i+1},t) + m\frac{\partial^2}{\partial t^2}y(x_i,t)\right]\right\},$$

$$\Delta_1 = \begin{vmatrix} e_{1k} & b_{1k} & c_{1k} & 0 \\ e_{2k} & b_{2k} & c_{2k} & 0 \\ e_{3k} & b_{3k} & c_{3k} & 0 \\ e_{4k} & b_{4k} & c_{4k} & 1 \end{vmatrix} = e_{1k}g_{11}(x_k) - e_{2k}g_{12}(x_k) - e_{3k}g_{13}(x_k). \tag{31}$$

$$\Delta_2 = \begin{vmatrix} 1 & e_{1k} & c_{1k} & d_{1k} \\ 0 & e_{2k} & c_{2k} & d_{2k} \\ 0 & e_{3k} & c_{3k} & d_{3k} \\ 0 & e_{4k} & c_{4k} & d_{4k} \end{vmatrix} = e_{2k}g_{21}(x_k) + e_{3k}g_{22}(x_k). \tag{32}$$

$$\Delta_3 = \begin{vmatrix} 1 & b_{1k} & e_{1k} & d_{1k} \\ 0 & b_{2k} & e_{2k} & d_{2k} \\ 0 & b_{3k} & e_{3k} & d_{3k} \\ 0 & b_{4k} & e_{4k} & d_{4k} \end{vmatrix} = e_{3k}b_{2k} - e_{2k}b_{3k} = e_{2k}g_{31}(x_k) + e_{3k}g_{32}(x_k). \tag{33}$$

$$\Delta_4 = \begin{vmatrix} 1 & b_{1k} & c_{1k} & e_{1k} \\ 0 & b_{2k} & c_{2k} & e_{2k} \\ 0 & b_{3k} & c_{3k} & e_{3k} \\ 0 & b_{4k} & c_{4k} & e_{4k} \end{vmatrix} = e_{2k}g_{41}(x_k) + e_{3k}g_{42}(x_k) + e_{4k}g_{43}(x_k). \tag{34}$$

$$\Delta = \begin{vmatrix} 1 & b_{1k} & c_{1k} & d_{1k} \\ 0 & b_{2k} & c_{2k} & d_{2k} \\ 0 & b_{3k} & c_{3k} & d_{3k} \\ 0 & b_{4k} & c_{4k} & d_{4k} \end{vmatrix} = b_{2k}c_{3k} - b_{3k}c_{2k} = G(x_k). \tag{35}$$

where

$$\begin{aligned} &g_{11}(x_k) = (b_{2k}c_{3k} - b_{3k}c_{2k}), \quad g_{12} = -(b_{1k}c_{3k} - b_{3k}c_{1k}), \quad g_{13} = -(b_{2k}c_{1k} - b_{1k}c_{2k}), \\ &g_{21}(x_k) = c_{3k}, \quad g_{22}(x_k) = -c_{2k}, \quad g_{31}(x_k) = b_{2k}, \quad g_{32}(x_k) = -b_{4k}, \\ &g_{41}(x_k) = b_{3k}c_{4k} - b_{4k}c_{3k}, \quad g_{42}(x_k) = b_{4k}c_{2k} - b_{2k}c_{4k}, \quad g_{43}(x_k) = b_{2k}c_{3k} - b_{3k}c_{2k}, \\ &G(x_k) = b_{2k}c_{3k} - b_{3k}c_{2k}. \end{aligned} \tag{36}$$

Find all values $y'''(x_k,)$, $y''(x_k,t)$, $y'(x_k,t)$ and $y(x_k,t)$, $k = \overline{1,n}$.

$$\begin{cases} y'''(x_k,t) = \dfrac{\Delta_1}{\Delta} = \dfrac{e_{1k}(b_{2k}c_{3k} - b_{3k}c_{2k}) - e_{2k}(b_{1k}c_{3k} - b_{3k}c_{1k}) - e_{3k}(b_{2k}c_{1k} - b_{1k}c_{2k})}{b_{2k}c_{3k} - b_{3k}c_{2k}}, \\ y''(x_k,t) = \dfrac{\Delta_2}{\Delta} = \dfrac{e_{2k}c_{3k} - e_{3k}c_{2k}}{b_{2k}c_{3k} - b_{3k}c_{2k}} \\ y'(x_k,t) = \dfrac{\Delta_3}{\Delta} = \dfrac{e_{3k}b_{2k} - e_{2k}b_{3k}}{b_{2k}c_{3k} - b_{3k}c_{2k}} \\ y(x_k,t) = \dfrac{\Delta_4}{\Delta} = \dfrac{e_{2k}(b_{3k}c_{4k} - b_{4k}c_{3k}) + e_{3k}(b_{4k}c_{2k} - b_{2k}c_{4k}) + e_{4k}(b_{2k}c_{3k} - b_{3k}c_{2k})}{b_{2k}c_{3k} - b_{3k}c_{2k}} \end{cases} \tag{37}$$

Solution has the form:

$$\begin{aligned} y(x,t) = -\frac{1}{2EJ}\sum_{k=1}(x_k + x_{k+1}) \Bigg\{ \left[p(L - x_k)y''(x_k,t) - py'(x_k,t) + m\frac{\partial^2 y}{\partial t^2}(x_k,t) \right] \times \\ \times H(x - x_k) - \left[p(L - x_{k+1})y''(x_{k+1},t) - py'(x_{k+1},t) + m\frac{\partial^2 y}{\partial t^2}(x_{k+1},t) \right] H(x - x_{k+1}) \Bigg\} + \\ + L^{-1}\left(s \cdot \alpha_3(x) + \gamma_3(x) + \frac{x^3}{6}A(s) + \frac{x^2}{2}B(s) + x \cdot C(s) + D(s) \right). \end{aligned} \tag{38}$$

4 Conclusion

The obtained general solutions of the differential equation of bending vibration of drill strings are used in the petroleum industry. Differential equations with partial derivatives are used to investigate the interaction of drill string bottom arrangement, cone bits and rock when drilling deep borewells in difficult geological conditions. These equations describe the non-lineor, axial, radial, parametric vibratians and oscillations bits in dynamic interaction with the rock. As well as dynamic and static stability of drill string equilibrium states at the rotary and turbine drilling methods, and more.

References

1. Kalinin P.V.: Mathematical modeling of drilling rig mechatronic complex.Abrtract, Novocherkassk (2010), (in Russian)
2. Gulyayev V.I., Borshch O.I.: Free vibrations of drill strings in hyper deep vertical borewells. J. Petrol Sci. Eng.78, 759–764 (2011)
3. Tyuiehodzhaev A.N.: Analytical solutions of nonlinear equations and differential equations with variable coeffiicients.In: Proceedings of the “Actual Psoblems of Mechanics and Engineering” IV International Scientific Conference,II,pp.40–57.Almaty (2014),(in Russian).

On a Thermodynamically-Consistent Nonlinear Model of Poroelasticity

A.S. Berdyshev[1], Kh.Kh. Imomnazarov[2], A.A. Mikhailov[2], M.A. Sultanov[3]

[1]Kazakh National Pedagogical University named after Abai, Almaty, Kazakhstan
[2]Institute of Computational Mathematics and Mathematical Geophysics SB RAS, Novosibirsk, Russia
[3]International Kazakh-Turkish University named after X.A.Yasavi, Turkestan, Kazakhstan
berdyshev@mail.ru,imom@omzg.sscc.ru,smurat-59@mail.ru

Abstract. One-dimensional direct initial-boundary value problem for a nonlinear system of the poroelasticity equations is considered. The theorem of local solvability of the classical solution to the problem is proved. The Frechet differentiability of the problem operator is proved too.

Keywords: hyperbolic system, inverse problem, Volterra equation, the porous medium, the coefficient of friction.

When studying many physical phenomena we have to deal with the movement of fluids in the elastically deformable porous media - Filtration. In such filtration processes, for example water seepage through the soil, the movement of oil in subterranean formations and others, the liquid moves in a branched system of interconnected pores. In permeable media, taking place in practice, (sand, clay, soil, peat, etc.) pore space has a very complicated and irregular structure, which, moreover, is usually unknown with sufficient accuracy, so it is clear that a direct description of the movement of fluid in all details would have considerable difficulties. However, in most cases, the characteristic linear dimensions of these problems are much greater than the characteristic pore size (in the case of granular medium such as sand - much greater than the characteristic grain size). Therefore, to describe the large-scale phenomena elastically deformable porous material can be regarded as a continuous medium, the characteristics of which (partial density, the fluid pressure in the pores, and others.) At each point are obtained by averaging over some neighborhood containing a sufficiently large number of pores. In mathematical modeling of seismic wave propagation in elastic media is usually assumed that the medium is perfectly elastically deformable and energy dissipation is neglected and porosity. On the other hand, there are a large number of works devoted to mathematical modeling of seismic wave propagation in saturated by fluid porous media based on linear models of Frenkel-Biot type [1,2].

The approach to the modeling of multiphase media based on conservation laws uses the self-consistent determination of forces and fluxes developed by Landau when describing two-velocity hydrodynamics of superfluid helium [3]. Detailed description of the derivation of the equations of the superfluidity theory can be found in [4]. In the case of using this approach, it suffices to assume the execution of only general physical principles: conservation laws and the principle of relativity of Galileo. Within the framework of conservation laws in work [5] is presented derivation of hydrodynamic equations for the classical media, and in work [6] derivation of the equations of two-fluid hydrodynamic model of two-phase media. In work [7] is presented a detailed analysis of issues related to the mathematical properties of the resulting equation systems.

In the case where the shear modulus $\mu = \mu(u_x)$ and coefficient of interfacial friction $\chi = \chi(u - \nu)$ the one-dimensional system of equations of poroelasticity can be written as

$$\rho_s u_t = \sigma_x - \rho_l^2 (u - \nu)\chi(u - \nu),$$

$$\sigma_t = \mu(u_x)u_x,$$
$$\rho_l\nu_t = \rho_l^2(u-\nu)\chi(u-\nu),$$

where u and ν are speeds of the elastic porous body with a constant partial density $\rho_s = \rho_s^f(1-d_0)$ and of the fluid with a constant partial density $\rho_l = \rho_l^f d_0$ respectively, d_0 is porosity, $u_t = \frac{\partial u}{\partial t}$, ρ_s^f and ρ_l^f are physical density of elastic porous body and fluid, respectively.

For convenience let us eliminate the stress tensor from the above system. We consider the following one-dimensional initial-boundary value problem for nonlinear system of equations of poroelasticity with respect to speeds u and ν:

$$\rho_s u_{tt} = (\mu(u_x)u_x)_x - \rho_l^2((u-\nu)\chi(u-\nu))_t, x \in (0,L), t \in (0,T), \quad (1)$$

$$\rho_l\nu_t = \rho_l^2(u-\nu)\chi(u-\nu), x \in (0,L), t \in (0,T), \quad (2)$$

$$u\mid_{t=0} = u_0(x), u_t\mid_{t=0} = u_1(x), x \in (0,L), \quad (3)$$

$$\nu\mid_{t=0} = 0, x \in (0,L), \quad (4)$$

$$\mu(u_x)u_x\mid_{x=L} = f(t), t \in (0,T), \quad (5)$$

$$u\mid_{x=0} = 0, t \in (0,T). \quad (6)$$

Here $f : [0,T] \to R$, $u_0 : [0,L] \to R$, $u_1 : [0,L] \to R$, further assume that performs the following: $\mu(\nu)$ is thrice continuously differentiable positive function, $\chi(\nu)$ is double continuous positive function.

Nonlinear wave equation of the form (1) ($\chi \equiv 0$ in the reversible approximation) arises in many problems. For example, in the case of string vibrations with elastic coefficient depending on the strain. In many models of mechanics of porous media, taking into account the energy dissipation, the coefficient of friction (permittivity) is a function of the velocity difference [7-9].

Further we are interested in the classical solution of initial boundary value problem (1) - (6), i.e., $u \in C^{2,2}([0,L]\times[0,T])$, $\nu \in C^{0,1}([0,L]\times[0,T])$, where $C^{k,m}([0,L]\times[0,T])$ is a space of k times continuously differentiable functions by variable x and m times continuously differentiable functions by variable t.

In this paper by means of ideas of work [10] is studied the direct problem for the one-dimensional dynamical system of equations of poroelasticity.

Problem statement and formulation of result

The problem determining u and ν from (1)-(6) at given μ, χ, ρ_s, ρ_l we will call one-dimensional direct dynamic problem for porous media. One dimensional dynamic problem for porous media, for determining u,ν, μ from (1)-(6) (at given χ, ρ_s, ρ_l) by additional information $\tilde{u} := u(L,\cdot)$ will be considered separately.

It is convenient to introduce new functions $\tilde{\mu}(s) = s\mu(s)$, $\tilde{\chi}(s) = s\chi(s)$. To study the properties of our model, we consider the operator F, mapping function $\tilde{\mu}$ on to the given $\tilde{u} := u(L,\cdot)$ - narrowing solutions u of the following initial boundary value problem

$$\rho_s u_{tt} = (\tilde{\mu}(u_x))_x - \rho_l^2(\tilde{\chi}(u-\nu))_t, x \in (0,L), t \in (0,T), \quad (7)$$

$$\nu_t = \rho_l\tilde{\chi}(u-\nu), x \in (0,L), t \in (0,T), \quad (8)$$

with initial conditions

$$u\mid_{t=0} = u_0(x), u_t\mid_{t=0} = u_1(x), x \in (0,L), \quad (9)$$

$$\nu \mid_{t=0}= 0, x \in (0, L), \tag{10}$$

and boundary conditions

$$\tilde{\mu}(u_x) \mid_{x=L}= f(t), t \in (0, T), \tag{11}$$

$$u \mid_{x=0}= 0, t \in (0, T). \tag{12}$$

Then function $\tilde{\mu}$ is defined from the solution of the operator equation

$$F(\tilde{\mu}) = \tilde{u}.$$

The derivative of operator F in some direction $\delta\tilde{\mu}$ is calculated as follows

$$F^{'}(\tilde{\mu})\,[\delta\tilde{\mu}] = \hat{u}(L, \cdot), \tag{13}$$

where functions $\hat{u}$, $\hat{\nu}$ are solution of the initial boundary value problem

$$\rho_s\hat{u}_{tt} = (\tilde{\mu}^{'}(u_x)\hat{u}_x)_x - \rho_l^2(\tilde{\chi}^{'}(u-\nu)(\hat{u}-\hat{\nu}))_t +$$

$$+(\delta\tilde{\mu}(u_x))_x, x \in (0, L), t \in (0, T), \tag{14}$$

$$\hat{\nu} = \rho_l\tilde{\chi}^{'}(u-\nu)(\hat{u}-\hat{\nu}), x \in (0, L), t \in (0, T), \tag{15}$$

with initial conditions

$$\hat{u} \mid_{t=0}= 0, \hat{u}_t \mid_{t=0}= 0, x \in (0, L), \tag{16}$$

$$\hat{\nu} \mid_{t=0}= 0, x \in (0, L), \tag{17}$$

and boundary conditions

$$\hat{u} \mid_{x=0}= 0, t \in (0, T), \tag{18}$$

$$\tilde{\mu}^{'}(u_x)\hat{u}_x + \delta\tilde{\mu}(u_x) \mid_{x=L}= 0, t \in (0, T). \tag{19}$$

In formulas (14)-(19) functions u,μ are solution of the initial boundary value problem (7)-(12). Assume that the following conditions are valid

$$u_0 \in C^3(0, L), u_1 \in C^2(0, L), f \in C^2(0, T), \tag{20}$$

and the compatibility conditions

$$(\tilde{\mu}^{-1} \circ f)(0) = u_0^{'}(L), (\tilde{\mu}^{-1} \circ f)^{'}(0) = u_1^{'}(L),$$

$$\rho_s(\tilde{\mu}^{-1} \circ f)^{''}(0) = (\tilde{\mu}(u_0^{'}))^{''}(L) - \rho_l^2\left[(u_1 - \rho_l\tilde{\chi}(u_0))\tilde{\chi}^{'}(u_0)\right]^{'}(L), \tag{21}$$

on the right boundary, and also

$$u_0(0) = u_1(0) = u_0^{''}(0) = u_1^{''}(0) = 0$$

on the left boundary.
Further assume that functions $\tilde{\mu}$, $\tilde{\chi}$ belong to the set

$$D(F) = \left\{ \begin{array}{l} \tilde{\mu}, \tilde{\chi} \in X \mid \tilde{\mu}^{'}(s) \geq \mu_0, \tilde{\mu}^{''}(s) \leq C, \tilde{\chi}^{''}(s) \leq C, \forall s \in [0, S], \\ \textit{and hold the compability conditions } (21) \end{array} \right\} \tag{22}$$

for some positive constants μ_0, C. Futher we denote by a positive constant that greater than the previous C,

$$X = \left\{\tilde{\mu} \in C^3(0, S), \tilde{\chi} \in C^2(0, S) \mid \tilde{\mu}(0) = 0, \tilde{\chi}(0) = 0\right\}, \tag{23}$$

where $S > 0$ Note that in the applications parameters of the media are often strictly monotonically increasing and smooth functions. The determination region *D(F)* and space *X,* defined by the above formulas (22),(23) satisfy these conditions. The assumption of smoothness of media parameters is also important for the effective solution of the original initial-boundary value problem. If $\tilde{\mu}, \tilde{\chi}$ are smooth enough, then in order to determine the media parameters can be applied Newton-type methods.

Theorem. Suppose that T is sufficiently small, S sufficiently large, condition (20) and D(F)is defined by formula (22).

Then, for any $\tilde{\mu}, \tilde{\chi} \in D(F)$ the problem (7)-(12) has a unique solution $u \in C^{3,2}([0, L] \times [0, T])$, $\nu \in C^{0,1}([0, L] \times [0, T])$ Consequently, the operator of the direct problem

$$F : D(F) \subseteq X \to C^2(0, T), \tilde{\mu} \longmapsto u(L, \cdot),$$

Where u, v is a solution of (7)-(12), is well defined. Moreover, for

$$X^{'} := X \cap C^4(0, s), D^{'}(F) := D(F) \cap C^4(0, s),$$

$$F : D^{'}(F) \subseteq X^{'} \to C^2(0, T)$$

is continuously differentiable according to Frechet and derivatives are calculated by formulas (13)-(19).

Remark 1. A similar result takes place for the homogeneous Neumann conditions instead of the Dirichlet boundary conditions at the left boundary x=0 which corresponds to the stress-free left boundary. In the proof of correctness (See below.) boundary conditions for $w = u_x$, $\tilde{w} = \nu_x$ have the following form

$$\tilde{\mu}(w) \mid_{x=L} = f(t), t \in (0, T),$$

$$w \mid_{x=0} = 0, t \in (0, T).$$

Thus functions u,μ are determined via functions $w, \tilde{w}$ by formulas

$$u(x, t) = \int_0^x w(\xi, t) d\xi + \frac{1}{\rho_s} \int_0^t \int_0^\tau (\tilde{\mu}(w))_x(0, \eta) d\eta d\tau +$$

$$+\rho_l^2 \frac{\rho_l}{\rho_s} \int_0^t \int_0^\tau \left[\tilde{\chi}(u - \nu)\tilde{\chi}^{'}(u - \nu)\right](0, \eta) d\eta d\tau,$$

$$\nu(x, t) = \int_0^x \tilde{w}(\xi, t) d\xi + \rho_l \int_0^t (\tilde{\chi}(u - \nu))(0, \eta) d\eta.$$

This system at a fixed x is a closed system of nonlinear Volterra integral equations of the second order by variable t.

Proof of the theorem

Let's introduce functions $\breve{u} = u_x, \breve{\nu} = \nu_x$. Differentiate both sides of (7), (8) by x and obtain the system of equations relatively $\breve{u}, \breve{\nu}$

$$\rho_s \breve{u}_{tt} = (\tilde{\mu}^{'}(\breve{u})\breve{u}_x)_x - \rho_l^2 \tilde{\chi}^{'}(u - \nu)\breve{u}_t - \rho_l^2 \left\{ \left[\tilde{\chi}^{'}(u - \nu)\right]_t - \rho_l \left[\tilde{\chi}'(u - \nu)\right]^2 \right\} (\breve{u} - \breve{\nu}),$$

$$x \in (0, L), t \in (0, T), \tag{24}$$

$$\breve{\nu}_t = \rho_l \tilde{\chi}^{'}(u - \nu)(\breve{u} - \breve{\nu}), x \in (0, L), t \in (0, T), \tag{25}$$

Assume that at the left boundary is given homogeneous Neumann condition (see. Remark 1) and using the condition (5), we obtain

$$\tilde{\mu}^{'}(\breve{u})\breve{u}_x \mid_{x=0}= 0, t \in (0,T),$$

$$\tilde{\mu}(\breve{u}) \mid_{x=L}= f(t), t \in (o,T),$$

or

$$\breve{u}_x \mid_{x=0}= 0, t \in (0,T), \tag{26}$$

$$\breve{u} \mid_{x=L}= \tilde{\mu}^{-1}(f(t)), t \in (0,T) \tag{27}$$

The initial conditions have the form

$$\breve{u} \mid_{t=0}= u_{0x}(x), \breve{u}_t^{'} \mid_{t=0}= u_{1x}(x), x \in (o,L), \tag{28}$$

$$\breve{\nu} \mid_{t=0}= 0, x \in (0,L), \tag{29}$$

In order to show the existence of solution of the nonlinear initial boundary value problem, we reduce the equation (24) to a standard form by using a smooth change of variables [4], using the characteristic curves $\frac{dx(t)}{dt} = \pm\sqrt{\hat{\mu}'(\hat{u})(x(t), t/\rho_s}$

Let us introduce a new function [11, 12]

$$\breve{u}(x,t) = U(\varphi(x,t) + \psi(x,t), \varphi(x,t) - \psi(x,t)), \tag{30}$$

Where $\varphi(x,t), \psi(x,t)$ satisfy the system

$$\varphi_t + \sqrt{\tilde{\mu}'(u_x)/\rho_s\varphi_x} = 0, \tag{31}$$

$$\psi_t - \sqrt{\tilde{\mu}'(u_x)/\rho_s\psi_x} = 0. \tag{32}$$

After simple changes the system of equations (24), (25) with respect to $\breve{\nu}$, U will take the following form

$$\breve{\nu}_t = \rho_l\tilde{\chi}^{'}(u-\nu)(U-\hat{\nu}), \tag{33}$$

$$U_{\zeta\zeta} - U_{\eta\eta} = \frac{1}{8}\left(\frac{\tilde{b}_x}{\tilde{b}} + \frac{\tilde{b}_t}{\tilde{b}\sqrt{\tilde{b}}} + \frac{\rho_l^2}{\rho_s}\frac{\chi_1}{\sqrt{\tilde{b}}}\right)\frac{1}{\psi_x}(U_\eta + U_\zeta) +$$

$$+\frac{1}{8}\left(\frac{\tilde{b}_x}{\tilde{b}} - \frac{\tilde{b}_t}{\tilde{b}\sqrt{\tilde{b}}} - \frac{\rho_l^2}{\rho_s}\frac{\chi_1}{\sqrt{\tilde{b}}}\right)\frac{1}{\varphi_x}(U_\eta - U_\zeta) + \frac{\rho_l^2}{\rho_s}\frac{\chi_2}{4\tilde{b}\varphi_x\psi_x}(U-\breve{\nu}). \tag{34}$$

where $\tilde{b} = \tilde{\mu}^{'}(\breve{u})/\rho_s$, $\chi_1 = \tilde{\chi}^{'}(U-\nu)$, $\chi_2 = \left[\tilde{\chi}^{'}(u-\nu)\right]_t - \rho_l\left[\tilde{\chi}^{'}(u-\nu)\right]^2$.

To show that this change of variables is a regular and from the class of C^2 at a sufficiently small interval $(0,\bar{t})$ at condition $\hat{u} \in C^2$, $\hat{\nu} \in C^1$ consider the determinant of the matrix Jacobi

$$det\begin{pmatrix}\varphi_x+\psi_x & \varphi_t+\psi_t\\ \varphi_x-\psi_x & \varphi_t-\psi_t\end{pmatrix}=det\begin{pmatrix}\varphi_x+\psi_x & -\sqrt{\tilde{\mu}'(\breve{u})/\rho_s}(\varphi_x-\psi_x)\\ \varphi_x-\psi_x & -\sqrt{\tilde{\mu}'(\breve{u})/\rho_s}(\varphi_x+\psi_x)\end{pmatrix}=$$

$$=-4\sqrt{\tilde{\mu}'(\breve{u})/\rho_s}\varphi_x\psi_x.$$

Show that the determinant of the matrix Jacobi is nonzero, i.e.

$$\psi_x\neq 0,$$

$$\varphi_x\neq 0.$$

From the characteristics of an ordinary differential equation (32) for ψ

$$t_\tau(\tau,\xi)=1, t(0,\xi)=\xi,$$

$$x_\tau(\tau,\xi)=-\sqrt{\tilde{\mu}'(\breve{u})(x(\tau,\xi),t(\tau,\xi)/\rho_s}, x(0,\xi)=0. \tag{35}$$

$$\psi_\tau(\tau,\xi)=0, \psi(0,\xi)=\xi,$$

obtain

$$t(\tau,\xi)=\tau+\xi, \psi(\tau,\xi)=\xi, \tag{36}$$

for $\tau\geq 0$, $\xi=t(0,\xi)\geq 0$.

By differentiating the second relation of (36), we obtain

$$1=\psi_\xi=\psi_x x_\xi+\psi_t t_\xi=\psi_x(x_\xi+\sqrt{\tilde{\mu}'(\breve{u})/\rho_s}).$$

Hence, we obtain $\psi_x\neq 0$. We similarly prove that $\varphi_x\neq 0$ Consequently, determinant of the matrix Jacobi is nonzero. On the other hand, limitation $\mid \psi_x \mid$ is performed until

$$x_\xi(\tau,\xi)\neq -\sqrt{\tilde{\mu}'(\breve{u})(x(\tau,\xi)),t(\tau,\tau+\xi)/\rho_s}.$$

This holds true for all t, such that $\tau=t-\xi$ less than certain $\tilde{t}>0$ which can depend only on $\|\breve{u}\|_{C^1}$

Differentiate the second relation of (35) by variable ξ. We obtain the first order ordinary differential equation with zero data of Cauchy relatively x_ξ We reduce this problem to the solution of the integral equation. Carrying out obvious estimates and using Gronwall inequality, we obtain the inequality

$$\mid x_\xi(\tau,\xi)\mid\leq e^{\frac{C\|u\|_{C^2}}{\sqrt[2]{c\rho_s}}}-1<\sqrt{c/\rho_s}\leq\sqrt{\tilde{\mu}'(\breve{u}(x(\tau,\xi),\tau+\xi))/\rho_s},$$

which is valid for

$$\tau\leq\tilde{t}=\frac{\sqrt[2]{c\rho_s}ln(\sqrt{c/\rho_s}+1)}{C\|\breve{u}\|_{C^1}}$$

Similarly can be proved the limitations of all derivatives up to second order from functions φ and ψ [10, 12].

According to theorem of inverse function the existence of the solution $\breve{u} \in C^{2,2}$, $\breve{\nu} \in C^{0,1}$ of problem (24) - (29) follows from the existence of solutions $U \in C^{2,2}$, $\breve{\nu} \in C^{0,1}$ of problem (33), (34) with converged initial and boundary conditions. To prove the existence of solution of the system (33), (34) let us use the Banach theorem [13]. Namely, we define a fixed point of the operator $M = (M_1, M_2)$, that maps function $U \in C^{2,2}$, $\breve{\nu} \in C^{0,1}$ in solving $M_1(U, \breve{\nu}) = Y$, $M_2(U, \breve{\nu}) = y$ from

$$Y_{\zeta\zeta} - Y\eta\eta = \frac{1}{8}\left(\frac{\tilde{b}_x}{\tilde{b}} + \frac{\tilde{b}_t}{\tilde{b}\sqrt{\tilde{b}}} + \frac{\rho_l^2}{\rho_s}\frac{\chi_1}{\sqrt{\tilde{b}}}\right)\frac{1}{\psi_x}(U_\eta + U_\zeta) +$$

$$+\frac{1}{8}\left(\frac{\tilde{b}_x}{\tilde{b}} - \frac{\tilde{b}_t}{\tilde{b}\sqrt{\tilde{b}}} - \frac{\rho_l^2}{\rho_s}\frac{\chi_1}{\sqrt{\tilde{b}}}\right)\frac{1}{\varphi_x}(U_\eta - U_\zeta) + \frac{\rho_l^2}{\rho_s}\frac{\chi_2}{4\tilde{b}\varphi_x\psi_x}(U - \breve{\nu}), \tag{37}$$

$$y_t = \rho_l\tilde{\chi}'(u - \nu)(U - \breve{\nu}), \tag{38}$$

with converged initial and boundary conditions. Notice that the right sides depend on U, $\hat{\nu}$, in not only linear way concerning $U_\eta + U_\zeta$, $U_\eta - U_\zeta$ but also in a nonlinear way through $\tilde{b} = \tilde{\mu}'(\breve{u})/\rho_s$, $\chi_1 = \tilde{\chi}'(U - \nu)$ and φ, ψ. Operator M is a compressible for the small values $\bar{t}(0 < t \le \bar{t})$ due to limitations of the right sides of (37), (38) by the norm $\|U\|_{C_{2,2}}$, $\|\breve{\nu}\|_{C_{0,1}}$. That implies the existence of the solution $u \in C^{3,2}$, $\nu \in C^{1,1}$ of nonlinear initial boundary value problem (1)-(6) and consequently due to

$$u(x,t) = \int_0^x \breve{u}(\xi, t)d\xi,$$

$$\nu(x,t) = \int_0^x \breve{\nu}(\xi, t)d\xi + \rho_l \int_0^t \left[\tilde{\chi}(u - \nu)\right](0, \tau)d\tau,$$

exists the solution $\breve{u} \in C^{2,2}$, $\breve{\nu} \in C^{0,1}$ of initial boundary value problem (24)-(29). The uniqueness is proved by a standard way [3] using theorem 4 from [4] for the system

$$\rho_s\hat{u}_{tt} = \left(\int_0^1 \tilde{\mu}(u_x^2 + (u_x^1 - u_x^2)\theta)d\theta\hat{u}_x\right)_x -$$

$$-\rho_l^2\left(\int_0^1 \tilde{\chi}(u^2 - \nu^2 + (u^1 - \nu^1 - u^2 + \nu^2)\theta)d\theta\right)_t,$$

$$\hat{\nu}_t = \rho_l\int_0^1 \tilde{\chi}(u^2 - \nu^2 + (u^1 - \nu^1 - u^2 + \nu^2)\theta)d\theta,$$

with homogeneous initial and boundary conditions for the difference of u^1, ν^1 and u^2, ν^2. solutions.

Similarly, can be shown a continuous dependence of the solution $u \in C^{2,2}$, $\nu \in C^{0,1}$ from the parameter $\tilde{\mu} \in C^3$.

To prove the differentiation by Frechet of the direct problem operator F, let us notice, that $F(\tilde{\mu} + \delta\tilde{\mu}) = \bar{u}(L, \cdot)$, where functions $\bar{u}$, $\bar{\nu}$ is a solution for initial boundary value problem (1)

(6) with (1)-(6), $\tilde{\mu} = \tilde{\mu} + \delta\tilde{\mu}$ functions $w := \bar{u} - u - u$, $\omega := \bar{\nu} - \nu - \nu$ are the solutions of initial boundary value problem:

$$\rho_s w_{tt} = (\tilde{\mu}^{'}(u_x)w_x)_x - \rho_l^2 \tilde{\chi}^{'}(u-\nu)w_t + G_x -$$

$$-\rho_l^2 \left[\left[\tilde{\chi}^{'}(u-\nu) \right]_t - \rho_l \left[\tilde{\chi}^{'}(u-\nu) \right]^2 \right] (w-\omega),$$

$$\omega_t = \rho_l \tilde{\chi}^{'}(u-\nu)(w-\omega),$$

with the zero initial and boundary conditions

$$\tilde{\mu}^{'}(u_x)w_x \mid_{x=L} = G(L,t),$$

$$w \mid_{x=0} = 0, t \in (0,T),$$

where

$$G = \tilde{\mu}(\bar{u}_x) - \tilde{\mu}(u_x) - \tilde{\mu}^{'}(u)_x(\bar{u}_x - u_x) + \delta\tilde{\mu}(\bar{u}_x) - \delta\tilde{\mu}(u_x).$$

Consequently, applying the characteristic conversion of the class C^2, known results for the wave equation and Gronwall's inequality, we obtain that the norm $\|w\|_{C^2}$ can be estimated through $\|\delta\mu\|_{c^3}$ [10]. That means the continuity of the operator F.

The continuity of derivatives by Frechet of the operator F can be proved similarly. Theorem is proved.

This work is financially supported by the grant of CS MES RK (number of the grant 3328/GF4)

References

1. Frenkel, Ya.I.: *To theory of seismic and seismoelectric phenomena in wet soil. Izvestia, Geogr. Geofis.,* **4(8)**, 133-150 (1944)(in Russian).
2. Biot, M.A.: *Theory of propagation of elastic waves in a Fluid-Saturated Porous Solid. I. Low-Frequency Range*. J. Acoust. Soc.Am., **28**, 168-178 (1956).
3. Landau, L.: *The theory of superfluidity of helium II . Zh. Eksp. Teor. Fiz.,* **11**, 592-605 (1941)
4. Khalatnikov, I.: *Theory of superfluidity*. Science, Moscow (1971) (in Russian).
5. Dorovsky, V.N.: *Continual theory of filtration. Sov. Geology and Geophysics* **7(30)**, 34-39. (1989)
6. Dorovsky, V.N., Perepechko, Yu.V.: *A hydrodynamic model for a solution in fracture-porous media. Geology and geophysics.***9(37)**, 123-134 (1996)(in Russian).
7. Blokhin, A.M., Dorovsky, V.N.: *Mathematical modelling in the theory of multivelocity continuum.* Nova Science, New York. (1995)
8. Dorovsky, V.N., Perepechko, Yu.V., Romensky, E.I.: *Wave processes in saturated porous elastically deformed media. Combustion, Explosion and Shock Waves*. **1(29)**, 93-103. (1993)
9. Zhabborov, N.M., Imomnazarov, Kh.Kh.: *Some initial boundary value problems of mechanics of two-velocity media*. Tashkent (2012)(in Russian).
10. Kaltenbacher, B.: *Identification of Nonlinear Coefficients in Hyperbolic PDEs, with Application to Piezoelectricity*. In: Kunisch, K., Leugering, G., Sprekels, J., Troltzsch, F. (eds.) Optimal Control of Coupled Systems of PDEs. Springer, **155**, 193-216 (2006)
11. Evans, L.C.: *Partial Differential Equations*. AMS. (1998)
12. Imomnazarov, Kh.Kh., Imomnazarov, Sh.Kh., Korobov, P.V, Kholmuradov, A.E *About one direct initial-boundary value problem for nonlinear one-dimensional poroelasticity equations*. Bull. Of the Novosibirsk Computing Center, series: Mathematical Modeling in Geophysics. Novosibirsk. **18**, 1-8 (2014)
13. Kolmogorov, A.N., Fomin, S.V. *Elements of the Theory of functions and Functional Analysis*. Moscow: Nauka (1968)

Numerical Study of the Discharged Heat Water Effect on the Aquatic Environment from Thermal Power Plant

Alibek Issakhov

Faculty of Mechanics and Mathematics, al-Farabi Kazakh National University,
av.al-Farabi 71, 050040 Almaty, Kazakhstan
alibek.issakhov@gmail.com

Abstract. The paper presents a mathematical model of the thermal load on the aquatic environment under operational capacity 200MW of thermal power plant. It is solved by the Navier-Stokes equation and transport equation for temperature an incompressible fluid in a stratified medium based on numerical method, the splitting method by physical parameters which approximated by the finite volume method. The numerical solution of the equation system is divided into four stages. At the first step it is assumed that the momentum transfer carried out only by convection and diffusion. Intermediate velocity field is solved by 5-step Runge-Kutta method. At the second stage, the pressure field is solved by found the intermediate velocity field. Poisson equation for the pressure field is solved by Jacobi method. The third step is assumed that the transfer is carried out only by pressure gradient. The fourth step of the transport equation for temperature is also solved as momentum equations, with 5-step Runge-Kutta method. The obtained numerical results of temperature distribution for operational capacity 200 MW of three-dimensional stratified turbulent flow were compared with experimental data. What revealed qualitatively and quantitatively approximately the basic laws of hydrothermal processes occurring in the reservoir-cooler.

Keywords: stratified medium, Navier-Stokes equation, operational capacities, thermal power plant, finite volume method, Runge-Kutta method, thermal discharge.

1 Introduction

Environment - the basis of human life, and the energy generated - is the basis of the modern world. However, the production of electricity adversely impact on our environment, worsening living conditions. Energy is the basis of different types of power plants. Electricity production in thermal power plants (TPP), hydropower plants (HPP) and nuclear power plants (NPP) is associated with adverse effects on the environment. Interaction energy and the environment has acquired new features, extending the influence of heat on the rivers and lakes. With the increasing use of coastal waters for the economic and social needs of the growing sources and vulnerability of coastal waters due to the harmful effects of excess concentration of natural substances. Pollution associated with the release of industrial products, etc. require special attention and management of coastal waters. Chemical plants and power plants use the coastal water in large quantities for cooling and throw away the water in the environment with higher temperature. In the paper Suryaman et al. [33] modeled circulation system of cold water from thermal power plant Kilakap which was built and has being operating since 2006, which uses the water of the Indian Ocean as a cooling unit. Water passing through the condenser, is poured back into the ocean through the drainage system. Above the temperature of the water in the ocean is poured from thermal power plant the temperature of the water. It is important that poured warm water with drainage circulating did not get back into the water absorbent water cooling system, since otherwise the temperature water absorbent will continue to grow, in turn causing a temperature increase drainage, etc. temperature rise water absorbent and drainage. Any rise in temperature water absorbent reduces cooling efficiency (capacitors), which eventually leads to a decrease in overall plant efficiency. The heated water

interacts with the natural conditions of the sea or rivers, affecting aquatic life. When the heat acts as a contaminant this called thermal pollutant. The temperature rise affects various physical and chemical properties of sea water such as density, viscosity, dissolved oxygen, salinity, turbidity, aquatic. Physical and chemical properties change directly affects the lives of marine organisms. Some sea creatures can counteract a rise in temperature, but not all organisms possible. The volume effect of the thermal water depends on the volume and temperature of water and poured seawater temperatures (near the drain), circulation flow around the drain. Heat transfer in coastal waters is part of the physical properties that depend on the tides, water depth, sea waves, river flows, salinity, heat source, coastal structures. In this paper Ali et al. [35] built interconnected numerical model, which is a three-dimensional temperature distribution of hot water thrown to standing water. This model is the relationship with the natural experiment, which was carried out on one side of one of the British Channel, using thermal cameras, as a source of shallow and stagnant water, and artificial experiment 10 times smaller, which was held in the laboratory. All three results give a good agreement. This model is used for calculating the temperature distribution in the channel when using water as a coolant channel for environmental purposes instead use conventional capacitors. After use water as the coolant water is returned again into the channel as a hot thermal dome discharged from the tube end. The model shows the heat-proportioned profile of the jet, which resets the thermal plume discharging horizontally into shallow and still receiving water. In the paper Becker et al. [34] used a mathematical model and numerical simulation to verify operation of the circuit water circulation and thermal circulation imposed by the developer of energy-station seaport Zeebrugge in Belgium, on the North Sea coast. Particular attention was paid to the water cooling, as the classical method of cooling the released warm water in the main river was impossible because the internal port (harbor) Zeebrugge, which actually was planned station is not supplied with water from the river. This inner reservoir filled with sea water is cut off from the outer harbor and the sea with two gateways (barriers). The cooling system was the following power-station was planned in the inner harbor of Zeebrugge in Belgium with indirect emissions into the North Sea. If there is a stratification, the lower part of the water is colder, and surface water interact with the environment may lose some of the heat is also part of the surface water enters the main harbor of Zeebrugge through the channel. It is shown that the stratification is created in inland waters. In the main harbor evacuation of heat is mainly due to evaporation and only 20% due to the release of the open sea. Under different atmospheric conditions and operating conditions of the plant have been carried out work to determine the increase in temperature in the harbor and at the entrance to energy plant. The expected increase in the inlet temperature of the plant was expected 1.6^0C and 6.6^0C, but substantially increase in temperature is between $3-4^0C$. It was found that the main influence on the circulation of the internal reservoir is atmospheric conditions. But in the case of atmospheric conditions on the coast of Belgium, the temperature rise is not hard and not serious.

2 Background

The development of local circulation is directly dependent not only on the thermal contrast of the water surface and land. But also significant role is played by local orographic conditions. Probability of breezes' formation on the shores of large bodies of water depends on their geographical location. Changes in the wind direction at the reservoirs and on shore are connected not only with the local circulation. Differences in the roughness of the water surface and land lead to a rotation of the movement direction of the air mass to the right. When the air reaches especially high shore, it tends to move along it, because roughness of the land bigger than water.

This gives the winds' rose the form of coastline. This effect is observed particularly clearly in narrow bays, at narrows of valley type reservoirs. One of the most effective methods of hydrodynamics study of the lake is a method of mathematical modeling. In some cases this may be the only tool to predict changes in the hydrological regime and lake ecosystems. For example, when studying the changes that may occur in spatial redistribution of water, while constructing waterworks and other events associated with the use of water objects. Mathematical models can be classified according to several criteria. It can be classified according to their model "dimension"[12]: one-dimensional (vertical or horizontal), two-dimensional (horizontal or vertical plane), three-dimensional model. The most simple - are one-dimensional models that commonly used for modeling of currents in rivers. Two-dimensional models are used to study wind and seiche flows, storm surges, etc. Lick [25] proposes to consider the following types of mathematical models of wind currents like: 1) integrated model (full flow), in which vertical integration over the flow is accounted but vertical profile of flows not modeled, 2) stationary models of wind currents for constant and variable density of water 3) non-stationary model for barotropic and baroclinic lakes. To study the wind currents Sheng et al. [26] divided the models to: Ekman, integrated by vertical direction, multi-level and multi-layered. In addition to these models the dynamic method and a variety of three-dimensional thermohydrodynamic models are used for calculation of lakes' flows. Previously the impact of thermal discharged water from power plant to reservoir-cooler were studied by [13-15, 17, 18]. There are many mathematical and numerical models have been developed to simulate distribution of temperature from power plant to reservoir - cooler. In recent years, some advanced numerical models [19-24] have been developed for coastal oceans and estuaries with improved performance. These models have been used to simulate circulation and transport process.

3 Reservoir-coolers

Reservoir-cooler is divided into the following groups by appointment, location and conditions of supply:
regulating reservoir on the waterways used not only for cooling circulating water, but also for seasonal or long-term regulation of the flow;
reservoir-cooler in watercourses without flow regulation, under construction just to create a surface sufficient to cool the circulating water;
reservoir-cooler on natural lakes and ponds;
filling reservoir constructed out of watercourse fed from nearby rivers.

The free surface of the reservoir-cooler not totally equal effectively involved in giving the heat coming from the hot water circulation. The amount of heat withdrawn per unit area of a portion of the reservoir surface depends on the water temperature in this region. Therefore, a picture of the temperature distribution on the surface for calculation of the thermal process in reservoir-cooler is necessary to be presented. Consequently, it is necessary to chart the warm water flow distribution from its point of discharge with the place of its intake. Circulation scheme in the reservoir-cooler is determined by its shape, the mutual arrangement of the discharge and intake constructions and by jet distribution and jet guide's facilities. Considering the modern powerful power plants the design of large reservoir-cooler with depths reaching tens meters, and with the volume of water in the hundreds millions of cubic meters we should be aware that in addition to the gradient flows caused by discharge of the circulating flow and intake of river water in reservoirs, there are also wind, density and compensation flow. Wind currents cause the water ebbs from the leeward side of the pond and surges it at the windward side. This occurs when the horizontal pressure gradient directed in the direction opposite to the wind, it is a

type of deep compensating flows. It is known that water has the highest density at 4^0C, but when heated its density decreases. The heat transfer into the water column due to molecular diffusion and thermal conductivity is very weak. Therefore, water temperature stratification is occurred by heating of the upper layers: the surface of water temperature is higher than in the deep layers, and this difference sometimes reaches 10^0C or more. Water temperature difference in the upper and lower layers may become stable with the discharged warm water to the surface of the reservoir. Hence, it leads to a bundle of threads having different density. This case raises the upper warm and deep cold flows, which can be multi-directional.

4 Mathematical modelling

In reservoir - coolers spatial temperature change is small (it usually does not exceed 20^0C). Corresponding change in the density is much smaller than the magnitude of the water density. Therefore, stratified flow in the reservoir - cooler can be described by the equations in the Boussinesq approximation, i.e. in the motion equations a variable of water density can be replaced by some constant everywhere except the members representing the Archimedean force. In view of the above, the starting point for describing the flow in the laminar regime is the Navier - Stokes equation and transport equation for temperature [1, 2, 3, 13-15, 31]. Compared to papers [13-15] in this work and in papers [1, 2, 3] stratification development is taken into account, which is added to the right hand side of motion equation and have the following form:

$$\frac{\partial u_i}{\partial t} + \frac{\partial u_j u_i}{\partial x_j} = -\frac{\partial p}{\partial x_i} + \nu \frac{\partial}{\partial x_j}\left(\frac{\partial u_i}{\partial x_j}\right) + \delta_{i3}\beta g(T - T_0) \tag{1}$$

$$\frac{\partial u_j}{\partial x_j} = 0 \tag{2}$$

$$\frac{\partial T}{\partial t} + \frac{\partial u_j T}{\partial x_j} = \frac{\partial}{\partial x_j}\left(\chi \frac{\partial T}{\partial x_j}\right) \tag{3}$$

where g the gravitational acceleration, β coefficient of volume expansion, u_i - velocity components, χ the thermal diffusivity, T_0- the equilibrium temperature, $T-$ the temperature deviation from equilibrium.

The system of equations are written in the Cartesian coordinate system in the physical space $x_i (i = 1, 2, 3)$, the three components of velocity u_i and pressure p are unknown functions, t - time, ν - the kinematic viscosity of the medium (molecular). Repeated indices should be the summarized in the system of equations (1) - (3) and below.

In the general case, the system of equations (1) - (3) in such way can not be solved because a turbulent model needs to be applied. Large eddy simulation method [4, 28] is used as the turbulent model. Averaged by Favre [4, 6, 7, 10] the system of equations (1) - (3).

This system of equations can be closed by Smagorinsky model [4, 16]. But in this study a dynamic model of Smagorinsky [3, 4, 6, 9] is used as a model of turbulence.

The finite volume method [6, 7] is used for the numerical simulation. We represent the Navier - Stokes equation and transport equation for temperature in the integral conservation laws form for arbitrary fixed volume $\Omega$with the boundary $d\Omega$ [6, 7, 8]:

$$\int_\Omega \left(\frac{\partial U}{\partial t} + \frac{\partial F_i}{\partial x_i} + \frac{\partial G_i}{\partial x_i} - B_i\right) d\Omega = 0, \tag{4}$$

where

$$U = \begin{pmatrix} 0 \\ u_j \\ T \end{pmatrix}, \quad F_i = \begin{pmatrix} u_i \\ u_i u_j + p\delta_{ij} - \tau_{ij} \\ v_i T \end{pmatrix}, \quad G_i = \begin{pmatrix} 0 \\ \nu \frac{\partial u_i}{\partial x_j} \\ \chi \frac{\partial T}{\partial x_j} \end{pmatrix}, \quad B = \begin{pmatrix} 0 \\ \beta g_i (T - T_0) \\ 0 \end{pmatrix}.$$

Now we perform a discretization of equation (1) in the control volume (CV) and the control surface (CS)

$$\sum_{CV} (\frac{\Delta U}{\Delta t}) \Delta\Omega + \sum_{CS} (F_i + G_i) n_i \Delta\Gamma = \overline{B_i} \Delta\Omega \tag{5}$$

5 Numerical algorithm

A good description of the topographic contours of the Zhyngyldy reservoir-cooler shore is required for hydrodynamic modeling. Splitting scheme by the physical parameters is used to solve Navier - Stokes equation and transport equation for temperature, which was proposed by Chorin [11] and used in [5, 8]. Discretization in form of (5) is used for the numerical implementation of the system of equations. At the first step it is assumed that the momentum transfer carried out only by convection and diffusion. Intermediate velocity field is solved by is 5-step Runge - Kutta method [29, 30, 32]. At the second stage, the found intermediate velocity field, forms pressure field. Poisson equation for the pressure field is solved by Jacobi method [6]. The third step assumes that the transfer is carried out only by pressure gradient [5, 11]. The temperature field is solved like the velocity field by 5-step Runge - Kutta method. The numerical algorithm is parallelized on high-performance system and a block partitioning computational domain is used for parallelization algorithm. Below we can see mathematical expressions of numerical algorithm for four stages (splitting scheme by the physical parameters):

I) $\int_\Omega \frac{\boldsymbol{u}^* - \boldsymbol{u}^n}{\tau} d\Omega = -\oint_{\partial\Omega} (\nabla(\boldsymbol{u}^n \, \boldsymbol{u}^* - \tau_{ij}) - \nu \Delta \boldsymbol{u}^*) n_i d\Gamma,$

II) $\oint_{\partial\Omega} (\Delta p) d\Gamma = \int_\Omega \frac{\nabla \boldsymbol{u}^*}{\tau} d\Omega,$

III) $\frac{\boldsymbol{u}^{n+1} - \boldsymbol{u}^*}{\tau} = -\nabla p,$

IV) $\int_\Omega \frac{T^* - T^n}{\tau} d\Omega = -\oint_{\partial\Omega} (\nabla \boldsymbol{u}^n \, T^* - \nu \Delta T^*) n_i d\Gamma.$

6 The results of numerical simulation

To study the vertical inhomogeneities in stratified reservoirs mathematical model was selected and numerical algorithm was developed. It is necessary to do numerical simulations and to compare the results with experimental data in order to check the correctness of the numerical algorithm and the possibility of their further application. Note that we have data only by the vertical distribution of temperature of Ekibastuz SDPP-1 Zhyngyldy Lake. However, these measurements were carried out in 2010 and for the operational capacity of 200 MW. So the verification of the models was carried out on these experimental data. In [27] it is noted that, despite the different weather conditions in different years, the vertical thermal structure of the water does not undergo changes cardinally. Therefore, at the first phase, a mathematical

model was validated by experimental data measured in 2010. The results were compared with experimental data. The results of numerical simulations of the temperature distribution along the depth of the reservoir and the experimental data for the operational capacity of 200 MW for different points on reservoir-cooler, which are presented in figure 1, are shown below in figures 2 - 3. The calculated spatial contour and the isolines of the temperature distribution at different times after the start of Ekibastuz SDPP-1 on the surface of water for the operational capacity 200 MW is shown on the figure 4. Figure 4 shows that the temperature distribution with distance from the discharge is approaching an isothermal condition. These results show that the temperature distribution is spread over a large area of reservoir-cooler. And also from the same figure it can be seen that an increase of thermal power plant's operational capacity, the area of thermal effect becomes directed in the same way, and leads to water warming of only one part of the reservoir, which has a negative effect on the performance of TPP. It to an increase in the operational capacity of Ekibastuz SDPP-1 of reservoir-cooler is not effective, fueling the western part of the reservoir, and the rest is not involved in cooling of heated water from thermal power plant that is resulted in the rapid warming of reservoir-cooler.

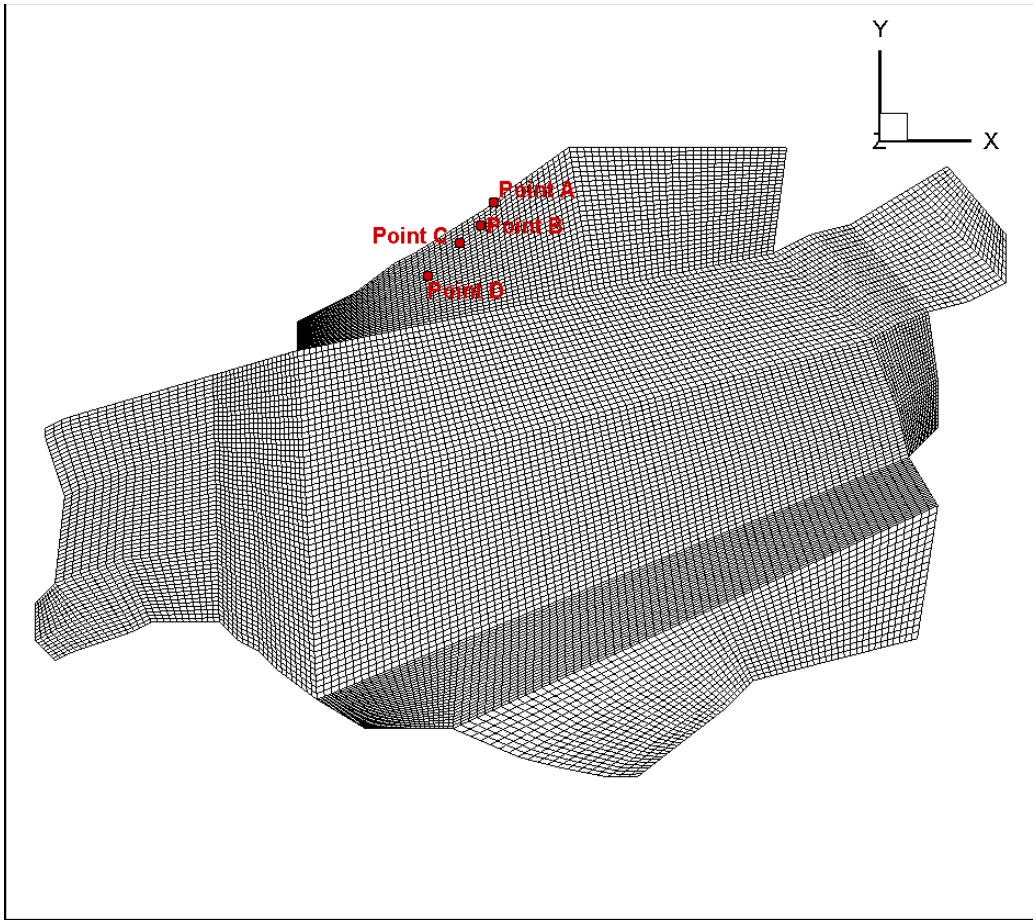

Fig. 1. Computational grid for Ekibastuz SDPP-1

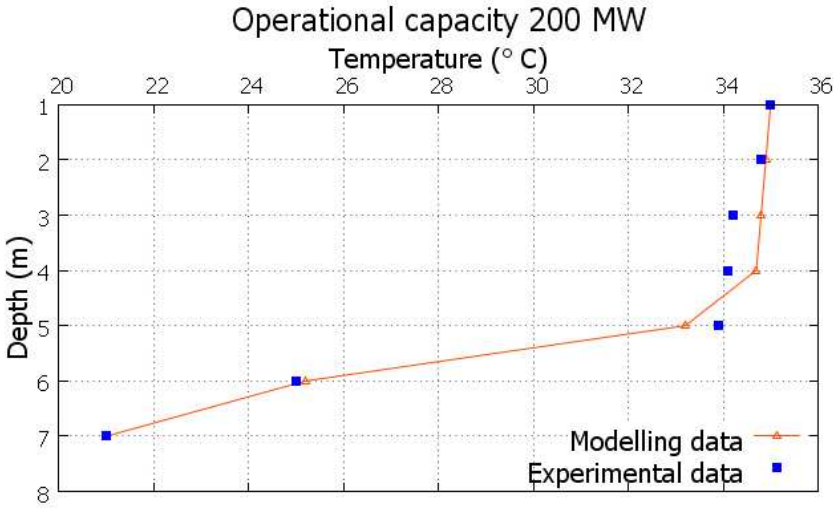

Fig. 2. Comparison of experimental data with simulation data for the operational capacity 200 MW at the point A.

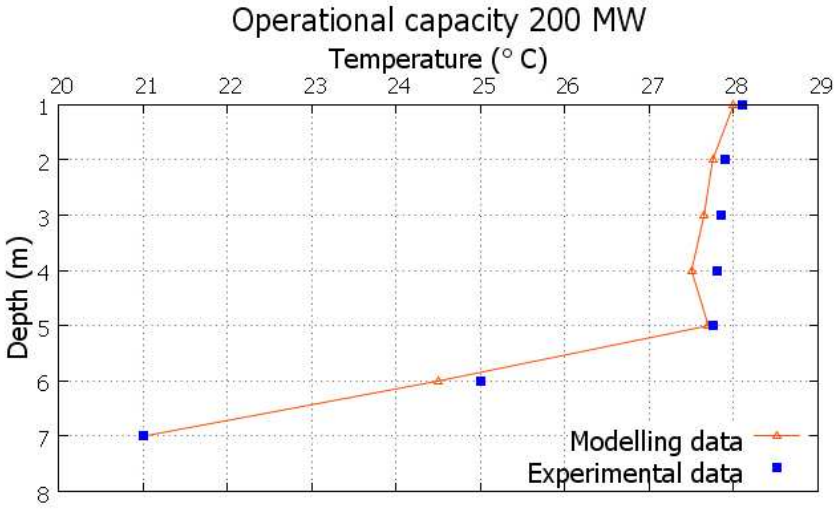

Fig. 3. Comparison of experimental data with simulation data for the operational capacity 200 MW at the point B.

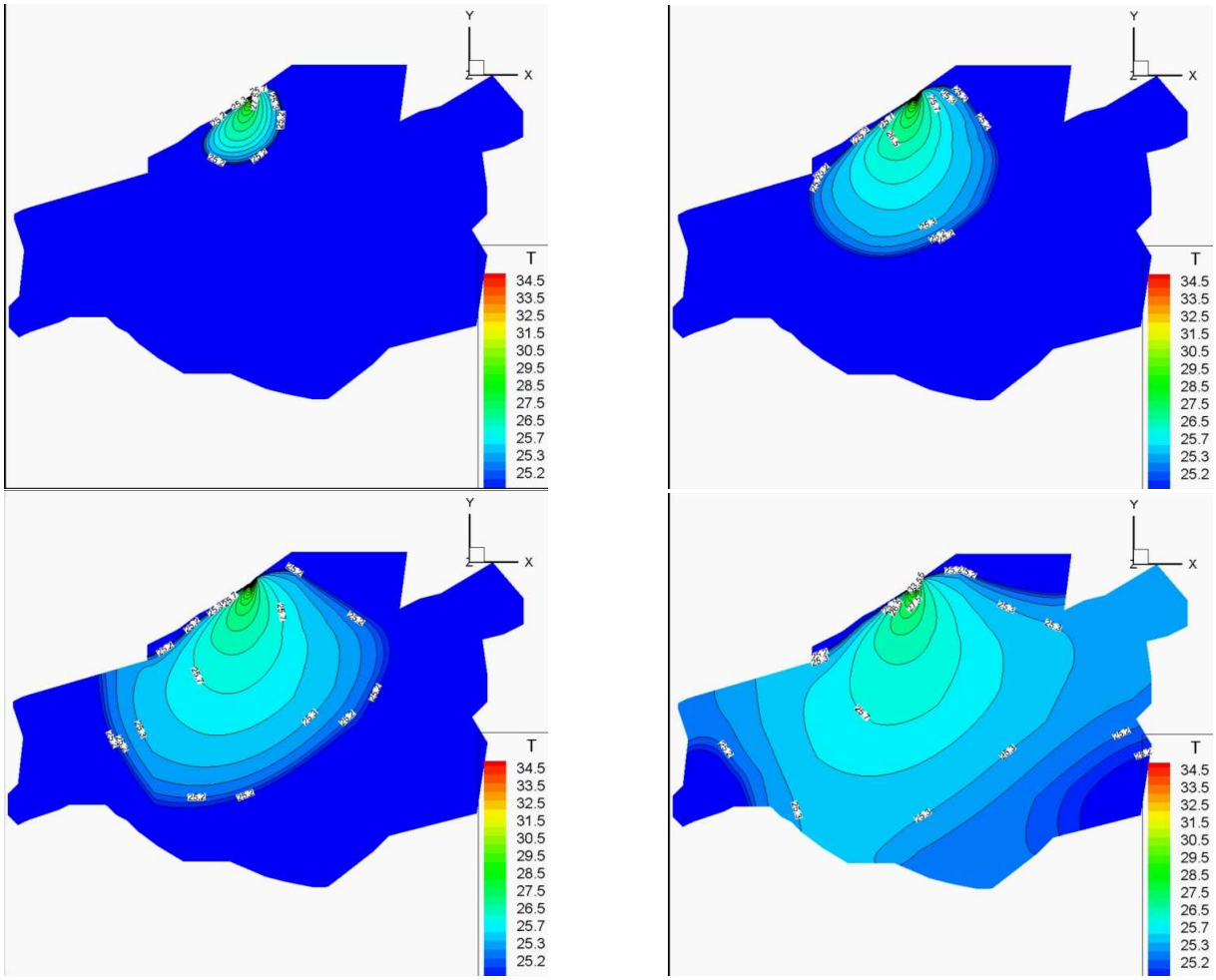

Fig. 4. The spatial contour and isolines of the temperature distribution at 1, 5, 12 and 24 h. after the start of Ekibastuz SDPP-1 on the surface of water for the operational capacity 200 MW.

Thus, the advanced three-dimensional model of a stratified turbulent flow reveals qualitatively and approximately quantitatively the basic laws of hydrothermal processes in the aquatic environment.

Figures 2-3 of the drawings shows that the numerical results agree with the experimental data. A difference in the upper layers can be explained by variations in weather conditions at various times of the day. And also from the figures 2-3 it can be seen that the calculated data from models show quite good results for the operational capacity 200 MW. Models allow us to determine the qualitative vertical structure, the position of the transition zone for the temperature values at the lower and upper layers. Note that mixing occurs under the influence of turbulence and mixing have a significant effect on the flow. The fact that the results are in good agreement with the experimental data says that an adequate simulation of the wind currents. The picture of the wind currents depends on the strength of the wind, stratification and reservoir geometry. A series of calculations were carried out, resulting in the obtained data on the nature of flows, which can be illustrated by some specific examples. One circulation zone is formed for a homogeneous fluid in the reservoir. Furthermore with the increase in the length of the reservoir increases the maximum speed of the water flow.

7 Discussions

LES is a more universal approach to close the system of equations which was filtered by Favre approach. A necessary condition for the performance of turbulent closures are "subgrid"model that correctly describes the dissipation of the kinetic energy of smoothed velocity fluctuations and the ability to simulate the circuit direct energy cascade from large to small eddies. This stage is the primary mechanism for the redistribution of energy in the inertial range of three dimensional homogeneous isotropic turbulence. The principal advantage of the LES from RANS is that, due to the relative homogeneity and isotropy of the small-scale turbulence, plotting a subgrid model is much simpler than the use turbulence models for RANS, when it is necessary to model the full range of turbulence. For the same reason, the hope for a "universal"subgrid model for LES is much more reasonable than a similar model for RANS. These important benefits of LES increase significantly computational cost associated with the need (also for Direct numerical simulation (DNS) case) of three-dimensional time-dependent calculations on sufficiently fine grids. Even also in cases where direct interest to the practice of the average flow is two-dimensional and stationary. On the other hand, for obvious reasons, the computational resources which are required to implement the LES, are much smaller than for the DNS. The degree of influence of different processes governing the formation of stratified flows and hydrothermal conditions in the entire body of water can be divided into two zones. The first (near) zone, directly adjacent to the water of outlet structures. The second is for the major part of the reservoir. In the near zone formation of the stratified flow is influenced by the processes of mixing discharged water with water from the reservoir. It should be regulated by creating a specific hydraulic regime in the outfalls. In the second zone of hydrothermal regime is formed primarily by the processes of heat transfer. The propagation of heat in this part of the reservoir is more dependent on the wind (direction and speed). When you spread the heated water in a cold environment density difference between the upper layer of warm water and bottom layer of cold water appears. This allows the use of a combined intake and discharge instead of building costly diversion canals to the discharge. Accordingly raises the problem of optimal choice of the geometrical and operational parameters of the reservoir - cooler for efficient work of power plant.

References

1. Issakhov, A.: Mathematical Modelling of the Influence of Thermal Power Plant on the Aquatic Environment with Different Meteorological Condition by Using Parallel Technologies. Power, Control and Optimization. Lecture Notes in Electrical Engineering. Volume 239, 165–179 (2013)
2. Issakhov, A.: Mathematical modelling of the influence of thermal power plant to the aquatic environment by using parallel technologies. AIP Conf. Proc. 1499, doi: http://dx.doi.org /10.1063/ 1.4768963, 15–18 (2012)
3. Issakhov, A.: Mathematical Modelling of Thermal Process to Aquatic Environment with Different Hydrometeorological Conditions. The Scientific World Journal, vol. 2014, Article ID 678095, 10 pages, doi:10.1155/2014/678095 (2014)
4. Lesieur, M., Metais, O., Comte, P.: Large eddy simulation of turbulence. New York, Cambridge University Press (2005)
5. Issakhov, A.: Large eddy simulation of turbulent mixing by using 3D decomposition method. Issue 4 (2011) J. Phys.: Conf. Ser. 318, 042051. doi:10.1088/1742-6596/318/4/042051, 1282–1288 (2011)
6. Chung, T. J.: Computational Fluid Dynamics. Cambridge University Press, (2002)
7. Ferziger, J. H., Peric, M.: Computational Methods for Fluid Dynamics. Springer; 3rd edition, (2013)
8. Kim, J., Moin, P.: Application of a fractional-step method to incompressible Navier-Stokes equations, J. Comp. Phys. 59, 308–323 (1985)
9. Roache, P.J.: Computational Fluid Dynamics, Albuquerque, NM: Hermosa Publications, (1972)
10. Peyret, R., Taylor, D. Th.: Computational Methods for Fluid Flow. New York: Berlin: Springer-Verlag, (1983)
11. Chorin, A.J.: Numerical solution of the Navier-Stokes equations. Math. Comp. 22, 745–762 (1968)
12. Abbaspour, M., Javid, A. H., Moghimi, P., Kayhan, K.: Modeling of thermal pollution in coastal area and its economical and environmental assessment. International Journal of Environmental Science and Technology, vol. 2, no. 1, 13–26 (2005)
13. Fossati, M., Santoro, P., Urrestarazu, S., Piedra-Cueva, I.: Numerical Study of the Effect of a Power Plant Cooling Water Discharge in the Montevideo Bay. Journal of Applied Mathematics, vol. 2011, Article ID 970467, 23 pages, doi:10.1155/2011/970467, (2011)
14. Fossati, M., Piedra-Cueva, I.: Numerical modelling of residual flow and salinity in the Rio de la Plata. Applied Mathematical Modelling, vol. 32, no. 6, 1066–1086 (2008)
15. King, I. P.: RMA-10 A finite element model for three-dimensional density stratified flow. Department of Civil and Environmental Engineering, University of California, Davis, California, USA, (1993)
16. Smagorinsky, J.: General Circulation Experiments with the Primitive Equations. Monthly Weather Review, vol. 91, issue 3, 99 (1963)
17. King, I. P.: Finite element modelling of stratified flow in estuaries and reservoirs. International Journal for Numerical Methods in Fluids. Volume 5, Issue 11, 943–955 (1985)
18. King, I. P.: Strategies for Finite Element Modelling of Three Dimensional Hydrodynamic Systems. Advanced Water Resources, Vol. 8, June, 69–76 (1985)
19. Yang, Z., Khangaonkar, T.: Modeling Tidal Circulation and Stratification in Skagit River Estuary Using an Unstructured Grid Ocean Model. Ocean Modelling, 28(1-3), 34–49 (2008)
20. Chen, C., Liu, H., Beardsley, R. C.: An Unstructured Grid, Finite-Volume, Three-Dimensional, Primitive Equations Ocean Model: Application to Coastal Ocean and Estuaries. Journal of Atmospheric and Oceanic Technology 01/2003; 20(1), 159–186 (2003)
21. Zheng, L., Chen, C., Liu, H.: A modeling study of the Satilla River estuary, Georgia. I: Flooding-drying process and water exchange over the salt marsh-estuary-shelf complex. Estuaries and Coasts 05/2003; 26(3), 651–669 (2003)
22. Isobe, A., Beardsley, R. C.: An estimate of the cross-frontal transport at the shelf break of the East China Sea with the Finite Volume Coastal Ocean Model. Journal of Geophysical Research 111:C03012. doi:10.1029/2005JC 003290.
23. Aoki, K., Isobe, A.: Application of finite volume coastal ocean model to hindcasting the wind-induced sea-level variation in Fukuoka bay. Journal of Oceanography 03/2007, 63(2), 333–339 (2007)
24. Weisberg, R. H., Zheng, L.: The circulation of Tampa Bay driven by buoyancy, tides, and winds, as simulated using a finite volume coastal ocean model. Journal of Geophysical Research 111:C01005, doi:10.1029/2005JC003067, (2006)
25. Lick, W.: Numerical models of lakes currents. -EPA-60013-76-020, (1976)
26. Sheng, Y., Lick, W., Gedney, R.T., Molls, F.B.: Numerical computation of three-dimensional circulation of Lake Erie: A comparison of a free-surface model and rigid-Lid. Model. - J. of Phys. Ocean., v.8, 713 – 727, (1978)
27. Dake, J.M.K.: Thermal stratification in lake: analytical and laboratory studies. Water Resour. Res. 5(2), 484-495 (1969)

28. Ferziger, J. H.: Large Eddy Numerical Simulations of Turbulent Flows. AIAA Journal, 15, 10.2514/3.60782, 1261–1267 (1977)
29. Jameson, A., Schmidt, W., Turkel, E.: Numerical Solution of The Euler Equations by Finite Volume Methods Using Runge-Kutta Time-Stepping Schemes. AIAA 14th Fluid and Plasma Dynamic Conference, Palo Alto, California (1981)
30. Sanderse, B., Koren, B.: Accuracy analysis of explicit Runge-Kutta methods applied to the incompressible Navier-Stokes equations. Journal of Computational Physics 231, 3041–3063 (2012)
31. Bork, I., Maier-Reimer, E.: On the Spreading of Power Plant Cooling Water in a Tidal River Applied to the River Elbe // Advances In Water Resources, Vol. 1, Issue 3, DOI:10.1016/0309-1708(78)90027-1, 161–168, (1978)
32. Issakhov, A.: Modeling of synthetic turbulence generation in boundary layer by using zonal RANS/LES method. International Journal of Nonlinear Sciences and Numerical Simulation, 15(2), 115–120 (2014)
33. Suryaman, Dh., Asvaliantina, V., Nugroho, S., Kongko, W.: Cooling Water Recirculation Modeling of Cilacap Power Plant. Proceeding of "The Second International Conference on Port, Coastal, and Offshore Engineering (2nd ICPCO) (2012)
34. Beckers, J.-M., Van Ormelingen, J.-J.: Thermohydrodynamical modelling of a power plant implementation in the Zeebrugge harbor. Journal of hydraulic research, 33 (2), 163–180, (1995)
35. Ali, J., Fieldhouse, J., Talbot, Ch.: Numerical modeling of three-dimensional thermal surface discharges. Engineering application of computational fluid mechanics. 5 (2), 201–209, (2011)

The Size of the Domain of Measurements is the Regularization Parameter in Continuation Problem

Sergey Kabanikhin[1,2] ⋆, Maktagali Bektemesov[3], and Maxim Shishlenin[4,2]

[1]Institute of Computational Mathematics and Mathematical Geophysics,
Acad. Lavrentjev av. 6, Novosibirsk, 630090, Russia
[2]Novosibirsk State University, Pirogova str., Novosibirsk, 630090, Russia
[3]Al-Farabi Kazakh National University, al-Farabi av. 71, Almaty, 050040, Kazakhstan
[4]Sobolev Institute of Mathematics, Acad. Koptyug av. 4, Novosibirsk, 630090, Russia
kabanikhin@sscc.ru,maktagali@mail.ru,mshishlenin@ngs.ru

Abstract. *We consider the 2-dimensional Cauchy problem for the Laplace equation. We employ the gradient method to minimize misfit function, which is a regularizing procedure for the stable determination of the solution. In each iteration step, mixed boundary value problems are solved. We show that the size of the domain of measurements is the regularization parameter. The more information contain the inverse problem data the more stable is the solution. Numerical results are presented and discussed.*

Keywords: continuation problem, Cauchy problem, Laplace equation, regularization, optimization

1 Introduction

The Cauchy problem of Laplace's equation arises from many physical and engineering problems such as nondestructive testing techniques, geophysics and cardiology [1,4,5,11]. The Cauchy problem is known example of ill-posed problem in the sense that a small change in the Cauchy data may result in a dramatic change in the solution [10,21,22,12]. Under an additional a priori boundedness condition, a continuous dependence of the solution on the Cauchy data can be obtained. This is called conditional stability [7,8,17,2,12].

Due to the severely ill-posedness of the problem, numerical computation is very difficult. In order to obtain a stable numerical solution for these kinds of ill-posed problems, many regularization methods have been proposed: the quasi-reversibility method [19,3], the Tikhonov regularization method [9], the boundary element method [24], and discretization [25], moment problem method [6], the iterative method [20,18,23], etc.

Some problems of interpreting gravitational and magnetic fields related to mineral exploration lead to ill-posed problems equivalent to the Cauchy problem for Laplace equation. Let us consider two examples.

Example 1 (Laplace and Poisson equation). Suppose that local part of the Earth can be described as the part of the half-space (see Figure 1). The inhomogeneity of the density distribution under the surface $x = 0$ of the Earth causes the gravitational field strength on the Earth's surface to deviate from its mean value (see left picture of Figure 2). Although these deviations are small in terms of percentage, they are reliably registered by physical devices (gravimeters). Gravimetric data are used in mineral exploration and prospecting.

The purpose of gravimetric exploration is to determine the location and shape of subsurface inhomogeneities based on gravimetric measurement data. If the distance between geological

⋆ This work was supported by the Russian Foundation for Basic Research (project No. 14-01-00208), the Ministry of Education and Science of the Russian Federation and the Ministry of Education and Science of the Republic of Kazakhstan, grant 1746/GF "Theory and numerical methods for solving inverse and ill-posed problems of natural Sciences".

bodies is greater than the distance between either of them and the surface of the Earth, then their locations correspond to the local maxima of the anomalies. Otherwise, the two bodies may be associated with a single local maximum (see left picture of Figure 2).

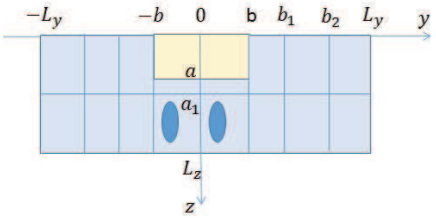

Fig. 1. Domain and two anomalies.

The main stage of prospecting consists in drilling the exploratory wells and analyzing the drilling data. If the shape of an anomaly leads us to the conclusion that it represents a single body, then a natural choice would be to drill in the center of the anomaly.

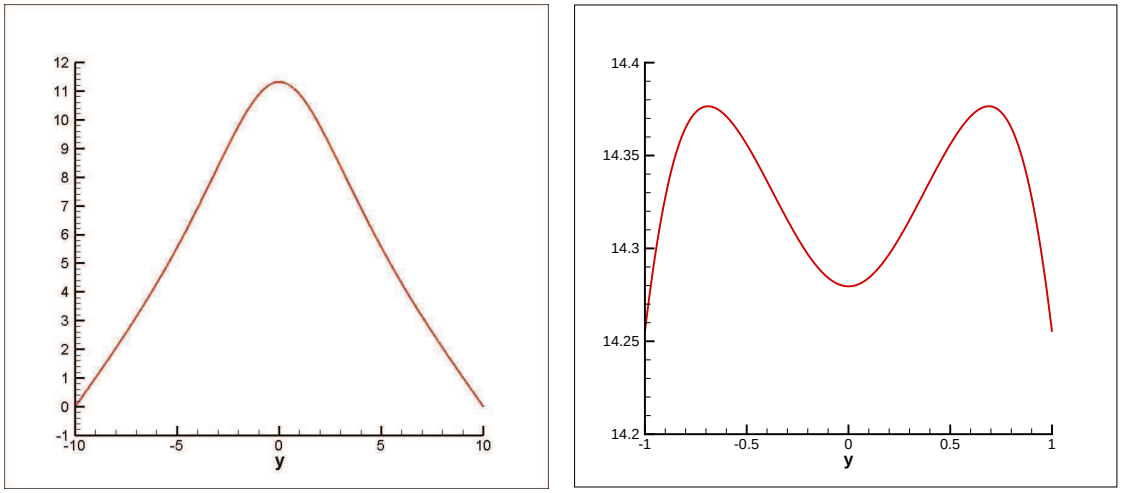

Fig. 2. Left — measured data $u(0, y)$. Right — the result of the continuation of Laplace equation solution $u(a_1, y)$.

However, if the conclusion is wrong, the decision to drill in the center will result in the well being drilled between the actual bodies that we are interested in.

This was often the case in the practice of geological exploration. Then it was proposed to calculate the anomalous gravitational field at a certain depth under the surface based on the results of the gravitational measurements performed on the surface of the Earth (i.e., to solve the Cauchy problem for Laplace equation).

If it turns out that the anomaly at that depth still has a single local maximum, then it is highly probable that the anomaly is generated by a single body.

Otherwise, if two local maxima appear as a result of numerical continuation, then we can conclude that there are two bodies, and the locations for drilling must be chosen accordingly.

Example 2 (Maxwells equation). A similar problem formulation arises when interpreting anomalies of a constant magnetic field, since the potential and the components of the field strength outside the magnetic bodies also satisfy Laplace equation.

In electrical sounding using direct-current resistivity methods, direct current is applied to two electrodes inserted into the ground and the potential difference on the surface is measured. It is required to determine the structure of the subsurface area under study based on the measurement results. If the sediment layer is a homogeneous conductive medium and the basement resistivity is much higher, then the electric current lines will run along the relief of the basement surface. Consequently, to determine the relief of the basement surface, it suffices to determine the electric current lines in the sediment layer.

In a homogeneous medium, the direct current potential satisfies Laplace equation. The normal derivative of the electric potential on the Earth's surface is equal to zero. The potential is measured. Thus, we again arrive at the Cauchy problem for Laplace equation.

2 Continuation problem for Laplace equation as the inverse problem

Continuation problem:

$$u_{zz} + u_{yy} = 0, \qquad (z, y) \in \Omega(a_1, L_y), \tag{1}$$

$$u_z(0, y) = 0, \qquad y \in (-L_y, L_y), \tag{2}$$

$$u(0, y) = f(y), \qquad y \in (-L_y, L_y), \tag{3}$$

$$u(z, -L_y) = u(z, L_y) = 0, \qquad z \in (0, a_1). \tag{4}$$

Here $\Omega(a_1, L_y) = \{(z, y) : z \in (0, a_1), y \in (-L_y, L_y)\}$.

Consider the ill-posed continuation problem as an inverse problem with respect to the direct problem (1), (2), (4) and the boundary condition on $z = a_1$:

$$u(a_1, y) = q(y), \qquad y \in (-L_y, L_y). \tag{5}$$

In the direct problem (1), (2), (4) and (13) it is required to determine $u(z, y)$ in $\Omega(a_1, L_y)$ from the function $q(y)$ given on the part of the boundary $z = a_1$ of the domain $\Omega(a_1, L_y)$.

The inverse problem consists of finding $q(y)$ using the additional information

$$u(0, y) = f(y), \qquad y \in (-L_y, L_y). \tag{6}$$

3 The estimate of the conditional stability

Theorem 1. Let q, $f \in L_2(-L_y, L_y)$. If the continuation problem (1)—(4) has a solution $u \in C^2(\overline{\Omega(a_1, L_y)})$, then it satisfies the inequality

$$\int_{-L_y}^{L_y} u^2(z, y)\mathrm{d}y \le ||q||^{2z/a_1}_{L_2(-L_y, L_y)} ||f||^{2(a_1 - z)/a_1}_{L_2(-L_y, L_y)}, \qquad z \in (0, a_1).$$

Theorem 2 (the rate of convergence with respect to the functional).

Assume that the problem $Aq = f$ with $f \in L_2(-L_y, L_y)$ has a solution $q_e \in L_2(-L_y, L_y)$.

If the initial approximation q_0 such that $||q_0 - q_e||_{L_2(-L_y, L_y)} \le C$, then the iterations q_n of the steepest descent method converge with respect to the cost functional, and the following estimate holds:

$$J(q_n) \le \frac{C^2}{n}, \qquad n = 1, 2, \ldots$$

Theorem 3 (the rate of the strong convergence)

Assume that the problem $Aq = f$ with $f \in L_2(-L_y, L_y)$ has a solution $q_e \in L_2(-L_y, L_y)$, and the initial approximation q_0 such that $||q_0 - q_e||_{L_2(-L_y,L_y)} \leq C$.

Then the sequence $\{u_n\}$ of solutions to the continuation problems converges to the exact solution $u_e \in L_2(\Omega(a_1, L_y))$ to the continuation problem and the following estimate holds:

$$\int_{-L_y}^{L_y} (u_n(z,y) - u_0(z,y))^2 \mathrm{d}y \leq C^2 n^{\frac{z-a_1}{a_1}}, \qquad z \in (0, a_1).$$

4 Optimization method

Let us introduce adjoint problem

$$\psi_{zz} + \psi_{yy} = 0, \qquad (z,y) \in \Omega(a_1, L_y), \tag{7}$$
$$\psi_z(0,y) = \mu(y), \qquad y \in (-L_y, L_y), \tag{8}$$
$$\psi(a_1,y) = q(y), \qquad y \in (-L_y, L_y), \tag{9}$$
$$\psi(z,-L_y) = \psi(z,L_y) = 0, \qquad z \in (0, a_1). \tag{10}$$

We introduce the operator

$$A : q(y) \to u(0,y), \qquad A : H^{\frac{1}{2}}(-L_y, L_y) \to H^{\frac{1}{2}}(-L_y, L_y).$$

Then the adjoint operator of A has the form

$$A^* : \mu(y) \to \psi_z(a_1, y).$$

Therefore, the inverse problem can be written in the operator form [**?**]

$$Aq = f.$$

We will find the solution minimizing the cost functional

$$J(q) = ||Aq - f||^2_{L_2(-L_y,L_y)}.$$

Note, that the $J'(q)$ can be calculated by the formula $J'(q)(z,y) = \psi_z(a_1, y)$, where $\mu(y) = 2(u(0,y) - f(y))$.

5 Numerical regularization. The size of domain is the regularization parameter.

In numerical calculations first we solve the following direct problem

$$u_{zz} + u_{yy} = F(z,y), \qquad (z,y) \in \Omega(L_x, L_y), \tag{11}$$
$$u_z(0,y) = g(y), \qquad y \in (-L_y, L_y), \tag{12}$$
$$u(L_x,y) = 0, \qquad y \in (-L_y, L_y), \tag{13}$$
$$u(z,-L_y) = u(z,L_y) = 0, \qquad z \in (0, a_1). \tag{14}$$

Continuation problem:

$$u_{zz} + u_{yy} = 0, \qquad (z,y) \in \Omega(a_1, b), \tag{15}$$
$$u_z(0,y) = 0, \qquad y \in (-L_y, L_y), \tag{16}$$
$$u(0,y) = f(y), \qquad y \in (-L_y, L_y). \tag{17}$$

For finding solution of the continuation problem we use sequence of the extending domains $\Omega(a_1, b) \subset \Omega(a_1, b_1) \subset \Omega(a_1, b_2) \subset \dots$

We will show that the size of the domain of measurement, namely, b_k can be treated as the parameter of regularization.

We reformulate the continuation problem (1) as the inverse problem. Let us consider the direct problem

$$u_{zz} + u_{yy} = 0, \qquad (z, y) \in \Omega(h, b), \tag{18}$$
$$u_z(0, y) = g(y), \qquad y \in (-b, b), \tag{19}$$
$$u(h, y) = q(y), \qquad y \in (-b, b), \tag{20}$$
$$u(z, -b) = q_1(z), \qquad z \in (0, h), \tag{21}$$
$$u(z, b) = q_2(z), \qquad z \in (0, h). \tag{22}$$

The inverse problem is to find functions $q(y)$, $q_1(z)$, $q_2(z)$ by known additional information about the solution

$$u(0, y) = f(y), \qquad y \in (-b, b). \tag{23}$$

Let $\boldsymbol{q} = (q, q_1, q_2)$.

Optimization method

$$\boldsymbol{q}_{n+1} = \boldsymbol{q}_n - \alpha J'(\boldsymbol{q}_n).$$

$$J'(\boldsymbol{q}_n) = (\psi_z(a_1, y), -\psi_y(z, -b), -\psi_y(z, b)).$$

We demonstrate numerically that the size of the domain of measurement b_k can be treated as the parameter of regularization.

Let $u_e(z, y)$ be exact solution of the direct problem (1) and $u_n^{(k)}(z, y)$ be approximate solution of the continuation problem (5) on n-th iteration in $\Omega(h, b_k)$.

We will estimate

$$\varepsilon_n = ||u_e - u_n^{(k)}||_{L_2(\Omega(a,b))}$$

and show that applying the more size of the domain of measurement $(-b, b) \subset (-b_1, b_1) \subset (-b_2, b_2) \subset \dots$ the solution of continuation problem becomes more stable in the domain $\Omega(a, b)$ (see Figures 3 and 4).

For numerical calculations we chose the following values: $L_z = 10$, $L_y = 10$, $a_1 = 1$, $a = 0.9$, $b = 1$, $b_1 = 2$, $b_2 = 3$, $b_3 = 4$, $b_4 = 5$, $b_5 = 6$, $b_6 = 7$, $n = 1000$, $\alpha = 0.5$, mesh size $N_z = 1000$, $N_y = 2000$.

$$F(z, y) = 200e^{-40(z-1.6)^2}(e^{-40(y-1)^2} + e^{-40(y+1)^2}).$$

The main volume of the function $F(z, y)$ is located in two small balls under the boundary $z = h$ (see Figure 1).

We see on Figures 3) and 4) that the size of the measured domain b_k is the regularization parameter. The more information contain the inverse problem data the more stable is the solution. The optimal parameter is b_5 with minimal residual.

Acknowledgments

This work was supported by the Russian Foundation for Basic Research (project No. 14-01-00208), the Ministry of Education and Science of the Russian Federation and the Ministry of Education and Science of the Republic of Kazakhstan, grant 1746/GF “Theory and numerical methods for solving inverse and ill-posed problems of natural Sciences”.

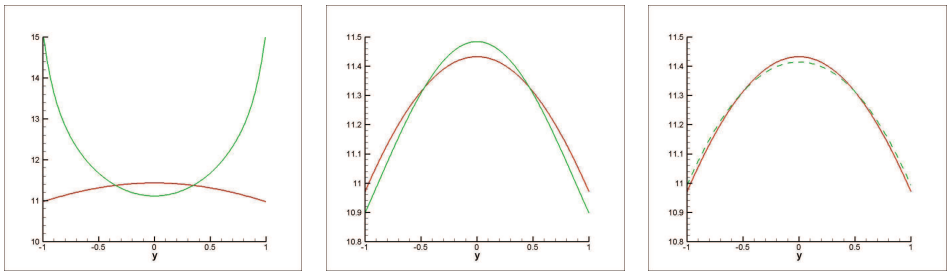

Fig. 3. Left — $u_n^{(1)}(a,y)$ and $\varepsilon_n = 0.435$. Center — $u_n^{(2)}(a,y)$ and $\varepsilon_n = 0.242$. Right — $u_n^{(3)}(a,y)$ and $\varepsilon_n = 0.154$.

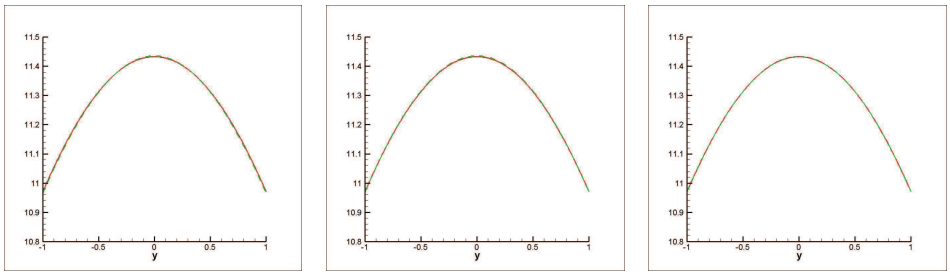

Fig. 4. Left — $u_n^{(4)}(a,y)$ and $\varepsilon_n = 0.086$. Center — $u_n^{(5)}(a,y)$ and $\varepsilon_n = 0.053$. Right — $u_n^{(6)}(a,y)$ and $\varepsilon_n = 0.055$.

References

1. Alessandrini, G.: Stable determination of a crack from boundary measurements Proc. Roy. Soc. Edinburgh Sec. A, 123, 961-вЂ“984 (1993)
2. Alessandrini, G., Rondi, L., Rosset, E., Vessella, S.: The stability for the Cauchy problem for elliptic equations, Inverse Problems. 25, 123004 (2009)
3. Cao, H., Klibanov, M.V., Pereverzev, S.V.: A Carleman estimate and the balancing principle in the quasi-reversibility method for solving the Cauchy problem for the Laplace equation, Inverse Problems, 25, 1–21 (2009)
4. Bukhgeim, A.L., Cheng, J., Yamamoto, M.: Stability for an inverse boundary problem of determining a part of boundary. Inverse Probl. 15, 1021-вЂ“1032 (1999)
5. Cheng, J., Yamamoto, M.: Local stability of a linearized inverse problem in detecting steel reinforcement bars. MatimyГЎs Mat. 21, 18-вЂ“33 (1998)
6. Cheng, J.,Hon, Y.C., Wei, T., Yamamoto, M.: Numerical computation of a Cauchy problem for Laplace's equation. ZAMM Z. Angew. Math. Mech. 81, 665–674 (2001)
7. Cheng, J., Yamamoto, M.: Unique continuation on a line for harmonic functions. Inverse Probl. 14, 869–882 (1998)
8. HГ o, D.N., Hien, P.M.: Stability results for the Cauchy problem for the Laplace equation in a strip. Inverse Probl. 19 833–844 (2003)
9. Engl, H.W., Hanke, M., Neubauer, A.: Regularization of inverse problems, Kluwer, Dordrecht (1996)
10. John, F.: Continuous dependence on data for solutions of partial differential equations with a prescribed bound., Commun. Pure Appl. Math. 13, 551–585 (1960)
11. Colli-Franzone, P., Guerri, L., Tentoni, S., Viganotti, C., Baruffi, S., Spaggiari, S., Taccardi, B.: A mathematical procedure for solving the inverse potential problem of electrocardiography. Analysis of the time-space accuracy from in vitro experimental data. Math. Biosci. 77, 353-вЂ“396 (1985)
12. Kabanikhin, S.I.: Inverse and Ill-Posed Problems, De Gruyter (2012)
13. Kabanikhin, S.I, Shishlenin, M.A., Nurseitov, D.B., Nursetova, A.T., Kasenov, S.E.: Comparative analysis of methods for regularizing an initial boundary value problem for the Helmholtz equation. Journal of Applied Mathematics. 2014, 7 pages (http://dx.doi.org/10.1155/2014/786326) (2014)
14. Kabanikhin, S.I., Gasimov, Y.S., Nurseitov, D.B., Shishlenin, M.A., Sholpanbaev, B.B., Kasenov, S.E.: Regularization of the continuation problem for elliptic equations. Journal of Inverse and Ill-Posed Problems. 21(6), 871–884 (2013)
15. Kabanikhin, S.I., Nurseitov, D.B., Shishlenin, M.A., Sholpanbaev, B.B.: Inverse Problems for the Ground Penetrating Radar. Journal of Inverse and Ill-Posed Problems. 21(6), 885–892 (2013)

16. Kabanikhin, S.I., Karchevsky, A.L.: Optimization method for solving the Cauchy problem for an elliptic equation. J. Inverse Ill-Posed Problems. 3, 21вЂ“46 (1995)
17. Kabanikhin, S.I., Schieck, M. Impact of conditional stability: Convergence rates for general linear regularization methods. J. Inv. Ill-Posed Problems. 16 (3), 267-282 (2008)
18. Kabanikhin, S.I., Karchevsky, A.L. Method for solving the Cauchy Problem for an Elliptic Equation. Journal of Inverse and Ill-posed Problems. 3(1), 21–46 (1995)
19. M.V. Klibanov and F. Santosa, A computational quasi-reversibility method for Cauchy problems for Laplace's equation, SIAM J. Appl. Math. 51 (1991), 1653– 1675.
20. Kozlov, V.A., Mazya, V.G., Fomin, A.V.: On iteration method for solving the Cauchy problem for elleptic equations, Zh. Vychisl. Mat. Fiz. 31(1), 64–74 (1991) (in Russian)
21. Lavrent'ev, M.M., Romanov, V.G., Shishatskii, S.P.: Ill-posed problems of mathematical physics and analysis, translated by J. R. Schulenberger, Translations of Mathematical Monographs, vol. 64, American Mathematical Society, Providence, R. I. (1986)
22. Lavrent'ev, M.M., Savel'ev, L.Ja.: Operator Theory and Ill-Posed Problems, Walter de Gruyter (2006)
23. Lesnic, D., Elliott, L., Ingham, D.B.: An iterative boundary element method for solving numerically the Cauchy problem for the Laplace equation, Eng. Anal. Bound. Elem. 20 123-вЂ“133 (1997)
24. НГ o, D.N., Lesnic, D.: The Cauchy for Laplace's equation via the conjugate gradient method. IMA J. Appl. Math. 65, 199–217 (2000)
25. Reinhardt, H.J., Han, H., НГ o, D.N.: Stability and regularization of a discrete approximation to the Cauchy problem of Laplace's equation. SIAM J. Numer. Anal. 36, 890–905 (1999)

Mathematical Modelling of Particle Motion under the Influence of Spacecraft Rocket Engine Supersonic Jets in Mars Environment

Anuar Kagenov *, Anatoliy Glazunov, and Ivan Eremin

National Research Tomsk State University,
36, Lenin Avenue, 634050 Tomsk, Russia
anuar@ftf.tsu.ru
http://www.tsu.ru

Abstract. The paper presents the results of mathematical modelling of landing a spacecraft (SC) "ExoMars"on the surface of Mars. During the numerical research the distance from which soil erosion is beginning to happen was revealed. The greatest destructive force of supersonic jets of propulsion systems (PS) are at a height of 1 meter and below. Qualitative and quantitative results of the behaviour of solid particles during the process of soil erosion under the influence of supersonic jets of PS while landing SC "ExoMars"on the surface of Mars were obtained.

Keywords: Mathematical modelling, Mars, spacecraft "ExoMars supersonic jet, solid particles

1 Introduction

Due to an increasing interest to the planet Mars, there are various space programs for study of outer space, nearest planets and satellites which are actively developed, such as the "Phobos-Grunt "ExoMars "Mars Scout "MAVEN "Curiosity"and etc. For this purpose, landing platform of SC, intended to explore Mars, is constantly designed and modified. While landing of supersonic jets of PS impingements with the Mars surface. This leads to erosion of the Mars soil, which in turn can form a cloud of dust away from the Mars. At low altitude, deposition of particles of dust on top of the spacecraft landing platform is also possible. These factors may adversely affect the correct operation of the on-board hardware and payload of SC. Therefore, during designing of the SC and PS, the behaviour of dust particles at different modes of PS and distances from the surface of Mars should be considered.

2 Physical and mathematical model

Considered in this paper SC "ExoMars"[1]. Figure 1 shows the configuration of the landing platform. It consists of platform, PS, radar, tanks of fuel and helium, thermal honeycomb panels, complex scientific equipment and mars rover. PS consists of four liquid rocket engines which can change direction of the thrust.

According to the planned descent of the spacecraft on the surface of Mars, the PS will start at an altitude of 600-1000 meters, and at a height of 10 meters the speed of descent is reduced to 2 m/s, and the PS must be operated at low thrust force [2]. With regards to the landing of SC, the program "ExoMars"has a number of requirements towards properties of soil in order to ensure a safe landing, and to achieve the objectives of the rover and the landing platform [3]. The place for landing should be ancient, have morphological and abundant mineral evidence of water activity, and contain sedimentary outcrops that should be allocated to the landing ellipse and have a small dusty cover.

* This research carried out in 2015 was supported by grant (No 8.2.45.2015) from "The Tomsk State University Academic D.I. Mendeleev Fund Program".

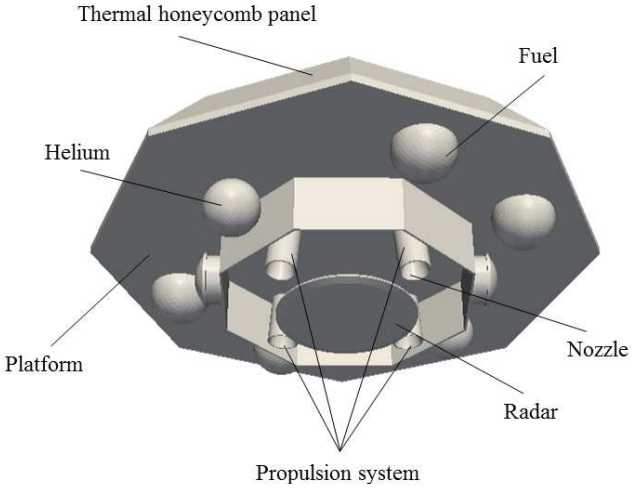

Fig. 1. Configuration of SC "ExoMars".

For mathematical modelling of SC landing on Mars the problem should be considered in three-dimensional unsteady viscous formulation, due to the complex configuration of SC, nature landscape, landing place and the presence of particles of soil, and sand in the atmosphere.

In the description of unsteady viscous compressible gas flow in a three-dimensional approximation of the laws dealt with conservation of mass, momentum and energy, were used the following assumptions: the gas was considered to be ideal, gravity was not considered [4,5,6]. The continuity equation:

$$\frac{\partial \rho}{\partial t} + \frac{\partial}{\partial x_j}\left[\rho u_j\right] = 0. \tag{1}$$

The momentum equation:

$$\frac{\partial}{\partial t}\left(\rho u_i\right) + \frac{\partial}{\partial x_j}\left[\rho u_i u_j + p\delta_{ij} - \tau_{ji}\right] = 0, \quad i = 1, 2, 3. \tag{2}$$

The energy equation:

$$\frac{\partial}{\partial t}\left(\rho E\right) + \frac{\partial}{\partial x_j}\left[\rho u_j E + u_j p + q_j - \tau_{ij}\right] = 0. \tag{3}$$

The ideal gas equation:

$$p = \rho R T, \tag{4}$$

where the viscous stress $\tau_{ij} = 2\mu S_{ij}$ and the trace-less viscous strain-rate

$$S_{ij} = \frac{1}{2}\left(\frac{\partial u_i}{\partial x_j} + \frac{\partial u_j}{\partial x_i}\right) - \frac{1}{3}\frac{\partial u_k}{\partial x_k}\delta_{ij}.$$

The total energy was defined by:

$$E = e + \frac{u_k^2}{2}. \tag{5}$$

Turbulent model $k - \omega$ SST was used [7], which included two equations.
The turbulence kinetic energy:

$$\frac{\partial(\rho k)}{\partial t} + \frac{\partial\left(\rho u_j k\right)}{\partial x_j} = P - \beta^* \rho\omega k + \frac{\partial}{\partial x_j}\left[\left(\mu + \sigma_k \mu_t\right)\frac{\partial k}{\partial x_j}\right]. \tag{6}$$

The specific dissipation rate:

$$\frac{\partial(\rho\omega)}{\partial t}+\frac{\partial(\rho u_j\omega)}{\partial x_j}=\frac{\gamma_t}{\nu_t}P-\beta\rho\omega^2+\frac{\partial}{\partial x_j}\left[(\mu+\sigma_\omega\mu_t)\frac{\partial\omega}{\partial x_j}\right]+ +2(1-F_1)\frac{\rho\sigma_{\omega 2}}{\omega}\frac{\partial k}{\partial x_j}\frac{\partial\omega}{\partial x_j}. \tag{7}$$

The turbulent viscosity was defined by the following equation:

$$\mu_t=\frac{\rho a_1 k}{\max(a_1\omega,\Omega F_2)}, \tag{8}$$

where

$$\Omega=\sqrt{2W_{ij}W_{ij}}, \tag{9}$$

$$W_{ij}=\frac{1}{2}\left(\frac{\partial u_i}{\partial x_j}-\frac{\partial u_j}{\partial x_i}\right). \tag{10}$$

Below are closure coefficients and auxiliary relations:

$$\nu_t=\frac{\mu_t}{\rho}, \tag{11}$$

$$F_2=\tanh\left(\arg_2^2\right), \tag{12}$$

$$\arg_2=\max\left(\frac{\sqrt{k}}{\beta^*\omega d},\frac{500\nu}{d^2\omega}\right), \tag{13}$$

$$P=\min\left(\mu_t S^2,10\beta^*\rho k\omega\right), \tag{14}$$

$$F_1=\tanh(\arg_1^4), \tag{15}$$

$$\arg_1=\min\left[\max\left(\frac{\sqrt{k}}{\beta^*\omega d},\frac{500\nu}{d^2\omega}\right),\frac{4\rho\sigma_{\omega 2}k}{CD_{k\omega}d^2}\right], \tag{16}$$

$$CD_{k\omega}=\max\left(2\rho\sigma_{\omega 2}\frac{1}{\omega}\left[\frac{\partial k}{\partial x_j}\frac{\partial\omega}{\partial x_j}\right],10^{-20}\right), \tag{17}$$

$$\sigma_k=F_1\sigma_{k1}+(1-F_1)\sigma_{k2}, \tag{18}$$

$$\sigma_\omega=F_1\sigma_{\omega 1}+(1-F_1)\sigma_{\omega 2}, \tag{19}$$

$$\beta=F_1\beta_1+(1-F_1)\beta_2. \tag{20}$$

$$\gamma_t=F_1\gamma_1+(1-F_1)\gamma_2, \tag{21}$$

where γ_1 and γ_2 represent the following constants:

$$\gamma_1=\frac{\beta_1}{\beta^*}-\frac{\sigma_{\omega 1}k_1^2}{\sqrt{\beta^*}}, \tag{22}$$

$$\gamma_2=\frac{\beta_2}{\beta^*}-\frac{\sigma_{\omega 2}k_2^2}{\sqrt{\beta^*}}. \tag{23}$$

Given the fact that the PS consists of liquid rocket engine, heat and mass transfer between the particles and the gas is not important and the task is necessarily to determine the behaviour of solid particles under the influence of the PS supersonic jets, and we can neglect the influence of

solid particles on the gas flow. In order to simplify the model, following assumptions were made: spherical particles are relied, due to the small size of the particles Magnus force was neglected, particles did not interact with each other [8].
The mass for each particle was defined by:

$$m_p = \frac{1}{6}\rho_p \pi D_p^3. \tag{24}$$

The velocity for each particle:

$$\frac{dx_{pi}}{dt} = u_{pi}. \tag{25}$$

The motion of particles was governed by Newton's law:

$$m_p \frac{du_{pk}}{dt} = \sum F_k. \tag{26}$$

Acting forces were considering gravity and drag:

$$\sum F_k = F_{Dk} + m_p g. \tag{27}$$

The drag force:

$$F_{Dk} = -\frac{u_{pk} - u_k}{\tau_p}. \tag{28}$$

The Reynolds number for particle:

$$\mathrm{Re}_p = \frac{\rho D_p \left| u_k - u_{pk} \right|}{\mu}. \tag{29}$$

The relaxation time provided Re<1 was described by following equation:

$$\tau_p = \frac{\rho_p D_p^2}{18\mu}. \tag{30}$$

Due to the significant impact of the drag force at high Reynolds numbers, the expression for the relaxation time was written as follows:

$$\tau_p = \frac{4\rho_p D_p}{3\rho C_D \left| u_k - u_{pk} \right|}. \tag{31}$$

where C_D- the drag coefficient depending on the Reynolds number:

$$C_D = \begin{cases} \frac{24}{\mathrm{Re}_p}\left(1 + \frac{1}{6}\mathrm{Re}_p^{\frac{2}{3}}\right), & \mathrm{Re}_p \le 1000; \\ 0.44, & \mathrm{Re}_p > 1000. \end{cases} \tag{32}$$

3 Solution methods

Geometry of SC "ExoMars"was created by Salome. Computation mesh automatic 3d tetrahedral mesh generator was generated. Mathematical modelling using open-source software OpenFOAM was done [9]. Numerical method of OpenFOAM is implemented utilizing finite volume method, mathematical model Riemann problem is based using approximate scheme HLLC [10]. Discretization in time was performed by the Runge Kutta method. Calculating trajectories of solid particles were carried out on a stationary gas field. In the gas field the calculation of particle trajectories is carried out in Lagrange formulation. Numerical investigations were done using supercomputer of National Research Tomsk State University SKIF Cyberia.

4 Results

Operation of PS at the minimum and maximum mode at 1, 0.5 and 0.3 meters was investigated. All characteristics of PS listed in [11]. The surface which located under the SC in the approximate form of the landscape of Mars was set. The parameters of the environment pressure, equal to 650 Pa and the temperature to 250 K, was set. Acceleration of gravity for solid particles was 3.711 m/s^2. Calculations of the supersonic flow of landing platform PS products of combustion before the release of a steady state were conducted. In figure 2 and 3 are shown streamlines for maximum and minimum mode at a height 0.3 meter.

There are presented two variants of calculation of solid particles trajectories in the paper. In the first variant, solid particles, evenly single layer, are spaced on the surface of Mars, after that they are subjected to force effects of supersonic jets at the maximum and minimum mode of PS for 0.2 seconds at heights of 0.3, 0.5 and 1 meters.

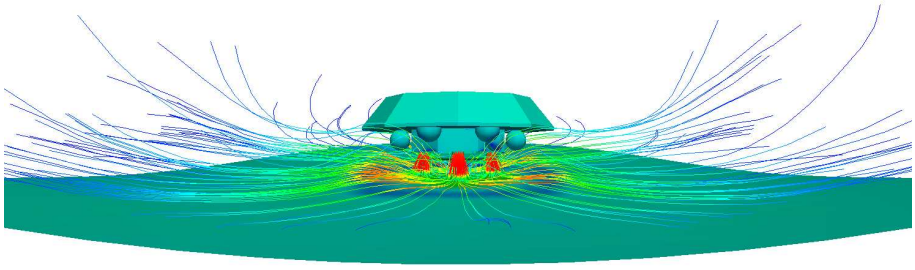

Fig. 2. Streamlines, maximum mode of PS, height 0.3 meter.

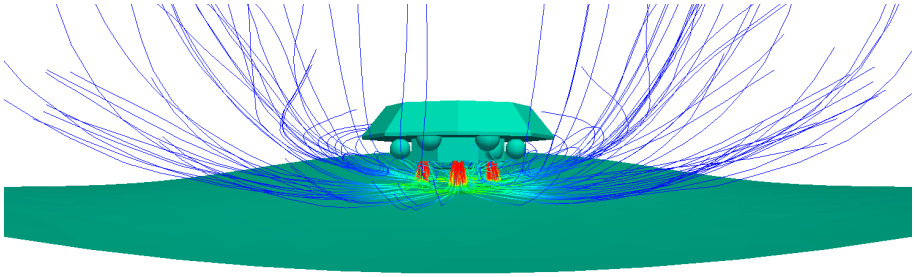

Fig. 3. Streamlines, minimum mode of PS, height 0.3 meter.

In the investigated areas of landing spacecraft "Viking "Pathfinder"and "MER the surface of Mars consists of bulk (1-10 μm), lumpy (5-3000 μm) of soil and sand (60-200 μm) [12], therefore, the diameter of particles in the numerical calculations was varied from 10 to 1000 μm. In figure 4, 5 and 6 are shown calculation results for solid particle with diameter of 10, 100 and 1000 μm under influence of PS supersonic jets at minimum mode on height 0.3 meter.

Numerical study showed that the particles with a diameter less than 100 μm can rise from the surface to a height of over 0.5 meters at the location of the spacecraft at an altitude of 0.3 meters. The trajectories of very small particles are similar to gas streamlines. Heavier particles, which diameter greater than 100 μm showed more inert behaviour in the gas flow and any lifting from the surface was not observed, not depending on the height and mode of PS. Landing of the

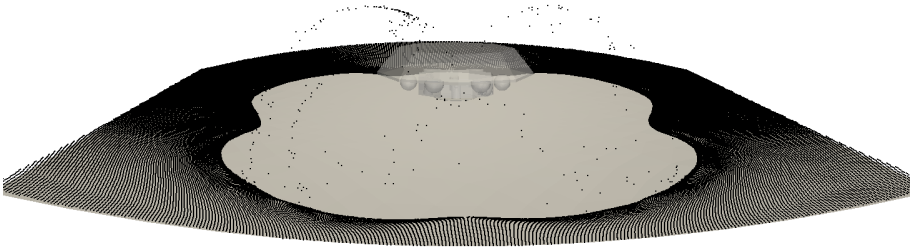

Fig. 4. Distribution of solid particles, diameter of particle 10 μm.

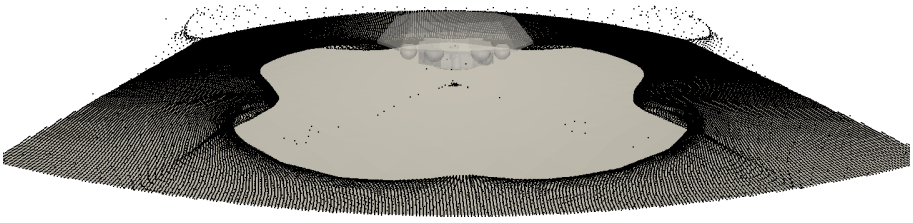

Fig. 5. Distribution of solid particles, diameter of particle 100 μm.

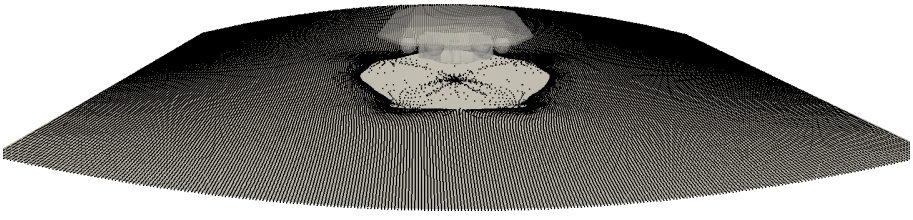

Fig. 6. Distribution of solid particles, diameter of particle 1000 μm.

SC from 10 to 1 meter height, it is possible to lift from the surface of Mars only solid particles diameter of 10-100 μm and dust. It's known about the frequent dust storms in different places of the planet Mars. Therefore, the assumption of a possible lifting of lighter solid particles from the surface of Mars and the possible content of the dust particles in the atmosphere are in the second variant. The field of solid particles was set in the form of cloud.

In this case, it is important to know; that the path of fine particles and quantitative results, show that sedimentation of solid particles and dust on the landing platform units is possible near the surface. Due to the relatively low speed which reduce the landing platform, pulse mode of PS; apparently, the largest particle deposition will occur at low altitudes and at the moment of landing of SC.

The initial distribution of solid particles is shown in figure 7. The particle diameter ranged from 10 to 100 μm, the previous results showed high inertia particles which size is above 100 μm. The time of influence of supersonic jets was 0.3 seconds at maximum and minimum mode of PS, for height 0.3, 0.5 and 1 meter. The calculation results of settled solid particles on the top part of the landing platform are shown in table 1, as a percentage of the total number of particles contained in a cloud.

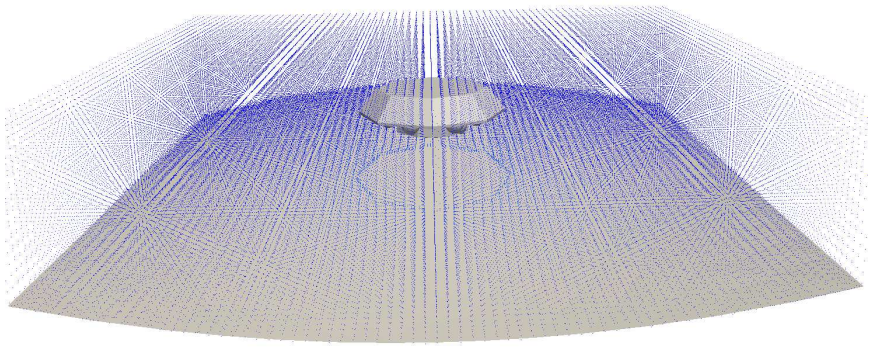

Fig. 7. The initial distribution of the solid particles.

Table 1. The percentage of settling particles on the spacecraft.

	Minimum mode of PS			Maximum mode of PS		
Height	10 μm	50 μm	100 μm	10 μm	50 μm	100 μm
0.3 m	1.1 %	1.2 %	1.35 %	1 %	1.4 %	2 %
0.5 m	0.9 %	1.2 %	1.4 %	1.1 %	1.65 %	2.6 %
1 m	0.5 %	1.5 %	2.5 %	1.9 %	2.1 %	3.5 %

Obtained the least amount deposited particles on top of the SC at maximum and minimum mode of PS with a diameter of 10 and 50 μm. Their value does not exceed 2 percent of the total number of particles. But the largest number of solid particles, deposited on the top of the SC,is particles with a diameter of 100 μm. At the minimum mode of PS at 1 meter, the content is about 3.5 percent. This behaviour means that lighter particles are less inert and quickly lured

by the gas flow, while heavy particles more inert and not so actively lured by the gas flow; in this case, some part of them is deposited under the action of gravity.

5 Conclusion

Three-dimensional mathematical modelling of SC "ExoMars"landing on the surface of Mars was done. Mathematical model and method of solution was implemented using open-source code OpenFOAM. Solid particles motion was obtained under influence of the supersonic jets of PS depending on the size of the solid particles and the mode of PS. In the first case, when located on the surface of Mars with a single layer of solid particles, numerical results showed that small particles were lured by gas flow due to low kinetic inertness. For heavy particles, which diameter exceeds 100 μm, the results showed that, lift solids from the surface of Mars were not observed regardless of the mode of PS and the height of the landing platform. In the second case, initial distribution of solid particles were in the form of a cloud with particles diameter 10 and 50 μm, numerical results showed that the percentage of settled particles on the top of SC did not exceed 2 percent of the total number of particles. The largest number of particles deposited on the top of SC was a particle with diameter of 100 μm. At minimum mode of PS, on a height of 1 meter, the content is about 2.5 percent, and 3.5 percent at the maximum. The differences between the percentages values are connected the impingement jets at different modes of PS.

References

1. Khartov, V.V., Martynov, M.B., Lukiyanchikov, A.V., Alexashkin, S.N.: Conceptual design of "EXOMARS-2018"descent module developed by Lavochkin association. VESTNIK NPO imeni S.A. Lavochkina. 23, 2, 5-12 (2014)
2. Likhachev, V.N., Fedotov, V.P.: Control of "EXOMARS"SC landing module motion during its descent and landing on Mars surface. VESTNIK NPO imeni S.A. Lavochkina. 23, 2, 58-64 (2014)
3. Jorge L. Vago, Leila Lorenzoni, Fabio Calantropio, Zashchirinskiy. A.M.: Selecting a landing site for the "EXOMARS-2018"mission. VESTNIK NPO imeni S.A. Lavochkina. 23, 2, 42-46 (2014)
4. Glazunov, A. A., Kagenov, A. M., Eremin, I. V., Kuvshinov, N. E.: Numerical study of the interaction of the spacecraft propulsion systems supersonic jets with the surfaces under conditions of Mars. Russian Physics Journal. вЂ“ Т. 57. вЂ“ в„– 8/2. 94-100 (2014)
5. Glazunov, A. A., Kagenov, A. M., Eremin, I. V., Tyryshkin I. M.: Mathematical modeling of the interaction of the spacecraft propulsion systems supersonic jets with the surfaces. Russian Physics Journal. Т. 56, в„– 9/3. 57-59 (2013)
6. Glazunov, A. A., Kagenov, A. M., Eremin, I. V., Tyryshkin I. M.: Application of OpenFOAM for calculates gas flows in nozzles and jets. Russian Physics Journal. Т. 56, в„– 9/3. 66-68 (2013)
7. Menter F. R.: Zonal Two Equation k-Π‰ Turbulence Models for Aerodynamic Flows. AIAA Paper 93-2906. 1598-1605 (1993)
8. Aurelia Vallier: Tutorial icoLagrangianFoam / solidParticle. CFD with Opensource Software, Assignment 3, 1-28 (2010)
9. OpenFOAM, `http://openfoam.com`
10. E.F. Toro: Riemann Solvers and Numerical Methods for Fluid Dynamics. Springer-Verlag Berlin Heidelberg, DOI 10.1007/b7976-1 10, 315-344 (2009)
11. Deryagin, Yu.A., Dubovitskiy, A.V.: Cruise engine of Versatile Space Tugs "Fregat "Fregat-SB". VESTNIK NPO imeni S.A. Lavochkina. 22, 1, 41-43 (2014)
12. M. P. Golombek., A. Huertas., J. Marlow., B. McGrane., C. Klein., M. Martinez., R. E. Arvidson., T. Heet., L. Barry., K. Seelos., D. Adams., W. Li., J. R. Matijevic., T. Parker., H. G. Sizemore., M. Mellon., A. S. McEwen., L. K. Tamppari., Y. Cheng: Size-frequency distributions of rocks on the northern plains of Mars with special reference to Phoenix landing surfaces. Journal of Geophysical Research: Planets. Volume 113, Issue E3, (2008)

Elongation Determination Using Finite Element and Boundary Element Method

Kisala P.*, Wojcik W.*, Kalizhanova A.**, Kashaganova G.**, Smailov N.**

*Politechnika Lubelska, Lublin, Poland
** K.I.SatpayevKazakh National Technical University, Almaty, Kazakhstan
{p.kisala;waldemar.wojcik}@pollub.pl,kalizhanova_aliya;guljan_k70;nur_aly.kz}@mail.ru

Abstract. This paper presents an application of the finite element method and boundary element method to determine the distribution of the elongation. Computer simulations were performed using the computation of numerical algorithms according to a mathematical structure of the model and taking into account the values of all other elements of the fiber Bragg grating (FBG) sensor. Experimental studies were confirmed by elongation measurement system using one uniform FBG.

Keywords: finite element method, boundary element method, fiber Bragg gratings, elongation distrubution

1 Introduction

Elongation measurement are very important in many practical cases [1]. Many differential speed measurement algorithms was introduced, showing how to solve eccentricity problems and that a bad processing but not slippage is the source of observed false elongation peaks [2]. In some cases the elongation sensor using optical elements is used [3,4,5]. A two-dimensional formulation within the scope of the boundary element method (BEM) was proposed for the determination of influence of shear and elongation on drop deformation [6]. Sometimes the Indirect Boundary Element Method (IBEM) is applied for the strain calculations eg. to study composites models [7] and scattering of elastic waves by cracks [8]. The finite element method is also widely used for the elongation determination [9], eg. in modelling and simulation of porcine liver tissue indentation [10] elasticity and fracture analysis [11] and also in many mechanical systems [12]. An efficient hybrid approach to study the deformation in known materials have been presented in our method. In this work the relative elongation is determined for the formed mechanical system using finite element method (FEM) and boundary element method. In addition, the results have been verified by measurements using FBG sensor. In this paper, the inverse problem solution is used to estimate the model parameters of elongation sensor in accordance with the method of measuring the elongation distribution [13,14]. To confirm the results obtained from FEM and BEM, measurements using FBG sensor have been performed. During measurements of the elongation distribution using inverse analysis it is important to build sensor model [15,16,17]. Direct measurements of described quantity are not possible due to lack of appropriate measurement system components (especially sensors), therefore the measurements are indirect [18,19,20,21,22]. In this case, it is essential to the use of optoelectronic devices, which process the available physical signals using specialized sensors, converts them into digital form, and then, according to the implemented numerical algorithms, converts it to the desirable quantity. In this paper we present an application of the finite element method and boundary element method to determine the distribution of the elongation and we implement the inverse analysis to the elongation determination.

2 Calculation method and measurement system

The elongation distribution of the sample material can be determined based on the distribution of the linear dimensions relative change in the considered area. The study lead to the use of information from the measured spectrum and the spectrum calculated by use of mathematical model. To perform the experiments laboratory testing tool was designed and manufactured. It allows for the metal specimens stretching. Bragg gratings were glued on the specimens. Elongation of the sample, moving into a grating, causing changes in the length of the grating period, which also changes its spectral characteristics, which possible to determine with photo spectrometer. The spectral characteristics of the grating allows to obtain the information about the elongation distribution even repeatedly differential along the measured length. Knowing the cross-section of the sample and the load the elongation was calculated at several points. For the calculation the finite element method and the boundary element method were used. FEM mesh is arranged in such a way that its greatest density occurred on the sample constriction. However, in the BEM the values of elongation were calculated on the external and internal edge of the specimen on its constriction. Presented method is shown in Fig. 1.

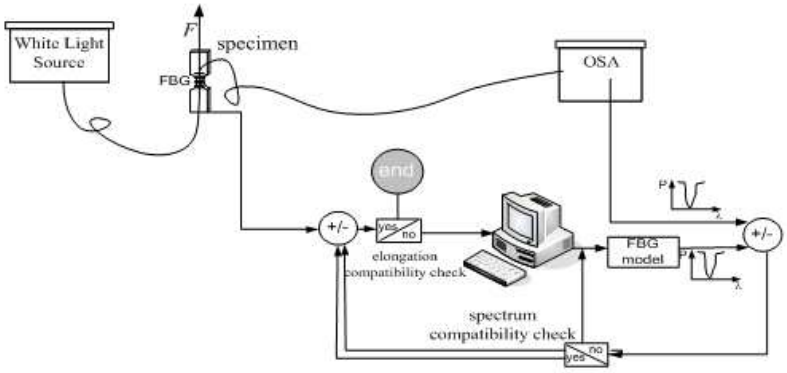

Fig. 1. Elongation determination system on the base of FBG model.

Light with wavelengths of 400-1700 nm is directed to an optical fiber in which the Bragg grating is written. The grating was glued to the sample, which is under tensile force F using the laboratory strain generator. After passing through an extended grating the modified spectrum is directed to an optical spectrum analyzer. At the same time the random distribution of the elongation is generated using simulated annealing algorithm. This random distribution is then introduced into the Bragg grating model. By means of a model and on the base of random elongation distribution the transmission spectrum of the grating is calculated. The modeled spectrum and actual spectrum (from optical spectrum analyzer – OSA) are then compared. In the case of spectral characteristics non-compliance, new values of the grating elongation distribution are selected in accordance with the simulated annealing algorithm. These are re-used to calculate a new transmission spectrum by means of a grating model. It is compared with the measured spectrum and the process is repeated until a predetermined accuracy is achieved or until a specified (suitably small) value of the objective function is achieved. Distribution of elongation, which will lead to the minimization of the objective function will be the most fitting for real. The next step is to check the compliance of the distribution determined using an algorithm with the theoretical one, resulting from tensile force F and the shape of the stretched specimen.

Knowledge of the force F and the shape of the specimen allows for calculation (using the FEM and BEM) the theoretical elongation distribution of the specimen and the grating. Fig. 2 shows the measurement system components.

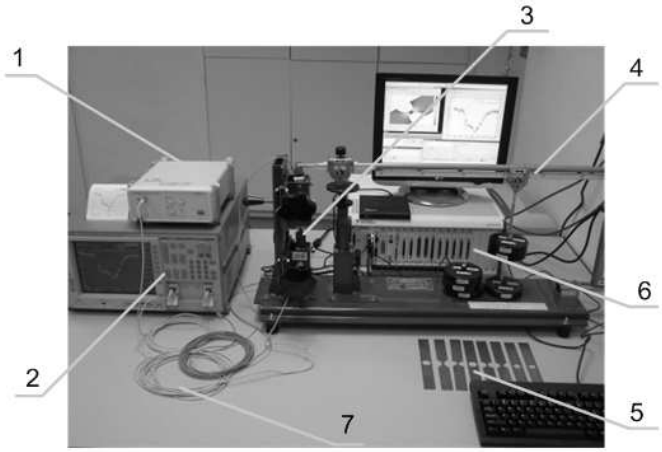

Fig. 2. Measurement system: 1 – light source, 2 – optical spectrum analyser, 3 – Bragg grating, 4 – elongation generator, 5 – specimens, 6 – PC with measuring card, 7 – fiber with FBG.

The coupled-mode equations were used in the simulation of the spectral response of the Bragg grating. The white light is the sensor model input. The input can be expressed as $R(-L/2)$. The output of the model is the light transmitted through the grating (grating's transmission spectrum), which can be expressed as $R(+L/2)$. The model parameters are as follows: the grating length L, the "DC" self-coupling coefficient σ, and the coupling coefficient k. There is no input signal that is incident from the right-hand side of the grating, i.e. $S(+L/2) = 0$, but there is a known signal value that is incident from the left side of the grating, i.e. $R(-L/2) = 1$ (Fig. 3).

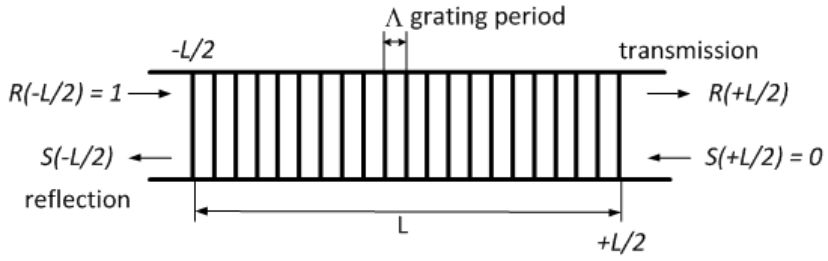

Fig. 3. The initial condition and calculation of the grating response to input field.

The grating is represented by the transfer matrix F_M. The light propagation process can be described by:

$$\begin{bmatrix} R\,(+L/2) \\ S\,(-L/2) \end{bmatrix} = F_M \begin{bmatrix} R\,(-L/2) \\ S\,(+L/2) \end{bmatrix} \tag{1}$$

$S(-L/2)$ is the signal reflected from the grating and the F_M matrix can be expressed as follows:

$$F_M = \begin{bmatrix} \cosh(\gamma_B L) - i\frac{\sigma}{\gamma_B}\sinh(\gamma_B L) & -i\frac{k}{\gamma_B}\sinh(\gamma_B L) \\ i\frac{k}{\gamma_B}\sinh(\gamma_B L) & \cosh(\gamma_B L) + i\frac{\sigma}{\gamma_B}\sinh(\gamma_B L) \end{bmatrix} \tag{2}$$

The individual elements of the F_M matrix can be described as follows.

The general "DC" self-coupling coefficient σ can be represented by:

$$\sigma = \delta + \overline{\sigma} - \frac{1}{2}\frac{d\phi}{dz}, \tag{3}$$

where $\frac{1}{2}\frac{d\phi}{dz}$ describes a possible chirp of the grating period, and ϕ is the grating phase. The detuning parameter δ can be represented by:

$$\delta = \beta - \frac{\pi}{\lambda} = \beta - \beta_D = 2\pi n_{eff}\left(\frac{1}{\lambda} - \frac{1}{\lambda_D}\right), \tag{4}$$

where$\lambda_D = 2n_{eff}\Lambda$ is the design wavelength for Bragg reflectance. For very weak gratings where $(\delta n_{eff} \to 0)$ we obtain:

$$\overline{\sigma} = \frac{2\pi}{\lambda}\overline{\delta n_{eff}}, \tag{5}$$

where $\overline{\delta n_{eff}}$ is the background refractive index change.

The coupling coefficient $k(z)$ can be represented by:

$$k(z) = \frac{\pi}{\lambda}\delta n(z) g(z) \nu, \tag{6}$$

where $g(z)$ is the function of apodization, and ν is the fringe visibility. The coupling coefficient $k(z)$ is proportional to the modulation depth of the refractive index $\Delta n(z) = \delta n(z) g(z)$.

In our case the grating was apodized and the apodization profile was given by the grating producer. The simulated grating apodization function was as follows:

$$g(z) = \exp\left[-a\left(\frac{z - \frac{L}{2}}{L}\right)^2\right]; \;\; z \in [0, L], \tag{7}$$

where a is the Gauss function width parameter and in our case $a = 80$.

γ_B can be expressed by the following equations:

$$\gamma_B = \sqrt{k^2 - \sigma^2}k^2 > \sigma^2 \tag{8}$$

$$\gamma_B = i\sqrt{\sigma^2 - k^2}k^2 < \sigma^2 \tag{9}$$

The grating FBG2 can be represented by a single transfer matrix describing its entire length because we assume a uniform temperature along the entire grating. There is therefore no need for the transfer function of light passing through FBG2 to depend on the position along the z axis. This assumption simplifies the mathematical model.

3 Calculations and measurements results

In Fig. 4 a shape of a used specimen has been presented, Fig. 5 presents elongation distribution of the specimen as a function of stress calculated on the basis of knowledge of the load, the specimen geometry and the type of material using MES and simulated (determined from indirect measurements on a laboratory). In contrast, in Fig. 6 the distribution of elongation for the same specimen as a function of stress using the boundary element method has been presented.

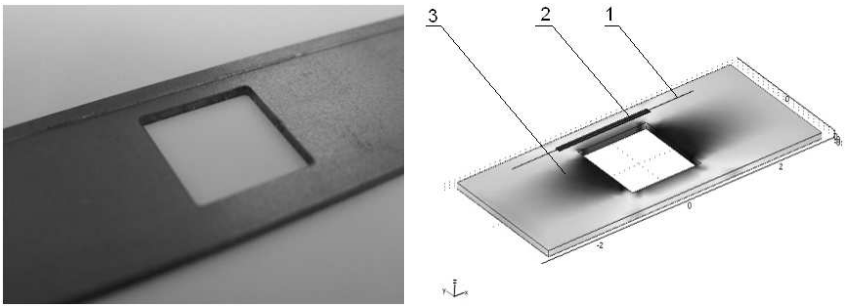

Fig. 4. Measured system: 1 – optical fiber with FBG, 2 – epoxy glue, 3 – specimen. a) real photo, b) system geometry in FEM.

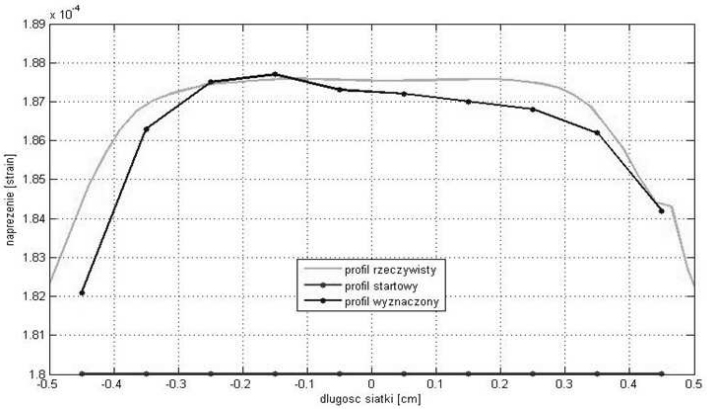

Fig. 5. Distributions of elongation in FBG.

In Fig. 5 elongation distribution characteristics of the Bragg grating have been presented. The profile determined as real was calculated using finite element method. The known tensile force and geometry of the specimen were used as the input quantities. The profile determined as measured was determined using Bragg gratings spectra, FBG model and simulated annealing algorithm. The algorithm does not know the force size and the specimen geometry. The process of determining the elongation distribution of Bragg grating began with a random initial value of tension, which was assumed constant throughout the length of the specimen.

The maximum value of the absolute error of the elongation determination was RMSD= 0.0092% for MES and RMSD = 0.0085% for BEM Fig. 6. It was calculated by accounting for the division of the grating into 10 sections using the following equation:

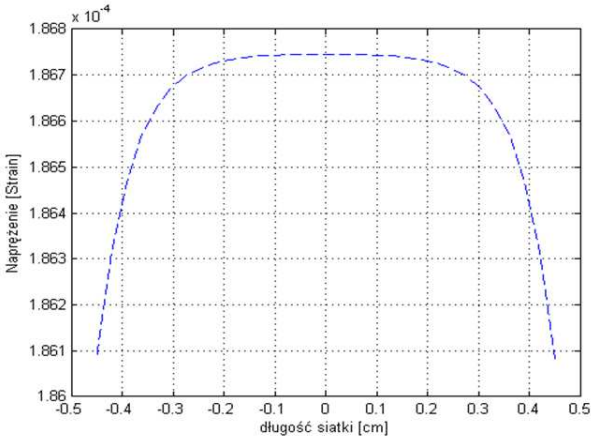

Fig. 6. The elongation distribution calculated using BEM.

$$RMSD = \left(1/10 \cdot \sum_{k=1}^{5} \varepsilon_C - \varepsilon_M\right)^{1/2} \tag{10}$$

This error was determined as the root square error and defines the difference between the calculated values of the elongation ε_C and the values obtained using the conjugate gradient algorithm ε_M.

4 Conclusions

The results of laboratory measurements and numerical calculations show that it is possible to apply the inverse analysis to determine the distribution of elongation using fiber optic sensors with Bragg gratings. It is possible to perform calculations using numerical algorithms performing calculations in accordance with the mathematical structure of the FBG model and taking into account the values of all model parameters. The boundary element and finite element method used in this paper, allows to obtain comparable results for the indirect measurement.

References

1. Fujii, H.; Namazu, T.; Inoue, S. R. Dembo, D. Rosen: "Development of the Novel Elongation-Measurement Device with In-Plane Bimorph Actuator for the Tensile Test" , Micro Electro Mechanical Systems, 2009. MEMS 2009. IEEE 22nd International Conference on, 1063-1066 (2009)
2. Granda, A.; Linera, F.M.F.; Vecino, G.; Diaz Canga, A., "Practical Speed and Elongation Measurement, Using Encoders, for a Temper Mill" , Industry Applications, IEEE Transactions on 50(1), 113-119 (2014)
3. Szustakowski, M.; Palka, N.; Kizlik, B., "Contrast of the fiber optic Michelson interferometer – a new prospect for elongation measurement" , Modern Problems of Radio Engineering, Telecommunications and Computer Science, 2004. Proceedings of the International Conference IEEE, 476-477 (2004)
4. Wolff, A.; Cramer, D.; Hellebrand, H.; Probst, I.; Lubitz, K., "Optical two channel elongation measurement of PZT piezoelectric multilayer stack actuators" , Applications of Ferroelectrics, 1994. ISAF '94., Proceedings of the Ninth IEEE International Symposium on, 755-757 (1994)
5. Yamashita, R.K.; Weiwen Zou; Zuyuan He; Hotate, K., "Measurement Range Elongation Based on Temporal Gating in Brillouin Optical Correlation Domain Distributed Simultaneous Sensing of Strain and Temperature" , Photonics Technology Letters, IEEE 24(12), 1006-1008 (2012)
6. Roger E. Khayat, A. Luciani, L.A. Utracki, F. Godbille, J. Picot, "Influence of shear and elongation on drop deformation in convergent-divergent flows" , International Journal of Multiphase Flow 26(1), 17-44 (2000)

7. Ursula Iturraran-Viveros, Francisco J. Sanchez-Sesma, Francisco Luzon, "Boundary element simulation of scattering of elastic waves by 3-D cracks" , Journal of Applied Geophysics 64(3-4), 70-82 (2008)
8. Yijun Liu, Naoshi Nishimura, Yoshihiro Otani, "Large-scale modeling of carbon-nanotube composites by a fast multipole boundary element method" , Computational Materials Science 34(2), 173-187 (2005)
9. Simon Chatelin, Caroline Deck, Felix Renard, Stephane Kremer, Christian Heinrich, Jean-Paul Armspach, Remy Willinger, "Computation of axonal elongation in head trauma finite element simulation" , Journal of the Mechanical Behavior of Biomedical Materials 4(8), 1905-1919 (2011).
10. Y.B. Fu, C.K. Chui, "Modelling and simulation of porcine liver tissue indentation using finite element method and uniaxial stress-strain data" , Journal of Biomechanics 47(10), 2430-2435 (2014)
11. Enqiang Lin, Hailong Chen, Yongming Liu, "Finite element implementation of a non-local particle method for elasticity and fracture analysis" , Finite Elements in Analysis and Design 93, 1-11 (2015)
12. Myrianthi Hadjicharalambous, Jack Lee, Nicolas P. Smith, David A. Nordsletten, "A displacement-based finite element formulation for incompressible and nearly-incompressible cardiac mechanics" , Computer Methods in Applied Mechanics and Engineering 274, 213-236 (2014)
13. Kisala, P. "Measurement of the maximum value of non-uniform strain using a temperature-insensitive fibre Bragg grating method" , Opto-electronics Review 21(3), 293-302 (2013)
14. Kisala, P. "Metrological conditions of strain measurement optoelectronic method by the use of fibre Bragg gratings"Metrology and Measurement Systems 19(3), 471-480 (2012)
15. M. Czerwinski, J. Mroczka, T. Girasole, G. Gouesbet, G. Grehan, Light-Transmittance Predictions Under Multiple-Light-Scattering Conditions. I. Direct Problem: hybrid-Method Approximation. Applied Optics 40(9), 1514-1524 (2001)
16. Mroczka J. and Szczuczynski D., "Simulation research on improved regularized solution of the inverse problem in spectral extinction measurements" , Applied Optics 51(11), 1715-1723 (2012)
17. Mroczka J. and Szczuczynski D., "Improved regularized solution of the inverse problem in turbidimetric measurements" , Applied Optics 49(24), 4591-4603 (2010)
18. Kisala P., "Generation of a zone chirp in uniform Bragg grating as a way of obtaining double functionality of a sensor"Metrology and Measurement Systems 19 (4), 727-738 (2012)
19. Mroczka J., "The cognitive process in metrology" , Measurement 46(8), 2896-2907 (2013)
20. Cieszczyk S., "Passive Open-Path FTIR Measurements and Spectral Interpretations for in situ Gas Monitoring and Process Diagnostics" , Acta Physica Polonica A 126(3), 673-678 (2014)
21. Cieszczyk S., "Non-Luminous Flame Temperature Determination Method Based on CO2 Radiation Intensity" , Acta Physica Polonica A 126(6), 1235-1240 (2014)
22. Swirniak G., Glomb G., and Mroczka J., "Inverse analysis of the rainbow for the case of low-coherent incident light to determine the diameter of a glass fiber" , Applied Optics 19(1), 4239-4247 (2014)

Computational Model of Thermo-Diffusive Processes in Electrodes by Arcing

Badr Munir[1], Baydaulet A.[2] Urmashev, Alexei A. Kavokin[2]

[1]GIK Institute of Engg. Sci. and Tech., Topi, Pakistan
[2]Al-Farabi Kazakh National University, Almaty, Kazakhstan
baydaulet.urmashev@mail.ru,kavokin_alex@yahoo.com

Abstract. The computational model of thermo-chemical processes in the body of plasmatron electrode working in the gas environment is investigated. Mathematical description and algorithm of numerical solution of the system of differential equations which describe electromagnetic, temperature and concentration fields into body of electrodes taking into account kinetic of phase transformation and chemical reaction in accordance with a state diagram, [1,2,9], is represented. The offered approach is simpler for computing in domain with unknown free boundary than the well-known Stefan approach, [7,8], of describing an analogous processes. The unknown kinetic coefficient is determined from the best fit exact self-similar and numerical solutions of one-dimensional case. As an instance the case of copper cathodes with the zirconium insertion in the environment of oxygen is considered. The calculations for various types of dependencies of gas diffusion coefficient from temperature are concluded. The results of calculations develop understanding of some features of oxidation process of electrodes.

Keywords: Mathematical model, phase transformation, thermo-chemical electrodes, plasmatron, Oxidation process.

1 Introduction

An example of multiphase process mathematical model is description of a heat and mass transfer occurring in metal which is being heated by an electric arch in the gas medium, [1, 2, 4]. The macroscopic model of physical and chemical transformations can be described as follows, [3]. There is a melting of metal at heating a surface of an electrode and, simultaneously there is a rise in the temperature which results in the free boundary between liquid and solid phases moving ahead deep into the electrode. At the same time there is a diffusion of gas in electrode and formation of new chemical compounds which can noticeably differ in the physical and chemical properties from each other and metal of the electrode. Moreover we shall name a phase of substance not only its solid or liquid state, but also different chemical or structural states e.g. α- and β- phases, which are typical for many metals,[5]. Mathematical model of counteraction of heat and diffusive processes in electrodes (cathodes) may be described by a system of equation,[3]:

$$div(\frac{1}{\rho} grad\psi) = 0 \tag{1}$$

$$\frac{\partial(c\gamma T)}{\partial t} = div(\lambda_i gradT) + F_t(C,T,X) + \frac{1}{\rho}(grad\psi)^2 \tag{2}$$

$$\frac{\partial C}{\partial t} = div(DgradC) + F_C(C,T,X) \tag{3}$$

where $\psi(r,z), T(t,r,z), C(t,r,z)$ - electric potential, integral temperature, and concentration of diffusing gas in cathode respectively. For more simple solution, it is supposed that the cathode has the form of the cylinder with infinite radius and length. The basic difference of system of

the equations (1) - (3) (with corresponding initial and boundary conditions) from offered earlier in [4], is refusal of allocation of areas of phases of substance with use both free boundaries and corresponding nonlinear boundary conditions (it is similar to Stefan problem, [4]). Instead of Stefan conditions, we have to use a system of ordinary differential equations which describes the kinetic of phases changes:

$$-\frac{\partial X_i}{\partial t} = K_i sign(X - X_{eq.i})|X - X_{eq.i}|^{P_i} \tag{4}$$

where X_i are the amounts of material in i-th phase; $X_{eq.i}$ are the equilibrium values of X_i which can be defined in accordance with state diagram [5], using known values of both temperature and total gas concentration C_{tot} in concrete domain of electrode: $C_{tot} = C + \sum N_j X_j$, and then total amount of a matter must obey the law of conservation of matter, i.e.:

$\sum_{\forall i} X_{0,i} = \sum_{\forall i} X_i = \sum_{\forall i} X_{eq.i} = const. \quad \forall t = 0$

where $X_{0,i}$ are the initial values of X_i by. K_i are the kinetics coefficients.

We also add sources F_i (or sinks) of heat and gas to the right side of equations (2) and (3):

$F_i(C, T, X) = \sum_i r_{L,i} \frac{dX_i}{dt}$,

where coefficients $r_{L,i}$ for equation (2) mean either either latent heat of respective phase reaction or stoichiometric coefficients for equation (3). The coordinates of phases boundaries for this model are defined from a state diagrams [5].

2 Modeling heat fields inside of Cu, Zr - electrode

For concrete calculation of processes in the $Cu, Zr-$ electrode the mathematical model has been preliminary simplified with a view of reception of analytical formulas which are more convenient for the further analysis. Let's result the brief description of the made simplifications:

At first, the contribution of JouleпγHs sources of heat in the temperature of cathode was estimated. Influence JouleпγHs sources insignificantly and is shown that in many practically interesting cases it can be neglected. For solution of equation for electrical potential $\psi(r, z)$ with constant electrical resistance ϕ:

$$\phi_{rr} + \frac{1}{r}\phi_r + \phi_{rr} = 0, \qquad (0 < r, z < \infty) \tag{5}$$

following boundary conditions were chosen:

$$-\frac{1}{\rho}\Psi_z|_{z=0} = i_0(r); \qquad \Psi_r|_{r=0} = 0; \qquad \Psi_r|_{r,z\to\infty} = U_k, \tag{6}$$

where $i_0(r)$ is given function of a current and density which we have chosen in a following form:

$i_0(r) = U_k + A_1(B_1^2 + r^2)^{-\frac{3}{2}}$.

Solution of (5)-(6) can be obtained as follows:

$$\Psi(r,z) = U_k + \rho\frac{A}{B}\left((B+z)^2 + r^2\right)^{-\frac{1}{2}}. \quad (7)$$

Coefficients A and B can be chosen from a condition that current $I_0(r)$, passing through a surface of the cathode with radius r_k,:

$I_0(r_k) = \frac{2\pi}{\rho}\int_0^{r_k} r\frac{\partial\psi}{\partial z}|_{z=0}dr,$

had preset values at two sizes r_k. In particular, it is possible to choose the first value $r_k = 0$, at which $I_0(r_k) = I_0$ - a total current through the cathode. The second value r_k, can be chosen from a condition that the current through a zirconium insertion has account an ε - part from total current I_0. Substituting (7) in these conditions, we find formulas for A and B:

$A = \frac{I_0}{2\pi}r_k\delta(1-\delta)^{-1/2}, \qquad B = r_k\delta(1-\delta^2)^{-\frac{1}{2}},$ where $\delta = 1-\varepsilon,$

For example, for typical values, [2], $I_0 = 150A$, $r_k = 0.2cm$, $\delta = 0.1$ we obtain $A = 0.48, B = 0.02$, and the corresponding density of the JouleпγHs heat sources is equal:

$$Q(r,z) = \frac{1}{\rho}(grad\psi)^2 = \frac{0.06}{((0.02+z)^2+r^2)^2}, \quad [Wt/cm^3], \quad (8)$$

It is possible to prove, using a principle of a maximum for the heat equation, that the increment of temperature due to JouleпγHs heat does not exceed value $maxT^* = \frac{\rho A^2}{2\lambda B^4}$ at $r = 0, z = 0$ and decreases at increase r and z. At the typical values specified above r, A, B and $\lambda = 0,2[Wt/cm{*}K]$ it is obtained that for temperature of a surface of the cathode 3000-4000 K, JouleпγHs heat brings no more than 10% from the general temperature and therefore, it can be not considered at calculations or it is possible to compensate due to partially increasing in temperature $T(0,0)$ at $r = 0$ and $z = 0$.

For next simplification we exclude thermal effects connected with phase processes from heat equation (2) since it allows use of a steady state model of temperature as it will be shown later on. For an estimation of time of approach of a steady state of temperature in our paper, [9], were used eigenvalues of a followed boundary problem:

$(c\gamma T)_i = \frac{1}{r}(\lambda T_z)_z + (\lambda T_z)_z, \quad (t > 0, 0 < z < z_0, 0 < r < r_0),$

$T(0,r,z) = 0; \quad -\lambda T_z(t,r,0) = f_0(r); \quad T_r(t,0,z) = 0;$

$T(t,r,z_0) = T_0(r,z_0); \quad T(t,r_0,z) = T_0(r_0,z),$

where $T_0(r,z)$ is solution of correspondent steady state task in infinite domain $(0 < r,z < 0)$ and $f_0(r)$ is given function of a heat flux through the surface of cathode. Time of achievement of quasi steady state has been estimated as $t >= 15-20s.$ for typical values of parameters: $? < 0.02(2\%), z_0 = 1cm, r_0 = 3cm, c\gamma = 2, J/(cm^3K)$. I.e. for practically real time (t >600 s.) it is possible to use with confidence the steady state form of the equation (2). Such assumption has helped to receive the approximate analytical solution of boundary problems for the equations (1) and (2).

This conclusion then was more accurately confirmed in paper [10], using numerical solution of heat distribution model which included also phases transformation processes. The kinetic coefficient $K = 0.3[1/s]$ is determined from the best fit exact self-similar and numerical solutions

of one-dimensional case,[6,7]. One can see on Fig.1 that the location of the free boundary close to steady state (curve 3 on figure) attained for about 1 second.

The analysis resulted above has allowed to simplify calculation of temperature in the cathode and to use following model:

$$\frac{1}{r}(\lambda r T_r)_r + (\lambda T_z)_z = 0; \qquad (0 < r, z, \infty), \tag{9}$$

with boundary conditions $T_z(r,0)$; $T_r(0,z) = 0$; $T(\infty) = T_0$, where $f(r)$ - known temperature of a surface of the cathode. Solutions of the equation (13) have been received for following type of dependence λ from T:

$\lambda = \frac{\lambda_0}{1+\lambda_1 T}$ and $f(r) = A_1(B_1^2 + r^2)^{-\frac{3}{2}}$,

$$T^a(r,z) = \frac{1}{\lambda_1}\left(exp\left(\frac{\lambda_1 a_1}{\lambda_0 a_2}((a_2+z)^2 + r^2)^{-\frac{1}{2}}\right) - 1\right), \tag{10}$$

where a_1 and a_2 are unknown parameters which can be calculated from a condition of known values of temperature of a surface of the cathode. From the equations (10) irrespective of choice parameters of λ it follows that the lines of constant temperature are defined by the equation $(a_2+z)^2 + r^2 = const$ and that simplifies the further calculations and determination of bounds of corresponding phases.

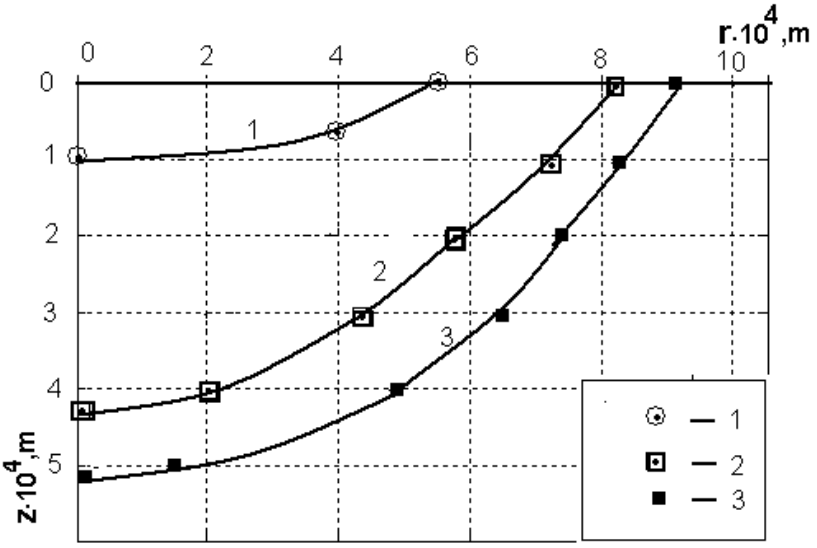

Fig. 1. Calculated, [6,7], coordinates of free boundary in thermo-cathode insertion vs time of arching, at different times: 1 ∼ 0.01s, 2 ∼ 0.1s, 3 0.5s. and K=0.3 [1/s]

Parameters a_1 and a_2 were defined from conditions of experimental data:

1. The temperature in the center of a cathode spot T(0,0) is close to temperature of boiling of zirconium (∼ 3500 СпуН), [2]
2. The temperature in a zone of contact between the zirconium insert and a body of the cathode $T(r_k, 0)$ should be a little below melting point of copper, i.e. about $1000^0 C$

Substituting corresponding values $T(0,0)$ and $T(r_k,0)$ in the equations (10), it is simple to find formulas for a_1 and a_2:

$$a_2 = r_k \left(\left(\frac{\ln(\lambda_1 T_{0,0}+1)}{\ln(\lambda_1 T_{r_k,0}+1)} \right)^2 - 1 \right)^{-\frac{1}{2}}, \quad a_1 = a_2^2 \frac{\lambda_0}{\lambda_1} \ln(\lambda_1 T_{0,0}+1); \tag{11}$$

These formulas completely define solutions (10) for calculation of temperature $T(r,z)$.

2.1 Diffusion of Oxygen into electrode

Let's consider further a part of model which describes process of oxygen diffusion inside the cathode. Taking into consideration only one stable stoichiometric chemical compound ZrO_2, we write down the equations (3), (4) as follows:

$$\frac{\partial C}{\partial t} = \frac{1}{r}\left(D(T) r C_r\right) + \left(D(T) C_z\right)_z - 2\frac{dX}{dt} \quad (t>0, 0<r<r_k, 0<z<z_0), \tag{12}$$

$$-\frac{dX}{dt} = K_x C \exp(-E_x/RT) sign(X - X_{eq}) |X - X_{eq}|^{\alpha}, \tag{13}$$

where C = C (t, r, z) - the ratio of quantities of atoms O/Zr, [%],in unit of volume ; $X = X(t,r,z)$ - relative quantity of phase $ZrO_2/(Zr+ZrO_2)$, [%], in unit of volume Initial and boundary conditions were

$$\begin{array}{lll} C(0,r,z)=0; & C_r(t,0,z); & -DC_r(t,r_k,z) = D_1 C(t,r_k,z); \\ C(t,r,0)=C_0; & -DC_z(t,r,z_0) = D_1 C(t,r,z_0), & \\ X(0,r,z)=0; & X_{eq} = 100[\%]. & \end{array} \tag{14}$$

Total concentration O_2 in the cathode, necessary for use of the state diagram, was determined as:

$$C_{tot}, at.\% = (C+2X)/(100+C+2X),$$

For calculation of diffusion coefficient, the dependences in [3] were analyzed:

$$\begin{array}{l} D_{0\to\alpha-z_r} = 5.4\exp(-50800/RT); \quad (T \in 400-1500^0 C), \\ D_{0\to\beta-z_r} = 0.98\exp(-41000/RT); \, (T \in 1050-1800^0 C), \end{array} \tag{15}$$

being based on the results from following approximation:

$$D(T), [cm^2/s] = \begin{cases} 1.10^{-10}, & T \le 1000^0 C, \\ 6.\exp(-25200/T), & 1000 < T \le 1860^0 C \\ 1.10^{-4}, & T > 1860^0 C \end{cases} \tag{16}$$

The Table 1 contains these values for comparison.

2.2 Numerical results

The solution of a task (12) - (14) has been obtained with the use of a usual explicit scheme of finite-difference method. For estimation of correctness and accuracy of calculations we have made comparison of the numerical solution with the exact solution (12)-14) at special values of parameters: $D = 1 * 10^{-4} cm^2/s$, $C_0 = 0.0254\%$, $K_x = 0$, which is defined by the formula:

$$C_1(t,r,z) = C_0 Erfc(z/\sqrt{(4Dt)})$$

Table 1. Comparison of approximation (15) and (16) for $D = D(T)$.

T^0C	$D_{0\to\alpha-z}$	$D_{0\to\beta-z}$	D(T)
500	1.10^{-22}		1.10^{-10}
1000	5.10^{-11}	1.10^{-9}	7.10^{-11}
1500	2.10^{-7}	1.10^{-6}	3.10^{-7}
1860	-	2.10^{-5}	1.10^{-4}

Table 2. Comparison of exact C_1 and calculated values Ccalc. at t=625 s.

z,cm	0	0.05	0.1	0.2	0.3
$C_1(t_0, 0, z)$	0.0254	0.0226	0.0198	0.0146	0.0010
$Ccalc(t_0, 0, z)$	0.0254	0.0226	0.0199	0.0149	0.0011

The result of comparison shown in Table 2, confirms good enough coincidence of exact and numerical solutions.

Finally, we have applied system of the equations (10),(12)-(14) to modeling of distributions of temperature and phases inside of the cathode, at following values of parameters:

$r_0 = 0.2cm, Z_0 = 0.5cm, T(0, 0, t) = 3500^0C$, $T(r_0, 0, t) = 1000^0C$, $C(r, 0, t) = 0.0254\%$, $K_x = 0.1$, $\alpha = 0.5$.

Solutions have been received for dependence (10) λ on T at $\lambda_0 = 3.4$, $\lambda_1 = 0.0025$. Results of calculations are shown in Figure 1, where the maximal values of depths (r=0) of melting zone and penetration of oxygen into a body of the cathode and also the relative concentration of phase ZrO_2 for various values of time are represented.

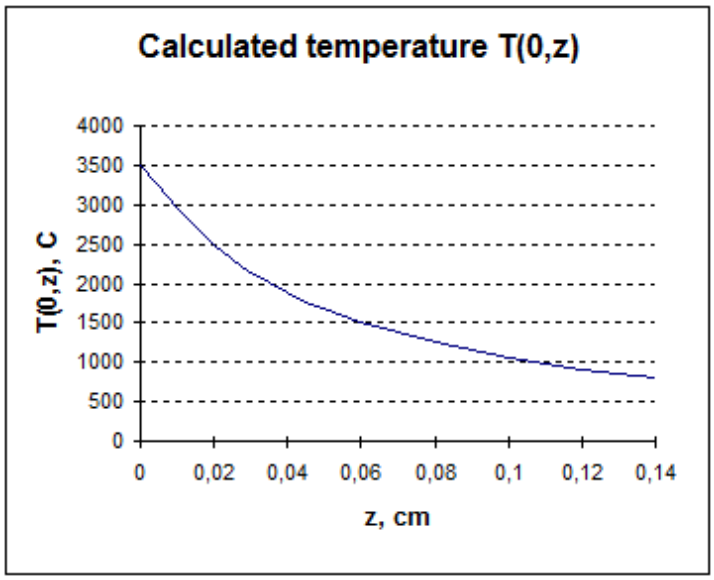

Fig. 2. Calculated temperature

From these results we can draw a conclusion that these maximal values depend basically on diffusion coefficient D (T). Hence there is no necessity to result other reasons for an explanation of the limited depth of penetration of oxygen inside zirconium insertion, and also the limited

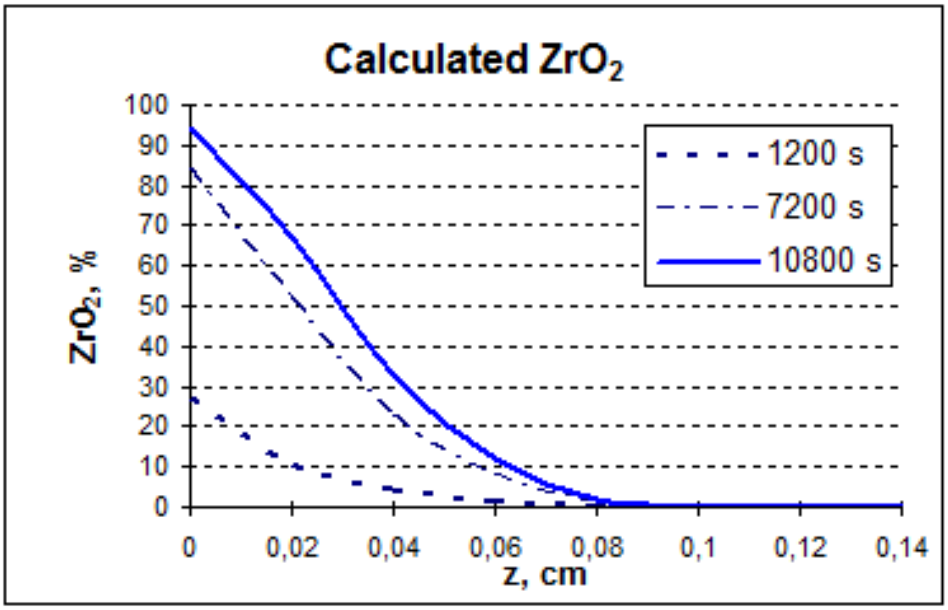

Fig. 3. Calculated Zirconium Dioxide ZrO_2/Zr_{total} at $r = 0$

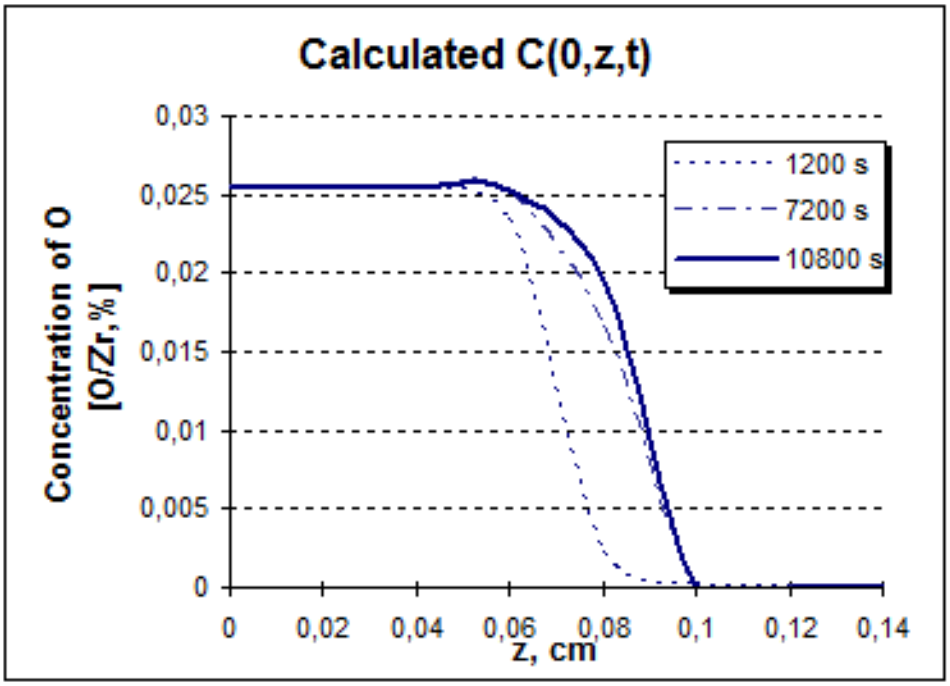

Fig. 4. Calculated O/ZR at $r = 0$

quantity of phase ZrO_2 even after long (few hours) work of cathodes. It quietly corresponds to the experimental facts [1,2,3].

References

1. Anshakov A.S., Kumenko D.O., Urbakh E.H., Urbakh A.E., *Investigation and development of high-efficient thermochemical cathodes for arc plasmatron.*// KORUS-2005, Electric Power Engineering, IEEE, 2005.p.310-312.
2. Zhukov M.F., Pustogarov A.B. et al., *Thermochemical cathodes.* - Novosibirsk, 1985. 126 pp.
3. Kavokin A.A., Kantaeva R.N., *Modeling of thermochemical and diffusive intraelectrode processes during arcing* , // Proc. Int. Symp. on electrical contacts, ISECTAпуЊ93. 1993, Almaty, Kazakhstan, pp 216-220.
4. Kharin S.N. et al., *Dynamics of thermophysical processes in the cathode at the electric arc influence* , // 6-th Int.conf, on Switching arc Phenomena, Lodz, Poland, 1985, pp. 259-262.
5. Fromm E., Gebhard E., *Gases and Carbon in metals*, Springer, Berlin 1976,,711 pp.
6. Kavokin A.A., Kharin S.N., Ya.Munir.,*Comparison Stefan's and kinetic models of phases transformation processes*, // Herald of Kazakh-British Univ., ISSN 1998-5655, #3(10),2009, pp 47-52
7. Kavokin A.A., Kazmi I.H., Munir B.,*Computational model of phase transformations in thermo-chemical cathodes using kinetic approach* ,// Key Engineering Materials (KEM), Trans Tech Publications, Switzerland , Vols. 510-511 (2012) pp 9-14.
8. Gupta S.C.,*The classical Stefan problem*, - Elsevier, 2003, p.p.385. 47-52
9. Kavokin A.A., Kazmi I.H., et al.,*Mathematical model of phase transformations in thermo-chemical cathodes with zirconium insertion*, // (P-45) in Proc.Int.conf. ISAM -2007, , Islamabad, Pakistan, Sep.2007. p.24
10. Kavokin A.A., Shpadi Yu.R.,*Model of thermo-physical intraelectrode processes including kinetics of phases transformation. (rus)*,)// Proc. The Int.Sci.Conf, пуЊDiff.equations and Math.physics.пуЊ Apr.2014, Institute of Math. and Math. Modelling, Almaty, Kazakhstan. P.277-279.

Numerical Modelling of Detached Flow Around a Car Body by Using Large Eddy Simulation Method

Alibek Issakhov and Yekaterina Khan

Faculty of Mechanics and Mathematics, al-Farabi Kazakh National University,
av.al-Farabi 71, 050040 Almaty, Kazakhstan
alibek.issakhov@gmail.com,h-katya@mail.ru

Abstract. This paper presents a mathematical model of detached flow around a car body by using large eddy simulation method, which is solved by the equations of Navier - Stokes for an incompressible fluid based on the method of splitting by physical parameters that can be discretize by the control volume method. In the first step it is assumed that the transfer of momentum carried out only by convection and diffusion. Intermediate velocity field is solved by 5-step Runge - Kutta method. At the second stage, the pressure field is solved based on the found intermediate velocity field. The algorithm is parallelized on high-performance systems. The obtained numerical results of three-dimensional detached flow around a car body reveals to approximate qualitatively and quantitatively the basic laws of hydrodynamics processes occurring in aerodynamics.

Keywords: Ahmed body, Navier-Stokes equations, finite volume method, Runge-Kutta method, pressure drag.

1 Introduction

As increasing the number of producing an automotive becomes evident automotive industry require more fuel efficiency as nowadays the problem is important for ecology and the costs. Most fuel efficiency depends on drag and to generate fuel efficient vehicle one must pay attention to drag reduction. As it is known the drag generally is made by pressure drag that generates at rear end [2]. Except drag force there are side force and lift force, that also have impact on vehicle stability. These forces are important to understand highly complex and often unsteady flows that are associated with the airflow over passenger cars. Velocities associated with vehicle dynamics coordinate system and aerodynamic forces and moments that act upon a vehicle associated with vehicle aerodynamics coordinate system are shown in figure 1.

The force coefficients are defined as

$$C_L = \frac{L}{\frac{1}{2}\rho V_\infty^2 A}, \quad C_D = \frac{D}{\frac{1}{2}\rho V_\infty^2 A}, \quad C_Y = \frac{Y}{\frac{1}{2}\rho V_\infty^2 A}$$

where C_L, C_D, C_Y is coefficient of lift, drag, side-force respectively, $\rho$is air density, $V$is velocity, $A$is reference area.

The moment coefficients are defined as

$$C_{MP} = \frac{P}{\frac{1}{2}\rho V_\infty^2 A l}, \quad C_{MR} = \frac{R}{\frac{1}{2}\rho V_\infty^2 A l}, \quad C_{MY} = \frac{Y}{\frac{1}{2}\rho V_\infty^2 A l}$$

where C_{MP}, C_{MR}, C_{MY} is pitch, roll, yaw moment coefficient respectively, l is a reference length.

The definition of forces and moments given in [2] follows. The forces may be considered to act along three, mutually perpendicular axes. Those forces are the drag, which is a measure of the aerodynamic force that resists the forward motion of the car, the lift which may act upwards or downwards; and the side force which only occurs in the event of a cross-wind or when the

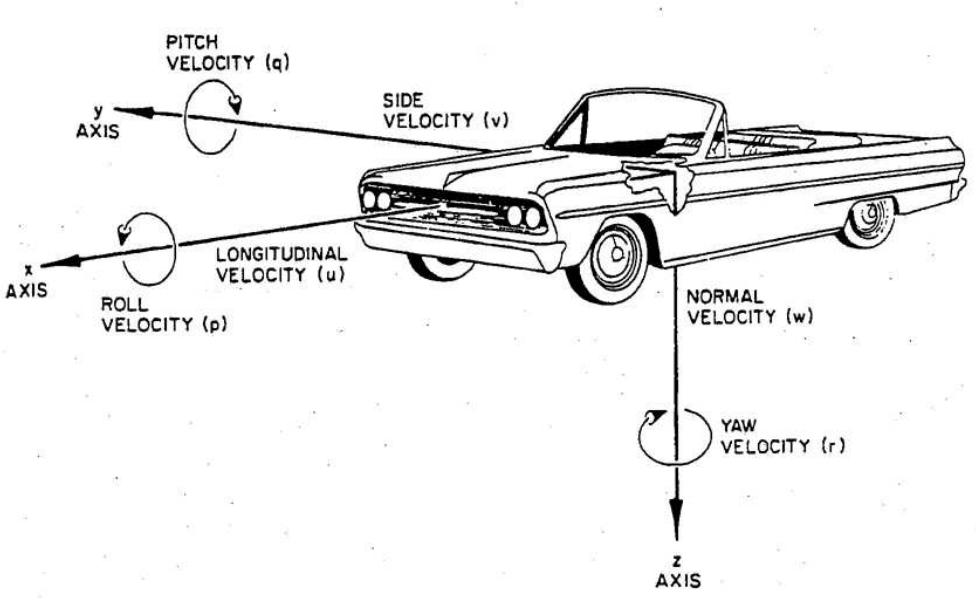

Fig. 1. Associated velocities of a vehicle

vehicle is in close proximity to another. The lift, drag and pitching moments are a measure of the tendency of those three forces to cause the car to rotate about some datum, usually the center of gravity. The moment effect is most easily observed in cross-wind conditions when the effective aerodynamic side force acts forward of the center of gravity, resulting in the vehicle tending to steer away from the wind. In extreme, gusting conditions the steering correction made by the driver can lead to a loss of control. As it is said in [2] the drag force is most easily understood if it is broken down into five constitutive elements. Surface drag or skin friction drag is a drag component that rise by generated frictional forces as air flows across the surface of the car. If the viscosity of air is considered to be almost constant the frictional forces at any point on the body surface depend upon the shear stresses generated in the boundary layer. Both the local velocity and the thickness and character of the boundary layer depend largely upon the size, shape and velocity of the vehicle. Induced drag force is created by changes in the character of the flow induced by force with a vertical component, lift. This force results to constraints imposed by realistic passenger space and mechanical design requirements. Practical requirements are also largely responsible for the creation of another drag source which is commonly referred to as excrescence drag. This is a consequence of all those components that disturb the otherwise smooth surface of the vehicle and which generate energy absorbing eddies and turbulence. Obvious contributors include the wheels and wheel arches, wing mirrors, door handles, rain gutters and windscreen wiper blades but hidden features such as the exhaust system are also major drag sources. Although some of these features individually create only small drag forces their summative effect can be to increase the overall drag by as much as 50%. Interactions between the main flow and the flows about external devices such as door mirrors can further add to the drag. This source is usually called interference drag. Another drag is that arising from the cooling of the engine, the cooling of other mechanical components such as the brakes and from cabin ventilation flows. Together these internal drag sources may typically contribute in excess of 10% of the overall drag. The most significant of the five in relation to road vehicles is the form drag or pressure drag which is the component that is most closely identified with the external shape of the vehicle. As a vehicle moves forward the

motion of the air around it gives rise to pressures. It is possible for two different designs, each having a similar frontal area, to have very different values of form drag (figure 2).

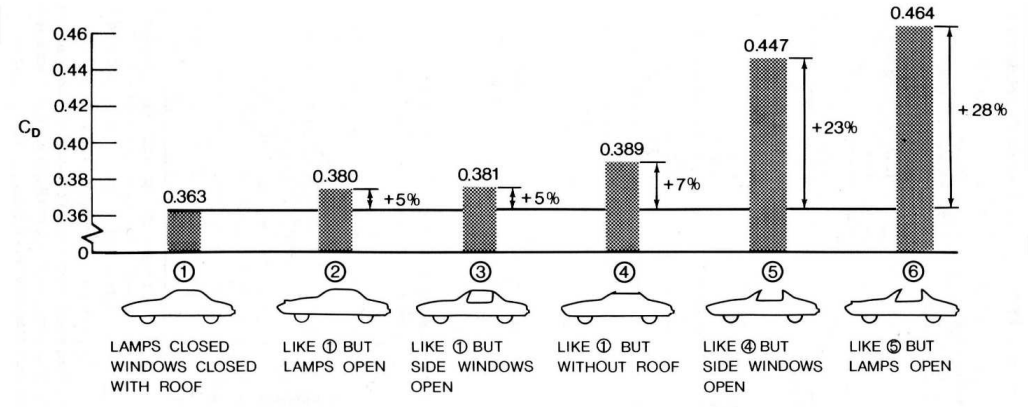

Fig. 2. Influence of a vehicle slightly changed form on drag coefficient

Ahmed benchmark model is the model that predicts most importance characteristics of the flow over a bluff body [1]. The Ahmed reference model is a car-like bluff body, representing a highly simplified 1/4 scale lower medium size hatchback vehicle with a slant back. Besides relatively simple geometry, the flow around Ahmed body retains some main features of the flow around real cars. The model's major attributes are 1044mm x 389mm x 288mm (Figure 3). The flow regimes are fully turbulent as the Reynolds number based on body length is usually too high. The flow around ground vehicle contains several separation regions.

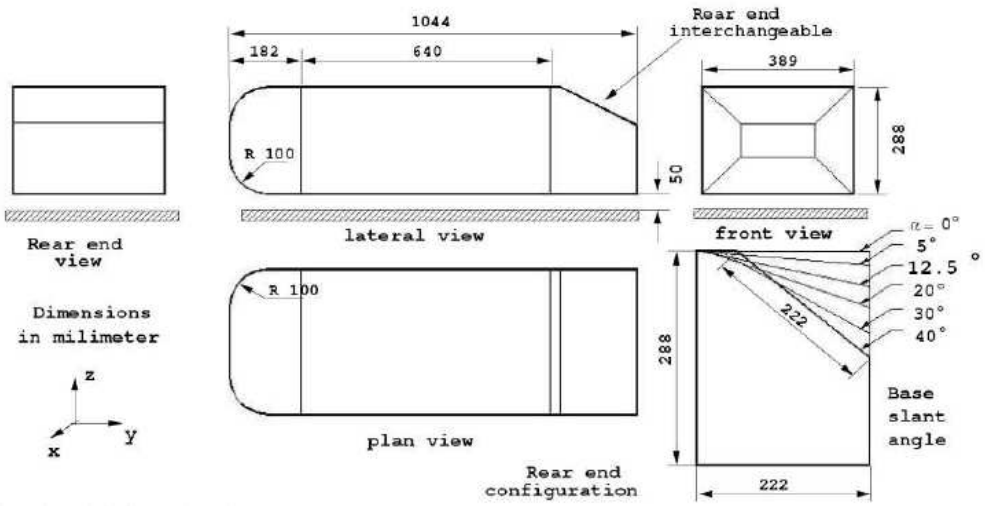

Fig. 3. Ahmed body reference model

Many experimental and numerical works have made in these area upon Ahmed body model and real cars. Numerical research can predict some aerodynamic characteristics and minimize

costs of experimental work. As experimental research providing qualitative and quantitative understanding numerical research is also important for interpreting the experiments and to obtain more complete understanding in flows around bluff body. From Ahmed experimental measurements in a wind tunnel [1] that most suitable for vehicle testing it was revealed that 85 percent of drag comes from pressure drag or form drag [1], generating at a rear end and detailed analysis were made upon the time averaged wake structure. The wake flow behind the vehicle is the flow region which represents major contribution to car's drag. For Ahmed used model based length Reynolds number was 4.29 million. It was only slant angle of changed geometric parameters.

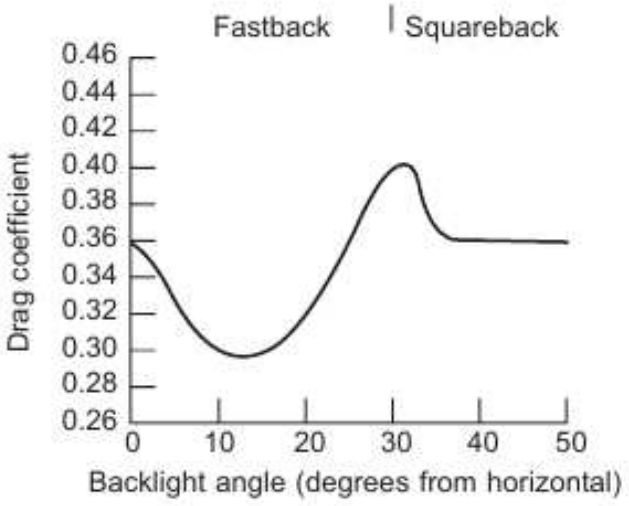

Fig. 4. Dependence between backlight angle and drag coefficient

Fig. 5. Squareback and hatchback profiles

There are other experimental works with use of Ahmed body reference model such as [3, 7-9]. The objective of the pioneer work of Ahmed et al. [1] was to study the influence of the slant angle at rear end. Their experimental and numerical work showed a clear influence of the rear slant angle to the time-averaged flow structures. Varying slant angle they found that the flow changes character at an angle about 30 degree [16]. From that moment there have been many works studying influence of different angles upon flow structure. From [2] figure 4

demonstrates the change in the drag coefficient of a typical vehicle with changing backlight angle. As the angle increases from zero (typical squareback) towards 15 degrees there is initially a slight drag reduction as the effective base area is reduced. Further increase in backlight angle reverses this trend as the drag inducing influence of the upper surface pressures and trailing vortex creation increase. As 30^0 is approached the drag is observed to increase particularly rapidly as these effects become stronger until at approximately 30^0 the drag dramatically drops to a much lower value. This sudden drop corresponds to the backlight angle at which the upper surface flow is no longer able to remain attached around the increasingly sharp top, rear corner and the flow reverts to a structure similar to that of the initial squareback. Lai et al. [4] were performed both experimental and numerical investigation to analyze the influence of the different rear diffuser angle on aerodynamic drag and wake structure. Also experimental and numerical investigation with use of CFD models were made by Korkischko et al. [6] for better understanding and validation between experiments and adequate numerical simulation. Large eddy simulation was performed by Das et al. [5] with a slant back angle of 25. Some numerical investigation involve RANS based models [10-15] and LES based models [16-20] to predict main features of the flow around ground vehicles.

2 Mathematical model

Therefore, flow around vehicle can be described by the equations in the Boussinesq approximation. For mathematical modeling of the system of equations are considered, which including the equations of motion and the continuity equation. The development of three-dimensional turbulent flow around vehicle is considered. Three-dimensional mathematical model is used for modeling of flow around vehicle [23, 24]:

$$\frac{\partial \overline{u_i}}{\partial t} + \frac{\partial \overline{u_j u_i}}{\partial x_j} = -\frac{\partial \overline{p}}{\partial x_i} + \nu \frac{\partial}{\partial x_j}\left(\frac{\partial \overline{u_i}}{\partial x_j}\right) - \frac{\partial \tau_{ij}}{\partial x_j}, \tag{1}$$

$$\frac{\partial \overline{u_j}}{\partial x_j} = 0, \quad (i = 1, 2, 3), \tag{2}$$

where $\tau_{ij} = \overline{u_i u_j} - \overline{u_i}\,\overline{u_j}$, g_i- gravitational acceleration, $\beta-$expansion coefficient, u_i – velocity components.

Smagorinsky turbulence model is used to close the system of equations (1) - (2) [21].
The finite volume method is used for the numerical simulation. For this purpose let us represent the Navier-Stokes equation and equation for the temperature in the form of integral conservation laws for arbitrary fixed volume Ω with boundary $d\Omega$ [23, 24]:

$$\int_\Omega \left(\frac{\partial U}{\partial t} + \frac{\partial F_i}{\partial x_i} + \frac{\partial G_i}{\partial x_i} - B_i\right) d\Omega = 0, \tag{3}$$

where

$$U = \begin{pmatrix} 0 \\ u_j \end{pmatrix}, \quad F_i = \begin{pmatrix} u_i \\ u_i u_j + p\delta_{ij} - \tau_{ij} \end{pmatrix}, \quad G_i = \begin{pmatrix} 0 \\ \nu \frac{\partial \overline{u_i}}{\partial x_j} \end{pmatrix}, \quad B = \begin{pmatrix} 0 \\ 0 \end{pmatrix}.$$

equation (3) can be written in this form

$$\int_\Omega \left(\frac{\partial U}{\partial t} - B\right) d\Omega + \oint_{\partial\Omega} (F_i + G_i) n_i d\Gamma = 0. \tag{4}$$

And we can write the equations (4) like

$$\int_{\Omega}\left(\frac{\partial U}{\partial t}\right)d\Omega+\oint_{\partial\Omega}(F_i+G_i)n_i d\Gamma=\int_{\Omega}B_i d\Omega. \tag{5}$$

Grid functions are defined at the cell center, and fluxes across the border in divided cells. Cell volume is denoted by the grid functions.

Now we perform a discretization of equation (5) by the control volume (CV) and control surface (CS)

$$\sum_{CV}(\frac{\Delta U}{\Delta t})\Delta\Omega+\sum_{CS}(F_i+G_i)n_i\Delta\Gamma=\overline{B_i}\Delta\Omega \tag{6}$$

or we can write the equation (7) in this form:

$$\sum_{CV}\Delta U\Delta\Omega+\sum_{CS}\Delta t(F_i+G_i)n_i\Delta\Gamma=\Delta t\overline{B_i}\Delta\Omega. \tag{7}$$

3 Numerical algorithm

Splitting method by physical parameters is used to solve the equation (1) - (2) [22, 23, 25, 28-30]. Discretization in form of (7) is used for the numerical implementation of the system (1) - (2). In the first step it is assumed that the transfer of momentum carried only by convection and diffusion. The intermediate velocity field is solved by 5-step Runge - Kutta method. In the second stage, the pressure field is found based on the found intermediate velocity field. Poisson equation for the pressure field is solved by Jacobi method. The third step it is assumed that only the transfer is carried out by pressure gradient. The algorithm is parallelized on high-performance systems. Simulations were made on cluster systems URSA and Cluster of Institute of Mathematics and Mechanics at the al-Farabi Kazakh National University.

I) $\int_{\Omega}\frac{\boldsymbol{u}^*-\boldsymbol{u}^n}{\tau}d\Omega=-\oint_{\partial\Omega}(\nabla\boldsymbol{u}^n\,\boldsymbol{u}^*-\nu\Delta\boldsymbol{u}^*)n_i d\Gamma,$

II) $\oint_{\partial\Omega}(\Delta p)d\Gamma=\int_{\Omega}\frac{\nabla\boldsymbol{u}^*}{\tau}d\Omega,$

III) $\frac{\boldsymbol{u}^{n+1}-\boldsymbol{u}^*}{\tau}=-\nabla p,$

4 Results of numerical simulation

There are experimental and numerical works of real cars of Basara B. [26], Manan et al. [27] and others. Manan performed both experimental and numerical investigation on small hatchback car model, named ADRENe. Experimental investigation was performed in conventional wind tunnel while numerical one was performed using Gambit as the preprocessing software and Fluent as the solver and post processor. There was a good agreement between experimental and numerical works on computed drag forces and pressure distributions over the entire range of air velocities, however, the agreement with the data for drag coefficient varies, which was appeared to suggest a higher degree of dependency on the details included in the geometric modeling, grid quality and elements selection. Evaluated drag coefficient for proposed exterior profile of ADRENe appeared to be of order of 0.4. This number of drag coefficient is acceptable for effective fuel savings. In

this work there was no accent on slant angle at rear end, but you can see it from figures of Manan et al. There is more other properties of the car that have influence on drag coefficient such as size of a car, wheels etc. Sometimes you just build a real car design, knowing about drag, test on drag coefficient and it comes out efficient in sense of drag coefficient and respectively fuel efficiency. Further it's presented numerical results obtained for Mercedes Gelandewagen car. In present work initial and boundary conditions were determined to solve the problems of flows around Mercedes Gelandewagen car. More than 800 000 grid points were used in simulations. Numerical results were obtained with LES technique using Smagorinsky SGS model. The Mercedes Gelandewagen car presented in this work is a squareback car model, but a wheel behind the car can create additional vortex, restricting car at moving and increasing pressure drag. As it's shown from figures 6 and 7 for this type of car with the slant angle of 0 degree we can see a small vortex in front of the car at low part of windshield that was discussed in M. Minguez et al. [19]. In this work it's shown the flow separates and then reattaches on the leading edge and at sharp edge between the roof of Ahmed body and the slant surface which slant was 25 degree at z=0 plane. Also it was observed that the flow around Ahmed body was turbulent and completely three dimensional with differences going from center to sides of the given model. The results presented in the given work are two dimensional with planes for the future of three dimensional one. As observed in experimental [3] and numerical works [19] the flow separates at the beginning of the slant and then reattaches in the middle of the slant. In M. Minguez et al. [19] work the flow separates at the two edges between the slant and the lateral surfaces of the Ahmed body. In the present study with given 0 degree of the slant angle Figures 6 and 7 show that the flow separates at the roof and the bottom of the rear end that lead to two large counter-rotating trailing vortices with time going by spreading farther in the wake.

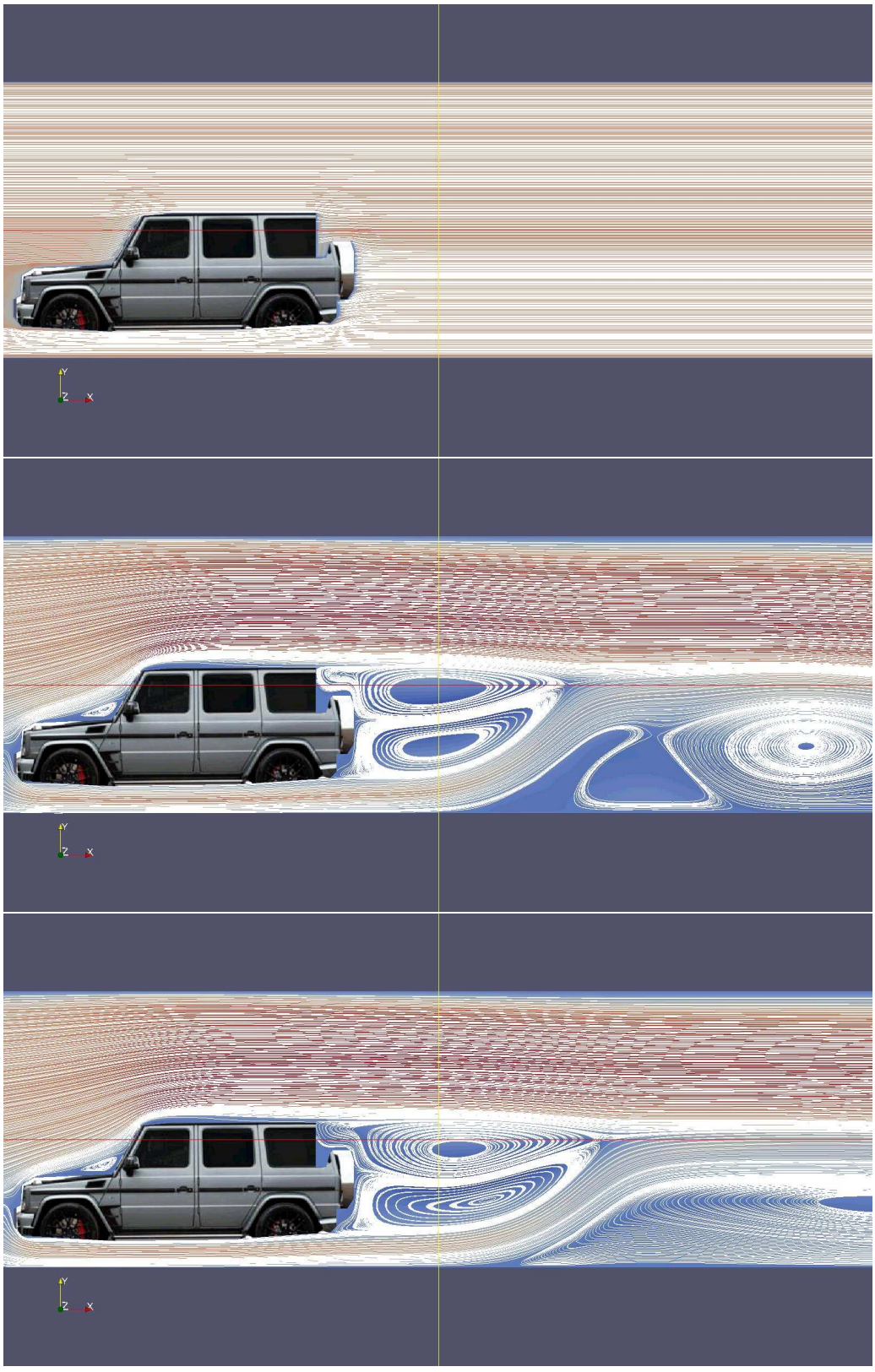

Fig. 6. Flow visualization with velocity profiles and streamlines at time: (a) t=0; (b) t=5; (c) t=10

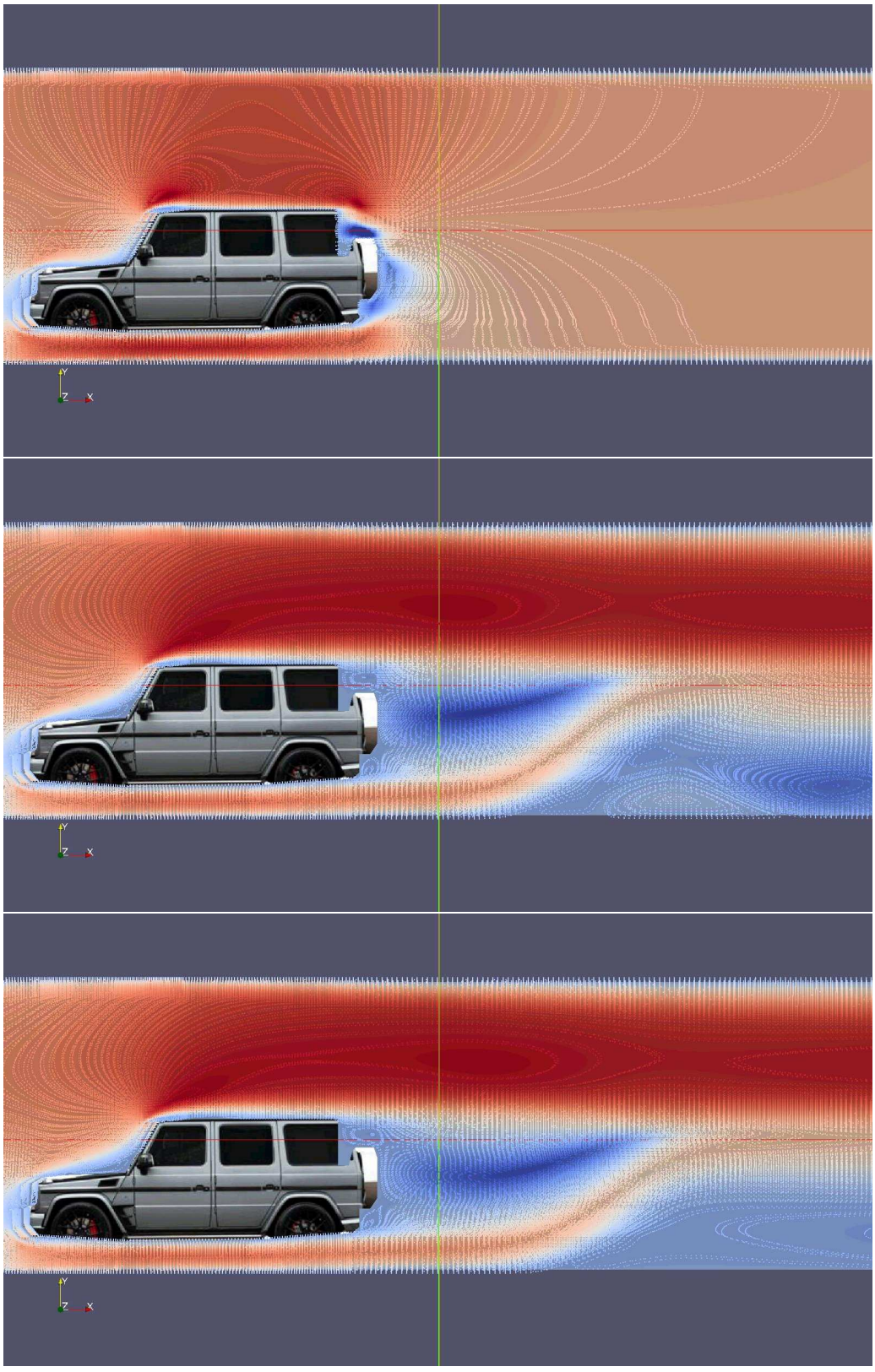

Fig. 7. Flow visualization with velocity profiles and particles at time: (a) t=0; (b) t=5; (c) t=10

References

1. Ahmed, S.R., Ramm, G., Faltin, G.: Some salient features of the time-averaged ground vehicle wake. SAE Paper 840300, (1984)
2. Happian-Smith, J.: Introduction to modern vehicle design. Transport research laboratory (TRL), UK
3. Lienhart, H., Becker, S.: Flow and turbulence structure in the wake of a simplified car model. SAE Paper 2003-01-0656, (2003)
4. Lai, Ch., Kohama, Y., Obayashi, Sh., Jeong, Sh.: Experimental and numerical investigations on the influence of vehicle rear diffuser angle on aerodynamic drag and wake structure. International Journal of Automotive Engineering 2, 47–53, (2011)
5. Das, P., Sayem, A.S.M., Islam, M.T.: Large-Eddy Simulation of the flow around an Ahmed reference model. Asian congress of Fluid Mechanics, 17-21 December, Dhaka, Bangladesh.
6. Korkischko, I., Romano Meneghini, J.: Experimental investigation and numerical simulation of the flow around an automotive model: Ahmed Body. 19th International Congress of Mechanical Engineering, Proceedings of COBEM2007, Brasilia.
7. Bayraktar, D., Landman, D., Baysal, O.: Experimental and computational investigation of Ahmed body for ground vehicle aerodynamics, SAE Report, 01-2742, (2001)
8. Spohn, A., Gillieron, P.: Flow separations generated by a simplified geometry of an automotive vehicle, IUTAM Symposium: unsteady separated flows. Toulouse, France, (2002)
9. Sims-Williams, D.: Experimental investigation into unsteadiness and instability in passenger car aerodynamics, SAE Report, 980391, (1998)
10. Manceau, R., Bonnet, J.P.: Workshop on refined turbulence modelling. 10th ERCOFTAC, (2002)
11. Gillieron, P., Chometon, F.: Modelling of stationary three-dimensional detached airflows around an Ahmed reference body. Third International Workshop on Vortex, ESAIM Proceedings 7, 173–183, (1999)
12. Durand, L., Kuntz, M., Menter, F.: Validation of CFX-5 for the Ahmed car body. CFX Validation Report No. CFX-Val 13/1002, (2002)
13. Han, T.: Computational analysis of three-dimensional turbulent flow around a bluff body in ground proximity. AIAA J. 27, 1213–1219, (1989)
14. Menter, F.R., Kuntz, M.: Development and application of a zonal DES turbulence model for CFX-5. CFX internal report, (2003)
15. Guilmineau, E.: Computational study of flow around a simplified car body. J. Wind. Eng. Ind. Aerodyn. 96, 1207–1217, (2007)
16. Krajnovic, S., Davidson, L.: Flow around a simplified car. J. Fluids Eng. 127, 919–928, (2005)
17. Howard, R.J.A., Pourquie, M.: Large eddy simulation of an Ahmed reference model. J. Turbul. 3(1), art no. 012, (2002)
18. Hinterberger, M., Garcia-Villalba, M., Rodi, W.: The aerodynamics of heavy vehicles: Trucks, Buses, and Trains. Applied and Computational Mechanics, New York, (2004)
19. Minguez, M., Pasquetti, R., Serre, E.: High-order large-eddy simulation of flow over the "Ahmed body"car model. Physics of fluids, 20(9), 095101, (2008)
20. Franck, G., Nigro, N., Storti, M., D'elia, J.: Numerical simulation of the flow around the Ahmed vehicle model. Latin American Applied Research 39, 295–306, (2009)
21. Lesieur, M., Metais, O., Comte, P.: Large eddy simulation of turbulence. New York, Cambridge University Press, (2005)
22. Issakhov, A.: Large eddy simulation of turbulent mixing by using 3D decomposition method. Issue 4 J. Phys.: Conf. Ser. 318. 042051. doi:10.1088/1742-6596/318/4/042051, 1282–1288, (2011)
23. Chung, T. J.: Computational Fluid Dynamics. Cambridge University Press, (2002)
24. Fletcher, C.A.: Computational Techniques for Fluid Dynamics. Vol 2: Special Techniques for Differential Flow Categories, Berlin: Springer-Verlag. (1988)
25. Issakhov, A.: Pryamoe chislennoe modelirovanie (DNS) turbulentnih techenii s ispolzovaniem parallelnih tehnologi. Bulletin of KazNU, 2(73), 81–91, (2012)
26. Basara, B.: Computations of automotive flows using the second-moment closure. European Congress on Computational Methods in Applied Science and Engineering ECCOMAS, Barcelona, (2000)
27. Manan Desai, S.A.: Channiwala and H.J. Nagarsheth. Experimental and computational aerodynamic investigation of a car. WSEAS TRANSACTIONS on FLUID MECHANICS, Issue 4, Volume 3, (2008)
28. Issakhov, A.: Mathematical Modelling of the Influence of Thermal Power Plant on the Aquatic Environment with Different Meteorological Condition by Using Parallel Technologies. Power, Control and Optimization. Lecture Notes in Electrical Engineering. Vol. 239, 165–179, (2013)
29. Issakhov, A.: Mathematical modelling of the influence of thermal power plant to the aquatic environment by using parallel technologies. AIP Conf. Proc. 1499, 15–18; doi: http://dx.doi.org /10.1063/ 1.4768963, (2012)

30. Issakhov, A.: Mathematical Modelling of Thermal Process to Aquatic Environment with Different Hydrometeorological Conditions. The Scientific World Journal, vol. 2014, Article ID 678095, 10 pages, doi:10.1155/2014/678095, (2014)

The Role of Thomson and Kohler Effects in Bridge Erosion of Electrical Contacts

S.N. Kharin, S. Kassabek

Kazakh-British Technical University, Kazakhstan, Almaty, Kazakhstan
Suleiman Demirel University, Kazakhstan,
staskharin@yahoo.com,kassabek@gmail.com

Abstract. Temperature asymmetry in opening electrical contacts due to Thomson and Kohler effects is an important factor influencing on the direction of material transfer and contact erosion at bridging and arcing, as well as on the duration of anode and cathode arc phases. The Kohler effects which occurs in relays due to tunnel mechanism of electrical conductivity through adhesive or passivating films may generate some times heat power comparable with Joule heating. The Thomson effect causes also the temperature displacement in closed contacts and in a liquid bridge that influences on the bridge erosion and arc evolution.
Mathematical model describing dynamics of temperature field in such electrical contacts is presented in this paper. Temperature dependence of Thomson coefficient is taken into account. Dimensionless criteria of Kohler, Thomson and Joule effects are introduced and discussed. It is shown that Kohler effects is most important in the range of low current. It enables to explain appearance of anode arc phase at the initial stage of arcing and also to evaluate its duration. Theoretical results are compared with experimental data with satisfactory coincidence.

Keywords: Thomson effect, Bridge erosion, Kohler effect, Joule heating.

1 Introduction

Evolution of electric arc between two contacts in relays, circuit breakers and other electrical apparatus depends essentially on phenomena occurring at pre-arcing stages of contact separation, especially at the initial phase of contact opening, which is accompanied by bridging [1]. For some contact materials Thomson and Kohler effects may play very important role and be responsible for the extra-heating and asymmetry of temperature field in contacts [2]. Mathematical models describing these phenomena are presented in the papers [3]-[5] at some simplifying assumptions. In particular Thomson coefficient is considered as averaged constant for whole temperature interval, from initial value to the melting point, while Kohler effect is described by axisymmetric stationary model. The main goal of this paper is to develop above mentioned models and consider the problems with temperature-dependent Thomson coefficient and non-stationary Kohler effect.

2 Non-stationary Kohler effect at the pre-bridging stage

The tunnel effect plays an important role in many fields of engineering applications and modern technologies such as electric vacuum devices, semi-conducting materials, super-conducting contacts, technology of thin films etc. Various problems of tunnel conductivity, magnitude of tunnel current, tunnel voltage across a contact film as well as properties of varied films have been investigated and much progress made in the understanding of these characteristics.

The modern tendency to use extra-low range of the current (about $10^{-4}A$ and less) in many fields of engineering leads to the situation when investigators are faced with new seriousproblems and phenomena that remain obscured at ordinary current range but come to the forefront if the current range is extra-low. The Kohler effect is one of them. The overheating of anode

in comparison with cathode due Kohler effect is not important at ordinary conditions. But it is essential at extra-low current, as it will be shown below. It leads to the thermal asymmetry in the microscopic molten bridge that appears between two electrodes during their opening just before arc ignition. If cathode and anode are of the same material the point of the bridge with maximum temperature is displaced toward anode, and when the temperature rises to the boiling point the bridge breaks at this point, and molten metal transfers from anode to cathode. After certain cycles of opening and closing operations one can see the formation of very thin pips (or spires) on the cathode and craters on the anode. This phenomenon, called bridge erosion, is very dangerous for micro-relays. Reducing of the current diminishes the volumes of the spires but not their height. Even the very thin spires are able to make sensitive micro-relays unreliable. The hypothesis that Kohler effect may be responsible for the bridge erosion of electrical contacts was proposed by E. Justi and H. Schultz. New aspects of this theory and corresponding mathematical models for stationary temperature fields are developed in the papers [4] - [5]. However dynamics of Kohler effect, which should be described by non-stationary mathematical models, is not investigated. It is very important for the understanding and calculation of relative contributions of Joule and Kohler components of contact heating and bridge erosion in the course of contact opening because experimental study of these phenomena is very difficult because of microscopic size of a bridge $(10^{-6} - 10^{-8}m)$ at extra-low current.

Let us consider a circular contact spot between cathode and anode covered with a thin (a few A^O) chemisorbed or adhesive films that are penetrated by the conduction electrons by means of tunnel effect, which creates a heat source on the interface between anode and film with specific capacity

$$\prod = j \cdot u_f = j^2 \cdot \sigma_f \quad (1)$$

A portion of liberated heat with the heat flux

$$\prod_c = \frac{\theta_f}{W} \quad (2)$$

flows back to the cathode through the film whereas the remainder part of the flux

$$\prod_a = \prod - \frac{\theta_f}{W} \quad (3)$$

flows into the anode. Here $\theta_f = \theta_2 - \theta_1$ is the temperature drop across the film between anode and cathode surfaces and is the specific thermal resistance across the film:

$$W = \frac{d_f}{\lambda_f} \quad (4)$$

The non-stationary heat conduction in a spherical contact for anode $(i = 1)$ and for cathode $(i = 2)$ can be described by the equations

$$\frac{\partial \theta_i}{\partial t} = a^2\left(\frac{\partial \theta_i}{\partial r^2} + \frac{2}{r}\frac{\partial \theta_i}{\partial r} + \frac{q}{r^4}\right), \ (i = 1, 2), \ q = \frac{I^2 p}{4\pi^2 \lambda} \quad (5)$$

The initial condition can be defined by the calculation of the temperature at the previous stage [4]. However it has a negligible influence on the following temperature dynamics, thus we can put

$$\theta \mid_{t=0} = f(r) = 0$$

The boundary conditions are

$$-\lambda \frac{\partial \theta_1}{\partial r} \mid_{r=r_0} = \frac{\partial \theta_2 - \partial \theta_1}{W} \mid_{r=r_0}, \quad -\lambda \frac{\partial \theta_2}{\partial r} \mid_{r=r_0} = \prod - \frac{\theta_2 - \theta_1}{W} \mid_{r=r_0} \text{ and } \theta \mid_{\infty} = 0$$

The solution of this problem can be found using Laplace transformation. In particular on the contact spot $r = r_0$ we get

$$\theta_1(r_0,t) = \theta_c(r_0,t) + \theta_K(r_0,t) - \tfrac{1}{2}\theta_f(r_0,t),\ \theta_2(r_0,t) = \theta_c(r_0,t) + \theta_K(r_0,t) + \tfrac{1}{2}\theta_f(r_0,t)$$

where $\theta_c(r_0,t)$ and $\theta_K(r_0,t)$ are the temperature components due to Joule heating and $\theta_f(r_0,t)$ due to Kohler heating respectively, and is the temperature drop across the film. If we introduce the dimensionless time (Fourier criterion) $\tau = \frac{a^2 t}{r_0^2}$, then these functions can be represented in the from: $\theta_c(r_0,t) = \frac{q}{2r_0^2}[1 - 2\eta(\sqrt{\tau}) + \varphi(\tau)]$, $\quad \theta_K(r_0,t) = \frac{\prod r_0}{2\lambda}[1 - \eta(\sqrt{\tau})]$
$\theta_f(r_0,t) = \frac{\prod r_0}{\lambda(1+\varepsilon)}[1 - \eta((1+\varepsilon)\sqrt{\tau})]$

where

$$\varepsilon = \tfrac{2r_0}{\lambda W}, \qquad \eta(\tau) = exp(\tau^2)\cdot erfc\ \tau,$$

$$\varphi(\tau) = \tfrac{2}{\sqrt{\pi}}\int_0^\infty exp(-z^2)[1 - \sqrt{\pi\tau}\cdot\eta(z+\sqrt{\tau})]\tfrac{dz}{+2z\sqrt{\tau}}$$

Fig. 1 depicts the dynamics of calculated temperature drop $\theta_f(r_0,t)$ for platinum contacts at the parameters: $I = 10A, \quad r_0 = 3.7\cdot 10^{-6}m$,
$\sigma_f = 4.4\cdot 10^{-3}\Omega\cdot m^2, W = 8.3\cdot 10^{-8}m^2\cdot^0 K\cdot W^{-1}$

.

The experimental measurement of Kohler temperature drop for stationary case at the same conditions carried out by R. Holm and I. Dietrich [2] gave the value $\theta_f = 500^0 C$, that agrees satisfactory with calculated value. One can see that if the Fourier criterion $\tau < 0.001$, than temperature drop is small and Kohler effect can be negligible. In other words Kohler effect is negligible if the duration of current pulse $t < \frac{0.001 r_0^2}{a^2}$. In contrast for $\tau < 0.1$, i.e. $t < \frac{0.1 r_0^2}{a^2}$, Kohler effect should be taken into account.

It is important for practice to compare the influence of Joule and Kohler components of heat generation on contact heating. That can be estimated using Kohler criterion,Ko , which was introduced in [5] as the ratio between contact film resistance $R_f = \sigma_f/\pi r_0^2$ and contact constriction resistance $R_c = \rho/2r_0$, i.e. $Ko = \frac{R_f}{R_c} = \frac{2\sigma_f}{\pi\rho r_0}$. The results of calculation of temperature drop across film in dependence on the Kohler criterion and τ is shown in Fig. 2

.

This result shows that overheating of the anode due to Kohler effect in considered case is not important if $Ko < 0.05$, however it becomes important for $Ko < 0.02$. If $Ko < 0.05$, then temperature drop θ_f depends essentially on time, thus in this case the stationary model presented in [5] can not be applied for estimation of Kohler effect.

The anode overheating due to Kohler effect is very important for the bridging phenomena accompanying the contact opening. Fig. 3 is evidence that anode temperature reaches the melting point $\theta_m = 1772^0 C$ at $\tau = 7$, while the cathode temperature at this moment $\theta_1(7) = 1200^0 C$, therefore the cathode remains for some time in the solid state and molten liquid bridge is forming from the anode material

.

It means that material transfer after bridge rupture (bridge erosion) occurs from anode to cathode, that was observed experimentally for Pt contacts. Hence Kohler effect may be responsible for the bridge erosion in Pt contacts.

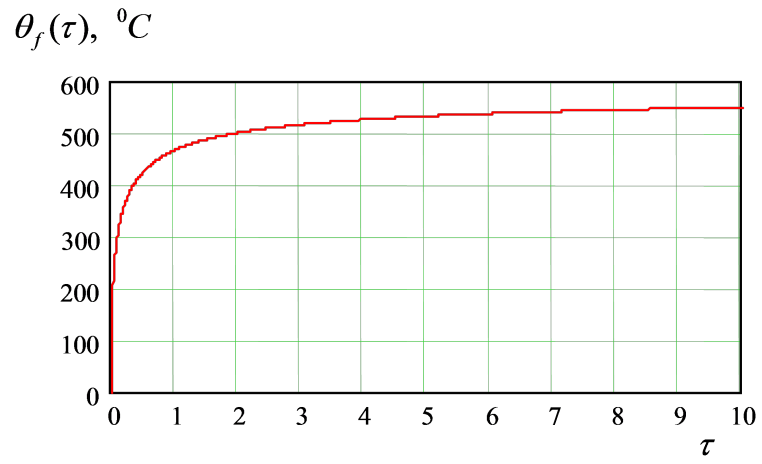

a)

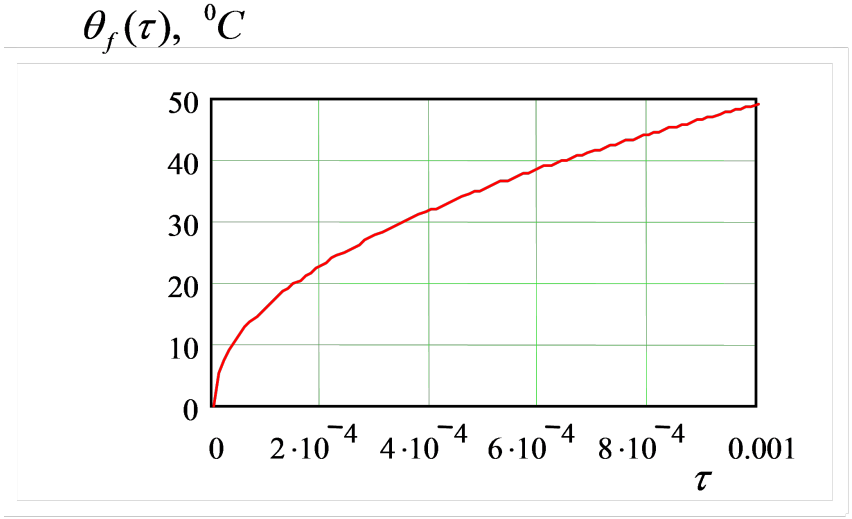

b)

Fig. 1. Dynamics of temperature drop across the film $\theta_f(r_0, t)$ due to Kohler effect for the interval $0 \leq \tau \leq 10$ (a) and for the interval $0 \leq \tau \leq 0.001$ (b)

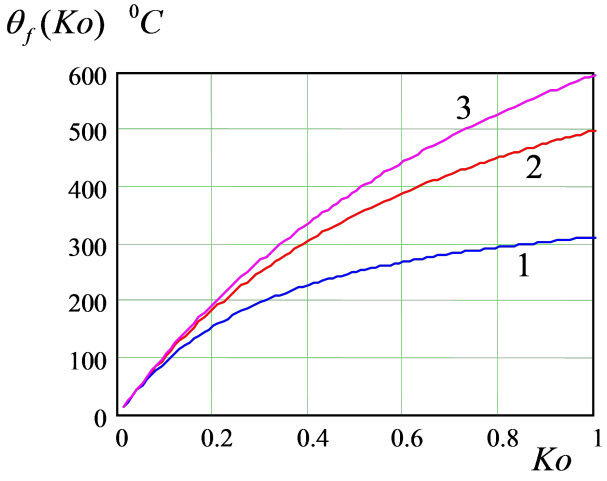

Fig. 2. θ_f versus Ko for $\tau = 0.1(1)$, $\tau = 1(2)$ and $\tau = 10(3)$

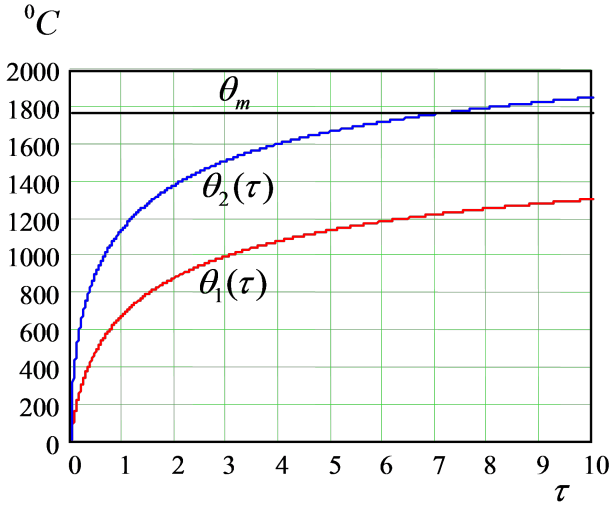

Fig. 3. Dynamics of cathode and anode temperature

3 Thomson effect

F. Llewellin Jones suggested that Thomson effect may be responsible for the displacement of temperature maximum in molten metal contact bridge from its geometrical center towards anode or cathode dependently on the sign of Thomson coefficient [6]. The assumption of constancy of Thomson coefficient considered in the model [4]-[5] is correct for copper, silver, gold, however for such materials like tungsten, platinum, and molybdenum temperature dependence of Thomson coefficient is very important and can not be averaged (see Fig. 4). Let us consider a molten bridge between opening contacts consisting of three zones (Fig. 5): visible part occupied the domain $D_1[-l \le z \le l, 0 \le r \le y(z)]$ and hidden parts D_2 and D_4 . The domains D_3 and D_5 inside anode and cathode are occupied by the solid metal zone. As a rule the Fourier criterion for thermal processes in a bridge is sufficiently large ($Fo \sim 10 - 10^2$) to apply quasi-stationary model of temperature field. The axial component of heat transfer due to metallic heat conduction is much greater than radial components due to convection and radiation into ambient gas.

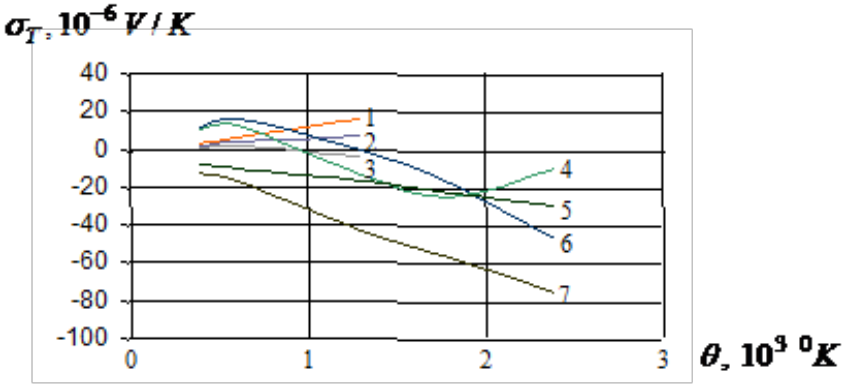

Fig. 4. The temperature dependence of the Thomson coefficient σ_T 1 - Ag, 2 - Cu, 3 - Au, 4 - Mo, 5 - Pt, 6 - W, 7 - Pd

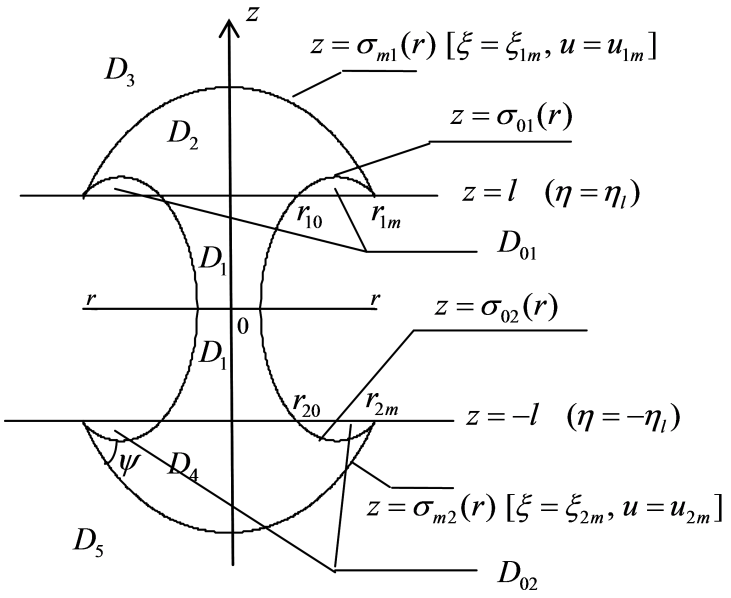

Fig. 5. The structure of molten metal bridge

Therefore the temperature field in the visible part of the bridge can be described by the quasi-stationary heat equation in the axial direction z. However the current density is different for different z:

$$j = \frac{I}{\pi y^2(z)}.$$

As well as the density of heat flux. To take into account this fact we use for the temperature of the visible part of a bridge the heat equation for a body with variable cross-section [4]:

$$\frac{1}{y^2(z)}\frac{d}{dz}[y^2(z)\frac{d\theta_1}{dz}] + \frac{\rho_{10}(1+\alpha_1\theta_1)I^2}{\pi^2\lambda_1 y^4(z)} = 0.$$

The heat equations for the domains $D_2 - D_5$ can be written in the form

$$\frac{\partial^2\theta_i}{\partial r^2} + \frac{1}{r}\frac{\partial\theta_i}{\partial r} + \frac{\partial^2\theta_i}{\partial z^2} + \frac{\rho_{i0}j^2}{\lambda_i}(1+\alpha_i\theta_i) = 0, \qquad i = 2,3,4,5$$

The boundary conditions on the interfaces $z = -l$ and $z = l$ are the conditions of continuity of temperature and heat fluxes. On the interfaces $z = \sigma_{ml}(r)$ and $z = \sigma_{m2}(r)$ the temperature should be equal the value of the melting point. These unknown interfaces should be found from the condition of continuity of heat fluxes between liquid and solid zones. Finally the temperature θ_3 and θ_5 should vanish at infinity.

The shape of the bridge is unknown a priori and should be found using the principle of minimum of bridge surface tension energy, i.e. the minimum of the functional

$$W(y) = 2\pi l \int_{-l}^{l} ky(z)\sqrt{1+y_z^2(z)}\,\mathrm{d}z$$

Solving corresponding Euler-Lagrange equation we can find the shape of the bridge in the form

$$y(z) = \frac{B}{2}exp(\frac{z}{A}) + \frac{A^2}{2B}exp(-\frac{z}{A})$$

The unknown constants A and B are defined using conditions of surface smoothness at the boundaries between visible and hidden parts of the bridge. Then we introduce instead of z the new dimensionless variable η by the formula

$$\eta = 2r_0 \int_{-l}^{z} \frac{\mathrm{d}z}{y^2(z)}$$

that enables to get a linear equation for the bridge.

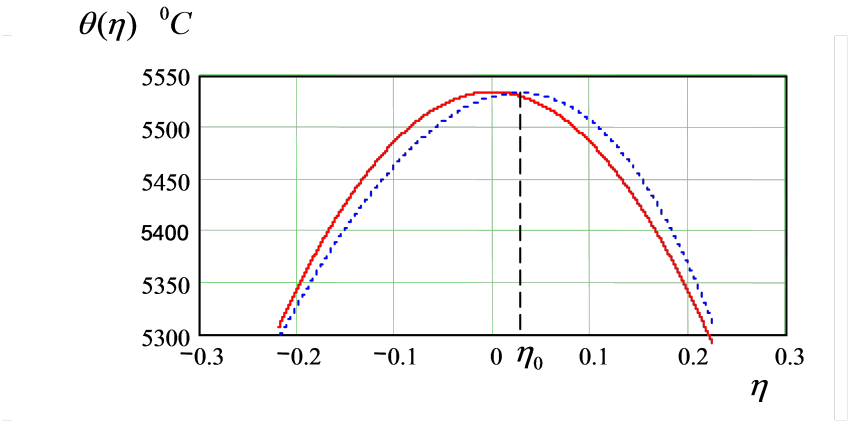

Fig. 6. Displacement of temperature maximum $\eta = \eta_0$ towards anode due to Thomson effect

The solution of heat equations for hidden parts of the bridge and for solid zones can be obtained by use of ellipsoidal isotherms [5], which enable us to reduce two-dimensional differential equations for radial and axial variables to one dimensional equation for the ellipsoidal coordinate ξ defined by the equation $\frac{r^2}{\xi^2+r_0^2} + \frac{z^2}{\xi^2} = 1$, and then simplify equations again by introduction of new dimensionless variable u =arctanξ/r_0. To get the solution satisfying the all boundary conditions the problem should be completed by two extra conditions. The first of them is the equality of the volume of bridge visible part D_1 and volumes $D_01 + D_02$ stretched out of liquid pool on the contact surfaces. The second condition is the given wetting angle ψ between surfaces $z = \sigma_{mi}(r)$ and $z = \sigma_{oi}(r)$. The analysis of this solution shows that displacement of temperature maximum in the bridge towards anode due to Thomson effect is about 10% of the bridge length (Fig. 6). It shows a good agreement with experimental results observed by F. Llewellin Jones [6].

4 Conclusions

1. Mathematical model described the influence of Thomson effect on contact heating in closed electrical contacts on the base of averaged values of Thomson coefficient is correct for such materials as Cu, Ag, Au, which have relatively week temperature dependence of Thomson coefficient. For W, Mo, Pt, Pd and other contact materials with large variation of Thomson coefficient non-linear heat equation should be used to estimate role of Thomson effect on contact heating.

2. In the range of low and extra-low contact force ($10^{-3} - 10^{-4} N$) and corresponding low range of film resistivity ($\sigma_f < 5 \cdot 10^{-13} \Omega \cdot m^2$) contact overheating due to Kohler effect may be much more than due to Joule heating. Non-stationary mathematical model of non-ideal quasi-metallic electrical contact enables to estimate dynamics of Kohler effect. This model may be applied in nano-technologies where transient extra-low current and contact spots are used.
3. The mathematical model of asymmetrical quasi-stationary liquid bridge between opening electrical contacts is elaborated, which takes into account the shape of the bridge depending on surface tension and phase transformation. The calculated values of the bridge geometry are in a good agreement with experimental data.
4. Thomson effect which creates a temperature asymmetry in the liquid bridge is estimated using the new mathematical model describing the conjugation of temperature fields in visible and hidden parts of bridge with solid phases. It was found that Thomson effect may play an important role for displacement of hottest temperature along the bridge and for contact erosion.

References

1. S.N. Kharin, "Post Bridge Phenomena in Electrical Contacts at the Initial Stage IEEE Transactions CPTMT - Part A, vol. 19, No 3, pp. 491 - 497, Sept.1996,
2. R. Holm: "Electric Contacts 4-th Edition, Springer Verlag, Berlin, 1981, pp 338-356
3. S.N. Kharin, Transient Thermophysical Phenomena at the Prearcing Period During Opening of Electrical Contacts. Proc.37-th Holm Conf. on Electrical Contacts, Chicago, 1991, pp. 53 - 65.
4. S.N. Kharin, Q.K. Ghori, M. Usman , "Significance of Thermoelectric Effects for the Bridge Transfer in Electrical Contacts Proc. INMIC'97 IEEE Conf., 1997, Islamabad , pp. 9 - 13
5. S.N. Kharin, Temperature Displacement in Electrical Contacts due to Kohler and Thomson effects, Proc. 9th International Conference on Switching Arc Phenomena (SAP-2001), Lodz, Poland, 2001, pp. 190-195
6. F. Llewellin Jones, Matter Transfer and the Microscopic Molten Metal Bridge, Proc. of the 14th International Relay Conference, Swansea, 1964, pp. 3–12

NOMENCLATURE

a^2 - thermal diffusivity of contact material, $m^2 \cdot s$
d_f - thickness of the film, m
I - electrical current, A
j - current density in contact spot, A/m^2
r_0 - radius of contact spot, m
u_f - the tunnel voltage across the film, V
W - specific thermal resistance across the film, $K^0 \cdot m^2/W$
α - temperature coefficient of electric resistivity, K^{-1}
λ - thermal conductivity of contact material, $W/m \cdot K^0$
λ_f - thermal conductivity of the film, $W/m \cdot K^0$
ρ - electrical resistivity of contact material, $\Omega \cdot m$
σ_f - the electric tunnel resistivity per unit area of the film, $\Omega \cdot m^2$
$\sigma - T$ - Thomson coefficient, V/K^0
θ_1 - cathode temperature, K^0
θ_2 - anode temperature, K^0
θ_f - the temperature drop across the film due to Kohler effect, K^0

Mathematical Modeling of the Destruction Process in the Fault Zone

Alexandr Kim and Yuriy Shpadi

JSC "National Center for Space Research and Technology Almaty, Kazakhstan
kim.as@mail.ru

Abstract. Developed a mechanics and mathematical model of tectonic fault with an area of engagement, which simulates the accumulation of strain and stress concentration in the source zone under constant influence of background stress. The distribution of stresses in the hard area of engagement, found the stress intensity factor at the edges. The regions in the area of beyond the structural stability of the rock, and their development over time. Identified the main directions of possible destruction of the environment in the area of the engagement.

Keywords: Mathematical Modeling, Destruction Process, Fault Zone

Fault zone characterized by the fact that they may be developed by shear strains. Weak resistance of the material change in the shape of the fault zone at low strain rates brings the body with a viscous fluid [1–3]. Assume that as a result of slow movements of two extended blocks relative to each other in a shear boundary and presence of "irregularities"in the contact surface of the accumulation of strain occurs on some parts of the boundary, stress relaxation and other areas "aseismic"movement in the third region.

In the approximation of generalized plane stress represent two long blocks in the form of two plates separated by a plane shear boundary, which corresponds to the case where the horizontal block size is much larger than the thickness. The plates can be represented in the form of two half-planes with a straight line of contact. On the line $y = 0$ the above-mentioned areas are located hook, stress relaxation, creep movements. Half-plane at infinity $y > 0$ and $y < 0$ are subjected to shear stresses $\sigma_{yx}^{\infty} = q$, $\sigma_x^{\infty} = 0$, $\sigma_y^{\infty} = 0$, is created in the background medium voltage $\tau_{yx} = q$. In an environment where traffic on the border of the shear occurs without dilating the shores of the gap displacements described x–component of the vector of mutual progress $a(x,t) = u(x,+0,t) - u(x,-0,t)$

$$v_+ - v_- = 0, \qquad -\infty < x < \infty \tag{1}$$

$$v_+ = v(x,+0,t), \qquad v_- = v(x,-0,t)$$

In the area of engagement the gap of displacement is zero

$$a(x,t) = 0, \quad \text{at} \quad y = 0, \quad |x| < l \tag{2}$$

In the area of aseismic slip tangential component of the stress tensor τ_{yx} depends on the x–component of the velocity vector of mutual progress shores. Here, this dependence is adopted by linear

$$\tau_{yx}^{\pm}(x,0,t) = \eta \frac{\partial a(x,t)}{\partial t}, \qquad l < |x| < L, \tag{3}$$

where η – effective viscosity in the area of aseismic slip (viscosity divided by the width of the fault zone). The "+"and "−"assigned to the limit values of the function at $y = 0$ for the upper and lower surfaces, respectively.

At the initial time the gap of movements in the area of aseismic slip is

$$a(x,0) = a_0(x), \qquad l < |x| < L \tag{4}$$

Regarding the function assume that it is continuous on the whole axis and has a bounded derivative, except for points $x = \pm l$, where it has an integrable derivative.

In the area of creep movements shear stresses coincide with background

$$\tau_{yx}^{\pm}(x,0,t) = q, \quad \text{at} \quad y = 0, \quad |x| > L \tag{5}$$

Superposition of the corresponding pass of the problem for $u(x,y,t)$ and for $v(x,y,t)$ a given $u^1(x,y,t)$ and for $v^1(x,y,t)$. In the future, consider the problem reduction, the index "1"is omitted.

The decision reduced the problem of motion of two half-clamped equivalent problem for the two semi-infinite collinear cuts in the elastic plane. A singular integral equation for this problem has the form [4].

$$\frac{2\mu}{\kappa+1}\frac{\partial a(x,t)}{\partial x} = \frac{\operatorname{sgn} x}{\pi\sqrt{x^2-l^2}}\left(\int_{-L}^{-l} - \int_{l}^{L}\right)\frac{\sqrt{\xi^2-l^2}}{\xi - x}\times$$

$$\times\left(\eta\frac{\partial a(\xi,t)}{\partial t} - q\right)d\xi, \qquad l < |x| < L \tag{6}$$

Transforming the right side of (6) and apply to both sides of the resulting equation Laplace transform with parameter p over time t, taking into account the above conditions (4) – (5), we obtain an integral equation in the image space

$$b(x,p) + \eta_* p\int_l^L L(x,\xi)b(\xi,p)d\xi = \frac{q}{p}f(x) - \frac{1}{p}\,a_0(x), \quad l < x < L \tag{7}$$

$$L(x,\xi) = \frac{1}{\pi}\ln\left|\frac{x\sqrt{\xi^2-l^2} + \xi\sqrt{x^2-l^2}}{x\sqrt{\xi^2-l^2} - \xi\sqrt{x^2-l^2}}\right|, \quad \eta_* = \frac{\kappa+1}{2\mu}\eta \tag{8}$$

$$f(x) = \frac{\kappa+1}{2\mu}\frac{1}{\pi}\left[L\ln\left|\frac{L\sqrt{x^2-l^2} + x\sqrt{L^2-l^2}}{L\sqrt{x^2-l^2} - x\sqrt{L^2-l^2}}\right| - \right.$$

$$\left. - x\ln\left|\frac{\sqrt{x^2-l^2} + \sqrt{L^2-l^2}}{\sqrt{x^2-l^2} - \sqrt{L^2-l^2}}\right|\right] \tag{9}$$

$$b(x,p) = a(x,p) - \frac{a_0(x)}{p}, \quad b(x,t) = a(x,t) - a_0(x), \quad l < x < L \tag{10}$$

Equation (7) is solved numerically-analytical method [4]. In the numerical analysis were adopted following parameters: $\mu = 3\cdot 10^{10} Pa$ – shear modulus; $l = 1\cdot 10^3 m$ – coordinate the right edge of the area of engagement; $L = 10\cdot 10^3 m$ – coordinate of the right edge of the zone of creep; $\eta_r = 10^{16} Pa\cdot c$ – viscosity of the material of the fault zone; $h_r = 10^2 m$ – width of the fault zone; $q = 2\cdot 10^5 Pa$ – background shear stresses; $T = 3.15\cdot 10^7 s = 1 year$ – time characteristic; $\kappa = 2$ – dimensionless; $t_p = T\cdot t(year)$ – time in seconds; $\eta = \frac{\eta_r}{h_r}$ – effective viscosity at fault; $a_0(x) = 0$ – initial displacement at the fault.

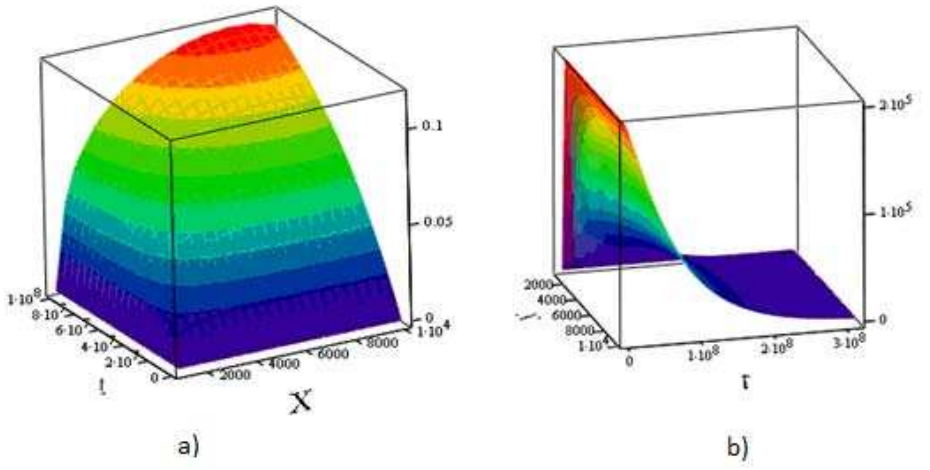

Fig. 1. Processes in the aseismic zone: a) – displacement on a fault; b) – stress relaxation in the aseismic zone.

The numerical analysis of the evolution of the concentration of stresses and displacements in fault closure shown in Figure 1. Figure 1a shows the displacement (by vertical, m) depending on the position in the aseismic zone (X-axis, m) and time (axis t, s). By colour highlighted the moving of the same level. Figure 1b presents the voltage (vertical axis) as a function of x and t.

As can be seen from Figures 1a and 1b at an early stage in the aseismic zone at a sufficient distance from the area of engagement is a uniform shift of the coast of the fault. As shown by the account over time voltage drop occurs in the aseismic zone and a significant (in this case about an order of magnitude) increase in the average level of stress in the toe area (if this level can be achieved, not interrupted by the destruction of the astillen).

The results of stress analysis in the vicinity of the left edge of the toe area are shown in Figure 2.

Figure 2a is a plot of the tangential stress intensity factor (vertical $Pa \cdot m^{\frac{1}{2}}$) in the vicinity of the left edge of the area of engagement versus time (axis t, s). Figure 2b stress distribution τ_{yx} in the vicinity of the left end ($x = -l$, $y = 0$) area zone of engagement depending on the distance from the end point of r ($r \ll l; -\pi < \theta < \pi$) at time $t = 10^8$ seconds, the vertical stress, Pa.

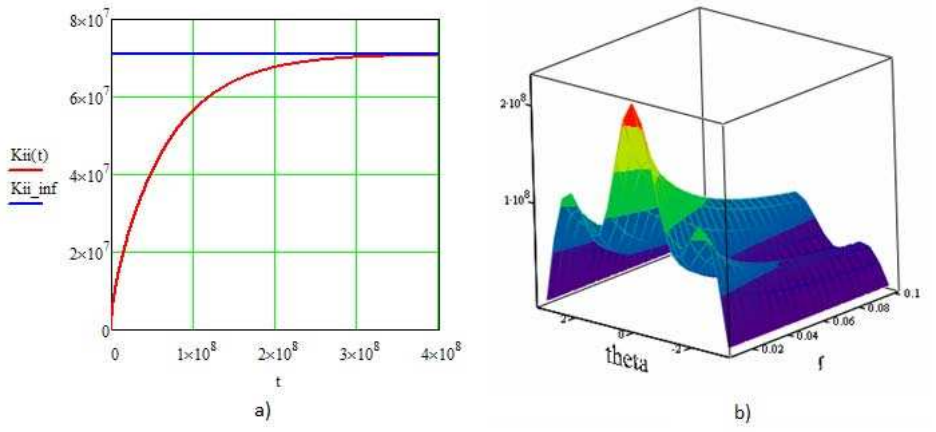

Fig. 2. Ratio of the intensity of shear stresses and stress distribution τ_{yx} near the left edge of the area of engagement.

Asymptotic formulas for the stress and displacement in the vicinity of the left edge of the toe of the form (to the right edge of the picture is symmetrical toe area) have the form [5]

$$\sigma_{xx} \sim -\frac{K_{II}}{\sqrt{2\pi r}} \sin\frac{\theta}{2}\left(2+\cos\frac{\theta}{2}\cos\frac{3\theta}{2}\right), \quad r \to 0, \quad -\pi < \theta \le \pi \tag{11}$$

$$\sigma_{yy} \sim -\frac{K_{II}}{\sqrt{2\pi r}} \sin\frac{\theta}{2}\cos\frac{\theta}{2}\cos\frac{3\theta}{2}, \quad r \to 0, \quad -\pi < \theta \le \pi \tag{12}$$

$$\tau_{yx} \sim -\frac{K_{II}}{\sqrt{2\pi r}} \cos\frac{\theta}{2}\left(1-\sin\frac{\theta}{2}\sin\frac{3\theta}{2}\right), \quad r \to 0, \quad -\pi < \theta \le \pi \tag{13}$$

$$u = \frac{K_{II}}{\mu}\sqrt{\frac{r}{2\pi}} \sin\frac{\theta}{2}\left(2-2\nu+\cos^2\frac{\theta}{2}\right) \tag{14}$$

$$v = -\frac{K_{II}}{\mu}\sqrt{\frac{r}{2\pi}} \cos\frac{\theta}{2}\left(1-2\nu+\sin^2\frac{\theta}{2}\right) \tag{15}$$

Figure 3 shows the evolution of the field outside the structural stability of rocks in the area of the left edge of the area of engagement.

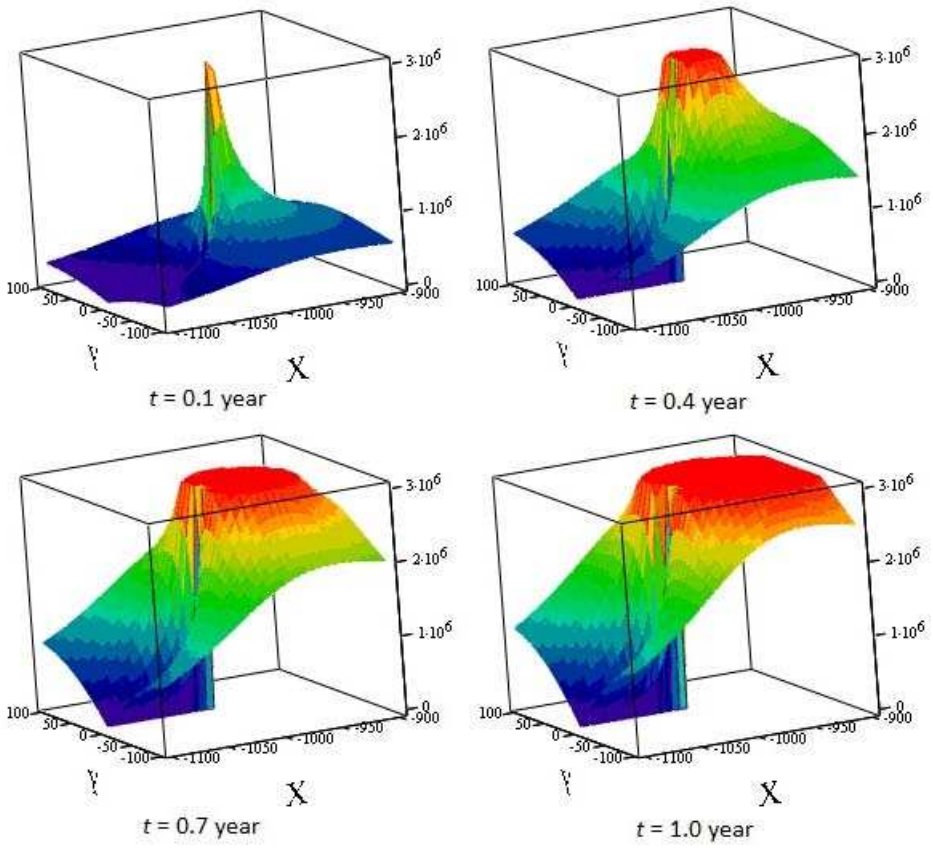

Fig. 3. Evolution of the field in the area of the barrier outside structural stability of rocks.

References

1. Sherman, S., Seminsky, K., Bornyakov, S., Buddho, V., Lobatskaya, R., Adamovich, A., Truskov, V., Babichev, A.: Faulting in the earth's crust. Shear zone // Novosibirsk: Nauka (1991)
2. Cherepanov, G.: A mechanism of fractures in the solid Earth // Proceedings of the Academy of Sciences of the USSR, Earth Physics, #9, pp. 3–12. (1984)
3. Adushkin, V.: Actual problems of geomechanics earth's crust. Electronic Scientific Information Journal "Herald DGGGMS RAS". 2001. #1 (16), pp. 1–33. (2001)
4. Kim, A.S.: Evolution of the stress-strain state in the tectonic fracture zone of the damping section. Proceedings of the international conference "Contribution of Koreans in science and technology in Kazakhstan Almaty, pp. 261-265 (1997)
5. Slepian, L.: Mechanics of grikes. L.: Shipbuilding (1981)

Modeling of Networks Flows of Grinshilds Types

Y. Amirgaliyev[1], A. Kovalenko[2], A. Kalizhanova[3], A. Kozbakova[3]

[1]Institute of Information and Computing technologies, Almaty, Kazakhstan
[2]Samara State University, Samara, Russia
[3] K.I.Satpayev Kazakh National Technical University, Almaty, Kazakhstan
amir_ed@mail.ru,alexey.gavrilovich.kovalenko@rambler.ru,{kalizhanova_aliya,ainur79}@mail.ru

Abstract. We consider flows distribution along networks, flows circulation described with Grinshilds type dependences. Those dependences identify the streams in traffic networks, in circuits of evacuation from the buildings. Applying game-theoretical approach and mathematical methods of hydraulic circuit theory, the tasks of searching balance state problems are set to solve that the cycle interrelationship methods are used.

Keywords: evacuation problem, urban territories, traffic accommodation, games theory, hydraulic circuit theory, Nesh, flow of Grinshilds type streams.

1 Introduction

Tasks having network arrangement have enormous significance for various social-economic and technological problems solution. A big share of it falls on flow problems. There exist integral guidelines of production and technical problems described with flow problems, for instance, hydraulic circuit theory. The key difference of those directions is in the causes defining flow progress. Thus, in water distribution systems, when the stream flows in the pipes with full storage the stream volume in the pipe is defined with pipe top and end piezometer heads. In that case, the flow along that pipe is the head receiver. If the flow moves along partial section pipe or along the channels, the pipeline flow magnitude coincides with intake.

To begin with, let's consider movement of people along building corridors during evacuation in an educational organization. Let's describe simulated conditions script.

Load flow task at organized evacuation. The building consists of many auditoriums, passages, staircases, building exit. There are trainees and a teacher in the classroom. Subsequent to evacuation signaling a teacher organizes trainees coming out from the lecture hall letting out one by one with specified intensity. Having left the classroom a trainee moves independently. His aim is to reach the exit within the shortest possible time. It is necessary to define movement intensity along all building sections. Below is the graph example of evacuation from the building see in the Fig. 3.

The movement of every stream pattern (a man) is defined with its aim and other stream components (people) movement. A person's aim is to reach destination within the shortest possible time, but the movement speed decreases due to the stream scope of other participant's movement. Those components interaction defines an overall stream movement. Generally, the motion is described with Nesh game-theoretical approach in normal form.

Problem of load flow in city traffic circuit.

City is the multiple of objects (micro regions, quarters, separate houses, enterprises, shops, entrance-exit points from the city, etc.) between which there circulates the traffic transporting different cargo and people.

Between those objects there are traffic mains consisting of street sections among the crossroads, entrance-exit points to and fro of enumerated objects along which we have traffic

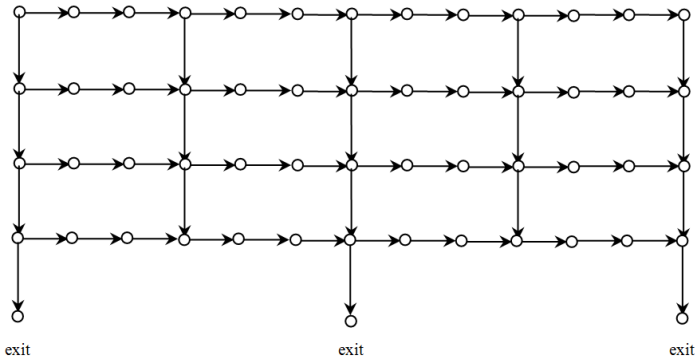

Fig. 1. Example of evacuated building.

movement. Assume that all objects are bound to entrance-exit points to the road from the quarters, via those places the quarters inlet and outlet the traffic, see an example on Fig. 2 Arrows show unit-direction motion lanes, circles show entrance-exit points.

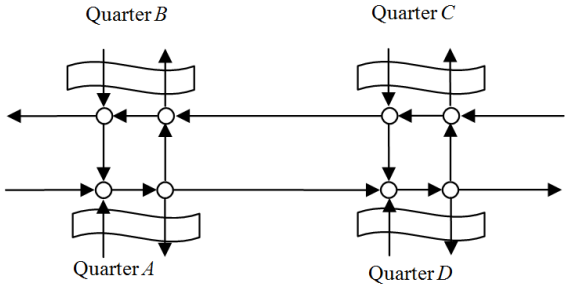

Fig. 2. Entrance-exit from the quarters.

Arrows show one-way traffic lanes along the road. Circles show transport flows access and exit points as well as flows connection and disconnection. At crossroads the streams are connected and disconnected. Total scheme of the crossroad is in the Fig. 3.

Similar to entrance-exit from the city:

Streams move along the roads between different points given above. Thus, the movement structure can be described as an oriented graph. Graph nodes are points of entry-exit from the crossroad, entry-exit from quarters, entry-exit from the city. Arcs of graph are the road sections between the nodes. Arrow direction denotes stream motion.

Nodes from which the stream enters the network are called the sources, the nodes into which stream enters from the network are outflows.

Let's assume that the flow consists of separate parts characterized with one movement path to draining. Transport units parts are similar and move uniformly, speed of those units at different arcs can be various. Each part represents the organized endless truck train in movement. Overall flow consists of multiple separate parts, let's denote the sum of flows from apex i to apex j as Q_{ij}. Parts' paths entering Q_{ij}, in general terms, are different. Let's consider that each part is controlled by a subject organizing the traffic.

Multiple of all subjects form multiple players I. Every $\gamma \in I$ player's strategy ξ_γ is a path from the source i to the outflow j out of all strategies' multiple - paths χ_γ, connecting those

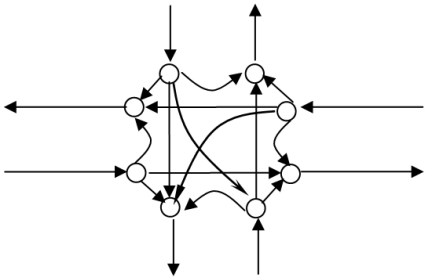

Fig. 3. Example of a crossroad.

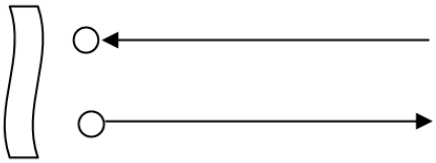

Fig. 4. Entrance-exit from the crossroad.

nodes. Every subject's criterion is motion time from i to j, its target is to minimize motion time of every transport unit, i.e. of all streams transport units. The criterion value is influenced by other players which path intercrosses with the γ player path. They increase the stream intensity at intercrossing sections thereby reducing motion speed and accordingly increasing time. As a result we obtain the game in the normal form:

$$G = \Big\langle I;\ \ \chi_\gamma, \gamma \in I;\quad \varphi_\gamma(\xi_1, \xi_2, \xi_3, \dots \xi_\gamma, \dots, \xi_{|I|}) \underset{\xi_\gamma \in \chi_\gamma}{\Rightarrow}$$

$$\underset{\xi_\gamma \in \chi_\gamma}{\Rightarrow} \min(\xi_1, \xi_2, \xi_3, \dots \xi_\gamma, \dots, \xi_{|I|}) \in \chi = \prod_{k \in I} \chi_k,\ \gamma \in I \Big\rangle,$$

Assume Nesh balance as the balance in the game [4].

Thereafter let us assume one more condition that I players multiple is infinite, of continual nature. In compliance with that the streams Q_{ij} will be broken down into the streams x_{ij}^{γ}, no matter how small is the magnitude.

2 Arc flow circulation analysis

It is obvious that in order the motion time all over the way to be minimal it is necessary that every participant's motion speed is maximum. But the speed magnitude of the motion participant is spontaneously affected with other participant's negative interference. They as well strive to speed maximizing upon selecting motion variables. Stream growth brings to the reducing of the considered participant's motion speed that leading to increase of his time.

Let us consider the motion only along one arc, therefore miss out all indices in respect of the arc. Let's introduce following designations: L – network section length, T – motion time along the section, x – stream – quantity of cars having passed through the road section per time unit, ρ – stream density – quantity of cars per length unit at one lane, s – amount of lanes on the road, w – stream speed, λ – average section length per one car on one lane.

According to the definition density is $\rho = 1/\lambda$. Assume w – motion participant speed, w_{max} – speed. Time spent by the participant upon driving along the path of length λ equals to $\tau = \lambda/v$. Participants amount per time unit is $\kappa = 1/\tau$. Therefore $x = \kappa s = \frac{1}{\tau}s = \frac{v}{\lambda} = w\rho s$. Assume the stream speed and density are interconnected through linear dependence $w/w_{max} + \rho/\rho_{maa} = 1$. It is the known Grinshield's formula.

This implies that $w = w_{maa}(1 - \rho/\rho_{maa})$, or $\rho = \rho_{max}(1 - w/w_{maa})$. Let's substitute it into the stream formula and obtain $x = sw\rho_{max}(1 - w/w_{maa})$. Resulting function is the parabolic curve branched downward, maximum is achieved at $w = w_{\max}/2$ and accordingly at $x_{max} = s(w_{max}\rho_{max})/4$. Thus we obtained maximum magnitude of the stream which can be passed along the arc.

Let's substitute instead of ρ its value expression and we obtain $w^2 - w_{max}w + (w_{max}/(s\rho_{max}))x = 0$. From Vieta formula we get $w = w_{max}(1 + \sqrt{1 - x/x_{max}})/2$ with account of everyone's strive to minimize its speed. It follows from here that motion speed along network section is expressed by given dependence: $\tau(x) = 2\tau_{min}/(1 + \sqrt{1 - x/x_{max}})$, where τ_{min} – minimum motion speed along the section in case the stream thereupon equals to zero. Function graph is given for illustrative purposes of that function $\tau(x) = 1/(1 + \sqrt{1 - x})$ (in the Fig. 5).

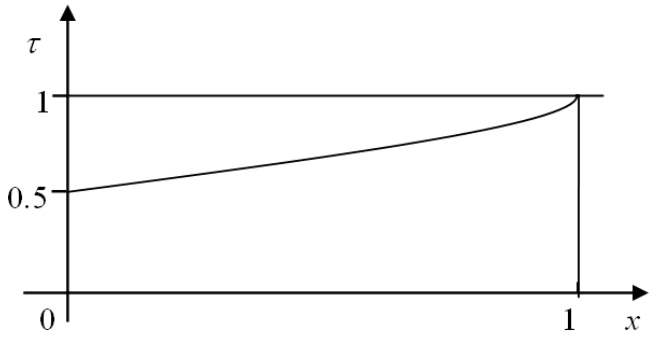

Fig. 5.

3 Layer concept, layer balance correlations and layer streams invariant transformation

3.1 Basic designations of graph theory used in the work

Assume $G = \langle E, V, H\rangle$ is an oriented graph, and V are end multiples, is function $H : V \to E \times E$. Let us name multiple components E the graph as nodes, multiple components of V as arcs. For each arc $v \in V$ the showing $H(v) = (h1(v), h2(v)), h1(v)$ the arc onset v, $h2(v)$ – the end. Let's denote $V^+(i) = \{v \in V/h2(v) = i\}$ – as arcs multiple entering the node i, $V^-(i) = \{v \in V/h1(v) = i\}$ – arcs multiple leaving the node i.

3.2 System decomposition – breakage of transport streams into layers

Assume i_0 is the top where the streams from other vertexes enter into. For instance, the enterprise employees where move in together, a big shop, cinema, etc., is in i_0. It is an exit from the building the evacuated subjects are directing to. If there are several exits let's introduce additional vertex.

Streams coming out from the vertex $i \in E$ and moving to the vertex $i_0 \in E$ denote as $q_i(i_0)$, for the vertex Total volume of the stream entering into i_0 will be $Q_{i_0} = \sum\limits_{i \in E} q_i(i_0)$. Let's denote $x_v(i_0)$ – stream along v moving to the vertex i_0. Total $S(i_0) = \langle G; i_0; q_i(i_0), i \in E; x_v(i_0), v \in V \rangle$ will be called the layer i_0. I.e., the circuit parts united into a single target to deliver the stream into the vertex i_0 enter into the layer. For every vertex $\sum\limits_{v \in V^+(i)} x_v(i_0) + q_i(i_0) = \sum\limits_{v \in V^-(i)} x_v(i_0)$ is true, flow volume along entering arcs of plus stream coming out from the vertex itself equals to flow volume moving along coming out arcs. Therefore

$$\sum_{v \in V^+(i)} x_v(i_0) - \sum_{v \in V^-(i)} x_v(i_0) = -q_i(i_0), \quad i \in E. \tag{1}$$

Following below is true for the vertex i_0 :

$$Q_{i_0} = \sum_{i \in E} q_i(i_0). \tag{2}$$

Correlation (1) is the First Kirchhoff law for the circuit. Let's denote the total stream $X_v = \sum\limits_{i_0 \in E} x_v(i_0)$ – the total stream flowing to the arc v. From (1) it follows

$$\sum_{v \in V^+(i)} X_v - \sum_{v \in V^-(i)} X_v = -\sum_{i_0 \in E} q_i(i_0), \quad i \in E. \tag{3}$$

Without restricting the generality let's assume that every vertex forms the layer, if for any vertex i_0 it does not exist, it means that $q_i(i_0) = 0$, $i \in E$. In the city traffic network (1), (2) are fulfilled for $i_0 \in E$. From equation (3) truth does not follow (1).

4 Single layer system study problem of evacuation

4.1 Search of initial permissible flows by means of maximum flow in the network

Balance algorithm idea is in searching initial permissible streams in the circuit with their subsequent transformation into the balance state. As every arc has restricted traffic capacity then we fulfill the existence of permissible streams with their search by means of maximum flow problem and solve with Ford-Fulkerson algorithm.

In the maximum flow problem the stream is allowed to pass from one initial vertex to another end vertex. All arcs have designed carrying capacity. To deduce the problem to this type let's add two fictitious peaks ii and kk. Let's connect ii to a stream source i_0. For it the carrying capacity equals to Q_{i_0}. Run-off from $q_i(i) > 0$ link via arcs with a vertex kk. For those arcs the carrying capacity equals to $q_i(i)$ accordingly. We obtain standard maximum flow problem, to solve it we apply any known algorithm. If it turns out that maximum flow is less than Q_{i_0}, one layer initial problem as well as the total problem accordingly have no solution. In that case minimal cut is beyond additional arcs.

If it has turned out that maximum flow equals to Q_{i_0} we obtain permissible flow which we transfer to balance state via invariant transformations.

4.2 Invariant transformation of layer streams

Let's consider a random cycle C. Let's pose a random sense of rotation coinciding with a certain arc in a cycle u. Let's construct generic function $sign_C^u(v)$:

$$sign_u(v) = \begin{cases} 0, \ \ if \ \ v \notin C \\ +1, \ \ v \in C, arc\ direction\ coincides\ with\ the\ cycle\ by\ pass\ direction, \\ -1, \ \ v \in C, arc\ direction\ is\ opposite\ to\ the\ cycle\ by\ pass\ direction, \end{cases}$$

Assume x_v, $v \in V$ satisfies correlation (1). Let's take a random number θ, for all $v \in V$, $\overline{x}_v = x_v + sign_C^u(v)\theta$, i.e. for cycles arcs the direction of which coincides with the one of rotation sense add θ to the magnitude of the stream x_v, for cycle arcs the direction of which is contrary to pass-by direction deduct xv. Then $\overline{x}_v$, $v \in V$ meets the correlation (1).

4.3 Second Kirchhoff law for a layer

Let's consider one layer of traffic flow from the source with a number i_0 into stream flow number j_0. Assume that at the motion the streams fall apart at vertex i and converge at vertex j. Assume some streams move the arcs which meet provision of First Kirchhoff law. There are minimum two ways of the stream to deliver from i to j, let's denote them $P1$ and $P2$. Assume that the time of motion $t1$ along the path 1 is more than the time of motion $t2$ along the path 2. Then a part of the stream switches to the path 2. There will be increase of the stream along the path 2 and accordingly the time along the path 2. Simultaneously the stream magnitude along the first path decreases and accordingly the motion time along it. Switching ends when congruence $t1 = t2$, or $t1 - t2 = 0$ is reached. In general terms, there shall be performed congruence $\sum\limits_{v \in V} sign_C^u(v)(\tau_v(x_v))$=0. In hydraulic circuit theory it is called as the Second Kirchhoff law. Its literary wording: In balance state the sum of the stream motion time change along the cycle equals to zero.

At random streams the equivalence does not work. Using invariant transformation of streams can be expressed as $NB_u(\theta)$=$sign_C^u(v)(\tau_v(x_v + sign_C^u(v)\theta))$=0. Cycle balancing problem is in the definition of θ, that $NB_u = 0$.

4.4 Framework construction, fundamental cycles system

It is known that if Kirchhoff law is applied to fundamental cycles system, it is performed at any cycle graph. Framework is a random tree, tops of which coincide with the ones of the assumed graph G, a framework example is given. Tree can be constructed by any algorithm, for instance, constructing the tree of the shortest paths with Dejkstra algorithm. Shortest paths mean the path lengths to the root. Arcs beyond the tree are chords. Chord and tree's arcs form a fundamental cycle $C(u)$ – a cycle, formed with a chord u. Let's set by-pass direction to every cycle coinciding with a chord. Function construction for the cycle $sign_u(v)$ is not complicated.

4.5 Limit calculation of argument function's variation

Let's break down $NB_u(\theta)$ into three parts: $NB_u(\theta) = NB_u^0(\theta) + NB_u^+(\theta) + NB_u^-(\theta)$. The first part $NB_u(\theta)$ consists of additive components with v, for which $sign_u(v) = 0$. The second part $NB_u^+(\theta)$ additive components with v, for which $sign_u(v) = 1$, the third part $NB_u^-(\theta)$ consists of additive components with v, for which $sign_u(v) = -1$.

1) It is evident that $NB_u^0(\theta) = 0$.

2) $NB_u^+(\theta) = \sum_{v\in V,\ sign_u(v)=1} \tau_v(x_v+\theta)$. As $\tau_v(x) > 0$ and ascendant per x (see Fig. 4), as $NB_u^+(\theta) > 0$ ascendant per θ. For all $v \in V$, $sign_u(v) = 1$ is performed as $0 \le (x_v + \theta) \le x_{max}$, or $-x_v \le \theta \le x_{max} - x_v$. Thus we obtain that

$$\theta = [\underline{\theta}^+, \overline{\theta}^+], \tag{4}$$

where $\underline{\theta}^+ = \max_{v\in V,\ sign_u(v)=1}(-x_v)$, $\overline{\theta}^+ = \min_{v\in V,\ sign_u(v)=1}(x_{max} - x_v)$.

3) In a similar way to 2 we obtain $NB_u^-(\theta)$ as an ascendant.

$$\theta = [\underline{\theta}^-, \overline{\theta}^-], \tag{5}$$

where $\underline{\theta}^- = \max_{v\in V,\ sign_u(v)=1}(x_{max} - x_v)$, $\overline{\theta}^- = \min_{v\in V,\ sign_u(v)=1} x_v$.

From considered cases 1)-3) and (4), (5) it proceeds that the function $NB_u(\theta)$ is ascendant and defined at the section $\theta \in [\underline{\theta}, \overline{\theta}]$, where $\underline{\theta} = \max(\underline{\theta}^-, \underline{\theta}^+)$, $\overline{\theta} = \min(\overline{\theta}^-, \overline{\theta}^+)$,

5 Searching algorithms of city transport system balance state

Given designs allow applying algorithms of consequent cycles balancing to search balance states of one layer. For example, we search the arc for which $NB_u(0) > \varepsilon$ (sufficiently small number), if there is no such an arc we stop the layer balancing and solve the task $NB_u(0) = 0$ for the problem and pass over to the algorithm execution over again. For multilayer systems the arc search is fulfilled along all layers and inside the layer accordingly.

Big experience in solving hydraulic circuits theory problems suggests that the offered approach is effective. For instance, city water system load flow problems, heat supply solution with a dimension about 1000 peaks and about 1500 arcs for 15 - 30 seconds at PCs give ground to assume that the load flow in road networks can be executed during appropriate time. Offered algorithms allow applying methods of parallelizing which bring wide prospects for using modern multiprocessor computer systems.

References

1. Kovalenko A.G., Khachaturov V.R., Raimzhanov Zh.D. Methodology of FES development on forming the utility system of urban territories // Proceedings of the 3rd international scientific-practical conference "Ecological safety of urban territories under conditions of sustainable development Astana. (2008).
2. Shvetsov V.I. Mathematical modeling of traffic streams // Automation and telemechanics. – No 11. (2003).
3. Smirnov N.N., Kisilyev A.B., Nikitin V. F., Yumashev M.V. Mathematical modeling of traffic streams // Mechanical-mathematical faculty of MSU. (1999).
4. Vasin A.A., Morozov V.V. Games theory and models of mathematical economics (study guide). – M.: MAKC Press, – 272 p. (2005).
5. Merenkov A.P., Hasilev V.Ya. Theory of hydraulic linkages. M., Nauka. 278 p. (1985).
6. Semyenov V.V. Mathematic modeling of megacities traffic streams dynamics (Mathematical modelling of transport streams dynamics of megacities. Preprint, Inst. Appl. Math., the Russian Academy of Science) IAM named after M.V.Keldysh RAS.
7. http://www.keldysh.ru/papers/2004/prep34/prep2004_34.html#tth_sEc4.

Geoinformation System on the Basis of Mathematical Model of the Microclimate of the Industrial City

M.N. Madiyarov[1], S. Sailarbek[2]

[1]East Kazakhstan State University named after S.Amanzholov,
Ust-Kamenogorsk, Kazakhstan
[2]East Kazakhstan State Technical University named after D.Serikbaev, Ust-Kamenogorsk, Kazakhstan
madiyarov_mur@mail.ru,ersal_7882@mail.ru

Abstract. In this paper we present an established Geoinformational System (GIS) based on mathematical models of the microclimate of the city, the transfer of impurities of pollutants in the atmosphere with the assimilation of measured data to assess the extent of air pollution in the industrial city, which is linked to the list of pollutants and monitoring data [1], [2]. Connection with the list of pollutants and monitoring data is provided by the database "Monitoring of air". Geoinformational system combines two object-oriented programs under Delphi 7.0. Programs automatically interact with a graphical editor "Surfer"allowing to build spread's isolines of concentrations of harmful substances in the atmosphere, as well as the cartographic analysis on the Mapinfo basis provided.
In order to solve the environmental problems of air protection, especially in industrial cities, there is a necessity of using GIS technology, with the help of which it could be possible to assess the impact of anthropogenic sources of pollution on air quality of the city, taking into account such factors as terrain, land-use category, differences in air temperature, atmospheric humidity and etc.

Keywords: Geoinformational System (GIS), atmosphere, pollution, database, mathematical model, the microclimate of the city, harmful substances, vehicular emissions

1 Introduction

The anthropogenic impact on the environment primarily affects the condition the air basin. Problems of the air basin's protection are a vast field of research at the intersection of science. The pollution of the surface layer of the atmosphere is the actual problem for today. The nature of the flow and dispersion of harmful substances and their compounds, which locally pollute the surface layer of air, is noticeably different from those phenomena in the free atmosphere. The solution of scientific and applied problems of environmental protection requires a detailed description of meteorological fields' structure and processes of harmful substances spreading into the air basin of the regions. Due to activities of large industrial enterprises in recent years, these problems are acute to humanity.

For Kazakhstan the urgency of this issue lies in the fact that with the rise of the economy more and more attention is paid to environmental protection and to introduction of new, environmentally friendly technologies in the workplace. Problem of air pollution is mainly in large industrial cities, where about a half the population of our Republic. 10 cities of Kazakhstan are considered to be the most polluted, 8 of which have a high level of air pollution.

In this regard, it is a great importance of the research of some patterns of spatial and temporal trends of meteorological aspects that affect air pollution in industrial cities. These studies provide an opportunity to carry out short-term air pollution forecasts and use them to regulate industrial and vehicle emissions. Without such studies it is impossible to identify the problem areas of cities and to make effective field observations in order to establish a system of control over the cleanliness of air. Characteristics of the atmospheric pollution now are mostly seen as meteorological variables. Therefore, the establishment of environmental air pollution

observation system and the analysis of the results are directly dependent on the conditions of distribution and transformation of contaminants in the atmosphere. It is necessary to define the basic principles of mutual businesses placements and residential areas, optimization of road junctions, planning new urban developments and maximum permissible emissions discovering.

The relevance of this work is determined by the need to process automation modeling air pollution in industrial centres, the creation of a geographic information system (GIS) to study the dynamics of contaminants in the air basin of a specific region, providing opportunities for computational experiments based on current information, and exploring different situations within the selected scenario.

It is known that the elements of GIS are computer network, database and mapping system of the real situation on the computer display. There have already been developed in the CIS geographic information systems to solve such problems, but they use only the methods for the calculation of emissions of harmful substances by OND-86 and to study the spread of harmful substances using the Gauss model torch, which does not describe the real condition of pollution, because it does not take into account the dynamics of microclimate change, characteristic of the studied area, vortex flow, topography. Therefore, the establishment of geographic information system on the basis of the mathematical 3D model of the microclimate of the city, especially the model adapted to the conditions of the industrial city located in the mountain area, is an urgent task. It should be noted that now there is practical interest of local forecasts, especially the possibility of increasing the concentration of harmful substances in the atmospheric boundary layer. Such an increase, which marked in a densely populated area of the industrial city, could be due to the adverse weather conditions for pollutants disperse, as well as the characteristics of building area and terrain. Therefore, the problem of air pollution must be solved depending on the meteorological factors. In times of increasing air pollution, it is necessary to apply the short-term measures to reduce emissions and their harmful effects.

At the present time a number of mathematical models based on the equations of turbulent diffusion is used for describing the scattering of impurities [29, 31]. Different types of models are used depending on the nature of the spatial scale and the processes of transfer and diffusion of pollutants. If the parameters of the model are constant (wind speed, diffusion coefficient, etc.) in the work [23] it is given the analytical solution of a system of equations in a one-dimensional and two-dimensional case, where the parameters a priori are unknown, and for their determination it is the need of applying parametric identification or other methods of measurement data processing [20, 28]. Due to the complexity of the equations describing the processes of air pollution, the focus is on methods for their numerical solution [19]. Sometimes, instead of the models presented by partial derivatives equations, regression models [18] based on experimental data processing research facility is used.

There is a many years' experience in the study of atmospheric pollution for today, held a series of field experiments to control the spread of impurities, received their basic patterns of transport and deposition[28, 31]. Conducting environmental activities put forward higher requirements for precision models for the calculation of the spread of pollutants in the atmosphere. Methods of calculating the impurities scattering is mainly suitable for the conditions of thermally homogeneous and smooth relief [28, 31]. However, a significant number of industrial facilities are located on the coasts of ponds or hilly areas. In such cases, the use of kinematic models, where the components of wind speed and other meteorological characteristics are defined, lead to large errors of scattering particles in the atmosphere. Therefore, it is quite clear the emerging interest in studying the migration process and dispersion of contaminants using hydrodynamic models describing physical processes in more detail [25].

From a physical and mathematical point of view the most difficult is to describe the transfer and diffusion to a distance of 200 km. This is due to the fact that the spectrum of atmospheric motions stored in the meso-scale range and depends essentially on orographic and thermal inhomogeneities of turbulence of the atmosphere, changes in the height of the inversion, etc. The work is devoted to this issue [21].

With the development of computer performance it is becoming possible to enter the physical factors into numerical models that bring them closer to the real atmosphere. It is first necessary to include an introduction to models the spatial and temporal changes in the atmosphere, detailed account of the processes in the boundary layer, the effect of radiation and turbulent transport and a number of other phenomena.

During the computational experiments for studying natural and anthropogenic factors it is required to formulate and solve numerically non-linear equations of the model of the microclimate, which should describe the evolution of the atmospheric processes in space with typical linear dimensions 50 x 50 km and over time, with periods of 1-3 days. In recent decades, mathematical modeling methods are increasingly beginning to be used to assess the effects of human impacts on the environment. It is obvious that success in solving the problems is largely dependent on the accepted basis for physical models and their mathematical formulations. These issues are adequately reflected in the works of G.I. Marchuk, V.V. Penenko, A.E. Aloyan, L.T.Matveev, R. PilвЂIke and others, where the models of local atmospheric processes are used for studying the various effects of natural and anthropogenic factors.

From a position of constructive realization of not hydrostatic model, taking into account the terrain can be divided into two groups. The first group of models use the Cartesian coordinate system, and to take into account conditions at the lower boundary - special methods for describing the interaction of air masses from the real surface topography [13]. In the second group of models the transform of coordinate system is used, in which the boundaries of the integration in the new coordinates match the coordinate surfaces.

Non-hydrostatic numerical models of the first group were built by K. Hirt, J. Kock and H. Orville, and the second group of numerical schemes is represented by models using the coordinate system conversion. Most preferred are the numerical scheme developed by T. Gal - Chen [18]. In these studies, it is given a numerical method for solving the equations of thermodynamics at the regular-type lower boundary of mountains. The advantage of the proposed in [5] schemes is that they are invariant in reference to the Cartesian and generalized coordinate systems. However, the appearance of new additional terms in the basic equations complicates its implementation.

At the present time to describe the dissipation of impurities uses a set of mathematical models based on the equations of turbulent diffusion [9, 10]. Different types of models are used depending on the nature of the spatial scale and the processes of transfer and diffusion of pollutants. If the parameters of the model are constant (wind speed, diffusion coefficient, etc.) in the work [23] it is given the analytical solution of a system of equations in a one-dimensional and two-dimensional case, where the parameters a priori are unknown, and for their determination it is the need of applying parametric identification or other methods of measurement data processing [19, 20]. Due to the complexity of the equations describing the processes of air pollution, the focus is on methods for their numerical solution. Sometimes, instead of the models presented by partial derivatives equations, regression models [18] based on experimental data processing research facility is used.

From a physical and mathematical point of view the most difficult is to describe the transfer and diffusion to a distance of 200 km. This is due to the fact that the spectrum of atmospheric motions stored in the meso-scale range and depends essentially on orographic and thermal

inhomogeneities of turbulence of the atmosphere, changes in the height of the inversion, etc. The work is devoted to this issue [25].

The works of many authors focus on climate modelling and the transfer and diffusion of contaminants harmful substances- Berlyand M.E., Marchuk, G.I., Penenko V.V., Aloyan A.E., Rao Shankar K., Seinfeld J.H., Kamenetz E.S., Tatarinov E.G., Ku J.Y. Rao Trivikramf S. There are the main results of these studies in the G.I. Marchuk's work, where the various models of transport and diffusion of substances, the basic equations describing these processes, identifying and solution properties are examined.

It was one of the first works executed by Arrago L.R. and Shvec M.E., which laid to the numerical solution of the equation of turbulent diffusion of heavy impurities. In the Berlyand's works and other for the study of atmospheric diffusion numerical methods have been applied. It has been subsequently developed a large number of models of atmospheric pollution, based both on the direct numerical solution of equations of conservation of momentum, heat and chemicals in the atmosphere (Marchuk G.I., Penenko V.V., Aloyan A.E., Zakarin E.A.) and in the approximate methods (Berlyand M,E., Danaev N.T., Abdibekov U. S., Bakirbaev B., Kamenetsky E.S., Tatarinov E.G.). The advantages and disadvantages of these models are revealed in their adaptation to the real terrain. The basis of the model describing mesometeorological processes and transport of harmful substances impuritiesis formed by equates of the atmospheric boundary layer. Atmospheric boundary layer equations are non-linear equations and their solution methods have common features with the equations of hydrodynamics. To address the multidimensional hydrodynamic equations in complex areas, Smagulov Sh.S., Zhumagulov B.T., Danaev N.T., Temirbekov N.M., Orunkhanov M.K., Kuttykozhaeva Sh.N. offered and mathematically substantiated new budget methods for solving corresponding differential equation.

For modelling the processes of air pollution of industrial regions and for solving regional environmental monitoring is the most effective to use geographic information systems. Works of Zakarin E.A., Muratova N.R and their students' are devoted to the creation of geographic information systems, basic research in computer graphics, expert systems and systems of digital cartography.The issues of digital cartography dedicated to the work of Kalabaeva N.B. This paper describes the creation of geographic information systems and digital mapping based on the creation of an automated cartographic and geodetic system.

This paper presents the results of research that have been conducted by the authors since 2003 till the next day.The aim of the project is to develop a mathematical model of the microclimate of major industrial cities of Kazakhstan; development of efficient numerical algorithms for solving climate model, because these equations are nonlinear and have no analytical solution; mathematical foundation created by the difference scheme; development of GIS for monitoring air pollution based on the model of the microclimate of the city.

As a result, the authors have created a new geographic information system, consisting of problem-oriented software packages, for modeling the spread of emissions of harmful substances from industrial plant, area sources and urban transport, with taking into account the influence of temperature and humidity of the air, water and the topography of the area containing the database and automatically interact with the graphical editor "Surfer"and geo-mapping system Mapinfo for constructing contours of concentrations of harmful substances and cartographic analysis of the numerical results. Also the opportunity of the graphical editor B«TecplotB» for getting scenarios of dynamics of air pollution is used.

2 Methodology

In the context of large industrial cities the level of contamination of surface air depends not only on the number of industrial and transport emissions, but also on the vertical and horizontal dispersion, which is mainly determined by meteorological factors. The weather conditions forecast conducive to the accumulation or dispersion of harmful impurities in the surface layer of air can become the basis of emissions regulation and ensure clean air.

The most important is the analysis of the synoptic conditions that determine the formation of high levels of air pollution, which represent a high risk to human health and the environment. First of all, they should include long periods with high levels of contamination. You need to select predictors, both as meteorological nature and technological, to create software for calculating scattering fields of main pollutants in the atmosphere of the city.

Evaluation of climate dispersion of pollutants in the atmosphere of the city of Ust-Kamenogorsk has allowed the following conclusions:

- to characterize the state of the atmosphere, which may occur at high concentrations of contaminants it stand out normal and abnormal weather conditions;
- under normal conditions, in the case of high-sources,it is unfavorable the existence of superadiabatic temperature gradient, when the result of the development of turbulent exchange takes place an intensive transfer of contaminants from the source to the surface, this may create their significant concentrations.

At the present time to describe the dissipation of impurities uses a set of mathematical models based on the equations of turbulent diffusion. Different types of models are used depending on the nature of the spatial scale and the processes of transfer and diffusion of pollutants [1, 2].

In this paper we present a geographic information system designed for the numerical simulation of pollutant dispersion from vehicles and industrial plants in the air. Consider the non-stationary spatial non-hydrostatic complete model of the city microclimate. The atmosphere is formally divided into two layers: the surface layer and the layer situated above. The initial system of equations can be written in the following form:

$$\frac{\partial u}{\partial t} + (\overrightarrow{u} \cdot \nabla)u = -\frac{\partial \pi}{\partial x} + lv + \frac{\partial}{\partial z}(\nu_u \frac{\partial u}{\partial z}) + \Delta u \tag{1}$$

$$\frac{\partial v}{\partial t} + (\overrightarrow{u} \cdot \nabla)v = -\frac{\partial \pi}{\partial y} - lu + \frac{\partial}{\partial z}(\nu_u \frac{\partial v}{\partial z}) + \Delta v, \tag{2}$$

$$\frac{\partial \omega}{\partial t} + (\overrightarrow{u} \cdot \nabla)\omega = -\frac{\partial \pi}{\partial x} - \lambda\theta + \frac{\partial}{\partial z}(\nu_\omega \frac{\partial \omega}{\partial x}) + \Delta\omega, \tag{3}$$

$$\frac{\partial \theta}{\partial t} + (\overrightarrow{u} \cdot \nabla)\theta + S\omega = -u(s\delta_x + \theta_x) - v(s\delta_y + \theta_y) + \frac{\partial}{\partial z}(\nu_\theta \frac{\partial \theta}{\partial z})\Delta\theta, \tag{4}$$

$$\frac{\partial u}{\partial x} + \frac{\partial v}{\partial y} + \frac{\partial \omega}{\partial z} = 0, \tag{5}$$

$$\frac{\partial \varphi}{\partial t} + di\nu\,\overrightarrow{u}\varphi + \delta\varphi = -\frac{\partial}{\partial x}\mu_1 \frac{\partial \varphi}{\partial x} - \frac{\partial}{\partial y}\mu_2 \frac{\partial \varphi}{\partial y} - \frac{\partial}{\partial z}\nu \frac{\partial \varphi}{\partial z} + f \tag{6}$$

at this point $\Delta = \frac{\partial}{\partial x}\mu_1 \frac{\partial}{\partial x} + \frac{\partial}{\partial y}\mu_2 \frac{\partial}{\partial y}$; $(\overrightarrow{u} \cdot \nabla)u = (u, v, \omega) \cdot (\frac{\partial u}{\partial x}, \frac{\partial u}{\partial y}, \frac{\partial u}{\partial z}) = u\frac{\partial u}{\partial x} + v\frac{\partial u}{\partial y} + \omega\frac{\partial u}{\partial z}$; $\overrightarrow{u}$ - wind speed's vector; λ, S - settings of convection and stratification; μ_1, μ_2 - horizontal

turbulence coefficients for momentum and quantity of heat; $\tilde{\theta}_x, \tilde{\theta}_y$ - horizontal gradients of potential background temperature, l - Coriolis parameter, $z = z_1 - \delta(x, y)$, z_1 - height above sea level, equation $z_1 = \delta(x, y)$ describes the relief, φ - number of impurities, falling from the atmosphere to the surface.

The system (1) to (6) for the city settled with the following boundary conditions:

$$u' = u^0,\ v' = v^0,\ \omega' = \omega^0,\ \varphi = \varphi^0\ at\ t = 0$$

$$u = f_1(y, z, t),\ v = f_2(y, z, t),\ \omega = 0,\ \frac{\partial\theta}{\partial x} = 0,\ at\ x = 0,\ 0 \le y \le Y,$$

$$\frac{\partial^2 u}{\partial x^2} = 0,\ \frac{\partial v}{\partial y} = -\frac{\partial u}{\partial x},\ \omega = 0,\ \frac{\partial\theta}{\partial x} = 0,\ at\ x = X,\ 0 \le y \le Y,$$

$$u = f_1(x, z, t),\ v = f_2(x, z, t),\ \omega = 0,\ \frac{\partial\theta}{\partial y} = 0,\ at\ y = 0,\ 0 \le x \le X, \tag{7}$$

$$\frac{\partial u}{\partial x} = -\frac{\partial v}{\partial y}0,\ \frac{\partial^2 v}{\partial y^2} = 0,\ \omega = 0,\ \frac{\partial\theta}{\partial y} = 0,\ at\ y = Y,\ 0 \le x \le X$$

$$u = 0,\ v = 0,\ \theta = 0,\ \omega = 0,\ \pi = 0,\ at\ z = H,$$

$$\omega = 0,\ h\frac{\partial u}{\partial z} = a_u u,\ h\frac{\partial v}{\partial z} = a_u v,\ h\frac{\partial\theta}{\partial z} = a_\theta(\theta - \theta_0),\ \varphi_0 = \frac{f_s + a_\theta\varphi_h v_h}{\beta + a_\theta v_h}\ at\ z = h,$$

at this point $a_u = \frac{\varphi_u(\xi_h)}{f_u(\xi_h\xi_0)}$, $a_\theta = \frac{\varphi_\theta(\xi_h)}{f_\theta(\xi_h\xi_0)}$; H - conventional atmospheric boundary layer height; X, Y - lateral boundaries.

Boundary conditions $u = f_1(y, z, t)$, $v = f_2(y, z, t)$ and conditions in the surface layer of the atmosphere model the physical meaning of these developments. And the remaining boundary conditions require perturbation smoothness and continuity equations performance in the neighborhood boundaries of integrated area.

The basis for the physical description of the surface layer of the atmosphere is Monin-Obukhov similarity theory [3] and the empirical features of the work [4].

Providing strong stability empirical functions are defined as linear [4]

$$\varphi_u(\xi) = (1 - 15\xi)^{-1/4}\ \varphi_\theta(\xi) = 0,74(1 - 9\xi)^{-1/2}$$

then

$$f_u(\xi, \xi_u) = ln\left|\frac{(\sqrt[4]{1 - 15\xi} - 1)(\sqrt[4]{1 - 15\xi_u} + 1)}{(\sqrt[4]{1 - 15\xi} + 1)(\sqrt[4]{1 - 15\xi_u} - 1)}\right| + arctg\sqrt[4]{1 - 15\xi} - arctg\sqrt[4]{1 - 15\xi_u},$$

$$f_\theta(\xi, \xi_0) = 0,74\left(ln\left|\frac{(\sqrt{1 - 9\xi} - 1)(\sqrt{1 - 9\xi_0} + 1)}{(\sqrt{1 - 9\xi} + 1)(\sqrt{1 - 9\xi_0} - 1)}\right|\right).$$

From the functions fiven above follows the boundary condition $z = h$.

A numerical algorithm for solving the system of equations (1) - (6) is developed, using the method of splitting into physical processes [5]. The difference of this method from the methods used in other studies is that at the first stage except advection, turbulent diffusion, the influence

of heat, moisture, and also taken into account the Coriolis force. In the second phase it is only the pressure force. The same as in the G.I Marchuk's work the transport equations along the trajectories of substance and turbulent exchange, the boundary condition for the complete problem are given. The system of equations is solved by the method of alternating directions. In the first stage of the method of splitting is an auxiliary field, which describes the characteristics of the eddy currents.

The transfer of Coriolis force from the second phase into the first yielded elliptic equation for determining the function π' , which does not contain mixed derivatives. To solve the aim of the second stage, taking into account the Coriolis force, as described by Marchuk G.I., on a differential level as well as on the subtractive, miscellaneous derivatives do not decrease, which complicates the equation for calculating the pressure.

The algorithm of numerical realization consists of the following three stages. In the first stage an advection-diffusion transport of substances is considered, taking into account the Coriolis force. In the second stage it is the harmonization of the coordination of mesometeorological fields. From the solution of these two phases the deviation of the background values of the components of the wind speed and temperature are determined. And in the third stage the equation of transport impurities harmful substances is solved. All required fields of meteorological and turbulent characteristics in the problem of transport and diffusion of impurities are determined from the solution of the previous stages.

The developed algorithm has been tested on the solution of the problem on a test of meso-meteorological processes that is developisng in the absence of background wind round the island without humidity processes in the atmosphere and in the soil [1, 2]. The results are fully consistent with the results obtained in [1, 2] works.

The new Geoinformational System (GIS) is established basing on mathematical models of the microclimate of the city, the transfer of impurities of pollutants in the atmosphere with the assimilation of measured data, in order to assess the extent of air pollution in the industrial city, which is linked to the list of pollutants and monitoring data. Connection with the list of pollutants and monitoring data is provided by the database "Local monitoring of air". Geographic Information System combines two object-oriented programs: B«Monitoring-EjectionsB» and B«Monitoring-DissipationB». Program automatically interacts with a graphical editor "SurferвЂ, allowing building spread's isolines of concentrations of harmful substances in the atmosphere, moreover the opportunity of cartographic analysis is provided. To ensure interactive models cooperation with user's graphical interface having integrated geographic information system based on Mapinfo the program "GEOEKOLOGY"in the design environment Delphi 7.0.is developed.

The software unit B«Monitoring-EjectionsB» - is designed for the collection, compilation, storing, processing information about the main sources of air pollution of industrial enterprises of the city, about the elements of the highway-road network (HRN) and the calculation of emissions of harmful substances by moving motor flux and the total concentration of harmful impurities in atmospheric air.

For the practical use of atmospheric dynamics models, transfer and diffusion of impurities in the air requires the creation of a special information database that contains information about the physical-geographical and climatic conditions of the studied objects, changes to the underlying surface of anthropogenic origin, as well as the parameters that define the sources of heat, moisture and contaminants impurities. The database"Environmental monitoring of air"was created. It consists of 4 main sections, which are interconnected between each other. The first section is vehicle ecology; the second section - industrial ecology; the third section - "a local air

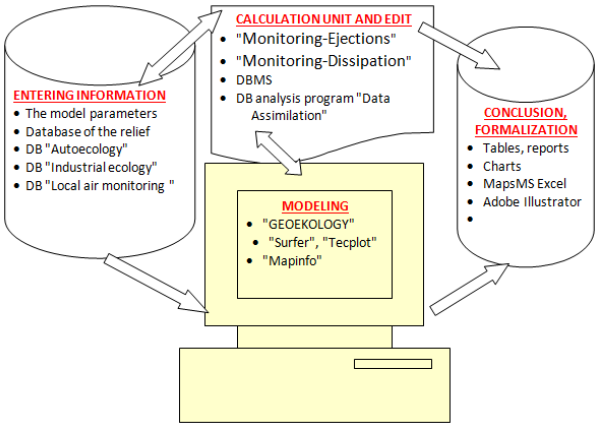

Fig. 1. GIS block-diagram

monitoring"stores time series of observations of meteorological data and air quality monitoring data; the fourth section - "land-use category and physical parameters".

The results of the "Monitoring-Dissipation block"are issued in the form of numerical values and stored in DAT-files, and for displaying in a graphical form of the numerical results use the Surfer program.

The program "Monitoring-Dissipation"during the work uses automated communication with the Surfer. The Surfer has a GS Scripter, which allows using the automation mechanism and to work with it through the application Delphi.

The program automatically creates a data file in the format XYZ grid file with the extension [.GRD], then creates a contour map of the grid [.GRD] of the[6] file.

3 Results

For the practical use of atmospheric dynamics models, transfer and diffusion of impurities in the air requires the creation of a special information database that contains information about the physical-geographical and climatic conditions of the studied objects, changes to the underlying surface of anthropogenic origin, as well as the parameters that define the sources of heat, moisture and contaminants impurities. To ensure interactive models cooperation with user's graphical interface having integrated geographic information system based on Mapinfo the program "GEOEKOLOGY"in the design environment Delphi 7.0.is developed and introduced into the GIS [3].

Picture 2 shows the main window where the menu of program management is.

As a result of the work of GIS above on our map there is a layer created by us, which is data visualization of air pollution of the city. At the picture 3 you can see the degree of contamination through its colouring corresponding to the area. The degree of contamination increases from light tones to darker ones.

With the help of the database "Category of land use and area relief"we can receive digital map of the area (Picture 4).

Numerical experiments were conducted using developed information technology, in which it was assumed that $\omega_g = 0$. As input parameters were used: $\beta = 0.0001$, $\mu_x = \mu_y = 320$ m2/s, $X = Y = 50000$ m, $\Delta x = \Delta y = 500$ m, $\Delta z = 2$ m, $\chi = 5$, $s = 6$ d/m, $z_u = 0.001$, $z_\theta = 0.00001$, $g = 9.8$ m/s2, $\bar{\beta} = 100$, $\delta = 0$.

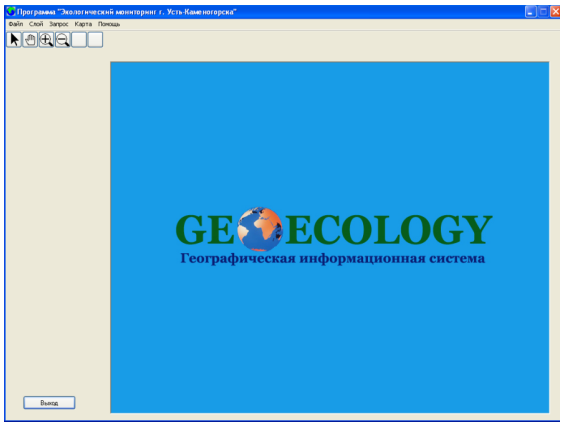

Fig. 2. The main window of the program

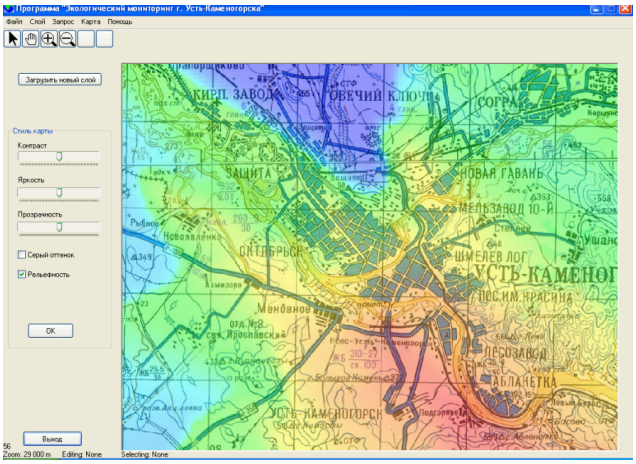

Fig. 3. Map with imposing layer of emissions

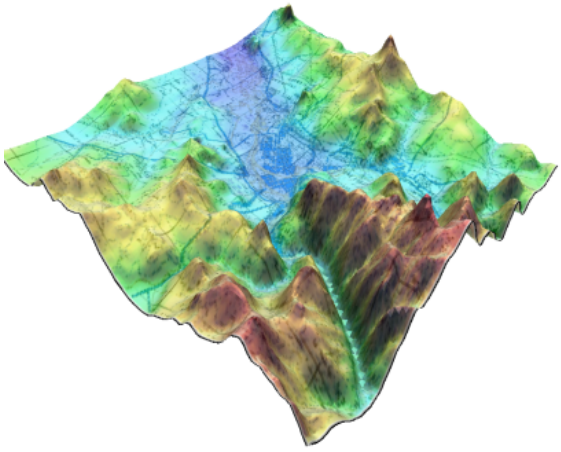

Fig. 4. Electronic map of the area

In carrying out numerical experiments for adversing weather conditions (wind speed - 1 m / s) on the third day with the southeast direction of the wind results showed the influence of the diurnal variation of the intensity of the TA, which subsides at night, resumes in the morning and reaches its maximum in the afternoon at peak hours.

Fig. 5. Air pollution in adverse weather conditions

References

1. Izrael Y.A. Changes in the global climate. The role of anthropogenic influences / Izrael Y.A. and [others] // Meteorology and Hydrology. - 2001. - p.– 5 .- P. 5-21.
2. Berlyand M.E. Modern problems of atmospheric diffusion and air pollution / Berlyand M.E. L.: Hydrometeo publishment, 1975. 448 p.
3. Berlyand M.E. Prediction and control of atmospheric pollution / Berlyand M.E. - L.: Hydrometeo publishment, 1985. - 272 p.
4. Landau L. D. Mechanics of continua / Landau L. D., E.M. Livshic. P: State technical publishment, 1953. - 273 p.
5. Kibel I.A. Introduction to hydrodynamic methods of short-term weather forecast / Kibel I.A. - M.: State technical publishment, 1957. - 357 p.
6. Gutman L.N. Introduction to the theory of nonlinear mesometeorological processes / Gutman L.N. - L. : Hydrometeo publishment, 1968. - 367 p.
7. Marchuk G.I. Mathematical modeling in the environmental problem / Marchuk G.I. .- M.: Science, 1982 .- 319 p.
8. Marchuk G.I. Clouds and climate / Marchuk G.I. and [others] .- L. : Hydrometeo publishment, 1986 .- 512 p.
9. Penenko V.V. Models and methods for problems of the environment / Penenko V.V., P●. Aloyan. Novosibirsk: Science, 1985. -254 p.
10. Penenko V.V. Numerical method of calculation of fields of meteorological elements of the boundary layer of the atmosphere // Penenko V.V. , P●. Aloyan // Meteorology and Hydrology.- 1976 .- p.– 6 .- P. 11-25.
11. Matveev L.T. Fundamentals of general meteorology. Atmospheric physics / Matveev L.T. - P>. : Hydrometeo publishment, 1980 .- 576 p.
12. Matveev L.T. Clouds' dynamics / Matveev L.T. - P>.: Hydrometeo publishment, 1981 .- 311 p.
13. Pielke R. A. Numerical Meteorological modeling / R. A. Pielke. New York: Academic press, 1984. - 211 p.
14. Smagulov Sh. S. The numerical solution of the Navier-Stokes equations for an incompressible fluid in channels with porous insert / Smagulov Sh. S., Danaev N.T., Temrbekov N.M. // Novosibirsk. -1995 . P. 36 .- p.– 5.
15. Smagulov Sh. S. Modeling of boundary conditions for the pressure and total head in problems of hydrodynamics using the method of fictitious domains / Smagulov Sh. S., Danaev N.T., Temrbekov N.M. // Reports of the Academy of Sciences of Russia. Moscow. - 2000. 374 .- p.– 5 . pp. 333-335
16. Smagulov Sh. Numerical methods of solution of Navier-Stokes equation in intricate regions / Sh. Smagulov and other // III international seminar of flame structure. - 18-20 September, 1990. - Alma-Ata. - P. 8-18.

17. Danaev N.T. About some numerical methods for solving the Navier-Stokes equations / Danaev N.T.and [others] // Numerical methods of continuum mechanics: Theses of reports Young Scientists School. Krasnoyarsk, 1989. вЂ“ P. 104-105.
18. Gal Chen T. On the use of a coordinate transformation for the solution of the Navier-Stokes equations / T. Gal Chen, C. J. Somerville // J. Comp. Phys .- 1985 .- V. 17 .- N 2 .- P. 209-228.
19. Zacharova I.M. Numerical simulation of the formation and development of radiation fog / Zacharova I.M. // .- Publ. 9 (52) .- 1975 .- P. 181-193.
20. Zacharova I.M. A mathematical model of the evolution of radiation fog / Zacharova I.M. // 1971. - publ. 23. - P. 157-175.
21. Orville H. D. Numerical simulation of the effects of cooling tower complexes on clouds and severe storms / H. D. Orville and other // J. Atmos. Environment. - 1981. - V. 15. - N 5. - P. 823-836.
22. Kogan E.L. Numerical simulation of clouds / Kogan E.L. and [others.] .- P. : Hydrometeo publishment, 1984 . 478 p.
23. Matveev L.T. On the theory of education and evaporation fog forecast / Matveev L.T., Soldatenko S.A. // Meteorology and Hydrology.- 1977 .- p.– 2 .- P. 24-31.
24. Aloyan A.E. The numerical experiment on the modeling of occurrence of fog and clouds in the atmospheric boundary layer / Aloyan A.E., Isayev G.I. // in book: Methods of mathematical modeling of the hydrodynamic problems of the environment. - Novosibirsk: Science, 1983. - P. 4-20.
25. Hiroyki O. Numerical calculation of three-dimensional model of land and Sea breezing in the case of constant eddy diffusitivs / O. Hiroyki, Tsutomu // Proc. 3. Pacif. Chem. Eng. Congz. - Seoul, May 8-11 .- 1989 .- V. 4 .- P. 401-406.
26. Yamada T. On the similarity functions A, B and C of the planetary boundary layer / T. Yamada // J. Atmos. Sci .- 1976 .- V. 33 .- N 5 .- P. 781-793.
27. Tapp M. C. A non вЂ“ Hydrostatic mesoscale model / M. C. Tapp, P. W. White // Quart Y. Roy. Meteorol. Soc. 1976 .- V. 102 .- p.– 432.
28. Carpenter K. M. An experimental forecast using an a non вЂ“ hydrostatic mesoscale model / K. M. Carpenter // Quart Y.Roy. Meteorol. Soc. .- 1976 .- V. 102 .- p.– 432.
29. Byzova N.L. Pollutant dispersion in the atmospheric boundary layer / Byzova N.L. - P>.: Hydrometeo publishment, 1989 .- 197 p.
30. Berlyand M.E. Modern problems of atmospheric diffusion and air pollution / Berlyand M.E. - L.: Hydrometeo publishment, 1975 .- 448 p.
31. Atmospheric turbulence and modeling of impurities' spread / under red. F.T.M. Neweast and H. Van Dope P>. : Hydrometeo publishment, 1985.- 350 p.
32. Yashimura T. Estimation of air pollutant concentration by the Galerkin finite element method / T.Yashimura, K. Nishina // Int. Y. Syst. Sci. 1983. - 14.–6 .- P. 661-672.
33. Yamada T. Numerical Simulation of valley Ventilation and pollutant transport / T.Yamada // Preprints to sevenths symposium on turbulence and diffusion. - Nov. 12-15. - Boulder Col. USA, 1995.

Численное исследование процесса разрядки природного газа из терморегулируемого слоя адсорбента

А.Б. Айтжан, Д.Т. Ыбыраймкул

Казахский национальный университет им. аль-Фараби, Алматы, Казахстан
aytzhan.aydyn@gmail.com,doskhan.ybyraiymkul@gmail.com

Аннотация. В данной статье решена задача численного моделирования терморегулируемого адсорбционного хранилища природного газа с учетом тепловых эффектов. В качестве математической модели процесса десорбции из слоя адсорбента взята система уравнений, состоящая из уравнений сохранения массы, сохранения энергии, кинетики адсорбции, закона Дарси, а так же уравнения Дубинина-Астахова. Вывод уравнений осуществлён пространственным осреднением основных уравнений. Решением взятой математической модели получены результаты численного решения, оказавшиеся близки к экспериментальным данным.

Ключевые слова: ANG, энергетика, хранение газа, десорбция.

1 Введение

Год за годом растет значимость природного газа в качестве основного источника топлива для автотранспорта, так как природный газ с экологической точки зрения является наиболее чистым видом топлива, по сравнению с традиционными видами, как бензин и дизель, к тому же природный газ является относительно недорогим видом источника энергии. Основным компонентом природного газ является метан ($CH_4, 95-96\%$), который имеет самую высокую удельную теплоту сгорания на единицу массы (55,2 МДж/кг) среди углеводородных источников энергии. Однако существуют проблемы в мобильном хранении природного газа связанные с безопасностью и оборудованием.

На сей день существуют три основных типа хранения газа. Наиболее распространенный способ хранения газа является, так называемый, сжатый природный газ (CNG – compressed natural gas). Давление в таком баллоне достигает 20 МПа. Хранение газа в сжатом состоянии ограничивается определенной формой баллона (цилиндр с закругленными краями) и определенных мер безопасности, в связи с большим давлением внутри. Чуть менее распространено хранение природного газа в сжиженном состоянии (LNG – liquefied natural gas). Данный тип хранения осуществляется в условиях умеренного давления, но при низких температурах, порядка 150 К, что так же является проблемой. Оба вышеописанных способа хранения природного газа опираются на дорогостоящее компрессионное или холодильное оборудование, что важно с экономической точки зрения. Хранение газа в адсорбированном состоянии (ANG – adsorbed natural gas) заключается в адсорбции газа в активированный уголь, являющимся наиболее безопасным способом кратковременного хранения, так как его функционирование происходит при небольшом давлении в 3.5 МПа и умеренной температуре в 300 К, однако в целях повышения эффективности такого хранилища, необходимо осуществлять терморегулирование. Определенно, для терморегулирования ANG хранилища необходимо определенное оборудование (термостат, датчики сбора данных и модули обработки информации), но, как оказалось, стоимость этого оборудования в цене уступает оборудованию для CNG и LNG. Это делает мобильное хранилище типа ANG более безопасным, и в то же время более экономичным. [1], [2]

Наряду с адсорбцией немаловажным является процесс десорбции. Так как речь идет о баллоне для оснащения газом автотранспорта, для соответствующего оснащения газом наиболее важным является скорость десорбции. Поэтому этой работе представлены результаты численного исследования кинетики десорбции метана из слоя адсорбента. В реализации численного решения рассматривается десорбция метана, так как природный газ на 95-96% состоит из метана.

2 Математическая модель

Для осуществления численного моделирования процесса кинетики десорбции из слоя адсорбента используются система уравнений, состоящая из уравнений сохранения массы, сохранения энергии, кинетики адсорбции, закона Дарси и уравнения Дубинина-Астахова.

2.1 Уравнение сохранения массы

Уравнение сохранения массы выведено при помощи пространственного осреднения с учетом притока газа:

$$\frac{\partial \rho_g}{\partial t} + \nabla \cdot (\rho_g \boldsymbol{u}_g) = S, \tag{1}$$

где S член определяющий приток массы газа десорбции:

$$S = -\frac{\rho_p}{\epsilon_b}\frac{\partial a}{\partial t}, \tag{2}$$

здесь плотность активированного угля определяется, как $\rho_p = \rho_s(1-\epsilon_t)$. В этом соотношении $\epsilon_t = \epsilon_b + (1-\epsilon_b)\epsilon_p$ — общая пористость, ρ_s — плотность скелета адсорбента, и a — величина адсорбции.

2.2 Уравнение движения

Для описания динамики течения газа используется закон Дарси:

$$\boldsymbol{u}_g = -\frac{K}{\mu_g}\nabla P, \tag{3}$$

где P– давление газа, μ_g – коэффициент динамической вязкости газа, K – коэффициент фильтрации слоя адсорбента.

2.3 Уравнение энергии

Результатом пространственного осреднения уравнения энергии является следующее уравнение:

$$(\epsilon_b \rho_g c_{p,g} + \rho_p c_{p,a} a + \rho_p c_{p,s})\frac{\partial T}{\partial t} + \epsilon_b \rho_g c_{p,g} \boldsymbol{u}_g \cdot \nabla T = -\nabla \cdot (k \nabla T) + \rho_p H_a ds \frac{\partial a}{\partial t}, \tag{4}$$

где $c_{p,g}$ – теплоемкость газа при постоянном давлении, $c_{p,a}$ – теплоемкость адсорбированного газа, $c_{p,s}$ – теплоемкость адсорбента, T – температура, $H_a ds$ – теплота адсорбции и $k = \epsilon_b k_g + (1-\epsilon_t)k_s$ – теплопроводность среды.

2.4 Уравнение кинетики сорбции и термодинамического состояния

Для описания кинетики адсорбции газа используется модель линейной движущей силы:

$$\frac{\partial a}{\partial t} = (a_e q - a) K_s exp(-\frac{E}{RT}), \tag{5}$$

где E – характеристическая энергия адсорбционной системы, $a_e q$ – равновесная величина адсорбции, R – газовая постоянная, K_s – эффективный коэффициент переноса массы.

Равновесная величина адсорбции определяется моделью Дубинина-Астахова

$$a_e q = \frac{W_0}{\nu_a} exp\left\{ - \left[\frac{RT}{E} ln\left(\frac{P_{cr}}{P} \left(\frac{T}{T_{cr}} \right)^2 \right) \right]^n \right\} \tag{6}$$

ν_a – удельный объем адсорбированного газа (метана), W_0 – максимальная величина адсорбции, и n – структурный параметр гетерогенности пористой среды. Для рассматриваемого адсорбента $n = 1$

Теплота адсорбции определяется равенством:

$$H_a ds = E \left[\left(ln\frac{W_0}{a\nu_a} \right)^{\frac{1}{n}} + \frac{\alpha T}{n} \left(ln\frac{W_0}{a\nu_a} \right)^{\frac{1-n}{n}} \right] + 2RT, \tag{7}$$

К этим уравнениям добавляется уравнение состояния идеального газа для задания плотности свободного газа:

$$P = \rho_g \frac{R}{M} T, \tag{8}$$

где M — молярная масса газа.

3 Постановка задачи

3.1 Описание ANG баллона

Конструкция реального баллона представляет собой стальной цилиндр, внутри которого находится прямоугольный канал из трубчато-пластинчатых теплообменников, целью которого является терморегулирование слоя адсорбента, находящегося между прямоугольными пластинами толщиной. Толщина пластины 0.1 мм, высота и ширина канала 112 мм, при расстоянии между пластинами 8.3 мм. Внешний и внутренний диаметры трубки 6 и 5 мм соответственно.В качестве адсорбента был взят активированный уголь порошкового типа Maxsorb III. Согласно геометрическим характеристикам слоя адсорбента, расставляются следующие начальные условия:

$$\begin{aligned} &\boldsymbol{u}_{g0} = 0 \left[\tfrac{m}{s} \right], \\ &P_0 = 3.5 \left[MPa \right], \\ &T_0 = 297 \left[K \right], \\ &a_0 = 0.23 \left[\tfrac{kg}{kg} \right], \end{aligned} \tag{9}$$

и краевые условия:

$$\begin{aligned} &\boldsymbol{u}_{g\Gamma} = 3.10 \cdot 10^{-5} \left[\tfrac{m}{s} \right], \\ &T_0 = 297 \left[K \right], \end{aligned} \tag{10}$$

для скорости и температуры трубки теплообменника соответственно.

Здесь, в целях упрощения, взята скорость выхода газа из слоя адсорбента, на самом же деле необходимо задавать отток газа массовым расходом.

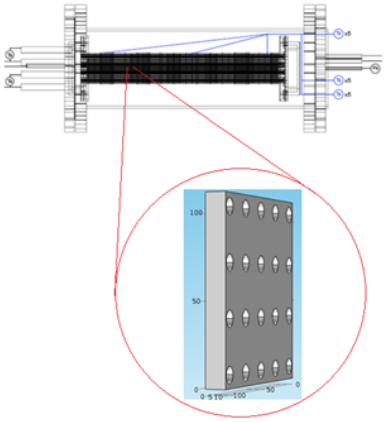

Рис. 1. Схема баллона для хранения адсорбированного газа.

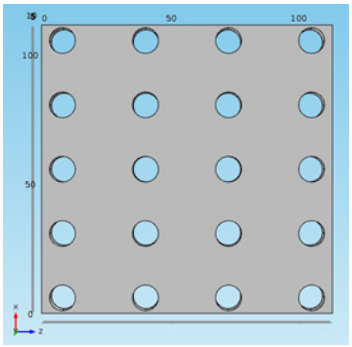

Рис. 2. Слой адсорбента.

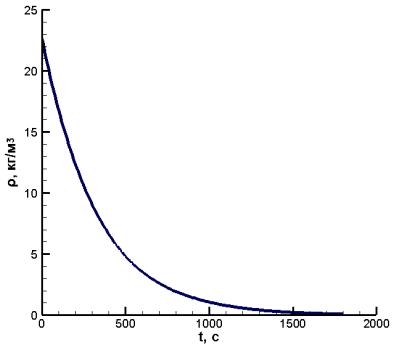

Рис. 3. Кривая изменения средней плотности свободного газа в слое адсорбента.

4 Результаты численного решения

Согласно сформулированной уравнениями (1) – (8) с начальными (9) и граничными (10) задаче произведено численное моделирование процесса десорбции метана при помощи пакета МКЭ-анализа Comsol Multiphysics.

Численное решение охватывает отрезок времени десорбции метана в течение 30 минут. За это промежуток времени манометрическое давление упало с 3.5 MPa до 13.7 kPa, плотность свободного газа упала с 22.66 до 0.1 $\frac{kg}{m^3}$, и величина адсорбции снизилась 0.23 до отметки 0.02 $\frac{kg}{kg}$.

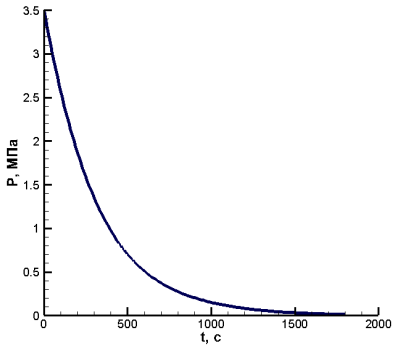

Рис. 4. Кривая изменения среднего давления в слое адсорбента.

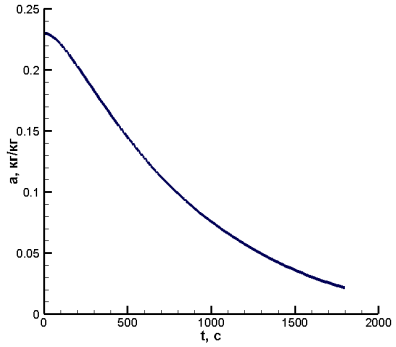

Рис. 5. Кривая изменения средней величины адсорбции в слое адсорбента.

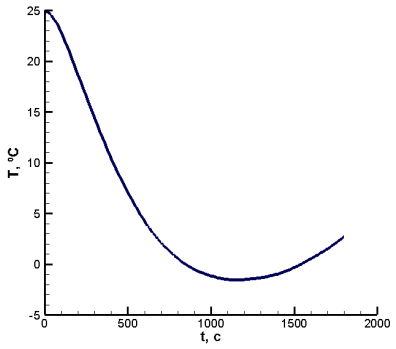

Рис. 6. Кривая изменения среднего значения температуры в слое адсорбента.

Весьма немонотонно ведет себя кривая температуры Рис. 6. Это можно объяснить тем, что первые 20 минут процесс десорбции гази проходит интенсивно, высвобождаясь от твердого скелета, температура падает из-за того что внутренняя энергия преобразуется. Этот процесс можно сравнить с процессом испарения, когда от поверхности отрываются частицы и при этом температура на поверхности падает. Начиная с 20 минуты интенсивность десорбции уменьшается, и поэтому влияние трубчатых теплообменников увеличивается, следовательно, температура в слое адсорбента повышается.

5 Заключение

Произведено численное моделирование процесса десорбции метана из слоя адсорбента терморегулируемого баллона типа ANG. Результаты численного решения показали ожидаемые результаты. Для сравнения, температура ведет себя немонотонно и во время эксперимента [3]. Использованная математическая модель оказалась адекватной к практическому применению.

Список литературы

1. Wegrzyn J, Gurevich M. Adsorbed storage of natural gas. // Appl Energy. 1996. – № 55(2). – P. 71-83.
2. Linares-Solano A. Adsorbed natural gas storage for alternative motor fuels. // materials from international conference of the 6th framework programme. –Warsaw, Poland, 2002.
3. Kazi A.F., Wai S.L., Kim C.N., Experimental investigations of adsorbed natural gas storage system with enhanced thermal management // International Journal of Modern Physics: Conference Series. 2012. – Vol 19. – P. 190-195.
4. Васильев Л. Л., Канончик Л. Е. Исследование теплообмена в баллоне с водородом, сорбентом и тепловой трубой // Матер. междунар. науч. форума. "VI Minsk International Heat and Mass Transfer Forum MIF 2008". – Минск: Дайк-Пресс, 2008.

О влиянии состава защитных газов на поведение электрической дуги и сварочной ванны

Жайнаков А., Султангазиева Р., Аманкулова Н.

Кыргызский Государственный Технический Университет
пр. Манаса, 66, Бишкек, Кыргызстан
{jainakov47,renasultangazieva,namankulova}@mail.ru

Аннотация. *Данная статья представляет собой численное исследование магнитогидродинамических процессов в электрической дуге и сварочной ванне при различном составе защитных газов, влияние состава защитной атмосферы на проплавление и формирование сварного шва. Рассчитаны коэффициенты переноса для сухого атмосферного воздуха с различными процентными содержаниями кислорода, азота, углекислого газа, паров воды, аргона при высоких температурах. С полученными коэффициентами переноса рассчитана система МГД уравнений в переменных "вихрь-функция тока". Проведен численный анализ результатов.*

Ключевые слова: Электрическая дуга, МГД уравнения, сварочная ванна, защитный газ, эффект Марангони, вихрь-функция тока

1 Введение

Электродуговая сварка в среде защитных газов один из наиболее распространенных видов сварки плавлением, используемый в индустрии. По сравнению с другими способами сварка в защитных газах обладает рядом преимуществ: высокое качество сварных соединений на разнообразных металлах и сплавах различной толщины; возможность сварки в различных пространственных положениях; возможность визуального наблюдения за образованием шва, высокая производительность, низкая стоимость при использовании активных защитных газов. При этом способе сварки в зону дуги подается защитный газ, струя которого, обтекая электрическую дугу и сварочную ванну, предохраняет расплавленный металл от воздействия атмосферного воздуха, окисления и азотирования. Вид защитного газа существенно влияет на качественные и экономические аспекты сварочного процесса. Правильно подобранные газовые смеси позволяют оптимально использовать положительные воздействия компонентов газовых смесей и таким образом существенно снизить влияние отрицательных последствий. Стандарт EN ISO 439 "Защитные газы для дуговой сварки и резки"учитывает и рассматривает различные возможные виды смесей, количество и виды их применения которых постоянно растет. Новый стандарт EN ISO 14175 "Применяемые в сварке материалы. Газы и газовые смеси для сварки плавлением и родственных процессов "более детально рассматривает многокомпонентные смеси в качестве защитных газов, которые в последние годы пришли на смену однокомпонентному газу -двуокиси углерода и аргона, и которые получают все большее распространение.Широкий диапазон используемых защитных газов и их смесей, обладающих значительно различающимися теплофизическими свойствами, обусловливает большие технологические возможности данного способа сварки. Сварка в смеси газов положительно сказывается на технологических свойствах сварочной дуги, повышает стабильность ее горения, происходит снижение размеров брызг и уменьшение потерь на разбрызгивание, уменьшается выпуклость шва. Качество сварных соединений в значительной мере зависит от содержания растворенных в металле, так называемых, вредных газов - водорода, азота и их соединений. Поэтому защитные газовые

смеси должны иметь в своем составе строго ограниченное количество вредных примесей. В промышленности широко применяются смеси с использованием Ar, CO_2 и O_2. Однако в настоящее время недостаточно изучено влияние состава защитной атмосферы на проплавление и формирование сварного шва, а также на плавление и перенос электродного металла. При сварке с газовой защитой зона сварки окружается защитным газом, подаваемым под небольшим давлением из сопла, концентрично расположенного к электроду. В качестве защитной среды служат инертные и активные газы и их смеси. В этом случае, доля теплоты, выделяемая за счет химических реакций в общем балансе теплоты незначительна. К активным газам, прежде всего, относят все кислородосодержащие газы, не только в атмосфере воздуха, но и выделяющиеся с нагретых элементов конструкции плазматрона в процессе его работы. Известно, что в состав сухого атмосферного воздуха входят O_2 (20 масс. %), N_2 (75 мас.%), CO_2 (0.046 мас.%) и др. Также могут находиться пары H_2O(1 мас.%).Воздушная плазма является самой экономичной, высоко энергетической и доступной, хотя образующиеся нитриды и озон значительно ухудшают санитарно-гигиенические условия труда. Также активно применяется воздух для плазменной резки металлов, так что фразой "воздушно плазменная сварка"сегодня все чаще подменяют термин воздушно плазменной резки посредством глубокого проплавления в зоне резания металла. При этом, расплавленный металл струей сжатого воздуха при этом непрерывно удаляется из полости рабочего среза.

1.1 Постановка задачи

На рисунке 1 приведена схема расчетной области.

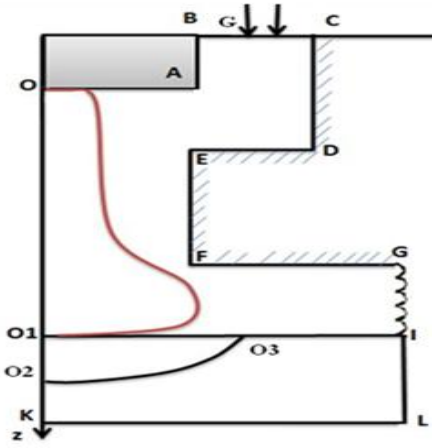

Рис. 1. Схема расчетной области

В модельной системе были сделаны следующие допущения:сварочная дуга и сварочная ванна обладают осевой симметрией, плазменная дуга находится в состоянии локального термодинамического равновесия, газ и расплавленный металл несжимаемы, течения ламинарные, поверхность сварочной ванны плоская. В объеме сварочной ванны рассматриваются четыре различные движущие силы - электромагнитная сила, поверхностное натяжение, вызванные температурными градиентами на поверхности сварочной ванны и, возможно, сила сопротивления газа, вызванная струей падающей плазмы, выталкивающая сила вызванная градиентом температуры в сварочной ванне. Таким образом, физические процессы в столбе

электродугового разряда и взаимодействующего с этим разрядом жидкого металла описываются одной и той же системой уравнений магнитной гидродинамики. Указанная система уравнений объединяет уравнение неразрывности,движения, энергии, уравнения Максвелла и закон Ома [1]:

$$div\left(\rho \boldsymbol{V}\right) = 0 \tag{1}$$

$$\rho\left(\boldsymbol{V}grad\right)\boldsymbol{V} = \rho\boldsymbol{g} + \boldsymbol{E}div\boldsymbol{D} + \boldsymbol{j}\times\boldsymbol{B} - grad\left(P + \frac{2}{3}\mu div\boldsymbol{V}\right) - 2div\left(\mu\dot{S}\right) \tag{2}$$

$$\rho\boldsymbol{V}grad\left(h + \frac{1}{2}V^2\right) = \boldsymbol{j}\boldsymbol{E} - \Psi + \boldsymbol{V}gradP + div\left(2\mu\dot{S} - \frac{2}{3}\mu div\boldsymbol{V} + \frac{\lambda}{c_p}gradh\right) \tag{3}$$

$$rot\boldsymbol{E} = 0 \;\; rot\boldsymbol{H} = 0 \;\; div\boldsymbol{B} = 0 \;\; \boldsymbol{E} + \boldsymbol{V}\times\boldsymbol{B} = \frac{\boldsymbol{j}}{\sigma} \tag{4}$$

В уравнение энергии для сварочной ванны добавляется слагаемое, которое может быть выражено как:

$$f_L = \begin{cases} 1 & T > T_l \\ \frac{T-T_s}{T_l-T_s} & T_s < T < T_l \\ 0 & T < T_s \end{cases} \tag{5}$$

T_s- температуры твердой фазы, T_l - до температуры жидкой фазы металла анода. С помощью программного пакета АСТРА и ТЕРРА рассчитан равновесный состав термодинамических функций и коэффициентов переноса многокомпонентной смеси сухого воздуха следующего состава O_2 (21 масс. %), N_2 (78 мас.%), CO_2 (0.07 мас.%),O_2 (0.93 мас.%): плотность $\rho = \rho(P,T)$, электропроводность $\sigma = \sigma(P,T)$,теплопроводность $\lambda = \lambda(P,T)$,вязкость $\mu = \mu(P,T)$,теплоемкость $C_p = C_p(P,T)$,энтальпия $h = h(P,T)$,излучение $\Psi = \Psi(P,T)$. Учитывается удельная теплота плавления. Исходная система МГД уравнений решается в переменных "вихрь-функция тока" ω - напряженность вихря, ψ- функция тока, χ - функция электрического тока, которые в случае цилиндрической системы координат и осевой симметрии определяются соотношениями:

$$\omega = \frac{1}{r}\left(\frac{\partial v}{\partial z} - \frac{\partial u}{dr}\right) \tag{6}$$

$$\frac{\partial\psi}{\partial r} = \rho ur \quad -\frac{\partial\psi}{\partial z} = \rho vr \tag{7}$$

$$\frac{\partial\chi}{\partial r} = rj_z \quad -\frac{\partial\chi}{\partial z} = rj_r \tag{8}$$

Для решения полученной системы дифференциальных уравнений необходимо задать граничные условия для данных функций по всему контуру, охватывающему расчетную область.

1.2 Граничные условия

Катод представляет собой цилиндр с плоским торцом, канал плазматрона - полый цилиндр с внутренним радиусом R_c, анодом служит обрабатываемое изделие. Между боковыми стенками катода и внутренними стенками сопла в аксиальном направлении подается поток газа. Распределение скорости в начальном сечении Z=0 определяется из уравнения движения изотермического газа, имеющий следующий вид в цилиндрических координатах:

$$\frac{dP}{dz} = \frac{1}{r}\frac{d}{dr}\left(r\mu\frac{du}{dr}\right) \tag{9}$$

Для определения значения градиента давления, используем интегральное условие сохранения расхода газа:

$$G = \int_{R_k}^{R_c} \rho u r dr$$

С учетом условий прилипания на боковых стенках катода и внутренней стенке сопла $u(R_c, 0) = 0$,$u(R_k) = 0$ запишем выражение для распределения скорости в нулевом сечении:

$$u(r,0) = \frac{2G\left(\frac{R_c^2-R_k^2}{\ln\frac{R_C}{R_k}}\ln\frac{R_C}{r} - R_C^2 + r^2\right)}{\pi\rho\left(R_c^2 - R_k^2\right)\left(\frac{R_c^2-R_k^2}{\ln\frac{R_C}{R_k}} - R_c^2 - R_k^2\right)} \tag{10}$$

Граничные условия по всей расчетной области:

BC:

$$\omega = -\frac{1}{r}\frac{\partial u(r,0)}{\partial r}, \quad \psi = \rho\int_{R_k}^{r} u(r,0) r dr, \quad h = h_0, \quad \chi = \frac{I}{2\pi}$$

BA:

$$\frac{\partial\psi}{\partial r} = 0, \quad \psi = 0, \quad h = h_0, \quad \chi = \frac{I}{2\pi}$$

CD,EF:

$$\frac{\partial\psi}{\partial r} = 0, \quad \psi = \frac{G}{2\pi}, \quad h = h_0, \quad \chi = \frac{I}{2\pi}$$

OA:

$$\frac{\partial\psi}{\partial z} = 0, \quad \psi = 0, \quad h = h_k, \quad \chi_k = \frac{I\int_0^r \sigma r dr}{2\pi\int_0^{R_k}\sigma r dr}$$

ED,FG:

$$\frac{\partial\psi}{\partial z} = 0, \quad \psi = \frac{G}{2\pi}, \quad h = h_0, \quad \chi = \frac{I}{2\pi}$$

GI:

$$\frac{\partial\omega}{\partial r} = 0, \quad \frac{\partial\psi}{\partial r} = 0, \quad \frac{\partial h}{\partial r} = 0, \quad \chi = \frac{I}{2\pi}$$

OK:

$$\frac{\partial\omega}{\partial r} = 0, \quad \psi = 0, \quad \frac{\partial h}{\partial r} = 0, \quad \chi = 0$$

O1O3:

$$\mu_p\omega_p = \mu_a\omega_a - \frac{1}{r}\frac{\partial\alpha}{\partial T}\frac{\partial T}{\partial r}, \qquad \psi = 0$$

$$\lambda_a\frac{\partial T_a}{\partial z} = \lambda_p\frac{\partial T_p}{\partial z} - \sigma_\varepsilon\varepsilon\left(T_a^4 - T_0^4\right) - W_v h_{fg} - j\varphi_a, \qquad \frac{\partial\chi_p}{\partial z} = \frac{\partial\chi_a}{\partial z}$$

Тепловые потери с поверхности сварочной ванны включают конвективные потери, радиационные потери и потери на испарение, T_0 - температура окружающей среды, σ_ε- коэффициент Стефана-Больцмана, ε - излучательная способность вещества, h_fg - удельная теплота испарения,W_v- скорость испарения, которая находится из следующего приближения:

$$\log W_v = A_v + \log P_{atm} - 0,5\log T$$

A_v - постоянная, зависящая от материала обрабатываемого изделия. Обоснование граничных условий для напряженности вихря представлено в работе [2]-[3]

2 Обсуждение результатов

Для изучения влияния свойств защитных газов на процесс электродуговой сварки рассчитаны коэффициенты для состава сухого воздуха. Как известно, термодинамические и транспортные свойства плазмы зависят от состава плазмы. Для однократно ионизированных атомов состав плазм определяется уравнением Саха, законом Дальтона и условиями квазинейтральности плазмы. На рис. 2- 4 представлены графики теплофизических коэффициентов для аргона [1] и расчетные коэффициенты для воздуха. Сложная форма кривой теплопроводности для воздуха (рис. 3а) объясняется тем, что полная теплопроводность плазмы является суммой теплопроводностей компонентов плазмы и диффузной теплопроводности, обусловленной переносом энергии диссоциации и ионизации в процессах диффузии составляющих плазмы из зоны высоких температур в низкотемпературную область, в которой происходит их ассоциации и рекомбинация.Ход кривой теплоемкости Ср (рис. 4а) отмечен пиками, соответствующими затратам энергии вначале на диссоциацию, на однократную и двукратную ионизацию компонентов.

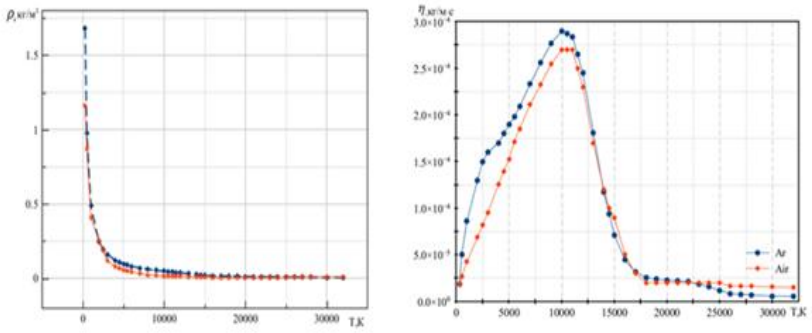

Рис. 2. Плотность (а) и вязкость (б)защитного газа

На рис. 5 показаны линии равных расходов газа в столбе электрической дуги. Газ подходит к столбу электрической дуги по каналу плазматрона в свободную область, где радиально растекается у поверхности анода, увлекая за собой потоки расплавленного металла сварочной ванны. Пристеночное течение газа у анода приводит к подсосу газа со стороны

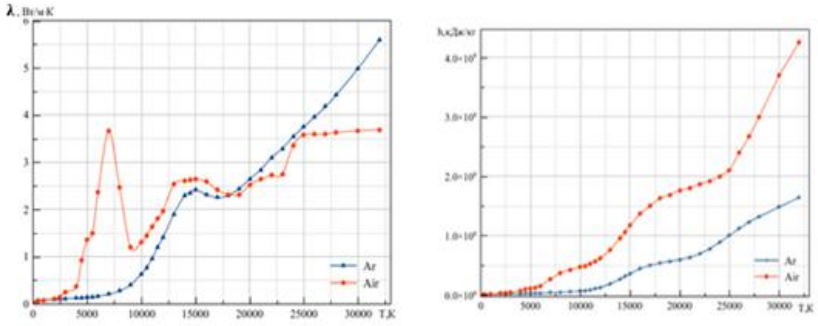

Рис. 3. Теплопроводность (а) и энтальпия (б) защитного газа

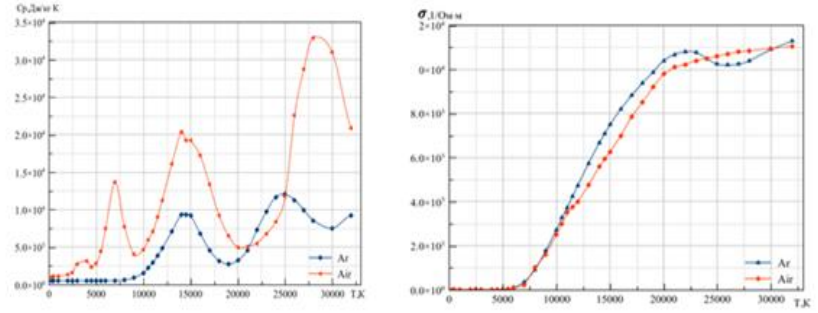

Рис. 4. Теплопроводность (а) и эектропроводность (б) защитного газа

свободной границы в результате действия сил вязкости и возникновению обратного течения у противоположной аноду стенки. Таким образом, в свободной области образуется тороидальный вихрь с застойной зоной по центру. Как показывают численные эксперименты, форма и размеры данного вихря зависят от величины расхода газа, геометрии и размеров плазматрона. Дуга в воздухе более сжата, меньшие поперечные размеры дуги обуславливают большое тепловое и силовое воздействие на обрабатываемое изделие. Замена аргона на воздух способствует повышению эффективности дуги, что связано с тем, что теплоемкость воздуха выше теплоемкости по отношению к Аг, и это, следовательно, должно привести к более высокой интенсивности тепловых потоков в расплаве металла.

На рис. 6 представлен характер течения потоков расплавленного металла сварочной ванны при силе тока в 150А. Как показано в работе [4] при малых силах тока вклад выталкивающей силы и силы Лоренца в конвекционную картину сварочной ванны незначительны. В объеме сварочной ванны расплавленный металл движется в одном направлении по часовой стрелке. Основными силами, обуславливающими потоки жидкости, являются силы поверхностного натяжения Марангони и силы вязкого взаимодействия с потоками плазмы. Градиент поверхностного натяжения является отрицательным, а конвективные течения на поверхности сварочной ванны центробежными. Силы вязкого взаимодействия также вовлекают потоки сварочной ванны в направлении от центра ванны к краям. Действие электромагнитных сил при данном токе пока не оказывает видимого влияния на картину в сварочной ванне.Выталкивающая сила Архимеда вносит несущественный вклад на фоне вышеуказанных сил. С увеличением силы тока до 200А в центральной части сварочной ванны образуется вихрь (рис. 7), движение которого обусловлено возросшей ролью электромагнитных сил, которые прокачивают потоки жидкого металла в вглубь ванны, образуя на

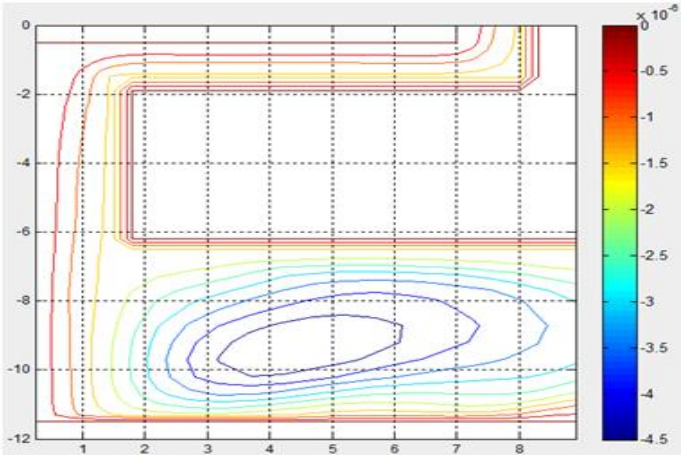

Рис. 5. Линии равных расходов газа, I=150A,G=10мг/сек

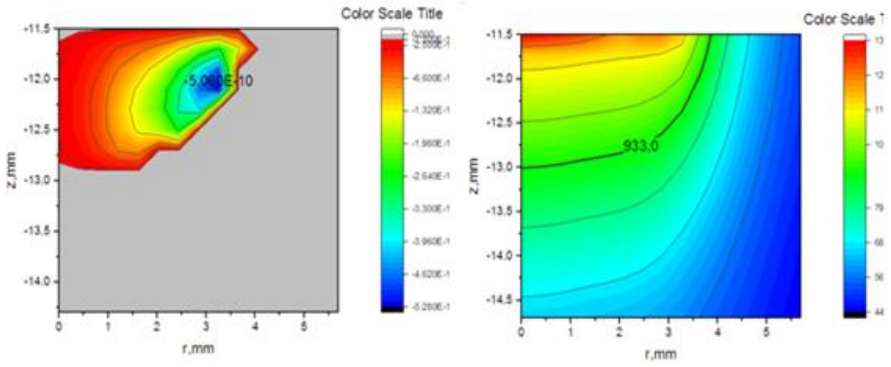

Рис. 6. Изолинии функции тока в сварочной ванне, I=150A

поверхности ванны конвективные потоки к центру ванны. У краев ванны сохраняется движение потоков расплавленного металла к краям, обусловленного вязким взаимодействием с потоками электрической дуги и термокапиллярной конвекцией. Таким образом, изменение характера и структуры гидродинамических потоков в сварочной ванне определяется в зависимости от направления силы Марангони,а также повышения роли лоренцевых сил при формировании течения расплавленного металла. При увеличении тока до 250A действие сил поверхностного натяжения увеличивается в сравнении с силой Лоренца и в объеме сварочной ванны вновь образуется только один вихрь, направленный на поверхности от центра ванны к краям, увеличивая радиальные размеры проплавленной области, а глубина проплавления практически не меняется. Дальнейшее увеличение силы тока до 300A также не влияет практически на глубину сварочной ванны, лишь увеличивается ее ширина из-за преобладания силы Марангони и сил вязкого трения. Параметры сварочной ванны при различных силах тока, расходе защитного газа G=100мг/сек для аргона и сухого воздуха показаны в таблице 1. По численным результатам видно, что проплавляющая способность дуги при использовании аргона в качестве защитного газа намного меньше, чем в случае, когда в роли защитного газа используется сухой воздух. Средний температурный градиент по сварочной ванне определяется как $T_a = \frac{T_{\max} - T_s}{R}$, где T_max-максимальная температура, R- радиус сварочной ванны. Температурный градиент и скорость кристаллизации являются важными параметрами при формировании сварочной ванны, влияющие на морфологию и

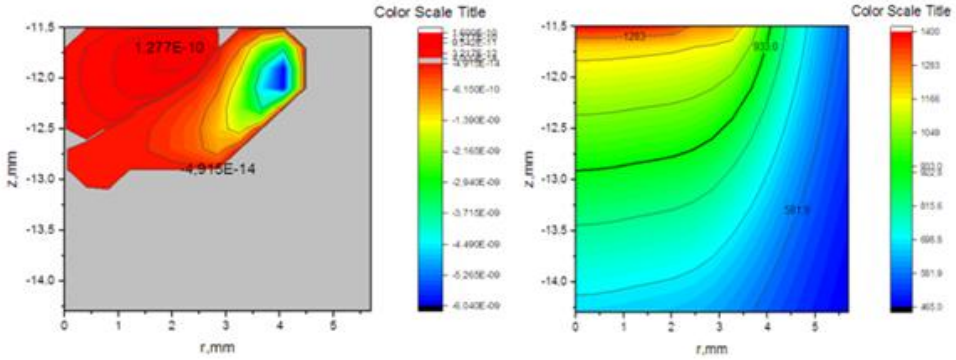

Рис. 7. Изолинии расхода и изотермы в сварочной ванне, I=200A

Таблица 1. Зависимость параметров сварочной ванны от рода защитного газа.

I, A	Сухой воздух		Аргон	
	Rv (мм)	Hv (мм)	Rv (мм)	Hv (мм)
I=150A	3,4	1,2	2,0	0,7
I=200A	3,5	1,4	2,3	0,9
I=250A	3,9	1,45	2,8	1,0

структуру кристаллизации сварочного шва. Когда отношение этих значений $\frac{T_{\max}}{R}$ увеличивается, шов меняется с равноосно-древовидного на ячеисто- древовидную форму и затем на ячеисто- зернистую форму. Таким образом, контроллируя данные параметры, а также варируя условия охлаждения, можно в некоторой степени влиять на процессы кристаллизации для достижения качественного сварного шва.

Список литературы

1. Под редакцией В.С.Энгельшта *Математическое моделирование электрической дуги*, Фрунзе: Илим,364 с. (1983).
2. Jainakov A., Usenkanov J., Sultangazieva R. *On joint modeling of processes in electrica arc plasma and melted metal*, 6 general assembly of federation of engineering institutions of Islamic countries,Almaty. (1999).
3. Жайнаков А.Ж., Султангазиева Р.Т., Усенканов Дж.О. *О влиянии термокапиллярной конвекции на параметры расплавленного электрической дугой металла*, Доклады 3 традиционной казахстанско-российской научно-практической конференции "Математическое моделирование научно-технологических и экологических проблем в нефтегазодобывающей промышленности Алматы (2000).
4. A.Moarrefzadeh, M.A.Sadeghi *Numerical simulation of copper temperature field in Gas Tungsten Arc Welding (GTAW) process*, Conference on robotics, control and manufacturing technology ISSN: 1790-5117-p.26.(2010).

Об асимптотики решений задачи теплопроводности с источником и нелинейным граничным условием

М.М. Арипов, З.Р. Рахмонов

Национальный Университет Узбекистана, Ташкент, Узбекистан
mirsaidaripov@mail.ru,zraxmonov@inbox.ru

Аннотация. Получено асимптотическое представление решения с компактным носителем задачи теплопроводности с несколькими нелинейностями, позволившее провести численный эксперимент. Установлены асимптотические поведения решения с комактным носителем. Решена важная проблема выбора подходящего начального приближения для построение итерационного процесса при численном изучение задачи теплопроводности, за счет установления качественных свойств решений.

Ключевые слова: асимптотика, критическая экспонента, режим с обострением, численный анализ.

1 Введение

Рассмотрим следующее параболическое уравнение

$$\frac{\partial u}{\partial t} = \frac{\partial}{\partial x}\left(\left|\frac{\partial u}{\partial x}\right|^{p-2}\frac{\partial u}{\partial x}\right) + u^{\beta}, \quad (x,t) \in R_+ \times (0,\ +\infty), \tag{1}$$

с нелинейным граничным потоком и начальным условием

$$-\left|\frac{\partial u}{\partial x}\right|^{p-2}\frac{\partial u}{\partial x}\ (0,t) = u^{q}(0,t), \quad t > 0, \tag{2}$$

$$u(x,0) = u_0(x) \geq 0, \quad x \in R_+, \tag{3}$$

где $p > 2$, β, $q > 0$, $u_0(x)$ - ограниченная, непрерывная, неотрицательная функция.

Уравнения (1) встречается в различных областях естествознание [3]. В частности, его можно рассматривать как модель распространение тепла с нелинейным коэффициентом теплопроводности зависящей от градиента, встречающей в химической реакции [1, 3]. Кроме того, уравнения (1) возникает при математическом моделировании диффузии в нелинейных средах, при исследование проблем течения жидкостей через пористые пласты, в задачах динамики биологических популяций, политропической фильтрации, образования структур в синергетике и в ряде других областях [2, 3].

Хорошо известно, что вследствие вырождения уравнения (1) при $u = 0$ может не имеет классического решения. Поэтому ее решение естественно понимать в обобщенном смысле из класса $0 \leq u, \left|\frac{\partial u}{\partial x}\right|^{p-2}\frac{\partial u}{\partial x} \in (R_+ \times (0,+\infty))$ и удовлетворящее уравнению (1) в интегральном смысле.

Исследованию различных качественных свойств решений задачи (1)-(3) для частных значений числовых параметров посвящено большое количество работ (см. [5-15] и приведенные ссылки там). Условия существования или несуществования глобального по времени решения задачи Коши для уравнения (1) были изучены в работах [5] и получены условие глобальной разрешимости:

$$\beta > 2p - 1$$

при достаточно малом $u_0(x)$. Доказано, что если $1 < \beta < 2p-1$, то любое нетривиальное решение взрывается за конечное время.

Значение $\beta_c = 2p-1$ принято называть критической экспоненты типа Фужита [4]. Многие аналогичные результаты были установлены для различных нелинейных уравнений параболического типа.

В работах [6], было впервые для задачи (1)-(3) в случае без источника установлено, что решение задачи (1)-(3) становятся неограниченными за конечное время, если $2\left(p-1\right)/p < q < 2\left(p-1\right)$. И были доказаны следующие утверждения:

– Решения задачи (1)-(3) является глобальным, если $0 < q \leq 2\left(p-1\right)/p$;

– Пусть $q > 2\left(p-1\right)$ и $u_0\left(x\right)$ достаточно мала, тогда решения задачи (1)-(3) является глобальным.

Свойств неограниченности решение для следующей модели реакции-диффузии с нелокальними нелинейностями

$$u_t = \Delta u^m + u^\beta, \quad (x,t) \in \Omega \times (0,T),$$

$$\frac{\partial u}{\partial \eta} = u^q, \quad (x,t) \in \partial\Omega \times (0,T)$$

$$u\left(x,0\right) = u_0\left(x\right), \quad x \in \Omega,$$

где $\Omega \in R^N$, были изучены в [7, 8].

В работе [10] изучено условие существование неограниченных и глобальных решений на основе построения нижних и верхних автомодельных решений. Показаны, что решение задачи является(1)-(3) неограниченным, если выполняется одно из следующих условий

1. $1 < \beta \leq 2\left(p-1\right)+1$, $2\left(p-1\right)/p < q < 2\left(p-1\right)$;
2. $\beta > 1$, $q > 2\left(p-1\right)/p$;
3. $\beta > 2\left(p-1\right)+1$, $q > 2\left(p-1\right)$;

Авторы работ [11] изучали задачу (1)-(3) для многомерного случая без источника. Ими получены критическая экспонента глобального существования решения

$$q_0 = 2(p-1)/p$$

и критическая экспонента типа Фужита

$$q_c = \left(1+1/N\right)\left(p-1\right)$$

с помощью построения нижних и верхних решений.

В работе авторов [12] исследованы задачи Коши для (1) и были получены главный член асимптотики автомодельных решений.

Целью данной работы является получение главного члена асимптотики автомодельных решений на основе метода эталонных уравнений [2], которая играет важную роль при исследовании качественных свойств изучаемых процессов. При критических значениях числовых параметров установлена асимптотика решений вблизи свободной границы. Предлагается способ выбора подходящего начального приближения для итерационного процесса при численных исследованиях решение рассматриваемой задачи (1)-(3).

2 Асимптотика решений автомодельных задач

Асимптотика автомодльных решений рассматриваемой задачи понимается в следующем смысле:

будем, говорит, что $\Phi_2(\eta)$ является асимптотикой функции $\Phi_1(\eta)$, если

$\lim\limits_{\eta\to\infty}\frac{\Phi_1(\eta)}{\Phi_2(\eta)}=1$ при $\Phi_2(\eta)\neq 0$ и $\lim\limits_{\eta\to\infty}\Phi_1(\eta)=0$ при $\Phi_2(\eta)=0$.

1. Случае $\beta\leq 1, q>2(p-1)$. Рассмотрим следующего автомодельного решения задачи (1)-(3)

$$u_1(x,t)=t^{\alpha}\varphi(\xi),\ \xi=xt^{-\gamma}, \tag{4}$$

где $\alpha=\frac{1}{1-\beta}$,$\gamma=\frac{p-1-\beta}{p(1-\beta)}$.

С помощью хорошо известного принципа сравнения решений можно показать, что $u_1(x,t)$ будет нижним решением задачи (1)-(3). Для этого функция $\varphi(\xi)$ должна удовлетворят следующей краевой задаче:

$$\frac{d}{d\xi}\left(\left|\frac{d\varphi}{d\xi}\right|^{p-2}\frac{d\varphi}{d\xi}\right)+\gamma\xi\frac{d\varphi}{d\xi}-\alpha\varphi+\varphi^{\beta}=0, \tag{5}$$

$$-\left|\frac{d\varphi}{d\xi}\right|^{p-2}\frac{d\varphi}{d\xi}\Bigg|_{\xi=0}=0. \tag{6}$$

Рассмотрим функцию

$$\bar{\varphi}(\xi)=\left(a-\frac{p-2}{p}\gamma^{\frac{1}{p-1}}\xi^{\frac{p}{p-1}}\right)_{+}^{\frac{p-1}{p-2}} \tag{7}$$

где $a>0$, $(y)_{+}=\max(0,y)$, которое строится на основе метода эталонных уравнений [2].

Покажем, что функция (7) будет асимптотикой решений задачи (5), (6).

Теорема 1. Решение задачи (5), (6) с компактным носителем при $\xi\to\left(\frac{ap}{(p-2)\gamma^{1/(p-1)}}\right)^{(p-1)/p}$ имеет асимптотикое представление

$$\varphi(\xi)\simeq\bar{\varphi}(\xi)(1+o(1))$$

Доказательство. Будем искать решение уравнения (5) в следующем виде

$$\varphi=\bar{\varphi}(\xi)w(\tau), \tag{8}$$

где $\tau=-\ln\left(a-b\xi^{\frac{p}{p-1}}\right)$, $b=\frac{p-2}{p}\gamma^{1/(p-1)}$, при этом $\tau\to+\infty$ при $\xi\to\left(\frac{ap}{(p-2)\gamma^{1/(p-1)}}\right)^{(p-1)/p}$, что позволяет исследовать асимптотическую устойчивость решения задачи (5), (6) при $\tau\to+\infty$.

Подставляя (8) в уравнение (5) с учетом (7) оно примет вид

$$\frac{d}{d\tau}(Lw)^{p-1}+\left(k_1\phi_1(\tau)-\frac{p-1}{p-2}\right)(Lw)^{p-1}+k_2Lw-k_3w\phi_1(\tau)-k_4w^{\beta}\phi_2(\tau)=0, \tag{9}$$

здесь и далее

$Lw=\frac{w}{p-2}-\frac{w'}{p-1}$, $\phi_1(\tau)=e^{-\tau}/(a-e^{-\tau})$, $\phi_2(\tau)=\frac{e^{-[(\beta+1)(p-1)-p]\tau/(p-2)}}{(a-e^{-\tau})^{p-2}}$, $k_1=\frac{p-1}{bp}$, $k_2=\frac{\gamma(p-1)}{(bp)^{p-1}}$, $k_3=\frac{\alpha(p-1)}{b^{p-1}p^p}$, $k_4=\frac{p-1}{(bp)^p}$.

Отметим, что изучение решений последнего уравнения является равносильным изучению тех решений уравнения (1), каждое из которых в некотором промежутке $[\tau_0, +\infty)$ удовлетворяет неравенствам:

$$w(\tau) > 0, \frac{w(\tau)}{p-2} - \frac{w'(\tau)}{p-1} \neq 0.$$

Проверим, что решение $w(\tau)$ уравнения (9) имеет конечный предел w_0 или нет при $\eta \to +\infty$. Пусть

$$\nu(\tau) = (Lw)^{p-1}.$$

Тогда для производной функции $\nu(\tau)$ имеем

$$v' = -\left(k_1\phi_1(\tau) - \frac{p-1}{p-2}\right)v - k_2L_1w + k_3w\phi_1(\tau) + k_4w^q\phi_2(\tau).$$

Для анализа решений последнего уравнения введем вспомготельную функцию

$$\theta(\tau,\mu) = -\left(k_1\phi_1(\tau) - \frac{p-1}{p-2}\right)\mu - k_2L_1w + k_3w\phi_1(\tau) + k_4w^q\phi_2(\tau) \tag{10}$$

где μ - вещественное число. Отсюда нетрудно видеть, что при каждом значении μ функция $\theta(\tau,\mu)$ сохраняет знак на некотором промежутке $[\tau_1, +\infty) \subset [\tau_0, +\infty)$ и при всех $\tau \in [\tau_1, +\infty)$ выполняется одно из неравенств

$$\nu'(\tau) > 0, \nu'(\tau) < 0.$$

Тогда анализируя (10) с учетом теоремы Боля [2] заключаем, что для функции $\nu(\tau)$ существует предел при $\tau \in [\tau_1, +\infty)$.

Произведем теперь предельный переход. Очевидно, что при $\xi \to (a/b)_-^{(p-1)/p}$

$$\lim_{\tau\to+\infty}\phi_1(\tau) \to 0, \lim_{\tau\to+\infty}\phi_2(\eta) \to 0,$$

Тогда с учетом последнего лимита и $w' = 0$ из (9) для w получим следующее алгебраическое уравнение

$$(p-1)\left(\frac{w}{p-2}\right)^{p-1} - k_2w = 0,$$

решения, которого является $w = 1$. Тогда в силу (8) $\varphi(\xi) \simeq \bar{\varphi}(\xi)$. Теорема доказана.

2. Случае $\beta > 2p-1$, $q < \frac{2(p-1)}{p}$. В этом случае автомодельное решение уравнения (1) ищется в виде

$$u_2(x,t) = t^\alpha\varphi(\xi),\ \xi = xt^{-\gamma},$$

где $\alpha = \frac{p-1}{2(p-1)-pq}$, $\gamma = \frac{p-1-q}{2(p-1)-pq}$. Известно [11], что решения задачи (1)-(3) при $\beta > 2p-1$, $q < \frac{2(p-1)}{p}$ является неограниченным. Согласно принципу сравнения решений для того, чтобы функция $u_2(x,t)$ была верхним решением, она должна удовлетворят следующему неравенству

$$\frac{\partial u_2}{\partial t} \le \frac{\partial}{\partial x}\left(\left|\frac{\partial u_2}{\partial x}\right|^{p-2}\frac{\partial u_2}{\partial x}\right), \qquad (x,t) \in R_+ \times R_+,$$

$$-\left|\frac{\partial u_2}{\partial x}\right|^{p-2}\frac{\partial u_2}{\partial x}\ (0,t) \le u_2^q, \quad t > 0.$$

Тогда, с учетом конкретного вида функции $u_2(x,t)$ для последних неравенств получим

$$\frac{d}{d\xi}\left(\left|\frac{d\varphi}{d\xi}\right|^{p-2}\frac{d\varphi}{d\xi}\right)+\gamma\xi\frac{d\varphi}{d\xi}-\alpha\varphi\geq 0 \tag{11}$$

$$-\left|\frac{d\varphi}{d\xi}\right|^{p-2}\frac{d\varphi}{d\xi}\Bigg|_{\xi=0}\leq\varphi^q(0). \tag{12}$$

Рассмотрим теперь следующую функцию

$$\bar{\varphi}(\xi)=K(a-\xi)_+^{\frac{p-1}{p-2}}.$$

где $K>0$, $a>0$, $(y)_+=\max(0,y)$. Имеет места

Теорема 2. Решение задачи (11), (12) с компактным носителем при $\xi\to a$ имеет асимптотикое представление

$$\varphi(\xi)\simeq C\bar{\varphi}(\xi),$$

где $C=\left(\frac{p-2}{p-1}a\gamma\right)^{1/(p-2)}\frac{p-2}{K(p-1)}$.

Теорема 2 доказывается аналогично доказательству теоремы 1.

3. Случае $pq<(p-1)(\beta+1)$, $q>2(p-1)$. Уравнения (1) допускает автомодельное решение вида

$$u_3(x,t)=(T+t)^{-\alpha}f(\xi),\ \xi=x(T+t)^{-\gamma},$$

где $\alpha=\frac{p-1}{qp-2(p-1)}$, $\gamma=\frac{q-(p-1)}{qp-2(p-1)}$. В этом случае решение задачи является глобальным, если $u_0(x)$ достаточно мало [11]. Поэтому, $u_3(x,t)$ будет верхним решением задачи (1)-(3), если

$$\frac{d}{d\xi}\left(\left|\frac{df}{d\xi}\right|^{p-2}\frac{df}{d\xi}\right)+\gamma\xi\frac{df}{d\xi}+(\alpha+\delta)f\leq 0 \tag{13}$$

$$-\left|\frac{df}{d\xi}\right|^{p-2}\frac{df}{d\xi}\Bigg|_{\xi=0}\geq f^q(0) \tag{14}$$

где $\delta=\frac{1}{2(p-1)}-\alpha$.

Рассмотрим функцию

$$\bar{f}(\xi)=\left(a-d(\xi+h)^{\frac{p}{p-1}}\right)_+^{\frac{p-1}{p-2}}$$

где $d=\frac{p-2}{p}\gamma^{\frac{1}{p-1}}$, $h>0$.

Теорема 3. Решение задачи (13), (14) с компактным носителем при $\xi\to(a/d)^{(p-1)/p}-h$ имеет асимптотикое представление

$$f(\xi)\simeq\bar{f}(\xi),$$

Теорема 3 доказывается аналогично доказательству теоремы 1.

Критический случай $pq=2(p-1)$. Этот случай является аналогичном продолжением 2-случая, когда $pq=2(p-1)$. В этом случае решение задачи (1)-(3) ищется в следующем экспоненциальном виде

$$u_4(x,t)=e^{\alpha(t-\tau)}\varphi(\xi),\ \xi=xe^{-\gamma(t-\tau)},$$

где $\alpha = \frac{p}{2p-1}$,$\gamma = \frac{p-2}{2p-1}$,

Для того , чтобы функция $u_4(x,t) = e^{\alpha(t-\tau)}\varphi(\xi)$, была нижным решением функция $\varphi(\xi)$ должна удовлетворять неравенствам.

$$\frac{d}{d\xi}\left(\left|\frac{d\varphi}{d\xi}\right|^{p-2}\frac{d\varphi}{d\xi}\right) + \gamma\xi\frac{d\varphi}{d\xi} - \alpha\varphi \geq 0 \tag{15}$$

$$-\left|\frac{d\varphi}{d\xi}\right|^{p-2}\frac{d\varphi}{d\xi}\Bigg|_{\xi=0} \leq \varphi^q(0). \tag{16}$$

Рассмотрим следующую функцию

$$\bar{\varphi}(\xi) = D\left(D^{m-1}\left(\frac{m}{m-1}\right)^{m+1} - \xi\right)_+^{\frac{p-1}{p-2}}.$$

Теорема 4. Решение задачи (15), (16) с компактным носителем при $\xi \to D^{m-1}\left(\frac{m}{m-1}\right)^{m+1}$ имеет асимптотику

$$\varphi(\xi) \simeq C\bar{\varphi}(\xi)(1 + o(1)),$$

где $C = \left(\frac{p-1}{p-2}\gamma\right)^{1/(p-2)}$.

Теорема 4 доказывается аналогично доказательству теоремы 1.

3 Численный анализ решений

При численном решение задачи (1)-(3) применяется итерационный процесс в котором основную роль играет выбор начального приближения в зависимости от значение числовых параметров и начального условия. Для численного решения задачи (1)-(3) уравнение (1) аппроксимировалось со вторым порядком точности по пространственным координатам и с первым порядком по t. При этом во внутренних шагах итерации значений узлов вычисляются методом прогонки. Хорошо известно, что итерационные методы требует наличия хорошего начального приближения, которое приведет к быстрой сходимости к искомому решению и сохраняет качественные свойства изучаемых нелинейных процессов, что является основной трудностью при численном решение задачи. Эта трудность в зависимости от значения числовых параметров уравнения преодолевается путем удачного выбора начальных приближений, в качестве которого при вычислениях брались выше установленные асимптотические формулы. На основе выше приведенных результатов были произведены численые расчеты. Ниже приведем некоторые результаты численных экспериментов.

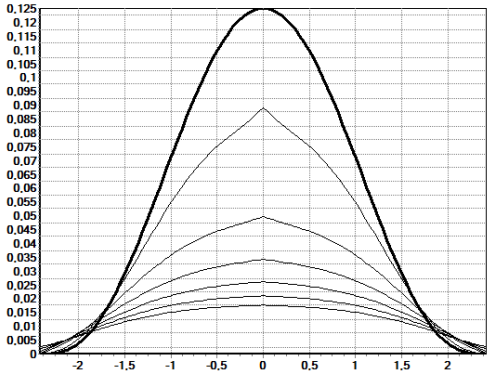

Рис 1. $p = 2.5$, $\beta = 2$, $q = 2.85$.

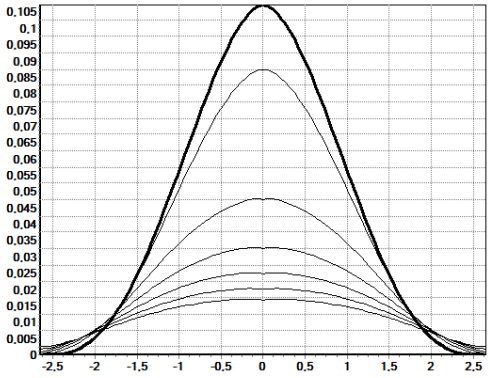

Рис 2. $p = 2.45$, $\beta = 2$, $q = 4$.

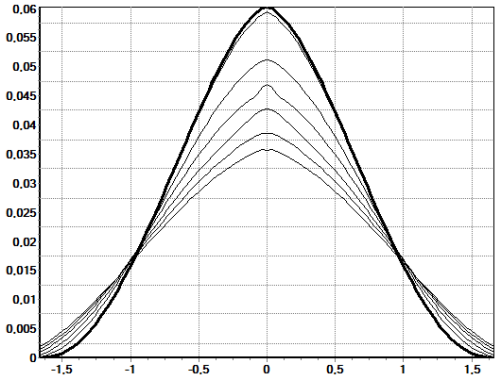

Рис 3. $p = 2.75$, $\beta = 2.5$, $q = 3.5$.

Результаты численных экспериментов показывают быструю сходимость итерационного процесса за счет удачного выбора предложенного нами начального приближения, сохраняя при этом свойсвто конечной скорости распространение возмущения.

Список литературы

1. Самарский А. А., Курдюмов С. П., Галактионов В. А., Михайлов А. П. Режимы с обострением для квазилинейных параболических уравнений. – М: Наука 1987. –477с.
2. Арипов М.М. Методы эталонных уравнений для решения нелинейных краевых задач. – Ташкент, Фан, 1988. –137 с.
3. Калашников А.С. Некоторые вопросы качественной теории нелинейных вырождающихся параболических уравнений второго порядка // УМН, 1987, т.42, Вып. 2 (254), 135-176.
4. Victor A. Galaktionov and Juan L. Vazquez. The problem of blow-up in nonlinear parabolic equations // Discrete and continuous dynamical systems, vol. 8, № 2, April 2002, 399-433.
5. Галактионов В.А. Об условиях несуществования в целом и локализации решений задачи Коши для одного класса нелинейных параболических уравнений // Ж. вычисл. матем. и матем. физ. Т. 23, № 6, 1983, 1341-1354.
6. Galaktionov V. A., Levine H. A. On critical Fujita exponents for heat equations with nonlinear flux boundary condition on the boundary // Israel J. Math. 94, 1996, 125-146.
7. A.D. Pablo, F. Quiros, J.D. Rossi, Asymptotic simplification for a reaction-diffusion problem with a nonlinear boundary condition // IMA J. Appl. Math. 67, 2002, 69-98.
8. X. Song, S. Zheng, Blow-up and blow-up rate for a reaction-diffusion model with multiple nonlinearities // Nonlinear Anal. 54, 2003, 279-289.
9. Li Z., Mu Ch. Critical exponents for a fast diffusive polytrophic filtration equation with nonlinear boundary flux // J. Math. Anal. Appl. 346, 2008, 55-64.

10. Zhongping Li, Chunlai Mu, Li Xie. Critical curves for a degenerate parabolic equation with multiple nonlinearities // J. Math. Anal. Appl. 359, 2009, 39-47.
11. Wanjuan Du and Zhongping Li. Critical exponents for heat conduction equation with a nonlinear Boundary condition // Int. Jour. of Math. Anal. vol. 7, 11, 2013, 517-524.
12. Арипов М.М., Рахмонов З.Р. К асимптотике решений одной нелинейной задачи теплопроводности с градиентной нелинейностью // Узб. Мат. Журн. 2013. № 3. 19-27.
13. Mersaid Aripov, Shakhlo A. Sadullaeva. To properties of solutions to reaction-diffusion equation with double nonlinearity with distributed parameters // Jour. Sib. Fed. Univ. Math. Phys. 2013. V. 6. № 2. P. 157-167.
14. Рахмонов З.Р. О поведение решений одной задачи нелинейной фильтрации с переменной плотностью и снелокальным граничным условием // Узб. Матем. Журн. № 1, 2015, 75-85.
15. Рахмонов З.Р. Об одной нелинейной задачи неньютоновской фильтрации в неоднородной среде с нелокальным граничным условием // Вестник КазНУ, Серия матем., мех., инф., № 3 (82), 2014, 45-56.

Обратная задача лечения организма бактериостатическим антибиотиком с измерением общей численности бактерий.

А.А. Азимов

Казахский национальный университет им. аль-Фараби, Алматы, Казахстан
anvar.aa@mail.ru

Аннотация. В настоящей статье рассматривается обратная задача, решение которой связано с необходимостью идентификации математической модели лечения организма бактериостатическим антибиотиком. Данная задача решалась посредством сведения ее к оптимизационной, и с использованием известных математических методов для упрощенной модели данного процесса вычислена производная по Гато функционала, характеризующего среднеквадратичное отклонение значения общей численности бактерий от результатов эксперимента, получена сопряженная система дифференциальных уравнений. На основе этих результатов был составлен и реализован алгоритм численного решения данной обратной задачи градиентным методом с дроблением шага. Были произведены и проанализированы результаты вычислений на модельных параметрах системы для различных значений искомого параметра.

Ключевые слова: Обратная задача, математическая модель лечения, градиентный метод.

1 Введение

Процесс лечения зараженного бактериями организма включает в себя три стадии: заражение, лечение, восстановление. На первой стадии организм подвергается заражению бактериями. Их численность растет сначала быстро, потом – всё медленнее, вплоть до установления некоторого предельного значения численности популяции. На второй стадии начинается лечение организма бактериостатическим антибиотиком, подавляющий рождаемость бактерий, в результате чего снижается их численность. Однако в результате мутаций появляются бактерии, не чувствительные к действию антибиотика. По мере сокращение исходной популяции бактерий происходит рост популяции мутантов. Эффективность антибиотика падает. На третьей стадии лечение прекращается. В отсутствии антибиотика менее жизнеспособная популяция мутантов постепенно вытесняется. Восстанавливается исходная популяция бактерий, чувствительных к действию антибиотика.

В [1] были рассмотрены математические модели для различных этапов данного процесса. В настоящей работе рассматривается только стадия лечения, которая описывается следующей системой дифференциальных уравнений:

$$\begin{cases} \dot{x}_1 = \left[\dfrac{a_1}{1 + cx_1\left(x_1^{\theta} - 1\right)} - b_1(x_1 + x_2) \right] x_1 + a_{12}x_2, \\ \dot{x}_2 = \left[a_2 - b_2(x_1 + x_2)\right] x_2 + \dfrac{a_{21}}{1 + cx_1\left(x_1^{\theta} - 1\right)} x_1, \end{cases}$$

где функции $x_1(t)$ и $x_2(t)$ – это численности основной популяции бактерий и бактерий-мутантов соответственно в момент времени t. Значения численностей обоих типов бактерий к моменту начала лечения считаются известными:

$$x_1(0) = x_{10}, x_2(0) = x_{20}.$$

Отметим, что эти начальные условия определяются экспериментально.

В системе через a_1 и a_2 обозначены приросты численности бактерий основной популяции и популяции мутантов соответственно, параметры b_1 и b_2 характеризуют их чувствительность к ограниченности жизненного пространства, а значение a_{12} – это прирост численности бактерий первого типа за счет мутаций из второго, a_{21} – наоборот. Параметр c показывает концентрацию, а θ – эффективность бактериостатического антибиотика.

Одной из трудностей использования данной модели является то, что значения многих параметров на практике невозможно измерить. В частности, неизвестны параметры c и θ, характеризующие концентрацию и эффективность антибиотика. Для этого на стадии лечения проводится ряд экспериментов по определению общей численности бактерий. Обратная задача состоит в отыскании неизвестных параметров так, чтобы решение рассматриваемых уравнений соответствовало результатам эксперимента.

2 Постановка обратной задачи

Для удобства последующих вычислений рассмотрим несколько упрощенную модель процесса лечения. Допустим, что в процессе лечения мутации происходят довольно редко. Тогда положим:

$$a_{12} = a_{21} = 0.$$

Рассмотрим выражение $1 + cx_1\left(x_1^\theta - 1\right)$, входящее в систему. Так как значение численности бактерий достаточно велико, то можно пренебречь единицами, входящими в него:

$$1 + cx_1\left(x_1^\theta - 1\right) \approx cx_1^{\theta+1}.$$

Введем обозначение

$$k = c^{-1}.$$

Учитывая это, можно переписать основную систему в следующем виде:

$$\begin{cases} \dot{x}_1 = \dfrac{ka_1}{x_1^\theta} - b_1(x_1 + x_2)x_1, \\ \dot{x}_2 = \left[a_2 - b_2(x_1 + x_2)\right] x_2, \end{cases} \tag{1}$$

с начальными условиями

$$x_1(0) = x_{10}, x_2(0) = x_{20}. \tag{2}$$

Таким образом, математическая модель лечения организма описывается задачей Коши (1)-(2).

Пусть экспериментально можно определить общую численность бактерий в любой момент времени $t \in [0, T]$, где T – момент окончания лечения, который мы можем выбрать сами. Что можно записать в виде следующего условия:

$$x_1(t) + x_2(t) = y(t), t \in [0, T], \tag{3}$$

где $y(t)$ – заданная функция, результат эксперимента.

Для простоты будем считать параметр θ известным. Тогда обратная задача формулируется следующим образом: необходимо определить значение параметра k так, чтобы соответствующее ему решение задачи Коши (1)-(2) удовлетворяло условию (3).

Полученную обратную задачу можно свести к эквивалентной ей оптимизационной задаче. Для этого рассматривается функционал, характеризующий среднеквадратичное отклонение значения общей численности бактерий от результатов эксперимента:

$$I(k) = \int_0^T (x_1(t) + x_2(t) - y(t))^2 \, dt. \tag{4}$$

Необходимо определить значение параметра k из условия минимума функционала (4), где функции $x_1(t)$ и $x_2(t)$ определяются как решение задачи Коши (1)-(2).

3 Производная функционала $I(k)$

Для решения полученной оптимизационной задачи воспользуемся градиентным методом. Для этого необходимо определить производную по Гато [2] функционала $I(k)$.

Дадим параметру k приращение $\sigma h : k + \sigma h$, где σ, h – некоторые числа. Обозначим через $x_1[k]$ и $x_2[k]$ решение задачи Коши (1)-(2), которое соответствует k, а через $x_1[k+\sigma h]$ и $x_2[k+\sigma h]$ – решение, соответствующее $k+\sigma h$. При этом для краткости опустим в записи аргумент t. Подставляя выражение $k + \sigma h$ в $I(k)$, получим:

$$I(k + \sigma h) = \int_0^T (x_1[k + \sigma h] + x_2[k + \sigma h] - y)^2 \, dt.$$

Обозначим:

$$\varphi_i(t) = x_i[k + \sigma h] - x_i[k], i = 1, 2,$$

причем, очевидно, что

$$\varphi_i(0) = 0, i = 1, 2.$$

Тогда получим:

$$I(k + \sigma h) = \int_0^T (x_1[k] + x_2[k] + \varphi_1 + \varphi_2 - y)^2 \, dt = \int_0^T (x_1[k] + x_2[k] - y)^2 \, dt +$$
$$+ 2 \int_0^T (x_1[k] + x_2[k] - y) (\varphi_1 + \varphi_2) \, dt + \int_0^T (\varphi_1 + \varphi_2)^2 \, dt.$$

Вычислим приращение функционала:

$$I(k + \sigma h) - I(k) = 2 \int_0^T (x_1[k] + x_2[k] - y) (\varphi_1 + \varphi_2) \, dt + \eta(\sigma),$$

где величина $\eta(\sigma) = \int_0^T (\varphi_1 + \varphi_2)^2 \, dt$ имеет более высокий порядок малости чем σ.

Обозначим через $f_i(x_1, x_2, k)$ правую часть i-го уравнения системы (1):

$$f_1 = \frac{k a_1}{x_1^\theta} - b_1(x_1 + x_2)x_1,$$
$$f_2 = [a_2 - b_2(x_1 + x_2)] \, x_2,$$

и найдем производную функции φ_i:

$$\dot{\varphi}_i = \frac{d}{dt}(x_i[k+\sigma h] - x_i[k]) = \\ = f_i(x_1+\varphi_1, x_2+\varphi_2, k+\sigma h) - f_i(x_1, x_2, k), i = 1, 2.$$

Разложим функцию $f_i(x_1+\varphi_1, x_2+\varphi_2, k+\sigma h)$ в ряд Тейлора по всем аргументам, получим:

$$\dot{\varphi}_i = \frac{\partial f_i(x_1, x_2, k)}{\partial x_1}\varphi_1 + \frac{\partial f_i(x_1, x_2, k)}{\partial x_2}\varphi_2 + \\ + \frac{\partial f_i(x_1, x_2, k)}{k}\sigma h + \eta_i(\sigma), i = 1, 2,$$

где слагаемое $\eta_i(\sigma)$ имеет более высокий порядок малости чем σ.

Найдем все частные производные, входящие в это выражение:

$$\begin{aligned}
&\frac{\partial f_1(x_1, x_2, k)}{\partial x_1} = -\frac{ka_1\theta}{x_1^{\theta+1}} - b_1(2x_1 + x_2),\\
&\frac{\partial f_1(x_1, x_2, k)}{\partial x_2} = -b_1x_1,\\
&\frac{\partial f_1(x_1, x_2, k)}{\partial k} = \frac{a_1}{x_1^{\theta}},\\
&\frac{\partial f_2(x_1, x_2, k)}{\partial x_1} = -b_2x_2,\\
&\frac{\partial f_2(x_1, x_2, k)}{\partial x_2} = a_2 - b_2(x_1 + 2x_2),\\
&\frac{\partial f_2(x_1, x_2, k)}{\partial k} = 0,
\end{aligned}$$

и подставим их в формулу для $\dot{\varphi}_i$:

$$\dot{\varphi}_1 = \left(-\frac{ka_1\theta}{x_1^{\theta+1}} - b_1(2x_1 + x_2)\right)\varphi_1 - b_1x_1\varphi_2 + \frac{a_1}{x_1^{\theta}}\sigma h + \eta_1(\sigma),$$
$$\dot{\varphi}_2 = -b_2x_2\varphi_1 + (a_2 - b_2(x_1 + 2x_2))\varphi_2 + \eta_2(\sigma).$$

Умножим полученные уравнения на произвольные функции λ_1 и λ_2 соответственно. Сложим полученные выражения, и проинтегрируем результат от 0 до T:

$$\int_0^T (\dot{\varphi}_1\lambda_1 + \dot{\varphi}_2\lambda_2)\, dt = \int_0^T \left\{ \left[-\left(\frac{ka_1\theta}{x_1^{\theta+1}} + b_1(2x_1 + x_2)\right)\lambda_1 - b_2x_2\lambda_2 \right]\varphi_1 + \right. \\ \left. + \left[-b_1x_1\lambda_1 + (a_2 - b_2(x_1 + 2x_2))\right]\varphi_2 + \frac{a_1\lambda_1}{x_1^{\theta}}\sigma h \right\} dt + \eta_3(\sigma),$$

где слагаемое

$$\eta_3(\sigma) = \int_0^T (\eta_1(\sigma)\lambda_1 + \eta_2(\sigma)\lambda_2)\, dt$$

имеет более высокий порядок малости чем σ.

Учитывая $\varphi_i(0) = 0$, применим к левой части этого выражение формулу интегрирования по частям:

$$\int_0^T (\dot{\varphi}_1\lambda_1 + \dot{\varphi}_2\lambda_2)\, dt = \varphi_1(T)\lambda_1(T) + \varphi_2(T)\lambda_2(T) - \int_0^T \left(\varphi_1\dot{\lambda}_1 + \varphi_2\dot{\lambda}_2\right) dt$$

Так как функции λ_1 и λ_2 – произвольные, то положим:

$$\lambda_1 = p_1(t), \lambda_2 = p_2(t),$$

где функции $p_1(t)$ и $p_2(t)$ определяются как решение следующей сопряженной системы дифференциальных уравнений:

$$\begin{cases} \dot{p}_1 = \left(\dfrac{ka_1\theta}{x_1^{\theta+1}} + b_1(2x_1 + x_2)\right) p_1 + b_2x_2p_2 - 2(x_1 + x_2 - y), \\ \dot{p}_2 = b_1x_1p_1 - (a_2 - b_2(x_1 + 2x_2))p_2 - 2(x_2 + x_2 - y), \end{cases} \tag{5}$$

с конечными условиями:

$$p_1(T) = 0, p_2(T) = 0. \tag{6}$$

Учитывая полученные выражения, можно переписать приращение функционала в следующем виде:

$$I(k + \sigma h) - I(k) = \sigma h \int_0^T \frac{a_1p_1}{x_1^\theta}\, dt + \eta_4(\sigma),$$

где $\eta_4(\sigma) = \eta_3(\sigma) + \eta(\sigma)$ также имеет более высокий порядок малости чем σ. Разделим это приращение на σ, и перейдем к пределу при $\sigma \to 0$:

$$\lim_{\sigma\to 0} \frac{I(k + \sigma h) - I(k)}{\sigma} = \lim_{\sigma\to 0} \left(h \int_0^T \frac{a_1p_1}{x_1^\theta}\, dt + \frac{\eta_4(\sigma)}{\sigma} \right) = h \int_0^T \frac{a_1p_1}{x_1^\theta}\, dt.$$

Следовательно, производная Гато функционала $I(k)$ будет иметь вид:

$$I'(k) = \int_0^T \frac{a_1p_1}{x_1^\theta}\, dt. \tag{7}$$

4 Градиентный метод

Система (1) представляет собой сложные нелинейные уравнения, которые не решаются аналитически. Поэтому и поставленную обратную задачу можно решить только численно. Для этого необходимо составить алгоритм ее численной реализации. Воспользуемся градиентным методом с дроблением шага [2]. Он включает в себя следующие этапы:

1) Задаем начальное приближение искомого параметра k_0.

2) Вычисляем соответствующее ему решение задачи Коши (1)-(2) – функции x_1 и x_2, а также p_1 и p_2 – решение сопряженной системы (5) с условием (6). Затем по известным значениям находим значение функционала (4) – $I(k_i)$ и его производной (7) – $I'(k_i)$.

3) Если $|I'(k_i)| + |I(k_i)| < \varepsilon$, где ε – некоторое маленькое положительное число, то останавливаем процесс и берем в качестве искомого параметра текущее значение k_i. В противном случае переходим к следующем шагу.

4) Находим следующее приближение: $k_{i+1} = k_i - \alpha I'(k_i)$

5) Вычисляем соответствующее этому k_{i+1} функции x_1 и x_2, а затем p_1 и p_2. После чего находим $I(k_{i+1})$ и $I'(k_{i+1})$.

6) Если выполнено условие монотонности $I(k_{i+1}) < I(k_i)$, то значение k_{i+1} берем в качестве следующего приближения и переходим к шагу 3. В противном случае дробим шаг $\alpha = \alpha/2$, и заново переходим к шагу 4.

Для решения основной и сопряженной систем дифференциальных уравнений применялся метод Рунге-Кутты 4 порядка, а для вычисления значения функционала и его производной – составная формула Симпсона [3]. Описанный алгоритм реализован на основе программного продукта Microsoft Visual C++ 2010 [4].

Расчетные значения параметров системы приведены в таблице 1.

Таблица 1. Значения расчетных параметров.

a_1	a_2	b_1	b_2	x_{10}	x_{20}	θ	ε	N	T
100	100	0.5	1	180	20	2.2	10^{-6}	1000	1

В качестве начального приближения взято значение $k_0 = 1000$. Результаты вычисления для различных k приведены в таблице 2.

Таблица 2. Результаты вычислений.

k	i	k_i	$\lvert J'(k_i)\rvert$	$J(k_i)$	$\lvert k_i - k\rvert$	$\lvert k_i - k\rvert/k$
0.01	56	0.01004047	0.000000963	0.000000000	0.00004047	0.004047
0.1	77	0.099919170	0.000000931	0.000000000	0.00008083	0.0008083
1	23	1.002019879	0.000000965	0.000000001	0.002019879	0.002019879
10	43	10.045635605	0.000000919	0.000000026	0.045635605	0.0045635605
100	21	100.29046198	0.000000235	0.000000042	0.290461983	0.0029046198

По таблице 2 видно, что значение искомого параметра восстанавливается, в целом, с хорошей точностью. С увеличением значения искомого параметра k, соответственно с уменьшением значения концентрации c, абсолютная погрешность вычислений возрастает. Относительная погрешность в свою очередь изменяется не значительно.

5 Заключение

Не смотря на то, что рассмотренная в данной работе обратная задача решалась при некоторых допущениях, она является важным этапом идентификации математической модели лечения зараженного бактериями организма. Однако для более детального уточнения модели необходимо рассматривать основную систему с учетом процесса мутаций и в случае с двумя неизвестными параметрами. Поэтому, последующие исследования будут связаны с решением обратных задач, наиболее приближенных к реальности. Помимо отмеченного, в них будет учтено то, что суммарная численность бактерий(результаты эксперимента)

известна только в отдельные моменты времени, и, следовательно, рассмотрен другой вид функционала. Полученные результаты необходимо применить к данным эксперимента.

Список литературы

1. С.Я. Серовайский, А.И. Ильин, Р.А. Исламов, С.Е. Касенов, Д.Б. Нурсеитов. Математическое моделирование популяций бактерий под действием различных антибиотиков с учётом мутаций // Сборник тезисов докладов Международной конференции "Поиск и разработка новых противоинфекционных лекарственных средств". 17-19 сентября 2014 г. АО "Научный центр противоинфекционных препаратов". – Алматы, 2014. – с. 49–51.
2. Васильев Ф.П. Методы оптимизации. – М.: Факториал Пресс, 2002. –824 с.
3. Демидович Б.П., Марон И.А., Шувалова Э.Э. Численные методы анализа. – М.: Наука, 1967. –368 с.
4. Подбельский В.В. Язык Си++. – М.: Финансы и статистика, 2003. –560 с.

Исследование фильтрованной функции плотности для моделирования крупных вихрей сложных турбулентных течений

М.К. Инкарбеков

Казахский национальный университет им. аль-Фараби, Алматы, Казахстан
inkarbekovm@gmail.com

Аннотация. Методология "фильтрованная функция плотности" (FDF) исследована и применена для моделирования крупных вихрей (LES) химически реагирующих турбулентных течений. В этой методологии, влияния нерешенных скалярных флуктуаций учитываются путем рассмотрения функции плотности вероятности подсеточных функций скалярных величин. В уравнении переноса для FDF эффект химических реакций находятся в замкнутом виде. Уравнение переноса для FDF решается численно Лагранжевым методом Монте-Карло. Консистенция FDF подхода, сходимость его Монте-Карло решения и эффективность замыканий использованных в уравнении переноса для FDF оцениваются путем сравнения с результатами прямого численного моделирования (DNS). Полученные FDF результаты хорошо согласуются с фильтрованными DNS результатами.

Ключевые слова: турбулентность, фильтрованная функция плотности, моделирования крупных вихрей, метод Монте-Карло, прямое численное моделирование.

1 Введение

Два статистических подхода были очень популярны в вычислении систем турбулентного горения [1]: (1) методы моментов и (2) методы функции плотности вероятностей (PDF). Первый подход рассматривает средние значения рассматриваемого течения через решения осредненных уравнений переноса [2]. Основной задачей в этом подходе является моделирование связи между неизвестными корреляциями в этих уравнениях и осредненными переменными переноса. Такие замыкания моментов используют комбинацию математического анализа и физического соображения. Несмотря на это, постройка окончательной математической модели требует дополнительных предположений и эмпирических взаимосвязей. В настоящее время, все полученные модели не являются универсально применимыми. В попытке исправить эти недостатки, достаточно много усилий были приложены на адаптацию этих моделей для определенных параметров течения. Второй подход, основанный на PDF, является весьма привлекательным в прогнозировании турбулентных реактивных течений, так как он преодолевает проблему замыкания связанную с химической реакцией. На практике, методы PDF стали применяться с помощью предложенных выше методов или через решение уравнения переноса, описывающее их дальнейшую эволюцию.

Значительные улучшения в вычислительных отраслях связанные с численными методами высокой точности облегчили моделирование простых турбулентных течений без турбулентных моделей. В этом подходе, известный как "прямое численное моделирование (DNS)" [3], все величины течения, включая самые мелкие турбулентные вихри, решаются напрямую. Такие моделирования стали ценными для фундаментальных исследований турбулентных течений для проверки моделей замыкания. Однако, из за высоких требований к размерам вычислительной сетки в реальных инженерных течениях, DNS не является широко

применимым для “практических” задач [4]. Трудности DNS заключаются в ограниченности компьютерных ресурсов. Количество требуемых сеточных узлов и временных шагов существенно превосходят современные вычислительные мощности.

Ниже представлена таблица 1, показывающая зависимость времени расчета от числа Рейнольдса для канала [5].

Таблица 1. Время расчета турбулентного течения в канале с DNS при различных числах Рейнольдса [5].

Re	$5 \cdot 10^3$	$5 \cdot 10^4$	$5 \cdot 10^5$	$5 \cdot 10^6$	$5 \cdot 10^8$
200 Mflop/s	68 дней	444 дней	610 лет	∞	∞
1 Tflops/s	13 дней	88 дней	122 года	∞	∞

Очевидно, что DNS позволяет получать результаты при современном развитии вычислительной техники только при малых числах Рейнольдса. Кроме этого существуют проблемы постановки граничных условий. Для описания случайного характера турбулентного течения необходимо адекватное задание нестационарных входных и выходных условий. С практической точки зрения, статистика, полученная с DNS, может быть использована для тестирования и калибровки моделей, базирующихся на осредненных уравнениях Рейнольдса.

При моделировании крупных вихрей (LES) [6], вместо того чтобы моделировать все турбулентные величины, как это делается в методе осреднения Рейнольдса, крупные вихри напрямую разрешаются на численной сетке и времени, а мельчайшие вихри подсеточного масштаба моделируются. Основной предпосылкой такого подхода является то, что наибольшие вихри несут максимум рейнольдсовых напряжений и должны быть рассчитаны. Мелкие же вихри содержат низкие значения рейнольдсовых напряжений, кроме того, мелкомасштабная турбулентность близка к изотропной и имеет близкие к универсальным характеристики, в большей степени подающиеся моделированию. Это приводит к некоторой степени облегченному решению по сравнению с решением DNS. В дополнении, предполагается что замыкание подсеточных величин в моделировании крупных вихрейявляются более универсальными чем осредненные величины Рейнольдса.

За последние три десятилетия значительный прогресс был сделан в моделировании крупных вихрей турбулентных течений [7]. Сравнительно, небольшая работа была выполнена в моделировании крупных вихрей химических реагирующих течений. Использование схем PDF для метода крупных вихрей было предложено Пейманом Гиви[8] и первое его фактическое применение было выполнено Маднием и Гиви [9]. Стивен Поуп представил концепцию “фильтрованная функция плотности (FDF)” [10], который по существу является PDF переменных величин подсеточной функции. С помощью математического определения FDF, Поуп демонстрирует [10], что эффекты химической реакции находятся в замкнутом виде в уравнении переноса FDF.

Одним из сложных вопросов в области энергетической и экологической исследований связано с точностью прогнозирования турбулентных реагирующих течений. Оптимальным средством захвата подробную, нестационарную физику таких потоков, как уже показала практика, является моделирование крупных вихрей (LES) [11]. Задачей в моделировании крупных вихрей является точное и последовательное моделирование величин подсеточной функции [12]. Методология, фильтрованная функция плотности (FDF), включая ее серию осредненной по плотности, фильтрованная функция массовой плотности, оказалось особенно эффективной для достижения этих целей [13]. Фильтрованная функция плотности, по

существу, является функцией плотности вероятности величин подсеточной функции. Поэтому фильтрованная функция плотности обеспечивает всю статистическую информацию касающуюся этих величин

2 Постановка

Мы рассматриваем несжимающиеся, изотермическое, турбулентное реагирующее течение жидкости, включающее N_S компонентов. Для математического описания процесса, основными переменными переноса являются вектор скорости $u_i(x,t)$ $(i=1,2,3)$, давление $p(x,t)$, и массовые доли компонентов $\phi_\alpha(x,t)(\alpha=1,2,...,N)$. Уравнениями, которые описывают перемещение этих переменных в пространстве и времени, являются:

$$\frac{\partial u_i}{\partial x_i}=0, \tag{1}$$

$$\frac{\partial u_i}{\partial t}+\frac{\partial u_i u_j}{\partial x_j}=-\frac{\partial p}{\partial x_i}+\frac{\partial \tau_{ij}}{\partial x_j}, \tag{2}$$

$$\frac{\partial \phi_\alpha}{\partial t}+\frac{\partial u_i \phi_\alpha}{\partial x_j}=-\frac{\partial J_j^\alpha}{\partial x_j}+\omega_\alpha, \tag{3}$$

где $\omega_\alpha(x,t)\equiv\hat{\omega}_\alpha(\Phi(x,t))$ химическая реакция для α компоненты, и $\Phi\equiv[\phi_1,\phi_2,...,\phi_N]$ обозначает скалярный массив. Предполагая Ньютоновское течение с законом Фика для диффузии, тензор напряжения вязкости τ_{ij} и массоперенос J_j^α представляются в следующем виде

$$\tau_{ij}=\nu(\frac{\partial u_i}{\partial x_j}+\frac{\partial u_j}{\partial x_i}), J_j^\alpha=-\Gamma\frac{\partial \phi_\alpha}{\partial x_j}, \tag{4}$$

где ν вязкость жидкости, Γ коэффициент диффузии, $\Gamma=\frac{\nu}{Sc}$, и Sc молекулярное число Шмидта.

В рамках LES используется осреднение по пространству, описываемое процедурой фильтрации [14]

$$\langle f(x,t)\rangle_L=\int_{-\infty}^{+\infty} f(x',t)G(x',x)dx', \tag{5}$$

где G функция фильтра, $\langle f(x,t)\rangle_L$ представляет фильтрованное значение переменной переноса $f(x,t)$, и $f'=f-\langle f\rangle$ обозначает флуктуацию f от филтрованного значения. После применение операции фильтрации к уравнениям переноса получается

$$\frac{\partial \langle u_i\rangle_L}{\partial x_i}=0, \tag{6}$$

$$\frac{\partial \langle u_i\rangle_L}{\partial t}+\frac{\partial \langle u_i\rangle_L\langle u_j\rangle_L}{\partial x_j}=-\frac{\partial \langle p\rangle_L}{\partial x_i}+\frac{\partial \langle \tau_{ij}\rangle_L}{\partial x_j}-\frac{\partial \langle T_{ij}\rangle_L}{\partial x_j}, \tag{7}$$

$$\frac{\partial \langle \phi_\alpha\rangle_L}{\partial t}+\frac{\partial \langle u_i\rangle_L\langle \phi_\alpha\rangle_L}{\partial x_j}=-\frac{\partial \langle J_j^\alpha\rangle_L}{\partial x_j}-\frac{\partial M_i^\alpha}{\partial x_j}+\langle \omega_\alpha\rangle_L, \tag{8}$$

где $T_{ij}=\langle u_i u_j\rangle_L-\langle u_i\rangle_L\langle u_j\rangle_L$ и обозначают подсеточное напряжение и подсеточный массовый поток, соответственно.

3 Стратегия замыкания

В методе LES нереагирующих течений проблема замыкания связана с $T_{ij} = \langle u_i u_j \rangle_L - \langle u_i \rangle_L \langle u_j \rangle_L$ $M_i^\alpha = \langle u_i \phi_\alpha \rangle_L - \langle u_i \rangle_L \langle \phi_\alpha \rangle_L$.В реагирующих течениях требуется дополнительная модель для $\langle \omega_\alpha \rangle_L$.Мы используем доступные на сегодняшний день замыкания, которые хорошо известны в нереагирующих течениях. Подсеточное напряжение моделируется через

$$T_{ij} - (\delta_{ij}/3)T_{kk} = -2\nu_t \langle S_{ij} \rangle_L, \tag{9}$$

где $\langle S_{ij} \rangle_L$ тензор деформации и подсеточная вязкость. Мы используем два вида замыкания для представления этой вязкости. Первый является таким же как традиционное замыкание Смагоринского [15]

$$\nu_t = C_s \Delta_G^2 \sqrt{\langle S_{ij} \rangle_L \langle S_{ij} \rangle_L}, \tag{10}$$

где Δ_G размер фильтра, C_s эмпирическая константа. Недостатки этого замыкания хорошо известны[16]. Чтобы избежать некоторых из этих недостатков, мы также использовали второй вид замыкания, в котором подсеточная вязкость определяется на основе модифицированной подсеточной кинетической энергии

$$\nu_t = C_K \Delta_G^2 \sqrt{|\langle u_*^i \rangle_L \langle u_*^j \rangle_L - \langle \langle u_*^i \rangle_L \rangle_{L'} \langle \langle u_*^j \rangle_L \rangle_{L'}|}, \tag{11}$$

где $u_i^* = u_i - \mathfrak{U}_i$, $\mathfrak{U}_i$−этолонная скорость в направлении x_i . Индекс L' обозначает фильтр второго уровня, который имеет размер больше первого уровня L . Это замыкание известно как модифицированная вязкость кинетической энергии (MKEV).

Типичная модель используется для замыкания подсеточного массового потока [17]

$$M_i^\alpha = \Gamma_t \frac{\partial \langle \phi_\alpha \rangle_L}{\partial x_i} = 0, \tag{12}$$

где $\Gamma_t = \nu_t / Sc_t$, Sc_t подсеточное число Шмидта.

4 Фильтрованная функция плотности

Ключевой момент в этой формулировке это рассмотреть скаляр неустойчивости основного скалярного массива $\Phi(x,t)$ в вероятностным методом. Для этого мы определяем «Фильтрованную функцию плотности» (FDF), обозначается P_L , как [18]

$$P_L(\Psi; x, t) \equiv \int_{-\infty}^{+\infty} \zeta[\Psi, \Phi(x', t)] G(x' - x) dx', \tag{13}$$

$$\zeta[\Psi, \Phi(x,t)] = \delta[\Psi - \Phi(x,t)] \equiv \prod_{\alpha=1}^{N_\alpha} \delta[\psi_\alpha - \phi_\alpha(x,t)], \tag{14}$$

где δ обозначает дельта-функцию и Ψ обозначает композиционную область скалярного массива. Значение $\zeta[\Psi - \Phi(x,t)]$ это «мелкозернистая» плотность [19], и (13) уравнение означает что FDF является пространственно фильтрованным значением мелкозернистой плотности. Таким образом, P_L дает плотность в композиционном пространстве жидкости вдоль x взвешенную фильтром G. При условии положительного ядра фильтра, P_L имеет все свойства ФПВ [19].

Для дальнейших разработок, определим "условно отфильтрованное значение" переменной $Q(x,t)$ по

$$\langle Q(x,t)|\Psi\rangle_L \equiv \frac{\int_{-\infty}^{+\infty}\zeta[\Psi,\Phi(x',t)]G(x'-x)dx'}{P_L(\Psi;x,t)}, \tag{15}$$

где $\langle\alpha|\beta\rangle$ означает фильтрованное значение α обусловлено β . Уравнение (15) имеет свойства

$$\text{(i) Для } Q(x,t)=c, \langle Q(x,t)|\Psi\rangle_L = c, \tag{16}$$

$$\text{(ii) Для} Q(x,t)\equiv\hat{Q}(\Phi(x,t)), \langle Q(x,t)|\Psi\rangle_L \equiv \hat{Q}(\Psi), \tag{17}$$

$$\text{(iii) Интегральное свойство} \langle Q(x,t)\rangle_L = \int_{-\infty}^{+\infty}\langle Q(x,t)|\Psi\rangle P_L(\Psi;x,t)d\Psi, \tag{18}$$

где c это постоянная, и $Q(x,t)\equiv\hat{Q}(\Phi(x,t))$ означает случай, когда переменная Q может быть полностью описана композиционным переменным $\Phi(x,t)$. От этих свойств следует, что фильтрованное значение любой функции скалярнной переменной (таких, как скорость реакции) получается интегрированием по композиционному пространству

$$\langle Q(x,t)\rangle_L = \int_{-\infty}^{+\infty}\hat{Q}(\Psi)P_L(\Psi;x,t)d\Psi. \tag{19}$$

Для того чтобы построить уравнение переноса для FDF, рассматривается производная по времени уравнения (13)

$$\begin{aligned}\frac{\partial P_L(\Psi;x,t)}{\partial t} &= -\int_{-\infty}^{+\infty}\frac{\partial\phi_\alpha(x',t)}{\partial t}\frac{\partial\zeta[\Psi,\Phi(x',t)]}{\partial\psi_\alpha}G(x'-x)dx' \\ &= -\frac{\partial}{\partial\psi_\alpha}\int_{-\infty}^{+\infty}\frac{\partial\phi_\alpha(x',t)}{\partial t}\zeta[\Psi,\Phi(x',t)]G(x'-x)dx'.\end{aligned} \tag{20}$$

В комбинации с уравнением (15), получается

$$\frac{\partial P_L(\Psi;x,t)}{\partial t} = -\frac{\partial}{\partial\psi_\alpha}\Big\{\Big[\Big\langle\frac{\partial u_i\phi_\alpha}{\partial x_i}\Big|\Psi\Big\rangle_L P_L(\Psi;x,t)\Big]. \tag{21}$$

Подставляя (3) в уравнение (21) получим:

$$\begin{aligned}\frac{\partial P_L(\Psi;x,t)}{\partial t} = \frac{\partial}{\partial\psi_\alpha}\Big\{\Big[&\Big\langle\frac{\partial\phi_\alpha}{\partial t}\Big|\Psi\Big\rangle_L + \Big\langle\frac{\partial J_i^\alpha}{\partial x_i}\Big|\Psi\Big\rangle_L \\ &-\langle\hat{\omega}_\alpha(\Phi)|\Psi\rangle_L\Big]P_L(\Psi;x,t)\Big\},\end{aligned} \tag{22}$$

в котором конвективный член может быть представлен в виде

$$\frac{\partial}{\partial\psi_\alpha}\Big\{\Big[\Big\langle\frac{\partial u_i\phi_\alpha}{\partial x_i}\Big|\Psi\Big\rangle_L P_L(\Psi;x,t)\Big] = \frac{\partial\langle u_i|\Phi\rangle_L P_L(\Psi;x,t)}{\partial x_i}. \tag{23}$$

Незамкнутый характер конвекции обозначается обусловленным фильтрованным значением скорости, который далее разлагается на разрешенный и подсеточный компоненты

$$\langle u_i|\Phi\rangle_L P_L = \langle u_i\rangle_L P_L + [\langle u_i|\Phi\rangle_L - \langle u_i\rangle_L]P_L, \tag{24}$$

так что уравнение (21) может быть выражено следующим образом

$$\frac{\partial P_L}{\partial t}+\frac{\partial \langle u_i\rangle_L P_L}{\partial x_i}=\frac{\partial[\langle u_i|\Psi\rangle_L-\langle u_i\rangle_L]P_L}{\partial x_i} +\frac{\partial}{\partial \psi_\alpha}\Big\{\Big[\Big\langle\frac{\partial J_i^\alpha}{\partial x_i}\Big|\Psi\Big\rangle_L -\langle\hat{\omega}_\alpha(\Psi)\rangle_L\Big]P_L(\Psi;x,t)\Big\}. \tag{25}$$

Это точное уравнение переноса для FDF и похож на уравнение, который был представлен Гао и О'Брайен [20]. Последний член в правой части этого уравнения за счет химической реакции и находится в замкнутом виде. Второе слагаемое в левой части представляет отфильтрованную конвекцию FDF в физическом пространстве, и также замкнут (известно что при условии $\langle u_i\rangle_L$). Незамкнутые члены связаны с первым слагаемым в правой части, обозначающей последствий неразрешенного подсеточного масштаба конвекции, и вторым слагаемым в правой части, представляющий влияние молекулярной диффузии.

Подсеточный конвективный поток моделируется

$$[\langle u_i|\Psi\rangle_L-\langle u_i\rangle_L]P_L=-\Gamma_t\frac{\partial P_L}{\partial x_i}. \tag{26}$$

Преимущество разложения (уравнение (24)) и последующего моделирования (уравнение (26)) в том, что они дают результаты, аналогичные тому, что в традиционном LES для первого момента FDF. Первыми моментами согласно уравнениям (24) и (26) являются

$$\langle u_i\phi_\alpha\rangle_L=\langle u_i\rangle_L\langle\phi_\alpha\rangle_L+[\langle u_i\phi_\alpha\rangle_L-\langle u_i\rangle_L\langle\phi_\alpha\rangle_L], \tag{27}$$

$$[\langle u_i\phi_\alpha\rangle_L-\langle u_i\rangle_L\langle\phi_\alpha\rangle_L]=-\Gamma_t\frac{\partial\phi_\alpha}{\partial x_i}. \tag{28}$$

Слагаемые в квадратных скобках в уравнении (27) - обобщенный скалярный поток в виде рассмотренных в традиционном LES [21]. Следовательно, уравнение (28) становится тождественным уравнению (12).

Замыкание для обусловленной подсеточной диффузии основано на линейной среднеквадратичной оценки (LMSE) [22] модели, которая также известна как IEM замыкание [23]. Модель включает разложение диффузионного члена в уравнении (25),

$$\frac{\partial}{\partial\psi_\alpha}\Big[\Big\langle-\frac{\partial}{\partial x_i}\Big(\Gamma\frac{\partial\phi_\alpha}{\partial x_i}\Big)\Big|\Psi\Big\rangle_L P_L\Big] =\frac{\partial}{\partial x_i}\Big(\Gamma_t\frac{\partial P_L}{\partial x_i}\Big)-\frac{\partial^2}{\partial\psi_\alpha\partial\psi_\beta}\Big[\Big\langle\Big(\Gamma\frac{\partial\phi_\alpha}{\partial x_i}\frac{\partial\phi_\beta}{\partial x_i}\Big)\Big|\Psi\Big\rangle_L P_L\Big]. \tag{29}$$

Первое слагаемое в правой части этого уравнения означает эффекты молекулярной диффузии в пространственном перемещении FDF. Второе слагаемое представляет собой диссипативную природу подсеточного скалярного смешивания. Модель среднеквадратичной оценки предполагает

$$\frac{\partial^2}{\partial\psi_\alpha\partial\psi_\beta}\Big[\Big\langle\Big(\Gamma\frac{\partial\phi_\alpha}{\partial x_i}\frac{\partial\phi_\beta}{\partial x_i}\Big)\Big|\Psi\Big\rangle_L P_L\Big]=-\frac{\partial}{\partial\phi_\alpha}[\Omega_m(\psi_\alpha-\langle\phi_\alpha\rangle_L)P_L], \tag{30}$$

где Ω_m является " частотой смешивания в подсеточном масштабе". Эта частота может быть связана с коэффициентом подсеточной диффузии и длины фильтра: $\Omega_m=C_\Omega(\Gamma+\Gamma_t)/\Delta_G^2$

. Второе значение уравнения (30) представляет собой выражение для общей подсеточной скалярной диссипации

$$\epsilon_\alpha = 2\Gamma\Big\langle \frac{\partial\phi_\alpha}{\partial x_i}\frac{\partial\phi_\alpha}{\partial x_i}\Big\rangle_L = 2\Omega_m(\langle\phi_\alpha^2\rangle_L - \langle\phi_\alpha\rangle_L^2), \tag{31}$$

Применяя полученные замыканиями (26) и (30), получаем смоделированное уравнение переноса для FDF

$$\frac{\partial P_L}{\partial t} + \frac{\partial\langle u_i\rangle_L P_L}{\partial x_i} = \frac{\partial}{\partial x_i}\Big[(\Gamma+\Gamma_t)\frac{\partial P_L}{\partial x_i}\Big]$$
$$+\frac{\partial}{\partial\phi_\alpha}[\Omega_m(\psi_\alpha - \langle\phi_\alpha\rangle_L)P_L] - \frac{\partial\hat{\Omega_\alpha}(\Psi)P_L}{\partial\phi_\alpha}. \tag{32}$$

Это уравнение может быть интегрировано чтобы получить уравнений переноса для моментов подсеточного масштаба. Уравнение для первого подсеточного момента, $\langle\phi_\alpha\rangle_L$, и обобщенная подсеточная дисперсия, $\sigma = \langle\phi_\alpha^2\rangle_L - \langle\phi_\alpha\rangle_L^2$ находятся

$$\frac{\partial\langle\phi_\alpha\rangle_L}{\partial t} + \frac{\partial\langle u_i\rangle_L\langle\phi_\alpha\rangle_L}{\partial x_i} = \frac{\partial}{\partial x_i}(\Gamma+\Gamma_t)\frac{\partial\langle\phi_\alpha\rangle_L}{\partial x_i} + \langle\omega_\alpha\rangle_L, \tag{33}$$

$$\frac{\partial\sigma_\alpha}{\partial t} + \frac{\partial\langle u_i\rangle_L\sigma_\alpha}{\partial x_i} = \frac{\partial}{\partial x_i}(\Gamma+\Gamma_t)\frac{\partial\sigma_\alpha}{\partial x_i} - 2\Omega_m\sigma_\alpha$$
$$+2(\Gamma+\Gamma_t)\frac{\partial\langle\phi_\alpha\rangle_L}{\partial x_i}\frac{\partial\langle\phi_\alpha\rangle_L}{\partial x_i} + 2(\langle\phi_\alpha\omega_\alpha\rangle_L - \langle\phi_\alpha\rangle_L\langle\omega_\alpha\rangle_L). \tag{34}$$

5 Решение FDF методом Монте-Карло

Решение уравнения переноса для FDF предоставляет всю статистическую информацию относительно скалярной переменной $\Phi(x,t)$. Это уравнение может быть решено эффективно с помощью Лагранжевого метода Монте-Карло [24]. Преимущество этого метода хорошо известен тем что в нем особо не проявляется численная диффузия. Основой Лангранжевого решения уравнения переноса для FDF является принцип эквивалентных систем. Две системы с разными мгновенными значениями могут иметь идентичную статистику, который полностью удовлетворяет уравнение переноса для FDF. В Лагранжевом методе Монте-Карло каждая частица перемещается согласно определенным уравнениям. Эти частицы подвергаются движению за счет конвекции из-за фильтрованной средней скорости потока, и диффундируют за счет молекулярной и подсеточной диффузии. Главный диффузионный процесс представляется в стохастической форме и описывается следующим стохастическим дифференциальным уравнением (СДУ)[24,25]

$$dX_i(t) = D_i(X_i(t),t)dt + E(X_i(t),t)dW_i, \tag{35}$$

где X_i Лагранжевое расположение стохастической частицы, D_i и E известные как коэффициенты “сноса” и “диффузии” соответственно, W_i означает процесс Винер-Леви.

$$E \equiv \sqrt{2(\Gamma+\Gamma_t)}, D_i \equiv \langle u_i\rangle_L + \frac{\partial(\Gamma+\Gamma_t)}{\partial x_i}. \tag{36}$$

Поэтому СДУ, которое определяет пространственное перемещение FDF, является

$$dX_i(t) = \Big(\langle u_i\rangle_L + \frac{\partial(\Gamma+\Gamma_t)}{\partial x_i}\Big)dt + \sqrt{2(\Gamma+\Gamma_t)}dW_i, \tag{37}$$

Композиционный состав частиц развивается одновременно благодаря действию подсеточного смешивания и реакции

$$\frac{d\phi_\alpha^+}{dt} = -\Omega_m(\phi_\alpha^+ - \langle\phi_\alpha\rangle_L) + \omega_\alpha, \tag{38}$$

где $\phi_\alpha^+ = \phi_\alpha(X_i(t), t)$ является скалярной величиной частицы с Лагранжевым вектором расположения X_i .

6 Результаты

Для того чтобы показать эффективность FDF модели, рассмотрена задача развивающегося по времени слоя смешивания. Этот слой состоит из двух параллельных потоков бегущих в противоположных направлениях с одинаковыми по абсолютной величине скоростями. Рассматривается реакция простого типа $A+B \to P$, в которой предполагается константная скорость химической реакции и течение считается изотермической. Реагенты A и B вводятся в верхний и нижний потоках соответственно.

Переменные течения нормированы относительно эталонных величин. Эталонными величинами в задаче развивающегося по времени слоя смешивания являются величины свободного потока и длина L_γ , которая определяется как $\delta_{\nu 0}/L_\gamma = 2.83$, где $\delta_{\nu 0}$ начальная толщина завихренности. Эталонные величины определяют число Рейнольдса $Re = U_\gamma L_\gamma/\nu$. Скорость химической реакции параметризуется с помощью числа Дёмклера $Da = K/(U_\gamma/L_\gamma)$.

Проведены DNS и LES расчеты. В методе DNS используется полностью конечно-разностный подход. Процедура в LES основана на методе Монте-Карло для решения уравнения переноса FDF, а фильтрованные гидродинамические переменные решаются конечно-разностным методом. Для 2D DNS расчета максимальным разрешением сетки является 433×577 точек с $Re = 500$ и $Da = 2$. В случае 3D DNS, расчет на сетке с колличеством узлов $217 \times 289 \times 133$ точек с $Re = 400$ и $Da = 1$.

FDF и LES- FD расчеты проводились на более грубой сетке с размером 74×98 для 2D случая, и $82 \times 108 \times 64$ точек для 3D. Для сравнения полученных результатов, DNS данные фильтрируются следующей функцией фильтра

$$G = (x' - x) = \prod_{i=1}^{N_D} \widetilde{G}(x_i' - x_i),$$
$$\widetilde{G}(x_i' - x_i) = \begin{cases} \frac{1}{\Delta_G} \text{ если } |x_i' - x_i| \le \frac{\Delta_G}{2} \\ \\ 0 \text{ если } |x_i' - x_i| > \frac{\Delta_G}{2} \end{cases} \tag{39}$$

в которой N_D обозначает размерность области.

Чтобы показать консистенцию FDF подхода и сходимость схемы Монте-Карло, результаты LES нереагирующих течений полученные с помощью FDF и LES-FD сравниваются. Так как точность метода конечных разностей хорошо исследована, такой сравнительный анализ дает возможность хорошо оценить производительность метода Монте-Карло.

На рисунке 1 представлены результаты LES для развивающегося по времени слоя смешивания, полученные с помощью FDF и LES-FD. Эти рисунки представляют простую визуальную наглядность консистенции FDF с помощью результатов полученных методом частиц в соответствии с результатами полученных с помощью LES-FD. В действительности

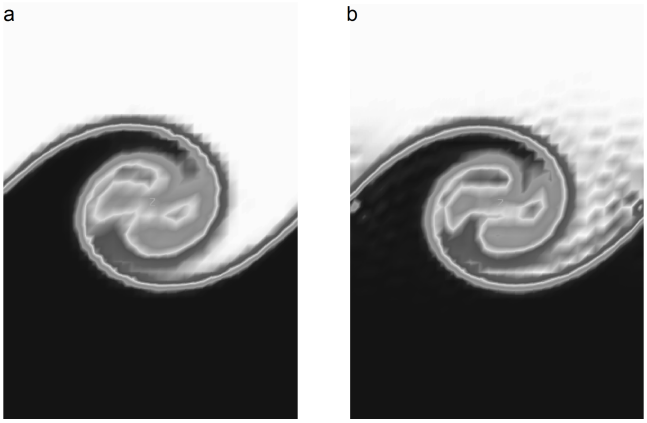

Рис. 1. Контур распределения фильтрованного скалярного поля. a – FDF и b – LES-FD.

результаты полученные методом Монте-Карло в какой-то мере более привлекательные, так как содержат меньше численную диффузию по сравнению с результатами LES-FD.

Для двумерного моделирования, значения фильтрованной массовой доли полученные методом Монте-Карло, согласуются с решением полученным с помощью метода конечных разностей. Это проиллюстрировано на рисунке 2, в котором показан Точечный график сравнения отфильтрованных значений скаляра полученных с помощью FDF и LES-FD.

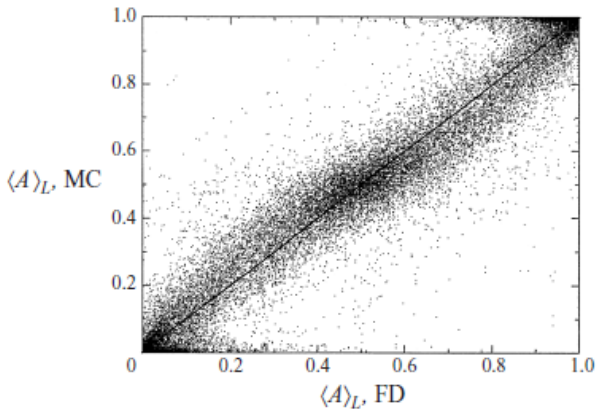

Рис. 2. Точечный график сравнения отфильтрованных значений скаляра полученных с помощью FDF и LES-FD.

Преимущество FDF подхода над традиционным LES-FD проявляется особенно в реагирующих течениях. Такая неконсистенция метода LES-FD, которая стимулирует использование FDF, проиллюстрировано на рисунке 3, где показано изменение массовой доли конечнего продукта со временем. Где также результаты LES расчетов сравниваются с данными DNS. По сравнению с LES-FD результаты LES показывают очень близкую согласованность с результатами DNS.

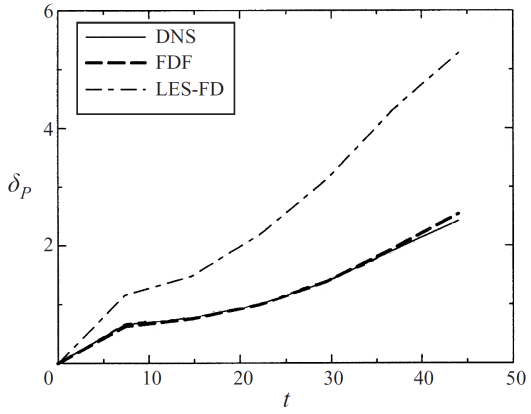

Рис. 3. Изменение массовой доли конечнего продукта со временем.

7 Заключение

Основной целью этой работы является исследование методологии “фильтрованная функция плотности” для моделирования крупных вихрей турбулентных реагирующих течений. Показано что FDF является мощным инструментом при моделировании реагирующих течений. Этот метод похож на метод функция плотности вероятности (PDF), который используется в подходе Рейнольдса. Основным преимуществом метода FDF, так же как в методах PDF, в том что эффект химических реакций получаются в замкнутом виде.

Смоделированное уравнение переноса для FDF решается численно Лагранжевым методом Монте-Карло. Показано что Лагранжевый метод Монте-Карло по сравнению с традиционным методом конечных разностей, хорошо подавляет эффект численной диффузии. Этот подход применен для LES задачи развивающегося по времени слоя смешивания. Полученные результаты сравниваются с результатами традиционного метода моделирования крупных методов, где влияния флуктуации подсеточного масштаба пренебрегаются, и с данными прямого численного моделирования (DNS) течения с идентичными значениями физических параметров. Консистенция FDF подхода и сходимость схемы Монте-Карло показываются с помощью сравнений с результатами LES-FD нереагирующих течений. Преимущество FDF над LES-FD проявляется при проведении сравнительного анализа с данными DNS. Показано что эффекты флуктуации подсеточного масштаба имеют большое влияние на решение фильтрованной скорости химической реакции. Таким образом, моделирование реагирующих турбулентных течений с помощью FDF имеет большую перспективу в будущем.

Список литературы

1. Libby, P.A., Williams, F.A. (Eds): Turbulent Reacting Flows, Academic Press, London, UK, chap. 5, pp. 185–218, 1994.
2. Jones, W. P., “Turbulence Modeling and Numerical Solution Methods for Variable Density and Combusting Flows”, in “Turbulent Reacting Flows” (P. A. Libby and F. A. Williams, Eds.) pp. 309–374, Academic Press, 1994.
3. Givi, P. “Spectral and random vortex methods in turbulent reacting flows. In Turbulent Reacting Flows” (P. A. Libby and F. A. Williams, Eds.), pp. 475–572. Academic Press, 1994.
4. Correa, S.M., “A Review of NOx Formation Under Gas-Turbine Combustion Conditions,” Combust. Sci. Technol., vol. 87, pp. 329-362, 1992.
5. Menter F.R. Methoden, Moeglichkeiten und Grenzen numerischer Stroemungsberechnungen. Numet. Erlangen, 2002.

6. R. S. Rogallo and P. Moin, "Numerical simulation of turbulent flow," Annu. Rev. Fluid Mech. 16, 1984.
7. Whither Turbulence? Turbulence at the Crossroads, Lecture Notes in Physics, edited by J. L. Lumley, Springer, New York, 1990, Vol. 357.
8. Givi, P. 1989 Model free simulations of turbulent reactive flows. Prog. Energy Combust. Sci. 15, 1–107.
9. Madnia, C. K. and Givi, P. Direct numerical simulation and large eddy simulation of reacting homogeneous turbulence. In Large Eddy Simulations of Complex Engineering and Geophysical Flows (ed. B. Galperin and S. A. Orszag), chap. 15, pp. 315–346. Cambridge University Press, 1993.
10. S. B. Pope. Computations of turbulent combustion: Progress and challenges. Proc. Combust. Inst., 23:591–612, 1990.
11. T. Poinsot and D. Veynante. Theoretical and Numerical Combustion. R. T. Edwards, Inc., Philadelphia, PA, second edition, 2011.
12. J. Janicka and A. Sadiki. Large eddy simulation of turbulent combustion systems. Proc. Combust. Inst., 30:537–547, 2005.
13. P. Givi. Filtered density function for subgrid scale modeling of turbulent combustion. AIAA J., 44(1):16–23, 2006.
14. A. A. Aldama, "Filtering techniques for turbulent flow simulations," Lecture Notes in Engineering (Springer, New York, 1990), Vol. 49.
15. J. H. Ferziger, "Higher level simulations of turbulent flows," Stanford University Report No. TF-16, Department of Mechanical Engineering, Stanford University, Stanford, California, 1981.
16. T. A. Zang and U. Piomelli, "Large eddy simulation of transitional flow," in Ref. 11, Chap. 11, pp. 209–227.
17. T. M. Eidson, "Numerical simulation of the turbulent Rayleigh-Benard problem using subgrid modelling," J. Fluid Mech. 158, 245 (1985).
18. S. B. Pope, "Computations of turbulent combustion: Progress and challenges," in Proceedings of the 23rd Symposium (International) on Combustion (The Combustion Institute, Pittsburgh, 1990), pp. 591–612.
19. S. B. Pope, "PDF methods for turbulent reactive flows," Prog. Energy Combust. Sci. 11, 119 (1985).
20. F. Gao and E. E. O'Brien, "A large-eddy simulation scheme for turbulent reacting flows," Phys. Fluids A 5, 1282 (1993).
21. M. Germano, "Turbulence: The filtering appraoch," J. Fluid Mech. 238, 325 (1992).
22. C. Dopazo and E. E. O'Brien, "Statistical treatment of non-isothermal chemical reactions in turbulence," Combust. Sci. Technol. 13, 99 (1976).
23. R. Borghi, "Turbulent combustion modeling," Prog. Energy Combust. Sci. 14, 245 (1988).
24. S. B. Pope, "Lagrangian PDF methods for turbulent flows," Annu. Rev. Fluid Mech. 26, 23 (1994).
25. H. Risken, The Fokker-Planck Equation, Methods of Solution and Applications (Springer, New York, 1989).

Характеристики переноса нейтронов в реакторе ИГР

Р.А. Иркимбеков, В.М. Котов и А.А. Байгожина

Филиал Института Атомной Энергии Национального Ядерного Центра РК, Курчатов, Казахстан
irkimbekov@nnc.kz,kotovvm@nnc.kz,baigozhina@nnc.kz

Аннотация. Создание расчетных кодов для проведения прецизионных расчетов реактора ИГР, на котором проводятся различные эксперименты в области безопасности ядерной энергетики, является жизненно важным при растущих потребностях в проведении реакторных экспериментов. В данной работе представлено описание динамической задачи переноса нейтронов в реакторе теплоемкостного типа и показан путь решения данной задачи с помощью компьютерного моделирования и применения современных кодов Монте-Карло. Представлен принцип проведения верификации расчетных моделей и показана достоверность получаемых данных.
Основным преимуществом использованного подхода является возможность расчета динамики различных параметров реактора, изменение которых невозможно отследить в процессе обработки экспериментальных данных.

Ключевые слова: ИГР, реакторный эксперимент, пространственная кинетика, компьютерное моделирование.

1 Введение

Реактор ИГР (Рисунок 1) - импульсный исследовательский ядерный реактор на тепловых нейтронах с гомогенной уран-графитовой активной зоной [1], [2]. Конструктивно реактор представляет собой кладку из графитовых блоков, собранных в колонны высотой $4.4m$, которая размещена в герметичном стальном цилиндрическом кожухе диаметром $3.1m$ с гелиевой средой. Общая масса графитовой кладки – $33870kg$. Графитовые блоки активной зоны пропитаны водным раствором уранилдинитрата. Форма активной зоны близка к кубической с размерами $1.4 \times 1.4 \times 1.4m$.

Реактор может работать в двух режимах: нерегулируемый режим самогасящейся нейтронной вспышки, и регулируемый режим. Для осуществления режима самогасящейся вспышки (Рисунок 2) реактору сообщается реактивность, превышающая долю запаздывающих нейтронов, величина которой определяет форму, амплитуду и полуширину вспышки; гашение вспышки происходит вследствие отрицательного температурного эффекта реактивности. Регулируемый режим осуществляется перемещением стержней регулирования, компенсирующих отрицательный температурный эффект реактивности по заданному закону. Форма, амплитуда и длительность регулируемого режима могут быть самыми различными (Рисунок 3) и определяются задачами испытаний исходя из условия не превышения температуры активной зоны $1400K$.

В связи с высокой востребованностью исследовательского реактора ИГР для проведения динамических экспериментов в обоснование безопасности энергетических реакторов, проблема создания современного специализированного программного обеспечения стоит наиболее остро. Работа этого реактора с гомогенной уран-графитовой активной зоной характеризуется множественными особенностями [3]:
- ассиметричное искажение поля нейтронов при работе системы регулирования мощности

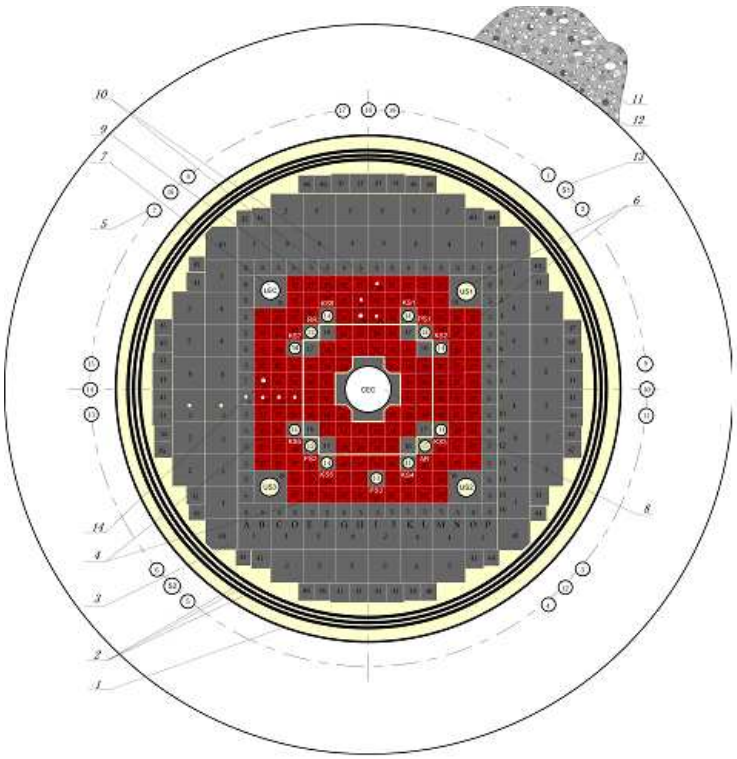

1 – кожух; 2 – экран боковой (три обечайки); 3 – отражатель; 4 – активная зона (неподвижная и подвижная части); 5 – канал ионизационной камеры (19 шт.); 6 – канал стержней регулирования (16 шт.); 7 – боковой экспериментальный канал; 8 – центральный экспериментальный канал; 9 – канал физических измерений; 10 – канал термоэлектрического преобразователя (9 шт.); 11 – биологическая защита; 12 – бак; 13 – канал счётчика нейтронов (2 шт.); 14 – канал источника нейтронов

Рис. 1. Реактор ИГР горизонтальное сечение.

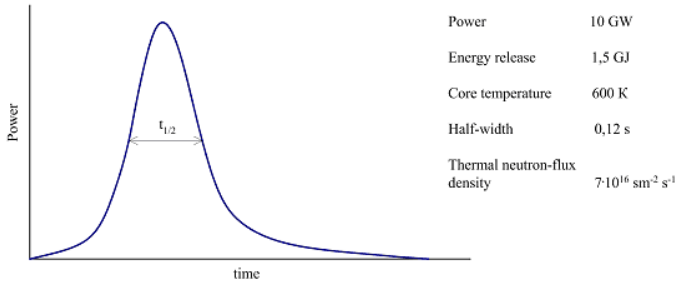

Рис. 2. Нерегулируемый режим.

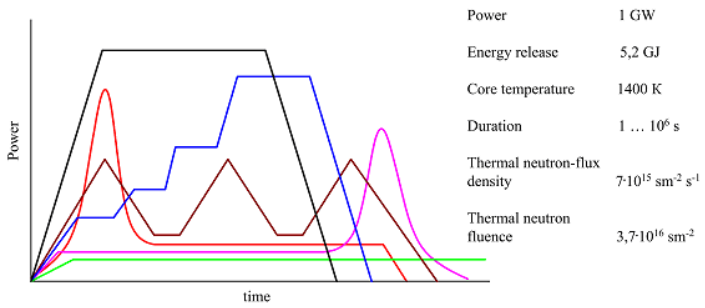

Рис. 3. Регулируемый режим.

реактора;
- изменение поля нейтронов в зависимости от температуры различных частей активной зоны реактора;
- регулирование плотности потока нейтронов в экспериментальных полостях с использованием пространственно удаленных от этих полостей детекторов нейтронов;
- широкий диапазон скорости изменения плотности потока нейтронов в зависимости от эксплуатационного режима.

При этом достоверный расчетный анализ в настоящее время возможен только для статических состояний активной зоны реактора. Нестационарные расчеты кинетических задач с изменяющимися параметрами реактора, такими как мощность, температура, реактивность, поле нейтронов, возможны только при значительном упрощении задачи [4], [5].В случае отсутствия возможности выполнения расчетных исследований процессов, происходящих в исследовательском реакторе во время экспериментов, существенно возрастает риск недооценки влияния различных факторов на результаты экспериментов. Данное обстоятельство приводит к ошибкам планирования экспериментов, вызывает необходимость применения консервативных подходов при обосновании и реализации экспериментов и, в конечном итоге, приводит к снижению качества проведения экспериментов.

2 Модель переноса нейтронов

Целью данной работы является разработка математической модели и расчетного кода пространственной кинетики для компьютерного моделирования изменения характеристик исследовательского импульсного графитового реактора ИГР.

Кинетический расчетный код, который планируется создать, позволит систематизировать на высоком качественном уровне накопленный опыт эксплуатации реактора ИГР. Использование такой программы повысит качество планируемых экспериментов и качество после экспериментального анализа.

Математическая модель основана на решении уравнений нейтронного баланса в элементарной ячейке и в узком энергетическом диапазоне. Математическая модель представлена в виде системы уравнений описывающих разогрев активной зоны, обмен нейтронами между элементарными ячейками и их термализацию. Это позволяет учесть специфические осо-

бенности системы регулирования мощности реактора, расположения экспериментальных полостей, изменения поля температуры и широкого диапазона эксплуатационных режимов.

Рассмотрим баланс нейтронов с энергией $E \in (Ei, Ei + dE)$ в элементарном объеме dV, распложенном в окрестности некоторой произвольной точки в пределах области активной зоны реактора ИГР.

$$\Delta n_{Ei} = n_{in} - n_{out} + n_{Ei+1} - n_{Ei-1} + n_{\nu} - n_a \tag{1}$$

Таким образом, можно вычислить нейтронный баланс в каждой элементарной ячейке в каждом элементарном диапазоне энергии нейтрона и составить карту температурной зависимости каждого слагаемого.

При решении задачи переноса нейтронов не применим классический набор параметров точечной модели кинетики, таких как реактивность, среднее время жизни мгновенных нейтронов, коэффициент реактивности. Вместо них используется набор параметров, которые должны переходить к классическим в случае точечной модели кинетики. Ниже приведено описание этих классических параметров и их аналоги в пространственной модели кинетики.

Реактивность.

Реактивность это производная величина от коэффициента размножения среды.

$$\rho = \frac{k-1}{k} \cdot \frac{1}{\beta} \tag{2}$$

В свою очередь коэффициент размножения это отношение эмиссии нейтронов к потерям нейтронов в системе в течение среднего времени жизни одного поколения нейтронов.

$$K_{eff}(t) = \frac{(1-P) \cdot \sum[(\nu_i \cdot \sigma_{ai} + 2\sigma_{2ni}) \cdot N_i(t)]}{\sum[(\sigma_{fi} + \sigma_{ai} + \sigma_{2ni}) \cdot N_i(t)]} \tag{3}$$

где, $N_i(t)$ - количество ядер $i-$ изотопа в момент времени t;
P - потери нейтронов в активной зоне реактора,
ν_i - число вторичных нейтронов i-го изотопа,
σ_{fi} - сечение реакции деления i-го изотопа,
σ_{2ni} - сечение реакции (n, 2n),
σ_{ai} - сечение реакции захвата нейтрона без деления.

Другими словами коэффициент размножения это параметр целой системы, которая не обменивается нейтронами с окружающей средой. Для описания отдельных пространственных зон, между которыми осуществляется перенос нейтронного поля необходимо перейти к набору параметров эмиссии и потери нейтронов в каждой ячейке. В результате записи баланса нейтронов получим систему уравнений пространственной кинетики:

$$\begin{array}{l} \frac{dn_{Ei,j}(t)}{dt} = [\nu_{Ei} J_{f,j}(1-\beta) - J_{a,j} + \sum S_j(m) - \sum S_m(j)] \cdot n_{Ei,j}(t) + \\ + S_{Ei+1} n_{Ei+1,j}(t) - S_{Ei} n_{Ei,j}(t) \end{array} \tag{4}$$

где $n_{Ei,j}(t)$ – концентрация нейтронов в фазовой ячейке (элементарная ячейка, взаимодействующая с другими элементарными ячейками в пространстве и ячейками на других

уровнях энергии нейтрона), $1/cm^3$;
$J_j = \sigma_j\ Nj\ V_{Ei}$ – скорость реакции на один нейтрон в фазовой ячейке, $1/c$;
$S_m(j)$ – ток нейтронов через площадь взаимодействия на один нейтрон в фазовой ячейке, $1/c$;
S_{Ei} – ток нейтронов между энергетическими уровнями, $1/c$;
индекс j – идентификатор пространственной ячейки под номером j;
индекс m – идентификатор пространственной ячейки под номером m;
индекс i – идентификатор уровня энергии нейтронов.

Как видно в данной системе нельзя перейти к уравнению, выраженному через коэффициент размножения и время жизни нейтронов, оставаясь в рамках пространственной модели. Но можно сделать это при сворачивании пространственной модели в точечную.

Среднее время жизни мгновенных нейтронов.

Этот параметр описывает время жизни нейтрона в системе в целом. Он зависит от вероятности нейтрона поглотиться в системе или покинуть ее. В случае пространственной кинетики данный параметр теряет смысл, поскольку в уравнении баланса нейтронов мы рассматриваем время жизни нейтрона в элементарной фазовой ячейке. Это время определяется, вероятностью вылета нейтрона из пространственной ячейки, поглощением, либо рассеянием. Таким образом, время жизни нейтрона в фазовой ячейке существенно меньше времени жизни нейтронов в реакторе.

Используемые параметры эмиссии поглощения рассеяния и потери нейтронов несут полную информацию о динамике изменения числа нейтронов со временем.

Температурный коэффициент реактивности.

Опираясь на систему уравнений баланса нейтронов в элементарной ячейке ТКР опишем снижением способности тепловых нейтронов отдавать свою энергию замедлителю. Параметры, связанные с нейтронными реакциями будем считать независимыми от температуры. Применительно к реактору ИГР это допустимо, поскольку композиция активной зоны реактора практически не имеет резонансов в тепловой области энергии. Перепишем уравнение (4) в соответствии с этими утверждениями:

$$\begin{array}{l}\frac{dn_{Ei,j}(t)}{dt} = [\nu_{Ei} J_{f,j}(1-\beta) - J_{a,j} + \sum S_j(m) - \sum S_m(j)] \cdot n_{Ei,j}(t) + \\ +S_{Ei+1}(T) n_{Ei+1,j}(t) - S_{Ei}(T) n_{Ei,j}(t)\end{array} \quad (5)$$

Снижение замедляющей способности с ростом температуры замедлителя приводит к смещению максимума в распределении плотности тепловых нейтронов в область более высоких энергий и как следствие изменению суммарного поглощения и эмиссии нейтронов.

При сворачивании пространственной модели в точечную, все коэффициент должны свернуться в значение классического ТКР реактора. В свою очередь классическое определение ТКР реактора ИГР сильно зависит от текущей конфигурации активной зоны.

Регулировочная характеристика органов регулирования.

Поскольку в классической кинетике регулировочная характеристика задана в терминах реактивности, то в данной модели регулировочная характеристика стержней должна быть пересчитана в фундаментальных параметрах – как влияние на количество поглощенных нейтронов (1). Таким образом, можно естественным образом моделировать интерференцию стержней регулирования.

Расчет выделенного тепла.

В модель кинетики входит температура элементарной ячейки для учета эффектов, связанных с изменением температуры. Поэтому важно рассчитать поле температуры в объеме активной зоны реактора. Поскольку эксперименты, связанные с разрушением модельной

сборки на реакторе ИГР, длятся в течение порядка ста секунд, то процесс разогрева активной зоны можно считать адиабатным. Это подтверждается в работе [6]. Функция, описывающая изменение температуры во времени задается в неявном виде в зависимости от динамики мощности:

$$\int W_j(t)dt = m_j \int C_p(T_j)dT_j \tag{6}$$

Таким образом, задача определения поля температуры по активной зоне сводится к решению задачи пространственного распределения мощности. Пространственно-временное распределение мощности будет отличаться от пространственно-временного распределения поля нейтронов вследствие наличия источников запаздывающего излучения мощности и переноса энергии γ-квантами и нейтронами.

Источники энергии в реакторе делятся на мгновенные и запаздывающие. Энергия мгновенных источников это энергия осколков деления и энергия мгновенных ?-квантов, выделяющихся при делении и при радиационном захвате нейтрона.

Около 90% тепловой энергии деления выделяется мгновенно или в течение одной миллисекунды. Оставшиеся 10% выделяются при распаде продуктов деления. Наиболее распространенная формула, описывающая остаточное выделение мощности формула Вэй-Вигнера не имеет параметров для описания запаздывающей мощности после кратковременных динамических нагрузок характерных для реактора ИГР. В случае представленной модели запаздывающее выделение энергии связанное с падением потока нейтронов учитывается естественным образом. Запаздывающее выделение мощности за счет распада источников β и γ излучений можно представить по аналогии с запаздывающими нейтронами введением концентрации активного элемента – источника запаздывающего излучения энергии.

Пространственное выделение энергии задано следующим образом:
- кинетическая энергия осколков деления и энергия, связанная с поглощением α и β излучения, выделяется в области деления мгновенно;
- энергия мгновенных и запаздывающих гамма квантов и гамма квантов выделяющихся при радиационном захвате нейтронов выделятся в соответствии с рассчитанным профилем мощности в MCNP;
- кинетическая энергия нейтронов преобразуется в тепловую энергию в области их рассеяния и поглощения;
- энергия нейтрино не преобразуется в тепловую энергию.

Составим система уравнений, описывающую выделение мощности в реакторе:

$$\begin{cases} W_i(t) = [((1-\gamma_m-\gamma_z-\beta_z)\, q_0 J_{f,j} + J_{s,j})\, n_j(t)] + \\ \ldots + \delta_{\gamma,j}[\lambda_w C_\gamma(t) + n_j(t) \sum(\gamma_m q_0 J_{f,j} + q_\gamma J_{\gamma,j})] + \lambda_w \beta_z C_{\beta,j} \\ \frac{dC_\gamma(t)}{dt} = \sum[\gamma \cdot q_0 \cdot J_{f,j} n_j(t)] - \lambda_w C_\gamma(t) \\ \frac{dC_{\beta,j}(t)}{dt} = \beta \cdot q_0 \cdot J_{f,j} n_j(t) - \lambda_w C_\beta(t) \end{cases} \tag{7}$$

$W_i(t)$ - мощность в момент времени t;
γ_m, γ_z, β_z- доля энергии мгновенного γ излучения, запаздывающего γ излучения и запаздывающего β излучения соответственно;
$\delta_{\gamma,j}$ - доля γ излучения в ячейке j;
$\lambda_w = 1c^{-1}$ - константа распада элемента запаздывающего излучения;
$C_\gamma(t), C_\beta(t)$ - концентрация источников запаздывающего излучения.

Таким образом, получим одно-групповое приближение для описания процесса выделения энергии с учетом запаздывания.

Система уравнений пространственной кинетики.

С учетом всего сказанного выше запишем систему уравнений пространственной кинетики с учетом шести групп запаздывающих нейтронов и одной группы источников запаздывающего теплового излучения:

$$\begin{cases} \frac{dn_{Ei,j}(t)}{dt} = [\nu_{Ei} J_{f,j}(1-\beta) - J_{a,j} + \sum S_j(m) - \sum S_m(j)] \cdot n_{Ei,j}(t) + \\ \ldots + S_{Ei+1}(T) n_{Ei+1,j}(t) - S_{Ei}(T) n_{Ei,j}(t) + A_{Ei} \sum \lambda_n C_n(t) \\ \frac{dC_{n,j}(t)}{dt} = \sum [\nu_{Ei} \beta \cdot J_{f,j} n_{Ei,j}(t)] - \lambda_n C_{n,j}(t) \\ W_i(t) = \sum [((1-\gamma_m-\gamma_z-\beta_z)\, q_0 J_{f,j} + J_{s,j})\, n_j(t)] + \\ \ldots + \delta_{\gamma,j} [\lambda_w C_\gamma(t) + n_j(t) \sum \sum (\gamma_m q_0 J_{f,j} + q_\gamma J_{\gamma,j})] + \lambda_w \beta_z C_{\beta,j} \\ \frac{dC_\gamma(t)}{dt} = \sum \sum [\gamma \cdot q_0 \cdot J_{f,j} n_j(t)] - \lambda_w C_\gamma(t) \\ \frac{dC_{\beta,j}(t)}{dt} = \sum [\beta \cdot q_0 \cdot J_{f,j} n_j(t)] - \lambda_w C_\beta(t) \\ \int W_j(t) dt = m_j \int C_p(T_j) dT_j \end{cases} \tag{8}$$

Запись в первой строке представляет собой систему уравнений баланса нейтронов в элементарной ячейке j в окрестности энергии нейтрона Ei с учетом шести групп запаздывающих нейтронов. Коэффициент ν отличен от нуля только в окрестности энергии нейтронов 2 МэВ и равен числу вторичных нейтронов деления. Коэффициент равен единице только в окрестности энергии нейтронов $0,5$ МэВ, во всех остальных случаях равен нулю. То есть эмиссия нейтронов в элементарную ячейку за счет мгновенных нейтронов деления и запаздывающих нейтронов возможна только при соответствующих энергиях.

Запись во второй строке представляет систему уравнений, описывающих динамику изменения концентрации источников всех групп запаздывающих нейтронов в элементарной ячейке j.

Запись в третьей строке представляет систему уравнений выделения энергии в элементарной ячейке j с учетом мгновенного выделения тепловой энергии за счет деления, за счет радиационного захвата нейтронов, за счет рассеяния нейтронов и за счет выделения запаздывающей тепловой энергии.

Запись в четвертой и пятой строке представляет систему уравнений описывающих динамику изменения концентрации источников запаздывающего энерговыделения.

Запись в шестой строке связывает интегральную мощность с температурой элементарной ячейки j.

3 Получение коэффициентов переноса нейтронов

Для определения аргументов системы уравнений (8) используем модель реактора ИГР, построенную для расчета в программе MCNP [7]. Данная модель максимально приближена к реальной конструкции реактора. Выполнена модернизация модели реактора ИГР в программе MCNP, которая заключалась в создании сетки конечных элементов, необходимой для нахождения аргументов системы уравнений пространственной кинетики.

Модель была разбита на параллельные ячейки. Область активной зоны разбита на ячейки размером $100X100X100mm$. Область отражателя разбита на ячейки с большим размером: $100X100X200mm$, $100X200X200mm$ и $200X200X200mm$. Ячейки формируются плоскостями $30X30X25$ плоскостей перпендикулярных каждой из координатных осей. Таким образом, получилось 3000 ячеек описывающих активную зону и 20184 ячеек описывающих весь реактор.

В ходе проведенных расчетов модернизированной модели получена база данных для создаваемого программного кода. База данных представляет собой текстовый файл с некоторой структурой выводимых данных по координатам, энергиям нейтронов и типе данных

(поток нейтронов, ток нейтронов или скорость реакции). На рисунке 4 показан вид файла данных.

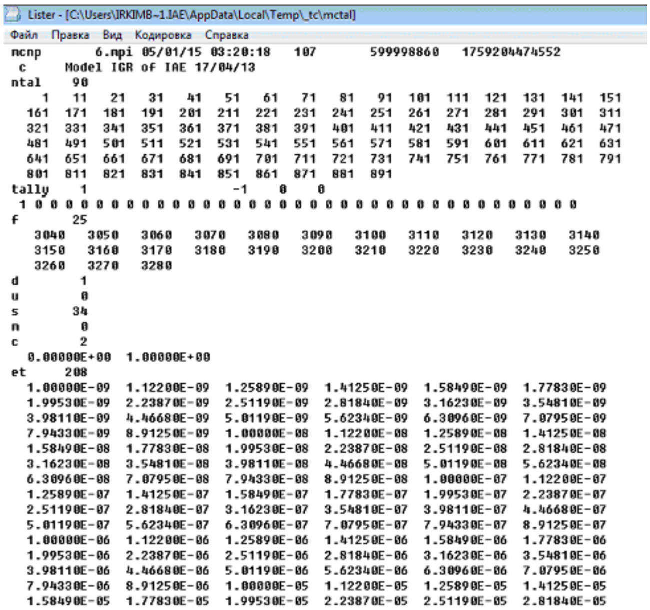

```
Lister - [C:\Users\IRKIMB~1.IAE\AppData\Local\Temp\_tc\mctal]
Файл  Правка  Вид  Кодировка  Справка
mcnp      6.mpi 05/01/15 03:20:18    107       599998860   1759204474552
 c     Model IGR of IAE 17/04/13
ntal    90
    1   11   21   31   41   51   61   71   81   91  101  111  121  131  141  151
  161  171  181  191  201  211  221  231  241  251  261  271  281  291  301  311
  321  331  341  351  361  371  381  391  401  411  421  431  441  451  461  471
  481  491  501  511  521  531  541  551  561  571  581  591  601  611  621  631
  641  651  661  671  681  691  701  711  721  731  741  751  761  771  781  791
  801  811  821  831  841  851  861  871  881  891
tally    1                  -1    0    0
 1 0 0 0 0 0 0 0 0 0 0 0 0 0 0 0 0 0 0 0 0 0 0 0 0 0 0 0 0 0 0 0 0 0 0 0 0
f       25
   3040   3050   3060   3070   3080   3090   3100   3110   3120   3130   3140
   3150   3160   3170   3180   3190   3200   3210   3220   3230   3240   3250
   3260   3270   3280
d        1
u        0
s       34
n        0
c        2
  0.00000E+00  1.00000E+00
et     208
  1.00000E-09  1.12200E-09  1.25890E-09  1.41250E-09  1.58490E-09  1.77830E-09
  1.99530E-09  2.23870E-09  2.51190E-09  2.81840E-09  3.16230E-09  3.54810E-09
  3.98110E-09  4.46680E-09  5.01190E-09  5.62340E-09  6.30960E-09  7.07950E-09
  7.94330E-09  8.91250E-09  1.00000E-08  1.12200E-08  1.25890E-08  1.41250E-08
  1.58490E-08  1.77830E-08  1.99530E-08  2.23870E-08  2.51190E-08  2.81840E-08
  3.16230E-08  3.54810E-08  3.98110E-08  4.46680E-08  5.01190E-08  5.62340E-08
  6.30960E-08  7.07950E-08  7.94330E-08  8.91250E-08  1.00000E-07  1.12200E-07
  1.25890E-07  1.41250E-07  1.58490E-07  1.77830E-07  1.99530E-07  2.23870E-07
  2.51190E-07  2.81840E-07  3.16230E-07  3.54810E-07  3.98110E-07  4.46680E-07
  5.01190E-07  5.62340E-07  6.30960E-07  7.07950E-07  7.94330E-07  8.91250E-07
  1.00000E-06  1.12200E-06  1.25890E-06  1.41250E-06  1.58490E-06  1.77830E-06
  1.99530E-06  2.23870E-06  2.51190E-06  2.81840E-06  3.16230E-06  3.54810E-06
  3.98110E-06  4.46680E-06  5.01190E-06  5.62340E-06  6.30960E-06  7.07950E-06
  7.94330E-06  8.91250E-06  1.00000E-05  1.12200E-05  1.25890E-05  1.41250E-05
  1.58490E-05  1.77830E-05  1.99530E-05  2.23870E-05  2.51190E-05  2.81840E-05
```

Рис. 4. Файл результатов расчета аргументов системы уравнений пространственной кинетики.

В первых двух строках представлены данные о модели и версии кода, в которой был проведен расчет. Третья строка показывает количество блоков данных и далее перечислены идентификаторы этих блоков. В каждом блоке содержатся данные о токах нейтронов через конкретный отрезок параллельных плоскостей создающих конечно-разностную сетку. Каждая плоскость разбита на клетки другими плоскостями.

В строке tally записан номер первого блока, далее задано количество блоков второго уровня, записано количество параллельных плоскостей и перечислены их идентификаторы. После ключевого слова et записано количество энергетических групп и перечислены их интервалы в мегаэлектровольтах. После этого идет основная часть блока содержащая последовательности значений соответствующих энергетической группе, плоскости и вырезанной поверхности на этой плоскости. После окончания блока начинается новый блок с ключевого слова tally.

4 Достоверность полученных результатов

Важным этапом при получении результатов компьютерного моделирования является их верификация. Достоверность полученных результатов невозможно проверить напрямую, но данные результаты содержат исчерпывающую информацию о конфигурации поля нейтронов и любые неточности в формировании этого поля могут повлиять на общие характеристики реактора.

В различных работах сделанных ранее верификация моделей реактора ИГР проводилась исключительно по результатам расчетов нескольких стационарных состояний. При работе над данным проектом было обнаружено, что такой подход имеет серьезный недостаток – невозможно четко определить систематическую погрешность модели. В случае получения

хорошей сходимости с экспериментом остается не исключенной значимая систематическая ошибка, поскольку в модели могут быть введены ряд ошибочных параметров, которые взаимно исключают связанные с ними реактивностные эффекты в стационарном состоянии, но могут проявлять себя в других конфигурациях реактора.

Для исследований, выполняемых в рамках данной работы необходимо быть уверенным в правильности моделирования конфигурации нейтронного поля. Поэтому верификация модели производится по различным параметрам.

Верификация по стационарным состояниям

Реактор имеет значительную высотную и радиальную несимметричность, и все органы регулирования взаимно влияют на вес друг друга. Это называется интерференцией органов СУЗ. Для проведения верификации по стационарным состояниям выполнены расчеты восьми конфигураций реактора отличающихся расположением органов регулирования, таблица 1.

Таблица 1. Конфигурации органов регулирования реактора ИГР в критическом положении

Индекс пуска	ПС1	ПС2	ПС3	АР	РР	КС	УС	Температура, ^oC
182Ф-8В	291	ввк	376	ввк	внк	внк	внк	13
182Ф-9В	491	ввк	193	ввк	внк	внк	внк	14
182Ф-10В	633	ввк	ввк	ввк	1386	внк	внк	13
182Ф-11В	793	ввк	ввк	ввк	994	внк	внк	17
182Ф-12В	976	ввк	ввк	ввк	787	внк	внк	19
182Ф-13В	1278	ввк	ввк	ввк	594	внк	внк	21
182Ф-15В	внк	263	ввк	ввк	545	внк	внк	14
182Ф-16В	внк	385	ввк	ввк	363	внк	внк	18

Экспериментальное измерение коэффициента размножения в критическом состоянии возможно с большой точностью 1.0000 ± 0.0001, что соответствует реактивности $\pm 0.02\beta$. При измерении конфигурации активной зоны возможны погрешности связанные с ошибкой измерения температуры $\pm 1.5K$ и ошибкой измерения положения органов регулирования $\pm 1mm$. Погрешность определения температуры дает неопределенность до 0.05β при расчете реактивности. Погрешность измерения положения органов регулирования дает неопределенность от 0β до 0.004β на каждый стержень в зависимости от расположения его нижнего конца. Погрешность расчета реактивности составляет $\pm 0.03\beta$ с доверительной вероятностью 95%. Таким образом, отклонение результатов расчета реактивности от результатов эксперимента не должно превышать $\pm 0.1\beta$ с вероятностью 95%. Данные верификации по стационарным состояниям представлены в таблице 2.

Таблица 2. Результаты верификации по критическим состояниям

Индекс пуска	182Ф-8В	182Ф-9В	182Ф-10В	182Ф-11В	182Ф-12В	182Ф-13В	182Ф-15В	182Ф-16В
Расчетные данные, β	-0.045	-0.073	-0.011	-0.043	-0.033	-0.016	0.013	0.049

Верификация по надкритическим состояниям

Извлечение органов регулирования из реактора с целью его перевода в надкритическое состояние ведет к значительному перераспределению конфигурации нейтронного поля и

изменению его спектра. Поэтому верификация модели по надкритическим состояниям позволит оценить правильность моделирования нейтронного поля при изменении композитного состава активной зоны. Данные верификации представлены в таблице 3. Отклонение результатов расчета реактивности от результатов эксперимента также не должно превышать 0.1β с вероятностью 95%.

Таблица 3. Результаты верификации по надкритическим состояниям

Индекс пуска	182Ф-8В	182Ф-9В	182Ф-10В	182Ф-11В	182Ф-12В	182Ф-13В	182Ф-15В	182Ф-16В
Экспериментальные данные, β	0.255	0.512	0.740	0.984	1.250	1.530	1.850	2.020
Расчетные данные, β	0.279	0.581	0.747	1.023	1.342	1.602	1.804	1.971
Разница, β	0.024	0.069	0.007	0.039	0.092	0.072	-0.046	-0.049

Верификация по динамическим характеристикам

С помощью моделирования точечной кинетики реактора ИГР [8], можно оценить качество расчета некоторых параметров реактора: время жизни мгновенных нейтронов, доля запаздывающих нейтронов, температурный коэффициент реактивности. Данные параметры влияют на высоту и ширину вспышки мощности в нерегулируемых режимах работы реактора. Эти данные можно оценить с достаточно высокой точностью. В таблицах 4, 5 представлены данные о расчетах реальных пусков и показано их соответствие экспериментальным данным. Погрешность измерения полуширины вспышки 10% погрешность определения амплитуды вспышки 15%.

Таблица 4. Результаты верификации по полуширине вспышки

Индекс пуска	182Ф-8В	182Ф-9В	182Ф-10В	182Ф-11В	182Ф-12В	182Ф-13В	182Ф-15В	182Ф-16В
Полуширина вспышки, с	144.5	42.0	17.9	6.73	2.00	0.968	0.593	0.492
Расчетные данные, с	144.5	43.0	17.7	6.38	1.91	0.956	0.566	0.510
Расхождение результатов	0.0%	-2.2%	1.3%	5.5%	4.5%	1.3%	4.8%	-3.5%

Таблица 5. Результаты верификации по амплитуде

Индекс пуска	182Ф-8В	182Ф-9В	182Ф-10В	182Ф-11В	182Ф-12В	182Ф-13В	182Ф-15В	182Ф-16В
Амплитуда вспышки, МВт	0.26	1.55	4.78	14.74	45.69	117.7	252.6	361.4
Расчетные данные, МВт	0.23	1.41	4.50	13.9	44.72	114.3	248.0	345.0
Расхождение результатов,	0.0%	-2.2%	1.3%	5.5%	4.5%	1.3%	4.8%	-3.5%

Таким образом, все расчетные данные согласованы с их экспериментальными значениями. Следовательно, при проведении нейтронно-физических расчетов ИГР в MCNP формируется поле нейтронов, которое достаточно точно описывает всевозможные эффекты, что в свою очередь дает основание считать, что все полученные аргументы уравнения пространственной кинетики будут соответствовать реальности.

5 Заключение

В результате проведенных работ была модернизирована модель и проведена верификация модели по параметрам в критическом и надкритическом состоянии реактора и верификация по динамическим параметрам реактора. Данные по верификации представлены в докладе. Показано, что результаты расчетов хорошо согласуются с результатами измерений соответствующих параметров.

Представлена система уравнений пространственной кинетики и показано, как данная система уравнений может быть свернута в точечную модель кинетики реактора. В ходе проведенных расчетов модернизированной модели получена база данных для создаваемого программного кода. Приведено краткое описание этой базы данных.

Работа выполнена при финансовой поддержке МОН РК по бюджетной программе "Научная и (или) научно-техническая деятельность подпрограмма "Грантовое финансирование научных исследований"приоритетное направление «Энергетика и машиностроение», тема «Исследование динамики нейтронного и температурного поля в импульсном реакторе теплоемкостного типа».

Список литературы

1. Курчатов, И.В. Импульсный графитовый реактор ИГР / И.В. Курчатов, С.М. Фейнберг, Н.А. Доллежаль // Атомная энергия. – 1964. – Т. 17, № 6. – С. 463-474.
2. Реактор ИГР [Интернет ресурс] // Официальный сайт Национального ядерного центра Республики Казахстан. – Курчатов, Казахстан.
3. В.М. Котов, А.М. Курпешева, Р.А. Иркимбеков Расчет характеристик ИГР // Атомная энергия. – Москва, август 2011. – том 111, выпуск 2. – с. 116
4. Иркимбеков Р.А., Вурим А.Д. Исследование зависимости значений температурного коэффициента реактивности от физического состояния активной зоны реактора ИГР. // Вестник НЯЦ РК, сер. Атомная энергетика и безопасность АЭС, вып. 3, Курчатов, НЯЦ РК, 2012.
5. Иркимбеков Р. А., Вурим А.Д. Изменение обратных связей реактора ИГР в сложных процессах – Материалы VI Междунар. конф. ICNRP'12, Алматы, 6 – 8 июня 2012.
6. Горин Н.В., Казьмин Ю.М., Васильев А.П., Павшук В.А. и др. Расчетно-экспериментальное исследование температурного поля кладки ИГР. – Атомная энергия, 2000, т. 88, вып. 4, с. 247 – 251.
7. Котов В.М., Иркимбеков Р.А., Курпешева А.М., Бенч-Марк модель реактора ИГР. – Сборник тезисов 8-ой Международной конференции «Ядерная и радиационная физика», Алматы, 20-23 сентября 2011 г., стр.37.
8. R.A. Irkimbekov, A.D. Vurim, L.K. Zhagiparova, P.L. Garner, N.A. Hanan, HEU/LEU IGR Reactor Kinetics. – Сборник тезисов 35-ой Международной конференции RERTR-2014, Вена, 12-16 октября 2014 г.

Численное моделирование нелинейных колебательных процессов в колоннах при бурении нефтегазовых скважин

Б.М. Мардонов[1], С.С. Аманов[1] и Л.А. Хаджиева[2]

[1]Ташкентский институт текстильной и легкой промышленности, Ташкент, Узбекистан
[2]Казахский национальный университет им. аль-Фараби, Алматы, Казахстан
batsam@list.ru,khadle@mail.ru

Аннотация. В работе исследуется поведение системы геометрически нелинейных бурильных колонн при динамических воздействиях. Предложена численная реализация метода конечных элементов для решения соответствующих краевых задач. Принимая колонны в виде балок, составлено выражение для энергии при изгибе и сжатии с учетом геометрической нелинейности деформирования. Формы балки в поперечном направлении представлены через полиномы Эрмита кубической степени. Установлено, что в случае геометрической нелинейности колонны одной и той же системе нагрузок соответствуют несколько различных деформированных состояний, устойчивых и неустойчивых. Нелинейность колонны может существенно изменить характер колебательных процессов в ее поперечном направлении. Происходит нарушение симметрии в прогибах штанги, что означает возможность появления потери устойчивости. Она может произойти при резких торможениях, реализуемых при высоких значениях параметра нелинейности. При этом вероятность перехода в состояние неустойчивости в начальные моменты времени снижается.

Ключевые слова: бурильная колонна, нелинейность, колебания, устойчивость, метод конечных элементов.

1 Введение

Нестационарные колебания геометрически нелинейных распределенных систем являются весьма сложной проблемой механики деформируемого твердого тела. Изучение проблем технологических процессов в нефтегазодобывающей отрасли выявило ряд малоизученных задач, к которым относятся вопросы учета как физически, так и геометрически нелинейных свойств буровых колонн, сопровождаемых различными видами осложнений (потерей устойчивости колонн, разрывами труб и др.), волновыми и колебательными процессами в элементах бурильных систем (БДС) [1],[2].

Источниками динамических воздействий на колонну могут быть крутящий момент от двигателя и повторно меняющиеся нагрузки при бурении с долотами режущего типа, осевые растягивающие нагрузки - от буровой установки и сжимающие нагрузки, сопровождаемые вибрациями - при работе долота на забое и т.д.

Все это предполагает рассмотрение колонны как нелинейной механической системы с бесконечным числом степеней свободы. Отсутствие аналитических способов исследования динамики работы такой системы, и, соответственно, оценки влияния колебаний на ее прочность и устойчивость при бурении вызывает практический интерес к данной проблеме.

В процессе работы бурильная колонна обычно теряет прямолинейную форму из-за потери устойчивости. Вопросам устойчивости бурильных колонн посвящены работы [3],[4], где изучены влияния сосредоточенной силы, собственного веса, внутреннего наружного давления, центробежных сил, деформационных свойств материала труб и других факторов на показатели их устойчивости.

При изучении динамической устойчивости бурильных колонн под действием динамических нагрузок появляются новые эффекты, связанные с характером их нагружения [3]. К

таким задачам, в частности, относятся быстрое нагружение колонны осевой сжимающей нагрузкой. Поскольку в таком динамическом процессе сжимающая сила может пробежать не только первое, но и более высокие критические значения, то при этом следует ожидать высших форм потери устойчивости. Эта особенность динамического процесса нагружения является важной, так как она связана с существенным повышением несущей способности колонны. Если же сжимающая нагрузка прилагается за короткое время, что соответствует ударному погружению колонны, в этом случае следует проследить процесс передачи усилий вдоль длины колонны, и таким образом, дополнительно учитывать силы инерции элементов колонны, отвечающие продольным перемещениям.

Для получения количественных решений нелинейных задач теории упругости часто приходится прибегать к численным методам, то есть представлять среду как дискретную модель. В этом случае дальнейшая идеализация при составлении уравнений или при их решении может и не понадобиться. Одним из таких подходов, основанных на идее кусочной аппроксимации непрерывных полей, является метод конечных элементов. Простота и общность этого метода, с разностными методами, делают его удобным средством решения широкого класса нелинейных задач [5]-[9].

2 Математическая модель

Исследуются колебания буровых штанг (колонн), возникающих при действии на колонны переменных во времени сжимающих нагрузок. Деформированное состояние буровой колонны полагается геометрически нелинейным, то есть допускается конечность деформаций. Принимаем колонну в виде весомого стержня. Определяем потенциальную энергию изгиба и продольного перемещения сечений стержня в случае его нелинейного деформирования U [3],[10],[11]:

$$\begin{array}{l} U = \frac{EI}{2}\int_0^l \left[\frac{\partial^2(v_1-v_0)}{\partial x^2}\right]^2 dx \\ +\frac{EF}{2}\int_0^l \left[\left(\frac{\partial u}{\partial x}\right)^2 + \left(\frac{\partial u}{\partial x}\right)\left(\frac{\partial v_1}{\partial x}\right)^2 + \frac{1}{2}\left(\frac{\partial v_1}{\partial x}\right)^4\right] dx\ . \end{array} \tag{1}$$

работу внешней силы P при вертикальном перемещении A_1, работу силы веса стержня при отклонении его от положения равновесия A_2:

$$\begin{array}{l} A_1 = \frac{P}{2}\int_0^l \left[\left(\frac{\partial v_1}{\partial x}\right)^2 - \left(\frac{\partial v_0}{\partial x}\right)^2\right] dx + \frac{Pl}{EF} \\ A_2 = -\frac{q}{2}\int_0^l \left[x + l\,(i-1)\right]\left(\frac{\partial v_i}{\partial x}\right)^2 dx\ . \end{array} \tag{2}$$

и кинетическую энергию T:

$$T = \frac{qF}{2g}\int_0^l \left[\left(\frac{\partial v_1}{\partial t}\right)^2 + \left(\frac{\partial u}{\partial t}\right)^2\right] dx\ , \tag{3}$$

где $v_0\,(x)$ - начальная форма изгиба, $v_1 = v_1\,(x,t)$ - полный прогиб стержня, $u = u\,(x,t)$ - продольное смещение сечений стержня, E - модуль Юнга материала стержня, l,F,I - длина, площадь поперечного сечения и момент инерции, q - погонный вес стержня.

Общая потенциальная энергия будет равна [3]:

$$П = U - A_1 - A_2\ .$$

Определим функцию Лагранжа как

$$L = T - П$$

Принимая $q = q(t)$ за обобщенную координату, составим уравнение Лагранжа II рода:

$$\frac{d}{dt}\left(\frac{\partial L}{\partial \dot{q}}\right) - \frac{\partial L}{\partial q} = 0 \,. \tag{4}$$

При этом прогибы балки $v_0 = v_0(x)$ и $v_1 = v_1(x,t)$ и продольное перемещение $u = u(x,t)$ могут быть представлены через произвольные функции, удовлетворяющие соответствующим начальным и граничным условиям.

3 Численная реализация модели

Рассмотрена краевая задача

$$v_1(x,t) = 0, \frac{\partial v_1(x,t)}{\partial x} = 0 \;\; (x = 0, x = l) \,, \tag{5}$$

$$\frac{\partial u}{\partial x} = \frac{P(t)}{EF} \;\; (x = 0) \,, \tag{6}$$

$$u = u_0(t) \;\; (x = l) \,. \tag{7}$$

Ее решение осуществляется методом конечных элементов. Для этого длину штанги разделяем на n конечных элементов (n+1 узлами) одинаковой длины a. Формы балки в поперечном направлении представляются через полиномы Эрмита кубической степени, которые имеют вид:

$$П_1 = 1 - 2\xi^2 + 2\xi^3, П_2 = a\left(\xi - 2\xi^2 + \xi^3\right), П_3 = 3\xi^2 - 2\xi^3, П_4 = a\left(-\xi^2 + \xi^3\right),$$

$$\xi = \frac{x}{a} \,.$$

Продольное перемещение в каждом элементе - через квадратичные функции:

$$N_1 = 1 - 3\xi + 2\xi^2, \;\; N_2 = 2\xi^2 - \xi \,.$$

Таким образом, прогиб произвольного элемента балки представлен в виде

$$v = П_1 q_i + П_2 q_{i+1} + П_3 q_j + П_4 q_{j+1} \,,$$

где q_i, q_j - прогибы, q_{i+1}, q_{j+1} - углы поворота в узлах элементов. Для выбранных n элементов общее количество неизвестных равно $2n$+2.

Продольное перемещение сечений элемента задано в виде

$$u = N_1 r_i + N_2 r_j \,,$$

где r_i, r_j - продольные перемещения узлов элемента.

Количество неизвестных перемещений узлов будет равно n+1. Таким образом, выбранная система конечных элементов в общем случае имеет $3n$+3 степеней свободы, отвечающих прогибам $v = q_i, v = q_j$, углам поворотов $v' = q_{i+1}, v = q_{j+1}$ и продольным перемещениям $u = r_i, u = r_j$, выступающим в качестве обобщенных координат. Для граничных условий (5)-(7), количество неизвестных становится равным $k = 3n + 3 - 6 = 3(n-1)$ $(n \geq 2)$.

Подставляя выражения $v = v(\xi, t)$ и $u = u(\xi, t)$ в формулы (1)-(3), определяем потенциальную энергию изгиба и продольного перемещения сечений стержня в случае нелинейного

деформирования U, работу внешней силы P при вертикальном перемещении A_1, работу силы веса стержня при отклонении его от положения равновесия A_2, а также кинетическую энергию T через полиномы Эрмита кубической степени.

Рассмотрен случай БДС с сосредоточенными массами (муфтами) m_i. При этом энергия балки и сосредоточенных масс представлена в виде

$$T_i = \frac{qF}{2g}\int_0^l \left(\left(\frac{\partial v_i}{\partial t}\right)^2 + \left(\frac{\partial u_i}{\partial t}\right)^2\right) dx + \frac{1}{2}m_i\left(\frac{\partial u_i(0,t)}{\partial t}\right)^2 ,$$

где $u_i = u_i(t)$ - перемещение i-ой массы, причем $u_n(l,t) = u_0(t)$ ($u_0(t)$ - перемещения нижнего конца n-ой балки).

Сумма потенциалов сил веса балки, сжатия P и сосредоточенных масс вычисляется по формуле

$$V_i = -\frac{q}{2}\int_0^l (x + l(i-1))\left(\frac{\partial v_i}{\partial x}\right)^2 dx - m_i g u_i(0,t) . \tag{8}$$

Для определения продольных перемещений штанги использована гипотеза Кирхгофа [12], согласно которой средние удлинения ε_{ix} каждой штанги не зависят от координаты x, а зависят только от времени. Тогда для деформации получаем выражение [12]:

$$\varepsilon_{ix} = \frac{\partial u_i}{\partial x} + \frac{1}{2}\left(\frac{\partial v_i}{\partial x}\right)^2 = \frac{1}{l}\left(u_i(l,t) - u_i(0,t) + \frac{1}{2}\int_0^l \left(\frac{\partial v_i}{\partial x}\right)^2 dx\right) .$$

Продольное перемещение i-ой балки представим в виде

$$u_i = r_{i-1}\frac{l-x}{l} + r_i\frac{x}{l} \;\; (i = 2\ldots n) , \tag{9}$$

где $r_{i-1} = r_{i-1}(t)$ и $r_i = r_i(t)$ соответственно перемещения начального и конечного сечений i-ой трубы (свечи), причем $r_n = u_0(t)$. На границах перехода труб выполняются условия непрерывности усилий:

$$EF\frac{du_i}{dx} = EF\frac{du_{i+1}}{dx} = k\left(u_{i+1}(0) - u_i(l)\right), \;\; EF\frac{du_1}{dx} = -P_0 .$$

В этом случае выражения потенциальной и кинетической энергий i-ой балки с учетом (8) и (9) имеют вид

$$U_1 = \frac{EI}{2}\int_0^l \left(\frac{\partial^2 v_i}{\partial x^2}\right)^2 dx + \frac{EF}{2l}\left[-\frac{P_0 l}{EF} + \frac{1}{2}\int_0^l \left(\frac{\partial v_i}{\partial x}\right)^2 dx\right]^2 , \tag{10}$$

$$U_i = \frac{EI}{2}\int_0^l \left(\frac{\partial^2 v_i}{\partial x^2}\right)^2 dx + \frac{EF}{2l}\left[r_i - r_{i-1} + \frac{1}{2}\int_0^l \left(\frac{\partial v_i}{\partial x}\right]^2 dx\right)^2 (i = 2...n), \tag{11}$$

$$T_i = \frac{qF}{2g}\int_0^l \left(\frac{\partial v_i}{\partial t}\right)^2 dx + \frac{1}{2}m_i\dot{r}_{i-1}^2 \; (i = 1...n, \; \dot{r}_0 = 0), \tag{12}$$

Подставляя выражения энергий в (4), получены системы $3n-3$ нелинейных уравнений для определения обобщенных координат $q_i = q_i(t), r_i = r_i(t)$ в обоих рассмотренных случаях, в частности, для $n = 3$.

4 Численные результаты

Получены кривые зависимости перемещения нижней части колонны по закону $u_0 = \frac{ln(kv_0t)+1}{k}$ (рис.1а) и продольное перемещение сосредоточенной массы по времени (рис.1б). В расчетах принято $n = 3,\ k = 1/m,\ v_0 = 2m/s,\ l = 1000m,\ D_1 = 140mm,\ D_2 = 128mm, E = 2 \cdot 10^5 MPa,\ \rho = \rho_0 F,\ \rho_0 = 7000kg/m^3,\ m_1 = m_2 = 40kg,\ P_0 = 485N$.

Определены зависимости поперечных перемещений узлов сопряжений q_1 и q_3 от времени для различных значений масс $m_1 = m_2 = m$ (рис.2).

Установлено, что сосредоточенная масса совместно с нижней частью колонны помимо поступательного движения совершает еще и колебательное движение. При этом установлено незначительное влияние наличия сосредоточенных масс на продольные смещения узлов сопряжения звеньев. Наличие сосредоточенных масс в узлах сопряжения звеньев колонн приводит к изменению частот и росту амплитуды их колебаний. Это указывает на изменение характера поперечных колебаний в местах муфтовых соединений отдельных свечей колонны при учете масс муфт.

5 Заключение

В результате анализа динамики буровой колонны под действием переменных осевых сил установлено, что наличие сосредоточенных масс практически не влияет на амплитуды продольных колебаний. При этом они могут оказать существенное влияние на поперечные колебания штанги. Наблюдается нарушение симметрии в прогибах штанги, что означает, возможность появления потери ее устойчивости.

Список литературы

1. Мардонов Б.М., Марданова Л.О. О вынужденных колебаниях звеньев бурильной динамической системы // Поиск-Ізденіс. Серия естественно-технических наук. – Алматы, 2001. – № 1, С. 217-220.
2. Мардонов Б.М., Бараев А.Б. Ахметов Н.М. Прикладные задачи механики бурения нефтегазовых скважин. Шымкент, 2013. – 172 с.
3. Вольмир А.С. Устойчивость упругих систем – М.: Физматгиз, 1963. – 880 с.
4. Барский И.Л., Бредихина Т.В., Генкина И.Н., Чайковская М.А., Шурова Н.Е. Математическое обеспечение для расчета статического изгиба и поперечных колебаний колонн труб в скважинах // Труды ВНИИБТ, вып. 60, 1985. – С. 38-43.
5. Зенкевич О. Метод конечных элементов в технике. – М.: Мир, 1975. – 541 с.
6. Образцов И.Ф., Савельев Л.М., Хазанов Х.С. МКЭ в задачах строительной механики летательных аппаратов. – М.: Высшая школа, 1985. – 392 с.
7. Оден Дж. Конечные элементы в нелинейной механике сплошных сред. – М.: Мир, 1976. – 464 с.
8. Turner M.J., Dill E.H., Martin H.C., Melosh R.J. Large deflection of structure subjected to heating end external loads. J. Aerospace Sce., 1960. – № 27, P. 97-102.
9. Glough R.W. The finite element method un plane tress analysis. J. Struct. Div. ASCE // Proc. 2nd Conf. Electronic Compilation, 1960.
10. Новожилов В.В. Основы нелинейной теории упругости. – М.-Л.: ОГИЗ, 1948. – 211 с.
11. Хаджиева Л.А. Модели нелинейных деформируемых систем. Практическое применение. – Алматы: Казак университеті, 2004. - 64 с.
12. Каудерер Г. Нелинейная механика. – М.: Иностр. лит., 1960. – 832 с.

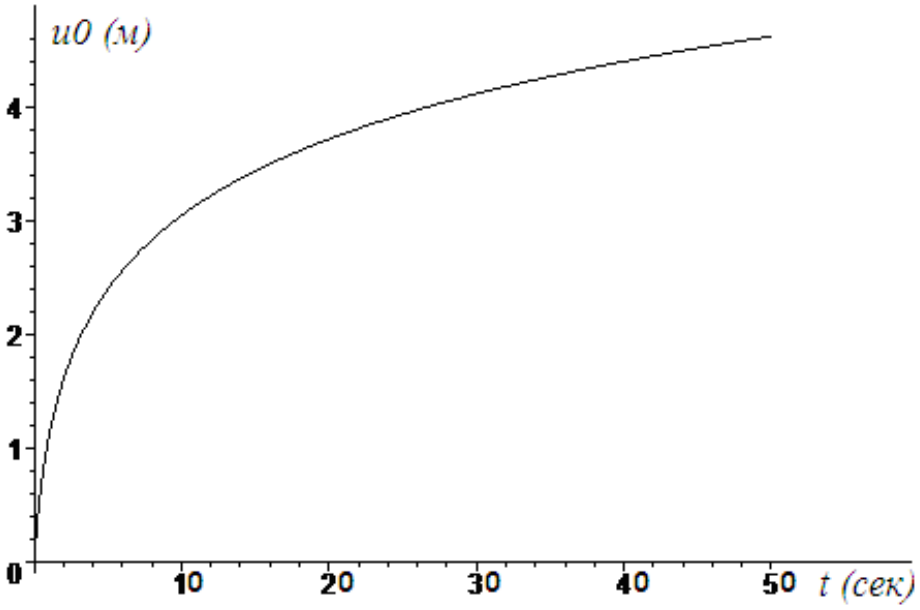

а)

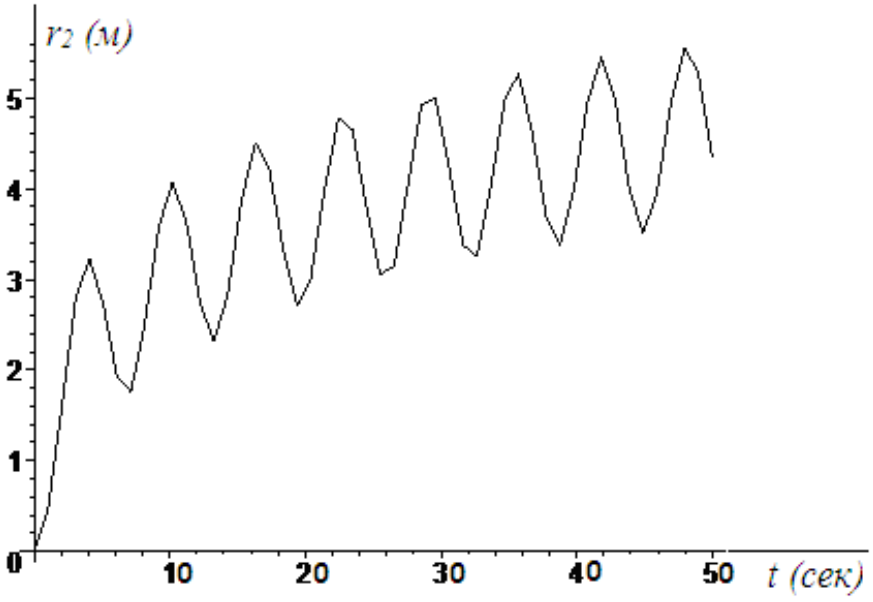

б)

Рис. 1. Зависимости перемещений нижней части колонны $u_0(t)$(м) и сосредоточенной массы $r_2(t)$(м) от времени t(сек).

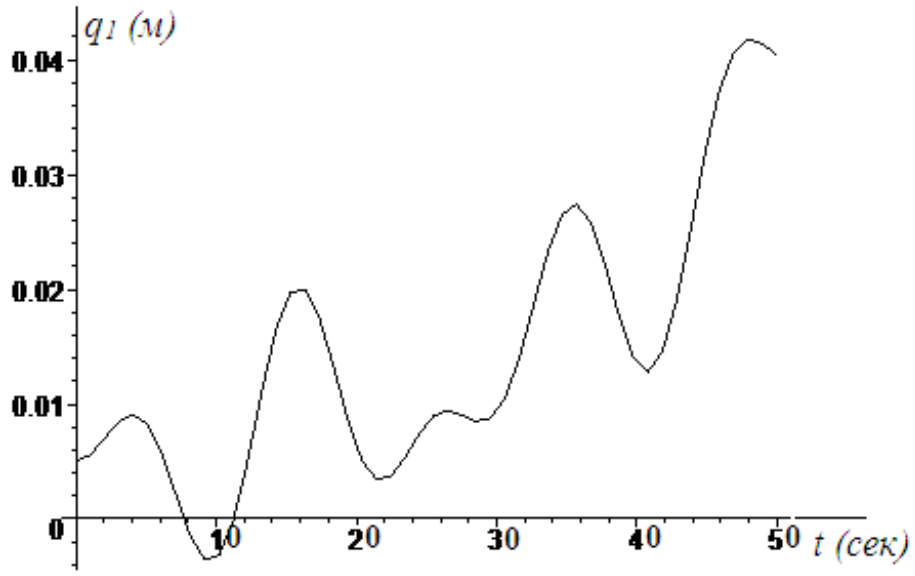

a)

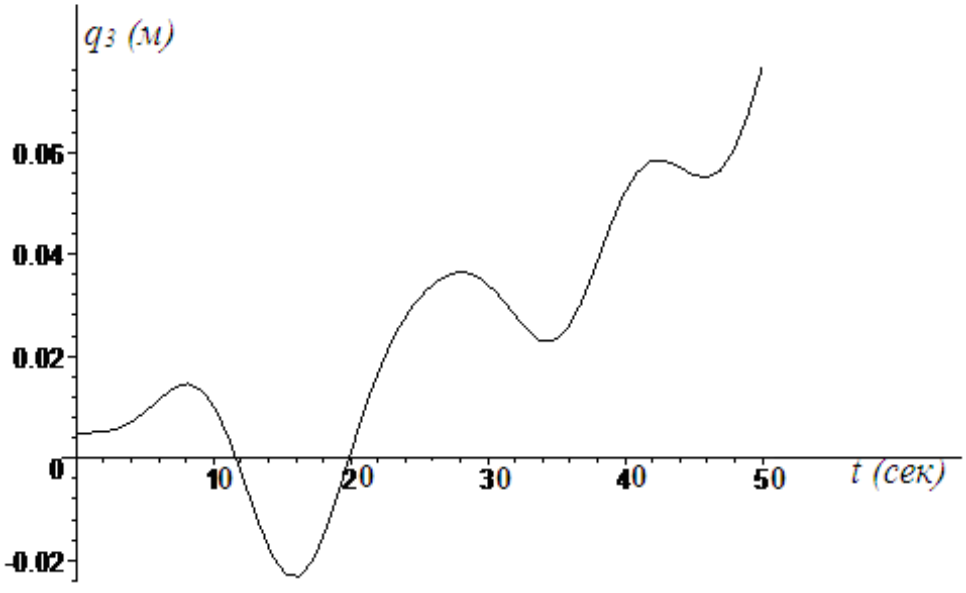

b)

Рис. 2. Зависимости поперечного перемещения узлов сопряжений q_1(м) и q_3(м) от времени t(сек) для различных значений массы m: a) m=0, b) m=40кг.

Комплекс программ NskMCNG для решения задач ядерно-геофизических технологий

А.И. Хисамутдинов[1], Б.В. Банзаров[2] и М.Ш. Урамаев[1]

[1] Институт нефтегазовой геологии им. А.А. Трофимука, Новосибирск, Россия
[2] Новосибирский Государственный Университет, Новосибирск, Россия
KhisamutdinovAI@ipgg.sbras.ru,banzarov@gmail.com,uramaevmsh@gmail.com

Аннотация. В докладе представлена программа NskMCNG, используемая для моделирования процессов распространения нейтронов и гамма-квантов в горных породах и системах типа «скважина-пласт», а также для моделирования показаний приборов ядерного каротажа. NskMCNG построена на основе моделей, привлекающих наиболее простые модели взаимодействий частиц со средой – аналитические индикатрисы и групповые сечения взаимодействий. За счет этого программа обладает высоким быстродействием и простотой кода. Это позволяет использовать программу для разработки методов и алгоритмов Монте-Карло для решения прямых задач, и алгоритмы для решения обратных задач. Верификация пакета проводилась различными способами, в том числе сравнениями с опубликованными данными, а также с помощью сравнительных расчетов проведенных программой Geant4. В докладе представлено описание комплекса программ, результаты верификационных вычислений, а также приведены некоторые задачи, которые решались с использованием данного комплекса.

Ключевые слова: Ядерная геофизика, методы Монте-Карло, программные комплексы, моделирование.

1 Введение

Моделирование распространения нейтронов и гамма-квантов востребовано при решении многих задач, связанных с методами ядерного каротажа. Среди основных можно выделить задачи: о распространении частиц в горных породах , о получении и уточнении принципиальных закономерностей; о выборе оптимальных параметров конструкций приборов; о восстановлении параметров горных пород по данным измерений. Для решения подобных задач требуются корректные постановки,численные методы, алгоритмы и программы. Востребованными и адекватными методами численного решения прямых задач уравнения переноса, включая и распространение нейтронов и гамма-квантов в условиях геофизического исследования скважин, являются в настоящее время методы Монте-Карло [1,2,3]. В различных странах, организациях, проектах и т.д. используется множество разнообразных вычислительных программ, алгоритмов и методов. Некоторые из них получили широкое распространение, например, комплексы MCNP и Geant4 [6,5]. Эти пакеты разработаны для наиболее точного моделирования процесса распространения частиц, и для этого они используют самые подробные системы ядерных констант, существующие на данный момент. Это позволяет получать с их помощью максимально возомжное соответствие с экспериментальными данными, что важно при анализе свойств конструкций новых приборов. При этом нет причин считать, что другие программы не нужны. В условиях, когда классы задач очень разнообразны, когда различны профессиональные уровни исполнителей, когда развиваются методы и алгоритмы, естественным является наличие некоторого количества независимых вычислительных программ. Например, когда не требуются очень детальные физические модели, но требуется гибкость и быстродействие, использование MCNP или Geant4 не будет эффективным из-за их сложности и трудоемкости. Говоря о гибкости,

мы подразумеваем возможность изменения кода программы для каких-то целей, нужных пользователям. Например, это необходимо при разработке новых алгоритмов Монте-Карло. Говоря о быстродействии, мы говорим о количестве траекторий, моделируемых и обрабатываемых программой за единицу времени. Высокое быстродействие позволяет использовать программу в алгоритмах для решения обратных задач. В 1965 году один из авторов настоящей программы разработал программу по моделированию задачи о гамма-гамма каротаже и провел численное решение. Позднее с участием также других авторов рассматривались численные решения и других задач ядерно-геофизических технологий. Постепенно формировался фонд алгоритмов и программ, относящихся к моделированию процессов переноса частиц в условиях ядерно-геофизических технологий. На базе этого фонда была разработана программа NskMCNG.

NskMCNG была разработана авторами в первую очередь для решения задач о принципиальных и важных закономерностях. Она также активно использовалась в связи с развитием методов Монте-Карло и методов решения обратных задач. Для этого не требовалось введения сложных геометрических и физических моделей. При ее разработке был использован некоторый минимум, позволяющий получать результаты, хорошо согласующиеся с экспериментальными закономерностями и близкие к результатам, полученным другими комплексами, но при этом NskMCNG обладает простым кодом и позволяет проводить быстрые расчеты. Простота кода позволяет использовать любые алгоритмы Монте-Карло, использующие как весовые оценки, так и оценки более широкого класса; например, - способа математических ожиданий. Быстродействие позволяет использовать NskMCNG для решения обратных задач о восстановлении параметров среды. То есть, программа обладает необходимой гибкостью и быстродействием, чтобы ее использование было более выгодно по сравнению с MCNP или Geant4 для определенного класса задач. Для NskMCNG получено свидетельство о государственной регистрации [4].

2 Структура программы

Комплекс NSKMCNG позволяет моделировать перенос частиц двух видов – нейтронов и гамма-квантов. Это делает возможным моделирование любого из методов ядерно-физического исследования скважин – ГГК, ННК, ИНГК, и пр. Геометрические возможности программы ограничены конфигурацией, состоящей из вложенных друг в друга цилиндрических объемов. Это позволяет с достаточной точностью воспроизводить скважинную геометрию, но при этом алгоритм розыгрыша длины пробега частиц имеет простой вид и не обладает высокой трудоемкостью. Физические свойства переноса в основном определяются взаимодействиями частиц с атомами среды. Для моделирования взаимодействий частиц со средой программа обеспечена набором групповых сечений для нейтронов с энергиями в отрезке [0, 14.1] МэВ [7] и набором точечных сечений для гамма-квантов в отрезке [0.03, 10] МэВ [8]. Для нейтронов используются две модели взаимодействий с атомами для разных энергетических диапазонов [1]. Для нейтронов с энергиями выше 0.215 эВ предусмотрено два типа рассеяния – упругое и неупругое. Упругое взаимодействие реализовано моделью взаимодействия упругих сфер с изотропным рассеянием в системе центра масс. Неупругое взаимодействие реализовано аналогичной моделью с изотропным рассеянием в лабораторной системе. Для энергий ниже 0.215 эВ используется диффузионная модель, реализованная односкоростным переносом с энергией 0.0252 эВ. Данная модель является вполне достаточной для исследования задач нейтрон-нейтронного каротажа. Для гамма-квантов рассматривается модель взаимодействия, использующая комптоновское рассеяние и фотопоглощение[1]. Данная модель приемлема для работы с задачами плотностного

гамма-гамма каротажа. Для корректного моделирования переноса гамма-квантов с энергиями выше 1.022 МэВ необходимо подключать процессы образования электрон-позитронных пар. Блок, реализующий оценки Монте-Карло, состоит из нескольких процедур, позволяющих вычислять функционалы от потока частиц, сосредоточенных на разных подмножествах фазового пространства. Доступно вычисление следующих функционалов – среднее по плоскому кольцу, среднее по цилиндрическому кольцу, и среднее по цилиндру. При вычислении средних используются различные весовые функции, в зависимости от которых вычисляемые средние значения являются либо средними потоками, либо средним количеством соударений, либо средним количеством поглощений.

3 Верификация программы

3.1 Перенос нейтронов

Модели, выбранные для описания переноса нейтронов, были подобраны таким образом, чтобы программа была пригодна не только для абстрактного изучения задач переноса, но также чтобы можно было рассчитывать зависимости, характер поведения которых близок к реальным. В данном параграфе мы приводим сравнительные эксперименты, демонстрирующие возможности программы. Верификацию моделирования нейтронного переноса рассмотрим на примере двух задач. В первой задаче мы вычислим временное распределение поглощений нейтронов в однородных средах и сравним его с табличными данными. Во второй задаче мы вычислим пространственное распределение тепловых нейтронов от источников разных энергий в однородных средах. Затем мы сравним их с данными, вычисленными программой Geant4.

В первой задаче рассмотрим однородную среду с известным составом и точечным источником, испускающим нейтроны с энергией 0.0252 эВ. На рис. 1 представлена зависимость частоты поглощений нейтронов от времени в чистой воде. Дял построенной зависимости вычислено экспоненциальное приближение (тренд), по показателю которого определяется среднее время жизни нейтронов в среде. Для чистой воды время жизни составляет 205 микросекунд. Аналогично были вычислены средние времена жизни в основных типах сред – песчанике, известняке с нулевой пористостью и известняке с 20%-й пористостью с порами, заполненными водой. Полученные значения представлены на табл. 1. В средней колонке находятся вычисленные данные. В правой колонке этой таблицы приведены средние времена жизни, опубликованные в [9]. Как видно, для этой задачи мы получаем высокое согласие вычисленных и табличных данных.

Таблица 1. Время жизни тепловых нейтронов в основных типах сред

Среда	Время жизни (числ.)	Время жизни (табл.)
Вода	205	206
Песчаник	1054	1086
Известняк 0%	633	643
Известняк 20%	448	452

Во второй задаче оцениваются пространственные распределения тепловых нейтронов. Рассматривался однородный песчаник с точечным источником с энергиями 0.0252 эВ, 1 МэВ и 4 МэВ. Вычислялись потоки нейтронов в точках на заданных расстояниях от источника. На рис. 2 представлены зависимости потока от расстояния для энергии источника

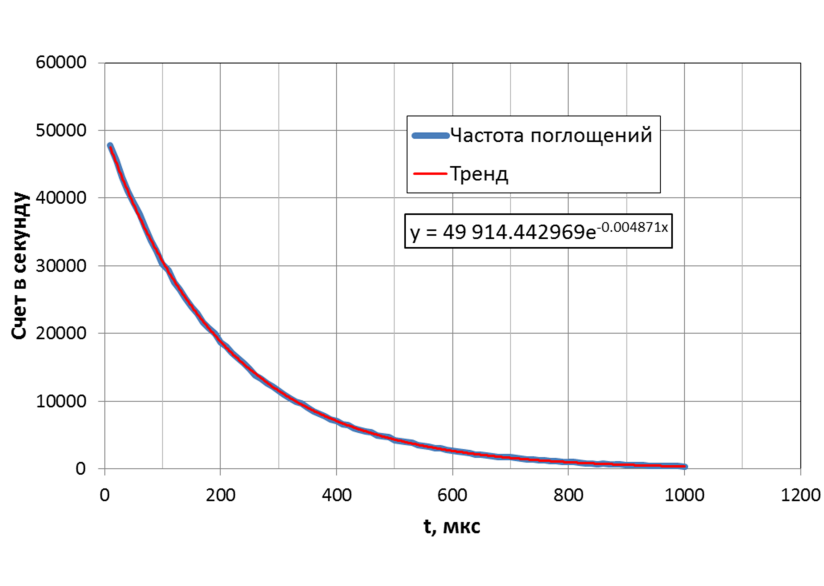

Рис. 1. Частота поглощений тепловых нейтронов в чистой воде.

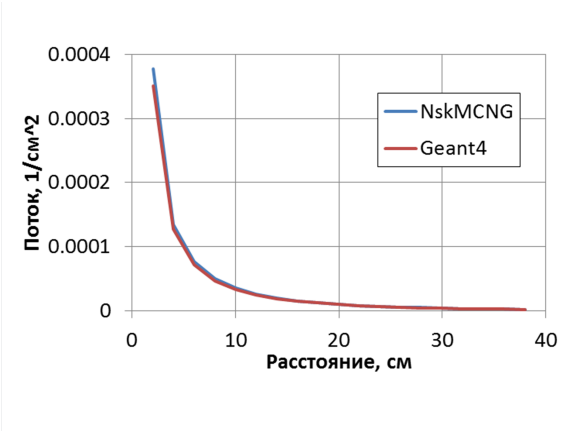

Рис. 2. Пространственное распределение тепловых нейтронов от источника 0.4 эВ

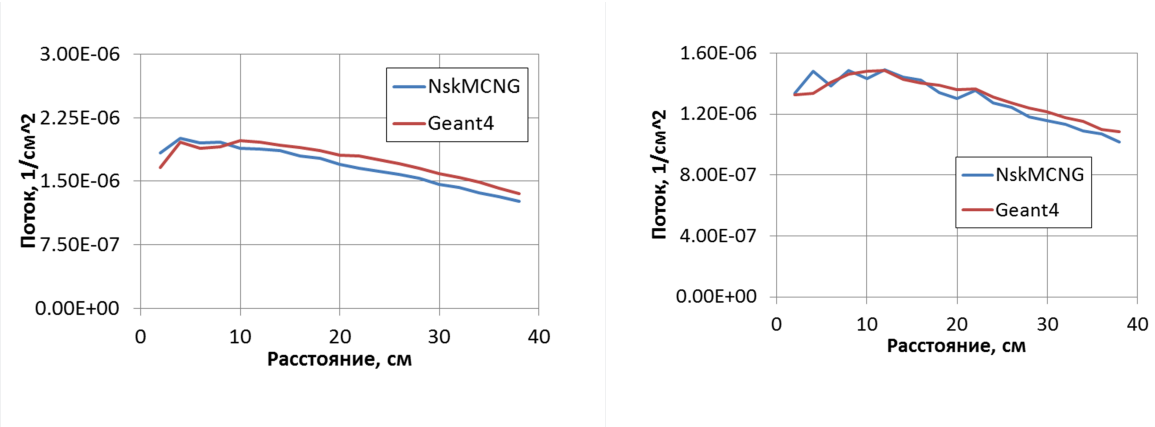

Рис. 3. Пространственное распределение тепловых нейтронов от источников высоких энергий. Левый график соответствует энергии источника 1 МэВ; правый график соответствует энергии источника 4 МэВ

0.0252 эВ. Сравнивались данные, полученные NskMCNG и Geant4. Из этого эксперимента и предыдущей задачи следует, что моделирование процесса диффузии тепловых нейтронов осуществляется с очень хорошим согласием с данными Geant4.

Рассмотрим теперь пространственное распределение нейтронов от источников с энергиями 1 и 4 МэВ. Построенные зависимости представлены на рис. 3. Сравнение NskMCNG и Geant4 демонстрирует, что характеры зависимостей соответствуют друг другу, и при этом кривые достаточно близки друг к другу.

Проводя эти сравнительные тесты, мы оценивали возможность использования NskMCNG при изучении задачи о нейтрон-нейтронном каротаже с источником Am-Be. Данный источник имеет широкий энергетический спектр, однако его средняя энергия близка к 4 МэВ. Результаты теста демонстрируют, что в рамках этой задачи моделирование процесса замедления и поглощения нейтронов проводится достаточно близко к тому, как это делается с Geant4.

3.2 Перенос гамма-квантов

Для верификации процесса моделирования распространения гамма-квантов в среде было рассмотрено две задачи – энергетическая и пространственная. Первая – анализ спектра гамма-квантов для изотропного моноэнергетического источника (662 кэВ), расположенного в однородной бесконечной среде (рис. 4). Вторая – анализ числа пересечений гамма-квантами концентрических сфер, расположенных вокруг изотропного источника рис. (5). Данные, полученные с NskMCNG были сравнены с данными Geant4. Из представленных графиков видно, что результаты моделирования совпадают с хорошей точностью в пределах погрешности метода Монте-Карло. В результате сравнения можно сделать вывод, что расчеты переноса гамма-квантов с NskMCNG для энергий ниже 662 кэВ не уступают в точности расчетам для Geant4. Таким образом, исследование задач, связанных с ГГК, можно осуществлять используя программу NckMCNG.

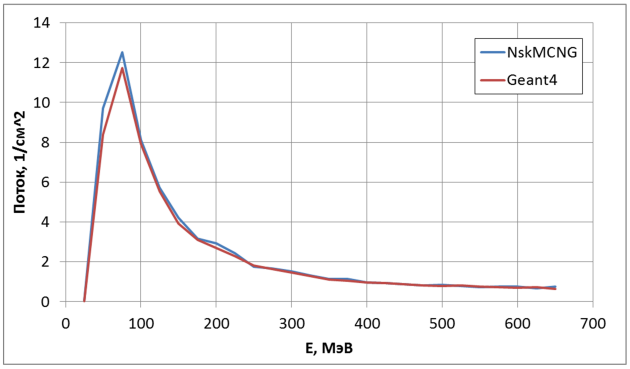

Рис. 4. Энергетическое распределение гамма-квантов в воде, вычисленное программами NskMCNG и Geant4

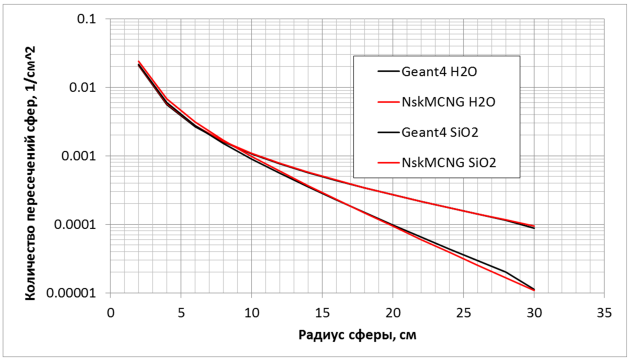

Рис. 5. Пространственное распределение гамма-квантов в воде и песчанике, вычисленное программами NskMCNG и Geant4.

4 Применение программы и ее развитие

Как было отмечено ранее, программа используется для решения трех различных типов задач. Во-первых, она является удобным инструментом для развития численных методов Монте-Карло для вычисления функционалов от решения уравнения переноса. В работе [10] построены алгоритмы способа математических ожиданий для вычисления средних от потоков нейтронов и гамма-квантов. Интегральные уравнения, соответствующие рассмотренной физической модели, имеют достаточно простой вид, что позволяло иметь дело с достаточно простыми конструкциями при работе с итерациями ядер уравнений.

Далее программа использовалась при изучении методов решения обратных задач о восстановлении параметров среды по данным различных видов каротажа. Среди подобных работ можно назвать [11] и [12]. В первой работе исследовался метод восстановления пористости по данным нейтрон-нейтронного каротажа, а во второй работе исследовался метод восстановления плотности по данным гамма-гамма каротажа. Оба метода основаны на итерационной процедуре, каждая итерация которой представляла собой решение прямой задачи. Здесь было особенно важно быстродействие программы, поскольку итерационные процессы составляли до десяти циклов, что было бы весьма трудоемко при использовании пакетов типа Geant4 или MCNP. В свою очередь в предыдущей главе было показано, что качество решения прямой задачи достаточно высоко, чтобы использовать программу для прямого моделирования.

Также NskMCNG применялась на ранних этапах для одного исследования неприжимного прибора плотностного гамма-гамма каротажа, см. работу [13]. Преимуществом NskMCNG перед Geant4 являлось ее быстродействие. Временные затраты на расчет одной траектории гамма-кванта у программы NskMCNG занимает в среднем 0,025 миллисекунд, что почти в 10 раз быстрее, чем у Geant4. По этой причине использование NskMCNG является выгодным при исследовании фундаментальных зависимостей, когда не требуется воспроизведение сложных геометрий среды и прибора. Разумный выбор программы для моделирования в зависимости от поставленной задачи позволяет добиваться оптимальных результатов.

Вместе с использованием программы непрерывно ведется процесс ее улучшения в тех областях, где она либо плохо согласуется с данными экспериментов, либо не имеет соответствующей функциональности. В первую очередь требуется корректный учет неупругих

взаимодействий нейтронов с атомами среды. Во-вторых, необходима подходящая модель, описывающая рождение гамма-квантов неупругого рассеяния и гамма-квантов радиационного захвата. В-третьих, необходимо подключение процессов образования пар при поглощении гамма-квантов. Это позволит проводить моделирование для проблем с импульсным источником с энергией 14.1 МэВ.

5 Заключение

В данной работе представлена программа NSKMCNG, разработанная для решения задач ядерной геофизики. Программу можно легко использовать при исследовании задач, связанных с построением методов для вычисления распределений нейтронов и гамма-квантов, а также с построением алгоритмов решения обратных задач для восстановления параметров сред по измерениям приборов ядерного каротажа. Для того, чтобы программу можно было легко использовать, были рассмотрены значительно упрощенные модели взаимодействия частиц с атомами среды (по сравнению с моделями, рассмотренными в MCNP или Geant4). Допущенные упрощения позволили, во-первых, упростить вид ядер рассеяния в уравнении переноса, что важно при разработке методов для его решения. Во-вторых, это значительно улучшает быстродействие, что важно при решении обратных задач, алгоритм которых требует решение прямых задач. Чтобы понять, насколько сильно упрощения изменяют решение по сравнению с полными моделями, был проведен ряд тестов, где сравнивались данные, полученные программой NskMCNG, с данными, полученными программой Geant4. Результаты сравнений продемонстрировали, что достигается достаточное согласие данных, чтобы считать допущенные упрощения корректными. Программа была использована в нескольких работах. Ее использовали для разработки методов Монте-Карло для вычисления средних по различным областям потоков, для разработки методов решения обратных задач, а также для исследования конструкции прибора литоплотностного каротажа. Опыт использования программы NskMCNG позволяет утверждать, что она имеет свою область эффективного применения, и что нужно продолжать ее развитие.

Список литературы

1. Хисамутдинов А. И., Стариков В. Н., Морозов А. А. Алгоритмы Монте-Карло в ядерной геофизике. Новосибирск: Наука, 1985, 158 с.
2. Алексеев Ф.А., Головацкая И.В., Гулин Ю.А. и др. Ядерная геофизика при исследовании нефтяных месторождений. М., Недра, 1978. 359с.
3. Резванов Р.А. Радиоактивные и другие неэлектрические методы исследования скважин.М., Недра, 1982, 368 с.
4. Банзаров Б.В., Хисамутдинов А.И. Novosibirsk Monte Carlo methods for Nuclear Geophysics problems, Свидетельство о государственной регистрации программы для ЭВМ №2010615224
5. Agostinelli S. et al. Geant4: a simulation toolkit // NIM A, 2003, vol. 506, pp. 250-303.
6. X-5 Monte Carlo Team. MCNP – A Monte Carlo N-particle Transport Code, Version 5. Los Alamos National Laboratory, 2003.
7. Абагян Л. П., Базазянц Н. О., Бондаренко И. И., Николаев М. Н. Групповые константы для расчетов ядерных реакторов. Москва, Атомиздат, 1964, 140 с.
8. Berger, M. J.; Hubbell, J. H.; Seltzer, S. M.; Coursey, J. S.; Zucker, D.S. XCOM: Photon Cross Sections Database (http://physics.nist. gov/). U.S. Secretary of Commerce, National Institute of Standards and Technology, 1998.
9. Ellis D., Singer J., Well Logging For Earth Scientists, 2007, Springer, 708 p.
10. Хисамутдинов А.И., Банзаров Б.В. Неимитационные оценки и улучшение способов математических ожиданий при статистическом моделировании переноса частиц // Вычислительные технологии. 2012. Т. 17. № 2. С. 99-114

11. Хисамутдинов А.И., Шишенина Э.А. Последовательные приближения по характерным взаимодействиям при восстановлении пористости по данным измерений нейтрон-нейтронного каротажа: Препринт // ИНГГ СО РАН – Новосибирск, 2010, 15 с.
12. Хисамутдинов А.И., Пахотина Ю.А. О компьютерном восстановлении плотности формации по данным измерений гамма-гамма метода: Препринт // ИНГГ СО РАН – Новосибирск, 2013, 21 с.
13. Урамаев М. Ш., Власов А. А. Моделирование неприжимного прибора ГГКП в метрологических образцах // Недропользование. Горное дело. Новые направления и технологии поиска, разведки и разработки месторождений полезных ископаемых: Материалы X Международного научного конгресса «ГЕО-Сибирь-2014»

Прогнозирование течения вокруг сооружения методом контрольных объемов

А.Ж. Жайнаков[1], А.Ы. Курбаналиев[2] и А.К. Калеева[2]

[1] Институт горного дела и горных технологий им. У. И. Асаналиева Кыргызского государственного технического университета им. И. Разакова, Бишкек, Кыргызстан
[2] Кызыл-Кийский гуманитарно-педагогический институт Баткенского государственного университета, г. Кызыл-Кия, Кыргызстан
jainakov-41@mail.ru,kurbanaliev@rambler.ru,Kaleeva79@mail.ru

Аннотация. В работе представлены результаты математического прогнозирования особенностей обтекания одиночной модели сооружения гексаэдральной формы воздушным потоком. Численное моделирование основано на усредненных по Рейнольдсу стационарных трёхмерных уравнениях Навье-Стокса. Для учета влияния турбулентных пульсаций на средние характеристики поля течения использовались двухпараметрические RANS модели турбулентности, основанные на гипотезе линейной и нелинейной вихревой вязкости. Проведено сравнение численных результатов с данными Европейского исследовательского сообщества по течению, турбулентности и горения ERCOFTAC и Архитектурного института Японии

Ключевые слова: Отрывные течения, RANS модели, OpenFOAM, метод контрольных объемов

1 Введение

Отрывные течения - одно из самых значимых явлений, наблюдаемых при вязком обтекании тел различных форм. Из-за имеющейся в среде вязкости кинетическая энергия потока около тела частично рассеивается так, что частицы жидкости не могут больше полностью противостоять существующему положительному градиенту давления и поток отрывается в поперечном направлении. Следовательно, в случае молекулярной природы механизма отрыва, отрыв потока происходит под действием положительного градиента давления и под влиянием ламинарных или турбулентных вязких напряжений. Таким образом, наличие вязкого трения приводит как к появлению сопротивления трения около обтекаемого тела, так и к возникновению локальных вращений в поле течения. Изменение пространственной структуры течения оказывает обратное действие на сам отрыв, которое проявляется в изменении подъемной силы и сопротивления тела. Поэтому исследование отрывных течений, с одной стороны, имеет большое практическое значение, а, с другой стороны важно для понимания основных проблем физики течения. При обтекании реальных пространственных тел, как правило, возникают трехмерные и нестационарные формы отрыва, изучение которых и представляет существенный интерес. Учитывая высокую стоимость лабораторных экспериментов, множество дополнительных осложняющих исследование факторов, влияющих на конфигурацию течения (неоднородность набегающего потока, шероховатость поверхности и т. д.), а также продолжающиеся положительные тенденции в развитии многопроцессорной вычислительной техники (повышение производительности и увеличение памяти) можно надеяться на расширение и углубление наших знаний об отрывных течениях путем численного решения трехмерных уравнений гидродинамики. Численное моделирование аэродинамических характеристик различных зданий и сооружений является достаточно трудоемкой задачей из-за сложной геометрической формы, а также из-за сложного

нестационарного течения, образующегося в результате их обтекания. При этом сложность обтекания предполагает выполнение не единичного, а целого ряда расчетов. Интерференция же спектра различных вихревых структур и масштабов между различными объектами еще более усложняет поставленную задачу. Поэтому точное моделирование предполагает использование эффективного, хорошо апробированного и верифицированного математического аппарата вычислительной гидродинамики с использованием высокопроизводительной вычислительной техники.

В данной работе приведены результаты численного моделирования обтекания воздушным потоком одиночной призматической модели сооружения с помощью открытого пакета OpenFOAM2.3[1], использующий метод контрольных объемов для дискретизации основных уравнений. Открытость исходного кода данного пакета предоставляет широкие возможности по изучению и доработке реализованных в нем математических моделей, методов решения систем линейных алгебраических уравнений, численных методов решения дифференциальных уравнений в частных производных методом контрольного объема.

2 Математическая модель

При отсутствии массовых сил, стационарное турбулентное течение несжимаемой жидкости описывается следующими усредненных по Рейнольдсу уравнениями Навье-Стокса[2, с. 294]:

$$\frac{\partial u_i}{\partial x_i} = 0, \frac{\partial u_i u_j}{\partial x_j} = -\frac{\partial p}{\partial x_i} + \frac{\partial}{\partial x_j}\Big(v\frac{\partial u_i}{\partial x_j} - \overline{u_i' u_j'}\Big)$$

Здесь u_i и u_i' - средняя и флуктуационная скорости в направлении оси x_i соответственно, p давление, v и ρ- кинематическая вязкость и плотность жидкости соответственно, а $\overline{u_i' u_j'}$- напряжения Рейнольдса, требующие моделирования.

Многие из моделей турбулентности, используемые на практике, основаны на понятиях турбулентной вязкости и турбулентной диффузии. Для течений общего вида, введенная Буссинеском турбулентная вязкость, связывающая напряжения Рейнольдса с градиентами осредненного течения, может быть записана в следующей форме [2, с. 294]:
$-\rho\overline{u_i' u_j'} = \mu_i\Big(\frac{\partial \overline{u_i}}{\partial x_j} + \frac{\partial \overline{u_j}}{\partial x_i}\Big) - \frac{2}{3}\rho\delta_{ij}k$, где μ_t−турбулентная динамическая вязкость, а кинетическая энергия турбулентности на единицу массы определяется как $k = \frac{1}{2}\big(\overline{u'^2} + \overline{v'^2} + \overline{w'^2}\big)$. Учет влияния турбулентных пульсаций на характеристики среднего течения производится на основе классических RANS-моделей турбулентности[3, с.66].

3 Численная модель

Расчетная область имела размеры 21bx13.75bx11.25b в направлениях осей x, y и z соответственно. Дискретизация расчетной области получается методом контрольного объема, который обеспечивает строгое соблюдение законов сохранения, и основные понятия метода напрямую соответствуют физическим таким величинам, как массовый расход, поток и т.д. [4, с. 24]. Расчетную область разбивают на некоторое конечное число непересекающихся гексаэдрических контрольных объемов таким образом, что каждая узловая точка содержится в одном контрольном объеме. Расчетная сетка (рис. 1) имела 60x45x39 ячеек по направлениям осей x,y и z соответственно.

Далее, дифференциальное уравнение интегрируется по каждому контрольному объему. Для вычисления интегралов используют линейно-кусочные профили, которые описывают изменение искомой величины между узловыми точками. Для дискретизации конвективного

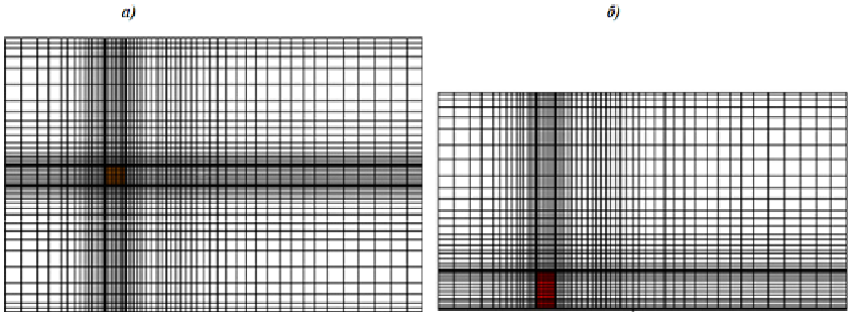

Рис. 1. Расчетная сетка: а) - вид сверху, б) - вид сбоку.

члена в уравнениях для трех компонент скорости, кинетической энергии k и скорости ее диссипации ε использована схема QUICK.

В качестве начальных условий во внутренних узлах расчетной сетки для скорости и давления заданы величины $u = 0$ м/с $p = 0$ Па. Как известно, для стационарного течения нет необходимости задания начальных условий. Однако определение начальных полей скорости и давления в пакете OpenFOAM является обязательным [1]. Кинетическая энергия турбулентности и скорость её диссипации имеют некоторые малые значения, которые обеспечивают хорошую сходимость численного решения на первых шагах интегрирования.

Входные граничные условия по возможности выбраны из экспериментальных данных. На выходе из канала продольные градиенты всех искомых переменных полагаются равными нулю. Гидродинамические граничные условия на твердых стенках канала для турбулентных величин ставились при помощи аппарата пристеночных функций, позволяющих снести граничные условия непосредственно со стенок в первый от стенки сеточный узел [2, с. 298].

Численное решение систем нелинейных уравнений проведено с помощью приложения simpleFoam пакета OpenFOAM, которое предназначено для стационарных турбулентных течений и использует известный алгоритм сопряжения скорости и давления SIMPLE[4, с. 84]. Для повышения устойчивости итерационного метода решения взаимосвязанных и нелинейных алгебраических уравнений, использовались следующие коэффициенты нижней релаксации 0,7 для U, k, ε, ω и 0,3 для p. Относительная ошибка сходимости итераций для всех рассматриваемых переменных была равной $\varepsilon = 10^{-4}$.

4 Результаты численных расчетов

Первой тестовой задачей является моделирование обтекания куба, расположенного в центре трехмерного канала [5, case 41]. Модель здания является куб, монтированный в центр нижней стенки канала с размером $390 \times 60 \times 5$ см. Куб с линейным размером $H = 2,5$см расположен на расстоянии 52H от входа канала, что обеспечивает развитое турбулентное течение в сечении $x = -5H$ вверх по потоку от препятствия. Число Рейнольдса, рассчитанное через высоту куба равно $8 \cdot 10^4$. Принятая система координат показана на рис. 2. Начало координат расположено в центре нижней грани подветренной стороны куба.

Сравнение результатов численных данных с соответствующими экспериментальными данными в сечении $x/H = 2$ приведено на рис. 3, где маркеры соответствуют экспериментальным данным ERCOFTAC[5, case 41], а сплошная линия представляет численные данные этой работы. Величины продольной (рис. 3а) и поперечной (рис. 3б) представлены в единицах средней входной скорости u_0 . Соответствие между расчетом и экспериментом

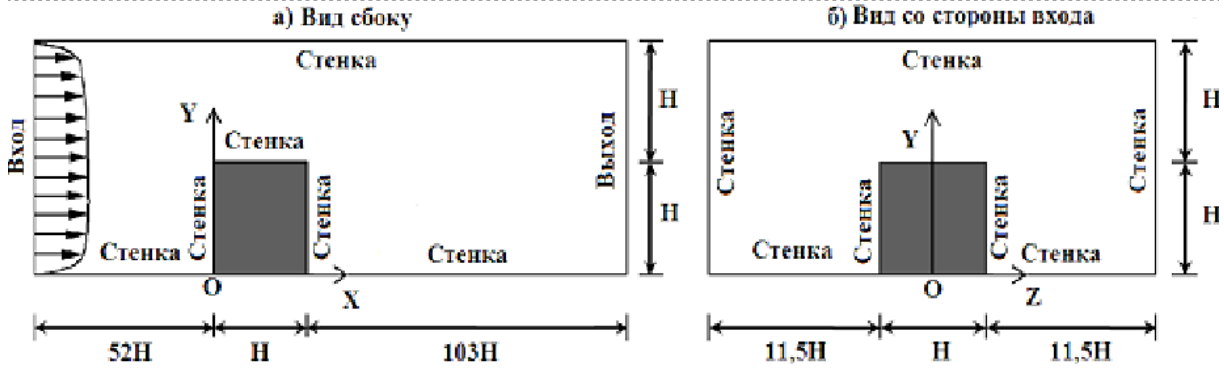

Рис. 2. Геометрия задачи и граничная условия.

следует признать удовлетворительным. На рис. 3 приведены линии тока продольной скорости в плоскости, перпендикулярной к оси y (при y=0). Видно, что численный расчет с приемлемой точностью воспроизводит три основные зоны обратных токов - перед кубом, за ним и над ним. Однако имеются некоторые отличия между численными и экспериментальными данными по длине рециркуляционных зон: размер зоны перед кубом занижен, а за кубом наоборот завышен.

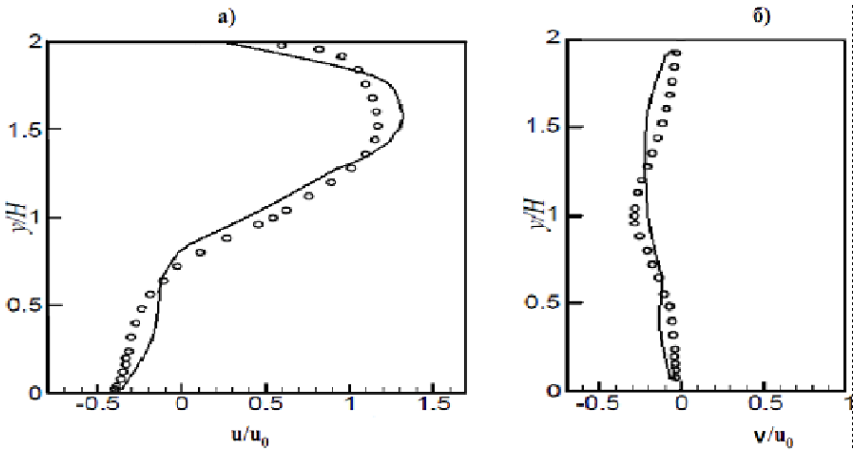

Рис. 3. Поперечные профили скорости.

5 Вторая тестовая задача

Второй тестовой задачей является моделирование обтекания призматической модели высотного здания[6, case A] с квадратным основанием. Начало координат расположено в центре нижней грани призмы высотой $h = 2b$, где $b = 0,08$ м - размер основания призмы (рис. 5).

Входные граничные профили x - компоненты скорости и кинетической энергии турбулентности представлены на рис. 6. Диссипация кинетической энергии турбулентности аппроксимирована при помощи формулы $\varepsilon = \sqrt{C_\mu} k \frac{du}{dz}$ в предположении, что генерация кинетической энергии турбулентности равна скорости её диссипации. Число Рейнольдса Re

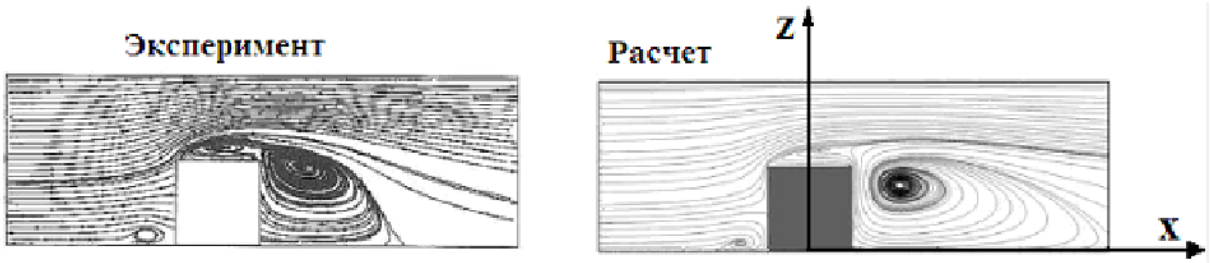

Рис. 4. Линии тока продольной скорости.

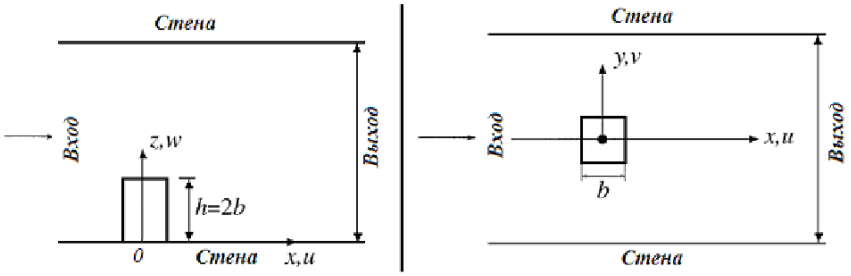

Рис. 5. Схема задачи без сохранения геометрической пропорции.

рассчитанное через высоту здания h и значение входной скорости u_0 при $z = h$ было равно 24000.

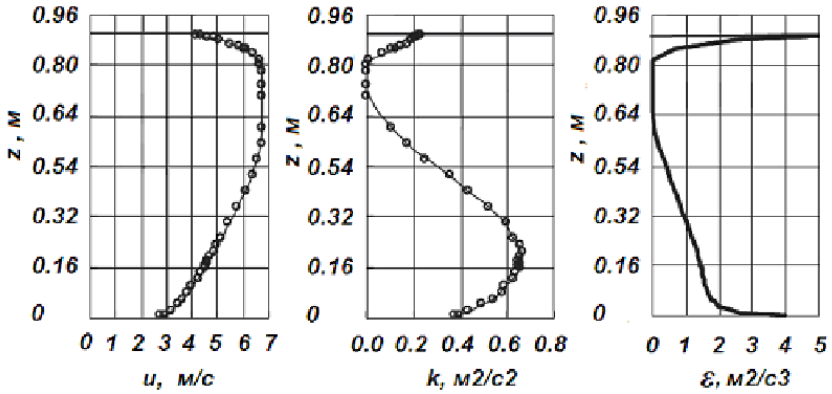

Рис. 6. Распределения входных условий для u, k и ϵ.

На рис. 7-9 представлено сравнение численных результатов с соответствующими экспериментальными данными по вертикальным профилям компонеты скорости при различных значениях координаты x. Практически все рассмотренные модели турбулентности дают приемлемые результаты. Однако имеются небольшие отличия между экспериментом и данными моделей $k - \omega$ и $k - \omega SST$ в области рециркуляционных течений.

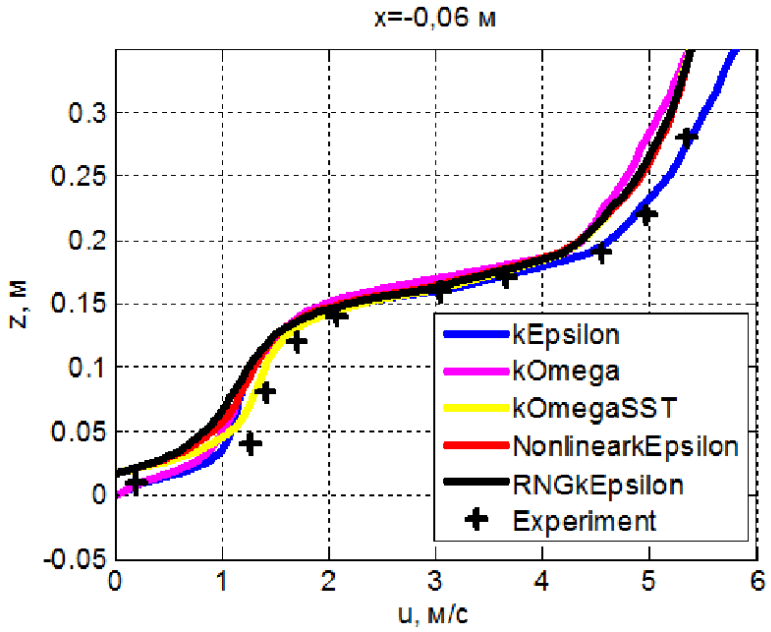

Рис. 7. Вертикальные профили скорости u при $x = -0,06$м.

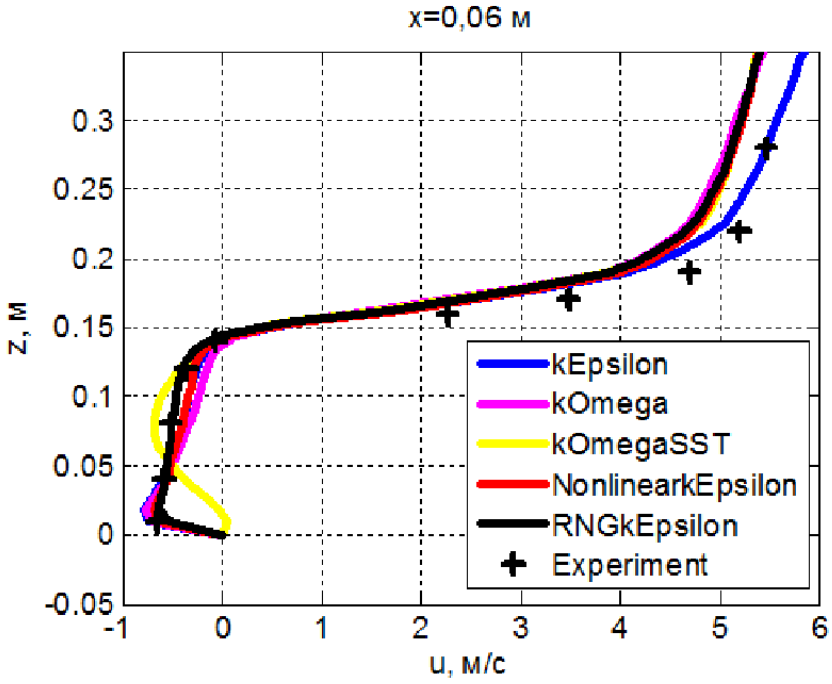

Рис. 8. Вертикальные профили скорости u при $x = 0,06$м.

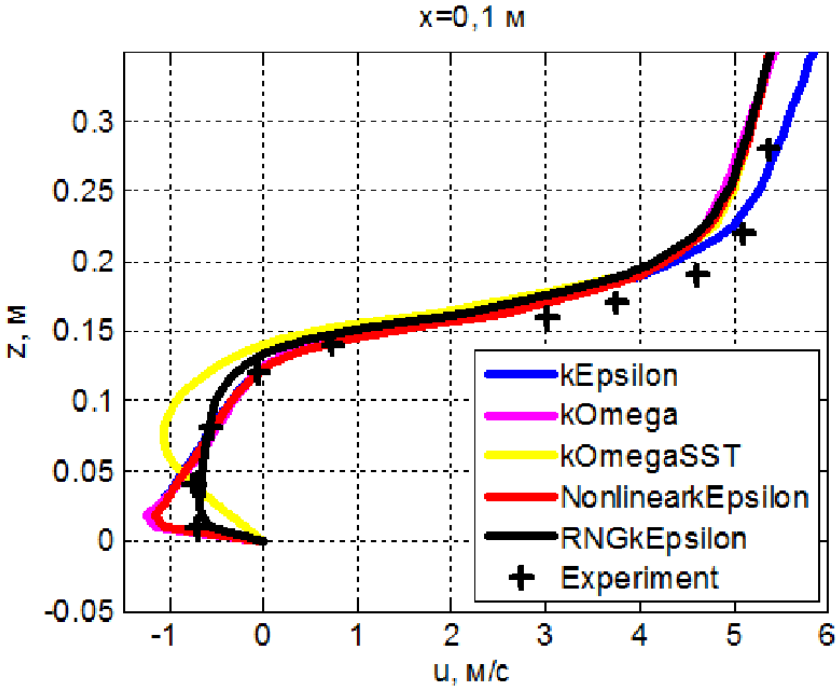

Рис. 9. Вертикальные профили скорости u при $x = 0,1$м.

6 Заключение

В целом, точность предсказания поля скорости вблизи призматической модели одиночного здания является удовлетворительной. Численные расчеты, полученные при помощи различных двухпараметрических моделей турбулентности адекватно (с небольшими отклонениями) повторяют характер изменения экспериментальных данных.

Список литературы

1. http://www.openfoam.org.OpenFOAM2.3.UserGuide.
2. Ferziger J.H., Peric M. Computational Methods for Fluid Dynamics // Springer Verlag, 2002. 423 p.
3. Versteeg H. K., Malalasekera W. An Introduction to Computational Fluid Dynamics // Edinburg: Pearson Education Limited, 2007.517p.
4. Патанкар С.В. Численные методы решения задач теплообмена и динамики жидкости: Пер. с. англ. -М.: Энергоатомиздат, 1984. - 152с.
5. European Research Community on Flow, Turbulence and Combustion Database. http://cfd.mace.manchester.ac.uk/ercoftac/
6. Guidebook for Practical Applications of CFD to Pedestrian Wind Environment around Buildings. http://www.aij.or.jp/jpn/publish/cfdguide/index_e.htm

К асимптотическому поведению решений нелинейных параболических систем уравнений недивергентного вида

М. Арипов, А.С. Матякубов

Национальный университет Узбекистана им. Мирзо Улугбека, Ташкент, Узбекистан
mirsaidaripov@mail.ru,almasa@list.ru

Аннотация. В данной статье изучается свойства решений нелинейных параболических систем уравнений недивергентного вида

$$\frac{\partial u_i}{\partial t} = u_i^{\gamma_i} \nabla \left(|\nabla u_i|^{\sigma} \nabla u_i \right) + \varepsilon \, u_{3-i}^{q_i} \quad (i = 1, 2) \, .$$

В работе используются: метод нелинейного расщепления, известный ранее для нелинейных параболических уравнений и систем уравнений в дивергентной форме, асимптотическая теория и асимптотические методы, основанная на различных преобразованиях.
Показано, что в зависимости от значения параметров нелинейной среды и размерности пространства возникают разные типы решений. Построены асимптотические представления автомодельных решений нелинейных параболических систем уравнений недивергентного вида, в зависимости от значения входящих в систему числовых параметров, найдены необходимые и достаточные признаки их существования.

Ключевые слова: нелинейные системы параболического типа, недивергентный, автомодельные решения, асимптотика решений.

1 Введение

Рассмотрим в области $Q = \{(t, x) : \ t > 0, \ \ x \in R^N\}$ параболическую систему двух квазилинейных уравнений недивергентного вида

$$\frac{\partial u_i}{\partial t} = u_i^{\gamma_i} \nabla \left(|\nabla u_i|^{\sigma} \nabla u_i \right) + \varepsilon \, u_{3-i}^{q_i} \, , \tag{1}$$

где $\sigma, \ \gamma_i, \ q_i \ (i = 1, 2)$ - положительные вещественные числа, $\varepsilon = \pm 1, \ u_i = u_i \left(t, x \right) \geq 0$ - искомые решения. Члены $\varepsilon \, u_{3-i}^{q_i}$соответствует наличию источников $(\varepsilon = +1)$ или стоков $(\varepsilon = -1)$, мощности которых равны $u_{3-i}^{q_i}$.

Система уравнения (1) описывает многие физические явление [1-9]. В частности, при $\gamma_i = 2, \ \sigma = 0, \ q_i = 3$ для одного уравнения в (1) оно встречается в физике плазмы [2]. Эта проблема возникает в модели резистивной диффузии силу свободной магнитного поля в плазме, удерживаемой между двумя стенами $0 < z < \infty$. Это магнитное поле имеет следующую форму $B_0 \left(\cos \phi, \sin \phi, 0 \right)$, где $\phi = \phi \left(z, t \right), \ B_0 = const.$

В работе [3] исследована задача Коши при $q_i = 0, \ \sigma = 0$, доказано существование единственного вязкого решения, а в работах [4,5] существование и единственность классического решения задача Коши при $\sigma = 0$, исследована в [4], а в [5] изучена свойство blow-up.

В работе [6] исследовано решение системы $(u_i)_t = u_{3-i}^{\gamma_i} \left((u_i)_{xx} + a u_i \right)$ с граничными условиями Дирихле, доказано существование глобального решения, установлены blow-up свойство решения.

В работе [7] исследовано положительные решения вырожденных квазилинейных параболических систем недивергентной форме

$$u_{it} = f_i \left(u_{i+1} \right) \left(\Delta u_i + a_i u_i \right), \ x \in \Omega, \ t > 0, \ i = 1, 2, ..., n-1,$$
$$u_{nt} = f_n \left(u_1 \right) \left(\Delta u_n + a_n u_n \right), \ x \in \Omega, \ t > 0$$

с однородной граничным условием Дирихле и положительным начальным условием. Локальное существование и единственность классического решения доказаны. Показано, когда $\min\{a_1, ..., a_n\} \leq \lambda_1$ (где λ_1 является первое собственное значение $-\Delta$ в Ω с однородным граничным условием Дирихле), то существует глобальная положительная классическая решения, и все положительные классические решения не имеет свойство blow-up.

В работах [8,9] в случае $\gamma_i < 1$, преобразованием $v_i(x,t) = (1-k)^{\frac{1-\gamma_i}{\gamma_i}} u_i^{1-\gamma_i}(x,t)$ система уравнений (1) редуцируется к системе с двойной нелинейностью в дивергентной форме и исследована некоторые свойства.

В настоящей работе построены асимптотические представления автомодельных решений системы (1) при $\varepsilon = -1$, в зависимости от значения числовых параметров, найдены необходимые и достаточные признаки их существования.

2 Асимптотики решений автомодельных системы уравнения (1)

Для построения автомодельных систем предлагается алгоритм нелинейного расщепления [1], для чего решения системы (1) ищется в виде

$$\frac{d\bar{u}_i}{dt} = -\bar{u}_{3-i}^{q_i}, \tag{2}$$

которая имеет решения вида

$$\bar{u}_i(t) = A_i\ (T+t)^{-n_i}, T > 0, \tag{3}$$

где

$$n_i = \frac{1+q_i}{q_1 q_2 - 1}\ , A_i = [n_i]^{-\frac{1}{1-q_1 q_2}}\ [n_{3-i}]^{-\frac{q_i}{1-q_1 q_2}}\ .$$

Здесь функции $\bar{u}_i(t)$- представляют собой "вклады"источников или стоков в решение системы (1).

Введем в (1) преобразование

$$u_i(t,x) = \bar{u}_i(t)\, w_i(\tau, x), \tag{4}$$

где

$$\tau(t) = \begin{cases} A_1^{\gamma_1+\sigma} \frac{(T+t)^{-n_1(\gamma_1+\sigma)+1}}{-n_1(\gamma_1+\sigma)+1}\ , & -n_1(\gamma_1+\sigma)+1 > 0, \\ A_1^{\gamma_1+\sigma} \ln(T+t)\ , & -n_1(\gamma_1+\sigma)+1 = 0, \\ A_1^{\gamma_1+\sigma} \frac{(T+t)^{-n_1(\gamma_1+\sigma)+1}}{n_1(\gamma_1+\sigma)-1}\ , & -n_1(\gamma_1+\sigma)+1 < 0. \end{cases}$$

Тогда относительно w_i получим систему уравнений

$$\frac{\partial w_i}{\partial \tau} = \varphi_i w_i^{\gamma_i} \nabla\left(|\nabla w_i|^{\sigma} \nabla w_i\right) + \psi_i \tau^{-1}\left(w_{3-i}^{q_i} + w_i\right) \tag{5}$$

при $n_1(\gamma_1+\sigma) = n_2(\gamma_2+\sigma)\ , \quad -n_i(\gamma_i+\sigma)+1 > 0,$

$$\frac{\partial w_i}{\partial \tau} = -\varphi_i w_i^{\gamma_i} \nabla\left(|\nabla w_i|^{\sigma} \nabla w_i\right) + \psi_i \tau^{-1}\left(w_{3-i}^{q_i} + w_i\right) \tag{6}$$

при $n_1(\gamma_1+\sigma) = n_2(\gamma_2+\sigma)\ , \quad -n_i(\gamma_i+\sigma)+1 < 0,$

а в случае $-n_i(\gamma_i+\sigma)+1=0$,

$$\frac{\partial w_i}{\partial \tau}=\varphi_i w_i^{\gamma_i}\nabla\left(|\nabla w_i|^{\sigma}\nabla w_i\right)+\psi_i\left(w_{3-i}^{q_i}-w_i\right), \tag{7}$$

где $\varphi_i=A_1^{-(\sigma+\gamma_1)}A_i^{\sigma+\gamma_i}$, $\psi_{\mathrm{i}}=\begin{cases}\frac{n_i}{-n_i(\sigma+\gamma_i)+1}, -n_i(\gamma_i+\sigma)+1\neq 0,\\ -A_1^{-(\sigma+\gamma_1)}n_i, \ -n_i(\gamma_i+\sigma)+1=0 \ \ (i=1,2).\end{cases}$

Полагая далее в (5)–(7)

$$w_i(\tau,x)=f_i(\xi), \tag{8}$$

$$\xi=\begin{cases}x\tau^{-\frac{1}{\sigma+2}}, \quad -n_i(\gamma_i+\sigma)+1\neq 0,\\ \sum_{i=1}^{N}\mu_i x_i-\tau, \ \ -n_i(\gamma_i+\sigma)+1=0 \ \ (i=1,2),\end{cases}$$

где $\xi-$автомодельная переменная, получим автомодельную систему уравнений

$$\frac{1}{\sigma+2}\xi\frac{df_i}{d\xi}+\varphi_i f_i^{\gamma_i}\xi^{1-N}\frac{d}{d\xi}\left(\xi^{N-1}\left|\frac{df_i}{d\xi}\right|^{\sigma}\frac{df_i}{d\xi}\right)+\psi_i\left(f_{3-i}^{q_i}+f_i\right)=0, \tag{9}$$

при $-n_i(\gamma_i+\sigma)+1>0 \quad (i=1,2)$,

$$\frac{1}{\sigma+2}\xi\frac{df_i}{d\xi}-\varphi_i f_i^{\gamma_i}\xi^{1-N}\frac{d}{d\xi}\left(\xi^{N-1}\left|\frac{df_i}{d\xi}\right|^{\sigma}\frac{df_i}{d\xi}\right)+\psi_i\left(f_{3-i}^{q_i}+f_i\right)=0, \tag{10}$$

при $-n_i(\gamma_i+\sigma)+1<0 \ \ (i=1,2)$,

$$\frac{df_i}{d\xi}+\mu\varphi_i f_i^{\gamma_i}\frac{d}{d\xi}\left(\left|\frac{df_i}{d\xi}\right|^{\sigma}\frac{df_i}{d\xi}\right)+\psi_i\left(f_{3-i}^{q_i}-f_i\right)=0, \tag{11}$$

при $-n_i(\gamma_i+\sigma)+1=0 \ \ (i=1,2)$. Здесь $\mu=\left(\sum_{i=1}^{N}\mu_i^2\right)^{\frac{\sigma}{2}+1}$.

Качественные свойства автомодельного систем уравнения (9) для одного уравнения были изучены в работе [10].

Ниже займемся изучением асимптотики решений автомодельных уравнений для системы (9)–(11). Для чего преобразуем исходную систему к относительно легко поддающемуся исследованию виду.

Для получения такой вспомогательной системы уравнений применим к уравнениям (9)–(11) следующее преобразования

$$f_i(\xi)=\overline{f}_i(\xi)y_i(\eta), \quad \eta=-\ln\left(a-b\xi^{\frac{\sigma+2}{\sigma+1}}\right), \tag{12}$$

где $\overline{f_i}(\xi)=\left(a-b\xi^{\frac{\sigma+2}{\sigma+1}}\right)^{\frac{\sigma+1}{\sigma+\gamma_i}}$, $(i=1,2)$, $a>0$, $b>0$, $y_1(\eta)$, $y_2(\eta)$ – искомые функции.

Теперь займемся асимптотикой решений системы уравнений (9)–(11) при $\xi\to\left(\frac{a}{b}\right)^{\frac{\sigma+1}{\sigma+2}}$.

После преобразования (12) системы (9)–(11) примет вид

$$\begin{gathered}y_i^{\gamma_i}\frac{d}{d\eta}\left(\left|\frac{dy_i}{d\eta}+a_{i0}(\eta)y_i\right|^{\sigma}\left(\frac{dy_i}{d\eta}+a_{i0}(\eta)y_i\right)\right)+a_{i2}(\eta)\left(\frac{dy_i}{d\eta}+a_{i0}(\eta)y_i\right)+\\ +a_{i1}(\eta)y_i^{\gamma_i}\left(\left|\frac{dy_i}{d\eta}+a_{i0}(\eta)y_i\right|^{\sigma}\left(\frac{dy_i}{d\eta}+a_{i0}(\eta)y_i\right)\right)+\\ +a_{i3}(\eta)y_{3-i}^{q_i}+a_{i4}(\eta)y_i=0 \quad (i=1,2).\end{gathered} \tag{13}$$

В которой $a_{i0}(\eta)=-\frac{\sigma+1}{\sigma+\gamma_i}$,

$$a_{i1}(\eta)=\begin{cases}\frac{N(\sigma+1)}{\sigma+2}\frac{e^{-\eta}}{a-e^{-\eta}}-\frac{(\sigma+1)(1-\gamma_i)}{\sigma+\gamma_i}, & \text{при } -n_i(\gamma_i+\sigma)+1\neq 0,\\ \frac{(\sigma+1)e^{-\eta}}{(\sigma+2)(a-e^{-\eta})}-\frac{(\sigma+1)(1-\gamma_i)}{\sigma+\gamma_i}, & \text{при } -n_i(\gamma_i+\sigma)+1=0,\end{cases}$$

$$a_{i2}(\eta)=\begin{cases}\frac{1}{\sigma+2}\left(\frac{\sigma+1}{b(\sigma+2)}\right)^{\sigma+1}\varphi_i^{-1}, & \text{при } -n_i(\gamma_i+\sigma)+1>0,\\ -\frac{1}{\sigma+2}\left(\frac{\sigma+1}{b(\sigma+2)}\right)^{\sigma+1}\varphi_i^{-1}, & \text{при } -n_i(\gamma_i+\sigma)+1<0,\\ \left(\frac{\sigma+1}{\sigma+2}\right)^{\sigma+1}(a-e^{-\eta})^{-\frac{\sigma+1}{\sigma+2}}\varphi_i^{-1}\mu^{-1}b^{-\frac{(\sigma+1)^2}{\sigma+2}}, & \text{при } -n_i(\gamma_i+\sigma)+1=0,\end{cases}$$

$$a_{i3}(\eta)=\begin{cases}\left(\frac{\sigma+1}{b(\sigma+2)}\right)^{\sigma+2}\frac{b\varphi_i^{-1}\psi_i e^{-s_i\eta}}{a-e^{-\eta}}, & \text{при } -n_i(\gamma_i+\sigma)+1>0,\\ -\left(\frac{\sigma+1}{b(\sigma+2)}\right)^{\sigma+2}\frac{b\varphi_i^{-1}\psi_i e^{-s_i\eta}}{a-e^{-\eta}}, & \text{при } -n_i(\gamma_i+\sigma)+1<0,\\ \left(\frac{\sigma+1}{b(\sigma+2)}\right)^{\sigma+2}\frac{b\varphi_i^{-1}\mu^{-1}\psi_i e^{-(\sigma+2)\eta}}{a-e^{-\eta}}, & \text{при } -n_i(\gamma_i+\sigma)+1=0,\end{cases}$$

$$a_{i4}(\eta)=\begin{cases}\left(\frac{\sigma+1}{b(\sigma+2)}\right)^{\sigma+2}\varphi_i^{-1}\psi_i\frac{be^{-\eta}}{a-e^{-\eta}}, & \text{при } -n_i(\gamma_i+\sigma)+1>0,\\ -\left(\frac{\sigma+1}{b(\sigma+2)}\right)^{\sigma+2}\varphi_i^{-1}\psi_i\frac{be^{-\eta}}{a-e^{-\eta}}, & \text{при } -n_i(\gamma_i+\sigma)+1<0,\\ -\left(\frac{\sigma+1}{b(\sigma+2)}\right)^{\sigma+2}\varphi_i^{-1}\mu^{-1}\psi_i\frac{be^{-\eta}}{a-e^{-\eta}}, & \text{при } -n_i(\gamma_i+\sigma)+1=0,\end{cases}$$

$$s_i=1+\frac{(\sigma+1)\,q_i}{\sigma+\gamma_{3-i}}-\frac{(\sigma+1)}{\sigma+\gamma_i}\quad(i=1,2)\,.$$

Здесь предполагалось $\xi\in[\xi_0,\xi_1), 0<\xi_0<\xi_1, \xi_1=\left(\frac{a}{b}\right)^{\frac{\sigma+1}{\sigma+2}}$.

Поэтому функция $\eta(\xi)$ обладает свойствами: $\eta'(\xi)>0$при $\xi\in[\xi_0,\xi_1)$, $\eta_0=\eta(\xi_0)>0$, $\lim\limits_{\xi\to\xi_1}\eta(\xi)=+\infty$.

Всюду в дальнейшем вспомогательная система уравнений (13) исследуется при следующем ограничении:

$$\lim_{\eta\to+\infty}a_{ij}(\eta)=a_{ij}^0\qquad(\mathrm{i}=1,\ 2;\ \ \mathrm{j}=0,1,2,3,4)$$

существуют, конечны и отличны от нуля, т.е. $0<\left|a_{ij}^0\right|<+\infty$.

В силу введенного преобразований (4),(8),(12) и свойства $\eta\to+\infty$, изучение решений системы (1) сводится к изучению тех решений системы (13), каждое из которых в некоторой окрестности $+\infty$ удовлетворяет неравенствам

$$y_i(\eta)>0,\qquad \mathrm{y_i'}+a_{i0}(\eta)\ \ y_i\neq 0\ \ (\mathrm{i}=1,\ 2)\,.$$

Займемся теперь исследованием асимптотики положительных, имеющих отличный от нуля конечной предел при $\eta\to+\infty$ решений системы (13).

3 Основные результаты

Введем обозначения:

$$c_{i1}=-\frac{1}{(\sigma+2)^{\sigma+2}(\sigma+\gamma_i)\,b^{\sigma+1}\varphi_i},\quad c_{i2}=\frac{1-\gamma_i}{(\sigma+\gamma_i)^{\sigma+2}},\quad c_{i3}=-\frac{\psi_i}{ab^{\sigma+1}(\sigma+2)^{\sigma+2}\varphi_i}\ ,$$

$$c_{i4}=\frac{1-\gamma_i}{(\sigma+\gamma_i)^{\sigma+1}}\ ,\ \ c_{i5}=-\frac{(\sigma+1)\,\mu^{-1}\varphi_i^{-1}}{(\sigma+2)^{\sigma+1}\,b^{\sigma+\frac{1}{\sigma+2}}a^{\frac{\sigma+1}{\sigma+2}}}\quad(i=1,2)\,.$$

Теорема 1. Пусть $(1+q_1)(\gamma_1+\sigma)=(1+q_2)(\gamma_2+\sigma)$, $s_i=0$ и $-n_i(\sigma+\gamma_i)+1>0$. Тогда решение системы уравнения (1) имеет асимптотику при $\xi\to\left(\frac{a}{b}\right)^{\frac{\sigma+1}{\sigma+2}}$

$$u_i(t,x)=A_i\ (T+t)^{-n_i}\left(a-b\xi^{\frac{\sigma+2}{\sigma+1}}\right)^{\frac{\sigma+1}{\sigma+\gamma_i}}y_i(\eta)\,,\quad y_i(\eta)=y_i^0+o(1)\,,\tag{14}$$

где $0 < y_i^0 < +\infty$ (i=1,2) и y_i^0 (i=1,2) являются соответственно корнями $z_i \quad (i = 1, 2)$ системы нелинейных алгебраических уравнений

$$c_{i1} + c_{i2} z_i^{\sigma+\gamma_i} + c_{i3} z_i^{-1} z_{3-i}^{q_i} = 0 (i = 1, 2). \tag{15}$$

Теорема 2. Пусть $(1 + q_1)(\gamma_1 + \sigma) = (1 + q_2)(\gamma_2 + \sigma)$, $0 < \gamma_i < 1$, $s_i > 0$ и $-n_i(\sigma + \gamma_i) + 1 > 0$. Тогда решение системы уравнения (1) имеет асимптотику при $\xi \to \left(\frac{a}{b}\right)^{\frac{\sigma+1}{\sigma+2}}$ вида (14), где $0 < y_i^0 < +\infty (i = 1, 2)$ и $y_i^0 (i = 1, 2)$ являются соответственно корнями $z_i (i = 1, 2)$ системы нелинейных алгебраических уравнений

$$c_{i1} + c_{i2} z_i^{\sigma+\gamma_i} = 0 (i = 1, 2). \tag{16}$$

Теорема 3. Пусть $(1 + q_1)(\gamma_1 + \sigma) = (1 + q_2)(\gamma_2 + \sigma)$, $0 < \gamma_2 < 1$, $s_1 = 0$, $s_2 > 0$ и $-n_i(\sigma + \gamma_i) + 1 > 0$. Тогда решение системы уравнения (1) имеет асимптотику при $\xi \to \left(\frac{a}{b}\right)^{\frac{\sigma+1}{\sigma+2}}$ вида (14), где $0 < y_i^0 < +\infty (i = 1, 2)$ и $y_i^0 (i = 1, 2)$ являются соответственно корнями $z_i (i = 1, 2)$ системы нелинейных алгебраических уравнений

$$\begin{array}{l} c_{11} + c_{12} z_1^{\sigma+\gamma_1} + c_{13} z_1^{-1} z_2^{q_1} = 0, \\ c_{21} + c_{22} z_2^{\sigma+\gamma_2} = 0 \end{array} \tag{17}$$

Теорема 4. Пусть $(1 + q_1)(\gamma_1 + \sigma) = (1 + q_2)(\gamma_2 + \sigma)$, $0 < \gamma_1 < 1$, $s_1 > 0$, $s_2 = 0$ и $-n_i(\sigma + \gamma_i) + 1 > 0$. Тогда решение системы уравнения (1) имеет асимптотику при $\xi \to \left(\frac{a}{b}\right)^{\frac{\sigma+1}{\sigma+2}}$ вида (14), где $0 < y_i^0 < +\infty (i = 1, 2)$ и $y_i^0 (i = 1, 2)$ являются соответственно корнями $z_i (i = 1, 2)$ системы нелинейных алгебраических уравнений

$$\begin{array}{l} c_{21} + c_{22} z_2^{\sigma+\gamma_2} + c_{23} z_1^{q_2} z_2^{-1} = 0, \\ c_{11} + c_{12} z_1^{\sigma+\gamma_1} = 0. \end{array} \tag{18}$$

Теорема 5. Пусть $(1 + q_1)(\gamma_1 + \sigma) = (1 + q_2)(\gamma_2 + \sigma)$, $\gamma_i > 1$, $s_i = 0$ и $-n_i(\sigma + \gamma_i) + 1 < 0$. Тогда решение системы уравнения (1) имеет асимптотику при $\xi \to \left(\frac{a}{b}\right)^{\frac{\sigma+1}{\sigma+2}}$ вида (14), где $0 < y_i^0 < +\infty$ (i=1,2) и y_i^0 (i=1,2) являются соответственно корнями z_i (i=1,2) системы нелинейных алгебраических уравнений

$$-c_{i1} + c_{i2} z_i^{\sigma+\gamma_i} - c_{i3} z_i^{-1} z_{3-i}^{q_i} = 0 (i = 1, 2). \tag{19}$$

Теорема 6. Пусть $(1 + q_1)(\gamma_1 + \sigma) = (1 + q_2)(\gamma_2 + \sigma)$, $\gamma_i > 1$, $s_i > 0$ и $-n_i(\sigma + \gamma_i) + 1 < 0$. Тогда решение системы уравнения (1) имеет асимптотику при $\xi \to \left(\frac{a}{b}\right)^{\frac{\sigma+1}{\sigma+2}}$ вида (1), где $0 < y_i^0 < +\infty (i = 1, 2)$ и $y_i^0 (i = 1, 2)$ являются соответственно корнями $z_i (i = 1, 2)$ системы нелинейных алгебраических уравнений

$$-c_{i1} + c_{i2} z_i^{\sigma+\gamma_i} = 0 (i = 1, 2). \tag{20}$$

Теорема 7. Пусть $(1 + q_1)(\gamma_1 + \sigma) = (1 + q_2)(\gamma_2 + \sigma)$, $\gamma_i > 1$, $s_1 = 0$, $s_2 > 0$ и $-n_i(\sigma + \gamma_i) + 1 < 0$. Тогда решение системы уравнения (1) имеет асимптотику при $\xi \to \left(\frac{a}{b}\right)^{\frac{\sigma+1}{\sigma+2}}$ вида (14), где $0 < y_i^0 < +\infty (i = 1, 2)$ и $y_i^0 (i = 1, 2)$ являются соответственно корнями $z_i (i = 1, 2)$ системы нелинейных алгебраических уравнений

$$\begin{array}{l} -c_{11} + c_{12} z_1^{\sigma+\gamma_1} - c_{13} z_1^{-1} z_2^{q_1} = 0, \\ -c_{21} + c_{22} z_2^{\sigma+\gamma_2} = 0. \end{array} \tag{21}$$

Теорема 8. Пусть $(1+q_1)(\gamma_1+\sigma) = (1+q_2)(\gamma_2+\sigma)$, $\gamma_i > 1$, $s_1 > 0$, $s_2 = 0$ и $-n_i(\sigma+\gamma_i)+1 < 0$. Тогда решение системы уравнения (1) имеет асимптотику при $\xi \to \left(\frac{a}{b}\right)^{\frac{\sigma+1}{\sigma+2}}$ вида (14), где $0 < y_i^0 < +\infty (i=1,2)$ и $y_i^0 (i=1,2)$ являются соответственно корнями $z_i (i=1,2)$ системы нелинейных алгебраических уравнений

$$\begin{array}{l} -c_{21} + c_{22} z_2^{\sigma+\gamma_2} - c_{23} z_1^{q_2} z_2^{-1} = 0, \\ -c_{11} + c_{12} z_1^{\sigma+\gamma_1} = 0. \end{array} \tag{22}$$

Теорема 9. Пусть $0 < \gamma_i < 1$ и $-n_i(\sigma+\gamma_i)+1 = 0$. Тогда решение системы уравнения (1) имеет асимптотику при $\xi \to \left(\frac{a}{b}\right)^{\frac{\sigma+1}{\sigma+2}}$ вида (14), где $0 < y_i^0 < +\infty (i=1,2)$ и $y_i^0 (i = 1,2)$ являются соответственно корнями $z_i (i=1,2)$ системы нелинейных алгебраических уравнений

$$c_{i4} z_i^{\sigma+\gamma_i} + c_{i5} = 0. \tag{23}$$

Доказательство. Полагая в системе (13)

$$v_i(\eta) = \left| \frac{dy_i}{d\eta} + a_{i0}(\eta) y_i \right|^{\sigma} \left(\frac{dy_i}{d\eta} + a_{i0}(\eta) y_i \right) (i=1,2) \tag{24}$$

получим тождество

$$v_i^{'}(\eta) \equiv -a_{i1}(\eta) v_i(\eta) - a_{i2}(\eta) v_i^{\frac{1}{\sigma+1}}(\eta) - a_{i3}(\eta) y_i^{-\gamma_i} y_{3-i}^{q_i} - a_{i4}(\eta) y_i^{1-\gamma_i} \quad (\mathrm{i}=1,2). \tag{25}$$

Рассмотрим теперь функцию

$$g_i(\lambda_i, \eta) \equiv -a_{i1}(\eta)\lambda_i - a_{i2}(\eta)\lambda_i^{\frac{1}{\sigma+1}} - a_{i3}(\eta) y_i^{-\gamma_i} y_{3-i}^{q_i} - a_{i4}(\eta) y_i^{1-\gamma_i} \quad (\mathrm{i}=1,2), \tag{26}$$

где $\lambda_i \in R$, $(i=1,2)$.

Пусть сначала $s_i = 0 (i=1,2)$. Тогда функция $g_i(\lambda_i, \eta)$ (i=1,2) сохраняет знак на некотором промежутке $[\eta_1, +\infty) \subset [\eta_0, +\infty)$ при каждом фиксированном значении λ_i (i=1,2), отличном от значений удовлетворяющих системе

$$-a_{i1}^0 \lambda_i - a_{i2}^0 \lambda_i^{\frac{1}{\sigma+1}} - a_{i3}^0 \left(y_i^0\right)^{-\gamma_i} \left(y_{3-i}^0\right)^{q_i} - a_{i4}^0 \left(y_i^0\right)^{1-\gamma_i} = 0 \quad (\mathrm{i}=1,2).$$

Пусть теперь $s_i > 0 (i=1,2)$. Легко видеть, что функция $g_i(\lambda_i, \eta)(i=1,2)$ при каждом фиксированном значении $\lambda_i (i=1,2)$, отличном от значений удовлетворяющего систему

$$-a_{i1}^0 \lambda_i - a_{i2}^0 \lambda_i^{\frac{1}{\sigma+1}} - a_{i4}^0 \left(y_i^0\right)^{1-\gamma_i} = 0 \quad (\mathrm{i}=1,2)$$

сохраняет знак на промежутке $[\eta_2, +\infty) \subset [\eta_0, +\infty)$.

А в случае $s_i < 0 (i=1,2)$ функцию $g_i(\lambda_i, \eta)(i=1,2)$ перепишем в следующим виде

$$g_i(\lambda_i, \eta) = -a_{i1}(\eta)\lambda_i - a_{i2}(\eta)\lambda_i^{\frac{1}{\sigma+1}} - a_{i3}(\eta) y_i^{1-\gamma_i} \left(y_i y_{3-i}^{q_i} - a_{i4}(\eta) a_{i3}^{-1}(\eta) \right) \quad (\mathrm{i}=1,2).$$

Отсюда ввиду

$$\begin{array}{l} \lim\limits_{\eta\to+\infty} a_{i1}(\eta) = -\frac{(\sigma+1)(1-\gamma_i)}{\sigma+\gamma_i}, \quad \lim\limits_{\eta\to+\infty} a_{i2}(\eta) = \frac{1}{\sigma+2} \left(\frac{\sigma+1}{b(\sigma+2)}\right)^{\sigma+1} \varphi_i^{-1}, \\ \lim\limits_{\eta\to+\infty} a_{i3}(\eta) = \infty, \quad \lim\limits_{\eta\to+\infty} a_{i4}(\eta) = 0 \quad (i=1,2) \end{array}$$

следует, что функция $g_i(\lambda_i,\eta)(i=1,2)$ сохраняет знак на промежутке $[\eta_2,\,+\infty)\subset[\eta_0,\,+\infty)$, где $\lambda_i\neq 0(i=1,2)$. Значит, функция $g_i(\lambda_i,\eta)$ (i=1,2) для всех $\eta\in[\eta_i,\,+\infty)\,(i=1,2)$ удовлетворяет одному из неравенств

$$g_i(\lambda_i,\eta)>0 \quad \text{или} \quad g_i(\lambda_i,\eta)<0(i=1,2). \tag{27}$$

Допустим теперь, что для функции $v_i(\eta)$ (i=1,2) предел при $\eta\to+\infty$ не существует. Рассмотрим случай, когда выполнено одно из неравенств (27). В силу колеблемости функции $v_i(\eta)$ (i=1,2) прямую $\bar{v}_i=\lambda_i$ (i=1,2) ее график бесконечное число раз пересекает на интервале $[\eta_i,\,+\infty)$ (i=1,2). Но это невозможно, так как на интервале $[\eta_i,\,+\infty)$(i=1,2) справедливо одно из неравенств (27) и поэтому из тождества (26) следует, что график функции $v_i(\eta)(i=1,2)$ пересекает прямую $\bar{v}_i=\lambda_i(i=1,2)$ только один раз на интервале $[\eta_i,\,+\infty)\,(i=1,2)$. Следовательно, для функции $v_i(\eta)(i=1,2)$ существует предел при $\eta\to+\infty$.

По предположению $y_i(\eta)$ (i=1,2) имеет представления (14), а функция $v_i(\eta)$ (i=1,2) определена согласно (24) и имеет предел при $\eta\to+\infty$. Тогда $y_i'(\eta)$ (i=1,2) имеет предел при $\eta\to+\infty$, причем равный нулю. Тогда $v_i(\eta)=\left|\frac{dy_i}{d\eta}+a_{i0}(\eta)\,y_i\right|^{\sigma}\left(\frac{dy_i}{d\eta}+a_{i0}(\eta)\,y_i\right)=\left|a_{i0}^0y_i^0\right|^{\sigma}a_{i0}^0y_i^0+o(1)$ (i=1,2) при $\eta\to+\infty$ и в силу (25) производная функции $v_i(\eta)$ (i=1,2) имеет предел, при $\eta\to+\infty$, который очевидно равен нулю.

Следовательно, необходимо, чтобы

$$\lim_{\eta\to+\infty}\left(a_{i1}(\eta)v_i(\eta)+a_{i2}(\eta)v_i^{\frac{1}{\sigma+1}}(\eta)+a_{i3}(\eta)y_i^{-\gamma_i}y_{3-i}^{q_i}-a_{i4}(\eta)y_i^{1-\gamma_i}\right)=0 \qquad (\mathrm{i}=1,2).$$

Отсюда легко убедиться в том, что при $s_i<0,\ -n_i(\gamma_i+\sigma)+1\neq 0$ (i=1,2) система (13) не может иметь решения $(y_1(\eta),\,y_2(\eta))$ с конечным не равным нулю пределом, при $\eta\to+\infty$, а при $s_i\geq 0,\ -n_i(\gamma_i+\sigma)+1\neq 0$ (i=1,2) для существования таких решений необходимо, чтобы соблюдалось условия теоремы 1,2,3,4,5,6,7,8 и при $-n_i(\gamma_i+\sigma)+1=0$ для существования таких решений необходимо, чтобы соблюдалось условия теоремы 9.

Следовательно, в силу введенного преобразований (4),(8),(12) решение системы уравнения (1) имеет асимптотику при $\xi\to\left(\frac{a}{b}\right)^{\frac{\sigma+1}{\sigma+2}}$ и имеет вид (14).
Теоремы доказаны.

4 Заключение

Предварительное качественное изучение автомодельных и приближенно-автомодельных систем уравнений важную роль играет для численного исследования нелинейных параболических систем уравнений недивергентного вида.

Обоснован метод нелинейного расщепления для нелинейных параболических систем уравнений недивергентного вида.

В зависимости от значения входящих в нелинейных параболических систем уравнений недивергентного вида параметров, получены асимптотические представления автомодельных решений.

Исследованы асимптотические поведения решений нелинейных параболических систем уравнений недивергентного вида.

Список литературы

1. Aripov M. Asymptotics of the solution of the Non-Newton Politropic Filtration Equation // ZAMM. – Berlin, 2000. – Vol.80, suppl.3. – P.767–768.
2. Friedman A. and Mcleod J.B. Blow up of solutions of nonlinear degenerate parabolic equations // Archive for Rational Mechanics and Analysis. – 1986. - Volume 96, Issue 1. –P. 55–80.
3. Zhou W., Yao Z. Cauchy problem for a degenerate parabolic equation with non-divergence form // Acta Mathematica Scientia. – 2010. - 30B(5). – P. 1679–1686.
4. Wang M. Some degenerate and quasilinear parabolic systems not in divergence form // J. Math. Anal. Appl. – 274(2002). – P. 424–436.
5. Wang M., Wei Y. Blow-up properties for a degenerate parabolic system with nonlinear localized sources // J. Math. Anal. Appl. – 343(2008). – P. 621–635.
6. Zhi-wen Duan, Li Zhou. Global and Blow-Up Solutions for Nonlinear Degenerate Parabolic Systems with Crosswise-Diffusion // Journal of Mathematical Analysis and Applications. – 244(2000). – P. 263–278.
7. Haihua Lu. Global existence and blow-up analysis for some degenerate and quasilinear parabolic systems // Electronic Journal of Qualitative Theory of Differential Equations. – 2009. – No. 49. – P. 1–14.
8. Садуллаева Ш.А. О свойствах решений одной системы взаимной реакции-диффузии с двойной нелинейностью // Материалы конференции "Предельные теоремы теории вероятностей и их приложения". – Фергана, 2011. – С. 243–246.
9. Aripov M., Sadulaeva Sh.A. To properties of solutions to reaction diffusion equation with double nonlinearity with distributed parameters // Jour. of Siberian Fed. Univer. Math. Phys. – 6(2013). – P. 157–167.
10. Chunhua J., Jingxue Y. Self-similar solutions for a class of non-divergence form equations // Nonlinear Differ. Equ. Appl. Nodea. – 2013. – Vol. 20, Issue 3. – P. 873–893.